

THE UNIVERSITY OF HULL

Monitoring and Modelling hydrological response and sediment yield in a North York
Moors Catchment: An Assessment of Predictive Uncertainty in a Coupled
hydrological-sediment yield model

being a Thesis submitted for the Degree of
Doctor of Philosophy

in the University of Hull

by

Margaretta S.A. Ayoung, BSc. (Hons.) UWI, 1993, MSc. Hull 1996.

March, 2001

Abstract

A fully distributed coupled hydrological-sediment yield model was developed. An assessment was made of the predictive uncertainty in the individual model predictions, as well as the uncertainty propagated from the primary hydrological model to the secondary sediment yield model, using the Generalised Likelihood Uncertainty Estimation (GLUE) methodology. The value of additional data, in the form of additional periods of flow data, as well as deterministic (based on landuse and soil type) and random spatial parameterisation of hydrological parameters in restricting model uncertainty of the spatially lumped model parameterisation were examined, using Bayesian updating.

The results revealed significant model uncertainty in both the hydrological and sediment yield models, with uncertainty bounds widest at peak flow and sediment flux, and predictive failure in recession flows, similar to other applications of GLUE methodology. Uncertainty in the sediment yield model was found to be due to uncertainty inherited from the hydrological model, as well as simplifying assumptions made about sediment removal and transport, and resulted in lower model efficiencies and generally poorer qualitative sedigraph fit.

The model validation exercise revealed that the calibrated 'optimum' parameter set was not 'optimum' for all validation periods and resulted in inaccurate spatial and temporal hydrological response predictions for the validation periods. This suggested that traditional split-sample model calibration methods may not be effective in capturing the true spatial and temporal variability of the system.

Successive periods of flow data were effective in reducing the calibration period uncertainty bounds. Similarly, the use of sediment yield predictions to update hydrological model uncertainty resulted in a reduction in hydrological model uncertainty. Spatially distributed parameterisation was found to also improve model predictions, resulting in a reduction in uncertainty bounds, particularly for soil-distributed parameterisation. However, stochastic parameterisation of spatially variable hydrological parameters provided equally acceptable predictions for both models, suggesting that a deterministic approach might not be required to capture the spatial variability in hydrological and sedimentological response in the study catchment, and that a stochastic approach may be adequate.

Acknowledgements

This thesis represents the culmination of four years of extensive field and laboratory studies into the hydrological and sedimentological response of a North York Moors catchment. It was not done in isolation, however, and I would like to acknowledge the contributions of the following people and institutions:

My supervisor, Dr. James Brasington, for academic guidance and advice throughout this research. Mr. Brendan Murphy, for advice and assistance in the field. The Environment Agency for allowing me access to the Kirkby Mills gauging station throughout the field programme, and providing me with data. My family, for their love and support.

This research was made possible by a 'Sir Brynmor Jones' scholarship from the University of Hull, and additional assistance from the Geography Department. I would also like to thank the following Trusts for the financial assistance they provided which permitted me to complete my PhD after my scholarship funding ended:

The Churches Commission for Overseas Students

The Leche Trust

Northern Foods

Table of Contents

Abstract	i
Acknowledgements	ii
Table of Contents	iii
CHAPTER 1 – Introduction	
1.0 Context of the Thesis	1
1.1 Uncertainty, Stochasticity and Randomness in Environmental Modelling	2
1.2 Uncertainty in Coupled Hydrological-Sedimentological Models	5
1.3 The Structure of the Thesis	9
CHAPTER 2 – Literature Review	
2.0 Summary	10
2.1 Introduction	10
2.1.1 Sediment Delivery	10
2.2 Temporal Issues in the Sediment Yield Process	11
2.3 Spatial Issues in the Sediment Yield Process	14
2.4 Problems of a Blackbox Concept	16
2.5 General Modelling Philosophies and approaches	17
2.5.1 Functionalist and Realist Approaches	18
2.5.2 Deterministic and Stochastic Approaches	21
2.6 Hydrological Modelling Approaches	22
2.7 Empirical Models	23
2.7.1 Empirical Hydrological Models	23
2.7.2 Empirical Sediment Models	25
2.8 Conceptual Models	27
2.8.1 Conceptual Hydrological Models	27
2.8.2 Conceptual Sediment Models	31
2.9 Physics-based Models	32
2.9.1 Physics-based Hydrological Models	32

2.9.2 Physics-based Sediment Models	39
2.10 Hybrid Models	43
2.10.1 Hybrid Hydrological Models	43
2.10.2 Hybrid Sediment Models	48
2.11 Conclusion	53
CHAPTER 3 – Farndale Catchment	
3.0 Summary	55
3.1 Farndale in its Regional Setting	55
3.2 Topography and Relief	58
3.3 Catchment Geology	63
3.4 Landuse	68
3.5 Soil Type	71
3.6 Hydrometry	81
3.6.1 Rainfall	81
3.6.2 Streamflow	86
3.6.3 Evapotranspiration	91
3.7 Catchment Turbidity and Suspended Sediment	92
3.7.1 Regional Sediment production	92
3.7.2 Suspended Sediment Monitoring in Farndale Catchment	98
3.8 Study Period Rainfall and Sediment Flux Analysis	102
3.8.1 Study Period Rainfall	102
3.8.2 Study Period Turbidity Data	104
3.9 Conclusion	109
CHAPTER 4 - Model Description	
4.0 Summary	111
4.1 The Hydrological Model	111
4.2 Hydrological Model Structure	116
4.3 Snowmelt Model Structure	126
4.4 Sediment Model	137
4.5 Uncertainty	146
4.5.1 Model Calibration and Uncertainty Analysis	146

4.5.2 Generalised Likelihood Uncertainty Estimation (GLUE)	147
4.5.3 Updating Likelihood Weights – Bayesian Updating	149
4.6 Summary of Model Developments	152
4.7 Model Implementation and Analysis	154

CHAPTER 5 – Lumped Spatial Parameterisation

5.0 Summary	155
5.1 Introduction	156
5.2 Model Implementation	159
5.3 Operational Testing	159
5.3.1 Hydrological Model Results and Analysis	159
5.3.2 Parameter Sensitivity Analysis	160
5.3.3 Model Calibration and Uncertainty Estimation	166
5.3.4 Model Validation	176
5.3.5 Bayesian Updating using flow data	191
5.4 Sediment Yield Model Results and Analysis	196
5.4.1 Parameter Sensitivity	196
5.4.2 Calibration and Uncertainty Estimation	198
5.4.3 Sediment Model Validation	210
5.5 Bayesian Updating and Error propagation in the coupled model	227
5.5.1 Updating hydrological predictions using sediment data	227
5.5.2 Propagation of Uncertainty to the Sediment Yield Model	236
5.6 Conclusion	238

CHAPTER 6 – Deterministic Spatial Parameterisation

6.0 Summary	240
6.1 Introduction	241
6.2 Distributed Parameterisation	242
6.3 Hydrological Parameter Sensitivity	248
6.3.1 Hydrological Model Calibration – results and Uncertainty Analysis	251
6.4 Model Validation	258
6.5 Sediment Model Calibration	272
6.6 Sediment Model Validation	286

6.7 Bayesian Updating using Sediment Data	310
6.8 Propagation of Uncertainty to the sediment Yield Model	321
6.9 Conclusion	325
CHAPTER 7 – Random Spatial Parameterisation	
7.0 Summary	327
7.1 Introduction	327
7.2 Method of Random Spatial Parameterisation	337
7.3 Results and Discussion	342
7.4 Conclusion	368
CHAPTER 8 – Discussion	
8.1 Introduction	369
8.2 Contribution to the GLUE methodology	371
8.3 The Way Forward	375
CHAPTER 9 – Conclusion	
9.1 Model Coupling	377
9.2 Model Uncertainty	378
9.3 The value of additional data	379
9.4 The value of spatially distributed data	381
9.5 Limitations	383
9.6 Thesis Conclusions	384
BIBLIOGRAPHY	386
APPENDIX 1	407
APPENDIX 2	423

CHAPTER 1 – Introduction

1.0 Context of the Thesis

In many areas of the world flooding and soil erosion represent significant environmental hazards with deleterious consequences for agriculture, property, infrastructure as well as posing a direct threat to human life (e.g., Blakie, 1985). Growing concern about recent acceleration in process rates, and non-stationarity of storm-event frequency and magnitude requires the development of rigorous, process-based, explanations of catchment dynamics in order to provide the basis for robust and reliable predictive strategies designed to minimise the impacts of flooding and sedimentation. This pursuit of process-based numerical simulation models has intensified over the last two decades. However, while significant progress has indeed been achieved in this direction, there is now growing awareness of the importance of a critical review of predictive capability from both operational and realist perspectives (Beven, 1993). A significant manifestation of this increased criticality is the recent emphasis on the development of new methods for open assessment of predictive uncertainty in environmental simulation models (Beven, 1989; Beven and Binley, 1992). This trend reflects the increasingly accepted view that parameter interaction, insensitivity, and inter-dependence, errors in model structure and observation data, lack of knowledge of boundary and initial conditions, non-linearity of threshold values, spatial and temporal lumping, all lead to uncertainty in model predictions.

One radical approach to the uncertainty dilemma promulgated by Beven (1993) is the complete rejection of an optimal model structure and parameterisation in favour of a ‘post-modern’ perspective emphasising a plurality of different, but *a priori*, equally acceptable model formulations. This approach holds to empirical reality through the systematic rejection of parameterisations or model structures through the iterative comparison of modelling and observed variables, measured relative to a statistical likelihood yardstick. At the heart of this approach lies an acceptance that while the catchment system can indeed be considered deterministic (at least at the macroscale), the inevitable incompleteness of model process description and in particular,

specification of spatially and temporally variable boundary conditions, implies the need for a stochastic treatment of catchment variability.

The assessment of model uncertainty is becoming increasingly important as an environmental planning tool (e.g. development on river flood plains), a disaster-preparedness tool, a design tool (e.g. in the construction of bridges, dams, etc.), a tool to calculate insurance premiums in high-risk areas and, hence, an important decision making tool in the environmental sciences (e.g. Bobba *et. al.*, 1996; Van Rompaey *et. al.*, 2001). Any assessment of model uncertainty must necessarily start with a general discussion of the concept of uncertainty and related concepts used in environmental modelling.

1.1 Uncertainty, Stochasticity and Randomness in Environmental Modelling

The use of probabilistic methods in modelling environmental systems started about 35 to 40 years ago – to a large extent growing out of the concepts of stochastic hydrology. Initially, the literature discussed variance and accuracy, rather than the concepts of uncertainty, stochasticity, or randomness and, by the mid-1980s, were used inconsistently. An attempt is made here to distinguish among the three.

Uncertainty

At the International Symposium on Uncertainty in Hydrological and Water Resource Systems (1972) several different definitions of uncertainty were presented. Moore and Brewer (1972) postulated that uncertainty is the result of insufficient information, reflecting our ignorance about the system under investigation, and may be reduced if more information becomes available. Ince (1972) suggested that uncertainty is the result of errors in field data and instrumentation difficulties, while Yu (1972) suggested that uncertainty, results from natural, random variations in parameters.

By the mid-1970s, the concept of uncertainty was at best unclear, and in some instances, the term was used interchangeably with error. For example, Burges and Lettenmaier (1975) defined one type of uncertainty as “the result of the choice of an incorrect model which has correct deterministic parameters”, while O’Neil and Gardner (1979) used the opposite approach by defining one source of error as

“uncertainty in model parameters”. In general, error can be defined as the difference between a computed or measured value and a ‘correct’ value. Error, as used in mathematical modelling, should therefore, be defined as the deviation of an output from some historical value or set of values, assumed to be ‘correct’ for that place, time and set of conditions, while factors which cause the deviation, and which can be identified and corrected, should be called “sources of error” (Tumeo, 1994). This concept remained pertinent and easily understood as long as it was believed that the purpose of an environmental model was to find a single, deterministic, “true” value, error. However, with the realisation that nature is not deterministic, by definition, the concept of the existence of a single, deterministic answer has been challenged by environmental modellers.

If uncertainty is simply considered to be the concept or condition of being in doubt about a value, then there is no judgement as to the “correctness” of a given value. In addition, the assumption that the error can be identified and corrected, distinguishes error from uncertainty. While error implies that there is a single “correct” value that can be found, uncertainty involves doubt, perhaps even about the idea of “correctness”, which may have profound consequences for the traditional concept of model validation and usefulness (Lund, 1992).

Hence, uncertainty, as applied to modelling, should imply only that a given value, may or may not occur in the future. Incomplete knowledge of the process, or failure to include all pertinent factors which impinge on the variable of interest, will result in uncertainty. Thus, increased knowledge, better understanding of natural processes, and more accurate representation of the environment, both in terms of model structure and accuracy of measurement, will all reduce uncertainty.

Stochasticity and Randomness

Stochasticity was not a popular term in the modelling literature until the early 1980s. Instead, most modellers spoke of “randomness” and most probabilistic modelling used Monte Carlo techniques (e.g. Freeze, 1975; Smith and Freeze, 1979a and b; Freeze, 1980). In general, it has become common to use the terms randomness and stochasticity as synonyms. However, there are important distinctions between these two concepts (Tumeo, 1994; Zielinski, 1991).

A process is random if, given complete knowledge of all previous outcomes, it is not possible to predict the next outcome. Because of the complex nature of environmental systems, natural processes rarely repeat exactly, even if all conditions are exactly the same. Hence at any one instant in time or point in space, there is a range of possible realisations of the process, and it is not possible to predict (within the range of possible outcomes) what the next outcome will be, even if all previous outcomes are known.

An important characteristic of randomness is its relationship to probability. If something is random and totally unpredictable, it is chaotic. This is not to be confused with chaos theories which, deal not with 'true chaos', but with randomness in general. If a process is random but its outcomes follow a pattern such that knowledge of the previous outcomes allows the identification of the probability of various outcomes in the next iteration, the process is stochastic. Hence stochasticity can be defined as random variations of processes over time and space, the magnitude, frequency, duration and/or other characteristics of which can be described by theories of probability.

Embedded in the concept of stochasticity is the idea that this random variation is mathematically describable by some probability distribution. This makes stochasticity a subset of randomness, which can be either probabilistic in nature (stochastic behaviour), or completely undefinable (chaos). In this context, the application of probability theory becomes most useful. One speaks of the "probability" of a given value or the chance that an event will occur. Stochasticity should be used to speak of the natural, probabilistic, random variability in environmental parameters and processes. It is then easy to see the distinction between stochasticity and 'randomness'.

These definitions also highlight the idea that "uncertainty" encompasses, but is not synonymous with, randomness and error. Model predictions can also be in doubt or "uncertain" due to errors in the data against which the model is calibrated, in the underlying assumptions and simplifications of the model, or in the parameter or input variables used. However, if all errors could be eliminated, there would still be

uncertainty. This is because “uncertainty” also arises from the fact that natural processes exhibit both stochastic and chaotic randomness.

The main approach to the evaluation of uncertainty in hydrology and water resources, has been to consider that the world is basically indeterministic, and must, therefore be modelled in terms of stochastic systems. This implies that stochasticity cannot be avoided at present, due to our limited understanding, but would give way to increasingly deterministic descriptions when our understanding improves. Uncertainty in hydrology and water resources, importantly includes directions of change, and dominating mechanisms. Moreover, according to the theory of chaotic systems, the time series of hydrological variables are unpredictable over long time horizons, which are inherently uncertain. Uncertainty in hydrology may result from the natural complexity and variability of hydrological systems and processes and from deficiency in our knowledge, and may pertain to magnitudes and spatio-temporal attributes of signals and states of hydrological systems (storages).

1.2 Uncertainty in Coupled Hydrological-Sedimentological models

Continued developments in computing power have had a largely two-fold impact on the fields of hydrological and sedimentological modelling. First, it has enabled the development of more complex models of both hydrological response and sediment yield, with increased physical understanding of processes. Second, it has enabled the application of techniques to assess the uncertainty in models. The results thus far have shown that such detailed physically-based models are prone to predictive uncertainty, and exhibit model equifinality whereby more than one parameter set and/or model structure can be an acceptable descriptor of the system under investigation.

In most environments, the geomorphological development of the landscape and processes of erosion, deposition and weathering, are dependent on the flow of water. Consequently, modelling of geomorphological processes must necessarily depend on the modelling of hydrological processes. In turn, the modelling of hydrological processes depends on the form of the landscape, which controls convergent and divergent flow paths, soil and vegetation development. This interaction of hydrological and geomorphological processes will shape the development of the

landscape over long periods of time within the context of climate, and tectonic change. On shorter timescales too, hydrological-sedimentological interactions are evident in the sediment delivery process. Thus the frequency and magnitude of overland flow over the hillslope controls the spatial and temporal distribution of soil erosion, while the quantity of suspended sediment carried in the flow may affect flow velocities (Govers, 1990; Torri and Borselli, 1991).

Equifinality in hydrological modelling refers to the possibility of obtaining more than one model structure and/or more than one parameter set which describe the system being modelled, equally well. Equifinality in geomorphological modelling, however, also relates to the difficulty of identifying and re-constructing the dominant processes responsible for the creation of a particular landform (Culling, 1957; Chorley, 1962, Haines-Young and Petch, 1983; Lane and Richards, 1996), at the time of morphological change. The interaction of discharge and sediment supply in channel change processes illustrates this problem. Sediment supply is determined both by patterns of erosion and deposition upstream, and by more local sediment supply from eroding banks. Catchment sediment yield reflects the interaction of discharge fluctuations with the availability of transportable sediment, and by the interaction of sediment supply, discharge, erosion and deposition patterns throughout the catchment. It may not be possible to define a particular discharge as dominant, because of the multiple discharge and sediment supply combinations that could cause change. This is supported by what is known about sediment rating curves, which rarely show a simple functional relationship between discharge and sediment transport rate (e.g. Bathurst, 1987, Walling and Webb, 1983, Moore and Clarke, 1983), because both bed sediment availability and upstream sediment supply affect point sediment transport rates. Hence, the response of the system to an imposed event depends on the 'conditioning' effect of previous events (Newson, 1980), which define the context that determines system response. This conditioning has a spatial manifestation, both because process patterns depend on a three-dimensional morphological initial condition and the spatial distribution of transportable sediment, and because of the time taken for the effects of a particular event to be propagated through the system.

Paola (1996) illustrated the dependence of sediment transport rate, at the basin scale, by treating a braided river as a stochastic system, and developing spatially averaged

equations for sediment flux through a procedure that is analogous to the Reynolds-averaging process in turbulence studies. Lane and Richards (1996) showed that morphology due to the interaction of previously imposed discharge and sediment supply, determines the way in which current sediment supply and discharge fluctuations interact to cause particular patterns of morphological change. The strong coupling between form and process is manifest as a spatially distributed feedback (e.g. Ashworth and Ferguson, 1986). In river catchments, such a feedback implies a state of continual change which results from continually changing the external process events (discharge, sediment supply) operating in the context of existing channel morphology and sedimentology (Lane, *et. al.*, 1996). The changes in morphology and sedimentology, caused by the process events, in turn, result in a different response to similar process events. The catchment can thus be envisaged as being on a trajectory, where what goes on in the future is critically dependent upon the spatio-temporal effects of what happened in the past, and what is happening at present. Hence, catchment morphology and sedimentology cannot be explained without including the imposed external conditions at particular points in space and time, as well as internal, primarily topographical and sedimentological, information (Schumm, 1991).

Only within the last six years have coupled models of hillslope and sediment production and transport and of channel form, discharge and sediment transport started to appear (e.g. Bathurst *et. al.*, 1995). In virtually all hydrological analysis and models that take some account of catchment topography, catchment characteristics are considered fixed (e.g. Beven *et. al.*, 1994, Refsgaard and Storm, 1995). Hence feedback between hydrology and geomorphology are not generally considered. While this was due to the lack of computing power, measurement techniques and data in the past, it is primarily attributable to a lack of interest of hydrologists in sediments (Lane and Richards, 1996). The topographic controls on flow pathways have only recently been reflected in the model structures used by hydrologists (e.g. Stephenson and Freeze, 1974; Beven and Kirkby, 1979; O'Loughlin, 1981; Abbott *et. al.*, 1986; Beven *et. al.*, 1995; Ambroise *et. al.*, 1996). In addition, the shorter time scales of hydrologically significant processes compared to geomorphologically significant events, as well as the relatively advanced understanding of hydrological processes, meant that hydrological modelling developed more rapidly than geomorphological modelling. Consequently, the assessment of hydrological model uncertainty has also

advanced more rapidly than that of sedimentological model uncertainty, and, given the lack of feedback representation, there has been no assessment, of the propagation of model uncertainty from the primary hydrological model, to the secondary sedimentological model in a coupled hydrological-sedimentological model.

Uncertainty and equifinality in geomorphological modelling is primarily due to the fact that geomorphological data is generally more difficult to obtain over sufficient periods of time and sequences of events to decide between multiple working hypotheses (or models). In addition, given the transience of geomorphological systems, their reliance on past and present processes, and the possibility of chaotic behaviour (Phillips, 1992), the trajectory of their development is difficult to reconstruct, on the basis of present day evidence alone. Beven argues therefore that dynamical systems theory, suggests that equifinality may not be an indication of poorly developed methodology, as Haines-Petch and Young (1983) suggested, but may be implicit in the nature of geomorphological systems.

While the interaction of hydrological and sedimentological processes within river catchments have been known and acknowledged, no attempt has been made to quantify the effect of explicitly coupling such models, on model uncertainty.

This thesis has four main aims:

1. To couple a fully distributed hydrological model to a dynamic fully distributed, conceptual sediment yield model.
2. To examine the uncertainty in the fully-distributed hydrological model, and the sediment yield model.
3. To examine the controls of spatially variable soil hydraulic parameters on hydrological and sedimentological response, and the effectiveness of spatially variable parameterisation in reducing model uncertainty. Two different approaches to spatially variable parameterisation are considered – deterministic and stochastic.
4. To examine the propagation of uncertainty from the hydrological model to the sediment yield model.

1.3 The Structure of the Thesis

Chapter 2 reviews the literature on sediment yield processes, and hydrological and sediment yield model development. Chapter 3 describes the physical characteristics of Farndale catchment - the study area, outlines the monitoring programme undertaken during the research conducted for this thesis, and examines the nature of hydrologic and suspended sediment storm response in the catchment. In Chapter 4, a detailed description of the coupled hydrological and sediment yield models are presented, as well as a discussion of the methodology employed in the analysis. The model results are presented in the next three chapters. Chapter 5 presents and discusses the results of the lumped spatial parameterisation calibration, validation and uncertainty assessment. Chapter 6 presents the results of the deterministic spatial parameterisation, and examines the effect of deterministic spatial parameterisation on model equifinality and uncertainty of model predictions, making direct comparison to the lumped parameterisation, to determine the added accuracy that deterministic spatial parameterisation offers. Chapter 7 presents the results of the random spatial parameterisation and, similarly to chapter 6, compares the effect of random spatial parameterisation on the accuracy of model predictions. A general discussion of the results is presented in chapter 8, and the thesis conclusions are presented in chapter 9.

Units

Throughout the thesis hydrographs are plotted in units of mm/hr in order to make them directly comparable to other reported work. The spatial distribution of soil moisture deficit is in m. Sediment flux timeseries is in $\text{gm}^{-2} \text{hr}^{-1}$ as in other work (e.g. Webb and Walling, 1993), while the spatial distribution of sediment depth is in m.

CHAPTER 2 – Literature Review

2.0 Summary

The objective of sediment yield modelling is to quantify the amount of sediment which is transferred, in a given time interval, from eroding sources through the channel network to the basin outlet (Ferro and Minacapilla, 1995). Catchment sediment yield is thus the result of spatially and temporally heterogeneous sediment availability, detachment and transport throughout the basin. In turn, fluvial soil erosion and sediment yield are governed by the processes of runoff generation. Many sediment-related models are, therefore, coupled to hydrological models, making them susceptible to the propagation of errors from the primary hydrological model. The inextricable link between hydrological and sedimentological processes is reflected in the concurrent development of modelling approaches in both fields. This chapter examines the processes governing catchment sediment yield, and reviews the development of hydrological and sedimentological modelling approaches including attempts to couple hydrological and sediment models.

2.1 Introduction

2.1.1 Sediment Delivery

The delivery of sediment to the catchment outlet can be considered as a two-component process, involving supply and transport phases, analogous to runoff generation and routing. A major component in sediment yield modelling is loss, or storage accounting, which is potentially very complicated. In general, only a fraction of the sediment eroded within a drainage basin finds its way to the basin outlet. The remainder is transferred to temporary or permanent storage on concave slopes, at the base of slopes, in swales, on the floodplain, or in the channel itself. The ratio of sediment delivered at the catchment outlet ($\text{t km}^{-2}\text{yr}^{-1}$) to gross erosion or sediment mobilisation within the basin ($\text{t km}^{-2}\text{yr}^{-1}$) is called the *sediment delivery ratio* (D_r).

The delivery ratio is the resultant of the various processes involved between on-site soil erosion and downstream sediment yield. The sediment delivery ratio for a

particular basin is influenced by a number of geomorphological and environmental factors, including the nature, extent and location of sediment sources, the relief and slope characteristics, drainage pattern and channel conditions, vegetation cover, landuse, soil texture (Walling, 1983) and climate. Many researchers (e.g. ASCE, 1975; Boyce, 1975; Maner, 1962) have reported an inverse relationship between sediment delivery ratio and basin area. ASCE (1975) suggested that the relationship could be modelled as a power function with the form:

$$D_r = kA^n \quad [2.1]$$

Where D_r is the sediment delivery ratio, A is the basin area, k and n are numerical constants, and the exponent, n , has been found to be in the range -0.01 to -0.25 (Richards, 1993; Ferro and Minacopilli, 1995). Variability of delivery ratio for a given basin area is due to the influence of local factors such as soil type and landuse. Boyce (1975) suggested that the inverse relationship can be explained by the ‘upland’ theory which argues that steep headwater areas are the main sediment-producing zones of a basin, and that as average slope decreases with increasing basin size, sediment production per unit area decreases. Richards (1993) attributes the inverse relationship to the increase in storage opportunities with increasing basin size, as the extensive floodplain and valley-fill development in large, high-order basins, buffers the effect of slope basal erosion and isolates the river from direct hillslope sediment supply. This results in a discontinuity in sediment transfer from slopes to rivers, which in turn results in a significant time lag between sediment production and output. Glymph (1954), Roehl (1962), and Williams (1977) all found similar inverse relationships between D_r and other basin morphometric factors such as relief or gradient. Richards (1993) argues, however, that it is difficult to uniquely identify catchment properties which influence D_r , as the methods of estimating D_r from morphometric analysis are generally unreliable because of the lack of standardisation of the procedures and time scales adopted for individual basins.

2.2 Temporal issues in the sediment yield process

The time lag between sediment production and output makes sediment delivery ratio sensitive to the temporal scale of measurement. There may be wide variability in the

intra-storm period for a given event, as well as between individual storms of comparable magnitude and duration, and between individual storms of varying magnitude and duration. This variability is reflected in the wide range of delivery ratios and residence times reported in the literature. Piest *et. al.* (1975) report a range of 6% to 72% over 7 years for one basin, indicating the sensitivity of D_r to variations in annual runoff and seasonal soil moisture status, and rainfall distribution. Trimble (1983) derived a delivery ratio of 6% for an 85 year period from measurements of the volume of alluvial fill between dated stratigraphic markers, while Walling (1983) reports ratios greater than 500% for storm period time scales, possibly due to channel erosion, and the re-mobilisation of sediment stored during previous events. Dietrich and Dunne (1978) report residence times (where residence time is the storage volume divided by throughput rate) in the valley floor of an Oregon basin ranging from 31 years in mobile gravel bars to 619 years in the channel zone, and 4933 years for the floodplain fill in total.

Patterns of sediment storage and re-mobilisation within the basin as a result of changing landuse practices may also account for temporal discontinuities in sediment delivery (e.g. Gurnell and Midgley, 1993). For example, severe soil erosion may occur during one period resulting in the accumulation of alluvium in the valley systems, which might be re-mobilised and transported out of the system, even when improved landuse practices are introduced, resulting in an increase, rather than the expected decrease in sediment yield. Such a response represents a considerable discontinuity in the erosion-sediment yield relationship when viewed on a timescale of less than or equal to 50 years or so (Walling, 1983). Even under more natural or undisturbed conditions, storage and re-mobilisation may occur in the delivery process. For example, when gradual accumulation is followed by the exceedence of either an extrinsic threshold during a catastrophic event, or an intrinsic threshold of stress or of strength of materials, episodic erosion and deposition results (Schumm, 1973). Schumm and Hadley (1957) used threshold-controlled flushing to explain epicyclic cut-and-fill in semi-arid basins. The concept of threshold exceedence forms the basis of the theory of channel extension by headward erosion (e.g. Montgomery and Dietrich, 1989; Montgomery and Foufoula-Georgiou, 1993; Dietrich *et. al.*, 1993; Montgomery and Dietrich, 1994). The process of headward cutting occurs as progressive in-filling of the hollow by colluvium initially encourages subsurface flow

and down-hollow migration of the stream head, until failure of the store exposes the subsoil or bedrock, and allows headward extension of the exterior link draining the hollow. Dietrich *et al.* (1986), suggest that the rate of accumulation of alluvium is proportional to sideslope gradient and to the difference between sideslope and hollow gradient. The rate of accumulation of colluvium therefore decreases with time as the cross-sectional area gradually increases due to infilling of the hollow. As hollow gradient gradually decreases, so too does the difference between the sideslope and hollow gradient. Hollow failure and hence sediment mobilisation occurs by landsliding when a critically unstable accumulation depth has developed and/or when a rainstorm capable of generating critical positive pore-water pressures occurs. Progressive changes in stability of these sediment stores (in hollow) are influenced by several mechanisms, which reflect the link between channel form and process.

Event Scale

The time lag between sediment production and output results in the incoherent phasing of sediment and water waves during a storm event and seasonally, which gives rise to complex hysteretic behaviour in the sediment load-discharge relationships (Walling and Webb, 1982; Oliver and Rieger, 1984; Bathurst, 1987; Williams, 1989). Exhaustion of sediment in progressive timesteps will also give rise to hysteresis (Walling and Webb, 1982; Moore and Clarke, 1983). Hence, the SSC-Q (suspended sediment concentration – discharge) rating curve approach may be flawed, as the suspended sediment yield may be out of phase with runoff in any given timestep.

In general, representation of the temporal variation of sediment delivery (and therefore sediment yield) requires the representation of four main types of processes.

1. The relatively gradual accumulation process which reflects soil development, weathering, and processes that re-distribute colluvium in the slope profile;
2. Hysteresis due to the time lag between discharge and sediment waves, and due to the effects of exhaustion;
3. The progressive and intrinsic changes which contribute to destabilisation of the store, and;

4. Mobilisation of the stored sediment, and delivery to the fluvial transport system by extreme extrinsic events of a meteorological and hydrological nature that can generate erosion by runoff or rapid mass movement.

2.3 Spatial issues in the sediment yield process

Spatial diversity of topographic, landuse and soil conditions within a basin could be expected to produce considerable local variations in sediment delivery response. The sediment delivery ratio, is a spatially lumped concept (Ferro & Minacapilli, 1995), but in reality sediments are produced from different sources distributed throughout the basin, each of which is characterised by detachment, transport, supply and availability (Richards, 1993). Burns (1979) suggested that each sediment source should be viewed as possessing a unique delivery potential, and that the probability of sediment being exported from a particular source should be a function of its relative position with respect to the stream and basin divide. In general, total basin sediment yield is derived from only a small proportion of the basin (e.g. Gregory and Walling, 1973), particularly when sediment sources are landslides feeding directly into the channel. Even when sediment is supplied by overland flow transport, the proportion of the basin affected is limited by the development of variable source or partial contributing areas of overland flow (Walling, 1983; Dunne and Leopold, 1978). Hence the magnitude of the sediment delivery ratio is related to the relative extent and characteristics of this zone rather than the characteristics of the entire basin. The delivery ratio can therefore vary through time, in response to changes in the extent of the contributing area, in a non-linear manner. For example, if the contributing area expands primarily in the riparian zone bordering the stream, the delivery ratio may decline as the probability of sediment being exported, is inversely proportional to the distance of the sediment source from the stream, and the relative position with respect to the stream and basin divide. If, however, the expansion was accompanied by a major increase in the density of the drainage network, the delivery ratio might increase. Moreover, the dynamics of a variable contributing area might be expected to embrace the re-mobilisation of sediment deposited within secondary source areas which remain disconnected from the stream network under normal conditions, but contribute to the network during extreme storm events (Walling, 1983).

An assessment of the spatial distribution and characteristics of sediment sources within the catchment is important to the assessment of sediment delivery. Inherent in Burns' (1979) concept of sediment source 'unique delivery potential' is the varying 'activation potentials' of sources. Wolman and Miller (1960) examined the relative importance of events of varying magnitude and frequency of occurrence in sediment mobilisation and landform evolution and found that although extreme events were important, there was a heavier dependency on both the magnitude and frequency of occurrence of individual events. They found that, irrespective of climatic and physiographic differences, 50% of the total suspended load is transported by flows which occur on average, one or more days per year, and the remaining 50% by less frequent flows. Half of the suspended sediment was found to be removed by low to moderate flows. Best (1986) reports that 5% of sediment stored in active, semi-active, and semi-stable deposits underlying the present channel and on the floodplain and terraces of a Californian creek was activated by flows 1m in depth, having a return of less than 10 years. 90% was classed as stable. He estimates that a ten-fold increase in the active-store sediment yield would occur if semi-stable deposits became more active. However, such deposits occur preferentially in wide valley sections where the competence of the necessary extreme events is reduced.

The activation potential of a source is also dependent on the characteristics of the stored sediment such as grain-size. Richards, (1993) suggests that since grain-size is itself inversely related to basin area, the delivery ratio-basin area relationship incorporates several self-cancelling effects. Williams (1975), in one of the few attempts to quantify the grain-size influence, suggests that as median particle size increases from 0.001mm to 0.1mm, the delivery ratio decreases from 37% to 6%, based on the model:

$$D_r = \exp(-\beta TD_{50}^{0.5}) \quad [2.2]$$

Where D_r is the sediment delivery ratio, D_{50} is the median particle size, T the travel time and β the routing coefficient.

Comparison of sediment source and particle size characteristics provides a more direct indication of the effect of particle size. Walling (1983) for example approximated the delivery ratio, D_r , using the percentages of clay (C%) in eroding soil and suspended sediment.

$$D_r = \frac{C\%_{soil}}{C\%_{sediment}} \quad [2.3]$$

assuming that the clay itself passes straight through the channel transport system. Suspended sediment delivery ratios of 30 – 50% are predicted with the above equation for basins up to 2.7km² and are lower for basins with sandier soils. Slattery and Burt (1997) report that the sediment size distribution of eroded sediment from an Oxfordshire basin was coarser than the size distribution of the sediment's primary particles for both stream sediments and surface runoff samples. This suggests that sediments were being transported to the outlet as aggregates. In addition, they found that the relationship between particle size of stream suspended sediment and discharge, was complicated by the influx of fines (silt and clay) by overland flow along vehicle wheelings, roads and tracks, and the entrainment of fine material from the bed and banks of the channel. This resulted in an increase in fines and a decrease in coarser material with increasing discharge, contrary to the traditional positive discharge-particle size relationship. If equation [2.3] is used to calculate delivery ratio in this catchment, then an artificially high value might be obtained.

2.4 Problems of a Blackbox Concept

The sediment delivery ratio is effectively a catchment-scale blackbox concept, which incorporates a variety of processes, each related to environmental variables in a specific manner, making it difficult to assess the importance of various controlling factors. Different morpho-climatic zones are characterised by different process assemblages, and thus have delivery ratios which reflect the dominant erosion processes occurring in each zone, as well as the morphology of the basin (Walling, 1983). It may therefore be necessary to distinguish the processes of sediment delivery from different types of sources by taking account of morphometric variables. In order to understand the linkages between source area erosion and downstream sediment yield, the various processes subsumed in the delivery ratio must therefore be

represented in detail. A sediment yield model must, therefore, take account of dynamic non-linear spatial and temporal variability of sediment delivery.

Walling and Webb (1982) suggest that any meaningful sediment yield model should include the following:

- A realistic representation of the storm runoff production, as the driving agent for sediment yield.
- A reproduction of the hysteretic behaviour of sediment concentration during the intra-storm period.
- Incorporation of the temporal variability of sediment availability in both the inter- and intra-storm periods.
- Incorporation of the partial/variable source area concept of storm runoff production, as a means of representing the spatial heterogeneity of sediment availability, exhaustion and recovery.

Bathurst and Wicks (1991) add that a practical sediment yield model should also be able to incorporate scenario modelling, as a tool to investigate catchment processes.

Given the importance of runoff representation in sediment yield modelling, as implied above, the following section will concurrently review developments in both hydrological and sediment yield modelling approaches.

2.5 General Modelling Philosophies and approaches

A system can be defined as a set of processes that converts an input variable(s) into an output variable(s), where a variable is a characteristic of the system that can be measured and that assumes different numerical values at different times (Clarke, 1973). Hydrological or sedimentological models are concerned with the relationships between hydrological or sedimentological variables that describe those aspects of the system's behaviour that are of interest to us, and can be described by the general equation:

$$y_t = f(x_{t-1}, x_{t-2}, \dots; y_{t-1}, y_{t-2}, \dots; a_1, a_2, \dots) + \varepsilon_t \quad [2.4]$$

Where the vector variable $\{x_t\}$ is the system input, the vector variable $\{y_t\}$ is the output, and a the system parameters. The function f defines the nature of the model and the error term, ε_t , is an expression of the lack-of-fit with observed reality. The processes that convert input hydrological variables to output hydrological variables can be physical, chemical and/or biological. Although hydrological systems are complex and heterogeneous, their integrated response to climatic inputs is relatively smooth and often stationary (Wheater *et. al.*, 1993). At the simplest level, a catchment hydrological system is the set of processes that convert climatic inputs to runoff outputs at the outlet, and include evapotranspiration, soil moisture storage, and groundwater recharge. A hydrological model representing this system can be as simple as a coupled volumetric loss function, and a time distribution function, to represent the various dynamic modes of catchment response (Wheater *et. al.*, 1993). Similarly, sedimentological response is relatively simple compared to the complexity and heterogeneity of the processes it incorporates, as is reflected in the relatively simple concept of the sediment delivery ratio. In general, sediment yield can be modelled using an erosion model and a mathematical operator that expresses the sediment transport efficiency of the hillslopes and the channel network (Renfro, 1975; Kirkby and Morgan, 1980; Walling, 1983). However, sedimentological models have the added complexity of representing non-linear stress-strain relationships where the same flows may not always generate the same sediment flux. Despite the simplicity of both these systems' responses and the relatively simple models that can be used to represent them, several different modelling approaches of varying complexity can be identified and are usually distinguished by their levels of mathematical and physical approximation and levels of spatial aggregation.

2.5.1 *Functionalist and Realist Approaches*

Both hydrological and sedimentological model development have occurred (to some extent) along the lines of changing needs and capabilities, as well as changing philosophies within both fields. It is important to recognise that any particular modelling approach should reflect the aims and philosophy of the modeller. Beck *et. al.* (1993) suggest that a modeller may take either a philosophical or pragmatic approach to modelling, depending on their aims and perspectives. In the *philosophical* approach the mathematical model is primarily used as a tool for

understanding processes and interactions in the natural system, while the *pragmatic* approach is concerned with the applicability of the mathematical model as a tool for decision-making. This dichotomy of approaches has previously been considered by O’Connell (1991) who identified the *descriptive* approach - analogous to the *philosophical* approach, and the *prescriptive* approach - analogous to the pragmatic approach.

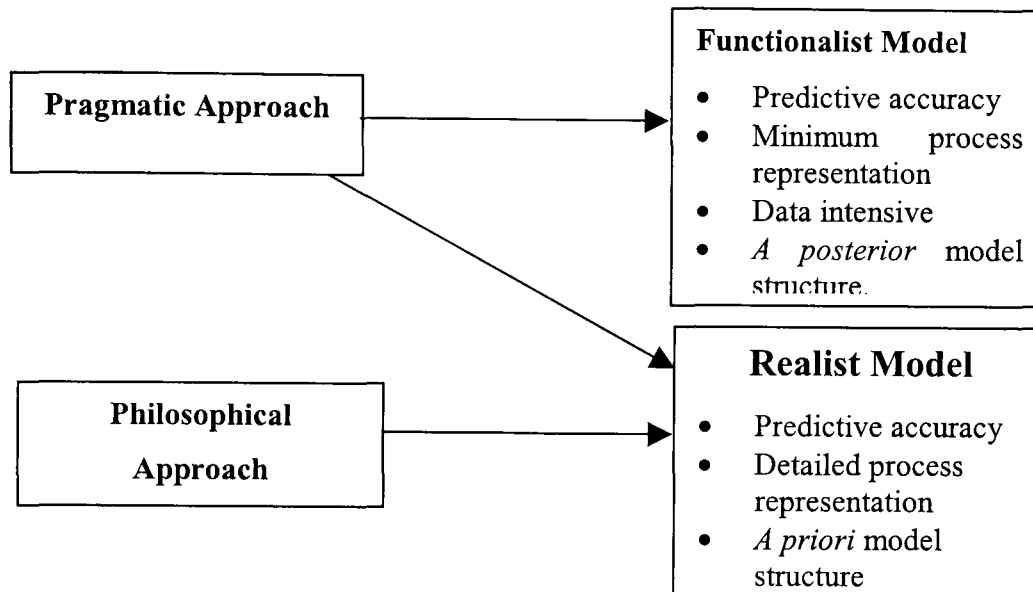


Fig. 2.1 The relationship between modelling approaches and model types.

Purely pragmatic perspectives of system modelling follow Bennett and Chorley’s (1978) *functionalist* methodology. Such models are based on the desire for accurate prediction of the system behaviour, even if it does not attempt to describe the processes and causative links of the natural system. Functionalist models are thus commonly based on a set of empirical or statistical relationships, and require no *a priori* description of the model structure, so that the model may adapt dynamically within a given simulation (Wood and O’Connell, 1985). These models require large amounts of historical data for model definition and/or calibration. They are widely applied in operational forecasting where the emphasis is on accurate predictions rather than system evaluation and understanding.

If the modelling approach is both philosophical and pragmatic, then the model is described as realist. Realist models are based on a desire to represent the dynamics of a system in terms of its governing processes and are therefore capable of both predicting and explaining system behaviour. Model structure is therefore defined *a priori*, and processes are represented in terms of the fundamental physical laws of

motion and thermodynamics, making explicit use of the principles of conservation of mass, energy and momentum. The model flow equations are physically-based, complex functions, which require prerequisite knowledge of the geometry of the region within which flow takes place, and the spatial and temporal distribution of its parameters and boundary conditions, as well as the spatial distribution of its initial conditions. Accurate analytical solutions to the governing equations are only usually possible where the boundary description is simplified to give regular symmetrical geometry and homogeneous, isotropic properties. Therefore it is only possible to obtain approximate solutions using numerical methods. The realist approach has been facilitated by developments in numerical schemes such as the finite difference methods (e.g. Freeze, 1971; Smith and Woolhiser, 1971), finite element methods, (e.g. Beven, 1977; Ross *et. al.*, 1979), integrated finite difference methods (e.g. Narashimhan and Witherspoon, 1977) and boundary integral methods (e.g. Lui and Liggett, 1979), in addition to increased computational power required for their implementation. The use of numerical rather than analytical solutions implies that continuous processes are represented in terms of discrete approximations of time and space. The scale of spatial and temporal ‘discretisation’ reflects a necessary compromise between the scale of physical observability of the system and the enhanced accuracy and stability of solutions that accompany the use of higher resolutions.

Because the system is described in terms of scientific laws and is spatially distributed, realist models provide the opportunity to examine the precise nature of the mechanics of the system as a whole, as well as elements of the system represented in each unit of spatial discretisation. This predictive capability may be used to couple one model’s set of process predictions to another model, the predictions of the first giving the boundary conditions of the second model. This coupling may, in principle, offer the potential for using a limited set of inputs to drive secondary processes. A relevant example is the coupling of an overland flow model, driven by hydrometeorological inputs, with sediment availability and transport equations for the prediction of the temporal and spatial patterns of soil erosion (e.g. Bathurst and Purnama, 1991; de Roo *et. al.*, 1996). Similar coupling has been used to provide more complex subgrid parameterisations of land-surface effects in GCMs (e.g. Famiglietti and Wood, 1991; Quinn *et. al.*, 1995a; Wood *et. al.*, 1992). Another significant aspect of realist models is that physics-based governing equations have parameters that are observable

properties of the natural system, and in principle should not require calibration. Hence realist models should be geographically-transportable, and applicable for ungauged catchments, with only minimum parameterisation. By extension, they should be capable of forecasting the effect of changes in processes due to changes in environmental conditions that are not directly observable (i.e. that haven't occurred as yet) - scenario modelling.

2.5.2 Deterministic and Stochastic models

Both functionalist and realist models may adopt either a stochastic or a deterministic structure. Clarke (1973) states that

“whether a model is stochastic or deterministic depends on whether or not it contains random variables.”.

while Chow (1964) states:

“If the chance of occurrence of the variables involved in such a process is ignored and the model is considered to follow a definite law of certainty but not any law of probability, the process and its model are described as deterministic. On the other hand, if the chance of occurrence of the variables is taken into consideration and the concept of probability is introduced in formulating the model, the process and its model are described as stochastic or probabilistic”.

Deterministic models therefore offer only one unique solution to a given set of inputs and internal state conditions, thus ruling out the choice of alternative or multiple solutions. They assume that one unique solution of the system does actually exist in nature. If any of the model's variables are described by probability distribution functions, on the other hand, then the model is said to be stochastic. Stochastic models represent model predictions as the combination of systematic and random components. The stochastic or probabilistic approach therefore acknowledges the fact that some parameters and processes may vary randomly in space and time, resulting in non-unique solutions. While this approach does not rule out choice, it does not guarantee it. That is, it merely suggests that there may be more than one solution to the system, but does not guarantee that there is. Kiesel (1969) said

“In the stochastic approach uncertainty by way of probability laws is woven into the fabric of hydrodynamic and phenomenological relations which define mean-value behaviour of a system with zero mean-square error”.

Hence commonly used methods of assessment of predictive uncertainty of deterministic models, which *a posteriori* attempt to ascertain the uncertainty in model output due to input variable and parameter variability (e.g. GLUE Beven and Binley, 1992), represent a fusion of the stochastic approach with the deterministic, in that, they acknowledge that the residual, ε_i in equation [2.4], may be stochastic. In this respect the deterministic and stochastic approaches complement each other as prescribed by Clarke (1973).

2.6 Hydrological Modelling Approaches

Three main types of hydrological (and sedimentological) modelling approaches can be identified: metric (or empirical), conceptual and physics-based (Beck *et. al.*, 1991). Distinction is made according to the extent to which the physical processes acting upon the input variable(s) to produce the output variable(s), are considered in the formulation of the function, $f(\cdot)$, of equation [2.4]. However, this distinction may be seen as somewhat artificial, since many of the “physics-based” process equations contain empirically derived coefficients, while the parameters of some explicitly empirical models may be shown to have physical relevance. For example, Darcy’s law, although derived from first principles by Hubbert (1940), is based on observation and laboratory experiments, and hence is empirical by strict definition (Clarke, 1973; Mandelbrot, 1970; Nelder *et. al.*, 1972). In a different context, the differential equations describing turbulent open-channel flow, derived by considerations of conservation of mass and momentum, require an estimate of Manning’s empirical roughness coefficient (Eagleson, 1970). At the other end of the spectrum, Diskin (1970), shows that quasi-physical interpretations for the parameters α and β of the linear regression $y_t = \alpha + \beta x_t + \varepsilon_t$, where x_t and y_t are annual rainfall and runoff from a catchment respectively, can be made.

The discussion that follows considers each of these modelling approaches in turn, in terms of their underlying philosophies and the changes in modelling demands and technological-capability that accompanied and/or facilitated their development.

2.7 Empirical Models

2.7.1 Empirical Hydrological Models

The main aim of empirical models is to accurately predict a given system's behaviour, without consideration of process description, or causation. The underlying philosophy is therefore pragmatic and the approach functional. Empirical models make no assumptions about the internal processes of the natural system, and represent the conversion of inputs to outputs as a set of 'black-box' transfer functions. They are data intensive and rely on the fit between observed and predicted data to 'define' model structure *a posteriori*. They are, therefore, most often used in operational forecasting, where accurate output is required, and where there is a need for rapid calculations to obtain forecasts well in advance of the event.

The first empirical approach in hydrology was the rational formula of Mulvaney (1851), used to calculate the peak discharge of the storm hydrograph, and may be expressed in the form:

$$Q_{peak} = ciA \quad [2.5]$$

Where, Q_{peak} is the maximum event discharge (in L^3T^{-1}), i is the rainfall intensity (in LT^{-1}) and A , the total catchment area (L^2). The coefficient c , is a dimensionless constant called the runoff coefficient which determines the portion of the total rainfall which becomes storm runoff.

The unit hydrograph theory of Sherman (1932) was the first attempt to simulate a complete streamflow hydrograph. The streamflow hydrograph is conventionally split into stormflow, $x_q(t)$, and baseflow, $x_s(t)$, response components. The unit hydrograph $h(t)$ is that part of the streamflow hydrograph that represents the stormflow response at time t to a unit input of rainfall excess $u(t)$, where rainfall excess is the total rainfall minus losses due to evapotranspiration, changes in storage and baseflow contributions. That is, it is the portion of the total rainfall that contributes to stormflow response. Stormflow is therefore the total number of unit hydrographs produced by effective rainfall, and is modelled as a linear, time invariant function of effective rainfall, i.e. its convolution with the unit hydrograph.



$$x_q(t) = \int_0^t h(t - \tau)u(\tau)d\tau \quad [2.6]$$

Total runoff is then simply the sum of the stormflow ($x_q(t)$) and baseflow ($x_s(t)$) components. This simple model meets the first basis requirements of a hydrological model as stated above, by representing the hydrological system as a loss function converting input to output. By using data from a range of events, the various dynamic modes of catchment response can be represented, thus meeting the second basis requirement. The main attraction of this model is the use of a linear relationship between stormflow and effective rainfall. Further developments of the model were undertaken in the 1950s and 1960s, focusing on linear response functions based on statistical and Fourier analysis (Dooge, 1973), and model identification methods (Nash, 1960; O'Donnell, 1966). An important development was the IHACRES approach of Jakeman *et. al.*, (1991), which uses Q_{t-1} as a form of API. This is important as a means of investigating what systems modelling reveals about the catchment response. Attempts at regionalisation (NERC, 1975) by characterising the UH for identifiable catchment physiographic and climatological characteristics followed, as well as characterisation of response to inter-storm variability (Wheater *et. al.*, 1982).

The time-area curve (Surkan, 1969) was developed as an extension of the rational model. This model uses a generalised knowledge of the catchment shape and topography to develop a synthetic catchment response. It couples the rational formula to a runoff routing model to represent the temporal distribution of the transfer of effective rainfall to the outlet. Routing is achieved by dividing the catchment into a number of isochrones and assigning a different effective (i.e. spatially uniform) velocity to each. Response to rainfall is simply related to the proportion of total rainfall excess generated within each isochrone (controlled by the coefficient c), and the travel time of runoff from the isochrone (controlled by the velocity). The time-area curve, can be considered to be the 'first' conceptual Instantaneous Unit Hydrograph based directly on catchment structure. The cumulative distribution function of the curve (which gives the percentage of the catchment responding to rainfall input at any given time) when differentiated, (or approximated by finite

differences) represents an IUH where its convolution with any measure of rainfall excess results in the prediction of stormflow.

2.7.2 Empirical Sediment Models

A common empirical approach to sediment yield modelling involves establishing a statistical relationship between concurrent sediment concentration and discharge at the basin outlet, using existing hydrometeorological and sediment yield data. The simplest relationship is the sediment concentration rating curves, which are usually given as log-log or power functions of the form,

$$\log c = b \cdot \log Q + \log a \quad \therefore \quad c = aQ^b \quad [2.7]$$

where, c is the sediment concentration (ML^{-3}), Q is the river discharge (L^3T^{-1}), and a and b are model parameters, most commonly obtained by non-linear regression analysis. Rating curves, however, often display a large degree of scatter (Walling and Webb, 1982; Pickup, 1988; Slattery and Burt, 1997). In addition, the method is prone to errors associated with data collection techniques, which are biased to the inter-storm period, when sampling is systematic and no attempt is made to fully characterise individual storm events. The recent use of turbidimetric methods of suspended-sediment concentration monitoring (e.g. Gippel, 1989; Brasington and Richards, 2000) offers the potential for high-resolution continuous sediment time-series allowing for more comprehensive parameterisations of the rating curve. These new data collection methods are, however, also prone to errors (see chapter 3). The variable phasing of discharge and SSC waves which results in hysteresis in the sediment delivery process, will also lead to considerable scatter in the rating relationship. Walling (1977), identifies different rating relationships with rising and falling discharges, in an attempt to account for the hysteresis, while Williams (1989) suggests a number of different rating relationships capable of modelling a wide variety of hysteretic behaviour. Another source of scatter in the rating curve is the variation in the spatio-temporal rate of sediment supply, which results from the underlying assumption inherent in the metric model approach, that the system is transport limited. Such behaviour, may be expected to be more significant over short

spatio-temporal scales and may be regularised with increasing scale (Brasington, 1997).

Another common empirical approach to estimate the average annual sediment yield of a basin, is to first estimate the average annual gross soil erosion or sediment supply, using the Universal Soil Loss Equation, USLE (Wischmeier and Smith, 1960), which is then multiplied by an estimate of catchment sediment delivery ratio, SDR. The USLE is the most widely used soil erosion model, and was developed from historical plot scale data in the USA. It is a multiplicative-factor model of soil erosion, which incorporates all the factors that are considered to be important in the erosion process. In its classic form the USLE is given by:

$$A = R.K.L.S.C.P \quad [2.8]$$

where A is gross erosion rate per unit area for a plot of specified size, not including the effects of gully or channel erosion, aeolian erosion and sediment re-deposition; R is the rainfall and runoff erosivity factor; K is the soil erodibility for a given soil type; LS is the topographic factor where L is the dimensionless slope-length factor, expressed as the ratio of soil loss from a slope, relative to the 22m slope used in the plot experiments, and S is the dimensionless slope gradient factor, again expressed as a ratio of the soil loss relative to a 9% slope used in the plot experiments; C is the dimensionless land-use factor expressed as a ratio of soil loss relative to a tilled fallow field; and P is a land management factor. All factors are derived empirically, which seriously limits the geographical transportability of this model. Wischmeier (1976) cautioned against using the USLE for purposes other than those for which it was designed, which is primarily to predict annual soil loss resulting from erosion and deposition on slope segments, but not deposition on the lower parts of the fields. It is therefore not useful for predicting sediment flux on a continuous basis. Many studies evaluating the USLE under specific conditions at different locations (e.g. Onstad *et al.*, 1976; Albaladejo and Stocking, 1989; Kramer and Alberts, 1986; and Freebairn *et al.*, 1989), failed to agree on the overall reliability of the model. Others (e.g. McIsaac *et al.*, 1987; and McCool *et al.*, 1987), investigating the effects of the topographic factor, LS , have concluded that the equation over-predicts on steep slopes, which is not surprising since the equation was designed for slopes from 3 to 18%, and < 122m

in length. Weltz *et al.*, (1987), Osborn *et al.* (1977), and Trieste and Gifford (1980), all showed that it under-predicted erosion on rangeland plots. Unfortunately, despite these findings, the USLE has gained widespread popularity as it is parametrically simple, easy to apply, conceptually appealing, and has a strong epistemological legacy (Risse *et al.*, 1993).

Further problems with estimating sediment yield using the USLE are encountered due to the method by which the sediment delivery ratio is determined, and the problems of spatial and temporal lumping inherent in the concept of sediment delivery ratio. The SDR required by the USLE must be specified *a priori*. In the absence of extensive field measurements SDR is estimated from existing empirical data. Several multiple-regression models have been developed to predict variations of the delivery ratio based on basin morphometric factors such as basin area, basin length, relief and channel slope. These relationships tend to exhibit a high degree of scatter and are therefore a major source of error in the model. In addition, there is a problem of non-standardised methods for deriving such relationships as mentioned earlier (section 2.2). Application of SDR models based on empirical morphometric relationships are inevitably dependent on the existence of an extensive database, further compounding the limited geographic transportability of the model.

2.8 Conceptual Models

2.8.1 Conceptual Hydrological Models

The early 1960s saw a change in modelling demands, particularly as the evaluation of potential consequences of environmental changes due to land-use and climate change became critical, largely due to an increased global environmental awareness and the upsurge in international treaties that sought to protect the environment (e.g. Stockholm, 1972). This change in demand was therefore accompanied by a divergence in model philosophy towards a more realistic perspective.

Conceptual models were developed to meet this changing demand, and were facilitated by the development of digital computers in the 1960s, which enabled the design of more quantitatively complex descriptions of hydrological systems based on an increasingly improved understanding of classical hydrological theory. These

models represent the first move away from event-based modelling toward an attempt to simulate continuous water balance within the catchment, and make explicit use of continuity equations to simulate response.

Dooge (1973) defines conceptual models as models that are based on a simple arrangement of a relatively small number of elements, each of which is a simple representation of a physical relationship. These so-called Explicit Soil Moisture Accounting models (ESMA) are commonly designed for continuous accounting for all water into, out from and stored within the soil. This is commonly achieved by representing components of the hydrological system, such as soil and vegetation, as a series of stores or reservoirs, connected by component processes of the hydrological cycle such as infiltration, evaporation, vertical and lateral subsurface flow and channel routing (Boyle *et. al.*, 2000). The number and configuration of the stores reflects the modeller's perception of the natural system, and the level of accuracy desired. Model structure is specified *a priori* – an improvement on the, statistically defined, *a posteriori* metric model structure. This subjective approach to the *a priori* specification of model structure of conceptual models has led to a wide range of model complexities. Process representation is often by quasi-physically based mathematical functions that link the model, only loosely, to the theoretical physical basis of the processes, and often assume some degree of linearity of the processes.

Another simplification employed in conceptual modelling is that of spatial lumping of model parameters. Spatially average properties allow a one-dimensional analysis of inputs and outputs over time. Input data therefore represent catchment totals, without taking account of within-catchment variability. The implications of such spatial lumping in hydrological modelling are discussed in the next section with respect to physics-based models.

Calibration of conceptual models

While conceptual models embody a representation of catchment processes, the parameters that govern the models' process functions are not usually directly observable. Consequently, parameter values must be identified, *a posteriori*, by the process of calibration, also termed system identification. This may be performed manually or using an automatic search algorithm. The first approach usually involves

the manual progressive refinement of model parameters until the user determines, usually by qualitative or semi-qualitative assessment, that the best fit has been achieved. This process allows the modeller to emphasise certain aspects of the model's predictive capability, which may be deemed to be more important than others for a given basin or time. The subjectivity that is involved in the qualitative assessment of the fit can be reduced through the use of an objective function and a definition of a criterion or criteria for the goodness of fit, as an aid to model assessment. Thus both the quality of the fit and the magnitude of the variance from the observed, can be determined. A common objective function used is the sum of squares of the residuals given by:

$$\varepsilon_t = \sum [Q_{pred} - Q_{obs}]^2 \quad [2.9]$$

Where Q_{pred} and Q_{obs} is the predicted and observed flows respectively. There are various optimisation criteria that may be used to terminate the search. For example, the model is said to be optimised when there is no further reduction of the value of ε_t by modifying the parameter values, or when there is no further change in predicted discharge ($dQ_{pred}/dt = 0$), or $F < x$, or after n steps.

Alternatively, an automatic parameter fitting, or optimisation procedure using computer algorithms that incorporate an objective function may be used to refine parameter estimates. This usually involves the use of iterative comparison of the observed and predicted hydrographs until the process converges on the optimised parameter set, according to some pre-determined criterion or criteria. The objective function is therefore critical to model calibration and the determination of model validity. However, the term “objective” may be somewhat misleading. Wheeler *et al.* (1986) noted that the shape of the objective function is determined by three factors: the field observations; the model structure and its parameters; and the type of estimator. The sensitivity of the objective function to these factors is due to the fact that the objective function makes certain assumptions about the residuals that are not always valid. For example the sum of squared errors makes the following assumptions about the residuals:

1. The mean, $\bar{\varepsilon}_t$, is zero and the variance, σ_ε^2 is constant (second-order stationarity). However, residual variance tends to increase as discharge increases (Douglas, 1974), and is therefore sensitive to high flows. If particular emphasis is to be placed on the model fit at peak flows, then a higher even power than the square of the error can be used (e.g. Chapman, 1970; Dawdy and Litchy, 1968)
2. The residuals are mutually un-correlated. Recession flows commonly show long sequences of identical values. Hence, if the emphasis is on low flows, then the objective function can be based on the logarithm sum of squares. Clarke (1973) suggests that a contributing factor may be the correlation between discharges automatically introduced where they are estimated from a fitted stage-discharge curve.
3. The residuals are normally distributed. Residuals commonly have distributions that are markedly skewed.
4. The log-likelihood given by:

$$\text{Log } L = \text{constant} - N \log \sigma_\varepsilon - \sum_t \varepsilon_t^2 \sigma_\varepsilon^{-2}$$

is approximately quadratic in the parameter values a_1, a_2, \dots in equation 2.4. However, several different surfaces have been characterised for the sum of squares.

Extensive research has been undertaken on different optimisation methods. Dawdy and Litchy (1968) and Chapman (1970) investigated alternatives to the sum of squared-errors. Sorooshian *et. al.* (1983) and Sorooshian and Gupta (1983) investigated least-squares and maximum likelihood methods, and found that a poor fit obtained using the maximum likelihood methods was accompanied by improved prediction, demonstrating the difference between calibration performance and predictability.

The main aim of model calibration – the identification of an optimal parameter set that provides a unique solution – is hardly ever achievable in practice (Hamon and Hannan, 1963) for a number of reasons.

1. Parameter compensation effects; interaction with model structure.
2. The presence of multiple solutions and discontinuities in the parameter hyperspace;
3. The dependence on input data.

At the root of the problems of model calibration of multi-parameter conceptual models is that the model complexity exceeds the information content of the available data (Wheater *et. al.*, 1986; Beck *et. al.*, 1990; and Jakeman and Hornberger 1993). This is termed ill-conditioning, and it implies that it becomes difficult to identify one optimum parameter set, due to the limited information contained within the observed data, compared to the assumptions of the model structure. This conflict reflects the earlier observation, that hydrological systems, although complex and heterogeneous, often exhibit relatively smooth and stationary behaviour, particularly in its integrated response. One solution to this problem is to simplify the model to an appropriate degree (e.g. Nash and Sutcliffe, 1970), by doing a preliminary assessment of model sensitivity to each parameter. The number of parameters to be optimised is then reduced by holding the insensitive parameters constant (e.g. Blackie and Eeles, 1978; Hornberger *et. al.*, 1985; Sorooshian and Gupta, 1985). Mein and Brown (1978) demonstrated that a thirteen parameter conceptual model could be successfully optimised using just three, with only marginal loss of accuracy. Alternatively, complexity can be reduced by altering the original model concepts, but at the risk of reverting to the metric approach, if the conceptual model is over-simplified.

2.8.2 Conceptual Sediment Models

Conceptual sediment yield models, like their hydrological counterparts, were developed to meet the growing need for detailed insight into internal process mechanisms, and to enable scenario modelling. Such models are based on a limited consideration of the physical processes of sediment detachment and transport, are parameterised empirically, and employ a large degree of spatial and temporal lumping.

The processes of sediment entrainment and transport, are complex, and are often represented by coupled hydrologic and sediment processes. The first attempt to represent the complex processes of sediment entrainment and transport by coupled hydrologic and sediment processes was the Stanford Sediment Model, SSM, of Negev (1967), which couples a rainfall-runoff model for the prediction of overland flow with representations of sediment detachment and transport rates. The SSM model, however, is limited by the use of spatially lumped parameters, which do not characterise the spatial variability of the processes. More recent attempts at such

integration include the soil erosion models of Morgan *et. al.*, (1982) and Brooks *et. al.*, (1993).

Conceptual sediment models recognised that the spatial discretisation of the sediment yield process allowed for the representation of within-basin variability in sediment source types and delivery ratios, and takes account of the fact that much of a basin's sediment yield is produced in only a small percentage of the total basin area. For example, low slope downstream areas have low delivery ratios (Boyce, 1975), and steep areas near main channels contribute to both erosion and sediment yield while steep fields remote from the channel network are characterised by local erosion but contribute little to sediment yield. Kling (1974) spatially distributed SDR using a neighbourhood function, based on the gradient between adjoining cells in a regular grid, and Boyce (1975) used catchment drainage structure in a similar manner. Dickinson *et. al.* (1986) derived local SDR for each discretised field unit within which the USLE is applied, based on Manning's n , the ground slope, and seasonal parameters defining the proportion and flowpath length of overland flow. This approach has two important advantages over those of Kling (1974) and Boyce (1975). Firstly, the spatial discretisation of SDR is at the same scale as the erosion model and, secondly, the SDR parameterisation takes account of seasonal variability in flow characteristics and hence in SDR.

2.9 Physically-based Models

2.9.1 Physically-based Hydrological Models

By the early 1970s it was recognised that conceptual models did not meet the requirements of a changing field that was becoming increasingly concerned with understanding hydrological processes, rather than merely predicting their behaviour. Models based on classical mechanistic equations of unsaturated (Richards' equation), saturated (Darcy's law) and open channel (St. Venant's equations) flow were used to describe hydrological processes. Solution to these non-linear continuous partial differential equations were made possible by developments of numerical approximation techniques, such as finite difference and finite element methods, which require spatial and temporal discretisation of the system under study. Further developments in computer power in the 1970s facilitated this computationally

intensive, distributed approach which was perceived as a marked improvement on spatially lumped conceptual models, and which led to the inter-changeable term “distributed models”. Freeze and Harlan (1969) proposed the first distributed model structure upon which most of the currently used models are based, while Freeze (1972) implemented the first computerised two-dimensional hillslope model. The solution of the process equations at each node within the discretised space domain allows the prediction of hydrological processes at a number of points within the catchment, thus enabling an assessment of the spatial distribution of hydrological response.

Another perceived advantage of physically-based models over other types is that, because model equations are based on hydrological laws, model parameters are, in theory, measurable in the field, thus eliminating the need for parameter optimisation. With parameter optimisation (and therefore the need for historical data) eliminated, this approach should permit a high degree of geographical transportability, an ability to simulate un-gauged catchments, and the ability to predict response under non-stationary conditions. In practice, however, model calibration is usually necessary, and is subject to many more problems than conceptual model calibration, as will be discussed later.

Given the distributed nature of physically-based models, model parameters representing distributed catchment characteristics such as land use, soil type, and geology can be measured and used as model inputs, thus allowing an assessment of the effect of these spatially distributed input variables. Spatial distribution also allows prediction of the effect of land use changes occurring over parts of the catchment. This is an important advantage as the change in hydrological response is dependent on the location of the land use change. For example, deforestation of an area on the catchment divide may have a very different effect from deforestation of a riparian contributing area in a valley bottom hollow (Beven, 1985). In addition, given the physical basis of their equations and their spatially distributed prediction capabilities, these models can potentially be used to forecast the highly spatially and temporally variable movements of pollutants and sediment within the catchment.

Despite the clear philosophical superiority of physics-based models (Howes and Anderson, 1988), and their aforementioned potential advantages over other types, their application and interpretation is far from straightforward. Indeed it has been strongly argued that many of the proposed advantages of catchment-scale distributed models remain largely unproven (Beven, 1985; Anderson and Rogers, 1987; Beven, 1989; Grayson *et. al.*, 1992).

The problems facing application of distributed hydrological models can be attributed to six main causes (Beven, 1985).

1. Model structure.
2. Spatial heterogeneity in system responses that are not well represented at the grid cell scale.
3. Errors in input data and output data used in model calibration or validation.
4. Over-parameterisation
5. Parameter interdependence.
6. Model equifinality

Model Structure and Spatial Heterogeneity

The main aim of physically-based models is to provide a fully deterministic description of hydrological processes. A full description of the three-dimensional heterogeneous flow pathways and spatially and temporally variable input and output processes that characterise a catchment, requires perfect knowledge of the physical characteristics of the entire system and accurate descriptions of the governing system processes. To achieve this, physically-based models require parameter values at every grid element and, to ensure model stability and convergence to the original differential equation, high resolution spatial discretisation and short time intervals. The computational requirements to facilitate this fully deterministic approach are enormous and often, simplifications are necessary. Such simplifications often include modifications to the model structure, the use of simplified process equations, and reduction in the number of grid elements used. Model structure simplification is usually achieved by a reduction in the dimensionality of process representation. For example, in the *Système Hydrologique Europeen (SHE)* model (Abbott *et. al.* 1986) channel flow and unsaturated flow are represented as one-dimensional processes, whilst overland and saturated subsurface flow is represented as two-dimensional.

Simplification of the St. Venant equations of open channel flow by the assumption of kinematic flow, or removal of diffusion terms, has often been employed. While the kinematic description of surface flow is computationally simpler than the full St. Venant equations, models based on these assumptions encounter problems. They cannot predict ‘looped’ rating curves, nor the backwater effects due to downstream disturbances that may be important in forecasting areas of flooding. In addition, they are subject to artificial ‘kinematic shock’ due to fast-travelling disturbances overtaking slower waves, as a result of neglecting the diffusive and inertial effects that would, in reality, obscure these ‘shocks’ (Beven, 1985). Simplifications are also used in subsurface flow descriptive equations. For example, Darcy’s equation for saturated subsurface flow, assumes (i) the only fluid involved in the flow is water; (ii) the porous medium is incompressible; (iii) the water is of constant density and viscosity; (iv) osmotic forces are negligible, and the governing forces are purely hydraulic; and (v) the medium is isotropic (and in some cases homogeneous) (Beven, 1985). In addition, Darcy’s equation does not account for the hysteresis observed in the relationships between hydraulic conductivity and soil moisture and capillary potential and soil moisture. The extensive field measurements required to characterise these relationships make it difficult to do so. As such further simplifications are often necessary in the specification of initial and boundary conditions, since these factors are rarely available from measured data. Mathematically convenient conditions are usually used which, in some cases, are also hydrologically reasonable, but which will, however, result in problems when this is not the case. Model application to complete catchment systems requires the specification of internal boundary conditions within the flow domain, e.g. between the reaches in a channel network or at the interface between a surface flow and an underlying porous medium. Instead, flow processes are often externally coupled using quasi-simultaneous solutions, rather than fully integrated ones (Freeze, 1978; Anderson and Rogers, 1987). This inability to accurately specify internal boundary conditions is a major problem encountered in the application of distributed models to complete catchment systems.

One major similarity between lumped conceptual models and physically-based distributed models is the use of effective or spatially lumped parameters. This is a reflection of the failure of physically-based models to realise their stated advantage of

having measurable parameters. In practice, full spatial parameterisation of a study area cannot be achieved at the required scale of model discretisation, as extensive field investigation is time-consuming and costly. Instead, point measurements are used to represent the entire unit of discretisation. The spatial lumping up of parameters to the grid-cell in this way assumes that the parameter value is homogeneous over the entire grid cell. This is not likely to be true given the spatial complexities of natural systems due to spatial variation in topography, soils, vegetation and rainfall inputs, at the sub-grid cell scale. The use of effective grid cell parameter values, therefore, means that the model cannot predict responses occurring over only a fraction of the grid square, nor the differential types of processes occurring at different parts of the grid square. Both of these shortcomings may result in the inaccurate prediction of response quantities and timing. However, the inability to represent differential types of processes occurring over a grid cell may also have very serious consequences for the type of response that is predicted where, for example, saturation overland flow, infiltration excess overland flow, inter-flow, and run-on all occur within a given grid cell.

Many of the papers which examined the effect of spatial variability of parameters on hillslope and catchment responses (e.g. Sharma and Luxmoore, 1979; Smith and Hebbert, 1979; Freeze, 1980; Sharma *et al.*, 1987; Binley *et al.*, 1989), groundwater systems (e.g. Bakr *et al.*, 1978) and soil water (e.g. Philip, 1980; Yeh *et al.*, 1986), have concluded that it is not possible to define a consistent effective parameter value to reproduce the response of a spatially variable pattern of parameter values. The primary reason is that a single parameter value cannot reproduce the heterogeneity of responses engendered by the variable catchment characteristics. While these studies suggest that equations more complex than physically-based equations are needed at the grid scale, they also suggest that statistical distributions of parameters based on field measurements may be used to effectively account for spatial variability of parameters.

More restrictive than the impracticality of extensive field measurements and the question of spatial representativeness of lumped grid-cell parameter values, however, is the question of applicability of these ‘observable’ parameters. Beven (1989) cautions that it may be dangerous to accept that equations based on the assumptions of

the small-scale physics of homogeneous systems are applicable at the grid cell scale. The lack of a clear theoretical basis for this lumping up of small-scale physics to the grid-cell scale, implies that application of these equations is conceptually based. This led Beven (1989) to suggest that the distributed modelling approach is in fact a lumped conceptual approach.

Model Calibration – Overparameterisation and Parameter Inter-dependence

The calibration of distributed models is potentially more difficult than that of conceptual models as they tend to have a larger number of parameters which may vary in time and space, and which may exhibit a greater degree of parameter interaction and heteroscedasticity. Similar to the calibration of conceptual models, the use of limited observed data to fit model predictions represents an imbalance between information content and the number of model parameters to be identified. Distributed models therefore suffer from over-parameterisation in a system simulation sense, resulting in *model equifinality* where multiple parameter sets result in the same model predictions (Grayson and Moore, 1992). *A priori* estimation or field measurements will allow some of the model parameters to be specified for input into the model. Bathurst (1986) suggests that measurements at a few “representative sites” may be sufficient to obtain an initial calibration of the model. He does not, however, specify how a representative site should be chosen, nor what measurement technique might be appropriate to obtain the required ‘effective’ grid-scale parameters. Given the large spatial and temporal variability of many hydrological parameters and the aforementioned impracticality of extensive field measurements, it is unlikely that sufficient measurements can be obtained to fully characterise the variability. Secondary data sources such as soil texture classifications, and remote sensed data have been used as alternatives to field measurements. Hydraulic conductivity, for example, can be derived from soil texture tables such as those of Brakensiek *et. al.*, (1981). Beven and Binley (1992) point out, however, that it may be dangerous to use these derived values of hydraulic conductivity as they are based on laboratory measurements that do not take account of soil structure, or spatial correlation in the field, and therefore add uncertainty to the model. Recent developments in remote sensing have resulted in the use of this data source as a means of obtaining spatially variable catchment parameters, on a grid cell scale. The analysis of RS images

involves the use of models to extract hydrologically effective parameter (or state variable) values, which may introduce additional uncertainty to the hydrological model. In addition, the parameters estimated at the grid scale of the image still assume that effective values indeed exist at this scale. In general, secondary data sources must be used with great care, as the methods by which they were derived may not be appropriate or accurate.

Another method of incorporating spatial variability is to use point measurements of the hydrological parameter to estimate a surface of parameter values at the required scale, by means of a smoothing method such as kriging (see section 7.1). This method requires some knowledge of the nature of the spatial variability of the parameter. In this way, the essential variability of the catchment can be constructed given sufficiently representative measurements. Again representativeness is difficult to define given the large spatial variability, short correlation lengths (e.g. Nielsen *et. al.*, 1973; Russo and Bresler, 1981) and non-stationarity of parameters such as hydraulic conductivity. Hence measured values may be dependent on the scale of measurement. As an alternative, completely random input/output fields have been widely applied in hydrology, using Monte Carlo simulations, to obtain multiple realisations of the output of deterministic models (e.g. Mejia and Rodriguez-Iturbe 1974; Wilson *et. al.*, 1979) and/or the physical properties of the watershed (e.g. Freeze, 1980) which may be stochastically varying in space (see Chapter 7).

While over-parameterisation is the result of the need to specify large numbers of parameter values, parameter interaction is inherent in the physics of hydrological systems. Any optimisation of parameters must, therefore, be subject to far greater problems of interaction than simpler lumped models. Beven (1985) argues that the assumption of ‘effective’ parameter values may be reasonable, given that bulk downslope flow processes will tend to integrate the effects of three-dimensional spatial variability of flow characteristics, but evidence of this is limited to theoretical work on groundwater flows (e.g. Dagan, 1979). He later points out however, that the same assumption may not be valid for infiltration and surface flows (Philip, 1980; Smith and Hebbert, 1979) and catchment response (Freeze, 1980), and would, in these cases, undermine the theoretical rigour of distributed models to some extent. Given the difficulties of over-parameterisation and parameter-interdependence, it is often

necessary to use ‘effective’ parameters. Given the importance of spatial variability in the behaviour of hydrological systems, the scale at which any such effective parameter values can be defined, must be carefully addressed before application.

The assessment of the uncertainty inherent in physically-based models due to their ‘lumped conceptual’ formulation, the simplification of model structure and process equations, and their over-parameterisation and parameter interdependence, should be treated as an integral part of any modelling approach. This is increasingly pertinent, as model predictions used in risk assessment may be subject to legal scrutiny (e.g. Blair, 1994). In addition, hydraulics engineering requires as wide a range of predictions as possible, in order to build reliable structures.

2.9.2 Physically-Based Sediment models

These models, akin to their hydrological counterparts, are based on an understanding of the physics of sediment yield processes and take the form of mathematical boundary-value problems, using equations governing the transfer of mass, momentum and energy (e.g. Abbott *et al.*, 1986; Beven, 1985). They use coupled representations of runoff production and hydraulic routing of overland and channel flow. The hillslope-erosion component of sediment yield is usually considered in detail and account is taken of one or more of the following: sheet and rill erosion, erosion by raindrop splash, overland flow, gullying, mass movement, bank and bed erosion. Examples of this modelling strategy include the Modified ANSWERS (Beasley *et al.*, 1982), SHESED-UK (Bathurst and Purnama, 1991), and LISEM (de Roo *et al.*, 1996).

Sheet and rill erosion processes have received the most attention in physically-based erosion modelling. Coupled models have been devised to represent rill and inter-rill processes (e.g. Foster *et al.*, 1977; Young and Onstad, 1982). However, the scale of representation used in these models, is usually too large to represent the scale of individual rill and inter-rill systems. In addition, the detail of representation of these, often indistinguishable, processes, is not complemented by the information content of measured data during calibration. Bathurst and Wicks (1991) suggest the use of effective grid cell parameters in rill modelling, in order to incorporate these processes in erosion models. This would have to be done via some theoretically plausible

method that allows for this lumping up to the grid cell scale. Attempts thus far, however, have been empirically based (e.g. Komura, 1976). Physical models of erosion due to large rills or gullies are based on consideration of the geotechnical factors affecting soil stability, the hydraulic factors affecting flow erosion and transport, and the hydrological factors determining soil moisture content and runoff (e.g. Nicklin *et. al.*, 1986).

Erosion by overland flow is usually modelled as a function of the exceedence of a critical shear stress at the eroding surface, when flow transport capacity exceeds the upstream sediment load (Lane *et. al.*, 1988). An equation of the form:

$$D_f = k_f (\tau - \tau_c)^b \quad [2.10]$$

is used, where D_f is the amount of sediment eroded, k_f is the overland flow soil erodibility coefficient which requires calibration, τ is the shear stress, τ_c is the critical shear stress and b is an exponent (=1 in SHESHED-UK). Critical stress is dependent on the nature of the soil. For non-cohesive soils, a number of relationships such as the Shields relationship (Simons and Senturk, 1977) can be used to account for spatial variability. Fewer alternatives exist for cohesive material, however (e.g. Kelley and Gultarte, 1981), although Yoo and Molnau (1982) applied the formula of Smerdon and Beasley (1961) based on percentage clay content and soil moisture with some success.

Wright (1987) discusses a detailed model of the spatial redistribution of soil by rainfall, considering the dispersion of raindrop splash droplets and the entrainment of mineral particles from a dis-aggregated soil mixture in the droplets. Most models, however, employ simpler representations. Soil detachment by raindrop splash on bare soil is usually given as a function of a soil erodibility coefficient and a rainfall parameter (e.g. Gilley and Finkner, 1985). Models such as SHESED-UK also account for the effect of spatial variability of ground cover on erosion by raindrop splash, as a function of vegetation heights, percentage canopy cover, interception, and raindrop diameter.

The physically-based approach to modelling erosion by mass movement uses geotechnical principles to define a safety factor, involving the two opposing forces acting on the soil mantle:

$$FS = \frac{\text{Resistance of soil to failure}}{\text{Downslope component of soil weight}}$$

When the downslope weight exceeds the resistance to shear ($FS < 1$), hillslope failure occurs. Soil strength and weight are dependent on soil moisture content, and most hillslope failures are triggered by the action of water (e.g. Addison, 1987; Jenkins *et al.*, 1988). Vegetation cover is also an important factor as resistance is dependent on the binding force exerted by vegetation (e.g. Megahan, 1983; Megahan and King, 1985). In general, the safety factor is naturally widely variable, and this as well as the lack of knowledge of subsurface conditions, introduces considerable uncertainty into the factor.

Physically-based representation of bank stability and erosion require both hydraulic and geotechnical analysis (e.g. Thorne, 1982) and the consideration of surface and subsurface factors affecting the soil moisture conditions. Models to date include that of Osman and Thorne (1988), which take account of removal of failed material and enables prediction of bank stability response to lateral erosion and degradation.

Physically-based sediment routing through the basin involves the representation of the mechanics of the various sediment entrainment and transport processes. In general, three main processes are required: (1) detachment, entrainment and delivery of hillslope sediment by overland flow to the channel system, (2) a component of sediment settling to account for lag between entrainment and delivery, and (3) a channel component for transport to the outlet. The overland flow component is the basic driving agent of hillslope sediment particle detachment and transport. Account must be taken of the spatial and temporal variation of flow velocity and depth, which determine the transport capacity of the flow. This usually involves application of the St. Venant equations for mass continuity and force-momentum (Woolhiser, 1975; Li, 1979). There is uncertainty, however, in the applicability of these equations to spatially variable shallow flow, and in the calculation of flow resistance as a function of soil and vegetation roughness and raindrop impact. In addition, the sediment

discharge relationship is important to account for the effect of sediment load on flow characteristics. Mean velocity, density, viscosity and unit discharge all tend to increase with sediment load. Govers (1990) proposed a correction factor for mean flow velocity:

$$u = \frac{u_{cw}}{(1 - c)} \quad [2.11]$$

Where u_{cw} is the mean flow velocity of clear water, and c is the volumetric sediment concentration. Torri and Borselli (1991) report that a better fit is obtained with a linear relationship, and even better when the sediment concentration used is the ratio of sediment volume to total volume of fluid. They derive mean flow velocity as a function of rate of increase or decrease in sediment concentration, grain density and water viscosity. Sediment transport by overland flow is therefore sensitive to the hydrological model used to determine runoff. Models which account for sediment deposition or settling usually involve an assessment of the transport capacity of the flow, as sediment is routed from cell to cell. When the transport capacity of the flow falls below the critical value, the sediment load is deposited. Channel routing requires representation of channel flow as the basic driving mechanism for sediment transport using the St. Venant equations, and the quantity of sediment being transported, using mass conservation (e.g. Chen, 1979). As with overland flow, account must be taken of the sediment discharge relationship to determine the capacity transport rates in terms of the flow components.

Like their hydrological counterparts, physics-based sediment yield models have the advantage, at least in theory, over other types of models of being geographically and temporally transportable, and should therefore be suitable for application to ungauged catchments and scenario modelling. In addition, because they are spatially distributed, they enable spatial predictions of on-site erosion rates, and their downstream effect. However, in addition to the problems of scale of representation, over-parameterisation, parameter interdependence and model equifinality, suffered by physics-based hydrological models, they may also incorporate errors associated with the description of sediment detachment and transport. Furthermore, errors in the representation of the hydraulic processes that drive soil erosion processes will be propagated to the sediment model. Sub-grid scale parameterisation requires soil

hydraulic and hydrodynamic roughness parameters as well as spatially heterogeneous sediment parameters which to date have been largely derived from laboratory-based soil physics, or highly invasive techniques. Alternative non-invasive remote sensing measurement techniques which may facilitate this spatial parameterisation, suffer from problems due to scale of representation and the methods of data extraction as discussed in the previous section. In addition, the complete representation of the spatial heterogeneity of the small scale topographic processes such as rilling and gullying, upon which the erosional and depositional processes depend, requires spatial discretisation that is computationally demanding and may lead to model over-parameterisation. Hence, models commonly use empirical factors to represent the estimated degree of these processes (e.g. Komura, 1976). These processes are however, evolutionary in nature and cannot be accurately represented by stationary parameterisations. Accounting for their dynamic nature requires simultaneous solution of hydraulic and sediment transport equations the boundary conditions of which are interdependent (e.g. Baird *et al.*, 1992, evolutionary RETIC model).

2.10 Hybrid Models

2.10.1 Hybrid Hydrological Models

The hybrid modelling approach was developed as a result of dissatisfaction with the performance of lumped conceptual models and the failure of the physics-based approach to realise its stated advantages. This approach is a combination of both the conceptual and physical approaches, and has as guiding principles, the parametric parsimony of lumped conceptual models, and the physical basis of the hydrological theory of physics-based models. Hybrid models are concerned with identifying the ‘ensemble’ average response of a catchment rather than the complete spatially distributed response. This is achieved by coupling quantitative geomorphological analysis with catchment streamflow response to surface runoff (Rodríguez-Iturbe and Valdes, 1979). One major advantage of hybrid models over other types is their reliance on topographic data as primary input data. The ready availability of topographic data either in the form of maps or in digital format in even the most data-poor areas, means that such models are highly geographically transportable. In addition, the focus on catchment average response means that calculations are not necessary for all grid-cells in the catchment, making them less computationally

demanding. Two main types of hybrid models can be identified: the Geomorphologic Instantaneous Unit Hydrograph (GIUH) (Rodríguez-Iturbe and Valdes, 1979), and topography-based and distributed function modelling approaches like TOPMODEL (Beven, and Kirkby, 1979), and TOPOG (Moore *et. al.*, 1988), and the distributed-function model by Moore and Clarke (1981).

GIUH

Rodríguez-Iturbe and Valdes (1979) and Valdes *et. al.*, (1979) presented a model that derives the unit hydrograph in terms of the geomorphological parameters of a basin. In their case, catchment geomorphological structure is defined by the Strahler stream ordering procedure, and the IUH is calculated as the probability that a drop of rainfall randomly imposed on the stream of order n will reach the outlet in time t . The ‘state’ of the raindrop is defined as the order of the stream in which the drop is located at time t , or the order of the stream to which the land drains directly, when the drop is still in the overland phase. All drops terminate in the highest numbered state $\Omega+1$ where Ω is the basin order, the extra state being the basin outlet, and undergo ‘transitions’ as they move from one state to the next. The probability that a drop makes any given transition is defined by the transition probability matrix for the drainage network $\mathbf{P} = [p_{ij}]$, where p_{ij} is the probability that the drop moves from state i to state j . The transition probabilities are governed by Markovian theory, while the time τ_{ij} that the drop spends in state i before making a transition to state j is a random variable defined by a probability density function $h_{ij}(\tau)$, which is independent of the destination state. Rodríguez-Iturbe and Valdes (1979) arbitrarily define an exponential distribution of travel times within each state, so that

$$f_{Tr\omega}(t) = K_{\omega} \exp(-K_{\omega} t) \quad [2.12]$$

where the parameter K_{ω} is given by $K_{\omega} = V / \bar{L}_{\omega}$, where V is a velocity parameter. Hence travel times can be computed for each transition of a raindrop on its journey to the outlet. The total travel time along a given path is the sum of travel times for each transition along the path, and the probability that the drop takes that particular flowpath, $P(s)$ is defined as:

$$P(s) = \theta_i P_{ij} P_{jk} \dots P_{l\Omega}$$

Where θ_i is the probability of a raindrop falling into a hillslope draining into a river of order i , and P_{ij} is the probability of the transition from a river of order i into a river of order j . The initial and transition probabilities are Horton's area and bifurcation ratios respectively. The probability density function for the travel time of any raindrop falling randomly within the catchment is given by,

$$P(T_B \leq t) = \sum P(T_s \leq t)P(s) \quad [2.13]$$

Where T_B is the travel time to the basin outlet, T_s is the travel time along path s , and S is the set of all possible flowpaths. The analytical IUH is defined by the derivative of equation [2.13] with respect to time.

The GIUH is limited by its reliance on the arbitrarily defined exponential distribution of travel times, and the use of a spatially and temporally constant velocity parameter. Flow velocity is spatially and temporally variable, and should at least distinguish hillslope from channel flow. The model treats the transition of rainfall to the outlet as stochastic and, although this is based on the catchment geomorphological structure, the GIUH remains essentially a rainfall-excess routing function similar to the linear routing metric models. Moreover, there is no attempt to address subsurface processes, which play an important role in catchment hydrological response, nor is there an attempt to explicitly account for variable source area theory.

Terrain-based approaches

Beven and Kirkby (1979) developed a topography-based model, TOPMODEL, based on the variable contributing area principle of Hewlett (1961), Hewlett and Hibbert (1967) and Dunne and Black (1970). It attempts to fully describe rainfall-runoff processes, based on the direct relationship between catchment topography and the spatial distribution of subsurface and surface flow pathways and runoff production (Anderson, and Burt, 1978), through a physically-based topographic wetness index. The wetness index, w_T is given by:

$$w_T = \ln\left(\frac{a}{T_0 \tan \beta}\right)_i \quad [2.14]$$

where T_0 [ML⁻²] is the transmissivity when the soil profile is saturated, a [L] is the upslope contributing area per unit contour length, and β is the local slope gradient, and i , represents any location within the catchment. Derivation of the index, which can be found elsewhere (e.g. Beven and Kirkby, 1979; Quinn *et. al.* 1995b) is based on three basic assumptions:

1. The water table is parallel to the surface. Hence the hydraulic gradient can be estimated by the surface slope;
2. Hydraulic conductivity decreases with depth or soil moisture deficit as a negative exponential function;
3. Continuity of subsurface flow. Hence flows can be represented by steady state water table positions.

The upslope contributing area reflects the tendency for water to accumulate at location i , whilst the local slope is a measure of the hydraulic gradient forcing water downhill through the point. Where a is high relative to $\tan \beta$, there will be a net accumulation of water. Therefore areas prone to saturation, can be identified by high values of the topographic index. TOPMODEL calculates the local soil moisture deficit, as a function of the catchment average soil moisture deficit, and the difference between the catchment-average and local index values.

$$S_i = \bar{S} + m \left[\gamma - \ln\left(\frac{a_i}{T_0 \tan \beta}\right)_i \right] \quad [2.15]$$

Where S_i is the local soil moisture deficit, \bar{S} is the catchment average deficit, m is a parameter, which controls the rate of exponential decline of soil transmissivity with soil moisture deficit, and γ is the catchment average topographic index, a [L] is the upslope contributing area per unit contour length, T_0 [ML⁻²] is the transmissivity when the soil profile is saturated, β is the local slope gradient, and i , represents any location within the catchment. This implies that areas of the catchment with similar values of the index behave in a similar manner and have the same soil moisture deficit. The topographic index is therefore a measure of ‘hydrological similarity’. Hence rather

than calculate individual values at each point, a distribution of soil moisture deficits can be obtained for each class of the index occurring in the catchment. For this reason this modelling approach is often described as semi-distributed. When S_i is zero the soil is saturated, and will produce saturation excess overland flow under rainfall. When $S_i < 0$ exfiltration or return flow occurs. The runoff contributing area is defined as the total saturated area, the extent of which is controlled by the catchment-average deficit, \bar{S} . This allows for a non-linear, dynamic variability of the contributing area as described by Dunne and Black (1970), and hence of runoff production. When the mean deficit is high, only areas with high values of the index contribute runoff, whereas when the deficit is low, low values of the index may also contribute. The model can also be used in full spatially-distributed mode, by mapping soil moisture and runoff generation back onto the soil-topographic index.

TOPMODEL has been successfully applied to a number of catchments world wide, particularly in humid temperate zones, e.g. upland UK (e.g. Beven *et. al.*, 1984; Quinn and Beven, 1993), New Zealand (e.g. Beven, 1993), the eastern USA (Hornberger *et. al.*, 1985) and western France (e.g. Bruneau *et. al.*, 1995). Applications to tropical catchments (e.g. Quinn, 1991; Brasington, 1997; Brasington and Richards, 1998) and to Mediterranean catchments (e.g. Sempre-Torres, 1990; Obled and Wendling, 1991) have also been successful. This relatively high level of geographical transportability of the model is due to the physical basis of model formulation, its parametric parsimony, and its reliance on readily available topographic data as a primary data source. Its main advantage is that 2 of its 5 parameters are defined by the topography and do not need identification. Of great advantage too, is the flexibility of the model to local adaptation. Indeed, Beven (1995) emphasises that TOPMODEL is a set of conceptual modelling tools, and not a static modelling package. Many researchers have used this to their advantage, when applying the model to individual catchments. Chapter 4 describes developments to TOPMODEL made by Brasington (1997), and further develops made within this thesis, for application to a catchment in the North York Moors, UK. Further discussion of the TOPMODEL modelling approach is given therein. Another topography-based model, TOPOG, is the approach by O'Loughlin (1981), which uses a similar topographic wetness index within a distributed vector-based model.

A related approach is that of Moore and Clarke (1981) who also proposed a distributed function approach to rainfall-runoff modelling. The basin was divided into an infinite number of stores of equal width, and of depth, s , described by a probability density function, $f(s)$ – assumed exponential, to represent the processes of interception and soil moisture storage by an algebraic expression, which is differentiable at each point in the parameter space. Gradient procedures are used for parameter estimation. Each store or storage element is closed at the bottom and opened at the top and when filled by rainfall, generates direct runoff, q . A weight is assigned according to the store depth to reflect the frequency of occurrence in the basin. Runoff is produced from each storage element only when the storage capacity is exceeded, and the extent of the contributing area is given by the integral of all cells producing runoff. Flow is routed to the outlet by a bivariate distribution of flow with store depth and time taken to reach the outlet. The depth of flow at the outlet is given by a convolution of contributing area and rainfall depth.

The model, while allowing for a distributed approach to runoff modelling, has no physical basis. In addition, the choice of an exponential distribution function of store depths is subjective. However, the method of runoff generation can be loosely linked to saturation excess overland flow, and the expansion and contraction of the runoff producing area, as the variable contributing area. This dynamic representation of runoff generation was later used (Moore and Clarke, 1983), to drive a sediment yield model (discussed below), in an attempt to represent the dynamic nature of the sediment delivery process.

The key similarity among these distributed function models is that they use a probability distribution function to describe the array of catchment stores and thus simulate a non-linear rainfall-runoff filter.

2.10.2 Hybrid Sediment Models

Topography-based approaches

Topography-based sediment yield models use parameters that are derived from digital terrain analysis, to model the spatial distribution of erosion hazard. These models make explicit use of the macro-scale link between surface topography, and erosional-

and hydrological-processes, identifying a generalised pattern of erosion, given a set of hydrologic boundary conditions.

Moore and Burch (1986a), describe a model based on a vector DEM arranged in irregular polygons, defined on the basis of topographically-derived streamlines. As such the model implicitly accounts for flow convergence and divergence by determining the difference in topographically-approximated upstream and downstream equipotentials of an element. Each flow element is bounded upstream and downstream by topographically-approximated equipotentials and on either side by adjacent streamlines. A wetness index after O’Loughlin (1986), similar to the TOPMODEL index, is used to determine the depth of runoff generation in each element for a given baseflow and rainfall intensity. The model assumes steady-state flow along non-preferential flow pathways, with no storage or attenuation of runoff. Moore and Burch (1986a), define sediment transport capacity on the basis of unit stream power theory. In turn, unit stream power is defined as the rate of potential energy expenditure per unit weight of water, and can be expressed mathematically by the product of average water velocity, V and energy slope, S ;

$$\frac{dY}{dt} = \frac{dX}{dt} \frac{dY}{dX} = VS \quad [2.16]$$

Y is the elevation above a datum, which also equals the potential energy per unit weight of water above a datum; X is the longitudinal distance and t is time. For steady uniform flow, the energy slope can be replaced by the water surface without introducing any errors.

They calculated flow velocity on the basis of Manning’s equation for uniform turbulent sheet flow, in which,

$$V = S^{1/2} n^{-1} D^{2/3} \quad [2.17]$$

and

$$q = VDW = S^{1/2} n^{-1} D^{5/3} W \quad [2.18]$$

where n is the Manning's roughness coefficient, and D is the depth of runoff generation in each element per unit area and W is flow width, V is average water velocity and S , the energy slope. The product DV - the volumetric discharge per unit width, q/W (L^2T^{-1}) - defines unit stream power in each element, VS (or P) as,

$$P = VS = q^{0.4} S^{1.3} n^{-0.6} \quad [2.19]$$

As the total sediment concentration is related to the intensity of turbulence, it is reasonable to assume that the rate of total sediment transport or the total sediment concentration is directly related to the unit stream power. Yang (1972) found that

$$\log C_t = A + B \log(VS - VS_{cr}) \quad [2.20]$$

provides the best correlation between total sediment concentration, C_t , and unit stream power VS , where A and B are coefficients, and VS_{cr} is the critical unit stream power required to start the movement of sediment particles. The difference between VS and VS_{cr} is the effective unit stream power, which is available to transport sediment. Following Yang (1972), sediment transport capacity, T , is related to unit stream power, and neglects the critical stream power required for incipient sediment motion, the relationship is reduced to a power function,

$$T = \gamma P^\beta \quad [2.21]$$

where, γ and β are empirical parameters related to the median eroded particle size and water temperature respectively. Yang (1972) showed that the response of a sediment particle to its surrounding turbulence and flow conditions decreases with increasing particle size. Hence a water flow capacity carrying fine material should use its power more effectively in transporting sediment than flow carrying coarse material. Consequently, the total sediment concentration of fine material should be higher than that of coarse material with equal unit stream power and water depth.

Moore and Burch (1986b) represented the influence of terrain on soil erosion by a dimensionless equation for sediment transport capacity, T ,

$$T = \left(\frac{A}{22.13} \right)^m \left(\frac{\sin \beta}{0.0896} \right)^n \quad [2.22]$$

By assuming that q is proportional to A_s , the topographic index $A_s \tan \beta$ is a measure of stream power. Hence, the dimensionless index of sediment transport capacity, T , becomes unity when the upslope area $A = 22.13 \text{ (m}^2\text{m}^{-1}\text{)}$ and the slope is 9%. This is the unit stream power based LS factor. The sediment flux per unit contour length, Y_b ($\text{kg m}^{-2}\text{s}^{-1}$) from an element is the product of q and T .

Moore and Burch (1986b) determined the spatial distribution of erosion and deposition, as a function of the difference between the sediment yield entering and leaving connected elements on a stream tube,

$$Y_r = \frac{(Y_b^i b_i - Y_b^o b_o)}{A_r} \quad [2.23]$$

where, Y_r is the net erosion or deposition, Y_b^i and Y_b^o are the sediment fluxes per unit contour width entering and leaving the element respectively, b_i and b_o are the contour lengths of the upstream and downstream element boundaries and A_r is the element area. Their application of a model to a research catchment gave qualitatively acceptable results. Mitasova *et al.* (1996) have also shown that the unit stream power based approach is especially appropriate for landscape scale erosion modelling, when the location of both areas with erosion risk and deposition potential is important.

Another approach to the topography-based hybrid model makes use of the geomorphic threshold theory of erosion, put forward by Schumm and Hadley (1957) to predict the spatial distribution of these erosional processes. Dietrich *et al.* (1992) define thresholds for erosion by landslides, Hortian overland flow, saturation excess overland flow and seepage erosion, based on static digital terrain analysis. Similar analyses have been used to determine the occurrence of gully erosion (Thorne *et al.*, 1986; Moore *et al.*, 1988) and the location of channel heads (Montgomery and Dietrich, 1989).

Hybrid models provide the compromise between empirical and distributed models. They provide spatially distributed predictions of erosional processes, with the use of fewer parameters than distributed models, and in the case of topographically-based models, utilise the macroscopic control exerted by topography on catchment-scale erosional processes within the catchment, hence providing the physical link between the processes and the model parameters. However, all of the topography-based models described here are essentially static models of potential erosion and, while useful in mapping erosion hazard, they fail to account for the dynamic temporal and spatial variability of the sediment delivery process.

Distributed function approaches

Moore and Clarke (1983) developed a dynamic sediment yield model, which describes sediment removal and transportation as supply- and transport-limited processes, based on distributed function theory. The model (a fully description of which is given in chapter 5), is coupled to the hydrological model of Moore and Clarke (1981) described above, and attempts to simulate the temporal and spatial dynamics of the sediment delivery process. In essence, they proposed that after an element of basin area has ceased to contribute to runoff, sediment that is available for future removal begins to be generated at a maximum rate R_0 , and thereafter at a rate defined by a two parameter exponentially-decreasing curve,

$$R(t) = R_0 \exp[-k(t - t_0)] \quad [2.24]$$

where k is the decay rate parameter. At time t , the depth of sediment is given by:

$$d(t) = \int_{t_0}^t R(\tau - t_0) d\tau = R_0 \int_{t_0}^t \exp[-k(\tau - t_0)] d\tau = R_0 k^{-1} [1 - \exp\{-k(t - t_0)\}] \quad [2.25]$$

As the inter-storm period lengthens, sediment will continue to accumulate at an exponentially-decreasing rate, asymptotically approaching a maximum depth,

$$d(\infty) = \frac{R_0}{k} \quad [2.26]$$

Sediment would remain on an element of basin area, until that element contributes to runoff, when the sediment would be completely removed. Hence a large storm occurring after long dry periods, will remove a larger quantity of sediment, while a similar storm following only shortly after will remove very little (Moore and Clarke, 1983). This represents the hysteresis observed in the temporal variability of sediment yield caused by variable sediment availability and exhaustion. Sediment is translated to the outlet either in the same manner as runoff, in which travel times are assumed to be exponentially distributed with time, or by individual distributions of travel times, based on an inverse Gaussian p.d.f., which Moore and Clarke (1983) show may be derived as a solution to the convection-dispersion equation for a Dirac delta function input, and is thus also related to the IUH.

The dependence of sediment availability on the length of the inter-storm period allows for the simulation of the temporal dynamics of the sediment delivery process, while the reliance of the sediment exhaustion on the runoff generated from individual stores, accounts for the spatial variability. The model is parametrically parsimonious, and easily optimised using gradient-based algorithms. However, the stochastic description of store depths and the reliance on an arbitrarily chosen travel-time distribution function, means that there is no direct assessment of deterministic patterns of sediment and hydraulic coupling. A fully-distributed physics based model, which represents the dynamic expansion and contraction of the variable contributing area, when coupled to this model would reduce the difficulties associated with the stochastic approach, and would provide a more appropriate representation of the spatial and temporal variability of the sediment yield process. This is a subject of this thesis. Chapter 4 describes a fully distributed physics-based hydrological model, which is coupled to this dynamic sediment yield model, to predict basin sediment yield.

2.11 Conclusion

This chapter examined the essential aspects of the sediment yield process and its environmental controls, and reviewed existing approaches to hydrological and sediment yield modelling. The sediment yield process is extremely complex and exhibits wide spatial and temporal variability, due to the dynamics of the subsumed sediment availability, detachment and transport processes. The reliance on runoff

generation processes underscores the primary importance of the spatial and temporal distribution of runoff generation, in sediment yield modelling. The wide range of existing hydrological models which reflect varied modelling approaches, highlights the need to choose an approach very carefully. In order to accurately represent the complex spatial and temporal variability of the sediment yield process, the underlying hydrological model must be capable of accurately representing the dynamics of runoff generation. Hence, a fully-distributed, physically-based hydrological model is required. Similarly, the sediment yield model must be capable of representing the dynamic spatial and temporal variability of sediment availability on the hillslopes, sediment entrainment, and transport through the basin. While most of the sediment models discussed above rely on some minimum description of the underlying hydraulics of the system, most remain essentially static models. Few models (e.g. Bathurst and Purnama, 1991; de Roo *et. al.* 1986; Moore and Clarke, 1983) have attempted to couple the processes of runoff generation and sediment yield, in a simultaneously spatially and temporally variable manner. The model described in chapter 4 is a fully-distributed physically-based model based on TOPMODEL theory. It predicts spatially variable runoff as a function of variable soil, land use, and rainfall, and incorporates a snowmelt model. This is coupled to the sediment yield model also described in chapter 4, which is a dynamic sediment yield model based on Moore and Clarke (1983) theory. The uncertainty associated with physics-based distributed models, discussed above, is assessed for both models, as well as the propagation of uncertainty from the hydrological model to the sediment yield model. The model is applied to a catchment in the North York Moors which is described in the following chapter.

CHAPTER 3 – Farndale Catchment

3.0 Summary

This chapter presents the environmental background of the study area, and examines the factors that affect its hydrology and geomorphology. The chapter begins with a description of Farndale catchment, the catchment of the River Dove, within its regional setting and includes a brief description of the geology of the region, followed by the geology of the catchment, its soil type, land use, climate, hydrology and contemporary sedimentological processes.

3.1 Farndale in its Regional Setting

Farndale, the catchment of the River Dove to Kirkbymoorside, is a 54.99 km² valley of the river Dove, one of a series of southerly flowing rivers draining off the North Yorkshire Moors into the Vale of Pickering (Fig. 3.1). It is separated from Bransdale catchment to the west, and Rosedale to the east by broad interfluves covered in characteristic moorland (Fig.3.2a).

The North York Moors is part of an isolated upland plateau bounded by the Vale of Pickering in the south, the Vale of York to the west, the North Sea coastline to the east and north-east and the Tees plain in the north-west. This plateau is dissected to form four ranges of hills; the Cleveland Hills in the north, the Hambleton Hills in the west, the Tabular Hills to the south and the North York Moors which stretch from west to east across the plateau.

The topography of the area reflects the nature of the rocks that crop out over its surface, much of which ranges from 300m O.D. to 460m O.D. The moorlands are mainly of Middle Jurassic sandstones and shales with Liassic clays forming the lower slopes. The oldest strata outcrop in the northwest, outer facing rim, becoming gradually younger towards the Vale of Pickering, where the topmost member of the Jurassic series, Kimmeridge clay, is exposed.

The south of the moorland slopes down to the foot of a well-defined broken north-facing escarpment, extending from the coast near Scarborough westwards to the Vale of Mowbray, the northern limit of the flat Tabular Hills, which also declines gradually southwards to the Vale of Pickering.

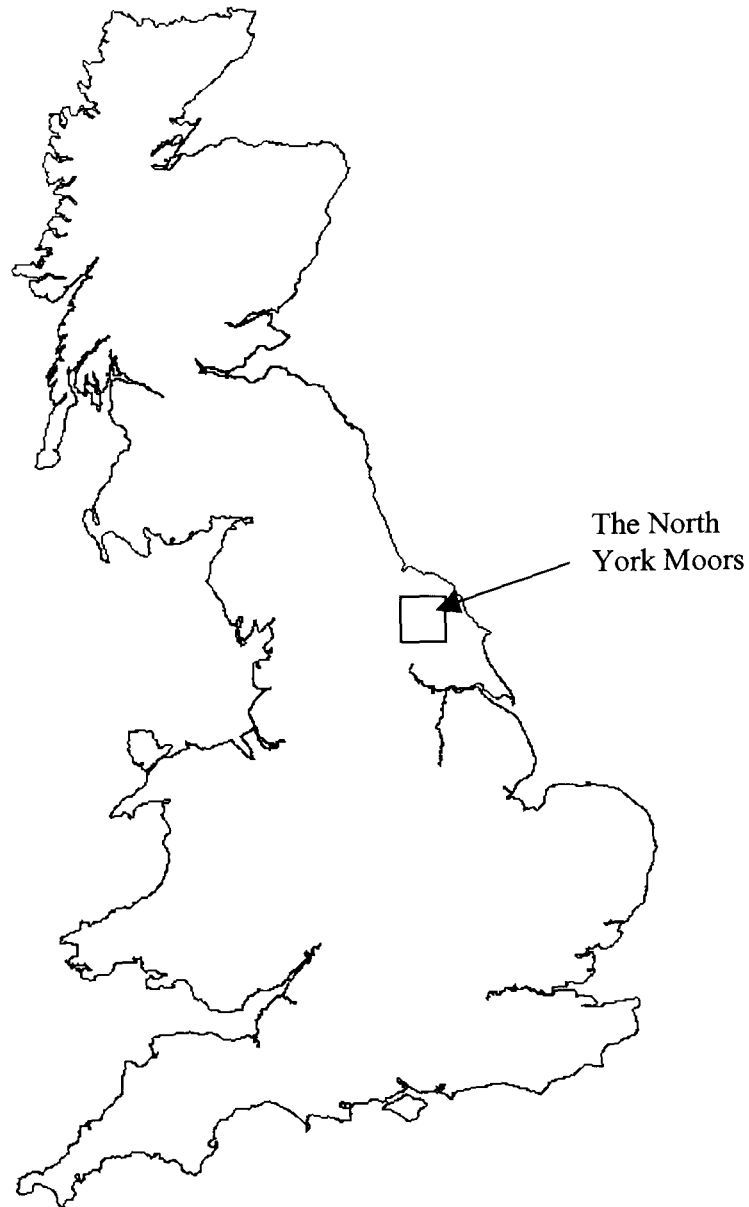


Fig. 3.1 Location of Farndale catchment.

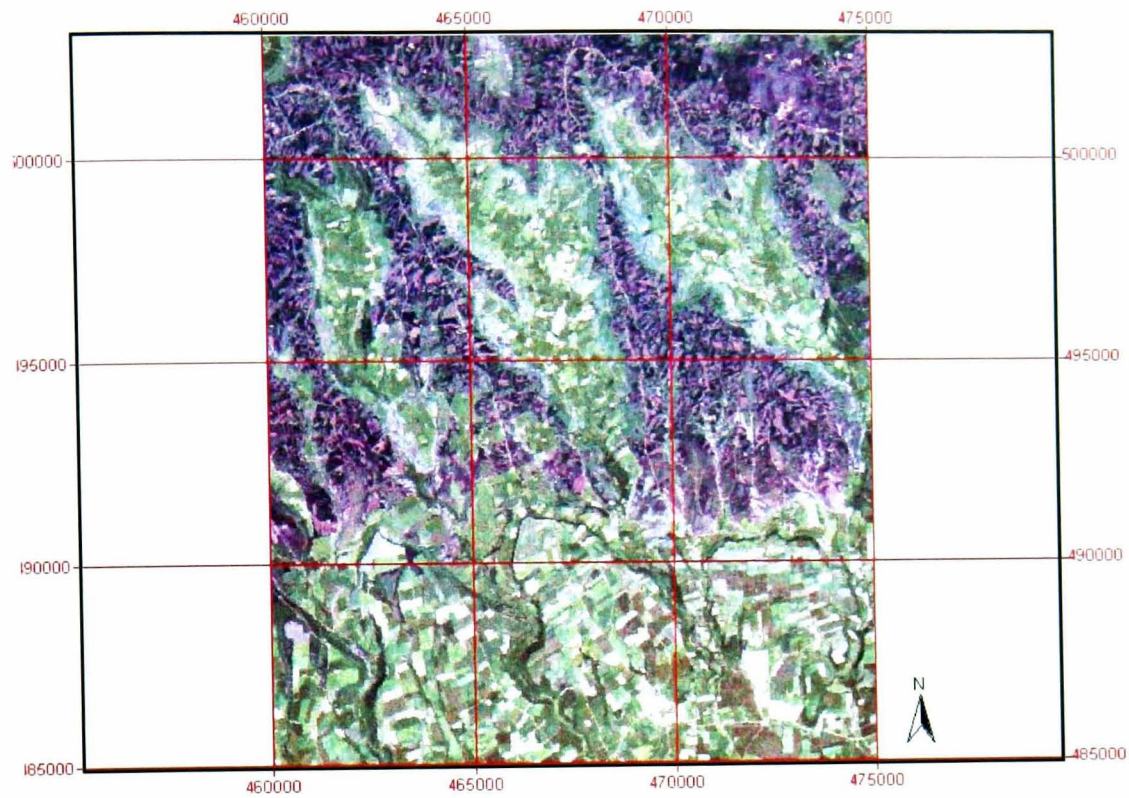


Fig. 3.2 a) Landsat TM image of Farndale Catchment showing Bransdale to the west and Rosedale to the east. (June 06 1992). b) In the north of Farndale Catchment looking west.

3.2 Topography and Relief

Farndale catchment ranges in altitude from 38.4m at the Kirkby Mills gauging station (705855, 486100) to 430m in the northwest of the catchment. The slopes are moderately to steeply sloping, and the valley bottom is wide.

DEM Construction

Digitised 10m contours were used in conjunction with spot heights and the digitised river channel network, within the TOPOGRID command in ARC/INFO. This is a finite-element procedure for interpolating grid DEMs from contours, spot heights and stream data, and other breaklines, which can be used to mark topographic discontinuities. The method has been extensively tested (Hutchinson and Dowling, 1991) and proved to be computationally efficient and capable of yielding globally smooth and accurate fits. This routine incorporates a drainage enforcement algorithm that automatically removes spurious sinks or pits, which may arise in near-channel areas where the interpolation procedure creates downstream dams in areas of narrow incision, thus maintaining the fidelity of the drainage network. These local anomalies are removed by raising cells in the sink to a level just above the lowest outflow point around the sinks so as to create a downslope gradient. In all operations a root mean square error (RMSE), a measure of fit of the DEM to the input elevation data, was set at 1.0m as a predefined tolerance for the interpolation. Nonetheless, it is important to note that all interpolation methods involve some degree of smoothing and the incorporation of errors.

DEM Resolution

There remains a preliminary assumption that DEMs used in such analysis are of high enough resolution to enable reliable description of hillslope flow routing. This requires that the DEM accurately captures the local scales of variability in hillslope morphology, which play an important role in the definition of flow pathways. Previous studies have shown that the TOPMODEL index is sensitive to DEM resolution. Quinn *et. al.* (1991) found significant differences in probability distributions of the topographic index computed from 12.5 and 50m grids. Zhang and Montgomery (1994) also found grid size to be a significant control. For a range of scales between 4 and 90m, they found that the mean of the topographic index increased progressively with grid size. The effects of both the topographic map scale

used to derive a DEM and the resolution of the DEM itself were analysed by Wolock and Price (1994), who again found the mean of the index to increase with grid size. In the case of changing map scale, they found that this was attributable to increases in the mean of the upslope contributing area and decreases in the mean slope gradient. By contrast, they found that the influence of DEM scale was most profound through its effect on the calculation of the contributing area. The effect of DEM resolution has been investigated in terms of the TOPMODEL hydrological predictions. Zhang and Montgomery (1994) found that the translation of the index distribution towards higher values as grid size increased, increased the rate of predicted peak streamflow and decreased the depth of the water table. Wolock and Price (1994) reported similar results and found that predicted hydrographs became more skewed as the ratio of predicted overland flow to subsurface flow increased for coarser DEMs.

A DEM with a grid size of 50m was constructed for Farndale catchment using the interpolation procedure described above, with the digitised river network forming breaklines. Following initial surface fitting, the ARC/INFO WATERSHED function was used to automatically re-delineate the watershed. The choice of a 50m sampling interval reflects an *a priori* compromise between data efficiency and the precision required to reflect the terrain, and is consistent with typical scales for DTA. Higher resolution is limited by the fundamental information content of the input data (1:25000 mapping at 10m intervals).

The 50x50m DEM comprises a matrix of 343 rows and 291 columns with a total of 21996 cells in the watershed and thus a total catchment area of 54,990,000m². The interpolation procedure identified 23 sinks, and the resultant DEM is shown in Fig. 3.3.

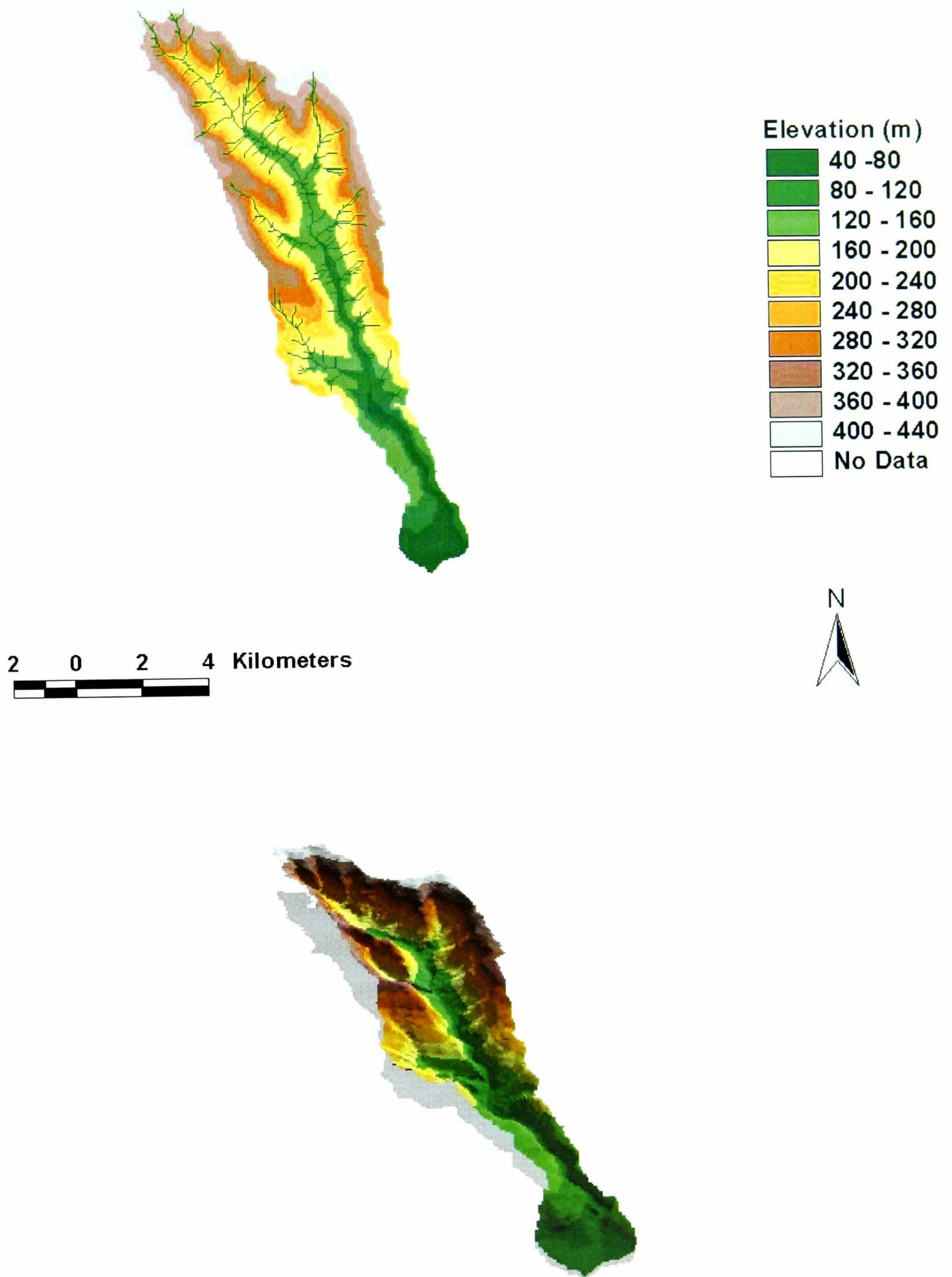


Fig. 3.3 a) Digital elevation model of Farndale catchment at 50m resolution. b) 3-D view of the DEM with shadow for effect.

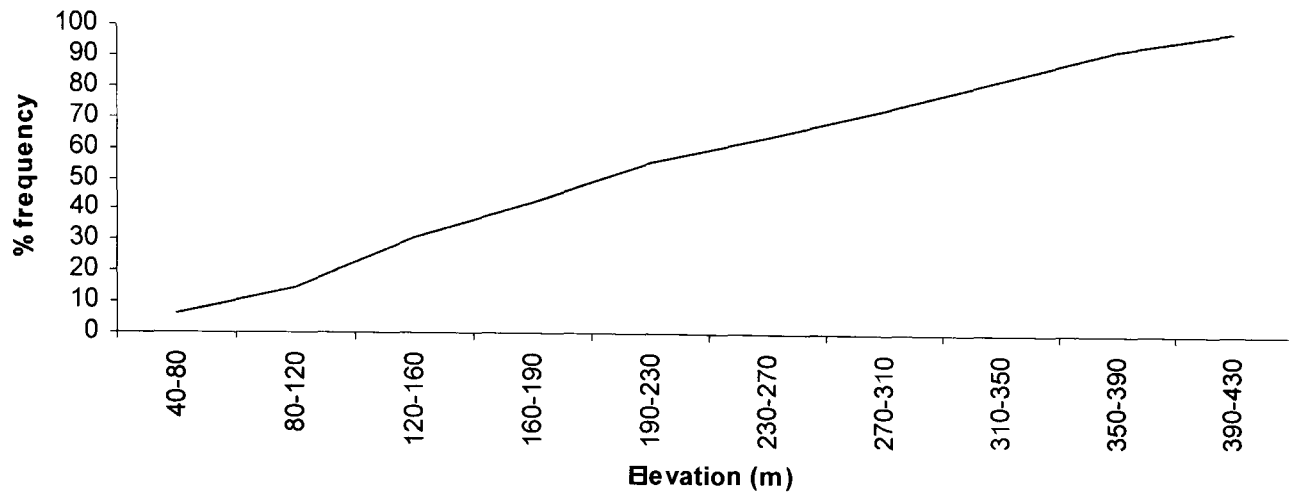


Fig. 3.4 cumulative frequency distribution of elevation.

Fig.3.4, the frequency distribution of elevation, shows that the relief is moderate with 75% of the catchment above 120m. There is an approximate decrease in elevation of 400m in 21km from the highest to the lowest point in the catchment.

Figures 3.5 and 3.6 show the spatial and frequency distributions, respectively, of slopes in the catchment. The steepest slopes are approximately midway between the wide valley floor and the flat ridgetops. The catchment, on the whole is gently undulating, with approximately 74% of the slopes less than 11° .

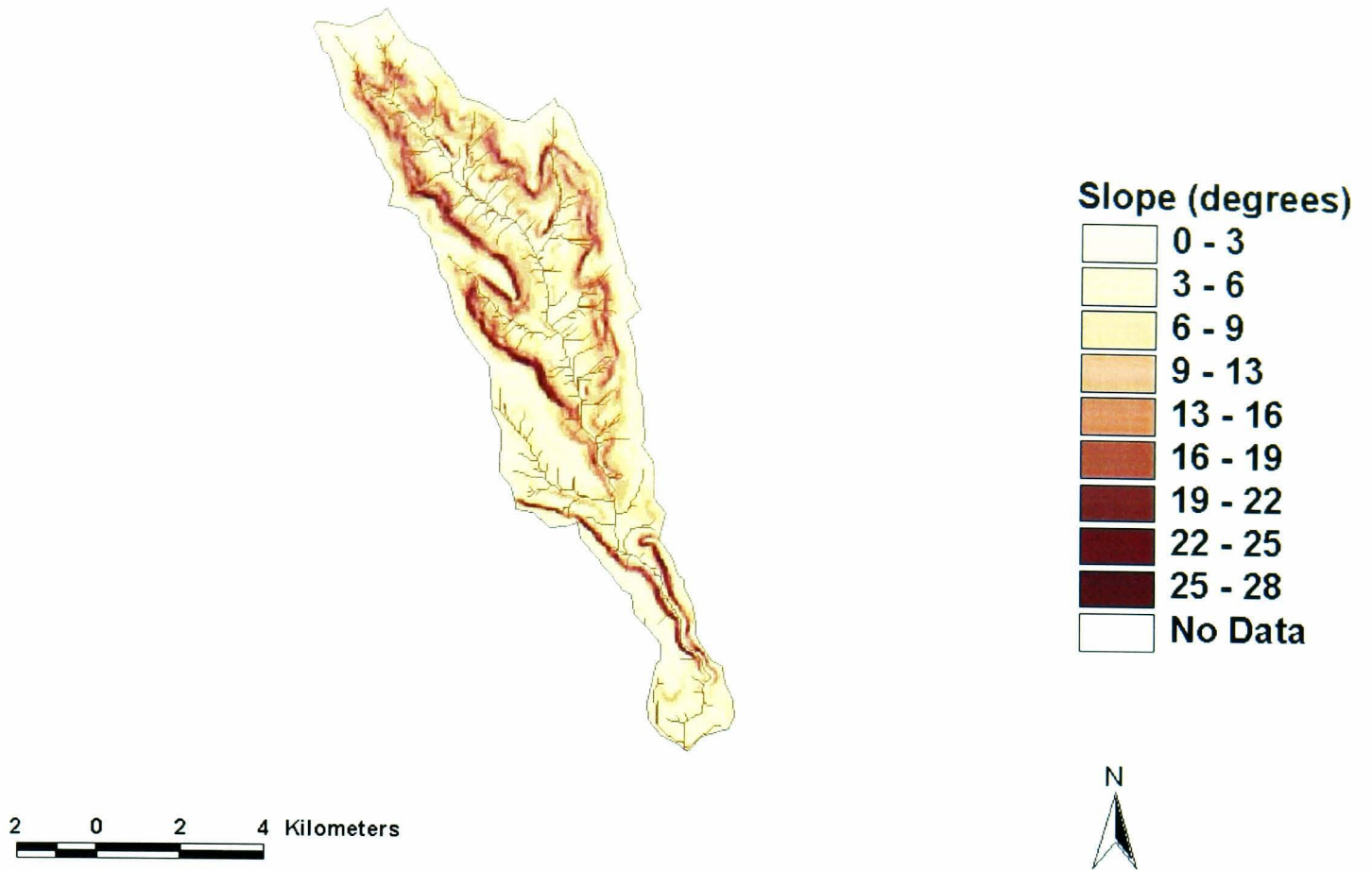


Fig. 3.4 Spatial distribution of slope in the catchment.

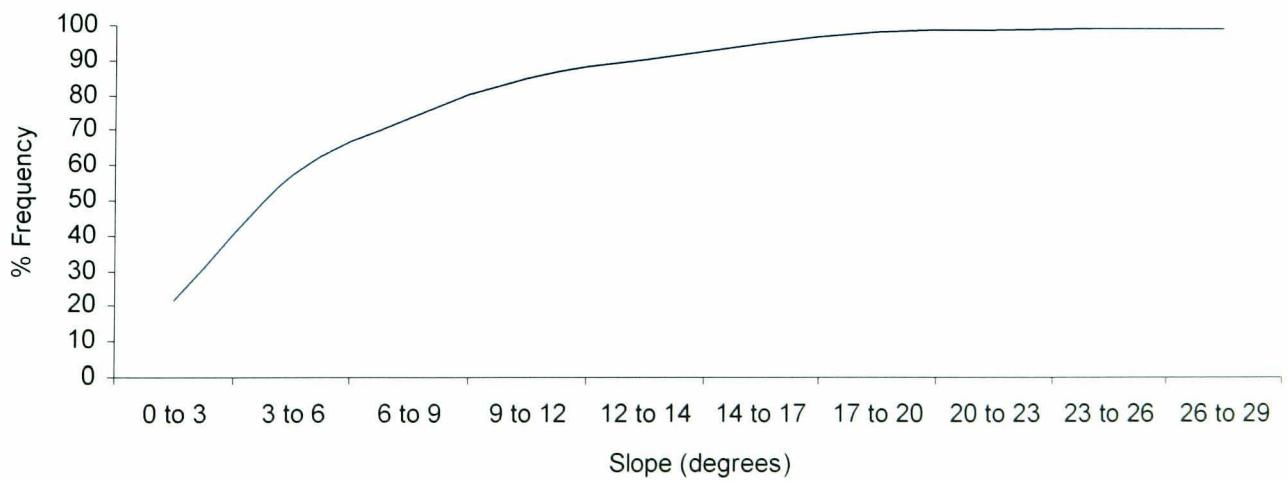


Fig. 3.5 Cumulative frequency of hillslope gradient.

3.3 Catchment Geology

The geology of Farndale catchment is Jurassic and is closely related to its relief. The youngest rocks occupy the highest ground and the oldest rocks, the valley floors, arranged in concentric inliers.

Fig. 3.6 is a geological map of Farndale catchment, and table 3.1, the key to geological symbols. There are four major stratigraphical divisions. The *Lower and Middle Lias* region, a relatively low level area located in the centre of the catchment, the *Upper Lias* region, a region of steep slopes, the *Middle Jurassic* region on ridge tops and the *Upper Jurassic* on the foothills in the south of the catchment. The Liassic beds of Northeast Yorkshire generally consist of clays and shales, with many subordinate ironstones, calcareous mudstones, limestones, and sandy beds, all deposited in the shallow muddy sea that came into being in Rhaetic times (Wilson, 1958, p.19).

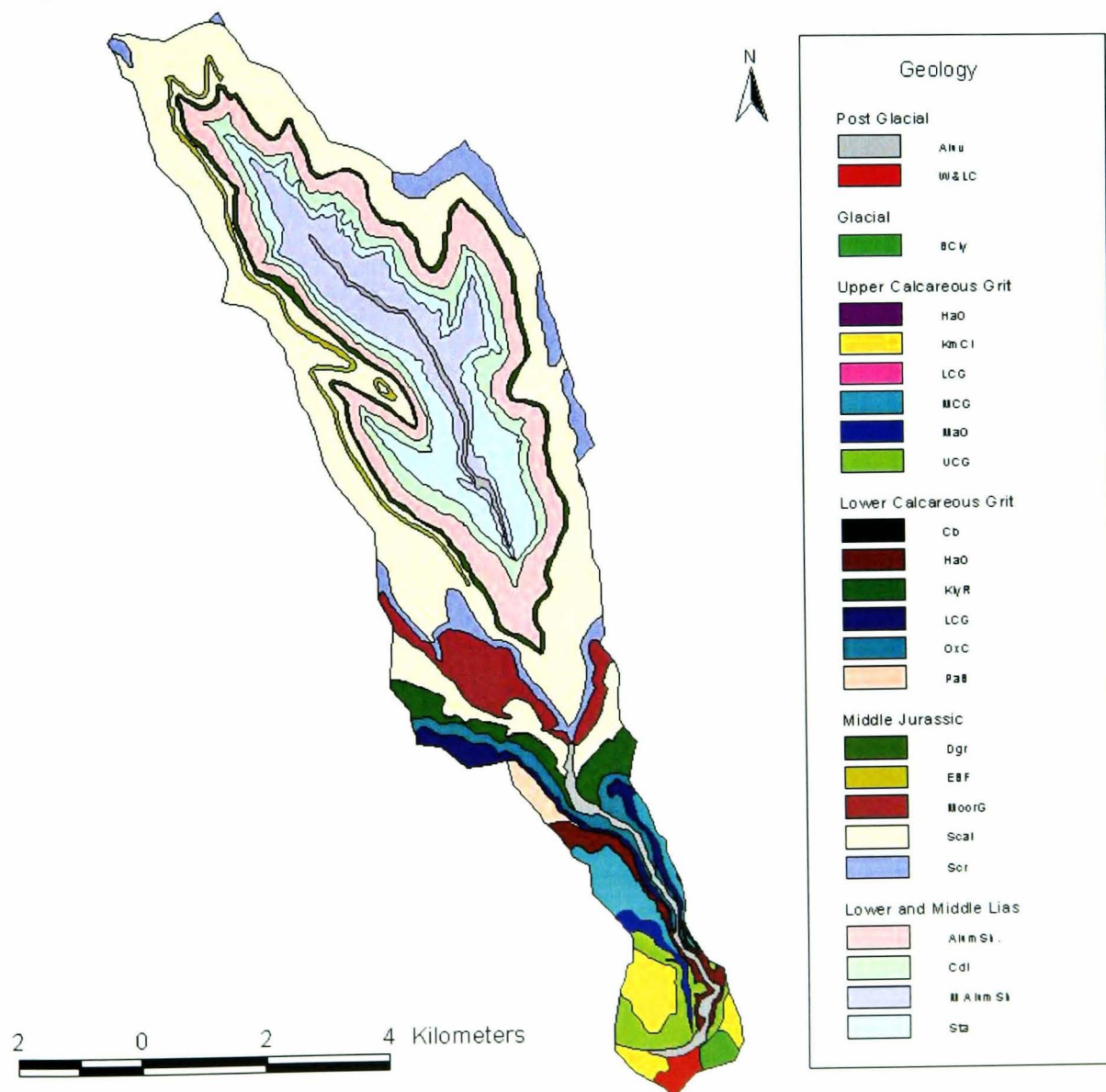


Fig. 3.6 Geology of Farndale Catchment.

Key to Geological Map

MAJOR GROUPINGS	SYMBOL	DESCRIPTION
Post-Glacial	Aluv	Alluvium
	W&LC	Warp and Lacustrine Clay
Glacial	BCly	Boulder Clay
Upper Calcareous Grit Coralline Oolite Formation (Upper Jurassic)	KmCl	Kimmerage Clay
	UCG	Fine-grained sandstone
	MalO	Malton Oolite - limestone
	MCG	Middle Calcareous Grit (sandstone, calcareous in part)
Lower Calcareous grit Formation (Upper Jurassic)	HaO	Hambleston Oolite (Oolitic limestone)
	PaB	Passage beds (mostly limestone)
	LCG	Mostly silicious sandstone
	OxC	Oxford Clay (mudstone)
	KlyR	Kellayways Rock
	Cb	Cornbrush -limestone & calc. Sandstone
UNCONFORMITY	UNCONFORMITY	UNCONFORMITY
Scarborough Formation (Middle Jurassic) Coal (Middle Jurassic)	Scal	Scalby Formation (estuarine sand)
	MrG	Moor Grit Member (mudstone, siltstone and sandstone), Quartz sandstone (Estuarine Shale)
	Scr	Scarborough formation (limestone, sandstone and mudstone) (formerly Grey Limestone)
	EBF	Eller Beck Fm (mudstone and sandstone with some ironstone and limestone)
	Dgr	Dooger Fm. (mostly ferroginous and calcareous sandstone)
UNCONFORMITY	UNCONFORMITY	UNCONFORMITY
	AlumSh	Alum Shales - Grey micaceous shales with Jet Rock.
	CdI (Middle Lias)	Cleveland Ironstone (mud, silt and sand with iron seams)
	Sta (Middle Lias)	Straithes sandstone (sandy siltstone and sandstone)
	M Alum Sh	Main Alum Shales - Grey pyritic shales

Table 3.1. Key to Geological Map (Fig. 3.3.1) showing symbols used in horizontal section on map face.

Lower and Middle Lias

Mainly an agricultural area, this region is located in the centre of the catchment. The main farming region is located along the River Dove channel which contains alluvium and terrace deposits of Flandrian clays, silts, sands and gravel.

The Middle Lias is comprised of an Upper Ironstone Series (Cleveland Ironstone) and a Lower Sandy (Straithe sandstone) series. The soils that have developed on this relatively low area vary from sandy and free draining to clays and water-logged gley soils, which generally provide good agricultural land. However, poor soils occur where material has accumulated by mass movement from the Upper Lias or where the Sandy series is poorly drained.

The slopes of this region, are gentle with gradients that range between 2 and 10 degrees. The steeper slopes, like the poorer soils, are often associated with hummocky accumulations of material derived from the upper Lias outcrop.

Soil erosion in the Middle and Lower Lias region is not extensive away from the river channels, largely because most of the land is used for pasture, and the thick vegetation cover and lack of disturbance, curtail the action of rain and frost (Imeson, 1970).

The Upper Lias Region

The Upper Lias outcrop encircles the Lower and Middle Lias as a belt of steeper land. Its lithology is characterised by dark grey shales, frequently exposed in gully and landslip features. The lowest horizon, the Grey Shale, ten metres thick and uncharacteristically soft, is usually overlain by material from the Jet Rock and Alum Shale above. The Jet Rock, ten metres thick, and the Alum Shale 37 metres thick are hard dense rocks which are difficult to distinguish in the field. The Alum Shale is the highest and most important outcrop of the Upper Lias in Farndale, and is located on slopes having gradients of between 16 and 28 degrees.

In general, soils developed on the Upper Lias are thin and free draining, with upper humic horizon and a lower zone of weathered shale separated by a thin brown soil. Exceptions to this occur where the soil has developed on solifluction material and on areas of poorly drained land, where gleyey or peaty soils are often found.

The Alum Shale and, to a lesser extent, the Jet Rock series, are characterised by a series of landslips and gullies, originating mainly at spring sites beneath the Dogger, which could be several thousand years old (Imeson, 1970). Alum Shale is therefore one of the most important sediment producing regions of the catchment. Over most of the Upper Lias region, the vegetation is dominated by bracken interspersed with woodland of Sitka and Norway spruce.

Middle Jurassic Region

The Middle Jurassic rocks occupy the highest areas of the catchment and encircle the Upper Lias area described above. They are comprised mainly of deltaic deposits but are interrupted by marine strata at three levels. Before the deposition of the Lower Deltaic series the beds at the top of the Lias were eroded. The deposits between this erosion surface and a similar surface higher up are known as the Dogger - a highly variable marine formation comprising conglomerates, sandstones, shales, limestones and ironstones.

The Dogger can be traced around the catchment as either a break of slope above the Alum Shale or by small outcrops of craggy boulders, fragments of which can be found in solifluction material and on the surface of most of the Lower slopes.

Above the Dogger, the lithologically complex Deltaic series form a relatively level moorland region. The deposition of the sediments, which occurred in shallow pools or freshwater lagoons, on the delta surface and in tributary channels, has resulted in a wide range of rock types occurring in close proximity. The Deltaic beds are divided into a Middle and Lower series by the marine sandstone of Eller Beck - 4.5 to 8m thick consisting of shales with a basal sideritic ironstone in the lower part, and a shaly sandstone in the upper part - which is present on the western side of the catchment, but is completely absent from the east.

Above the Middle Deltaic series the Fossiliferous Grit faces of the Grey Limestone series (Scarborough formation), a marine horizon, caps the interfluvial areas of the catchment in the north and east with thick spreads of grit. According to Fox-Strangways (1892, p. 244)

' This causes a great change in the country; for where these great spreads of fossiliferous grit occur, long flat dip slopes are seen, which are usually very dry, except where covered by peat, and the wet Estuarine Clays have a much narrower outcrop; but further east where the grit is absent a large area is formed of low round hills of estuarine strata, with simply a belt of Grey limestone series beneath; the country bleak and wet in the extreme '

The slopes of the moorland region are fairly gentle. The interfluves are particularly level with gradients seldom steeper than eight degrees. The gradients gradually steepen until at the Dogger outcrop they are generally between 12 and 16 degrees. Exceptions occur where the Eller Beck is crossed and where seepage faces, gullies and bogs, form local relief features.

The soils on the Deltaic series are as varied as the lithology so that coarse sands and clays occur in close proximity. In most places the mineral soil is covered by a peaty humic deposit a few centimetres to a few metres thick. This acid mineral-poor horizon, has often been eroded away to expose the sands and clays below. The soils of the moorland area are closely related to local relief, and drainage features to the type and condition of the moorland vegetation, the present and past exposure of the soil by burning, and any subsequent erosion by frost, rain and wind. The drainage of the moorland is related to conditions of cover, vegetation, soil, slope and erosion. In general, where the heather is unburnt and a thick humic subsoil exists, there may be little surface runoff. Hence rainfall is intercepted and evaporated, or transmitted as throughflow to the seepage bogs and faces found at various levels downslope (Imeson, 1970). Only those areas beneath the main seepage bogs support permanently flowing streams. The vegetation of the moorland area is dominated by heather in various stages of development after burning, except at seepage sites and waterlogged land along certain reaches of the main river channels.

The Corallian outcrop is horse-shoe shaped, open to the coast, and peripheral to the faulted Vale of Pickering Syncline (Kent, 1980). Here it consists of three formations - the Lower Calcareous Grit, the Coralline Oolite and the Upper Calcareous Grit, in upward succession (Wright, 1972). The 'grits' consist largely of fine-grained calcareous sandstones, and are neither true grits nor true limestones (Kent, 1980). There are variations in lithology in both grits and oolites. Oolites, however, exhibit

more marked variations in the nature and abundance of faunas. These small areas of Deltaic series in the south of the catchment, provide quite good agricultural land.

3.4 Landuse

Fig. 3.7 shows the spatial distribution of landuse within the Farndale catchment, derived from the Landsat TM image from June 1992 (Fig. 3.2). Landsat Thematic Mapper detects reflected radiation from the earth's surface in the visible and near infra red wavelengths using 7 spectral bands. Band 1 penetrates water for bathymetric mapping along coastal areas, and is useful for soil-vegetation differentiation and for distinguishing forest types. Band 2 detects green reflectance from healthy vegetation. Bands 1 and 2 together detect in the visible portion of the spectrum and are useful for detecting cultural features such as roads. Band 3 detects chlorophyll absorption in vegetation, while band 4 detects near-IR reflectance peaks in healthy green vegetation and water-land interfaces. Together, Bands 3 and 4 can be used in the discrimination of land/water and vegetation, while bands 5 and 7 are useful for vegetation and soil moisture studies and for discriminating between rock and mineral types. Band 6 is the thermal band and is designed to assist in thermal mapping and soil moisture and vegetation studies.

The Landsat image was analysed in ERDAS Imagine. Based on landuse maps and general knowledge of the catchment, it was determined that five broad classes can be identified. These are heather, bracken, woodland, cultivated and grassland. The geo-referenced and rectified image was classified, into 5 classes using unsupervised classification. The catchment is made up of 20.24, 19.70, 16.73, 22.96, and 20.37% of heather, bracken, woodland, grazing and cultivated respectively. The resulting classified image was validated by a field visit to verify the boundaries of each landuse type. This image is used to spatially distribute hydraulic conductivity by landuse, in order to assess the effect of spatially distributed landuse on the prediction of catchment hydrological response. Details of the field survey and implementation of the spatially distributed parameterisation are given in section 6.2.

Fig. 3.7 shows that heather is located mainly on the catchment interfluvies on flat to gentle slopes overlying peaty soils, estuarine sands and sandstones. Its location in the headwaters of the catchment overgrowing gully formations suggests that it plays an

important role in soil erosion and sediment supply within the catchment. Bracken interspersed with woodland is on steeper slopes downslope of the heather. On these steeper slopes, the topographic controls on runoff processes may overshadow the influence of bracken and woodland on runoff and soil erosion. Given their higher hydraulic conductivities than heather, they may also serve to reinforce those topographic controls. Grazing is downslope of bracken and woodland. Compaction and exposure of soil under this landuse can potentially result in lower infiltration rates and hence higher runoff and erosion rates. Agricultural crops are grown on the valley floor and in the south of the catchment. This landuse is a major source of sediment due to its location on the floodplain. In addition, disturbance of the topsoil during cultivation makes it a high sediment producing area. Erosion under some of these landuses is considered in more detail in section 3.7.1 below.

Remote sensing has been used increasingly as a source of spatial data on vegetation cover, topography and soils (Fryer, *et. al.*, 1994; Giles *et. al.*, 1994), and even soil moisture and precipitation (e.g. Engman and Gurney, 1991; Corr, 1993; Hogg *et. al.*, 1993; Lin *et. al.*, 1994). The main advantage of remote sensed data is that it provides spatial data in a digital format, and is therefore easily integrated into GIS. Rango *et. al.*, (1983) showed that the accuracy of landuse classification obtained from Landsat images was around 90%. The spatial resolution of Landsat TM (30 x 30m) enables the easy incorporation of this into the 50 x 50m grid cell model developed here.

However, remote sensed data can be prone to error due to the calibration and quantification of derived information, as well as the spatial resolution of the data (e.g. Sader *et. al.*, 1995).

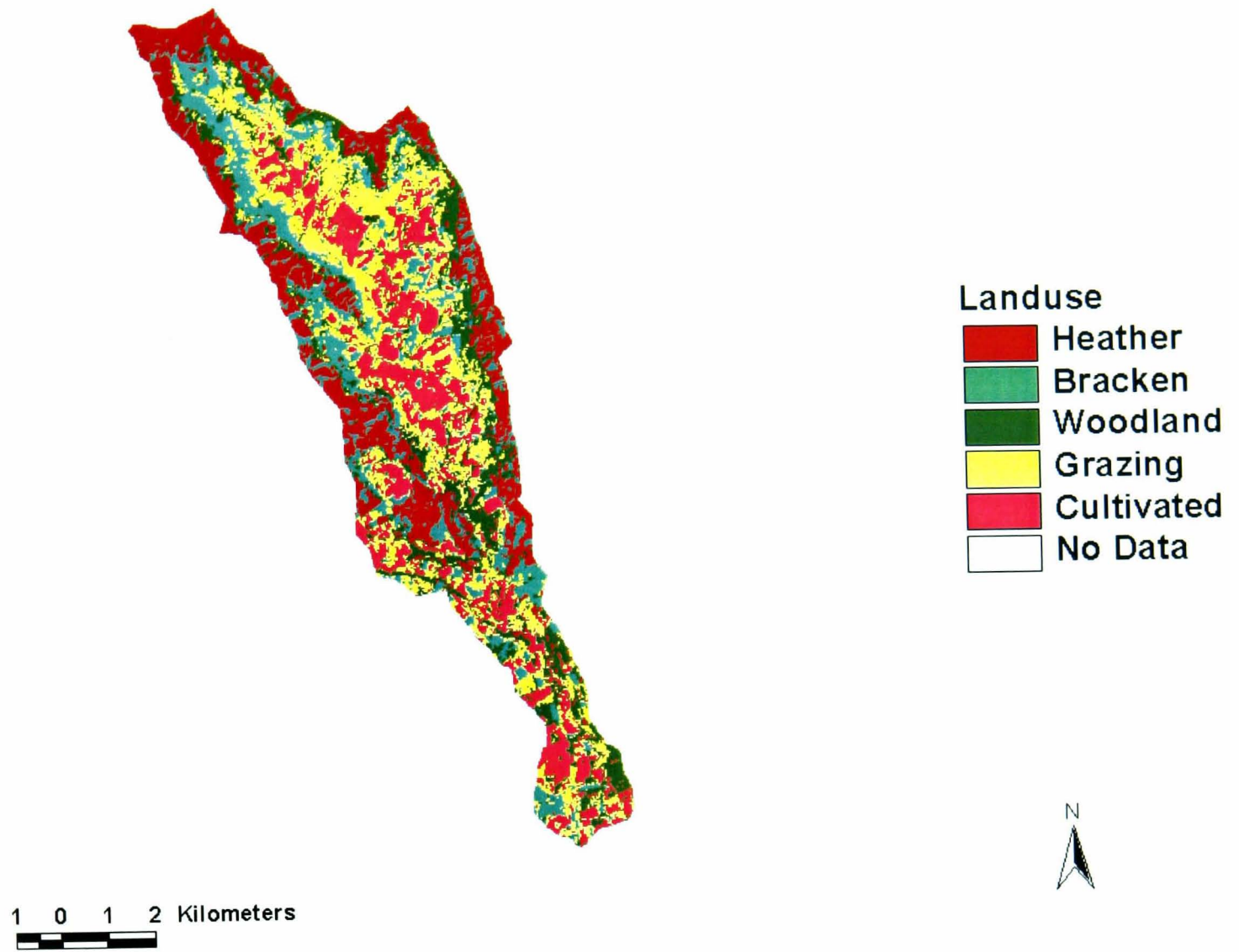


Fig. 3.7 Spatial distribution of Landuse in Farndale derived from Landsat TM

3.5 Soil type

Fig. 3.8 is a map of soil type derived by digitising soil maps for the catchment. Each soil type is discussed in the context of its location within the catchment, its water retention capacity, and its predominant landuses.

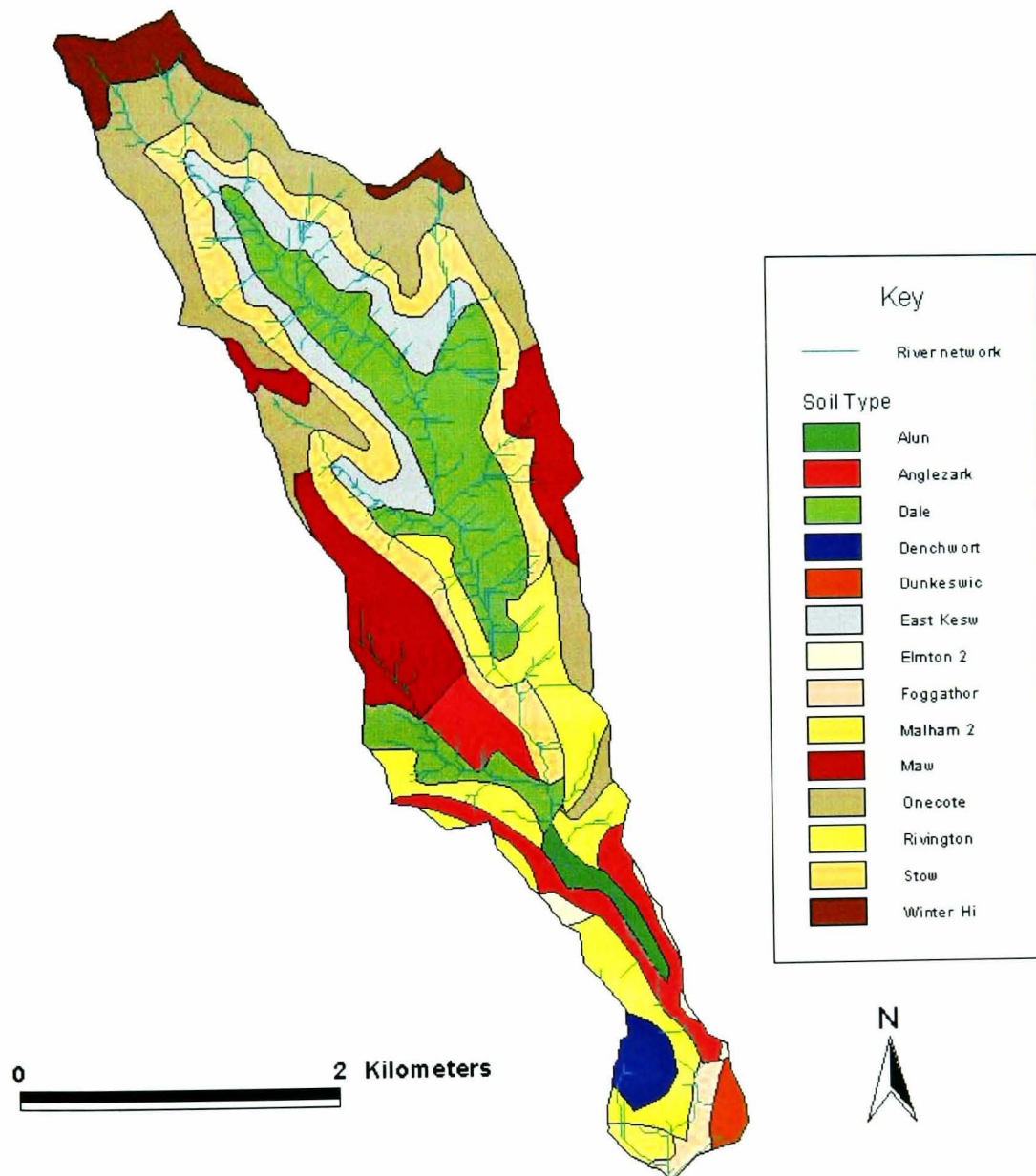


Fig. 3.8: Soil Type distribution in Farndale Catchment (original source: Soil Survey of England and Wales, 1983 1:250,000).

Association Name	Soil Type	% Heather	% Bracken	% Woodland	% Grazing	% Cultivated	Wetness Class
Alun		4.3	0.9	39.5	22.2	33.1	I
Anglezarke	Humo-ferric podzols	24	16.4	27	19	13	V
Dale	Pelo-stagnogley soils	2.8	9.9	9.5	30.6	47.2	IV
Denchworth	Pelo-stagnogley	0	1.1	15.0	17.4	66.5	IV
Dunkeswick	Typical stagnogley soils	0	1.7	37.0	19.0	42.0	IV
East Keswick2	Typical brown earths	0	15	8.7	44	32	I
Elmton2	Brown rendzinas	0.5	28	43	22	7	II
Foggarthorpe	Pelo-stagnogley soils	0.2	12.6	31.8	22.05	33.3	III
Malham2	Typical Brown earths	0.8	36.03	4.4	28.0	32.0	I
Maw	Humus-ironpan stagnopodzols	52	24	11.16	6.0	7.0	V
Onecote	Cambic stagnogley soils	37	28	22	12	1.0	VI
Rivington 1	Typical brown earths	7.0	19.2	17.86	27.0	29.0	II
Stow	Typical brown earths	8.0	29.0	22.0	33.0	8.0	II
Winter Hill	Raw oligo-fibrous peat soils	87.0	10.0	2.0	0	0	VI

Table 2: Soil types in Farndale Catchment, showing landuse and wetness class

Wetness Classes

I – soil profile is not waterlogged within 70cm depth for more than 30 days in most years.

II – soil profile is waterlogged within 70cm depth for 30-90 days in most years.

III – soil profile is waterlogged within 70cm depth for 90-180 days in most years.

IV- soil profile is waterlogged within 70cm depth for more than 180 days, but not waterlogged within 40cm depth for more than 180 days in most years.

V- soil profile is waterlogged within 40cm depth for 180-335 days, and is usually waterlogged within 70cm for more than 335 days in most years.

VI – soil profile is waterlogged within 40cm depth for more than 335 days in most years.

Alun Association

The Alun association is found in the channel and along the floodplain in the southern part of the catchment at 55 to 116m O.D. on flat to gently sloping land. It consists of coarse and fine loamy brown alluvial soils, comprising the Alun series, which occurs on floodplains, and Enborne and Trent series, which occur in hollows. The underlying geology is predominantly alluvium and Oxford Clay. These soils are well drained and readily absorb winter rain-water, but flooding may occur in Enborne and

Trent soils because these are located in depressions which suffer from surface ponding in winter. The landuse is 40% woodland, 33% cultivated and 22% grazing.

Anglezarke Association

The Anglezarke association is found at 45 - 250m O.D., mainly in the southern parts of the catchment on slopes of 3-8°, extending south-eastward from the west, downslope towards the outlet. It is also found further north in a V-shaped formation from western to eastern slopes of 12-17°. The underlying geology is Moor Grit (29%), Coralline Oolite (26%), Eller Beck Formation (23%) and Oxford Clay (10%). The Anglezarke association is made up of humus-enriched subsoils with a thin ironpan in some places, and contains the Anglezarke series and the Revidge series. The Revidge series comprises shallow peaty soils with the bedrock within 30cm at high altitudes, and deeper soils containing bleached subsurface horizons and dark humus-enriched subsoil or ironpan, at lower altitudes. Most of the association has a long field capacity period. Excess winter rainfall is not readily absorbed by saturated peaty or humus topsoils so there is rapid winter run-off. The semi-natural vegetation is heather moor (24%), in which heather (*Calluna vulgaris*) predominates, with bell heather (*Erica cinerea*), bilberry (*Vaccinium myrtillus*), and cowberry (*V. vitis-idaea*) in some places (MAFF, 1984). Regular controlled burning has preserved heather over large areas. Woodland accounts for 27% of the landuse, bracken for 16%, grazing 19%, and cultivated, 13%.

Dale Association

The Dale association occurs on gently to moderately sloping valley sides, and on the valley floor in the centre of the northern floodplain at 80-160m O.D. and slopes of 5-8°. It also occurs further south at 75- 290m O.D. on western slopes of 3-12°. The underlying geology is predominantly Alum Shale (41%) and Staithes Formation (26%). The chief soils are surface-water gley soils. The Dale series, pelo-stagnogley soils are usually found where there is no Head, often on convex slopes. The main soils are seasonally waterlogged where undrained, depending on rainfall. Excess winter rain forms shallow, lateral, subsurface flow (Jarvis *et. al.*, 1984). The Dale series exhibits variable droughtiness under grass. The highest land of the central northern occurrence of this soil is predominantly in permanent grass. At lower altitudes there is cereal growing with ley grassland, while wooded areas are found on

the western slopes further south. Most soils of this association are slightly acid and tree growth is limited by shallow rooting caused by surface wetness. Planting is mainly Sitka or Norway spruce and some hardwoods with amenity value, namely ash, sycamore and elm, can be grown in sheltered places.

Denchworth Association

The Denchworth Association is located in the south west of the catchment near Kirkbymoorside at 57 to 126m O.D. on slopes of 0 – 13° over Kimmerage Clay (80%) and Corallian rocks (20%). The association consists mainly of the Denchworth and Lawford series, but also present are the Evesham series, the Wickham series, and the Oxpasture series.

The Denchworth soils comprise stoneless, strongly mottled clays with slowly to moderately permeable topsoils, while Lawford soils comprise clays that contain stones and small amounts of sand in their topsoils. Wickham soils have loamy upper horizons, and the other associated soils also have clayey subsoils. Most of these soils are prone to waterlogging for long periods during winter, due to their slowly to moderately permeable topsoils. When waterlogged, runoff is mainly by lateral flow, usually surface runoff, and the land does not readily absorb excess winter rainfall (Jarvis *et. al.*,1984).

Landuse is mainly cultivated (66%), grazing (17%), and scattered trees (15%). On grassland, surface wetness and weak soil bearing strength limit stocking density and grazing period, although moderately good yields of grass are possible. The soils poach easily and yields are reduced where grazing is ill-timed. The Denchworth soils are acid in the surface where un-limed, but pH increases gradually with depth and the soil is often neutral or alkaline within 1m depth.

Dunkeswick

The Dunkeswick association occurs in the south-eastern extreme of the catchment over Corallian Rock, Kimmerage Clay and Boulder Clay, on slopes of 0 – 4°, at 47 – 90m O.D., and is dominated by stagnogley soils in greyish brown drift. It comprises mainly Brickfield series and Dunkeswick series. These soils are slowly permeable, the clayey subsoil impeding percolation and causing rapid run-off of winter rainwater.

They are therefore seasonally waterlogged for long periods in winter. Landuse is mainly cultivated (42%) woodland (37%) and grazing (19%).

Elmton 2

The Elmton 2 association is found in the south of the catchment on the western and eastern divides on flat to gentle slopes (0-4°) at elevations of 83-176m O.D. overlying Corallian rocks. This association includes well-drained soils overlying limestone at various depths. Its main members are fine loamy and fine silty shallow stony Elmton soils, typical brown rendizinas within 30cm of the limestone in some places and within 80cm in others. Because of the permeable substratum at shallow depth, winter rain is readily absorbed. Run-off is slight, but may increase where clayey subsoils are thicker. This has resulted in some erosion on slopes. On the eastern divide this soil supports non-coniferous trees (43%) in isolated strips as stoniness and the presence of bedrock at shallow depth restricts rooting. These soils are too shallow and dry for vigorous growth of softwoods and because of their calcareous nature, conifers show chlorosis. Other landuses are bracken (28%), rough grazing and grassland (22%).

East Keswick 2 Association

In Farndale, this association occurs at 115-280 m O.D. on slopes of 0-25°, on both southeast- and southwest-facing slopes, in the north of the catchment. It consists predominantly of coarse and fine loamy typical brown earths in drift, derived from the underlying Jurassic shales (Alum Shale, Mica Shale), interbedded with sandstones (Estuary Sand), on steep valley sides or escarpments. It comprises the East Keswick series, the Wick series, Neath series, Rivington and Belmont series. The soils are absorbent and, despite the steep slopes, there is little winter run-off. Landuse is mainly poor grassland (44%), scrub (15%) or managed deciduous and coniferous woodland (9%) and some arable fields (32%).

Foggathorpe 2 Association

This association is located in the centre of the southern tip of the catchment at 38–84m O.D. on slopes of 0–16°, over Corallian rock, alluvium, and glaciolacustrine clay. It is dominated by the slowly permeable clayey and fine loamy over clayey soils, and comprises mainly the Foggathorpe series, which is very strongly mottled and often clayey throughout, but may have thin fine loamy topsoil locally. Seasonal

waterlogging occurs, resulting in rapid runoff of winter rainwater. The large clay content and surface wetness restricts cropping to cereal (33%) on better drained soils, grass (22%) and woodland (32%).

Malham 2 Association

Located in the south-western extreme of the catchment at 39–50m on flat ground, this association comprises mainly well-drained soils in silty aeolian drift, interspersed in places with bare limestone. It readily absorbs winter rainwater, but rapidly becomes saturated, remaining water-logged for long periods in winter. Landuse is scrub (36%), cereal (32%), and grazing/grassland (28%).

Maw Association

The Maw association is found on eastern slopes at 200-400m O.D. and of 0-20°, and at the same altitude on steeper western slopes of 20-29°. The association consists mainly of the Maw series – humus-ironpan stagnopodzols, and the Gelligaer series - ferric stagnopodzols, over sandstones and grits. It normally occurs on long narrow ridges, under cool humid, exposed conditions on land rising from lower ground, where stagnohumic gley soils of the Onecote and Wilcocks associations predominate. In Farndale, it occurs uphill of the Onecote association. Soils are waterlogged for long periods during growing season, resulting in rapid winter runoff.

Heather, dominated by bell-heather is abundant (52%). Acid-tolerant grasses and mosses are found. The soil is at field capacity for more than 225 days (MAFF, 1984). Hence patches of marsh are found. The soils can support trees once remedial measures such as burning of heather, rotavating, and subsoiling have been undertaken. Small patches of woodland (11%) occur on the east-facing slopes. Deep cultivation is necessary to break the ironpan and improve drainage and aeration. Tree growth declines above 300m and is restricted to Sitka spruce, Scots pine, hybrid larch and Douglas fir.

Onecote

The Onecote association is found on west-facing slopes of 3-20° at 200-400m O.D., on south- and southwest-facing slopes, 8-28° at 360- 440m O.D., and on steep east facing slopes of 20-30° at 360-400m O.D. It consists of loamy and clayey cambic

stagnohumic gley soils, on shale or mudstone and thin local drift. The clayey Onecote series passes to clay or mudstone within 80cm depth whereas the Ipstone series is loamy over clay and the Wilcocks series entirely loamy (MAFF, 1984). These soils have a peaty or humose surface and slowly permeable, strongly gleyed subsurface horizons. The Onecote series is found where there is little or no drift, while the Wilcocks and Ipstones series are common where Head, partly derived from adjacent sandstones and grits, masks the underlying mudstones (MAFF, 1984). The raw oligo-fibrous peat, Winter Hill, is found on hilltops in the north-east, adjacent to the Onecote soils.

In high rainfall, the peaty surface horizon quickly becomes waterlogged for long periods, so run-off can be rapid. These soils are at field capacity an average of 215 days per year in the North York Moors (MAFF, 1984). Marsh occurs on steeper slopes and on hilltops. Large areas of hydrophilous heather (37%) are supported along with bracken (28%) and scattered trees (22%). Moderate grass yields occur, on lower ground on the west-facing slopes (12%). The land is only marginally suited to grassland, however, as the large retained water capacity of the topsoil easily causes rutting and poaching (MAFF, 1984). Burning, rotavating and reseedling is necessary to reclaim moorland and accommodate rough grazing by sheep, but over-grazing may lead to poaching.

Rivington 1 Association

This association occurs in the south of the central floodplain at 40–240 m O.D. on slopes of 3 – 28°, in an east-west direction just north of the escarpment, and along the western margin in a north-south direction towards the outlet at 40–120m O.D. on slopes of 0-9°. The topsoil consists of a dark greyish-brown, slightly stony sandy loam or sandy silt loam, and extends to 0-20cm. This overlies a yellowish brown, slightly to moderately stony sandy loam or sandy silt loam with a weak medium subangular blocky structure at 20-50cm. At depth (>50 cm) hard or soft sandstone or extremely stony sandy loam can be found. Excess winter rainwater passes downwards easily through the permeable substrate. In the south of the catchment, the land is given over to grassland and some scattered trees. Further north, narrow strips of mixed woodland are supported, and on the valley floor, landuse is grass, arable, cereal, winter grazing and mixed woodland. During times of low rainfall, this soil can

become drought prone under grass and arable crops. This draughtiness, combined with the stoniness of the soil, limits tree growth.

Stow Association

The Stow association occurs adjacent to, and downhill from, the Maw and Dale associations in the north of the catchment at an altitude of 200-300m O.D. on steep (14-20°) slopes. It is composed mainly of clayey or loamy soils formed from Jurassic mudstones and siltstones. The chief soil, the Stow series, typical non-calcareous pelsols, has a clayey, water-retentive topsoil which is slowly permeable, resulting in seasonal waterlogging. Lateral subsurface flow occurs in winter on slopes steeper than 8°, with less runoff on steeper slopes. These soils are traditionally grassland soils, and are also used for grazing (33%) in the summer on the steeper slopes but, some areas are covered by scrub, woodland, or bracken (29%). Steep slopes and weed-growth are the main limitations to tree planting.

Winter Hill

This association is located on the high ridge tops in the north and north-east of the catchment at 400-430m O.D., on land which is flat to gently sloping, with underlying peat, which has filled in the hollows and produced a smooth undulating surface. The association is predominantly made up of the Winter Hill series, comprising blanket peat with moss and cotton-grass remains, along with the Floriston series, comprising raised peat with moss remains, and Longmoss series, comprising basin peat with grass and sedge remains. These soils are almost permanently waterlogged (soil moisture deficit of less than 40mm) making them increasingly vulnerable to gully erosion, and mass flow (MAFF, 1984). Land degradation on these soils can be manifested as parallel or network patterns of gullies, and peat bogs up to 6m deep (MAFF, 1984). The main channel originates here, and is maintained by headward cutting. Where severe erosion has occurred, the ground is often covered by grey sand and loose angular blocks of sandstone or gritstone, and an ironpan, originally beneath the peat and pre-dating it, may be exposed at the surface. Small inclusions of stagnohumic gley soils occur at the peat margins.

This association, in general, has little agricultural value because of wetness, unpalatable vegetation and the short grazing season. Landuse is mainly heather

(cross-leaved and bilberry) (87%), and rough grazing (10%). Where heather is burned in the interest of grazing, gully erosion can be exacerbated (Imeson, 1970; MAFF, 1984).

Soil Type grid

The soil type grid used in the analysis is derived by using soil texture tables (Avery, 1980), to derive average saturated hydraulic conductivity values in the top 100cm of each soil type. The soils are then grouped into six classes. Table 3.2 is the table of estimated saturated hydraulic conductivity values, and Fig. 3.9 is the new re-classified soil type grid. The implementation of the reclassified grid in the spatial parameterisation of the model is discussed in chapter 6.

Association Name	Soil Type	Saturated Hydraulic Conductivity
Alun		0.02502
Anglezarke	Humo-ferric podzols	0.1332
Dale	Pelo-stagnogley soils	0.00450
Denchworth	Pelo-stagnogley	0.00461
Dunkeswick	Typical stagnogley soils	0.06390
East Keswick2	Typical brown earths	0.00262
Elmton2	Brown rendzinas	0.00882
Foggarthorpe	Pelo-stagnogley soils	0.00432
Malham2	Typical Brown earths	0.01930
Maw	Humus-ironpan stagnopodzols	0.52900
Onecote	Cambic stagnogley soils	0.00461
Rivington 1	Typical brown earths	0.04013
Stow	Typical brown earths	0.00461
Winter Hill	Raw oligo-fibrous peat soils	0.00004

Table 3.2: Saturated hydraulic conductivity values for different soil types derived from soil texture tables of Avery (1980).

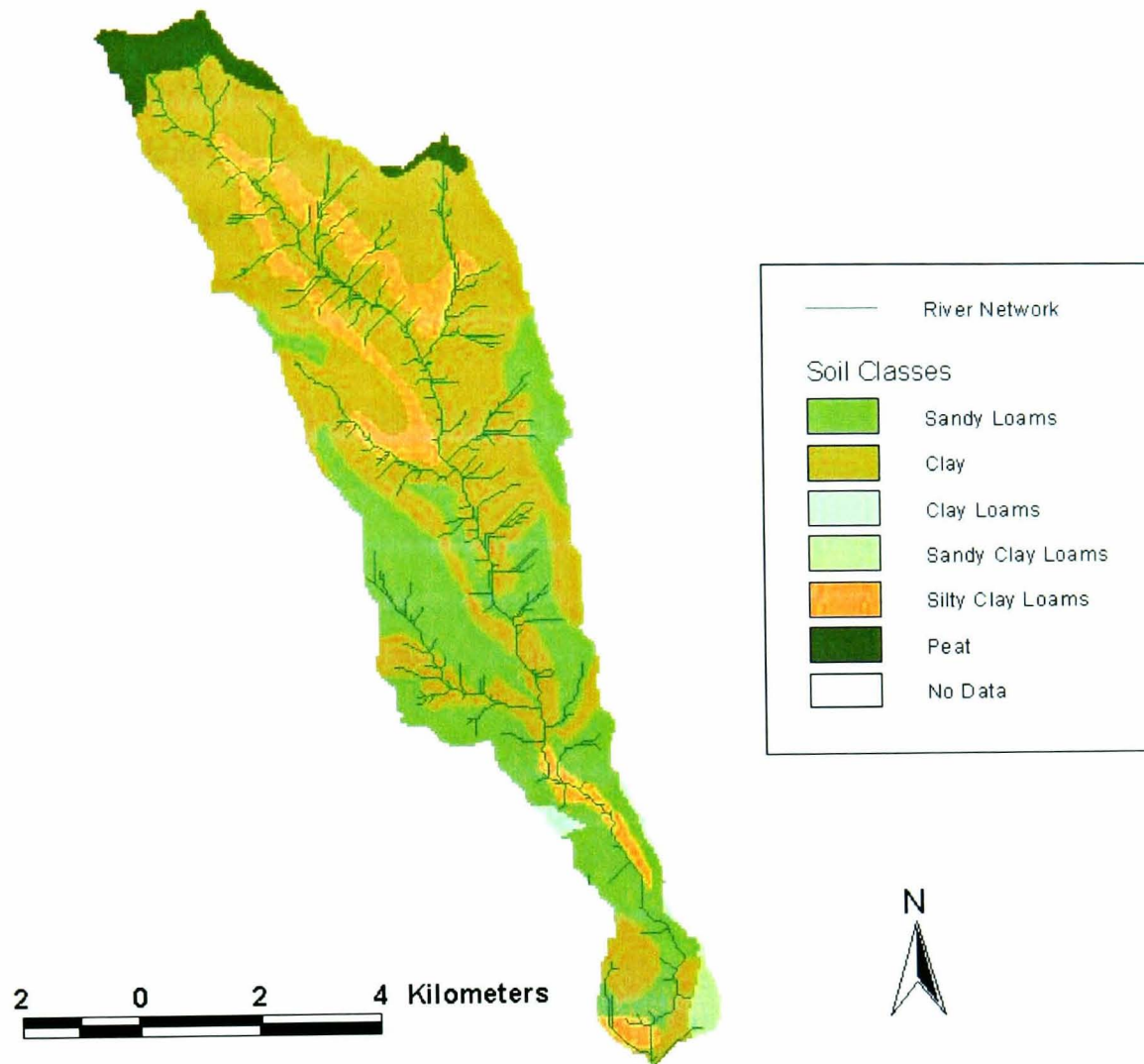


Fig. 3.9 Reclassified soil type map showing spatial distribution of saturated hydraulic conductivities derived from Avery (1980) soil texture tables.

3.6 Hydrometeorology.

3.6.1 Rainfall

Rainfall records from a continuous tipping-bucket rain gauge at Church Houses gauging station (467000, 497600) in the north of the catchment at an elevation of 150m, was made available by the Environment Agency. Fig. 3.10 below shows the location of the rain gauge and flow gauges within the catchment.

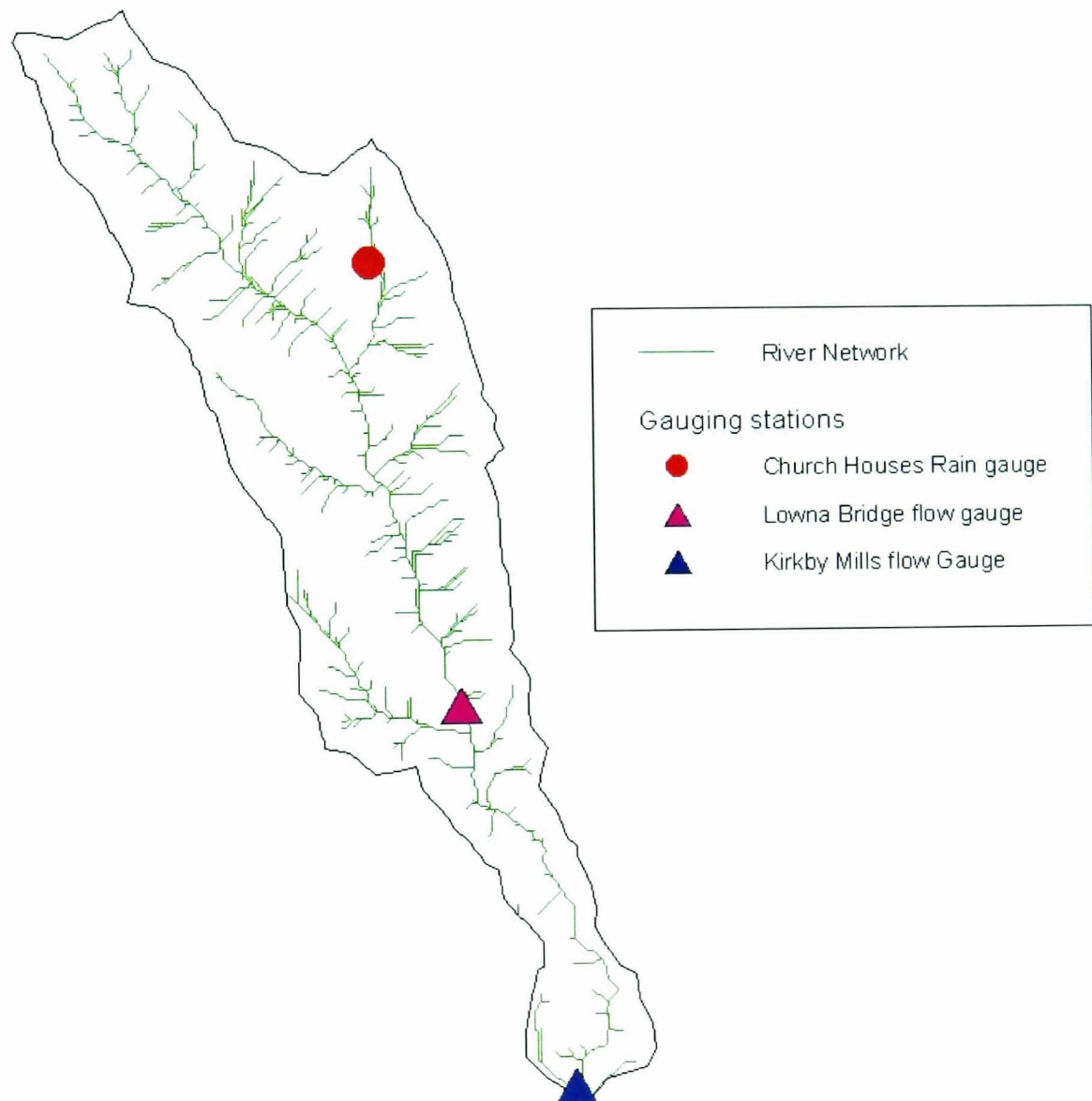


Fig. 3.10 The Location of gauging stations within the catchment.

The average annual rainfall for 1989 to 1998 is 0.812m, with 62% falling in winter (defined as 01 September to 28/29 February of the following year) (Figs. 3.11 and 3.12). Fig. 3.13 shows the distribution of rainfall for September 1994 to September 1995, for which an event analysis was done (the large gap in the data from April to May 1995 is due to equipment failure at the gauging station). An event here refers to any rain falling after a dry period and continuing for at least an hour and of at least 0.0002m in magnitude. Fig. 3.14 shows the variation of storm duration, mean rainfall intensity and peak rainfall intensity with time, as well as the variation of mean and peak rainfall intensities, and storm depth with storm duration, for a typical year - 1994/95. There were 371 events for the year. Of these 63% (234) occurred in winter. Storm duration shows distinct seasonality. Winter events vary between 1 hour and 17 hours in duration, 95% of which are 9 hours or less, and summer events vary in duration from 1 hour to 8 hours with 95% of events 7 hours or less.

Peak rainfall intensity also exhibits seasonality, though this is less apparent at a cursory examination of the plot. All but two winter events have peak intensities ranging from 0.0002 mhr^{-1} to 0.004 mhr^{-1} , while all but four summer events range from 0.0002 mhr^{-1} to 0.0028 mhr^{-1} . The highest peak rainfall intensities occur at the end of January and February, both having peak intensities of 0.006 mhr^{-1} , and both occurring during 3 hour events. Comparable summer events occur in late May (0.0056 mhr^{-1} and 0.0048 mhr^{-1} , during 4 and 3 hour events), and mid-July (0.0056 during 1 hour and 0.0046 mhr^{-1} during a 2 hour event). The occurrence of events with comparable peak rainfall and duration in summer and winter is useful when comparing flow generation under different soil antecedent moisture conditions (see fig. 3.20).

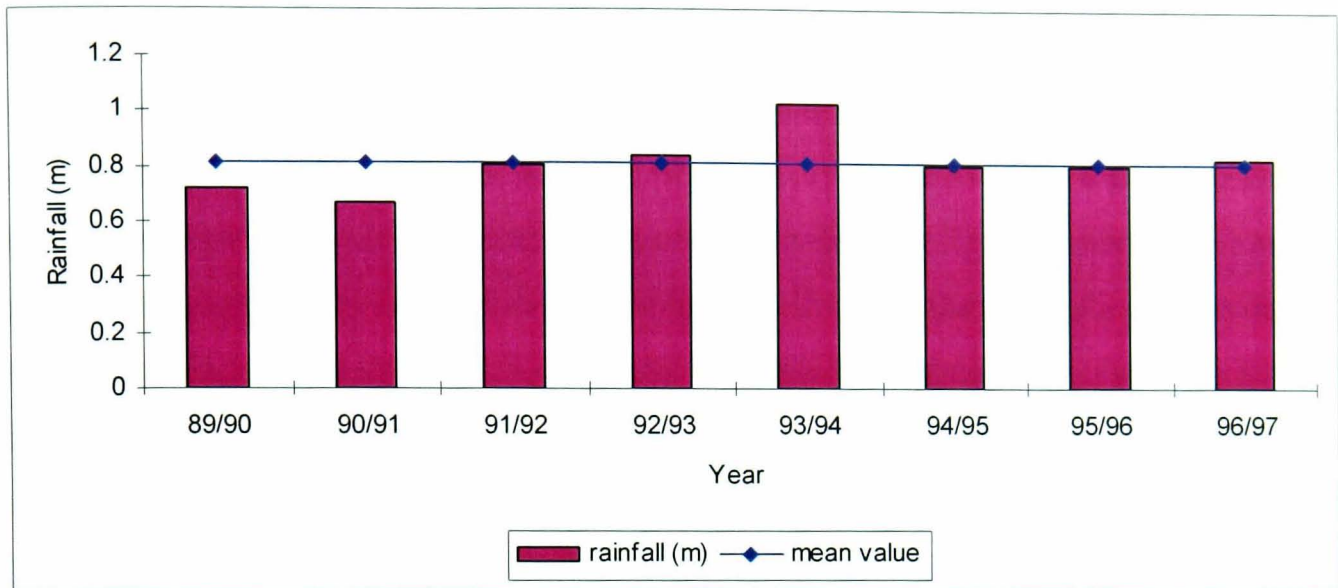


Fig. 3.11 Total annual rainfall.

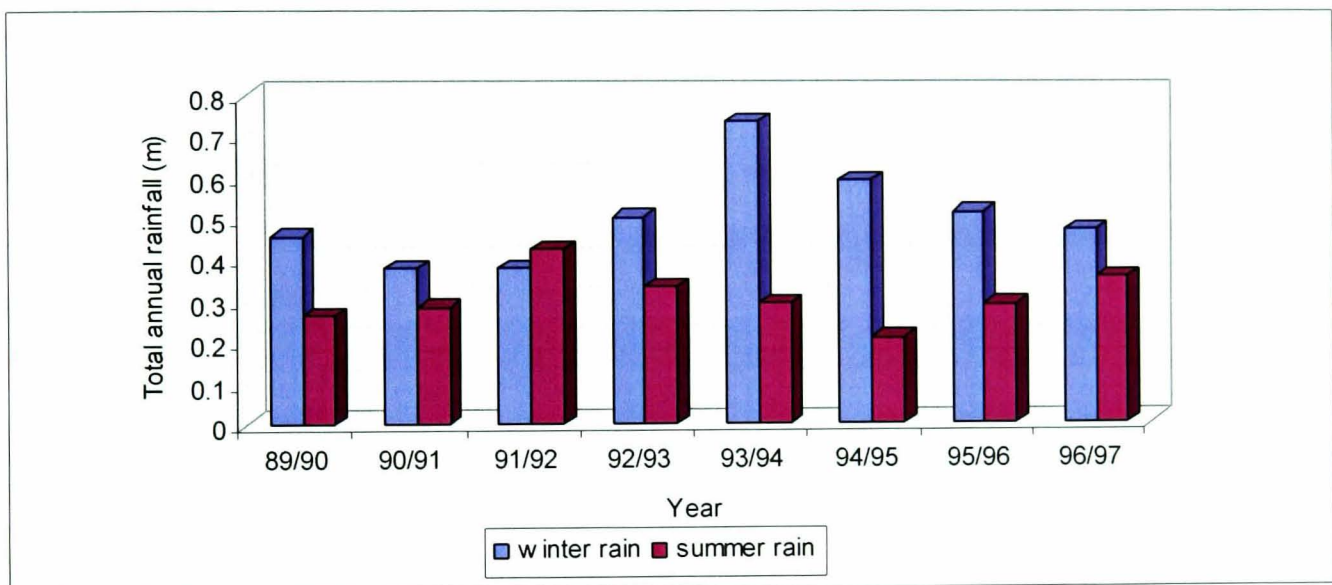


Fig. 3.12 Seasonal Rainfall (89-97)

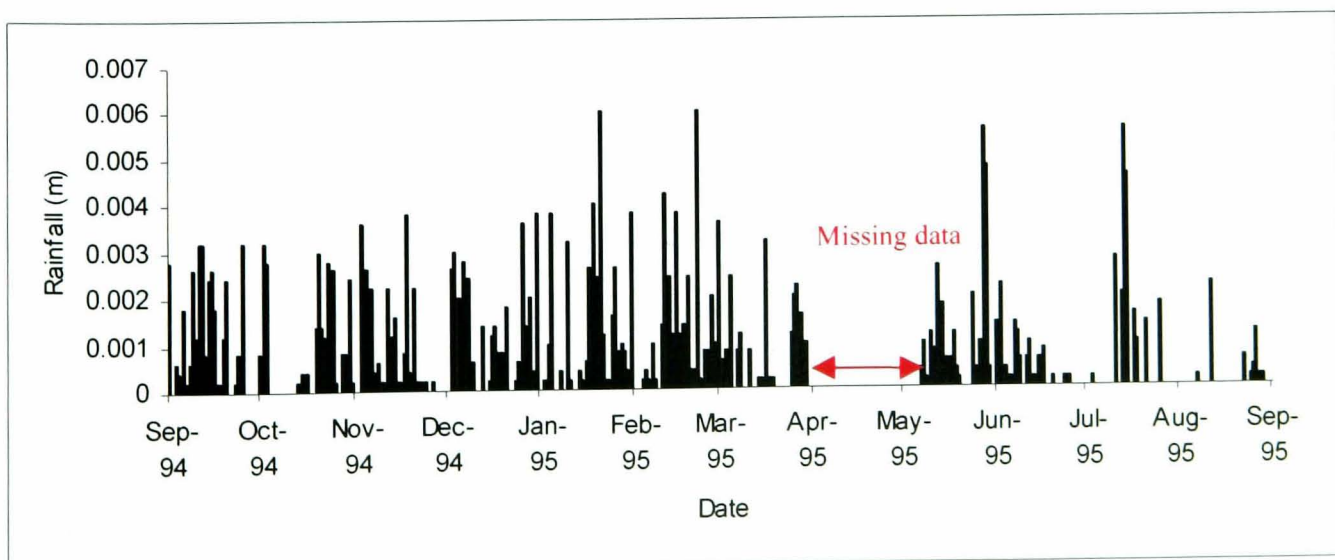


Fig. 3.13 Times series of Rainfall for Sept. 1994 to Sept. 1995

Mean rainfall intensity was found to have little seasonal variability, and a strong inverse relationship with storm duration. Events of 1-hour duration show the largest variation in mean rainfall intensity with values ranging from 0.2 mmhr^{-1} to 5.6 mmhr^{-1} . Total rainfall depth showed a strongly positive relationship with duration. The maximum depth of rain (0.03m) occurred during one of the 17hour events. The event analysis presented here is based on data originally at 15 minute intervals, lumped to 1 hour intervals. While a 1hour interval is the smallest that can possibly be used in the hydrological model (due to computational requirements etc.), it represents an aspect of temporal lumping, which could introduce uncertainty to model predictions. The 1hour July event of magnitude 0.0056m, for example, suggests that a smaller temporal scale might be needed in order to accurately represent rainfall patterns. The temporal lumping of rainfall data will inevitably result in the masking of important trends in rainfall, which will, in turn, affect hydrological and sedimentological predictions. During actual observations of events at the Kirkby Mills gauging station, periods of flashiness were observed. Hence, intervals of at least 15 minutes are necessary in order to accurately characterise elevated flow and suspended sediment concentrations here.

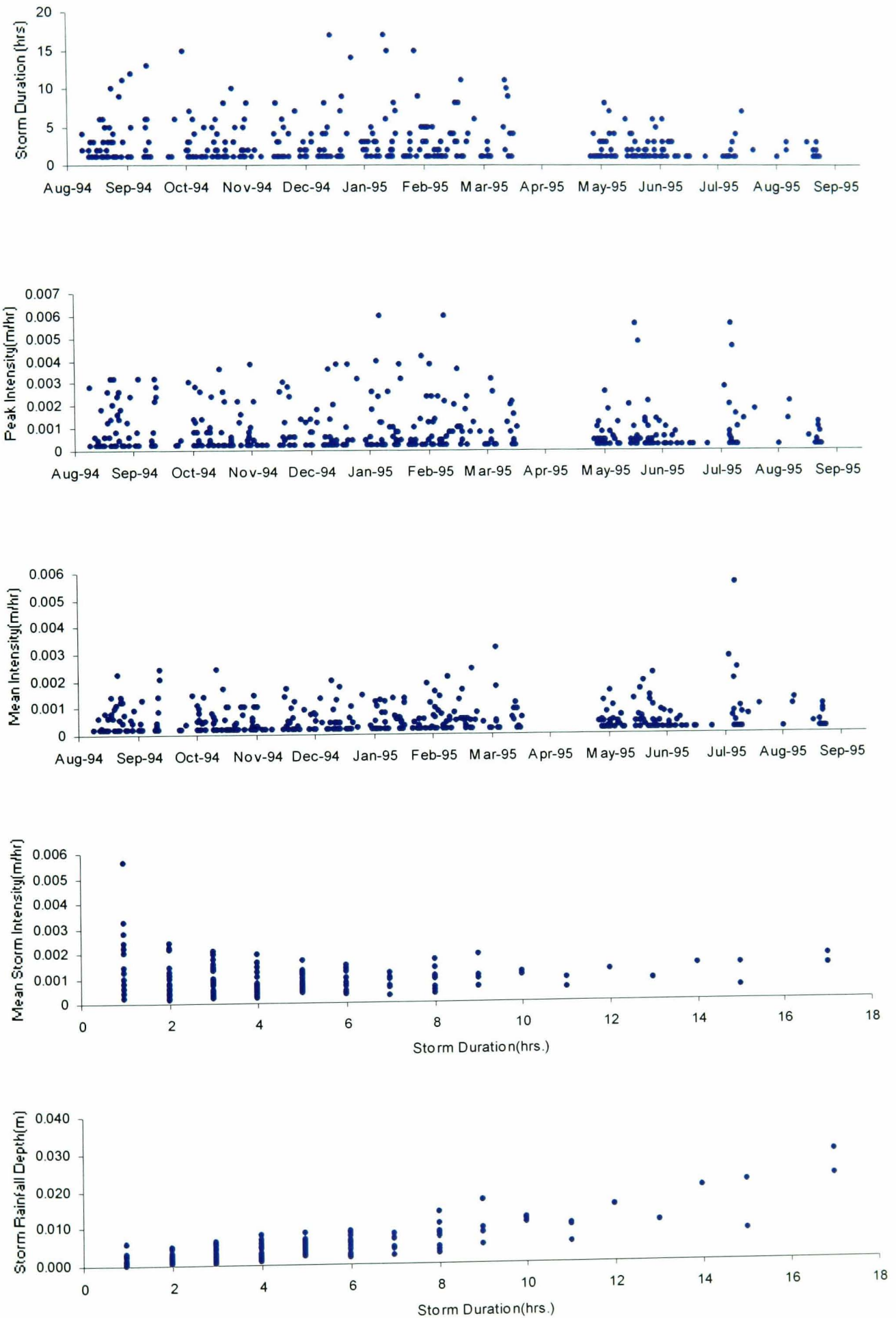


Fig. 3.14 Rainfall event analysis for September 1994 to September 1995.

3.6.2 Streamflow

Runoff records for Kirkby Mills gauging station were obtained for 1988 to 1998, and stage data for Lowna Bridge gauging station were obtained for 1994 to 1998 (Fig. 3.10). The weir at Lowna Bridge is a Triangular profile (Crump) weir, the geometry of which gives an essentially constant coefficient of discharge and a high modular limit (75%). The slopes are 1:2 (vertical to upstream face), and 1:5 (on downstream face). The equation used to convert stage to discharge, Q , at Lowna was

$$Q = C*(H+A)^B \quad [3.1]$$

Where C is a coefficient = 12.566, H is the gauged head or depth of flow in metres, A is the head correction factor = 0.004 and B is a constant = 1.544. Values were supplied by the EA and are based on long-term weir characterisation experiments.

The weir at Kirkby Mills gauging station is a flat-V triangular weir with a 1:10 cross slope and profile of 1:2 upstream and 1:5 downstream. The crest width is 3.0 m and the difference between the lowest crest level and upstream slab level is 0.6m. It is constructed to measure flows of 0.1 to 40.0 cumecs.

Figs. 3.15 and 3.16 show strong seasonality in the runoff values corresponding to the seasonality in the rainfall and evapotranspiration (discussed below) values. On average 66.0% and 70.0% of the total annual runoff at Kirkby Mills and Lowna Bridge respectively, occur in winter. The average winter runoff coefficient for Kirkby Mills and Lowna Bridge (runoff/rainfall) are 53.3% and 60.0% respectively, while the average summer runoff coefficients are 46.0% and 52.2%. Fig. 3.18 shows that in 1991/92, 1992/93, and 1994/95, the summer runoff coefficient was higher than the winter. In 1991/92, the higher summer runoff coefficients can be attributed to the higher rainfall values recorded for summer than for winter. In addition, large depths of summer rain are more readily converted to runoff by increased hillslope velocities on land where compaction is caused by grazing and machinery, and where land is left bare after harvesting arable crops close to the catchment outlet. The higher summer runoff coefficients for 1992/93 can be attributed to the fact the summer runoff for this year is exceptionally high (0.1927m), while the rainfall value is about average

(0.333m). The 1994/95 summer coefficient is also exceptionally high due the missing rainfall data for April 4th to May 2nd 1995.

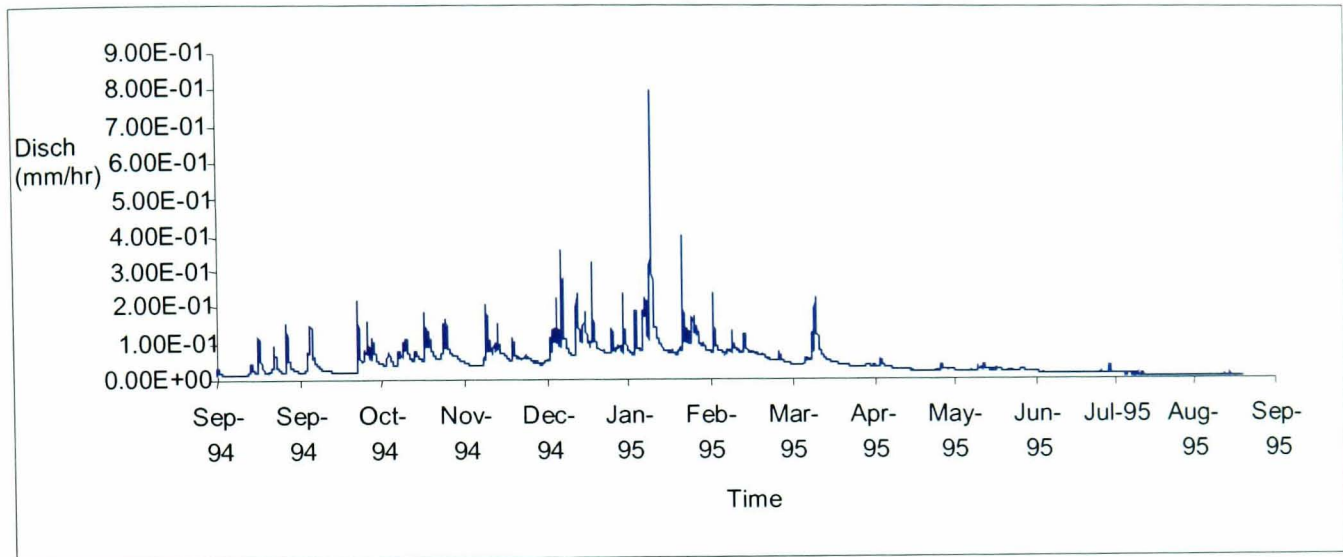


Fig. 3.15 Runoff for Sept. 94 to Sept 95 at Kirkby Mills gauging station

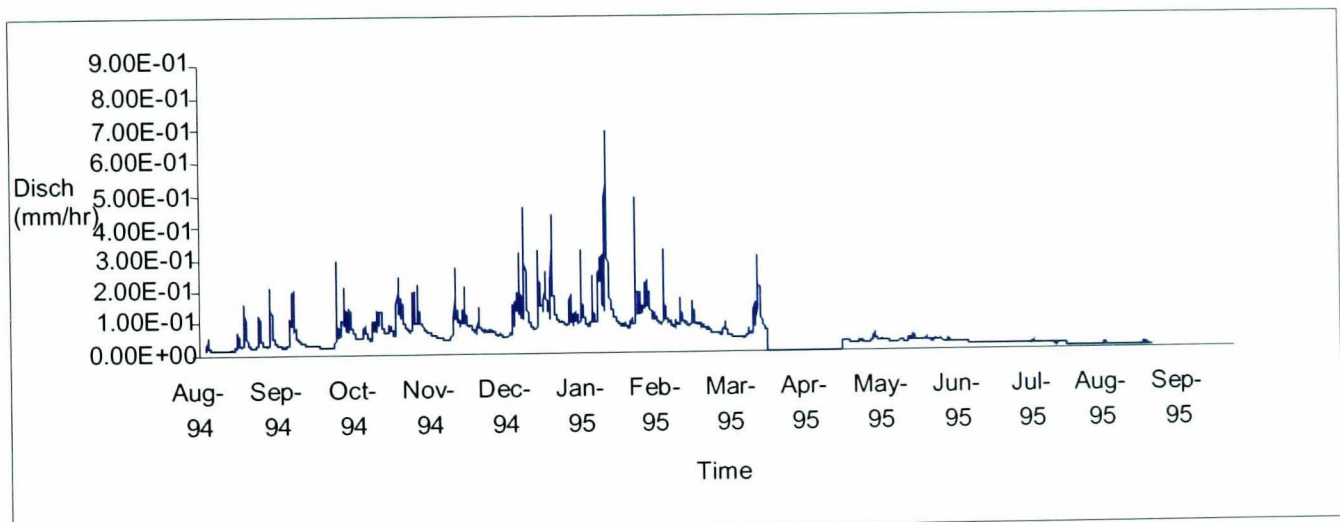


Fig. 3.16 Runoff at Lowna Bridge gauging station for Sept 1994 to Sept. 1995

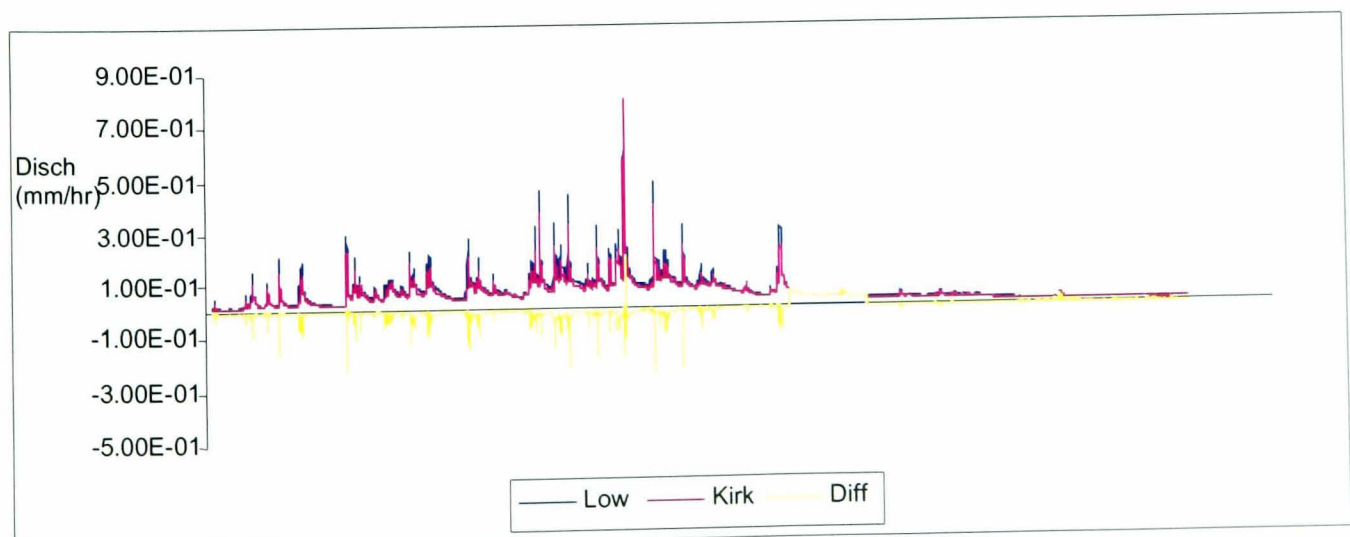


Fig. 3.17 Time series of discharge in cumecs for Lowna Bridge and Kirkby Mills

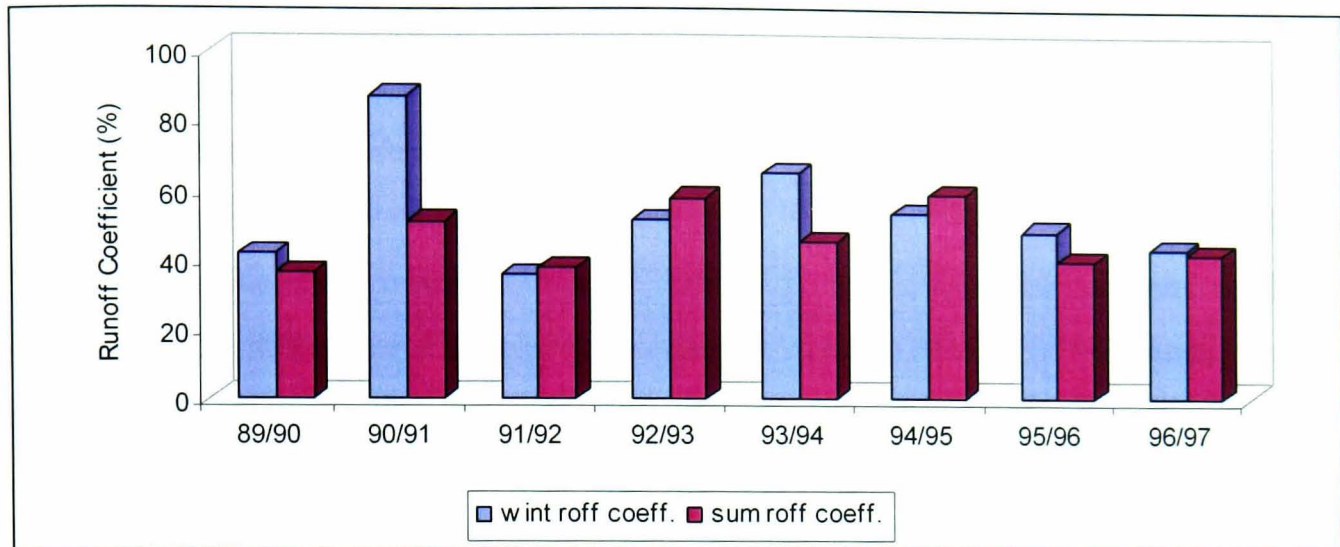


Fig. 3.18 Seasonal runoff coefficient for Kirkby Mills 1989-1997

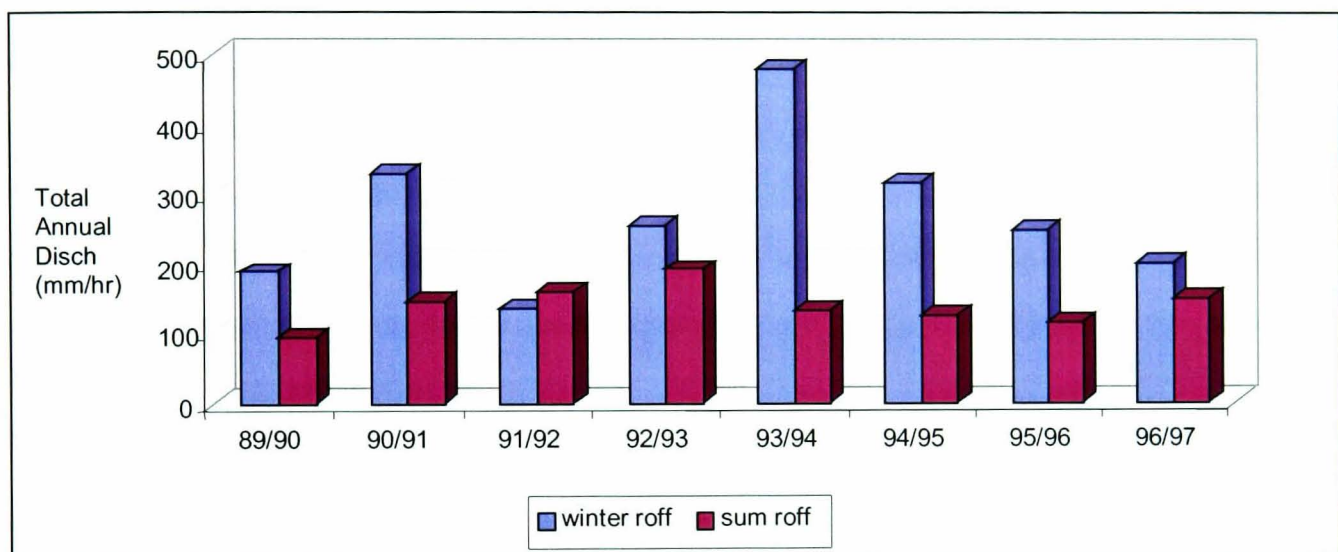


Fig. 3.19 Total annual discharge for Kirkby Mills.

The Lowna Bridge and Kirkby Mills gauging stations are at the upstream and downstream extremes of the Corallian limestone respectively. Comparison of the discharge at these two stations therefore allows an assessment of the possible loss of runoff over the Corallian Limestone. Figure 3.17 is a plot of discharges (in cumecs) at the two sites and the difference between the two. It shows that, during winter, discharge at Lowna Bridge exceeds that at Kirkby Mills close to the discharge peaks. Closer examination of this trend revealed that this occurs just as the hydrograph begins to rise for each event. This is because Lowna attains peak flow before Kirkby Mills, and at these times there appears to be an inversion of flow or a loss of water. However the fact that total discharge at Kirkby Mills is always greater than at Lowna Bridge indicates that there is negligible loss to groundwater over the limestone.

As mentioned above, the occurrence of storms of comparable magnitude and duration during winter and summer allows for an assessment of the effects of antecedent soil moisture conditions on runoff generation. Fig 3.20 is an analysis of runoff generated for events of the same magnitude occurring in January, February and May. The January event is a 3-hour rainfall event with a peak value of 0.006m and total rainfall of 0.0023m. This resulted in a well-defined hydrograph, with 14.1mmhr^{-1} and 11.3mmhr^{-1} of runoff recorded at Lowna Bridge and Kirkby Mills respectively, and elevated flows lasting approximately 2hours. The February event is also 3hours, with a peak of 0.006m and total rainfall of 0.0015m, and resulted in 13.4mmhr^{-1} and 11.5mmhr^{-1} at Lowna Bridge and Kirkby Mills respectively, with elevated flows lasting for 2days. The May event was a 4hour event with a peak of 0.0056m and total rainfall of 0.0026m. This event resulted in 4.94mmhr^{-1} and 3.96mmhr^{-1} of runoff at Lowna Bridge and Kirkby Mills respectively, with elevated flows lasting for 4 days. These results reflect the effect of antecedent soil moisture conditions on runoff depths and duration. During winter when the soil moisture content is high, high intensity events result in quick, sharp peaks. An event of the same magnitude occurring in summer results in lower, less sharp peaks over a longer period of time, as much of the rainfall goes into replenishing depleted soil moisture leaving little for runoff. Any hydrological model must be able to account for differences in response due to varying antecedent soil moisture content.

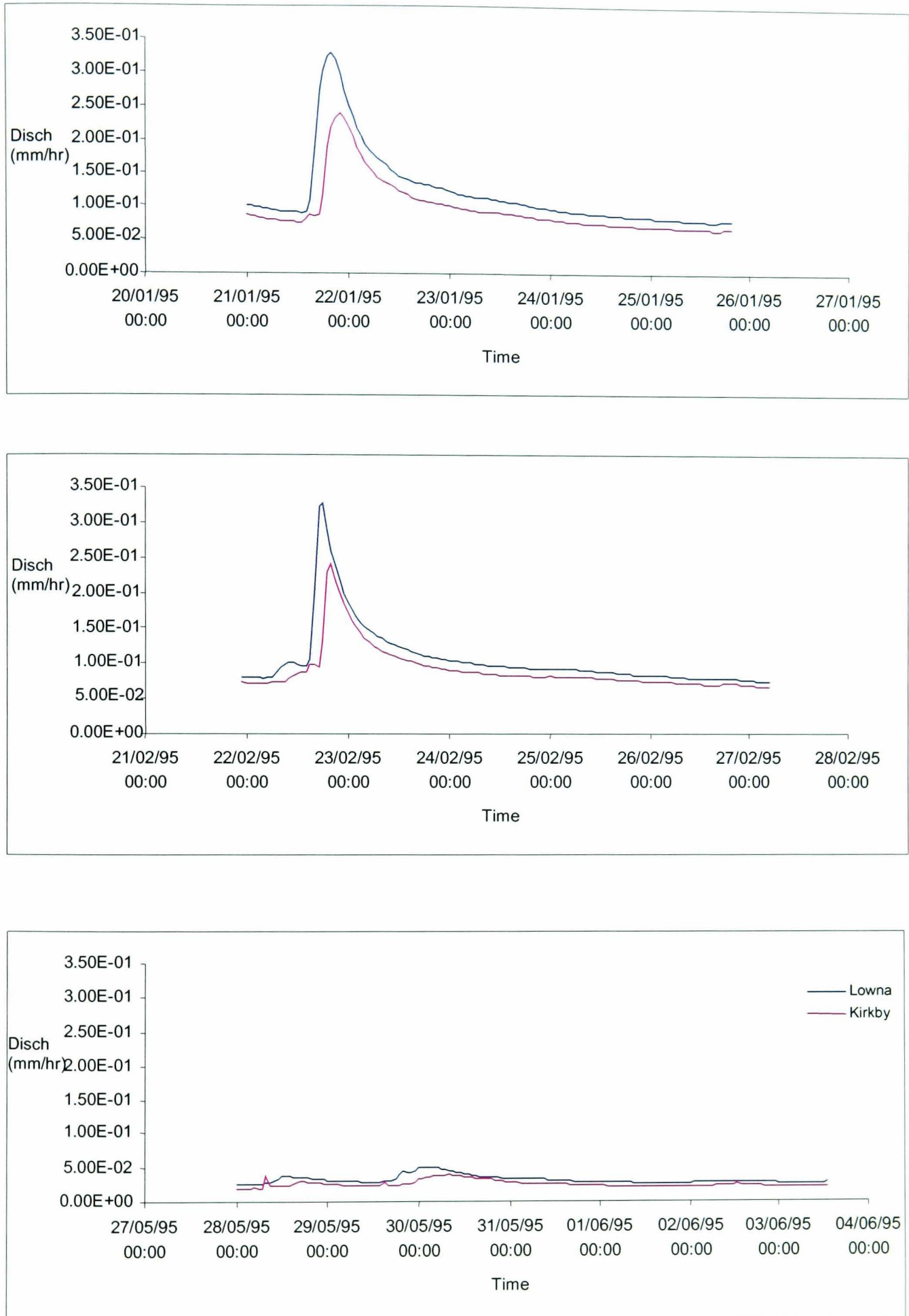


Fig. 3.20 Hydrographs for January, February and May 1995.

3.6.3 Evaporation

Monthly MORECS potential evaporation data (Thompson *et. al.*, 1981) for the catchment was obtained from the EA (sourced from the UK Meteorological Office). MORECS provides site-average annual evaporation estimates for major land cover types, major soil types and soil moisture conditions. Values are based on the Penman-Monteith model (Penman, 1948; Monteith, 1965) with aerodynamic data from the nearest local synoptic stations.

Daily potential evaporation was calculated as follows. The monthly mean PE was calculated and assigned to the middle day of each month. The PE for each day was then calculated by linear regression between the median monthly values. Hourly PE was then calculated by distributing the daily total around a mid-day maximum between 06:00 and 18:00 hours, based on a sine distribution. Fig. 3.21 shows the resulting distribution for 1994/95.

This strongly seasonal distribution of evapotranspiration is responsible for the strong seasonality in hydrological response. Figures 3.15 and 3.16 show that discharge is lowest during summer when evapotranspiration is highest, and highest in winter when evapotranspiration is lowest.

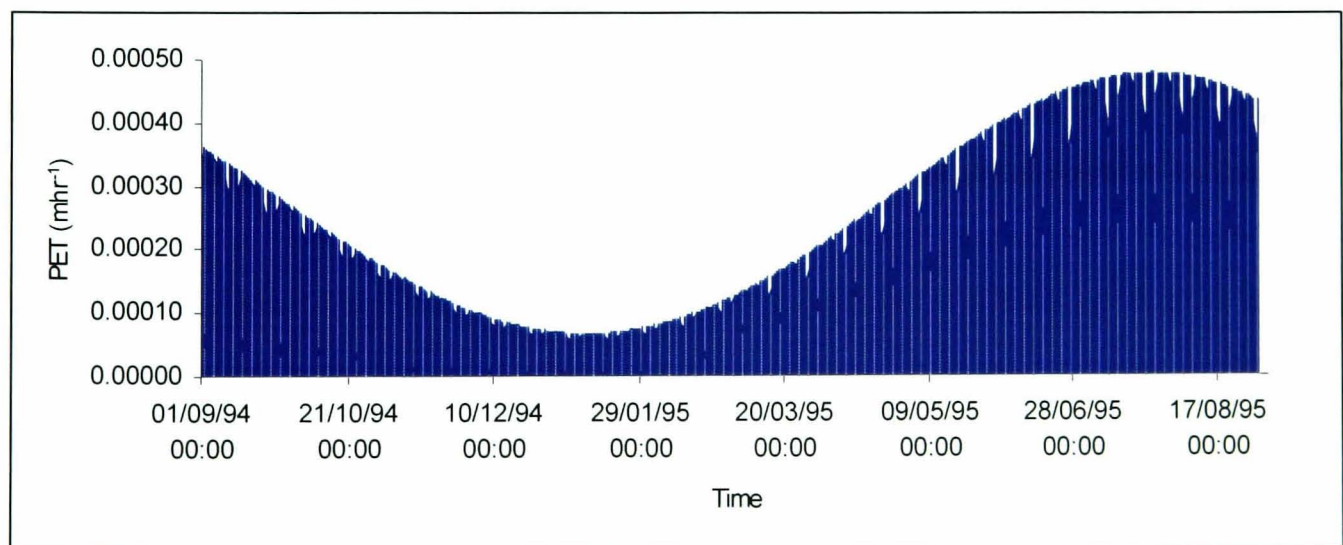


Fig. 3.21 Hourly evapotranspiration for Farndale catchment.

3.7 Catchment Turbidity and Suspended Sediment

3.7.1 Regional sediment production

Imeson (1970) investigated sediment production under the major land uses in Bransdale catchment. Given the similarities in geology, soil type and landuse of the two catchments, his findings are relevant to Farndale catchment. This discussion is based mainly on his findings.

Erosion under Heather

The main factors which influence erosion of soil under heather can be summarised as:

1. Stage of plant growth
2. Amount of cover
3. Height of heather
4. Soil conditions

All of which are interrelated. Imeson (1970) found no correlation between soil loss and slope, and no significant difference between soil loss in the summer and the winter. He said that winter and summer losses are possibly similar because wind erosion is important in the summer when the surface is dry.

He, however, found significant correlation between heather height and soil loss. Under fully developed heather i.e. complete cover of 30-40cm high heather, the upper soil is composed of decaying heather litter, spongy and fibrous at the surface and increasing in density with depth until, depending on local conditions, at 20-40cm, a horizon of consolidated peat nodules, 5-10cm in diameter, is often reached. Fairly dense nodules or agglomerations, often coated with sand grains, are thought to represent a horizon of water movement beneath the surface. Gullies in these areas, when over-grown with fully-developed heather seldom, if ever, transmit running water.

Heather when burnt completely would result in subsequent erosion to form a landscape of sandy wastes and peat pedestals. Less severe burning results in a fairly rapid re-growth of heather. Severe erosion may follow burning, however, and this results in complete failure of heather or various stages of re-colonisation. The nature of the soil and heather cover reflect the recent history of heather burning, and the

intensity of subsequent erosion. Hence heather burning and erosion influence the rate of soil erosion and the type of material being removed.

Imeson (1970) found that there was net local accumulation of sediment under a fully developed heather cover, with a maximum rate of accumulation of 5.04 mm per year. Fully developed heather intercepts and protects the soil from rain, wind and frost, minimising erosion. In addition, the fibrous spongy soil favours infiltration, which is aided by stem-flow from the heather. He concluded, however, that although the accumulation rates observed were high, the litter is capable of a large amount of compaction, and hence a long period of measurement might record a lower rate of accumulation as the litter decomposed and settled.

Less thick heather, or heather re-colonising burnt land, contained less litter and many patches of bare ground, where burning and erosion occurred recently, and showed lower rates of accumulation. Imeson (1970) reported net sediment accumulation under less thick heather at a rate of 0.75mm per year, between August and April, and some loss between April and August.

The greatest losses were found to occur at the other end of the spectrum of heather re-growth and colonisation. That is, under most recently burnt heather, where the heather was under 15cm high and formed an incomplete cover protecting about 10-20% of the ground surface, the greatest loss was recorded where the heather was thinnest on the ground. Although the erosion rate was high (9.68 mm per year), the eroded material was found to be made up of fibrous, loosely packed heather remains and, to a lesser extent, of peat aggregates about 0.5mm in diameter both of which have low density. The next highest rate of erosion was from heather 5-7cm high and covering 20-75% of the ground surface. Imeson (1970) found that the larger amount of cover accounted for the lower rate of loss, since more litter is supplied to the ground to compensate for decomposition and since greater protection is afforded from erosion.

Hence the loss or accumulation of material beneath heather in Bransdale was found to be variable and related to the amount of cover under 'fully developed' heather, which offers good protection against erosion. Where the heather cover is incomplete,

accumulation is less, so that when the cover is 50-80%, accumulation gives way to erosion.

Bracken

Bracken occupies most of the steep slopes on the Upper Lias, and forms a thick canopy of fronds protecting the ground surface. However, in winter, dead and decaying plants leave the surface exposed. Beneath the bracken canopy, is a spongy, humic soil built up from successive annual accumulations of litter. Soil loss and accumulation under bracken reflect the annual cycle of bracken growth and decay. Imeson (1970) reports seasonal variation in soil loss and accumulation, with an average accumulation depth of 8.2mm in winter when the ground was partially exposed, while beneath the canopy of bracken fronds, in summer, when no litter was added to the surface, an average loss of 3.8 mm occurred. Thus, it appears that the breakdown of litter takes place more rapidly in the winter than in the summer, probably because the effective precipitation is higher (Imeson, 1970). However, because freshly accumulating litter is less dense than that being removed or compacted, the combined effect of litter accumulated and decayed over a year, was to raise the litter surface by an average of 3.7mm. Imeson (1970) found that while the density of bracken growth is an important factor, the height of the bracken and the slope of the ground do not correlate with surface change. The importance of bracken density suggests, therefore, that the rate of decomposition and solution of litter is fairly constant, no matter what the cover.

Hence it appears that bracken covered areas supply relatively little sediment to the catchment rivers, even where the bracken cover has been partly destroyed. The material lost from bracken litter during decomposition and compaction probably reaches the rivers in solution rather than in suspension.

Woodland

Woodland is interspersed with bracken on the steep slopes. Imeson (1970) found that under bracken growing under woodland canopy, sediment accumulates at a rate of 6.2mm per year, slightly higher than the rate of accumulation under bracken growing on its own. Where the ground cover is thick, even on steep slopes, the accumulation of material takes place and surface erosion is minimal. Conversely, on uncovered

ground, particularly on steep slopes and near to the trunks of trees, surface erosion is locally important.

The woodland in Farndale occupies steep slopes, which are subject to landsliding. This is especially so where the Alum Shale outcrops along the river bank. Whether landslides are associated with the undercutting of slopes, or with the steadily increasing thickness of weathered soil and litter beneath the woodland cover is not known.

Grass

Grass in the moorland comprises mainly common rush (*J. conglomeratus*), heath rush (*J. squarrosus*), *Nardus stricta* and low unidentified and grazed broad-leaved grass. Imeson (1970) found that surface change varied between a loss of 2 mm per year, to an accumulation of 1.5 mm per year. Some losses, occurred in peaty soil where the grass is fine, and forms only a little cover. However, the loss recorded beneath *Nardus* is either due to movement caused by plant growth or, less likely, to the breakdown of subsurface peat (Imeson, 1970).

Gully erosion

Most of the heather moorland is criss-crossed by shallow intermittent channels ranging in depth from 10 – 20 cm to 3 –4 m. These gullies cut across areas of different vegetation and because they are minor, erosive forms which are sensitive to anthropogenic activities, they warrant a separate discussion. Imeson (1970) summarised the general properties of moorland hydrology and gully formation as follows:

1. In some places, particularly where the heather cover is fully-developed, gullies are overgrown and intermittent, while elsewhere, particularly downslope of heavily eroded burnt ground, gullies may be very active. The overgrown gullies in areas of thick heather are shallow and only rarely carry water.
2. Most gullies have a humic topsoil which overhangs a sandy subsoil. Frequently the gully bed or low gully sides are composed of clay, in which case, the gully is wide with relatively gentle slopes, which is not what might be expected if running water was the main agent of gully enlargement (Schumm, 1960).

3. Bands of clay in the Deltaic series are important in preventing the downward movement of water which consequently moves laterally in sandy soil horizons higher in the profile.
4. Where peat directly overlies clay, water may flow underground.

Imeson (1970) suggested that the development of the gully features on the moorland area almost certainly occurs in response to hydrological changes caused by burning. The erosion that occurs in response to burning, depends upon constraints imposed by slope variability, soil characteristics and topographic details inherited from the former heather cover. Destruction of the forest soil as a result of repeated burning and grazing during the initial colonisation of the moorland by heather would have resulted in extensive and widespread gully erosion.

The hydrology of the ‘fully developed’ heather moorland, as described above, is such that interception and evaporation are high. The soil is seldom exposed to rain, frost or wind, and surface runoff and gulying are minimal due to rapid infiltration into the thick fibrous peaty litter. Hence, water entering the soil will remain in the peaty surface material if the subsoil is clay, or alternatively, pass through the peat if unconsolidated sand deposits lie below. If there are overgrown gully features and the water-table in the heather soil is high enough, water will move laterally into these channels where it will either collect or move slowly downslope, according to the degree of gully infilling (Imeson, 1970). Water trapped in the peat by a clay boundary below will move slowly downslope in the peat, probably along horizons of peat agglomerations and voids. If sand underlies the peat, infiltration will continue downwards until impermeable clay horizons are reached, before moving downslope. Due to the deltaic origin of the underlying rocks, sand and clay subsoils occur in close proximity. Thus water will move frequently between the peat and sand deposits wherever those are resting on clay.

The downslope movement of water in the peat and sand might be concentrated in places by minor topographic irregularities and by former gullies. The concentration of subsurface drainage is suggested by the peat agglomeration horizon and by the observed rapid movement of water from thin bands of sand, after heavy rainfall, into drainage ditches (Imeson, 1970). Eventually, at the boundary of the fully developed

heather, or where a clay subsoil narrows the depth of water movement, seepage bogs and seepage faces might be located.

Where the heather cover has been burnt, the hydrological conditions will be greatly modified, and favourable conditions will be established for the development of seepage faces and gullies. Lower interception and transpiration, causes an increase in the amount and rate of infiltration, unless of course, the fibrous peaty soil surface has been burnt away. In addition, as infiltration increases, the thickness of the surface layer of peat is reduced. If burning has been very severe and the less permeable lower horizons of peat exposed to erosion, intense rain, frost and wind will speed this reduction. Increased infiltration rates and amounts will concentrate the throughflow of water into shorter, more intense periods. Where this throughflow passes from a peaty soil resting on sand to a peat soil resting on clay, a perched water table may develop. Gradually peat and then peat and sand, above clay, will be removed and a seepage face develops. If the throughflow is concentrated, gully-head features might be expected to form. Such gully-heads and seepage faces will enlarge and retreat, and water draining from them will wash over an increasing area of exposed clay downslope. Water on this exposed clay will be concentrated into small channels, which will be extended when the water flows to sand or peat deposits downslope.

One implication of the association of gully formation with hydrological processes is that gullies, although they produce a considerable amount of sediment, are transient features depending on anthropogenic activity for their continued importance.

3.7.2 Suspended Sediment Monitoring in Farndale Catchment

The greatest source of error in the estimation of catchment sediment yield is the inability to continuously monitor suspended sediment concentration. Water sampling at unrealistically high frequencies would be required to accurately characterise temporal trends in basin sediment yield. To partially overcome this issue of temporal lumping, *in situ* optical turbidimeters can be used along with concurrent discharge data to estimate suspended sediment concentration. Turbidimeters measure turbidity as a function of the attenuation or scattering of an incident beam of radiation between a source and a receiving optical surface (Gippel, 1989, 1995). Given flow data and a turbidity-SSC rating relationship, accurate estimates of SS yield can be obtained. However, the relationship between turbidity and suspended sediment concentration is complicated by variations in particle size, particle mineralogy and water colour. Infra-red attenuation meters (Gippel 1989) have been developed to limit some of these complications and have been used in this study.

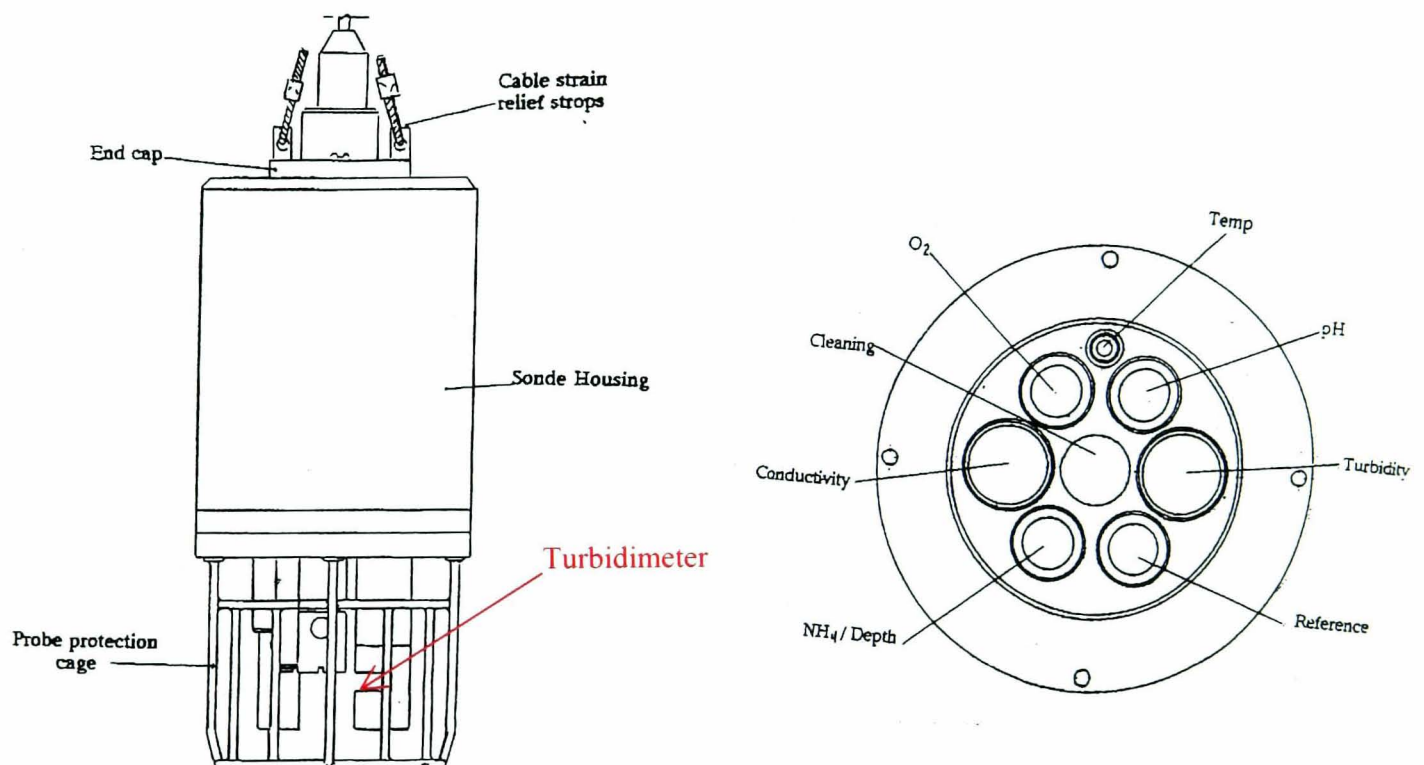


Fig. 3.22 ELE multi-meter containing IR turbidimeter.



Fig. 3.23 Arrow showing the location of the ELE probe. Looking upstream from Kirkby Mills weir.

Two different types of IR turbidimeters were deployed at Kirkby Mills gauging station just upstream of the weir along a stable stretch of the river. The first is an ELE 200 series turbidimeter with a dynamic range of 0 – 500 NTUs (Fig. 3.22). This probe operates on an Infra Red absorption technique with compensation for ambient light temperature. It was deployed approximately 8m upstream of the weir, midway between the banks, and approximately mid flow (Fig. 3.23). The probe was calibrated in the laboratory with Formazine solution for the high calibration (500 NTUs) and clean turbid-free water for low calibration (0 NTUs). Resolution is a function of the optical system, and is 1 NTU. Turbidity in NTUs is recorded at 15-minute intervals and logged on a data logger. Prior to taking the reading, the probe is automatically cleaned ensuring that the optical surfaces are free of particles. However, readings can be affected by air bubbles on the optical surfaces which build up when temperature rises, and cleaning does not reduce this effect.

The second are two Partechs, which generate a 0 –5 mA signal, and are attached to the side wall of the weir. These probes were initially calibrated in the laboratory using sediment from the catchment, and allows for full scale deflections of 3g/l. SSC (in mg/l) is logged every 15 minutes as the average of 10 second readings taken two minutes preceding the sampling time.

Probe Calibration

The turbidity – SSC relationship was determined in two ways. Laboratory calibrations using known concentration of sediment from the catchment, and dip sampling concurrent with turbidimeter readings. Laboratory calibration was done, by making up known concentrations of suspended sediment, and determining the rating relationship for known increments of suspended sediment. Soil samples taken from the bank close to the outlet, were first wet sieved, separated into three different fractions, $< 63\mu\text{m}$, $63 - 150\mu\text{m}$ and $> 150\mu\text{m}$, and heated in an oven at 130°C to remove organic matter. Particles were kept in suspension using a motorised mixer. It was found that particles $> 63\mu\text{m}$ were not kept in suspension sufficiently long to obtain effective readings. This is due to the fact that a simple laboratory mixer cannot simulate the magnitude of turbidity that would bring larger particles into suspension. Fig. 3.24a and b show the probe calibration results for the ELE and Partech probes respectively. The ELE probe was found to have a 1:1 relationship with suspended sediment concentration. The accuracy of these readings are limited by the 1 NTU increments of measurement, that this probe allows. Both Partech probes were found to follow a typical S-curve relationship with sediment concentration, although Partech 2 shows several spurious readings. This rating curve was used to program the logger so that readings were taken in mg/l, whereas the ELE probe data had to be processed after collection.

Dip sampling was done, by taking water samples concurrently with data logging, which were analysed in the lab, using millipore infiltration experiments. Instantaneous, depth-integrated samples were taken close to the probes using a 500ml bottle on a long pole. Samples were taken at least on every visit (every three weeks), and more frequently during events. Field calibration of this kind is necessary in order to characterise the variability in probe response, which may arise due to variations in sediment source areas with time of the event, size of the event, and type of flow. The use of concurrent depth-integrated samples, and time-averaged logged turbidity, however, may also result in inaccuracies in the rating curve derive by this method. Values obtained by this method were used to cross-check the probe readings.

Parameter measured (units)	Location	Probe	Measurement timestep	Monitoring period
Turbidity (NTUs)	Outlet (467000,497600)	ELE 200series turbidimeter	Every 15 minutes	10/98 to 03/99
SSC (mg/l)	Outlet (467000, 497600)	Partech	Every 15 minutes	02/99 – 04/99 and
Infiltration Rates (mm/hr)	Throughout catchment	Ring Infiltrometer		

Table 3.3 Summary of monitoring programme.

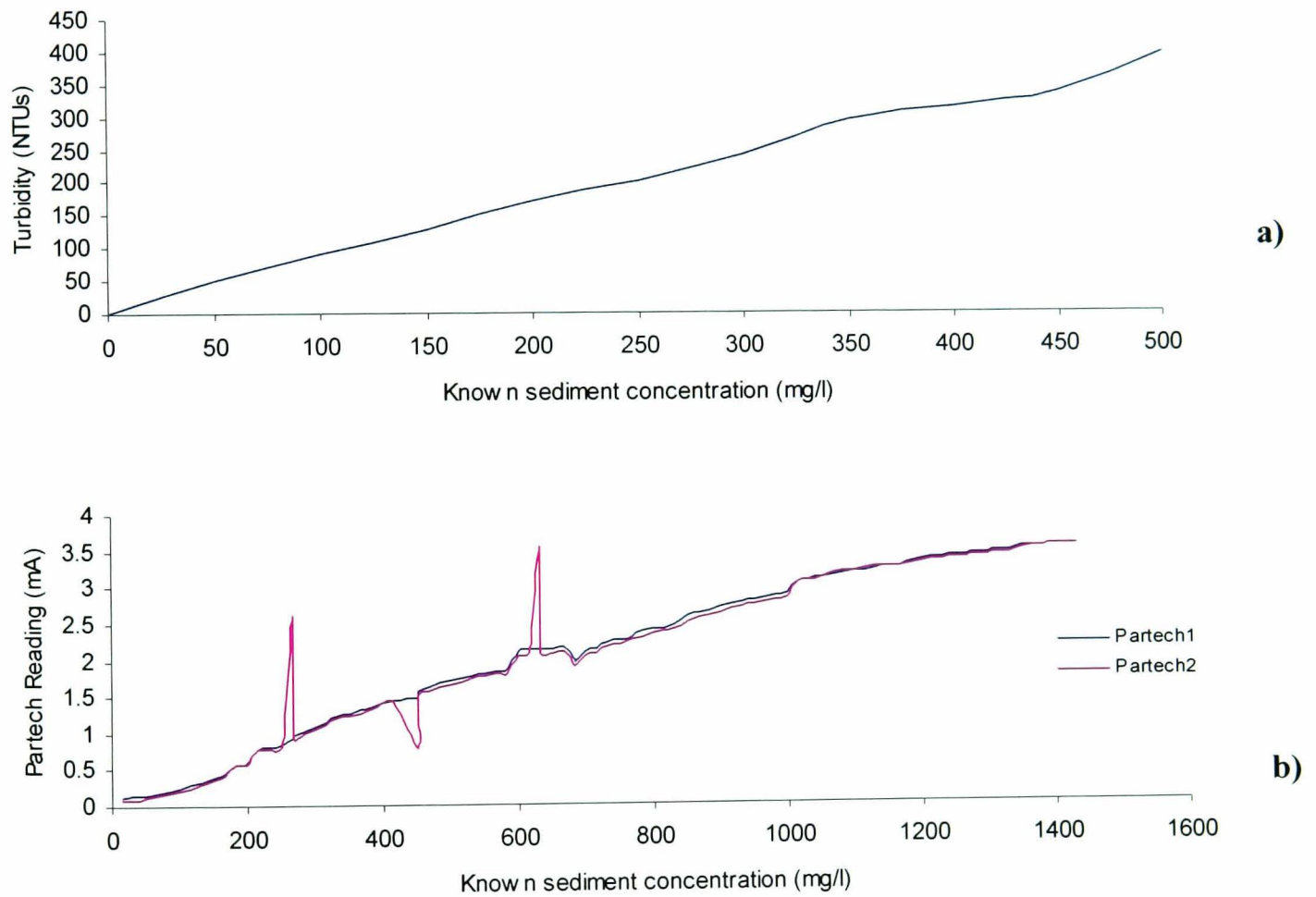


Fig. 3.24 a) Turbidity-sediment concentration rating curve for the ELE probe.

b) Current-sediment concentration rating curve for the Partech probes.

3.8 Study Period Rainfall and Sediment Flux Analysis

3.8.1 Study Period rainfall

The calibration and validation events used in this study are taken from the period October 1998 to March 1999 (Fig. 3.25). An analysis of the rainfall for this period is presented here.

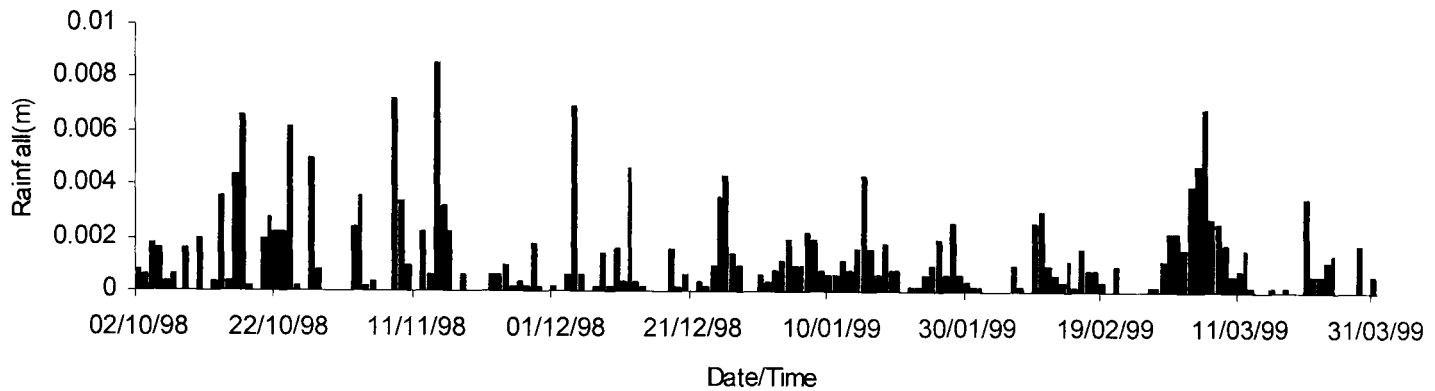


Fig. 3.25 Rainfall for October 1998 to March 1999.

Fig. 3.26 shows the temporal variation in duration, peak intensity and mean intensity, as well as the mean intensity and rainfall depth plotted against storm duration. The temporal distribution of storm duration shows that most events are less than 20 hours in duration, except one, which occurred on the 04/03/99 and was 92 hours in duration. Peak intensities are highest in mid-November and lowest in February. A peak intensity of 0.007mhr^{-1} corresponds to the 92-hour event. The mean intensity is highest in November. The 92-hour event has a relatively low mean intensity mainly because of the long duration over which the total rainfall is averaged. The maximum storm depth for all other events is 0.03m, but a total depth of 0.19m is obtained for the 92-hour event. That is, six times greater than what would be expected for this time of year.

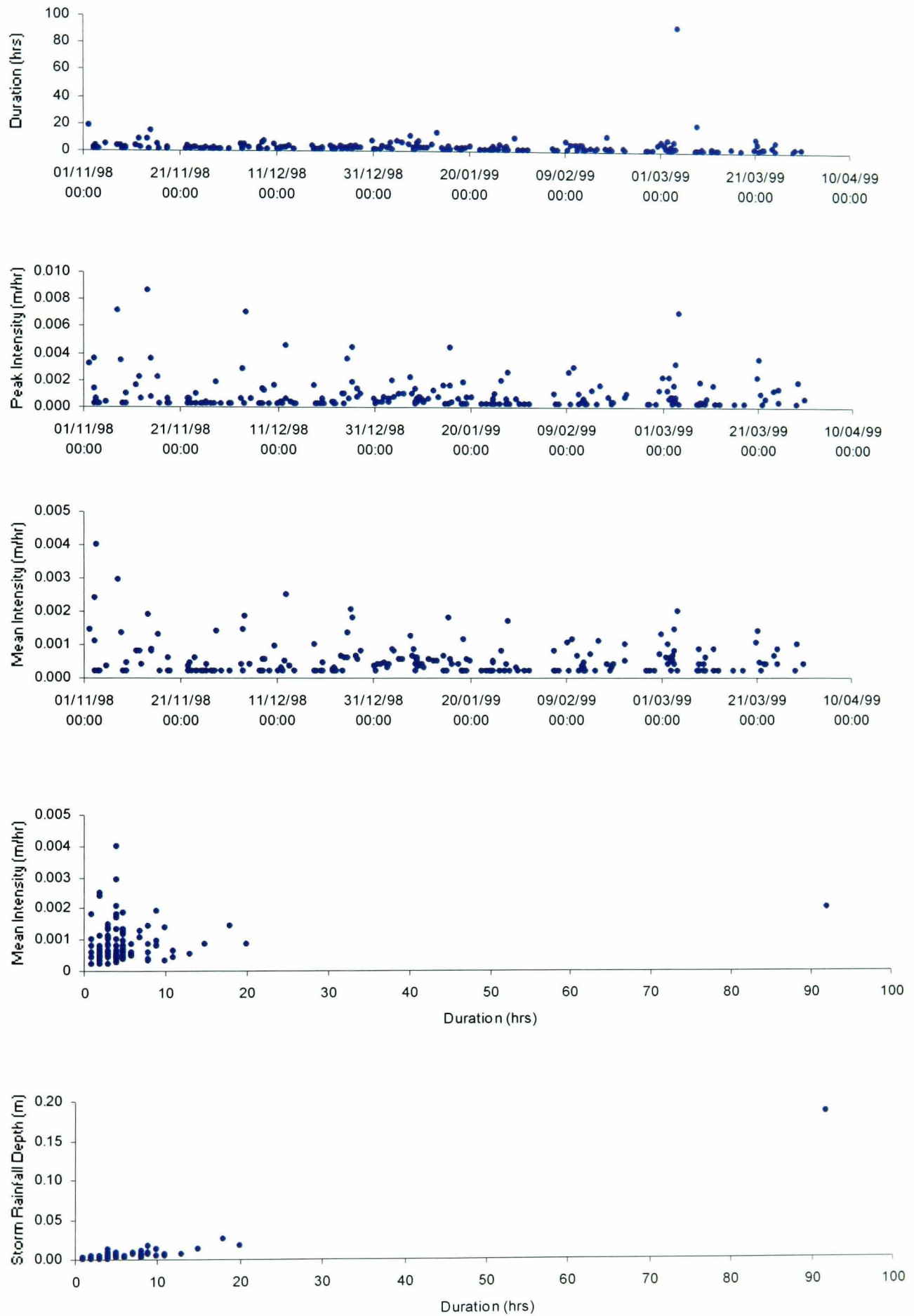


Fig. 3.26 Rainfall event analysis for October 1998 to March 1999.

3.8.2 Study Period Turbidity data

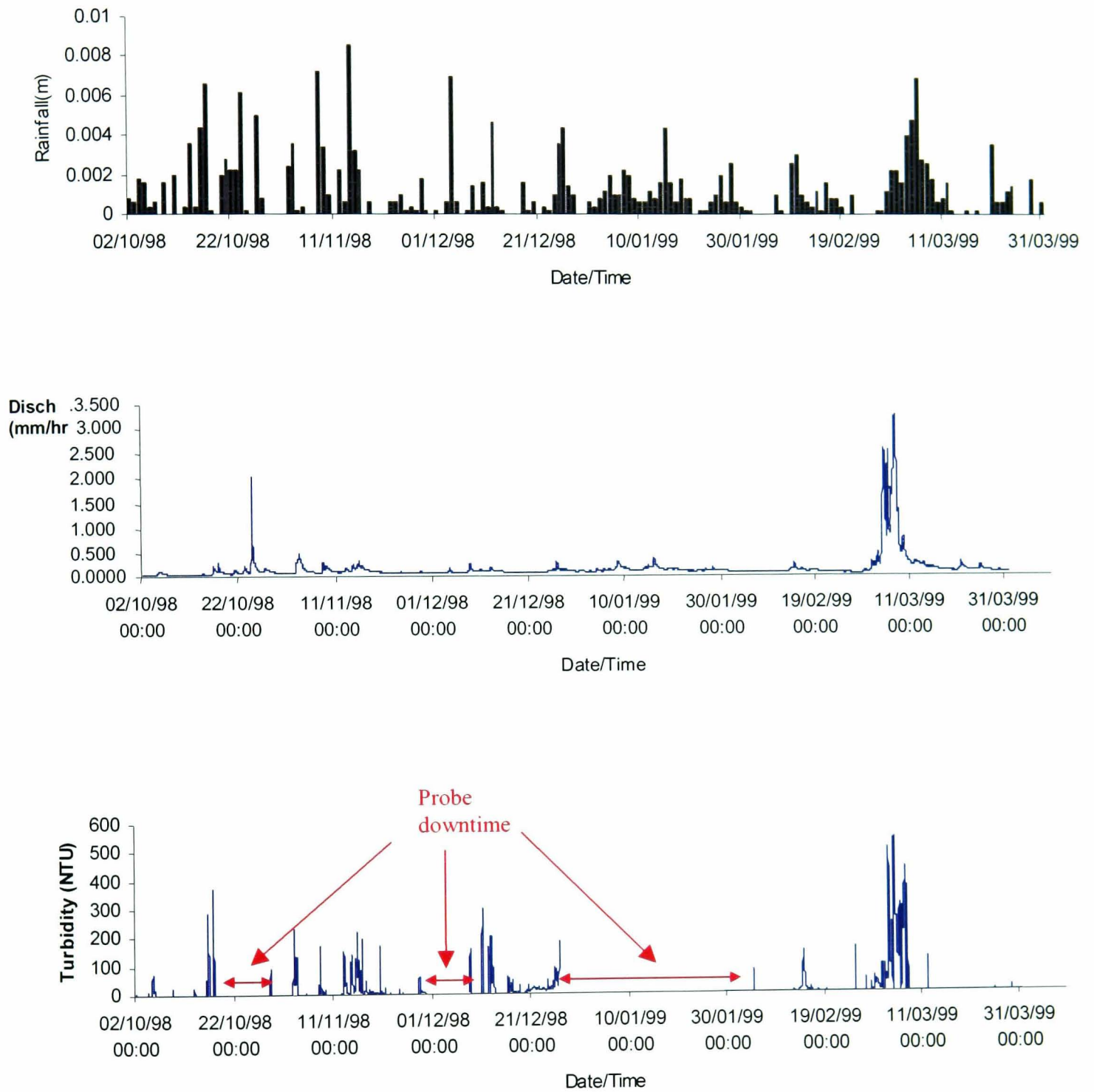


Fig. 3.27 Time-series of rainfall, discharge and turbidity data for October 1998 to March 1999.

Fig. 3.27 shows the time-series of rainfall, discharge and turbidity data for October 1998 to March 1999 for the ELE probe. The arrows indicate missing data corresponding to probe down-time. After particularly large events in late December – and January, the probes exceeded their dynamic ranges and had to be re-calibrated.

The plot is dominated by the large double-peaked event in late February – early March when a 1 in 50 year flood event occurred in Farndale. This extreme flooding was caused by a combination of prolonged high intensity rainfall and rapidly melting snow. The discharge peaked at four times its normal maximum. This event is dealt with in more detail in the event analysis that follows.

The suspended sediment concentration/Discharge Relationship

The suspended sediment concentration/discharge relationship or rating curve for a drainage basin reflects the overall pattern of erosion and sediment delivery operating in the upstream area and provides a useful and readily accessible starting point for isolating and interpreting salient features of basin sediment response (Walling and Webb, 1982). The following features are found to provide the most information about sediment accumulation and transport:

1. Seasonality of the quantity and quality of SSC, provides information about the dominant processes from one season to the next, and the dominant source areas.
2. Hysteresis or exhaustion effects operating during individual events, and during a sequence of events, gives an indication of the temporal and spatial controls on sediment availability.

The considerable degree of scatter observed in the SSC/discharge plot (fig.3.28) is associated with, the variable phasing of discharge and SSC waves which leads to hysteretic, and exhaustion effects. The poor correlation is also due to the fact that the data is for the wet period of 1998 (November 1998 to March 1999), since no summer data are available. Hence a proper assessment of the seasonality of the relationship is not possible. Another source of scatter in the rating curve is the variation in the spatio-temporal rate of sediment supply, which results from the underlying assumption inherent in the rating curve method, that the system is transport limited. Such behaviour, may be expected to be more significant over short spatio-temporal scales and may be regularised with increasing scale (Brasington, 1997).

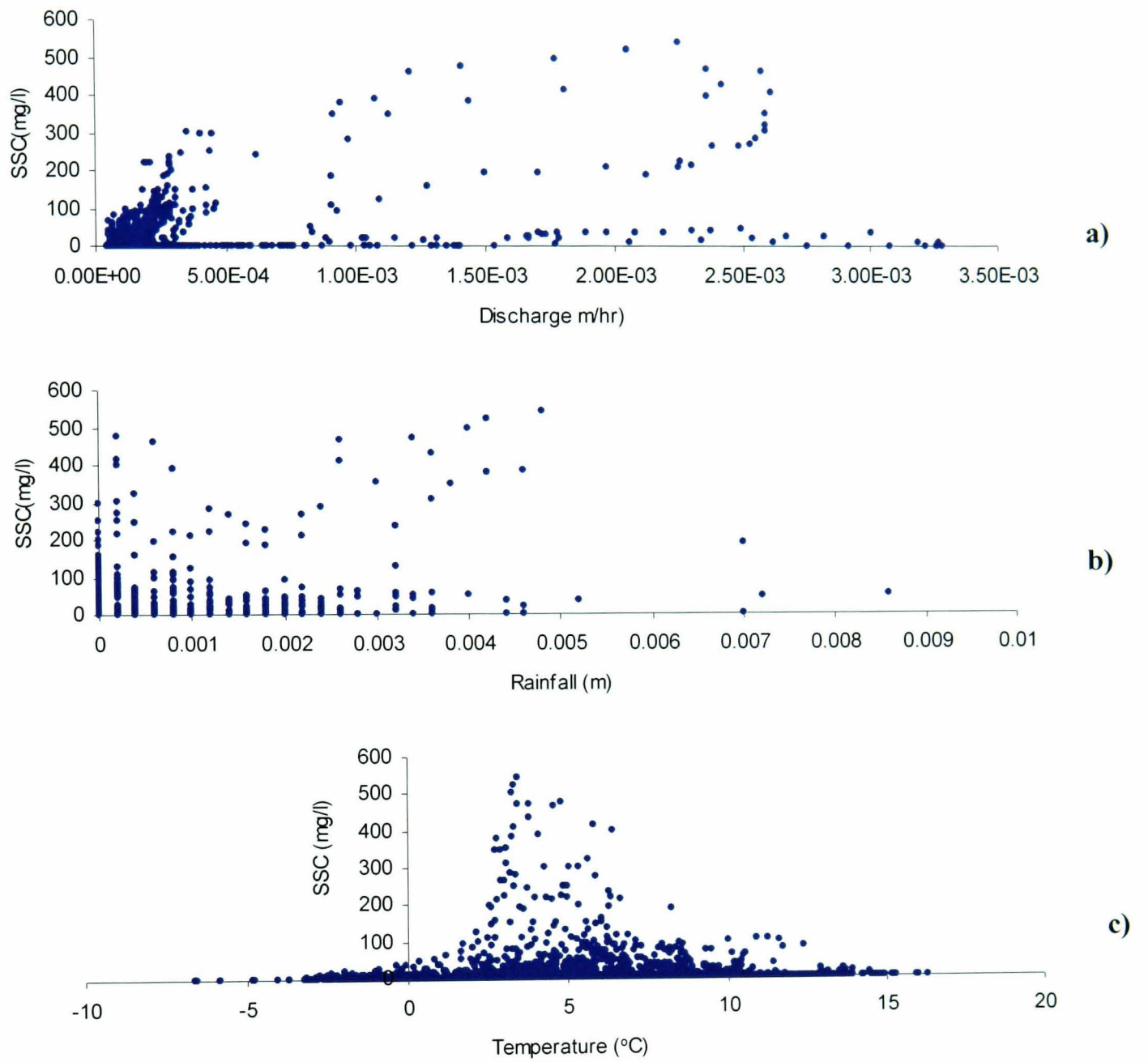


Fig. 3.28 Scatterplots of Suspended Sediment Concentration versus a) discharge b) rainfall c) temperature

A rather poor correlation is obtained for the SSC/rainfall relationship (Fig. 3.28b). Imeson (1970), working in the neighbouring Bransdale catchment, found that only the rainfall during the 24-hour period before sampling is important, reflecting the greater speed of runoff from the catchment. He reports a poor correlation between rainfall intensity and duration indices and sediment concentration, which he attributed to the fact that the rainfall data used was from the Farndale Vicarage in Farndale catchment, which was not representative of rainfall in Bransdale. His findings imply that antecedent rainfall, and hence moisture content, are more important than intensity and duration of rainfall. This is in keeping with the variable source area concept, whereby runoff is produced from areas that are already wet or nearly so at the start of an event. Since sediment is carried by runoff, then the amount of sediment produced depends on the area producing runoff. This is also in keeping with the Moore and Clarke (1983, 1984) approach to sediment availability, based on the inter-storm period.

However, there must be a trade-off between sediment accumulation during the inter-storm period and the cells actually producing runoff (and hence sediment) as the duration of the inter-storm period increases. That is, the longer the inter-storm period, the more sediment is accumulated as the catchment dries up. However, when precipitation occurs, there would be fewer cells with the requisite moisture content to produce runoff (and hence sediment). Hence, the longer the inter-storm period, the longer the rainfall duration required to allow as many cells as possible to 'fill up' to produce runoff and mobilise sediment. Hence the poor correlation with rainfall intensity and duration found here for Farndale catchment, suggests that the rainfall data for Church Houses located in the catchment may not be representative of the entire catchment. The dependence of the correlation between the intensity and duration and SSC on the length of the inter-storm period is indicative of the inter-dependence of hydrometeorological parameters, which makes it difficult to determine and isolate the important parameters.

The poor correlation between temperature and sediment concentration (Fig. 3.28c), is due to the fact the all of the data is for a wet period, and suggests that intra-seasonal variations in sediment concentration are masked by variations due to other more important factors.

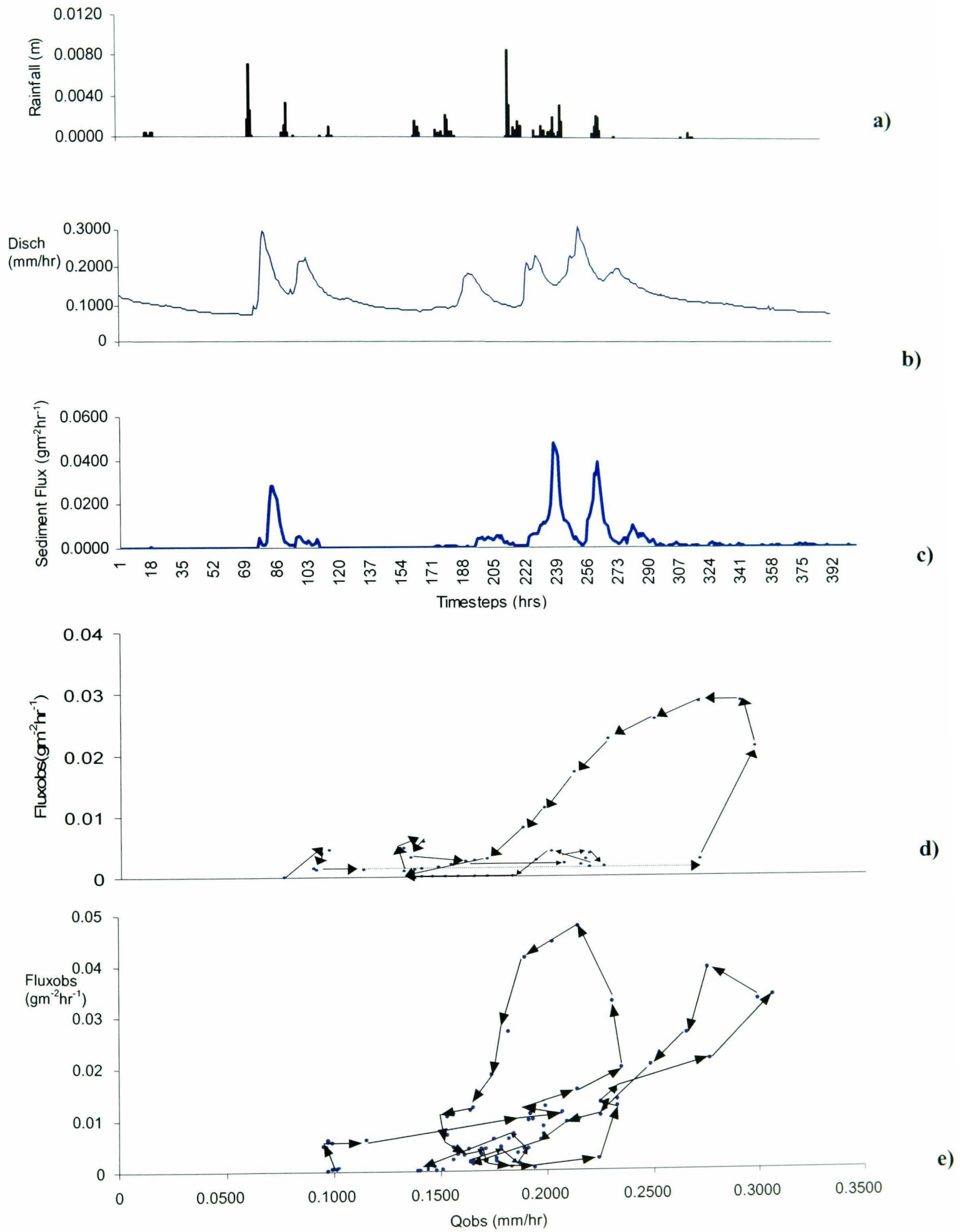


Fig. 3.29 Sediment flux-discharge relationship for different peaks in one event.

Fig. 3.29d and e are the sediment concentration – discharge for different peaks for an event on 04/11/98 to 21/11/98. For the first peak (Fig. 3.29d), as discharge increases on the rising limb, sediment flux does not rise significantly. This is probably because the initial flow is from the more frequently saturated riparian areas immediately adjacent to the channel, which would not contribute significantly to sediment input due to their lower rates of sediment accumulation than hillslope areas. In addition, it could be attributable to sediment sources being located in the distal regions of the catchment. As flow continues to increase, however, channel-hillslope coupling occurs and sediment derived from the hillslopes, carried by overland flow reaches the channel, and subsequently the outlet. On the falling limb, sediment flux is higher than on the rising limb because, even though flow is decreasing, sediment derived from further upslope is delivered to the outlet, at a delayed rate.

For the double peaks (Fig. 3.29e) both hysteresis and exhaustion are observed. As flow increases on the first rising limb, sediment begins to increase slowly at first, then more rapidly. The maximum sediment flux occurs just as flow begins to fall. Again, sediment flux is greater on the falling limb. Sediment flux increases more slowly on the second rising limb of the double peak, and although a higher maximum discharge is obtained for this peak, the maximum sediment flux is lower than that of the first peak. This indicates a decrease in sediment availability due to exhaustion during the first peak, and an insufficient replenishment period.

3.9 Conclusion

The chapter described the physical characteristics of the study catchment in terms of its geology, soil type and land use. There is large spatial variability in catchment soil type and land use, both of which will exert some control on local, and catchment hydrological and sedimentological response. Land uses are such that topographical controls might be reinforced given the location of decreasingly permeable land uses from the hillslopes towards the valley floor. The configuration, however, opens up the possibility for run-on processes where land uses of higher permeability are located downslope of land uses with lower permeability, and return flow, where the opposite is true. Soil type variability is more pronounced, and may actually obscure topographical controls on catchment response. In addition, the location of heather,

which can be a major source of sediment at certain stages of its development, on peaty soils in the headwaters of the catchment, where there is extensive gully erosion, suggests that the controls of land use and soil type on catchment hydrological and sedimentological response may be interdependent and mutually reinforcing.

The chapter also described and analysed catchment hydrometeorological and sedimentological characteristics, and discussed the monitoring programme implemented during the period of this research. Catchment hydrometeorology is characterised by seasonal rainfall, runoff and evapotranspiration. Suspended sediment yield exhibits inter- and intra-storm variability, indicating a strong dependence on sediment availability and runoff generation. The following chapter describes the coupled hydrological-sediment yield model, and the analysis methodology employed.

CHAPTER 4 – Model Description

4.0 Summary

This chapter describes the coupled hydrological-sediment yield model developed as the basis of the thesis, and the methods of analysis. The hydrological model presented here is a fully-distributed terrain-based model, based on TOPMODEL (Beven and Kirkby, 1979) concepts, which represents water fluxes on a cell-by-cell basis using a regular grid discretisation of the catchment. It is directly coupled to a conceptual sediment yield model similar to that developed by Moore and Clarke (1983, 1984), which represents catchment sediment yield as a sediment availability- and transport-limited process. The methods of model calibration, validation and uncertainty estimation, based on the Generalised Likelihood Uncertainty Estimation (GLUE) (Beven and Binley 1992) and Bayesian Updating techniques, are discussed.

4.1 The Hydrological Model

The hydrological model developed and employed here differs from TOPMODEL in a number of significant respects. Firstly, rather than the distributed function approach of TOPMODEL, water fluxes are modelled on a cell-by-cell basis using a regular grid discretisation of the catchment. This approach relaxes the steady-state assumption of TOPMODEL, and allows for dynamic variation in the upslope contributing area, heterogeneous recharge rates and spatially non-uniform rainfall. These developments were reported by Brasington (1997). In addition, to reflect local hydrological processes, a simple, but spatially-distributed snowmelt model has been developed to account for the seasonal melt contributions to runoff.

As stated in section 2.10.1, the fundamental assumptions underlying the derivation of topographic index of hydrological similarity used in TOPMODEL are:

1. exponential decline in hydraulic conductivity below the soil surface with increasing depth or moisture deficit.
2. downslope hydraulic head can be approximated to the ground-surface slope, implying that the water table is parallel to the surface.
3. Steady-state flow.

These assumptions and the restrictions they impose are outlined in detail below.

Exponential Decline of Transmissivity with Depth

TOPMODEL uses an exponential decline of transmissivity with depth or soil moisture deficit so that $T = T_o \exp(-fz_i)$, where T_o is the transmissivity at saturation, z_i is the local depth to the water table (which is replaced by S_i for soil moisture deficit) and f is a scaling parameter (equal to $1/f$ or m when soil moisture deficit is used) controlling the rate of decline. Beven (1984) has shown that this model is an acceptable simplification for a variety of soil data sets (though not everywhere), which, if available, could be used to derive the local transmissivity profiles. More commonly, however, m is parameterised from recession curve analysis (Beven *et al.*, 1994). Beven *et al.*, 1994 suggest that the $1/Q$ vs. T relationship is a straight line with gradient $1/m$. An analysis of hydrograph recession curves for some catchments may, however, reveal violation of this assumption (e.g. Ambroise *et al.*, 1996). Ambroise *et al.* (1996) have shown how the index approach can be extended to linear and parabolic transmissivity profiles, resulting in different indices $[(a/\tan \beta)$ for the linear case and $\sqrt{(a/\tan \beta)}$ in the parabolic case]. Lamb *et al.*, (1996) provide a means of using an arbitrary recession curve within a generalised TOPMODEL framework. Kirkby (1997) demonstrates that the exponential transmissivity profile has advantages when the subsurface downslope saturated flow equation - a kinematic wave equation under assumption 2 above - is solved for the transient case. The exponential case, for uniform recharge rates has only short-lived transients and rapidly approaches a uniform flow per unit upslope area. Transients are much longer lived for other profiles such as the linear and parabolic cases proposed by Ambroise *et al.*, (1996). In these cases, the quasi-steady-state dynamics of the TOPMODEL assumptions may not be appropriate and might be expected to have an effect on the parameter values required.

Beven *et al.* (1984) have previously applied TOPMODEL to Hodge Beck – the catchment adjacent to the Dove. Their results suggested that the form of the index was appropriate for this catchment, and reasonably implies that it may be appropriate for the adjacent Dove catchment. This is corroborated by examination of the recession $1/Q$ vs. T relationship for the Dove catchment (Fig. 4.1), which shows a

linked recession between $1/Q$ and T and suggests that an assumption of exponential hydraulic conductivity decline with depth is appropriate.

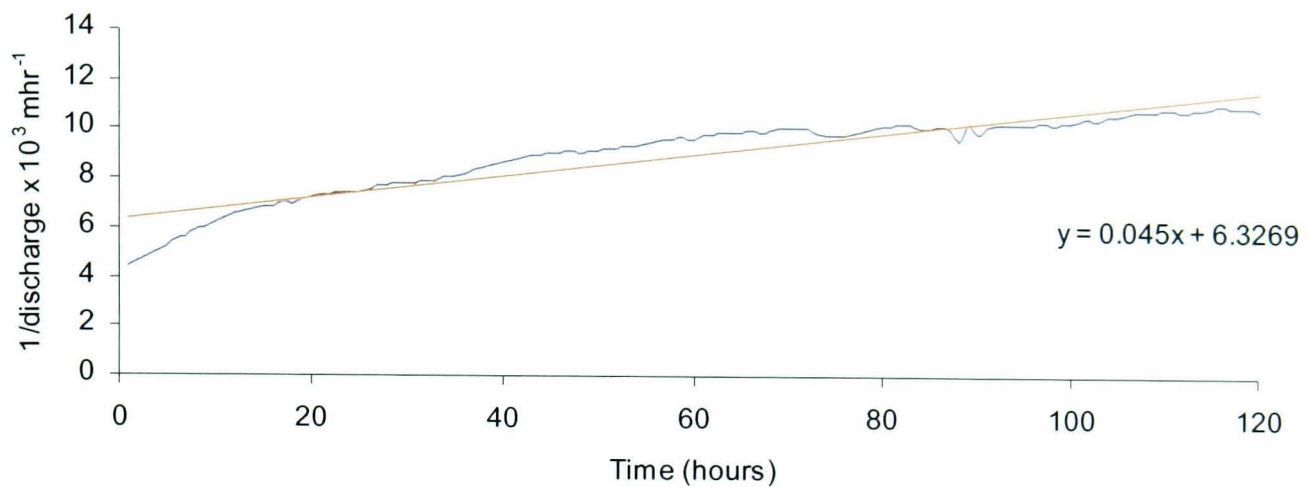


Fig. 4.1 Observed recession $1/Q$ vs. T relationship (blue line) for Farndale catchment, approximated by the linear relationship (red line) $y = 0.045x + 6.3269$. m can therefore be approximated as $1/0.045 = 0.022$.

Approximation of the hydraulic gradient by the slope

This assumption may hold for thin soils over an impermeable bed on moderate slopes that are not subjected to excessive drying (Ambroise et. al. 1996). However, it may not hold for deeper soils or soils which exhibit a strong spatial or temporal change in recharge rate. Rapid recharge to a shallow water table at the base of the slope, with slower recharge further upslope, can lead to ground water ridging (Sklash and Farvolden, 1979). Spatial variability in recharge may also be caused by irregularities in the bedrock.

Quinn *et al.*, (1991), showed, that this assumption can be relaxed by introducing a ‘reference level’ based on a characteristic water table shape, which may deviate from the surface topography, and which may be used to define an ‘effective’ $\ln(a/\tan\beta)$ distribution against which local water table depths can be adjusted. Also implicit in this assumption is the assumption of the dependence of flow pathways on the topographic component of total soil water potential alone. This may hold for slopes $> 25^\circ$, for which subsurface hydrological patterns can be adequately described by topographic variations (Anderson, 1982). However, Anderson (1982) demonstrated

that subsurface flow pathways on shallower slopes ($<10^\circ$) may be more sensitive to the distributions of soil matric potential.

Steady-State Assumption

Within TOPMODEL, the local soil moisture deficit is given by:

$$S_i = \bar{S} + m \left[\gamma - \ln \left(\frac{a_i}{T_0 \tan \beta} \right)_i \right] \quad [4.1]$$

where S_i is the local soil moisture deficit, \bar{S} is the catchment average deficit, m is a parameter, which controls the rate of exponential decline of soil transmissivity with soil moisture deficit, and γ is the catchment average topographic index, a [L] is the upslope contributing area per unit contour length, T_0 [ML⁻²] is the transmissivity when the soil profile is saturated, β is the local slope gradient, and i , represents any location within the catchment. Equation 4.1 implies that all points within the catchment with a similar value of the topographic index also have a similar relationship between the local depth to the water table and the mean depth, and that these points will therefore respond in a similar way to the same inputs. As the catchment wets and dries, the saturated zone is then predicted to expand and contract in accordance with the pattern of the topographic index values. Essential to the analysis of subsurface flow in TOPMODEL, is the assumption that the specific upslope area, a_i , is a surrogate measure of the subsurface flow rate at any point in the landscape. This assumption, however, is only valid if the drainage flux has reached steady state conditions; i.e. every point is receiving drainage from its entire upslope contributing area. In reality, however, this is rarely, if ever, the case. In addition to topography, other factors such as vertical recharge, evapotranspiration and deep seepage to groundwater, all of which may be highly spatially variable, may also affect soil water content, and hence upslope contributing area. Steady state conditions may be achieved if recharge to the water table occurs at a constant rate for the length of time required for every point on a catchment to reach subsurface drainage equilibrium. However, most points on a catchment only receive flow contributions from a fraction of their total upslope contributing areas, due to the low subsurface flow velocities, which results in a

subsurface flow regime that is in a state of dynamic non-equilibrium (Barling *et al.*, 1994). Kirkby and Chorley (1967) concluded that

'The low velocities of throughflow introduce a situation which is different from that obtained during general overland flow..... A slope profile 270 m long thus needs one hour to come to a steady state of overland flow, but requires 1350 hours of rainfall to come to a steady state of throughflow. In practice, therefore, steady state flows are never achieved during through flow for drainage basin slopes. As a result throughflow discharges do not increase linearly downslope, except in a very narrow zone close to the divide. Instead, the flow is almost independent of the distance downslope over much of the hillslope profile, but steadily increases with time throughout the storm'. [p. 7].

Hence, most rainfall events are much shorter than the timescale required for a catchment or hillslope to achieve steady state flow conditions.

Variable rates of deep seepage to groundwater associated with the spatial variability in soil structure due to the presence of macropores may also influence the rate of downslope flow and hence upslope contributing area. Jones (1986) has shown that wetness indices are not good predictors of soil water when soil piping plays an important role in the hydrological response of a catchment. In addition, irregularities in the bedrock may lead to development of a perched water table, which will make it difficult to assess the effective area draining through a point, a , which may itself vary with the wetting and drying of the catchment (Burt and Butcher, 1986; Barling *et al.*, 1994).

Spatially variable evapotranspiration may also affect soil moisture content and hence, the effective upslope contributing area, especially in large catchments. Ladson and Moore (1992) report significant seasonal differences in the spatial distribution of soil moisture on agricultural fields in Kansas prairies, with little spatial variability in summer, resulting in relatively uniform response to rainfall, and large variability in winter, resulting in non-uniform response. Large catchments with large spatial variability in evapotranspiration rates will exhibit variations in effective upslope area, seasonally as well as during a given event. This temporal variability in upslope area cannot be modelled by a static topographic index.

The result of unsteady-state conditions is that hydrologically similar points in a catchment may respond differently to the same inputs. This suggests that upslope contributing area is not the sole factor affecting local rate of downslope flow. Field studies conducted by Burt and Butcher (1986) suggests that slope shape is a more sensitive control of hillslope runoff, which led them to question the validity of the index, formulated solely on the basis of upslope area and local gradient.

When used as the primary model in coupled hydrology-soil erosion models, the hydrological model must be able to predict the specific location of saturation, as well as the dynamic expansion and contraction of these zones, as local variations in saturated areas controls sediment availability, removal and transport. The relaxation of the steady state assumption will allow for dynamic soil moisture accounting on a cell by cell basis, and hence for the dynamic accounting of sediment accumulation and yield.

4.2 Hydrological model Structure

The conceptual foundation of the model is identical to TOPMODEL. It retains the simple gridded spatial discretisation, which allows distributed soil, vegetation and rainfall-evaporation data to be manipulated and stored within a GIS, and facilitates simple mathematical computational methods of data integration. This spatial discretisation is achieved using a Digital Elevation Model (DEM) constructed from 1:25000 topographic OS maps, described in section 3.2.

Each grid cell into which the catchment is divided contains an individual ‘patch model’ of the hydrological system, which represents an idealised vegetated soil profile (Fig. 4.2). It consists of a topsoil root zone store and a gravity store incorporating a dynamic transition zone between the root zone and the water table – identical to the patch model used for each $\ln(a/\tan\beta)$ increment in TOPMODEL. Water fluxes into and out of each grid-cell are based on the same concepts for TOPMODEL and are thus mathematically simple and parametrically parsimonious.

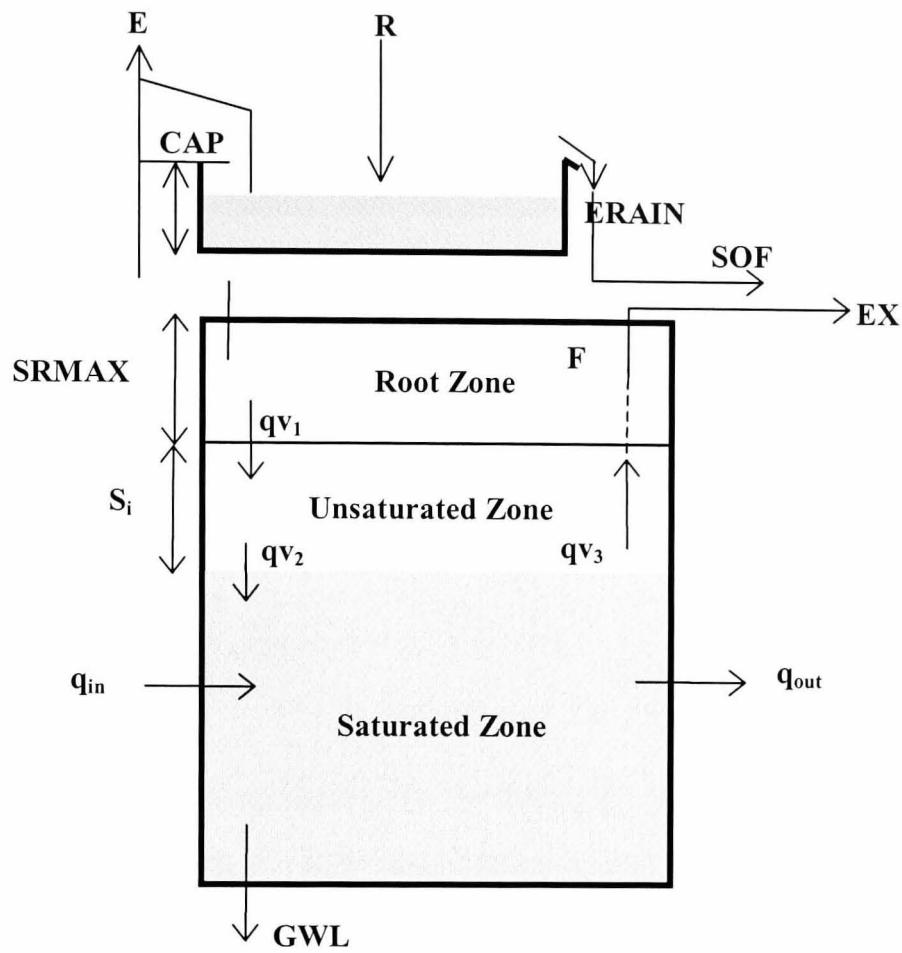


Fig. 4.2 Patch model structure showing water fluxes for a grid-cell

R is the rainfall; *E* is evaporation; *ERRAIN* is interception excess; *F* is infiltration; *SOF* is saturation-excess overland flow; *EX* is exfiltration runoff; *qv1* is vertical flow from the root-zone; *qv2* is vertical unsaturated recharge to the saturated zone; *qv3* is vertical upward water flux representing a rise in the water table; *q_{in}* is the saturated zone flux in to the grid cell and *q_{out}* is saturated zone flux out; *GWL* is groundwater seepage losses; *CAP* is the capacity of the interception store; *SRMAX* is the capacity of the root zone store and *S* is the saturated zone deficit.

Unsaturated Zone fluxes

The unsaturated zone comprises a fixed capacity root store, defined by SRMAX in fig. 4.2, and a dynamic transition zone – the unsaturated zone (gravity store) - between the base of the routing zone and the water table. Infiltration into the root zone is allowed at the potential rainfall rate, but no account of infiltration-excess is taken, although an infiltration excess routine could easily be incorporated (Brasington *et al.*, 1998). Recharge to the saturated zone is taken as the Darcian flux at the base of the unsaturated zone, and is governed by the vertical hydraulic conductivity, K . Under the assumption of an exponential decline in K with soil moisture deficit, this is given by:

$$K_i = K_{0_i} \exp\left(\frac{-S_i}{m}\right) \quad [4.2]$$

where K_i is the local vertical hydraulic conductivity K_{0_i} is the local vertical hydraulic conductivity at saturation, S_i is the local soil moisture deficit, and m is a parameter, which controls the rate of exponential decline of soil transmissivity with soil moisture deficit. m can be estimated by comparing the shapes of observed and predicted recession curves, but care must be taken as similar shapes of recession curves can be obtained under different sets of transmissivity profile assumptions (Ambroise, 1996). Different assumptions about recharge rates may also lead to different curves. In nearly all TOPMODEL studies, m has been assumed to be spatially constant. Saulnier *et al.* (1997a), however, has shown that this assumption can be relaxed to take account of differences in local rates of decline of transmissivity with water table depth, if m is known everywhere in the catchment.

If the estimated vertical hydraulic conductivity exceeds the available unsaturated zone storage (SUZ) the actual vertical flux, q_v , is limited accordingly. This simple description of unsaturated zone flow can be substituted by an alternative model, such as the one used by Brasington *et al.* (1998), comprising a grid-based model where the unsaturated flux is computed using the Brooks and Corey (1964) relationship.

Evaporative losses from the root zone are, as in TOPMODEL, computed as a function of the local storage deficit and a modified Penman potential rate (accounting for transpiration), so that

$$AE_i = (E_0 \cdot ETF_i) \left[\frac{SRZ_i}{SRMAX_i} \right] \quad [4.3]$$

where E_0 is the Penman potential evaporation, ETF is an evapotranspiration correction factor and SRZ_i is the local root zone moisture content and $SRMAX_i$ is the root zone capacity. Although not considered here, all components of equation 4.3 could be made locally variable, including E_0 which could be modified to reflect spatial variation in land-use and topographic conditions (see Wigmosta *et al.*, 1994). Any remaining evaporative potential is used to draw water from the saturated zone at the potential rate.

Saturated Zone Fluxes

Saturated zone fluxes are calculated individually for each grid cell through the application of local continuity equations. Each grid cell can exchange water with its eight neighbours, receiving flows from upslope and discharging downslope. In each cell, transient conditions are approximated by a series of local steady-state solutions based on hydraulic gradients estimated from the ground surface slope. Saturated fluxes into and out of each cell are based on the same kinematic approximation for subsurface flow used in TOPMODEL;

$$q = T \tan \beta \quad [4.4]$$

where q is the subsurface flux per unit contour length (m^2t^{-1}), T is the profile transmissivity (m^2t^{-1}) and $\tan \beta$ is the hydraulic gradient estimated from the local surface slope. Contour lengths along cardinal and diagonal directions are differentially weighted according to the geometric design used in the multiple direction flow-partitioning algorithm. As in TOPMODEL, transmissivity is calculated as the depth integral of the saturated hydraulic conductivity which, under the assumption of isotropy and a negative exponential relationship with soil moisture deficit is,

$$T_0 = \int_{s_d} K_0 \exp\left(\frac{-S}{m}\right) ds \quad [4.5]$$

So that,

$$T_0 = -K_0.m \exp\left(\frac{-S_d}{m}\right) + K_0.m \quad [4.6]$$

where T_0 is the transmissivity of the saturated soil profile, K_0 is the saturated hydraulic conductivity, S_d is the soil moisture deficit when the saturated zone is entirely empty and m is a parameter, which controls the rate of exponential decline of soil transmissivity with soil moisture deficit. If the term $\exp(-S_d/m)$ in equation 4.6 is assumed to be negligible, transmissivity can be found as:

$$T = T_0 \exp\left(\frac{-S}{m}\right) \quad [4.7]$$

where $T_0=K_0.m$. T_0 is usually assumed spatially constant, and is calibrated from existing data when no soil data is available. Calibrated T_0 values, however, tend to be very large, and are dependent on the grid scale of the DTM used in the derivation of the index. Beven (1997) advances a number of reasons for the high calibrated or effective T_0 values. First, vertical conductivity measurements made at finite depths, may not accurately characterise soils in which the downslope transmissivity decreases rapidly with depth to the water table, for which the appropriate value might be much higher than the measured value. Secondly, it has been found that ‘more normal’ conductivity values used in Darcian finite element simulations result in unrealistically slow recession curves (e.g. Binley and Beven, 1992). Thirdly, downslope transmissivity values may be high where preferential downslope flow pathways exist due to piping (e.g. Gilman and Newson, 1980). Fourthly, the calibrated transmissivities may reflect the effective wave speeds in the catchment more than the mean velocities of flow, and wave speeds in near-saturated soils may be much faster than Darcian velocities. In addition, pressure transmission at the wave speed beneath the water table, may be sufficient to induce a rapid response of the saturated zone to changes in hillslope recharge rates, without the need for extensive connectivity of high conductivity flow pathways. Finally, a high T_0 value can compensate for any overestimation in the effective a value of the combined soil-topography index $\ln(a/T_0 \tan \beta)$. Saulnier (1997b), for example, shows that the significant increase in the

calibrated T_0 value with DTM grid size is greatly reduced if the valley bottom ‘river’ grid elements are not allowed to accumulate area from upstream, i.e. are restricted to the local hillslope a values. If this compensation mechanism is important and if a catchment has dynamic a values, then the effective T_0 values might also be dynamic.

Local flow routing

Flow into a cell, $q_{in(x,y)}$, occurs from all upslope directions (i.e. negative slopes with respect to the central cell) according to:

$$q_{in_{x,y}} = \sum_{i=1}^g T_{0_i} |\tan \beta_i| \exp\left(\frac{S_i}{m_i}\right) \quad [4.8]$$

where x,y are 2-d Cartesian co-ordinates of the central cell, g is the number of upslope cells and i refers to each of the upslope cells. Subsurface flow out of the cell, $q_{out(x,y)}$ to all downslope neighbours is then determined by:

$$q_{out_{x,y}} = \sum_{i=1}^{8-g} T_{0_{x,y}} |\tan \beta_{x,y}| \exp\left(\frac{S_{x,y}}{m_{x,y}}\right) \quad [4.9]$$

Wigmosta *et. al.* (1993) described a similar explicit finite difference scheme for kinematic subsurface flow. An approximate stability criterion for this explicit solution requires that the predicted wave propagation per unit time remains smaller than the grid cell dimension (see Kirkby, 1997). The continuity equation for each cell is,

$$S_{t+1} = S_t + GWL + q_{out} - q_{in} - q_v \quad [4.10]$$

where S_{t+1} is the soil moisture deficit in the next timestep, S_t is the soil moisture deficit in the current timestep, GWL is the rate of seepage to deep groundwater, q_{out} and q_{in} are the fluxes out of and into the cell in the current timestep and q_v is the net vertical flux from the unsaturated zone to the saturated zone. In the absence of field data, this flux is taken to be spatially uniform, although unlike the TOPMODEL formulation this may be made variable if data are available. It should be noted therefore, that this formulation applies to a perched rather than a free-surface

groundwater table. The GWL is estimated directly during calibration, and strictly following equation 4.2 could be used to estimate the total profits storage deficit, S_d , using

$$GWL = K_0 \exp\left(\frac{-S_d}{m}\right)$$

and therefore,

$$S_d = -m \ln\left(\frac{GWL}{K_0}\right) \quad [4.11]$$

where S_d is the soil moisture deficit when the saturated zone is entirely empty, m is a parameter, which controls the rate of exponential decline of soil transmissivity with soil moisture deficit, K_0 is the saturated hydraulic conductivity and GWL is loss to groundwater. To ensure consistency with this approach, seepage losses should cease at this deficit. If field data are available, for the depth and porosity at the permeability break above which a perched water table is thought to develop, equation [4.11] could, alternatively, be rearranged to estimate GWL . This would, of course, ignore the heterogeneity and secondary porosity, which are likely to be responsible for deep seepage losses.

Runoff Generation

Two runoff delivery processes are distinguished. First, saturation excess runoff, Q_s , is produced when the vertical recharge, $Q_{v(x,y)}$ exceeds the available storage capacity of the soil profile, so

$$\text{if} \quad Q_{v(x,y)} > S_{x,y}$$

then

$$Q_{s(x,y)} = (Q_{v(x,y)} - S_{x,y}) - (SRMAX_{x,y} - SRZ_{x,y}) \quad [4.12]$$

where $SRMAX_{x,y}$ is the root zone capacity, and $SRZ_{x,y}$ is the root zone storage at grid cell x,y . Second, subsurface contributions to streamflow, Q_b , due to exfiltration, occurs when the net balance between the lateral subsurface fluxes exceeds the residual

storage deficit of the whole soil profile. If the saturated zone deficit is reduced to zero, any remaining storage in the root-zone store is depleted and the excess is exfiltrated above the ground surface. Rainfall onto already saturated areas is arbitrarily assigned as channel precipitation and is considered jointly with exfiltration runoff. No channel system is imposed on the model, and the exfiltration process is maintained purely by the downslope redistribution of soil water. In addition, the effects of draw-down near seepage faces are ignored. These simplifications reflect the aim of the model formulation to represent the macroscopic controls on flow processes.

Total flow generated from each cell is the summation of the component flows,

$$Q_{x,y} = Qs_{x,y} + Qb_{x,y} \quad [4.13]$$

Catchment Flow Routing

Runoff generated by each cell is routed to the catchment outlet using a spatially-distributed convolution integral,

$$Q(t) = \int_A \int_0^t Q(x, y, \tau) h(x, y, t - \tau) d\tau dA \quad [4.14]$$

where $Q(t)$ is the hydrograph of catchment area A , at time, t , τ is the time lag, and $h(x, y, t)$ is a spatially-distributed instantaneous response function, which is determined by the nature of the flowpath taken to the outlet. The unit hydrograph is identified by dividing the catchment into hillslope and channel areas, based on a rasterised channel network. This is computed using the ARC/INFO command STREAMLINE, and the digitised river network. This vector-raster transformation is weighted by a flow-direction matrix, which refines the accuracy of the line-grid conversion and minimises the number of adjacent pixels assigned as river cells. This problem may arise for sinuous rivers or near network bifurcation where a simple line-to-grid rasterisation may overestimate channel area.

Two parameters, V_h and V_c are used to describe time-averaged flow rates for hillslope and channel areas respectively, and the response function, $h(x,y,t)$ is the Dirac delta function

$$h(x, y, t) = \delta \left[\frac{l_{h,x,y}}{V_h} + \frac{l_{c,x,y}}{V_c} \right] \quad [4.15]$$

Where l_h and l_c are the length of the flowpath over hillslope and channel elements respectively (fig. 4.3a and b). These are determined directly from a DEM using the ARC/INFO command FLOWLENGTH, in which the length of flowpath toward the catchment outlet is determined for each cell, summing the distances moving cell-to-cell along a topographically-defined path of steepest descent. The hillslope and channel flowpath lengths and flow velocities, V_h and V_c , are assumed to be time-invariant. This simplification clearly fails to account for transient effects of channel expansion and variation in flow velocity with depth (although this will be implicitly compensated by the tendency for exfiltration runoff in near- or in-channel cells). The calibrated flow velocities should therefore be regarded cautiously, and need not necessarily reflect actual observable flow rates, but rather, the spatio-temporally averaged wave speeds which will be significantly biased in calibration by the spatial distribution of runoff generation. Nonetheless, despite the obvious limitations, this two-component distributed unit hydrograph is a conceptual improvement over simple time-area unit hydrographs based on Euclidean flow lengths, which take no account of differential hillslope and channel conductivity. Furthermore, the method is easily parameterised and requires only two calibration parameters and a DEM. A more complex approach along similar lines has been described by Maidment *et al.* (1996) which accounts for variable flow rates based on reach-scale variation in hydraulic roughness.

All simulations are started, when possible, following a dry period, so that observed flow can be assumed to consist of exfiltration discharge alone. However, unlike TOPMODEL, initial conditions in the saturated zone cannot be set analytically, and instead, are estimated by allowing the catchment to dry from a fully saturated condition until the predicted exfiltration runoff equals total observed flow. This method implicitly defines the initial conditions for both unsaturated stores and the saturated deficit.

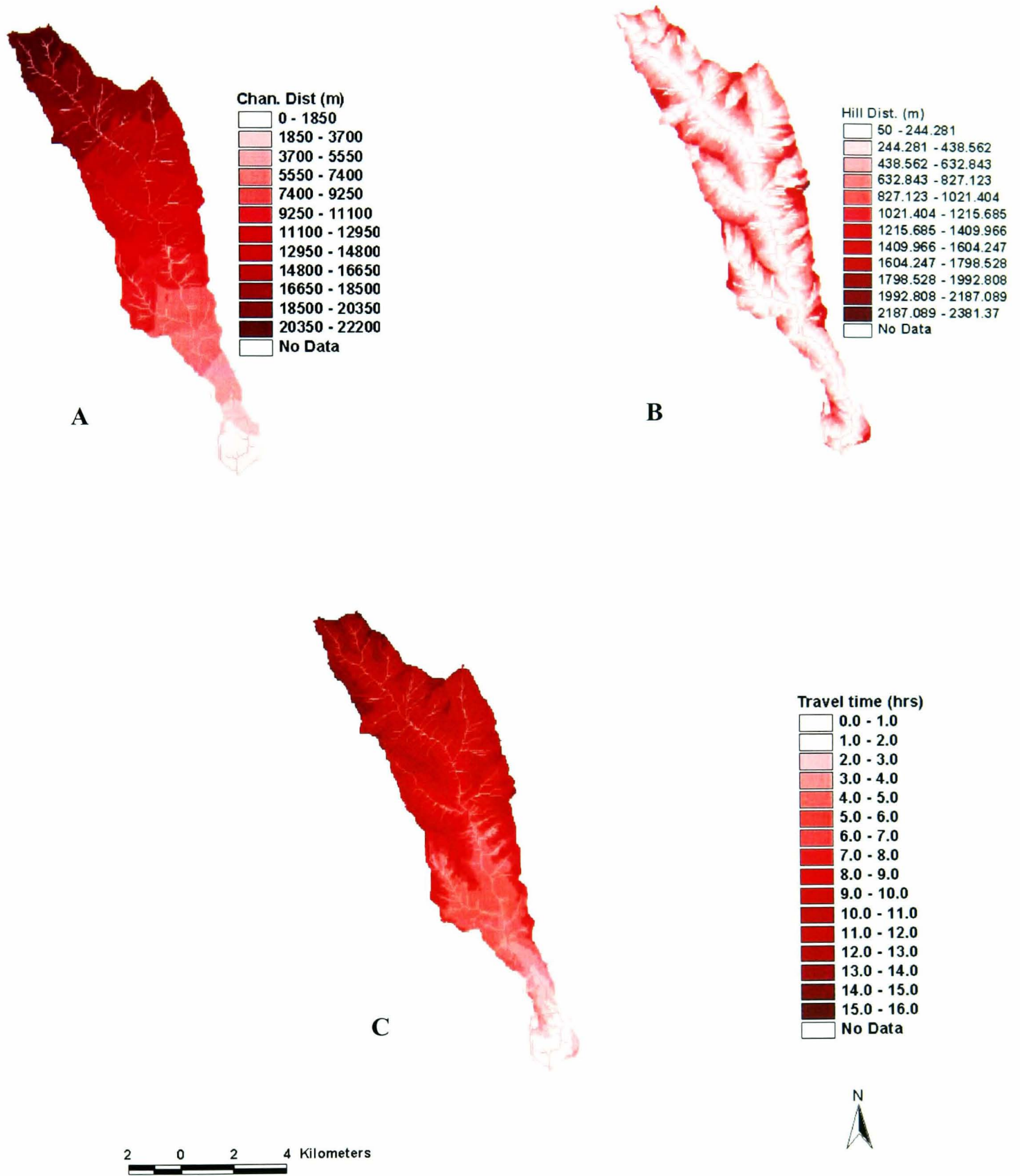


Fig. 4.3 Spatial distribution of A) channel distance B) hillslope distance C) total travel time to outlet

4.3 Snowmelt model

Preliminary visual examination of the observed and modelled hydrographs for winter 1994/95 (Fig. 4.4) revealed major discrepancies due to snowmelt and runoff on frozen soils, similar to those described by Ward (1984) for the Catchwater Drain in Holderness, East Yorkshire.

Fig. 4.4b shows a number of occasions (points 1, 2, 3, 4) when a peak in one hydrograph is associated with a virtual lack of response in the other. While some of these misfits may be attributed to model error or the quality of the input data, an examination of temperature and solar radiation for the same period suggests that some may be attributable to snow accumulation and melt during the winter months. The result is that modelled discharge peaks and time to peak, which are precipitation-dependent, precede the corresponding observed peak, whose timing is temperature-dependent. That is, snow falls, and is recorded as precipitation, hence the model responds to this input. However, the precipitation falling in that timestep is stored on the ground and does not actually contribute to runoff at that time. Hence the observed hydrograph does not record a peak in this timestep. When the temperature rises above freezing, and the snow melts, however, the peak occurs, lagging behind the precipitation (snowfall) event. When large amounts of snow falls and is stored for long periods, the effect of the resulting lagged runoff may be devastating, especially if it occurs concurrently with rainfall. Jackson (1977) noted that while the depth of snow lying on the ground at any given time is usually insufficient to produce large snowmelt floods in the United Kingdom, some of the major floods on rivers here have followed the melting of a snow cover. The large peak in fig. 3.25 is one such event, which occurred concurrently with heavy rainfall of long duration in the North York Moors in winter 1998/1999, resulting in a 1 in 50 flood with peak flow four times the average for that time of year.

Another reason for discrepancies between modelled and observed hydrographs is runoff on frozen soils. Sustained periods of low temperatures are capable of freezing the soil and the subsurface moisture contained within it, thereby temporarily reducing infiltration rates and increasing direct runoff. This results in faster and larger peak flows, when near enough to the channel system, or slower and smaller peaks, when in

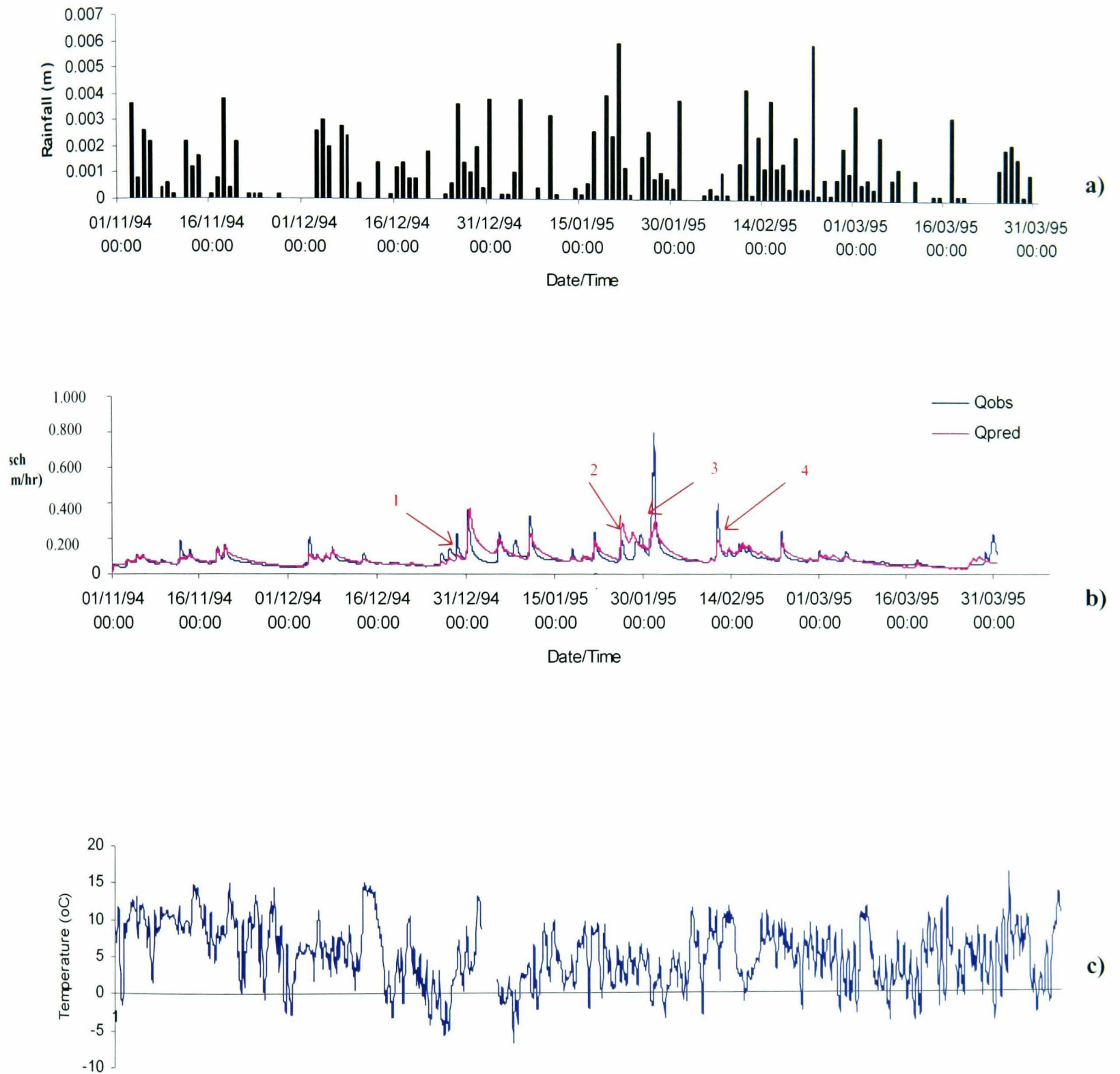


Fig. 4.4 Preliminary calibration of hydrological model for 11/94 to 03/95. a) Rainfall; b) observed and predicted hydrographs; c) temperature

the distal hillslope regions of the catchment, where lower infiltration rates will result in lower recharge to the water table, and hence lower subsurface storm flow.

The World Meteorological Organisation (WMO) (WMO, 1986) identified snowmelt models as conforming to two model categories: the snowmelt model, and a transformation model. The snowmelt model simulates the processes of snow-accumulation and snowmelt, while the transformation model takes snowmelt and any rainfall, and translates them to the basin outflow. Snowmelt and transformation models can be either lumped or distributed. Distributed models attempt to account for the spatial variability in basin physical and hydrological characteristics by dividing the basin into discrete sub-areas, while lumped models use basin-wide effective parameters. There are generally three approaches to basin discretisation. They are, in order of increasing complexity and data requirements, discretisation by: (a) elevation zones; (b) basin characteristics such as slope, aspect, soils, vegetation and elevation; and (c) a fixed or variable length, 2- or 3-dimensional grid.

Models are described as empirical if they are based on the temperature index approach, and more deterministic if they use an energy balance approach. The energy balance approach uses an equation of the form (US Army, 1956):

$$H_m = H_{sn} + H_{ln} + H_c + H_e + H_g + H_p + H_q \quad [4.16]$$

where

H_m = energy available for snowmelt;

H_{sn} = net shortwave radiation;

H_{ln} = net longwave radiation;

H_c = convection heat flux;

H_e = latent heat flux;

H_g = conduction of heat from the ground;

H_p = heat content of precipitation; and

H_q = change in energy content of the snowpack.

The minimum data requirements of the energy balance approach are measurements of air temperature, incoming radiation, vapour pressure, and wind speed (Anderson,

1976). Limited availability of some of these data, and of techniques to extrapolate point measurements to areal mean values, have limited application of this approach. A few basin scale models that use the full energy balance approach include the Institute of Hydrology Distributed Model, IHDM (Morris, 1980) and the Système Hydrologique Européen, SHE (Jonch-Clausen, 1979). Some models, like the Precipitation Runoff Modelling System, PRMS (Leavesley *et. al.*, 1983) and the Snowmelt Model, MELTMOD (Leaf and Brink, 1973) use a modified version of the energy balance approach.

A highly simplified, empirical approach is the temperature index approach, which has the general form:

$$M = C_m (T_a - T_b) \quad [4.17]$$

where M is the snowmelt (mm); C_m is the melt factor ($\text{mm}^\circ\text{C}^{-1}$), T_a is the air temperature ($^\circ\text{C}$) and T_b the base temperature ($^\circ\text{C}$). It is assumed that several of the individual energy-budget components in equation [4.16] are integrated in C_m and T_a . This assumption can be substantiated by the incorporation of knowledge of the relationships between these parameters and measurable spatial and temporal variations in basin and climatic characteristics. C_m may be spatially distributed by vegetation as in the HBV (Bergström, 1976) and Snowmelt Runoff Model, SRM (Martinec *et. al.*, 1983), as well as temporally distributed for each snowpack as a function of density as in the SRM (Martinec *et. al.*, 1983). Account may also be taken of seasonal variations in day length as in the UBC (Quick and Pipes, 1977), CEQUEAU (Charbonneau *et. al.*, 1977), the National Weather Service River Forest System, NWSRFS (Anderson, 1973) and Streamflow Synthesis and Reservoir Regulation Model, SSARR (US Army, 1975). One of the most widely used temperature index models is the degree-day model. It calculates the daily depth, M (cm), by multiplying the number of degree-days, T ($^\circ\text{Cd}$), by the degree-day ratio, a (equivalent to C_m in equation 4.17). A degree-day is defined as a departure of one degree per day in the daily mean temperature from an adopted reference temperature (same as $(T_a - T_b)$ in equation 4.17).

Snowmelt model structure

The snowmelt model developed for application here is a distributed ‘conceptual’ snowmelt model, which attempts to account for:

1. Storage of precipitation during snow accumulation,
2. The lag between the snowfall event and its contribution to catchment hydrological response,
3. The effects of rain falling onto frozen ground.

For hourly snowmelt depth computations, the degree-day method cannot be used because it is radiation, rather than temperature, which is mainly responsible for variations at smaller time intervals. In addition, the degree-day method does not take account of nightly freezing of meltwater and its detention in the snowpack. The data requirements for the alternative complete energy balance approach, however, could not be met. Hence the model used here is based on Bengtsson (1984) for hourly snowmelt, which is similar to the degree-day method, complemented by the radiation component. It uses the simplified equation:

$$M = a_T T + M_R (1 - r) - G \quad [4.18]$$

where

M = hourly snowmelt depth (m)

a_T = coefficient ($\text{m}^\circ\text{C}^{-1}\text{hr}^{-1}$);

T = temperature integrated over time ($^\circ\text{Chr}$)

M_R = global radiation converted to hourly meltwater depth (m)

r = albedo as a decimal fraction.

G = is the net outgoing longwave radiation converted to hourly meltwater depth (m), to account for nightly re-freezing of the surface snow layer (Martinec and Quervain, 1975).

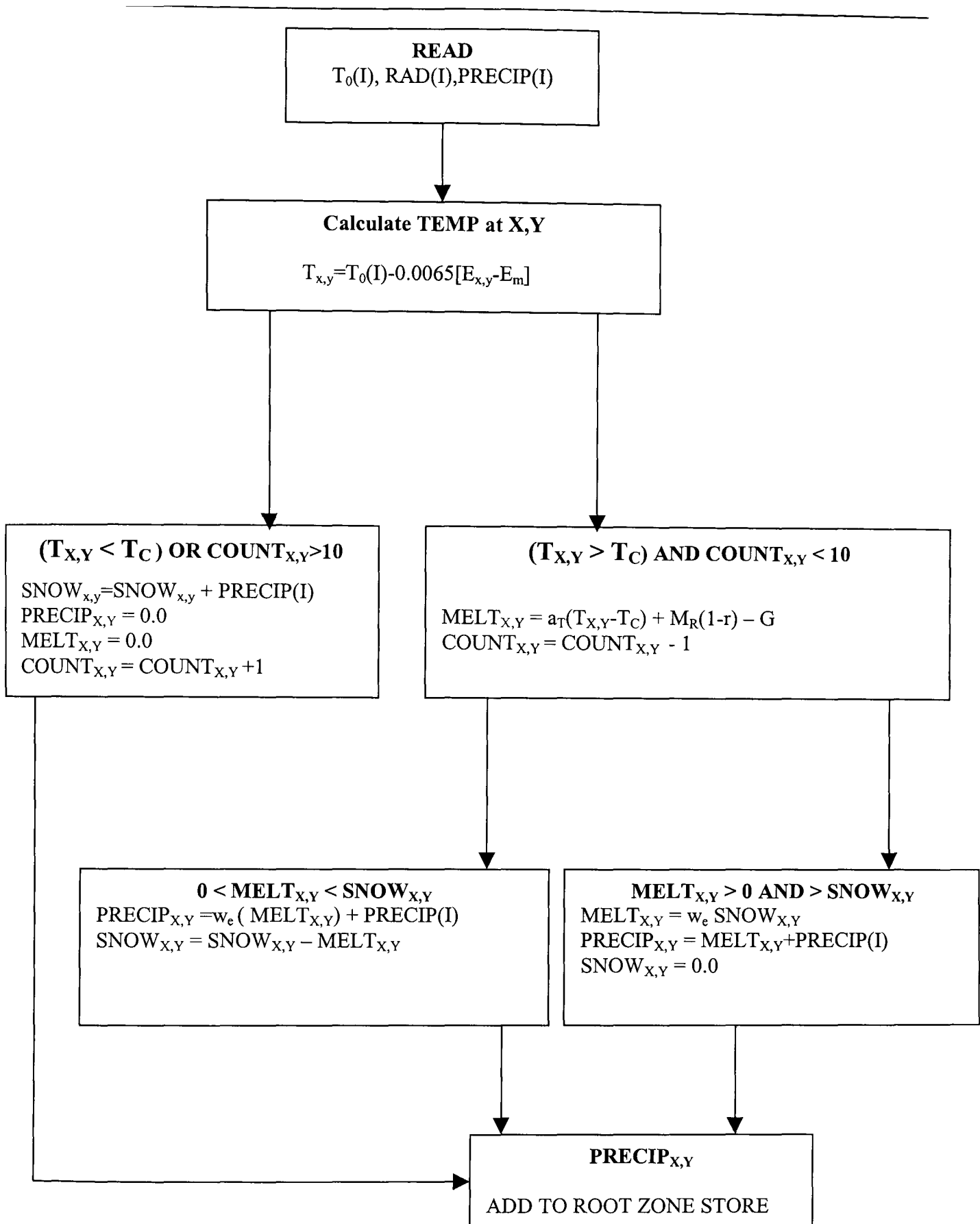


Fig. 4.5 Flow chart of snowmelt model. Converts temporal inputs of temperature, radiation and precipitation to spatially-distributed precipitation.

Fig. 4.5 is a flow chart of the snowmelt model. Hourly measurements of temperature, global radiation and precipitation are used as inputs to derive spatially and temporally variable temperature, snow accumulation, snowmelt and precipitation for each catchment grid cell. The spatial distribution of air temperature is affected by elevation and slope aspect. Air temperature usually decreases with increasing elevation at an average lapse rate of $-6^{\circ}\text{Ckm}^{-1}$. However, the variation about this average can be large and is related to climatic region, season, type of air mass and other meteorological conditions. The occurrence of an inversion can reverse the typical lapse rate-elevation relation, which results in an increase in air temperature with increasing elevation. A constant lapse rate of $-6.5^{\circ}\text{Ckm}^{-1}$ is used to spatially distribute point measurements of hourly temperature according to the elevation of individual grid cells. This is given by:

$$T_{x,y} = T_0 - 0.0065(E_{x,y} - E_m) \quad [4.19]$$

where $T_{x,y}$ is the temperature of a grid cell at elevation $E_{x,y}$, T_0 is the temperature at the meteorological station which is at elevation E_m . A count is taken of the number of hours when the temperature is below a critical value, T_c . If $T_{x,y}$ is less than the critical temperature, T_c , or if there are greater than ten hours prior to which temperatures were below critical value (that is, even if T_{xy} is greater than T_c in the time step being considered), any precipitation falling in that timestep is added to any snow already on the grid cell and stored there until the temperature rises above T_c or the number of hours prior to which the temperature was below critical, is reduced to less than ten. Hence,

$$\text{Snow}_{x,y} = \text{Snow}_{x,y} + \text{precip} \quad [4.20]$$

The precipitation falling on that grid cell is reset to zero along with melt. In this way precipitation is spatially distributed and temporally restricted by temperature. When the temperature of the grid cell rises above T_c , and $\text{Count}_{x,y}$ is reduced to less than 10 hours, potential snowmelt is calculated according to:

$$\text{Melt}_{x,y} = a_t(T_{x,y} - T_c) + M_R(1 - r) - G \quad [4.21]$$

This is the depth of snow that would be converted to water, limited by availability. If the depth of snow on the grid cell is less, then all of the available snow is removed. M_R is derived as follows. A daily average of 1Wm^{-2} of incoming radiation would produce 0.03cm of snowmelt water (Kustas *et. al.*, 1994). Hence an hourly average of 1Wm^{-2} would produce $0.03/24$ cm or 1.25×10^{-5} m of snowmelt. This factor is multiplied by the hourly incoming global radiation value, to give M_R – the global radiation converted to hourly melt water depth.

G , the outgoing long-wave radiation is given by:

$$G = \varepsilon(\sigma T_k^4) \quad [4.22]$$

where ε is snow emissivity (=0.985), σ is the Stefan Boltzman constant ($=5.67 \times 10^{-8} \text{Wm}^{-2}\text{K}^{-4}$), and T_k is the absolute temperature at x,y ($T_k = T_{x,y} + 273$) in Kelvin.

The depth of snow removed is converted to a water equivalent by multiplying by a factor w_e . Hence,

$$Melt_{x,y} = w_e Melt_{x,y} \quad [4.23]$$

w_e can be found using the method of Jackson (1977) for deriving the water equivalent for snowmelt in the United Kingdom, as a function of altitude and return period of the snow event.

$$w_e = c_{rp} [w_{msl} + c_a (E_{x,y})] \quad [4.24]$$

where c_{rp} is a correction factor for return period relative to a 5 year return period, w_{msl} is the water equivalent at mean sea level, and c_a is a correction factor for altitude above mean sea level. As there is no explicit way to account for the loss when snow is converted to melt water equivalent, and because no loss was observed in the water balance for the catchment (section 3.7.1), a water equivalent factor of 1 was used. This implies that the entire snow depth identified for removal by equation 4.21 is

converted to melt. Clearly this is a limitation of the model. However, it is thought that the difference in magnitude between a water equivalent calculated as a fractional value of w_e and that calculated using a value of 1, is less significant than the lag time associated with the melting event and, since it is the timing of the melt that is of greater consequence to the hydrological response of the catchment, this might not be an unreasonable assumption. The only parameter that requires calibration is the melt coefficient, a_T , which controls the contribution made by temperature, to the melt process.

The parameter a_T can be derived from lysimeter measurements where available in combination with the degree-day ratio. Martinec (1989) computed a_T from daily lysimeter snow depth measurements, and net outgoing radiation. a_T is 1/24 of the degree day value which is reported to be in the range 0.2-0.5 cm °C⁻¹day⁻¹. Based on this, the preliminary value of a_T was set at 8.33×10^{-5} m°C⁻¹hr⁻¹. The depth of melt water is added to any rain falling in that timestep, which is then added to the root zone, to be routed in the manner described above.

Runoff from frozen, or near frozen soil is accounted for as a function of the number of hours prior to, and including the timestep under consideration, for which the temperature was below the critical temperature. If $Count_{x,y}$ is greater than 0 but less than 10°C, the soil is considered frozen, and 95% of the total precipitation in that period is added to the root zone, and allowed to infiltrate, while 5% is added to direct runoff. This is purely arbitrary, but is meant to represent the period before and after snowfall conditions when the soil is frozen, but precipitation is not snow, and the infiltration of rain falling onto the soil is reduced.

The model has many limitations. Firstly, the variability of a_T has not been taken into account. Martinec (1960) found that a_T varies with snow density and shows substantial deviations during periods of extremely high or low wind speeds. The dependence on density is due to the change in albedo with change in density, and hence the change in the age of the snow. Older snow has a higher density and a lower albedo, which increases the gain of heat from radiation. Higher density is also associated with higher water content, and hence lower thermal quality of snow (where thermal quality is the ratio of the amount of heat required to produce a given volume

of water from snow, to the amount of heat required to melt the same volume of water from pure ice at 0°C (Rodda, 1985)). Ice, which also has a high density, but high thermal quality is likely to have a reverse effect on a_T . In addition, a_T is affected by changes in the radiation balance due to vegetation, slope angle and aspect.

Secondly, the radiation component is only considered to be a function of altitude, but is also controlled by slope, aspect, vegetation, and the age of the snow. Swift (1976) developed a procedure to extrapolate measured or estimated values of incoming solar radiation for a horizontal surface to the slope and aspect of each basin sub-area. Remote sensing also provides a source of spatially distributed radiation measurements. Measures of cloud cover from sequential GOES images and computed potential solar radiation can be used to estimate daily values of incoming solar radiation (Allen and Mosher, 1986). However, image analysis techniques may introduce additional uncertainty to the model.

Thirdly, wind speed is not considered as a factor in radiation component. Wind and vapour pressure are important components in any snowmelt model as the turbulent heat exchange is a major snowmelt energy source in open areas and alpine type environments (Leavesley, 1989). Point measurements of wind speed, which is most commonly available, are however inadequate to fully characterise the spatial variability in energy balance, and hence snowmelt, due to this factor. The relationship of wind and vapour pressure with vegetative cover and terrain are, in fact, needed. Wind and vapour pressure may be important in the study catchment since it is an upland area located near the windy east-coast of the UK.

Fourthly, the use of a constant critical temperature to determine snow accumulation and melt may not adequately represent the temporal variability of the processes. T_c may vary seasonally and will obviously be sensitive to the temporal scale of discretisation, and should ideally be optimised. However, T_c is assumed here to be 0°C. In addition, the seasonal variability in temperature lapse rate is not considered.

Problems associated with the accuracy of input data are particularly significant. The WMO (1986) concluded that precipitation distribution assumptions and the determination of the form of precipitation were the most important factors in

producing accurate estimates of runoff volume in snowmelt models. Charbonneau *et al.* (1981) concluded that the spatial distribution of precipitation was more important than the selection of model approach. Precipitation measurements are prone to errors due to the effects of wind on precipitation gauge catch efficiency and redistribution of snow on the ground. When snow falls, it might not be recorded in the timestep in which it occurs, but may remain on the raingauge until the temperature rises, and it melts, resulting in incorrect rainfall depths for both the period in which the event occurred, and the period when it is recorded. Precipitation gauge catch deficiencies for solid precipitation can range from about 45% at a wind speed of 16kmhr^{-1} to more than 70% at wind speeds greater than 32kmhr^{-1} for unshielded gauges; a shield reduces these errors by about one third to one half (Larson and Peck, 1974). This poses a major problem for any snowmelt model when applied to a catchment in which rain and snowfall are not recorded as distinct events.

Despite these difficulties, the model may provide a possible improvement in the prediction of catchment hydrological response. While snowfall in the catchment is not significant in terms of duration and depth of snow, the timing of snowmelt events may sometimes be crucial to hydrological response. It is therefore important to take account of the annual snowmelt contribution to basin response. The model used here, attempts to account for the lag in the timing of the snowfall event, and the response, using physically based radiation and temperature components, making it somewhat physically-based. In addition, the decreased infiltration on frozen soils is accounted for by a more conceptually based approach. The model is therefore capable of improving the timing and quantity of snowmelt runoff, and consequently of catchment hydrological response, in a spatially distributed manner. This is important for the coupled hydrological-sediment yield model, which depends on accurate spatial and temporal predictions of runoff.

4.4 Sediment Yield Model

Examination of the observed sedigraph (section 3.8.2), revealed considerable scatter in the SSC/discharge plot (fig.3.26) associated with the variable phasing of discharge and SSC waves which leads to hysteretic, and exhaustion effects, and reflects the fact that sediment yield is an availability-limited process. The variation in spatio-temporal rate of sediment supply, also contributes to scatter in the rating curve, and results from the underlying assumption inherent in the rating curve method, that the system is transport limited. Most events have steep rising limbs and a more gradual recession, which indicates that sediment in suspension is not necessarily intimately mixed with the transporting flow. Variations in particle size will cause variability in rates of transport, and may result in settling out within the channel. Thus the sediment yield model was developed to represent sediment yield as a dynamic, availability- and transport-limited process.

Moore and Clarke (1983) and Moore (1984) describe a model, which represents sediment yield as an availability- and transport-limited process. This rather conceptual model was selected over more physically-based sediment yield models, due to its parametric parsimony, and its ready conversion to a fully distributed format. Fig. 4.6 shows the flowchart of the essential components of the hydrological model and its explicit coupling to the sediment yield model. The distributed, gridded format of the hydrological model enables a fully distributed dynamic format of the sediment yield model instead of the distributed function approach of Moore and Clarke (1981; 1983). Coupling is achieved by explicitly linking runoff generation with patterns of sediment accumulation and removal.

Sediment Accumulation and Availability

It is proposed that the available sediment, $L = L(t)$, may be viewed as a depth which accumulates over time until partial or complete removal by detachment and transport processes. Hence once S_{t+l} in equation [4.10] is greater than zero, sediment begins to accumulate as a function of the time since the cell last produced runoff. Thus, sediment availability is akin to the increasing depths of unconsolidated sediment broken up by heating, cooling, and mechanical and biological disturbance, which makes loose, friable material near the surface available for entrainment. The rate at

which sediment is made available, $R(t)$ is taken to decrease exponentially as the amount of sediment currently available, increases, so that

$$R(t) = \frac{dL}{dt} R_0 - KL = R_0 \exp[-K(t - t_0)] \quad [4.25]$$

where R_0 (in mhr^{-1}) is the initial (maximum) rate of increase in sediment availability at time t_0 when no sediment is available after a long period of intense rainfall. (Figure 4.7a); K (in hr^{-1}) is the availability rate constant which determines the rate of decrease of accumulation rate, and L (in m) is the depth of available sediment (figure 4.7b). Integrating equation [4.25] over the interval $(t-\Delta t, t)$ gives:

$$L(t) = \exp(-K\Delta t)(L(t - \Delta t) + [1 - \exp(-K\Delta t)]R_0 / K) \quad [4.26]$$

Since, by definition, no sediment is available at time t_0 ($L(t_0) = 0$), considering the interval (t_0, t) allows equation [4.26] to be simplified to

$$L(t) = \frac{R_0}{K} [1 - \exp(-K\Delta t)] \quad [4.27]$$

where in this case $\Delta t = t - t_0$. Between storms, sediment available for transport is therefore envisaged to increase at an exponentially decreasing rate, asymptotically approaching a maximum of $L(\infty) = R_0 / K$ (Figure 4.7b).

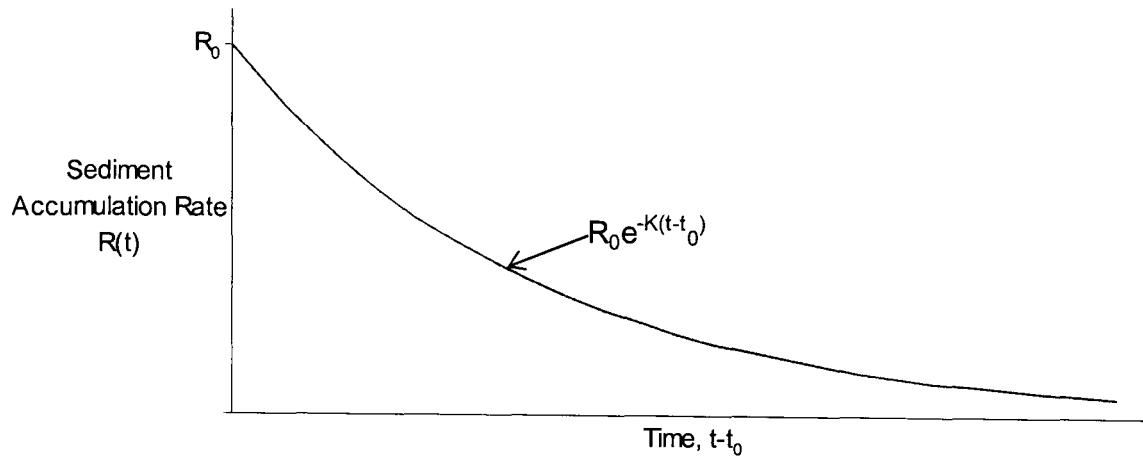


Fig. 4.7a Sediment accumulation rate curve.

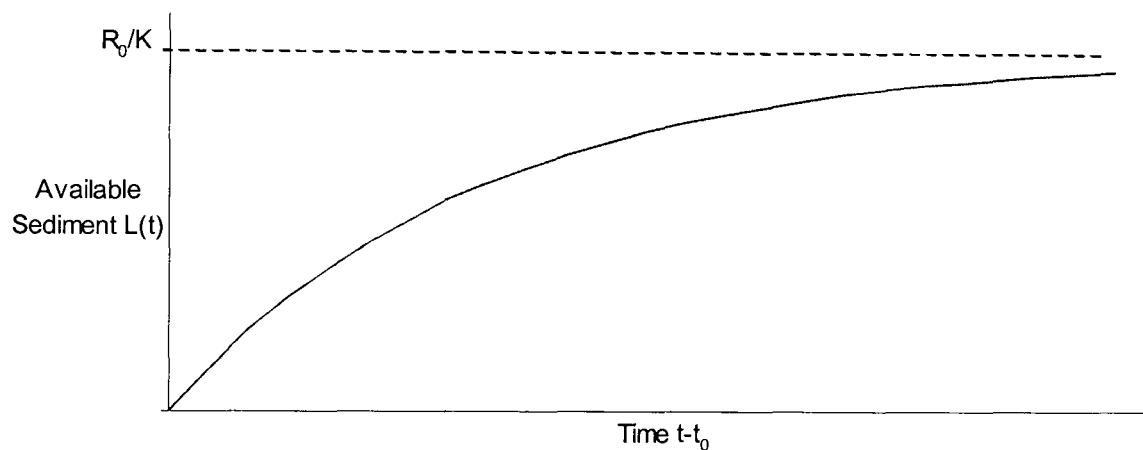


Fig. 4.7b Sediment availability curve.

No river system is imposed on the model. The use of initial soil moisture deficit as the criterion for sediment accumulation in a given timestep ensures that channel cells do not accumulate sediment. This also allows for the dynamic expansion and contraction of the contributing area of sediment sources associated with the expansion and contraction of the runoff contributing area within the basin, which is in agreement with the observations of Brune (1950), Gregory and Walling (1973), and Wall *et. al.* (1979), that only a small portion of the catchment contributes to sediment yield. Sediment is more likely to be removed from a basin during a particular storm from a zone near to, and often contiguous with, the channel and also in closer proximity to the basin outlet.

Sediment Removal

The model allows sediment removal when overland flow occurs in hillslope cells and when saturation from above (i.e. due to rainfall input) occurs in exfiltrating cells. Hence, the model represents particle entrainment, but ignores bedload and channel erosion. All exfiltrating cells are assumed to be channel cells and may only contribute sediment during a rainfall event. That is, if a cell is contributing exfiltration flow in the current timestep, but had accumulated sediment in previous timesteps, then no sediment is removed until the cell contributes to saturation excess during a rainfall event. Walling and Webb (1982) showed that sediment yield was more closely related to stormflow runoff than total runoff. Hence the assumption of storm period removal of sediment from exfiltrating cells may not be unreasonable given that these marginal exfiltrating cells are likely to be significant sediment sources, due to location in the riparian zone. This approach allows for the dynamic movement of channel cells, into and out of the channel, and hence the expansion and contraction of the sediment accumulation zones along the channel. Ignoring the role of exfiltration runoff in the sediment removal process, in this way, facilitates the separation of saturation-excess and exfiltration runoff into distinct processes, which affect sediment removal differently. This is desirable since it is suspended sediment flux that is of interest here. However, it also ignores the possibility of modelling sediment removal due to shallow return flow, which may be generated at the base of saturated hillslopes, and re-suspension of in-channel fines, both of which may be significant to the sediment yield of the catchment.

All sediment on a cell producing runoff is removed in the timestep in which runoff is produced. This is a limitation of the model, as only a fraction of the available sediment may, in fact, be removed from the grid cell, either because runoff is only produced on a portion of the grid cell, or because the erosive power of the runoff produced is capable of removing only a fraction of the available sediment. If the former is true, then it is a limitation of the hydrological model to predict within grid cell variability in runoff mechanisms, which is partly due to the scale of discretisation, and partly to the lack of explicit representation of interflow processes. If the latter is true, then it is a limitation of the sediment yield model and the lack of representation of the spatial variability in the erosive power of runoff. While methods such as the unit stream power, described in section 2.10.2, have been successfully used to account

for the variability in local sediment entrainment and removal, it is essentially a static model which would be difficult to implement within the dynamic framework applied here, as it would require the knowledge of both runoff and sediment, entering and removed from each grid cell in each timestep. The trade-off between accuracy and computing requirements, however, precludes the implementation of this type of approach here.

Sediment Routing

Moore and Clarke (1983) suggested the use of the inverse Gaussian density as a suitable function to describe the distribution of translation times of direct runoff and sediment, $f(t)$ and $f_s(t)$, because:

1. Its shape is unimodal and positively skewed.
2. The heavy-tailed nature of the density agrees well with observed hydrograph recessions, without the need for identifying and separating a base flow component.
3. It may be derived as the solution of the convection-diffusion equation for a Dirac delta function input, and thereby related to the Saint Venant equation of open channel flow in linearized form.
4. It is characterised by only two parameters, which can be related through the linearized Saint Venant equation to the physical characteristics of the stream channel.

The form of the density is

$$f(t; \mu, \lambda) = \left(\frac{\lambda}{2\pi t^3} \right)^{1/2} \exp\left\{ -\frac{\lambda(t - \mu)^2}{2\mu^2 t} \right\} \quad t > 0$$

$$f(t; \mu, \lambda) = 0 \quad \text{otherwise} \quad [4.28]$$

The parameters μ and λ are positive and of dimension [T], and may be related to the linearized Saint Venant equations (for flow in a rectangular channel and neglecting inertia terms)

$$\frac{1}{2} \frac{A_0 C^2 H_0^2}{Q_0} \frac{\partial^2 p}{\partial x^2} - \frac{3 Q_0}{2 A_0} \frac{\partial p}{\partial x} = \frac{\partial p}{\partial t} \quad [4.29]$$

at $x=L_0$, by the relations

$$\mu = \frac{2L_0 A_0}{3Q_0} \quad [4.30]$$

$$\lambda = \frac{L_0^2 Q_0}{A_0 C^2 H_0} \quad [4.31]$$

where Q_0 , H_0 and A_0 are the reference flow, depth, and cross-sectional area; C is the Chézy coefficient, and L_0 is the characteristic length. Equation [4.31] is of the form of the convection-diffusion equation:

$$\frac{1}{2} \sigma^2 (\partial^2 p / \partial x^2) - v(\partial p / \partial x) = \partial p / \partial t \quad [4.32]$$

for which the inverse Gaussian density equation [4.29] is a solution. The dependent variable $p=p(x,t)$ may be used to represent either the translated flow or translated sediment at time t and at a distance x from its point of origin. This distance may be taken as $x=L_0$ and regarded as a characteristic translation length of the basin. The parameters of the convection-diffusion equation are related to those of the inverse Gaussian density by $\mu=L/v$ and $\lambda=L_0^2/\sigma^2$ at $x=L_0$. The relative importance of convection and diffusion is governed by the ratio of μ and λ . A component to account for settling is also included, as a sink term in the convection-diffusion equation.

Here, sediment is routed to the outlet using a spatially distributed convolution integral

$$Q_{sed}(t) = \int_0^t \int_{A_0} Q_{sed}(x, y, t) h_{sed}(x, y, t - \tau) d\tau dA \quad [4.33]$$

where $Q_{sed}(t)$ is the sedigraph of the catchment A at time t , $Q_{sed}(x,y,t)$ is the depth of sediment from a grid cell at (x,y) arriving at the outlet at time, t and $hsed(x,y,t)$ is a spatially-distributed instantaneous response function, which is determined by the nature of the flowpath taken to the outlet, based on the same distribution of hillslope and channel flowpath lengths, described in section 4.2. This instantaneous unit sedigraph, $hsed(x,y,t)$, defines the mean translation time for the depth of sediment removed from a given cell. It is the Dirac delta function:

$$hsed(x, y, t) = \delta \left[\frac{l_{h,x,y}}{V_h^{sed}} + \frac{l_{c,x,y}}{V_c^{sed}} \right] \quad [4.34]$$

This gives a mean translation or arrival time of t_a . However, unlike flow, all sediment removed from a given grid cell does not arrive at the outlet at the same time. A log-normal distribution is used to determine the distribution of arrival times at the outlet where the mean of the distribution is the mean arrival time for the grid cell. The mean arrival time from the source t_a and total depth of sediment removed, define the shape of the distribution of sediment. Hence the sediment arriving from a given grid cell will be distributed according to:

$$Q_{sed}(x, y, t) = \frac{Sedrem(x, y)}{St\sqrt{2\pi}} \exp \left[- \left\{ (\ln t - M)^2 / 2S^2 \right\} \right] \quad [4.35]$$

where $\mu = e^{M+S^2/2}$

$$\sigma^2 = e^{S^2+2M} (e^{S^2} - 1)$$

and M and S are the mean and standard deviation of the corresponding normal distribution. $Sedrem(x,y)$ is the total depth of sediment removed from the grid cell. Clearly, μ is the mean arrival time, t_a . σ is set at the unit of temporal discretisation of one hour. For simplicity, a unit log-normal distribution is defined such that the maximum number of timesteps that sediment from any grid cell can take to reach the outlet, is set to 10 hours, and sediment can arrive only one hour before the peak at mean arrival time. Hence:

$$\sum_{t=t_a-1}^{t=t_a+8} sed(x, y, t) = 1 \quad [4.36]$$

where $sed(x, y, t)$ is the fraction of one unit depth of sediment from a grid cell at (x, y) arriving at the outlet at time $t = t_a + d$, where d is the delay in hours ($d < 9$). This unit log-normal distribution is then used with the mean arrival time to determine the rate at which sediment arrives at the outlet. For example, for a given cell, the fraction of sediment arriving at the outlet one hour before the mean arrival time, is the total depth of sediment removed, multiplied by the factor for $t = t_a - 1$ in equation [4.36]. Hence, re-writing equation [4.35],

$$Qsed(x, y, t) = Sedrem(x, y, t) * sed(x, y, t) \quad [4.37]$$

The sediment arriving at the outlet from all cells contributing in that timestep are summed, and converted to sediment flux in $gm^{-2}hr^{-1}$.

The method does not implicitly account for settling, but the lag between sediment arriving at the mean arrival time and sediment delayed, may be interpreted as temporary settling and remobilization. While the method employed here does not explicitly make use of any physical attributes of the catchment to account for the shape of the wave, it is in agreement with the general shape of the distribution prescribed by Moore (1984), for translation time. This method is simpler to implement within a finite difference scheme than the Inverse Gaussian method, and requires no additional parameters to be defined. A limitation of the approach, however, is the use of a fixed unit log-normal distribution to define the shape of the sediment arrival times. Clearly, different sediment sources and different events will require varying numbers of hours for translation to the outlet, resulting in distributions of different shapes – more peaked for sediment arriving from a grid cell close to the outlet, and less peaked for cells in the distal areas of the catchment.

4.5 Uncertainty

The models described above will be implemented within an uncertainty analysis framework.

4.5.1 Model Calibration and Uncertainty Analysis

It has become increasingly accepted that many different parameter sets, from different parts of the parameter space are capable of producing equally ‘acceptable’ simulations for a single model – the concept of model equifinality discussed earlier. As discussed in section 2.9.1, traditional calibration procedures which seek to identify a global optimum parameter set to describe a system, encounter difficulties due to over-parameterisation, parameter interdependence, parameter insensitivity and model equifinality when applied to distributed models. Binley and Beven (1992) suggest that the natural interdependence and interchange-ability of different mechanisms of catchment hydrological response may be the cause of parameter autocorrelation, heteroscedasticity and insensitivity observed in global parameter optimisation techniques. Hence, it might be possible to obtain similar hydrographs for different combinations of response mechanisms.

Beven (1989), in a critical discussion of the physically-based distributed modelling approach and its associated calibration problems, suggested that modellers reject the traditional presumption that one unique model structure and parameter set can be identified, and instead, concentrate on the estimation of predictive uncertainty, and how it can be restrained.

Beven (1989) and Beven and Binley (1992) propose a methodology for calibration and uncertainty estimation of distributed models based on generalised likelihood measures, which incorporates, and attempts to account for, equifinality in distributed models. The so-called Generalised Likelihood Uncertainty Estimation (GLUE) procedure is based on the premise that any model/parameter set combination is an equally likely simulator of a given system. Beven and Binley (1992) suggest therefore that it is only possible to make an assessment of the likelihood or possibility of a particular parameter set being an acceptable simulator of the system. The procedure includes a means of incorporating additional observations to update the

likelihoods – Bayesian updating. This section describes the model calibration and predictive uncertainty assessment methodology using GLUE and Bayesian updating.

4.5.2 Generalised Likelihood Uncertainty Estimation (GLUE)

GLUE incorporates a Monte Carlo method, based on running a large number of simulations of a given model with different parameter sets, drawn randomly from specified parameter probability distributions. Each simulation is assigned a likelihood weight, L , based on one or more of a number of different qualitative and quantitative measures of the correlation between the observed and predicted response. A simulation or given parameter is classified as *behavioural* or *non-behavioural* (*sensu stricto* Hornberger and Spear, 1981) if L is greater than zero, and if L is zero respectively, based on some *a priori* knowledge of the system, or a statistically-minimum acceptable level of performance. All simulations with L greater than zero are retained and the likelihoods summed and scaled to unity to give a probability distribution function for the corresponding parameter sets. The new re-scaled likelihoods are then used to weight the model predictions generated at each timestep and the distribution function of predictions is calculated to gauge predictive uncertainty. Previous experience with GLUE for hydrologic models suggests that the probability distributions of predicted discharges are rarely Gaussian, and confidence limits derived from estimates of the variance are likely to be inappropriate (*Freer et al.*, 1996). Therefore, for each timestep of the simulation, confidence limits are derived by extracting percentiles from the distribution of model predictions, which may reasonably be expected to cover a comprehensive range of model predictions (e.g. 5 and 95 %). GLUE implementation requires *a priori* definition of the likelihood measure(s) to be used, and the initial range or distribution of parameter values to be considered.

Choice of Likelihood measure

The likelihood function chosen must have some specific characteristics, which can be used to distinguish between *behavioural* and *non-behavioural* simulations. Beven and Binley (1992) stress that the term likelihood, as used here, should be interpreted in a very general sense, and not under the strict assumptions implied in maximum likelihood theory (Clarke, 1994). In general, the likelihood measure is of the form:

$$L(\Theta_i | Y) \quad [4.38]$$

where L is the likelihood measure, i is the i^{th} model, Θ_i is a particular parameter set, and Y is the observed data variable. Hence expression [4.38] is the likelihood measure for the i^{th} model associated with a particular set of parameters Θ_i , conditioned on the observed data variables Y .

Various goodness-of-fit functions can be used as likelihood measures for GLUE (Beven and Binley, 1992; Freer *et. al.*, 1996), such as model efficiency, sum of squared errors, sum of absolute error, and scaled maximum absolute error. The choice of likelihood measure is subjective and, because each study is unique, it is important that the likelihood function used is appropriate to the study area, and reflects both the observations available as well as the purpose for which the model is required. The choice of a rejection criterion is somewhat arbitrary and may affect the uncertainty bounds computed. Lamb *et. al.*(1998), however, found that relaxation of the rejection threshold to define a larger proportion of the total number of behavioural simulations resulted in only slight modifications to uncertainty bounds. This they attributed to large discrepancies between the ‘best’ simulations and the ‘worst’ simulations, particularly when conditioned on a combination of observed variable (flow and water table levels in this case), so that most of the simulations fell within the tails of the cumulative distributions of L , and have little effect on the location of the uncertainty bounds.

Initial distribution of parameters

The ranges over which parameters are initially defined are also usually subjective. They must, however, be broad enough to ensure that the model behaviour will span the range of observations, and reflect the distribution function of the parameter values over the range. This may be done, by using a set of parameter values that reflect our prior knowledge of the parameter values, or more normally perhaps, a set of assumptions consistent with all lack of prior knowledge about what might be appropriate values (Beven and Binley, 1992). Where there is little prior knowledge, a uniform distribution over the chosen range may be used to define a suitable ‘reference’ or standard prior distribution. While it may be thought that the choice of a

uniform distribution may not be appropriate for some parameters, it is not critical, as the likelihood distribution which defines acceptable simulations should implicitly reflect any non-linearity, and condition the probability bounds accordingly. Furthermore, since parameter sets rather than individual values are evaluated, any parameter interaction effects are implicitly accounted for in the procedure.

As mentioned earlier, GLUE analysis can also be used to evaluate different model structures. If the observed hydrological response still falls outside the calculated uncertainty limits after evaluation of a wide range of parameter values, and if this predictive failure cannot be accounted for by measurement errors, then model structure or the imposed boundary conditions may be in error. If this is the case, then the model can be redeemed, by redefining the likelihood function used, to produce wider uncertainty limits. Hence it is important to have a well-defined likelihood measure, as the uncertainty limits will depend on the definition used. It may therefore be necessary to try several different likelihood functions, before a failing model is discarded as having a poor model structure. If the uncertainty limits are drawn too narrowly, then a comparison with observations will suggest that the model structure is invalid, while if they are drawn too widely, then it might be concluded that the model has little predictive capability. In order to determine whether poor model performance is due to errors in input data measurements, some measure of the errors due to input data measurement errors has to be undertaken.

4.5.3 Updating Likelihood Weights –Bayesian Updating.

A key advantage of the GLUE approach is that it allows for revision of the likelihood values and hence the refinement of prior beliefs in the unknown parameter, as additional data becomes available. Recalculation of the distribution function associated with the parameter sets is carried out using Bayes' equation in the form (Fisher, 1922):

$$L_p(\Theta | Y) = L_y(\Theta | Y)L_0(\Theta) \quad [4.39]$$

where $L_o(\Theta)$ is the prior likelihood distribution for a parameter set Θ , $L_y(\Theta|Y)$ is the calculated likelihood function of the parameter sets given the set of new observations, Y , and $L_p(\Theta|Y)$ is the posterior distribution of parameter sets. Bayes' equation in this form presupposes that the likelihood distribution has a cumulative value of unity. It can be applied on a sample by sample basis, as each sample parameter set is associated with its own prior likelihood, and its own likelihood function value, making it easy to use within a Monte Carlo procedure.

Bayesian updating allows for a gradual reduction in the number of parameter sets that have posterior likelihood values significantly greater than zero, thus constraining the number of acceptable simulations of the catchment. This approximates to convergence on an optimal set of parameter values in traditional model calibration. However, GLUE explicitly allows that the 'optimal' set of parameter values may vary from period to period of observation and will reflect evolution of posterior likelihood distribution with the addition of new observations. It also allows for the possibility that there may be more than one region of high likelihood values in the parameter space. Hence an 'optimal' parameter set and the appearance of convergence to an 'optimal' set is not likely. As more observations are taken into account, behavioural parameter sets are retained, and non-behavioural parameter sets are excluded, and replaced by behavioural sets by resampling the response surface. Because sampling is done uniformly along each parameter axis, new sample sets may be added by continuing to sample uniformly along each axis from the posterior distribution defined by the existing sets of values. Beven and Binley (1992), using a likelihood function based on the sum of squared errors for the Gwy catchment, found that the distribution of predicted discharges appeared approximately Gaussian at some timesteps and highly skewed at others, thus precluding the normal calculation of uncertainty limit as a function of the variance of the predicted values. They also note that from timestep to timestep the position of any particular simulation run within the distribution will vary. Hence, a run that over-predicts in one timestep may under-predict in another, due to interaction between individual parameters and the dynamics of the model. This implies that the uncertainty limits cannot be related directly to a variance of estimation for individual parameter values, but must be associated with a set of parameter values.

Bayesian updating is a means of overcoming the problem of ill-conditioning mentioned above and in sections 2.9.1 and 2.9.2, whereby model complexity is not matched by the information content of the observed hydrograph – often the only source of calibration data. Different types of observed data can be utilised in different ways to refine the model. Franks *et al.*, (1997) suggest the use of information of saturated areas extent as a source of measurable or observable data about the internal state variable. They used Radar remote sensed data in combination with the TOPMODEL index to derive a Saturation Potential Index (SPI), which was used to update likelihood values for discharge predictions. The use of remotely sensed data as a secondary data source in this way is not ideal, as the method of data extraction from remote sensed images is a potential source of additional error. Nevertheless, they report a reduction in the range of predicted discharges, thus constraining the number of feasible parameter sets. Lamb *et al.*, (1998) used three different types of data to modify likelihood measures within TOPMODEL. They used observed flow, continuously logged borehole water levels, and more extensive (over 100) spatially distributed water table depth data. They showed how distributed likelihood measure, L changes, as different types of observation data are considered. While they report a reduction in uncertainty bounds when data from a second flow observation period was used on the same data, they found that the use of observed water level data to update uncertainty within TOPMODEL, served to widen the uncertainty bounds rather than constrain them. They report that the largest change in likelihood distributions was obtained for m and K_0 , the most sensitive parameters in TOPMODEL, both resulting in a change in the likelihood bounds. The less sensitive saturated zone parameters $SRMAX$ and t_d were least affected, with their parameter distributions reverting to the uniform distribution curves, while the effective porosity was modified, but with little refinement to the uniform prior distribution. The failure of water level data to restrict the uncertainty bounds, in this case, illustrates the fact that, although internal state variables are, in theory, a better test of model performance in validation exercises, most require measurements at scales much smaller than the grid or catchment scale, which are rarely available. Hence predictions and measurements refer to different, incommensurate quantities, making validation difficult. Lamb *et al.*, (1998) used spatially lumped measurements of water table depths, but attributed the failure to constrain uncertainty to the need to incorporate a distributed soils component or empirical correction factor into TOPMODEL, to better relate the topographic index to

measured water table depths, as also suggested by other studies (e.g. Jordan, 1994; Lamb *et. al.*, 1997; Seibert *et. al.*, 1997).

It may be necessary to determine the value of each type of additional data in the modelling procedure, before use in uncertainty updating. This can be done objectively using uncertainty measures that are associated with the predictions, but which are insensitive to the sampling limitations of the Monte Carlo procedure, such as the Shannon Entropy measure, H , and the U-uncertainty measure (Klir and Folger, 1988).

Bayesian updating may also be useful in scenario modelling. The posterior distributions obtained from Bayesian updating may be used directly to evaluate the uncertainty limits for future events for which observed data may not be available. If however, the changed conditions to be considered involve changing parameters or boundary conditions, then there will clearly be additional uncertainty associated with the changed conditions relative to a model calibrated using the GLUE procedure to the present condition of the catchment (Beven and Binley, 1992). A subjective definition of prior likelihood weights associated with the realisations for the new conditions will be required.

4.6 Summary of Model developments

The hydrological model used here is based on TOPMODEL (Beven and Kirkby, 1979) with developments by Brasington (1997), while the sediment yield model is based on that of Moore and Clarke (1983) and Moore (1984). Further model developments made as the basis of this thesis are:

1. Implementation of a snowmelt model based on the hour-to-hour degree day method to include a conceptual model of runoff from frozen soil developed here.
2. Coupling the sediment yield model and the hydrological model.
3. Bayesian updating of the hydrological model uncertainty using sediment yield model predictions and the evaluation of uncertainty propagated from the hydrological model to the sediment yield model.

Snowmelt Model Implementation

The model of Bengtsson (1984) for hourly snow melt, is implemented within a fully distributed topography-based hydrological model, which provides the framework for distributing air temperature as a functions of elevation and hence the distribution of snow accumulation and melt. The method of implementation reflects the perceptual model of snow accumulation, snowmelt and runoff from frozen soils within this upland UK catchment. The proportioning of the spatially distributed precipitation, comprising rainfall and melt-water, into direct runoff and infiltration is done in a unique manner, which attempts to capture the pattern of variability in response with temperature.

Hydrological and Sediment Yield model coupling

The sediment yield model used here is based on that of Moore and Clarke (1983) and Moore (1984), but makes use of the fully-distributed framework of the hydrological model to drive sediment availability and removal rather than their original distribution function approach. The log-normal distribution function adopted here to translate eroded sediment to the outlet is a unique alternative to the inverse-Gaussian approach used by Moore and Clarke (1983) which retains the positively-skewed, unimodal, and heavy-tailed properties of the inverse-Gaussian density function, but is easier to implement within the finite difference framework of the hydrological model.

Bayesian Updating and Evaluation of Propagated Uncertainty

Model calibration and validation are done within the GLUE framework with Bayesian updating using both hydrological response, and sediment yield data. The use of additional flow periods to update model uncertainty has been previously reported (Beven and Binley, 1992; Freer *et. al.*, 1996; Franks *et. al.*, 1997; Lamb *et. al.*, 1998). However the use of data from a secondary model to update hydrological uncertainty has never been reported. This novice approach is an attempt to evaluate the importance of secondary data in reducing uncertainty in primary hydrological models. The analysis also presents an assessment of the uncertainty propagated from the primary hydrological model to the secondary sediment yield model, which has not been previously reported. This approach attempts to acknowledge the need to evaluate and reduce uncertainty in the primary hydrological model before coupling with a secondary model – a need ignored in model coupling to date.

4.7 Model Implementation and Analysis

All model developments have been conducted within FORTRAN F77. The GLUE procedure was implemented using the NAG subroutines within FORTRAN. Appendix 1 contains a complete FORTRAN listing of the coupled model. While the procedure is computationally demanding, one advantage of the GLUE methodology is the ability to use as many realisations as possible to calibrate the model. Hence it was decided that, in the interest of minimising computational time, the minimum required number of simulations would be used. Given that the model is fully distributed, requiring computations at each of 94622 grid cells (241x392), it was decided that only 1000 simulations would be used, this being a reasonable compromise between model speed and accuracy. Even so, each 1000 runs of the model took a minimum of three days on a SUN OS 5.6 workstation.

The model described above is implemented to examine uncertainty in model predictions for a lumped spatial parameterisation as well as spatially distributed parameterisations.

The simplifying assumption of subsurface-flow dynamics as a function of surface topography, used in the hydrological model, limits the representation of spatial heterogeneity of hydrological response due to factors other than topography. Spatial variability of local soil transmissivity, soil structure, soil depth etc., will cause differences in the temporal and spatial variability of hydrological response. When introduced to the model these factors will give spatially and temporally variable model predictions that might be different from spatially lumped observations. Of great importance, is the possible improvement in the spatial pattern of response, that spatially variable parameterisation may offer.

Two approaches are used to assess effect of spatial heterogeneity on model predictive uncertainty – deterministic parameterisation based on landuse and soil type data and random parameterisation.

The results of the analysis for the spatially lumped parameterisation, deterministic spatial parameterisations, and random spatial parameterisation respectively are presented in the next three chapters.

CHAPTER 5 – Lumped Spatial Parameterisation

5.0 Summary

The results of lumped landuse, soil and rainfall parameterisation of the model described in chapter 4 are presented. The procedure adopted is based on the GLUE and Bayesian methods discussed in chapter 4 and can be summarised as follows:

1. *Hydrological model calibration.* GLUE analysis was done using 1000 Monte Carlo simulations. The results were used to assess parameter sensitivity and to determine the degree of uncertainty as explained below. Uncertainty bounds were derived and the ‘optimum’ parameter set determined for the calibration period. Validations were done on two other events.
2. *Sediment model calibration.* Keeping hydrological parameters constant at the ‘optimum’ values obtained in 1 above, GLUE analysis was carried out varying the sediment yield parameters (1000 simulations). Uncertainty bounds were obtained, and the ‘optimal’ sediment yield parameter set determined.
3. *Bayesian Updating.* Using the ‘ideal’ sediment parameters as fixed input, the model was run with all of the original randomly selected hydrological parameter sets. The behavioural hydrological parameter sets for which the sediment yield predictions were also behavioural were retained, and used to determine the posterior likelihoods of the hydrological model. The hydrological model uncertainty was then updated in two ways. First, new uncertainty bounds were derived, based on a simple rejection of the previously behavioural hydrological parameter sets that prove to be non-behavioural for the sediment yield model. Second, Bayesian updating was done using two different hydrological-sediment yield combined likelihood measures.
4. *Error propagation.* The propagation of predictive uncertainty from the hydrological model to the sediment yield model was assessed, by determining the uncertainty bounds for constant ‘ideal’ sediment parameters and varying hydrological parameters.

The chapter is organised as follows. The choice of events used for model calibration and validation are discussed in the introduction. The hydrological model calibration results, including the analysis of the snowmelt model are presented, followed by the model validation, which is followed by the calibration and validation of the sediment yield model. Each calibration and validation begins with a parameter sensitivity analysis, followed by an uncertainty analysis and the results of spatial predictions. The final section deals with the Bayesian updating of likelihoods, and the propagation of error in the coupled model.

5.1 Introduction

The analysis is conducted on three events with fairly different characteristics, from November 1998 to March 1999 – the period for which both suspended sediment concentration data and flow data are available (Table 5.1). Model calibration is conducted on Event 1, a 405hr event from 04/11/98 at 23:00 to 21/11/98 at 19:00, which has a total rainfall depth of 0.0704m, maximum intensity of 0.0086mhr^{-1} , total observed runoff, 0.050813m, and runoff coefficient of 72.18%. This event was chosen for model calibration as it represents a relatively typical early-winter event in terms of total rainfall depth and discharge, based on an analysis of 10 years worth of data for the catchment. In addition the highest rainfall intensity for the year occurs during this event. Also of great importance is the fact that it contains periods of precipitation at sub-zero temperatures, which can be used to test the snowmelt model performance.

The first validation event - Event 2 - is a 324hr event from 10/12/98 at 07:00 to 23/12/98 at 19:00, which has a total rainfall of 0.022m, maximum intensity of 0.0046mhr^{-1} , observed runoff of 0.028034m corresponding to a runoff coefficient of 127.4%. This is actually a relatively small event with rainfall depth and intensity, typical of a summer storm, which provides the opportunity to examine model performance on a low intensity event. While it isn't directly comparable to a summer event, given that both antecedent soil moisture deficit, and evapotranspiration rates, would be lower than that of an equivalent summer storm, it will give some indication of low flow performance.

The second validation event - Event 3 - is a 500hr event from 21/02/99 at 11:00 to 14/03/99 at 07:00, which has a total rainfall depth of 0.2542m, and maximum intensity of 0.007mhr^{-1} . The maximum duration is a 91-hour period, during which 0.1854m of rain fell. A total observed runoff of 0.241m and potential evapotranspiration of 0.115m during the event suggest that 0.1018m more runoff occurred, than was available. This is attributable to the melting snow that had been on the ground for approximately one week prior to the rainfall event. The combination of melting snow and high intensity, long-duration rainfall resulted in the severe flooding of the North York Moors. Model validation on an event of this magnitude will be a test of the capability of the model to perform well in extreme events.

Event Characteristics	Event 1	Event 2	Event 3
Total rainfall depth (m)	0.0704	0.0220	0.2542
Maximum Intensity (mhr^{-1})	0.0086	0.0046	0.0070
Total runoff (m)	0.0508	0.0280	0.2410
Runoff coefficient (%)	72.18	127.40	94.81
Potential Evapotranspiration (mhr^{-1})	0.09229	0.0505	0.115
Total sediment flux (gm^{-2})	1.125	0.217	25.16
Maximum sediment flux ($\text{gm}^{-2}\text{hr}^{-1}$)	0.048	0.011	1.220
Event Duration (hrs)	405	324	500
Dates	11/98	12/98	02/99 – 03/99

Table 5.1 Characteristics of events used in the analysis.

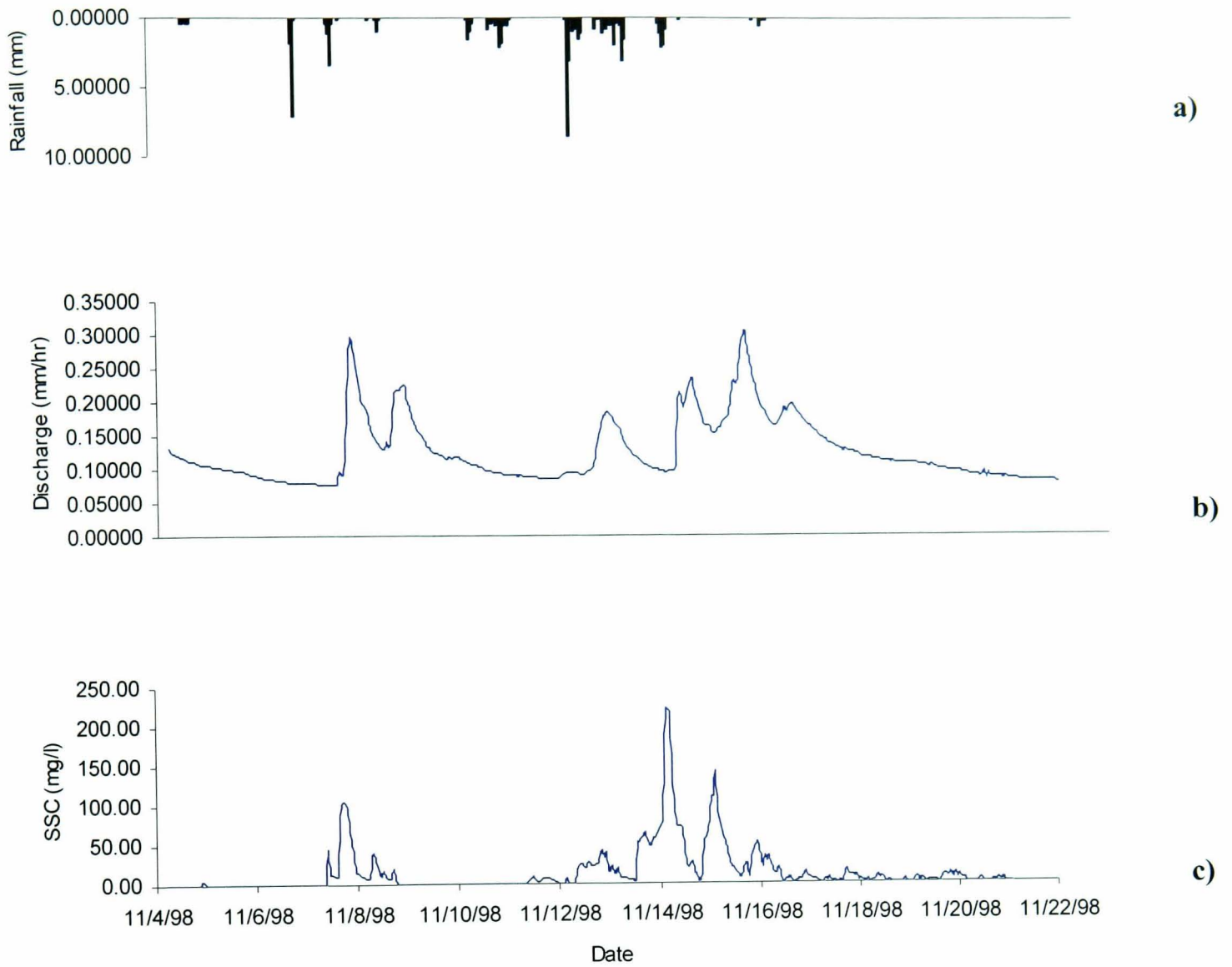


Fig. 5.0 a) Rainfall b) Discharge and c) Suspended Sediment Concentration for the calibration period – Event 1.

5.2 Model Implementation

Initial Conditions

Unlike TOPMODEL, initial conditions in the saturated zone cannot be set analytically, and instead, are estimated by allowing the catchment to dry from a fully saturated condition until the predicted exfiltration runoff equals total observed flow. All simulations are started, when possible, following a dry period, so that the total observed flow could be assumed to consist of exfiltration discharge alone. This method implicitly defines the distributed initial conditions for both unsaturated stores and the saturated zone deficit.

5.3 Operational Testing - Sensitivity Analysis, Parameter Calibration and Uncertainty Estimation

5.3.1 Hydrological Model Results and Analysis

The lumped hydrological model has a minimum of eight parameters, which include the TOPMODEL parameters, K_0 , m , $SRMAX$, the water loss parameters, GWL and ETF , the routing parameters V_h and V_c , and the snowmelt parameter, SMF . Table 5.2 summarises the function of each model parameter. The snowmelt factor was calibrated manually, and its value fixed at 9.4×10^{-5} for the remainder of the analysis. The model response was found to be relatively insensitive to SMF .

Parameter	Units	Function
m	m	Defines the rate of change of conductivity with soil moisture deficit. It may also be interpreted as a recession coefficient and the effective depth of the soil profile
K_0	mhr^{-1}	Saturated hydraulic conductivity of the soil profile when just saturated
$SRMAX$	m	Root zone storage capacity
GWL	mhr^{-1}	Defines the rate of seepage losses from the base of the perched water table
ETF	N/a	Evapotranspiration factor
V_h	mhr^{-1}	Velocity of flow on the hillslope
V_c	mhr^{-1}	Velocity of flow in channel
SMF	N/a	Snowmelt factor

Table 5.2 Summary description of model parameters.

5.3.2 Parameter Sensitivity Analysis

An analysis of parameter sensitivity was conducted using the Monte Carlo results in two different ways. First, scatterplots were constructed for each parameter by plotting parameter values for each simulation against model efficiency. The use of scatterplots is a departure from traditional methods of parameter sensitivity analysis such as factor perturbations. Such traditional methods do not permit evaluation of parameter interdependence and interaction. The use of Monte Carlo simulations, in which all parameters are varied simultaneously, implicitly incorporates both parameter interdependence and interaction, and the stochastic nature of parameter variability. The output from this analysis does not yield a one-to-one mapping of parameter values to model efficiencies, but specifies a range of model efficiencies that can be obtained for a given parameter value, accepting uncertainty in the remaining parametric framework of the model. Scatterplots can provide a good visual assessment of the performance of individual parameter values, and any trends within the data, when there is a discernible difference in model efficiencies for different parameter values. Fig. 5.2 shows the scatterplots for five of the model parameters, conditioned on Event 1. These are discussed later in conjunction with the results of the second method of sensitivity analysis – the Generalised Sensitivity Analysis (GSA).

Generalised Sensitivity Analysis

Generalised Sensitivity Analysis (Hornberger and Spear, 1981), is a further approach, utilising random searches in an attempt to evaluate combinational parameter sensitivity. The results are categorised as either behavioural, B, or non-behavioural, \bar{B} (Fig. 5.1). An indication of sensitivity is then obtained for each parameter θ , by summing the likelihood of these two categories and scaling to unity. The result is used to construct probability distributions for each parameter. In addition, the likelihood weights from the entire set of simulations are summed and scaled to unity to derive the *a priori* ‘parent’ probability distributions created for each parameter.

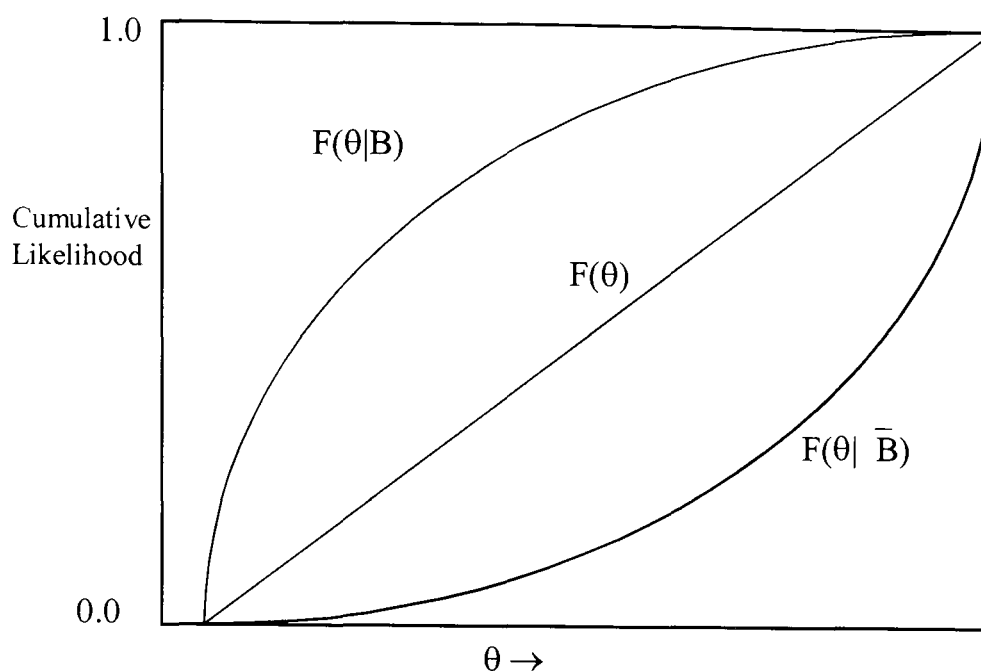


Fig. 5.1 Definition diagram for GSA; after Hornberger and Spear (1981); $F(\theta)$ = parent; a priori distribution for parameter θ ; $F(\theta|B)$ = distribution of θ in the behavioural category; $F(\theta|\bar{B})$ = distribution of θ in the non-behavioural category.

This parent probability distribution can be likened to a null hypothesis, and the degree (or lack) of separation between the behavioural and non-behavioural simulations can then be used to infer the significance of a parameter within the model. That is, if behavioural and non-behavioural distributions are similar then the parameter is insensitive. Hornberger and Spear (1981) applied GSA to evaluate sensitivity in a simple parametric eutrophication model. They were then able to rank parameters in order of sensitivity using the statistical significance of separation measured by the nonparametric Kolmogorov-Smirnov two-sample test.

The specification of a criterion used to separate B from \bar{B} in GSA, like GLUE is subjective. In order to reduce this subjectivity, the Monte Carlo simulations can, alternatively, be grouped into a number of sets corresponding to ranked intervals of likelihood function, and not simply into two categories (Freer, *et. al.*, 1996). Here, cumulative likelihood (the likelihood measure is described in section 5.3.3) distribution functions for the key model parameters were derived for six classes of model efficiency, as follows: $eff < 0\%$; $0\% \leq eff < 20\%$; $20\% \leq eff < 40\%$; $40\% \leq eff < 60\%$; $60\% \leq eff < 80\%$; $eff \geq 80\%$. The number of simulations in each group was:

323; 76; 72; 135; 296; 98 respectively. Although no group is recognised to directly reflect non-behavioural simulations, group 1 ($eff < 0$) represents parameterisations in which model predictions are non-informative (i.e. containing less information than the mean observed flow) and as such this distribution provides a baseline for comparison.

Results of Sensitivity Analysis

The scatterplots (Fig. 5.2) demonstrate that high efficiencies can be obtained throughout the full range of $SRMAX$ and ETF . Although high efficiencies can also be obtained for a broad range of K_0 and $CHV2$ values, both parameters show slight peaks; K_0 peaks at approximately 275mhr^{-1} , and $CHV2$ at approximately 0.5ms^{-1} . The most sensitive parameter is m , with only a limited range between 0.04 and 0.06m for which high model efficiencies are obtained.

An examination of the GSA plots shown in Fig. 5.3 reveals a high degree of separation between the distributions of high and low efficiency groups for m . For $eff < 0\%$, the distribution rises steeply from $m=0.01\text{m}$ and attains a cumulative likelihood of 1 at $m=0.02\text{m}$, implying that low values of m (0.01m and 0.02m) yield very low model efficiencies. Distributions for efficiencies between 20% and 60% show increasingly higher values at which cumulative likelihood of 1 is attained. Distributions for efficiencies greater than 60%, however, indicate no changes in cumulative likelihood until values between 0.04m and 0.06m. As such, this result confirms the earlier observation that m values between 0.04m and 0.06m are good simulators of the system.

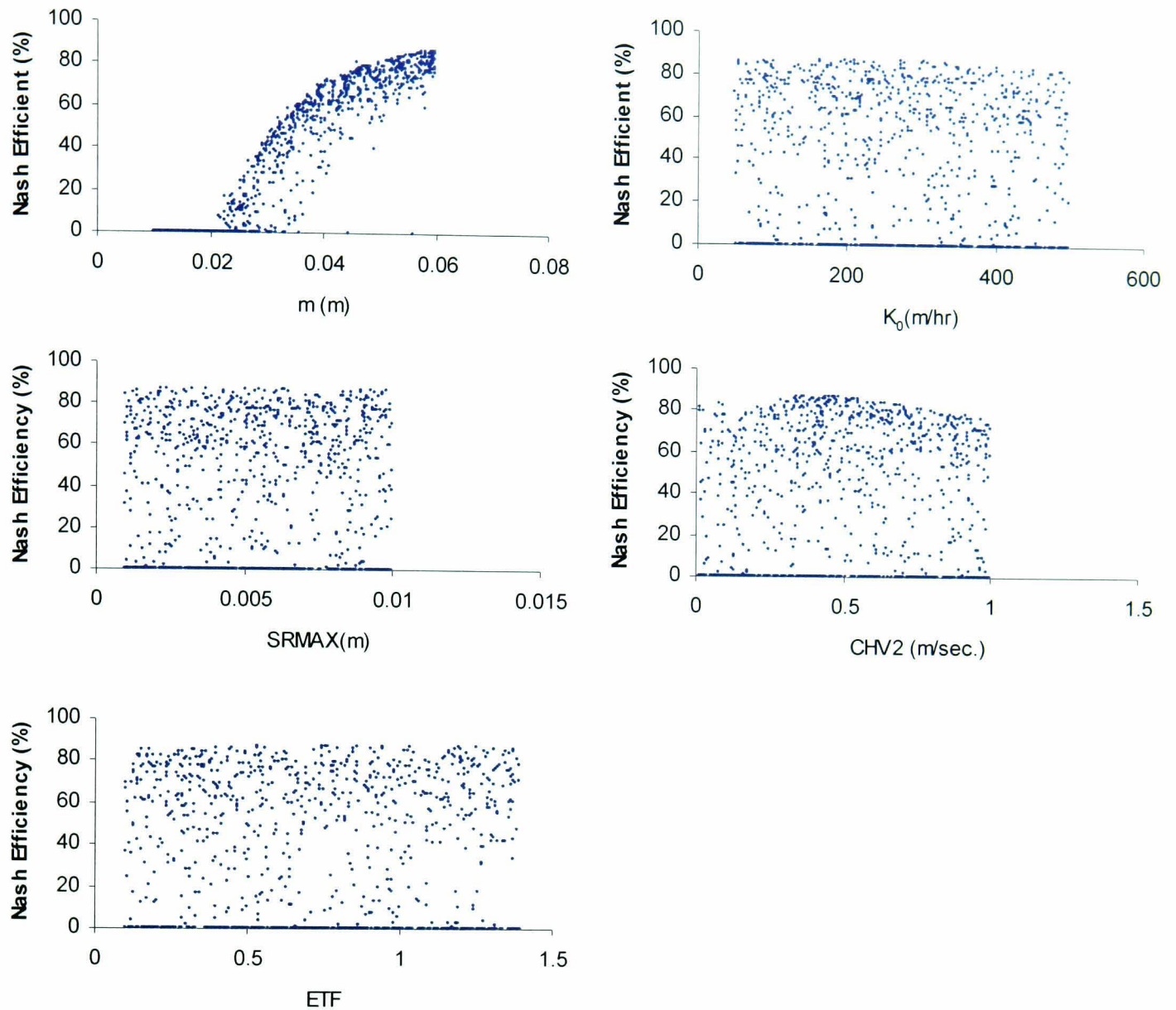


Fig. 5.2 Scatterplots of five of the model parameters against model Efficiency for calibration event – Event 1 (04/11/98 to 21/11/98).

K_0 shows considerably less sensitivity than m . Distributions of all efficiencies plot to approximately straight lines, with very little variability between high and low efficiencies. This is confirmed by the scatterplot which shows that the entire range of values of K_0 can give the entire range of efficiencies, with only a slight peak apparent at $K_0 = 275\text{mhr}^{-1}$. This peak is only just discernible in the GSA plot in which the distribution for $eff > 80\%$ shows a slightly larger degree of separation from the other distributions at approximately $K_0=275\text{mhr}^{-1}$.

Of the five parameters, SRMAX shows the smallest degree of separation with similar distributions for all five classes. Even for $eff > 80\%$ the distribution is spread across

the entire range of values considered - a trend also evident in the efficiency scatterplot. Similar results have been obtained in other TOPMODEL applications (e.g. Lamb *et. al.*, 1998).

The channel flow velocity parameter, $CHV2$, exhibits more separation between behavioural and non-behavioural simulations, indicating sensitivity in two distinct areas of the sampled parameter range. For $eff < 0\%$ the cumulative likelihood increases rapidly from $CHV2 = 0$ to 0.2ms^{-1} , while $eff > 80\%$ shows little response. The cumulative likelihood of $eff > 80\%$ then rises rapidly from approximately $CHV2=0.35$ to 0.7ms^{-1} , and then less rapidly above 0.07ms^{-1} , while the increase in $eff < 0\%$ is much slower. Parameter sensitivity is lowest at approximately $CHV2=0.46\text{ms}^{-1}$ where the distributions for $eff < 0\%$ and $eff > 80\%$ intersect. ETF , similarly, shows two distinct areas of higher sensitivity and an area of reduced sensitivity. The distribution for $eff < 0\%$ rises rapidly for $ETF=0.1$ to 0.2 while there is little response for $eff > 80\%$. The distribution for $eff > 80\%$ then rises rapidly from $ETF=0.3$ to 0.7 , while that of $eff < 0\%$ rises less rapidly. Sensitivity is a minimum at $ETF=0.5$.

The model parameters can thus be ranked according to sensitivity, as follows:

$m > ETF > CHV2 > K_0 > SRMAX > CHV1$. This pattern reflects the role played by m in determining the exact form of the hydrograph recession. The relative importance of ETF reflects the dependence of hydrological response on evapotranspiration rates as is evident in the distinct seasonality in the hydrograph due to the higher evapotranspiration rates in summer than in winter (see section 3.6.3). The sensitivity of $CHV2$ reflects its importance as a control in flow routing, and hence the timing of hydrograph peaks. The relative insensitivity of K_0 is perhaps indicative of its interaction with m in controlling recession rates. Hence, the high sensitivity of m might have masked the sensitivity of K_0 .

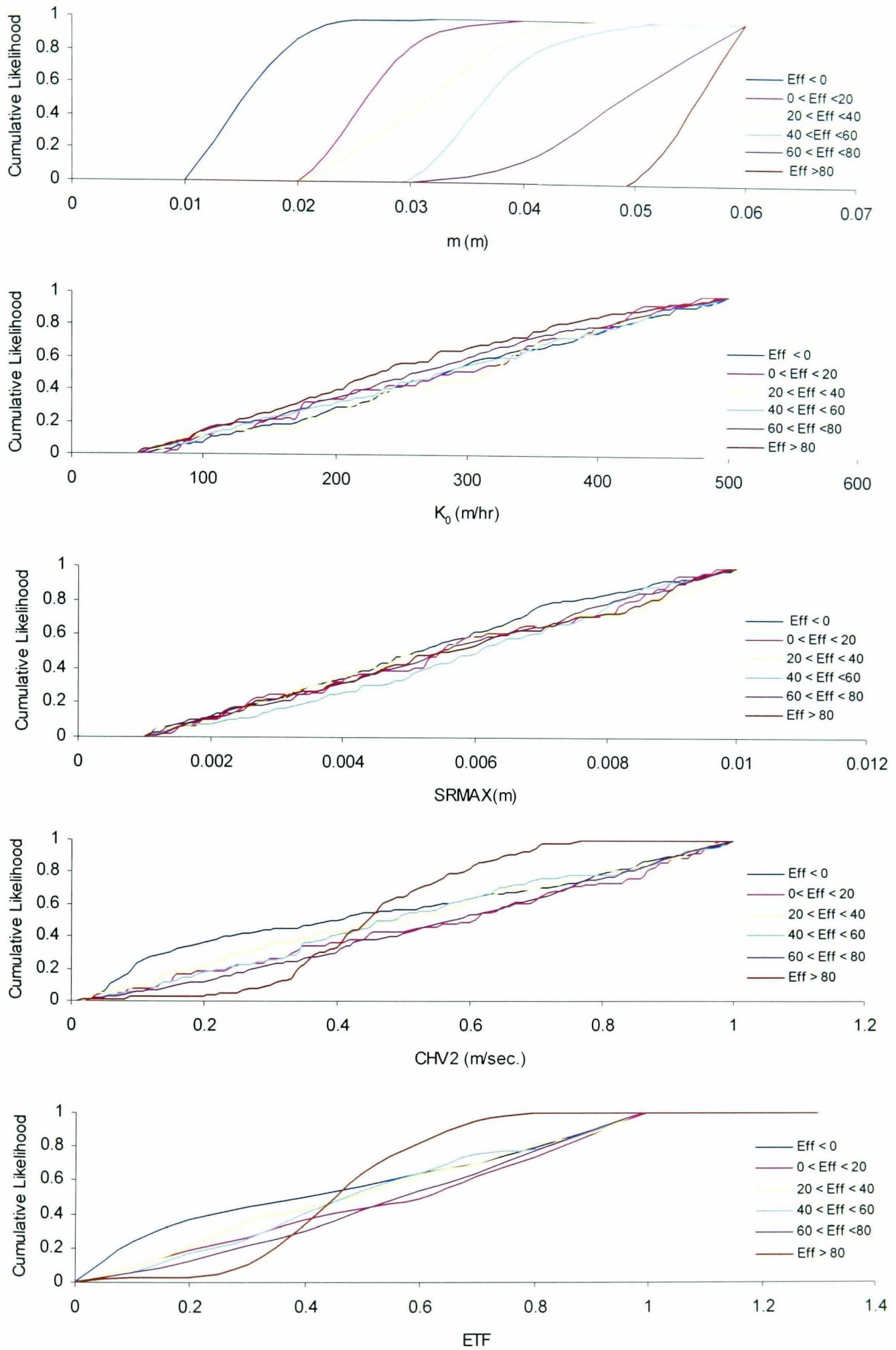


Fig. 5.3 Generalised Sensitivity Analysis plots for five model parameters conditioned on event 1.

5.3.3 Model Calibration and Uncertainty Estimation

The likelihood measure chosen for the GLUE analysis is the model Nash efficiency after Nash and Sutcliffe (1970).

$$Eff(\%) = 100 * \left[\frac{(Q_{obs} - Q_{pred})^2}{(Q_{obs} - \bar{Q}_{obs})^2} \right] \quad [5.1]$$

A rejection criterion of 40% for the hydrological model was arbitrarily selected in order to perform the analysis on well-conditioned simulations. Following the procedure outlined by Beven and Binley (1992), likelihood weight was assigned to all behavioural simulations where:

$$L_i = \frac{Eff_i}{\sum_1^{N_b} Eff_i} \quad [5.2]$$

in which L_i is the likelihood weight, Eff_i is the efficiency of the i^{th} behavioural simulation and N_b is the number of behavioural simulations. If the simulation is non-behavioural ($Eff < 40\%$), then L_i is given a value of -1 and rejected from the analysis.

The likelihood is then assigned to the discharge obtained for each timestep in the given behavioural simulation, and all discharges and likelihoods for a given timestep, are grouped together. Frequency distributions of discharges for each timestep in the event are constructed and the 95% confidence intervals are derived, and used to construct the uncertainty bounds of the event, resulting in an envelope of possible predictions rather than a single hydrograph.

Fig. 5.4 shows the results of the hydrological model calibration on Event 1. The number of behavioural simulations obtained, N_b , is 529 (from 1000 simulations). The uncertainty bounds of Fig. 5.4c are widest at peak flow – in particular the fourth peak - but narrower for recession flow. There are periods during the calibration, particularly during recession flows, when the observed discharge falls outside of the 95% limits, indicating significant predictive failure.

This uncertainty in peak flows may be due to the insensitivity of K_0 , which governs the rate of vertical recharge to the saturated zone and hence, along with m , controls peak flow. As discussed above, there is a wide range of K_0 values for which behavioural simulations are obtained, and hence, a wide range of behavioural peaks predicted. The smaller uncertainty bounds in the recession flow point to the fact that m , which is the primary control on recession flow, is a much more sensitive parameter, which gives behavioural simulations for only a small range of values. The timing of the peaks is very good, pointing to the sensitivity of the routing parameter $CHV2$.

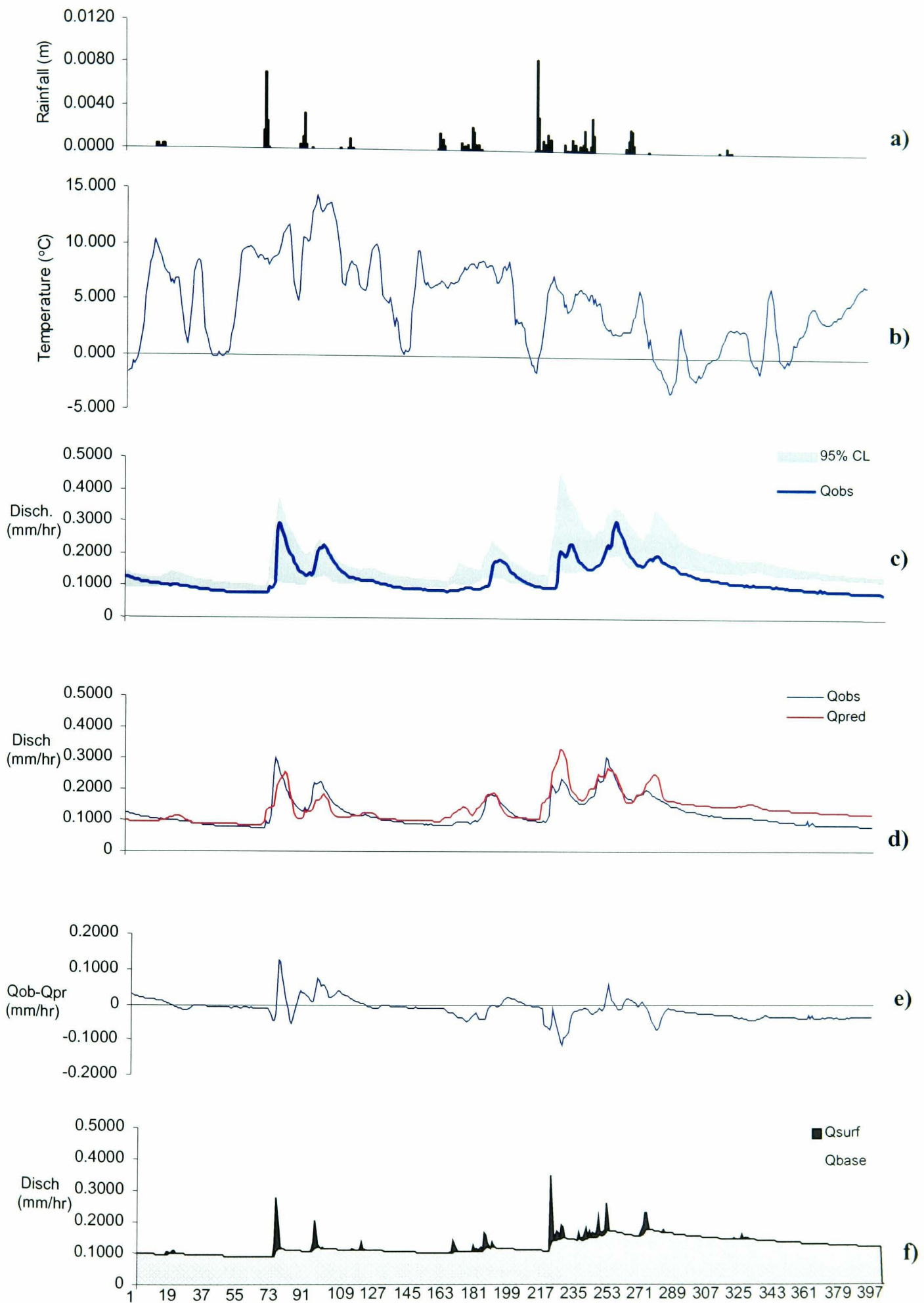


Fig. 5.4 Calibration results for storm 1 (/11/98 - /12/98). (In f) Q_s is surface runoff Q_b is baseflow).

The effect of changing the rejection criterion was examined (Fig. 5.5) using efficiencies of 0%, 20%, 30%, 40%, and 60%. The number of behavioural simulations, N_b , obtained for each rejection criterion was: 677; 601; 573; 529; 394 (from 0% to 60% respectively). There is no reduction of the predictive failure, with change of rejection threshold, but marginally narrower uncertainty bounds were obtained for a rejection efficiency of 60% (Fig. 5.5e). Hence relaxing the rejection threshold to define a larger proportion of the total number of behavioural simulations resulted in only slight modifications to uncertainty bounds, and no improvement in the predictive failure of the modelled recession flow. This insensitivity to rejection threshold may be attributable to large discrepancies between the ‘best’ and the ‘worst’ simulations, such that the simulations fall within the tails of the cumulative distributions of L , and have little effect on the location of the uncertainty bounds, as was also found by Lamb, *et. al.*, (1998). It may also be due to the relatively small number of iterations undertaken, and the relatively narrow range of parameter values sampled which, when combined, will restrict the possible parameter combinations used, thus resulting in relatively ‘similar’ parameter sets with hence ‘similar’ simulation efficiencies.

It is important to note that the rejection criteria used are based on an evaluation of the model performance for simulation of streamflow alone. Beven (1993) suggests that other qualitative criteria may be incorporated into GLUE. For example, parameter sets that predict behaviour inconsistent with the modeller’s perceptual model of catchment response, could automatically be excluded from the behavioural set. The GLUE methodology also offers the potential to incorporate multiple measures of model performance, so that streamflow predictions can be considered together with internal state predictions compared to observations of soil moisture (or water table). Water table depths are, however, not always readily available, as is the case here, and are expensive and time-consuming, to effectively characterise.

Also noteworthy is the fact that more than one data set can be used to evaluate behavioural parameter sets. Here, the validation events are used to further refine the uncertainty bounds, thus allowing for further rejection or acceptance of parameter sets.

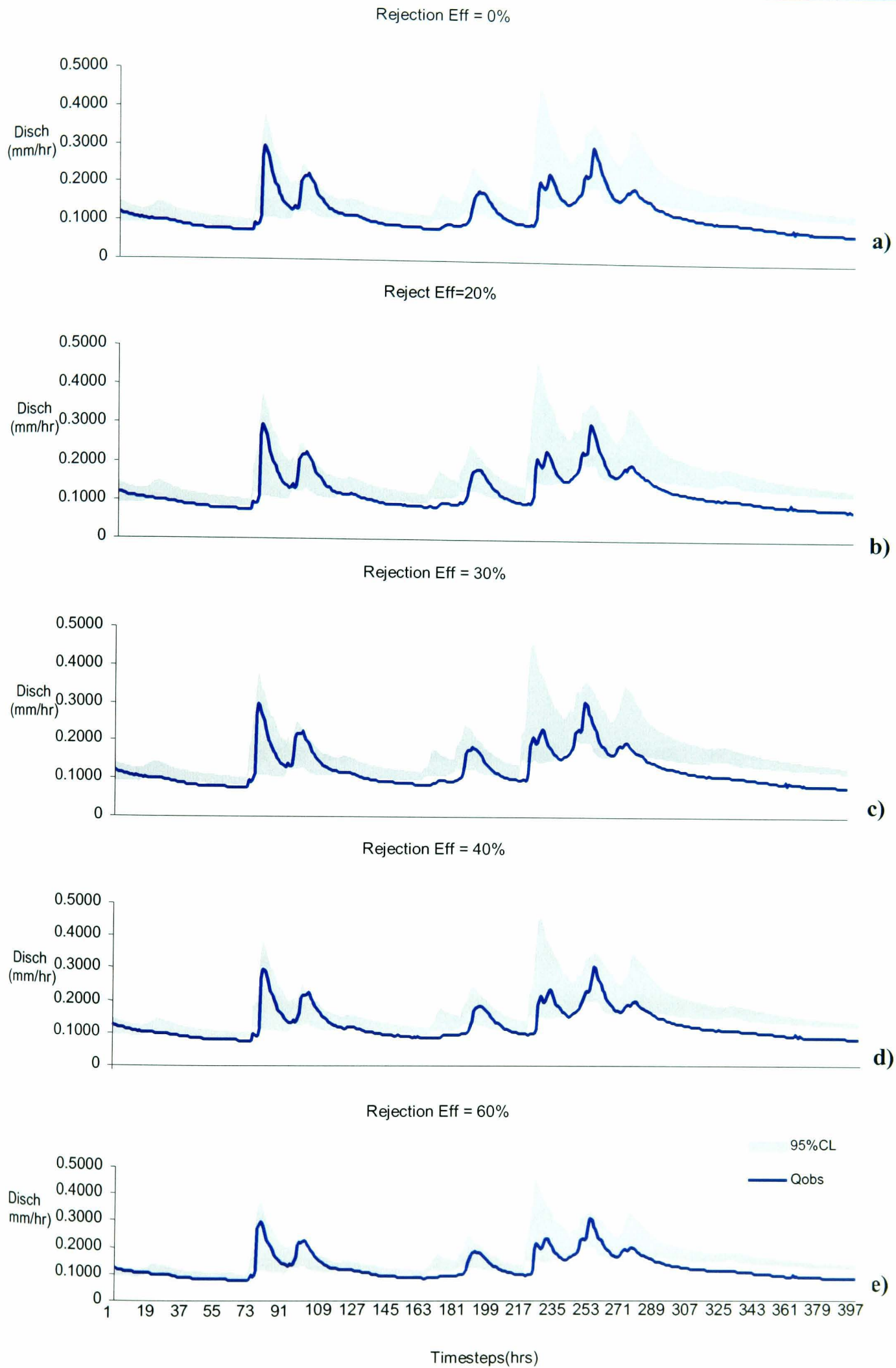


Fig. 5.5 95% Confidence limits for rejection efficiencies of 0%, 20%, 30%, 40% and 60%.

m (m)	K₀ (m/hr)	SRMAX (m)	CHV2 (m/s)	ETF	Nash Eff (%)
0.05947	271.7395	0.00372	0.46237	0.76232	87.16151
0.05962	210.49420	0.00237	0.46859	0.75772	87.01835
0.05896	163.35056	0.00326	0.36382	1.24867	86.91273
0.05989	303.30136	0.00625	0.35659	0.74380	86.75705
0.05809	196.10312	0.0050	0.43418	0.53289	86.74942
0.05964	236.53275	0.00505	0.34070	0.86118	86.69132
0.05936	54.57312	0.00922	0.45260	1.0317	86.66538
0.05752	163.09613	0.00221	0.44739	1.18920	86.45853
0.05905	331.19006	0.00578	0.47678	0.90394	86.41485
0.05690	86.66100	0.00891	0.41555	1.1995	86.03596

Table 5.3 The ten ‘best’ parameters sets as conditioned on event 1.

Table 5.3 lists the top ten parameter sets according to model efficiency. There is very little variability in the value of m for the top ten simulations, which confirms the sensitivity of m within the model. $CHV2$ also shows very little variability, while K_0 shows the widest variability.

Fig. 5.4d, a plot of the observed and ‘optimum’ hydrographs, shows that 87% of the observed flow is accounted for, with 4.05% of flow predicted being saturation excess overland flow, and 95.95% baseflow. This is confirmed in Fig. 5.4f, which shows that baseflow dominates the response for most of the event.

Analysis of Snowmelt Model performance

An examination of the temperature curve (Fig. 5.4b) suggests that the over-prediction of the fourth peak and the predictive failure of recession flow might be related to snowmelt, or runoff from frozen soils. The fourth peak is the result of precipitation occurring at the highest annual intensity, at sub-zero temperatures, suggesting a snowfall event. Hence the fourth observed peak is small, compared to the fifth peak, which would have occurred when the snow melted. However, the model over-predicts peak four and under-predicts peak five, suggesting a failure of the snowmelt model to fully characterise the accumulation and subsequent melting of the snow. Closer examination of the temperature curve, however indicates that there is only a small period during precipitation when the temperature is below zero – the critical

temperature used in the snowmelt model. Hence, the model would have accumulated snow when precipitation occurred, but would have allowed it to melt in the next timestep when the temperature increased above zero. The fact that this isn't reflected in the observed hydrograph suggests that a critical temperature of zero may not be adequate to characterise the event, which might be better represented by a higher critical temperature. An analysis of the effect of varying the critical temperature for snowfall (Fig. 5.6a) shows that the use of critical temperatures increasingly higher than 0°C results in no improvement in model prediction. The effect of runoff from frozen soil was also investigated as a possible explanation for the predictive failure, especially in the recession flow. The model allows for reduced infiltration on frozen soil if there are between 5 and 10 hours prior to the rainfall event, for which temperatures are sub-critical. Fixing the critical temperature at zero (given the insensitivity to different critical temperatures, it was felt that this should be retained), the number of prior sub-critical temperatures was varied as follows: between 2 and 10, 3 and 10, 4 and 10. Fig. 5.6b shows that there is no change in prediction with number of prior sub-critical temperatures. The lack of sensitivity to critical temperature, and to the number of prior hours of sub-critical temperatures, is perhaps attributable to errors in input data associated with the inefficiency of raingauges in recording snowfall, or any of the problems associated with snowmelt modelling as discussed in chapter 4. Fig. 5.6c is a plot of hydrographs for different percentages of total precipitation that is allowed to runoff directly due to reduced infiltration on frozen soil. As the percentage of direct runoff increases, the predicted recession decreases, but the larger the peak flows, resulting in an improved recession, but increased predictive failure in the peaks. A possible improvement may be to use a melt water equivalent factor (w_e in equation 4.23) less than 1, but to allow the 'loss' to occur only in the direct runoff component, but retain the reduced infiltration rate component. This loss would have to be accounted for in the water balance of the catchment, perhaps by using temporally variable Penman evaporation (E_0 in equation 4.3) to reflect the variable loss rates.

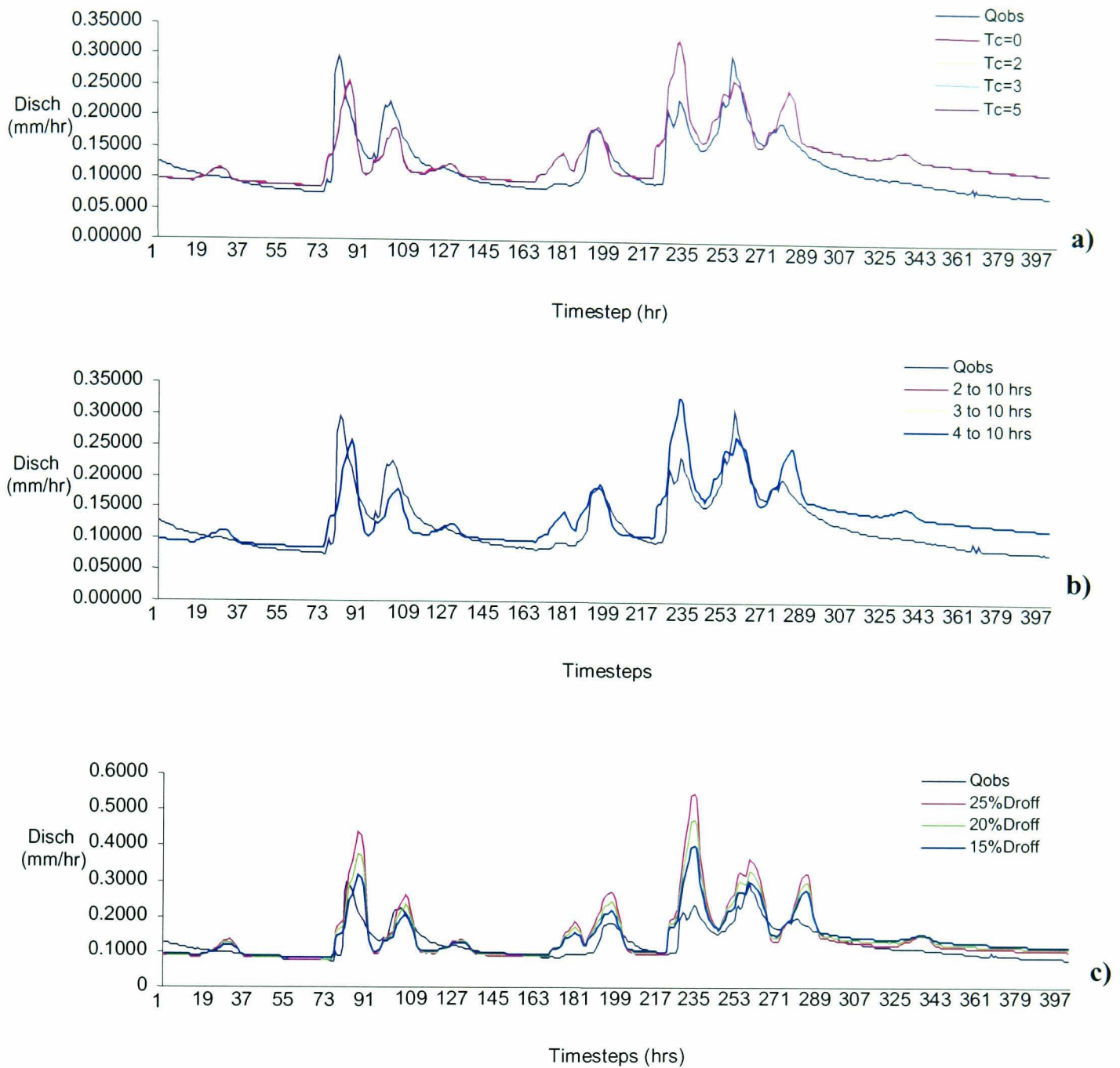


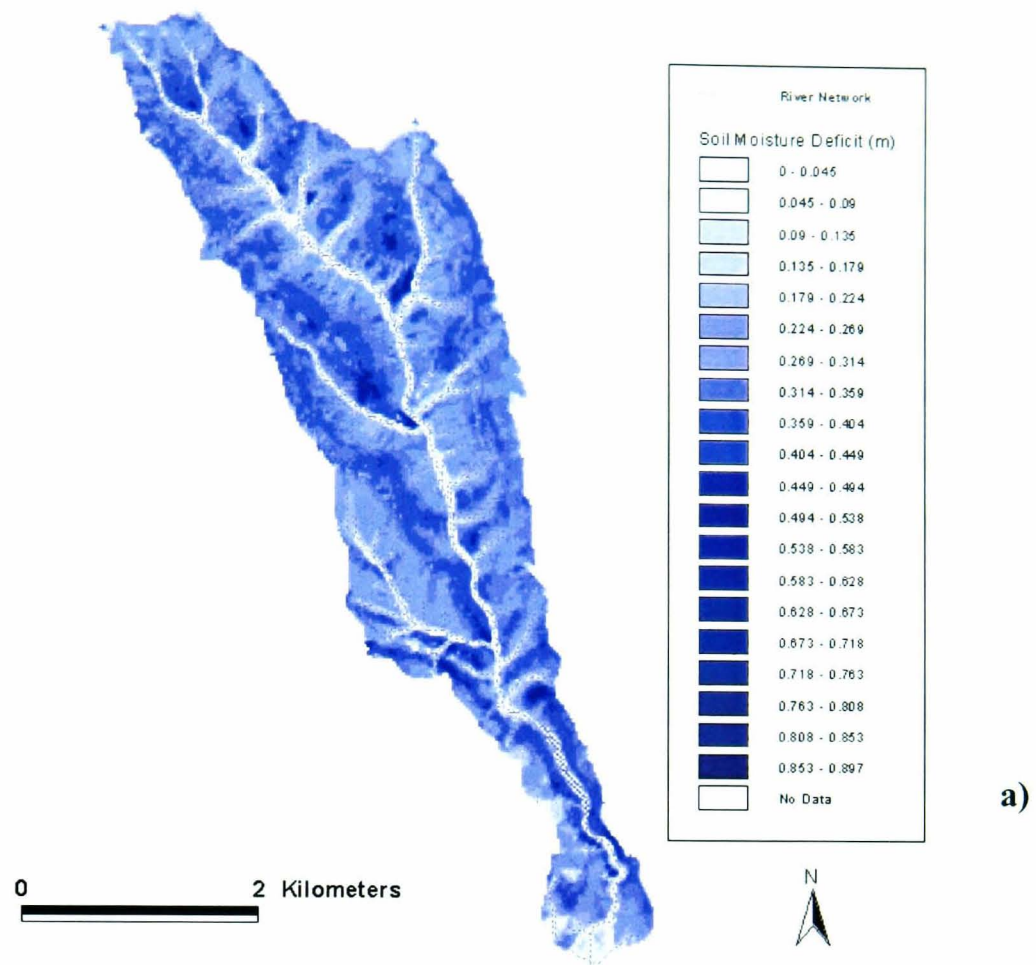
Fig. 5.6 a) Hydrographs for different critical temperatures plotted with observed hydrograph. Hydrographs are identical for different T_c .
 b) Hydrographs for different numbers of sub-critical hours. Hydrographs are identical.
 c) Hydrographs for different percentage direct runoff from frozen soils.

Model spatial predictions

In terms of interpreting model processes and considering the potential for secondary process coupling, the spatially distributed predictions generated by the model are of great importance. Maps of soil moisture deficit during the driest and wettest periods of the simulation are presented in Fig. 5.7. Fig. 5.7a shows that the contributing area represented by the lowest soil moisture deficit occurs in areas of topographic convergence within the riparian zone. The number of saturated or near saturated cells (moisture deficit of 0 – 0.045) is 807 or 3.7% of the total catchment area. During the wettest timestep, the contributing area expands only marginally, with the number of saturated or near-saturated cells increasing to 977, or 4.4% of total catchment area.

This pattern is indicative of the dominance of topography as a control on subsurface flow, and hence on soil moisture deficit, when lumped soil parameters are used. The difference between the soil moisture deficit at dry and wet timesteps is minimal, and indicates that the event was perhaps not sufficiently large to cause a significant change in the extent of the contributed contributing area. This limited expansion of the contributing area would be reflected in the spatial distribution of sediment accumulation and removal.

Soil Moisture Deficit - driest timestep



Soil Moisture Deficit - wettest timestep

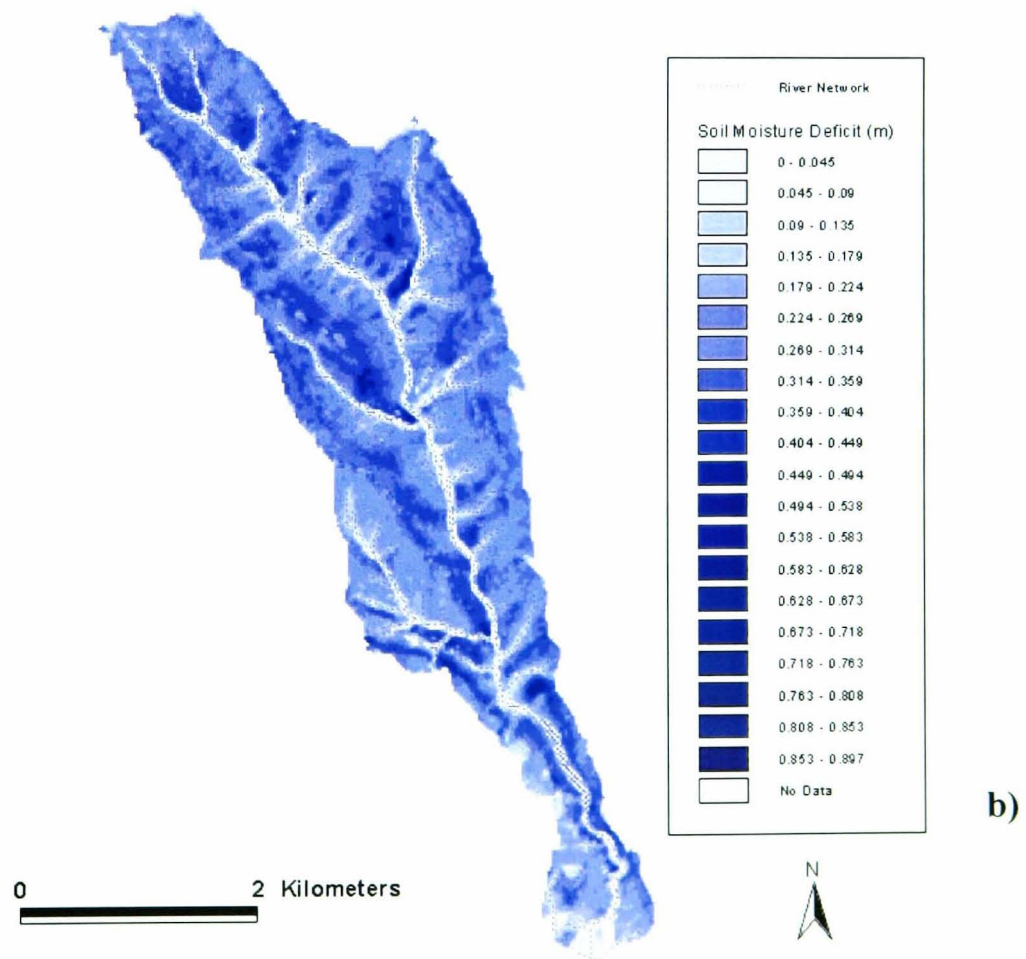


Fig. 5.7 Moisture deficit maps at a) the driest period (T=35); b) the wettest period of storm1 (T=236).

5.3.4 Model Validation

The main aim of model validation is to ensure that the model makes accurate predictions outside the calibration period (Tsang, 1991; Flavelle, 1992; Refsgaard and Knudsen, 1996). Traditional model validation methods include, and are in most cases restricted to, split-sample testing (Popper, 1959). Morczkowski *et. al.*, 1997 argue, however, that the main weakness of the split-sample test, when applied to streamflow data alone, is that it typically validates the same response to which it is calibrated. Klemes (1986) and Kuczera *et. al.* (1993) suggest that the split-sample test should be one of a list of validation methods which should be employed in any given modelling exercise.

Validation of the hydrological model was approached using two distinct methodologies. First, traditional split-sample testing (Popper, 1959) whereby the ‘optimal’ parameter set obtained in the model calibration, is applied to the validation event. Second, through a framework of uncertainty analysis based on Bayes’ theorem (Beven and Binley, 1992). In this later approach, the 1000 parameter sets from the model calibration which comprise the randomly selected parameter values, are applied to the validation events, and uncertainty bounds and ‘optimal’ parameter sets determined for these validation events. If the uncertainty bounds are comparable to the calibration uncertainty bounds, and if similar parameter sets are found to give the ‘optimal’ efficiency, then the model has been successfully validated. This is a test of the applicability of the original range of parameter values used in the calibration to other periods. The results of the validation experiments are then used to update the calibration likelihoods. This is a move away from the conventional model validation exercise in which one ‘optimal’ parameter set is applied to the validation event, and the original calibration rejected or accepted on the basis of the goodness-of-fit to the validation event. It is also an acknowledgement of the fact that one ‘optimal’ parameter set cannot be used to describe catchment conditions for one event, and is therefore much less likely to be a sufficient descriptor for all events.

Validation 1

Fig. 5.8 is the result of a simple split-sample test in which the ‘optimal’ calibration parameter sets are used as input to event 2. A Nash Efficiency of 71.88% was obtained. Fig. 5.8b shows that the peaks are well timed, although the first two peaks

and much of the recession are under-predicted while the last is over-predicted. Baseflow accounts for most (98%) of the runoff during this event.

Fig. 5.9 is a plot of the 90% confidence envelope constructed using the same 1000 simulations used in the calibration. The number of behavioural simulations ($\text{eff} > 40\%$), N_b , was 965. An examination of the uncertainty bounds reveals that the upper limit only just encloses the observed curve for the first 200 timesteps.

Table 5.4 shows that there is wider variability in m for the 10 ‘best’ simulations of the validation period than was obtained for the calibration (Table 5.3). This is confirmed by the scatterplot of efficiency for m (Fig. 5.10), which has a wider range of values for which high ($>80\%$) efficiencies are obtained, compared to the corresponding plot for the calibration period (Fig. 5.2).

Table 5.4 also shows that larger values of K_0 are included in the ten ‘best’ parameter sets, compensating for the lower m values than obtained for event 1.

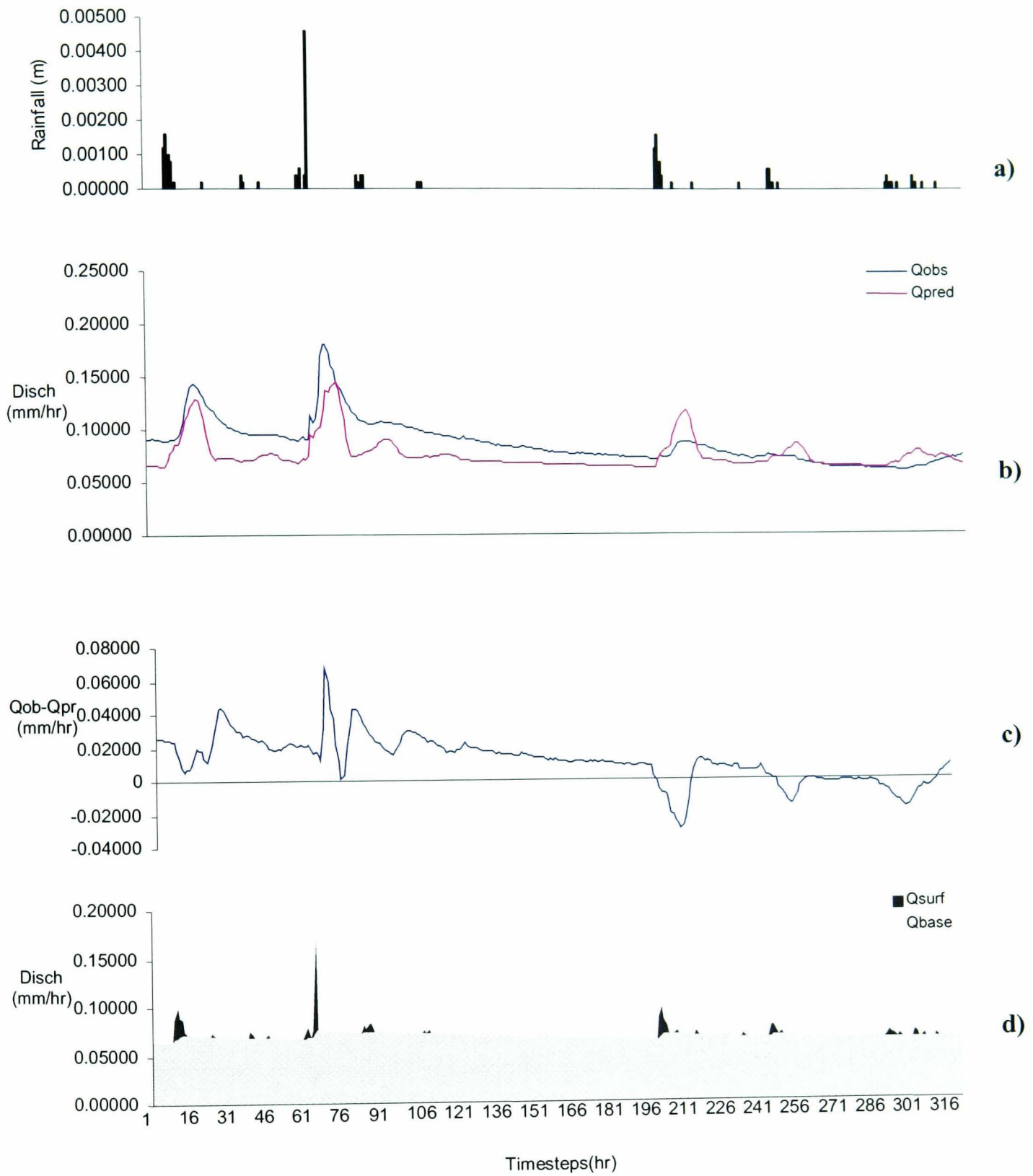


Fig. 5.8 Results of validation 1 (10/12/98 to 23/12/98).

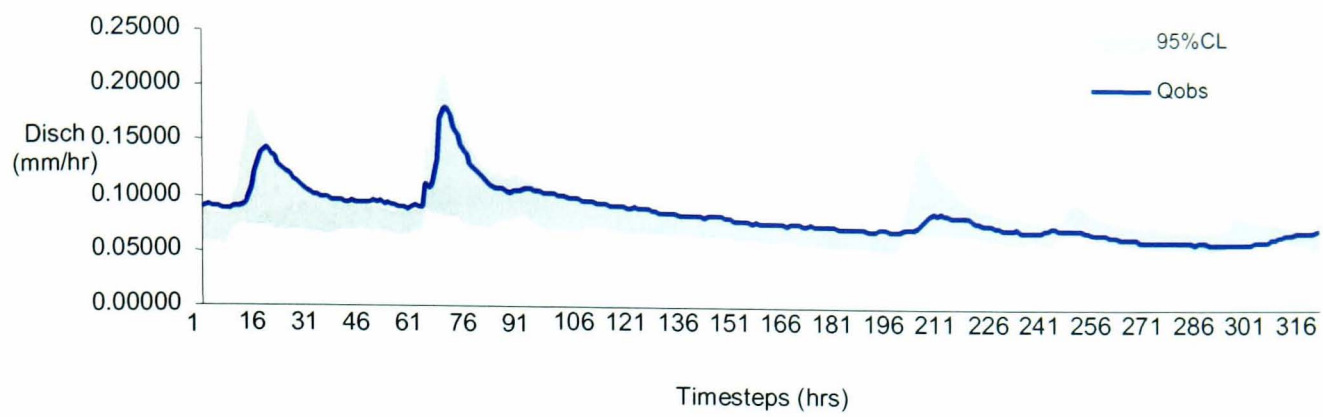


Fig. 5.9 Uncertainty in validation 1 – event 2 (10/12/98 to 23/12/98).

m (m)	K_0 (m/hr)	SRMAX (m)	CHV2 (m/s)	ETF	Nash Eff (%)
0.05732	412.351	0.00459	0.4229	0.37655	99.55007
0.05981	166.0129	0.00112	0.2653	0.79122	99.51612
0.05573	218.1714	0.00384	0.3567	0.36791	99.44867
0.03975	293.9092	0.00841	0.2630	0.98793	99.12032
0.04899	491.1028	0.00227	0.3519	0.11262	99.02666
0.04066	469.6501	0.00747	0.2731	0.5725	98.39889
0.03569	473.858	0.00335	0.3081	0.56035	98.34869
0.03505	419.9638	0.00403	0.2959	0.99356	98.32602
0.03822	264.4012	0.00854	0.3694	0.96893	98.23631
0.04319	417.3187	0.0096	0.1933	0.63274	98.12333

Table 5.4 The ten ‘best’ parameter sets as validated on event 2.

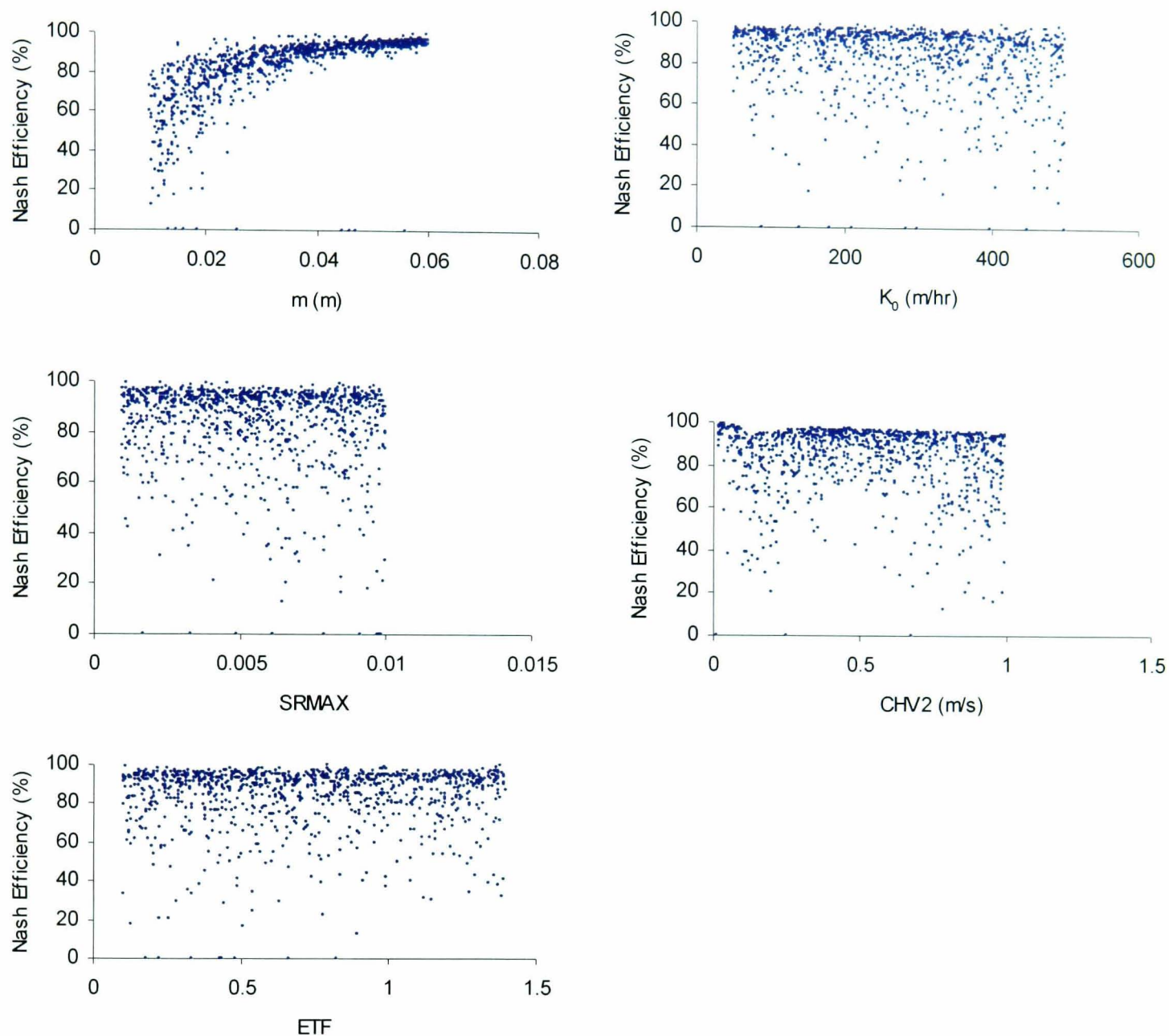
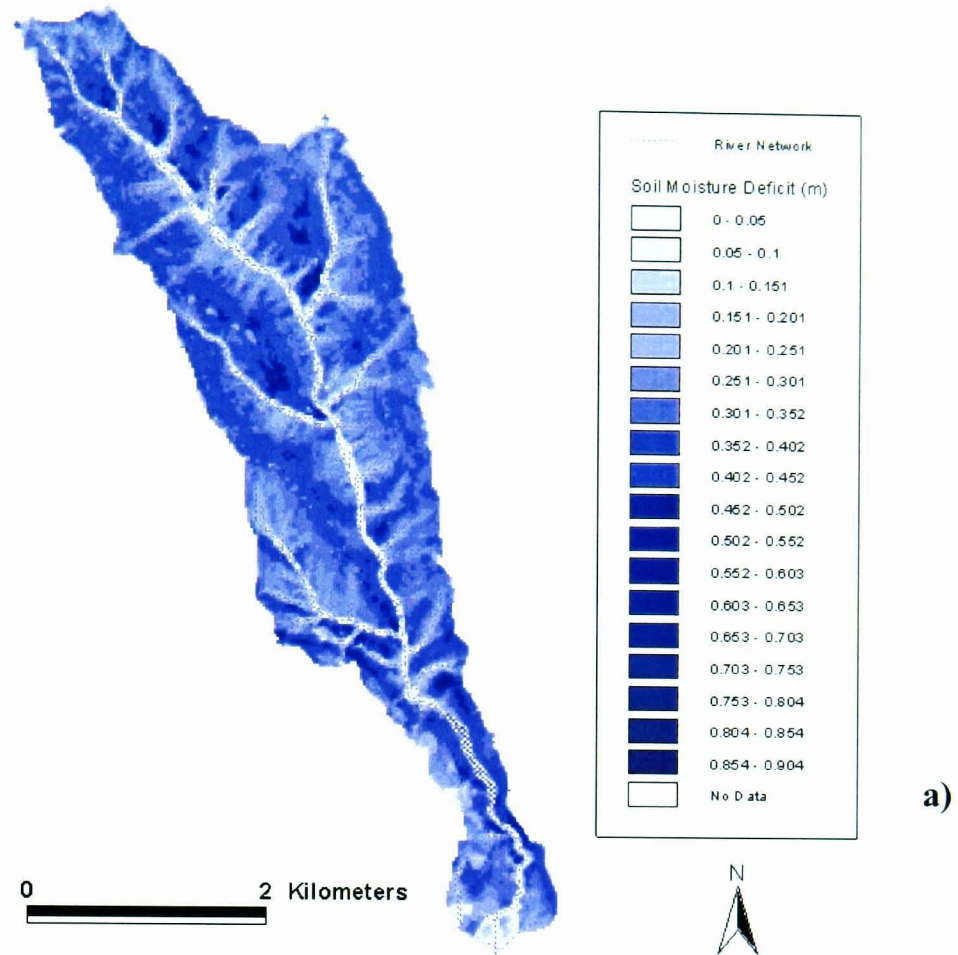


Fig. 5.10 Scatterplots of efficiencies vs. parameter values for validation 1 (10/12/98 to 23/12/98).

SRMAX and *ETF* show high efficiencies throughout their ranges. While *CHV2* shows high efficiencies for the entire range of values, efficiencies $> 40\%$ are obtained at approximately 0.45 to 0.50ms^{-1} . At $CHV2=0.5\text{ms}^{-1}$, all but one simulation are greater than 75% .

Soil Moisture Deficit - driest timestep



Soil Moisture Deficit - wettest timestep

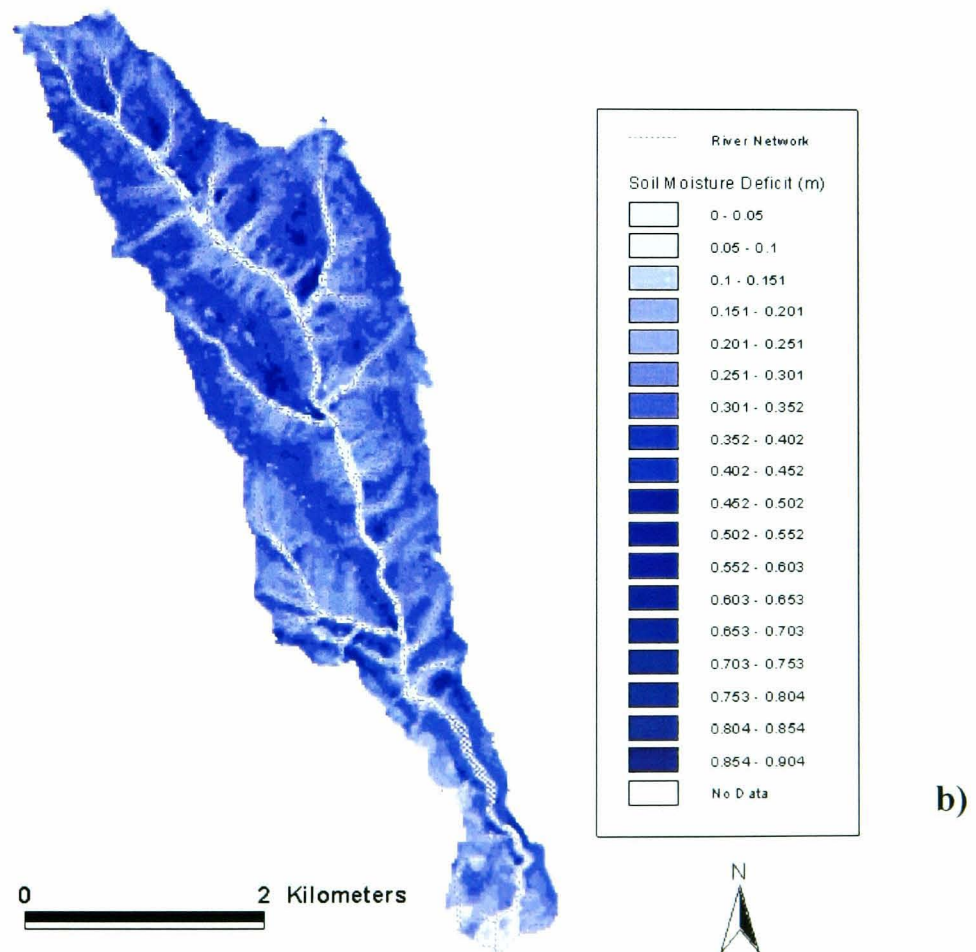


Fig. 5.11 Spatial distribution of soil moisture status at the a) driest and b) wettest timesteps for validation 1.

Similar to the calibration results, the spatial distribution of soil moisture deficit for the validation event (Fig. 5.11) shows little difference between the contributing area for the dry and wet period. During the driest interval a total of 789 cells or 3.6% of the catchment was saturated or near-saturated, while 815 cells or 3.7% of the catchment was saturated or near-saturated during the wettest interval. Again, saturated areas are predominantly along the riparian area in topographically convergent cells. The restriction of the saturated cells to the riparian zone again reflects the fact that this event is quite small, with only 0.022m of rainfall and 0.02803 total runoff occurring over a 324-hour period. With a maximum rainfall intensity of 0.0046mhr^{-1} and a calibrated saturated hydraulic conductivity of 412.35mhr^{-1} , most of the rainfall will infiltrate quickly, but runoff production will be low, as only topographically convergent cells will have the necessary upslope contributing areas to generate runoff.

Validation 2

The second validation was done on event 3. Fig. 5.12 shows the results of the split-sample test for this validation period. A model efficiency of 45.55% was obtained. The hydrograph fit is qualitatively poor with less than 50% of the variance in Q_{obs} explained by the simulation (Fig. 5.12c and d). None of the three major peaks are well predicted, and the recession flow is over-predicted. Fig. 5.12e suggests that baseflow dominates even at peak saturation.

The GLUE analysis (Fig. 5.13) predicts that the 90% confidence intervals enclose the first and second peaks, but not the third. Table 5.5 shows that ten ‘best parameter sets are again characterised by lower m values, lower K_0 and higher $CHV2$ values than the ten ‘best’ calibrated parameter sets. This is corroborated by the scatterplots for this event (Fig. 5.14). Nash efficiency for m peaks at 0.02m and then decreases steadily with increasing m . The lower m and K_0 values suggest a shallower, less permeable soil depth resulting in faster time to saturation and hence runoff production. It is representative of the inability of the soil to deal with the high, long-duration infiltration rates of the rainfall. $CHV2$ shows a steady increase in efficiency from $CHV2=0$ to 1ms^{-1} . The increased $CHV2$ values characterise the faster travel times to the outlet, which will result when runoff from hillslopes, not normally saturated and hence normally controlled by the lower hillslope velocities, are taken to the outlet at increased overland flow velocities. That is, when hillslope cells are ‘converted’ to channel cells when they become saturated, runoff from them occurs at channel velocities. Thus more cells than originally assigned, are characterised by channel velocities. This suggests that the use of a static channel network on which the assignment of hillslope and channel velocities is based, might not be appropriate. A more dynamic system that allows for the expansion of the channel and the corresponding increased travel velocity, would more effectively reflect the dynamic spatial and temporal variability of flow velocities.

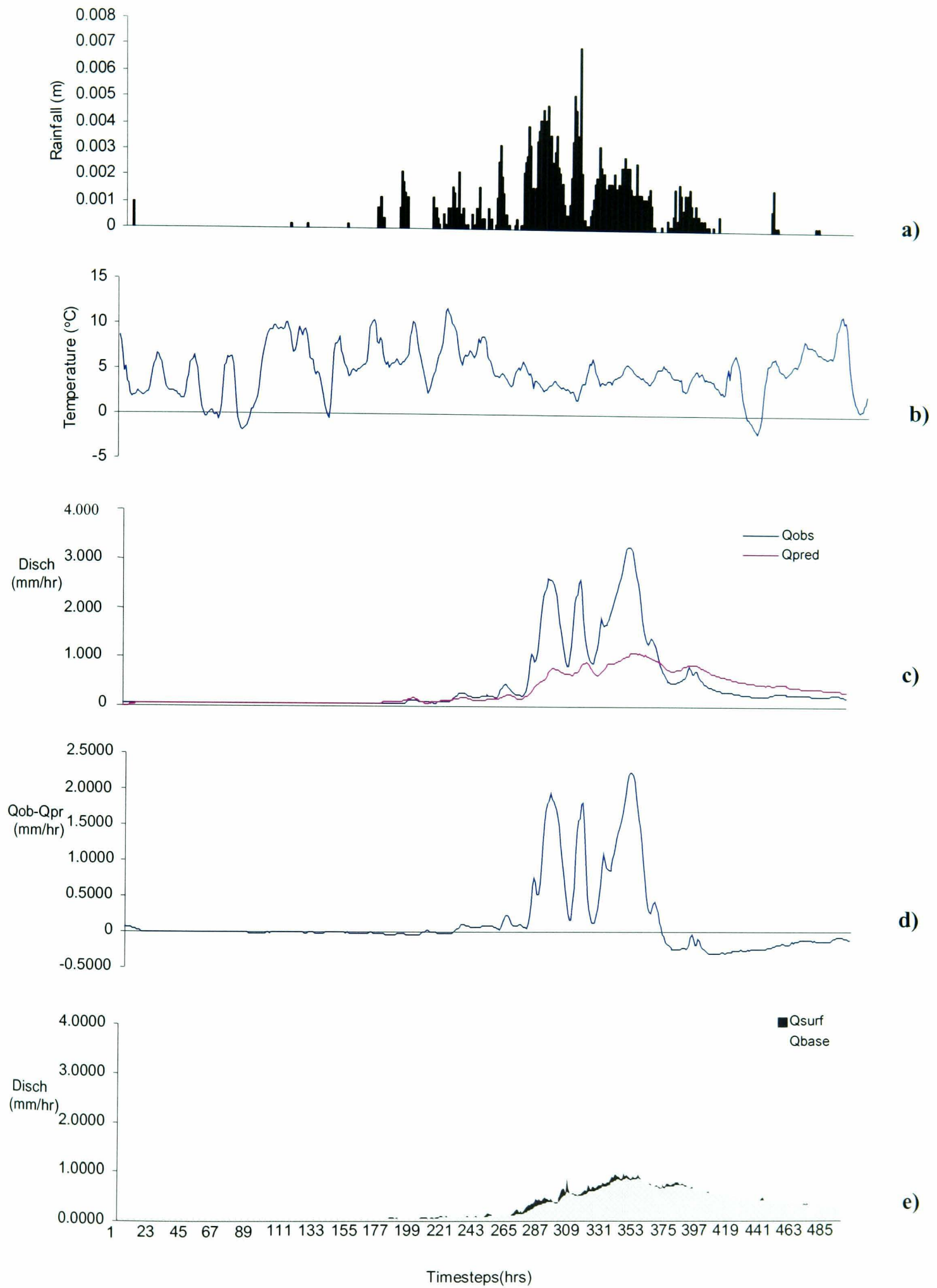


Fig. 5.12 Results of validation 2 (21/02/99 to 14/03/99) using 'optimal' calibrated parameter set..

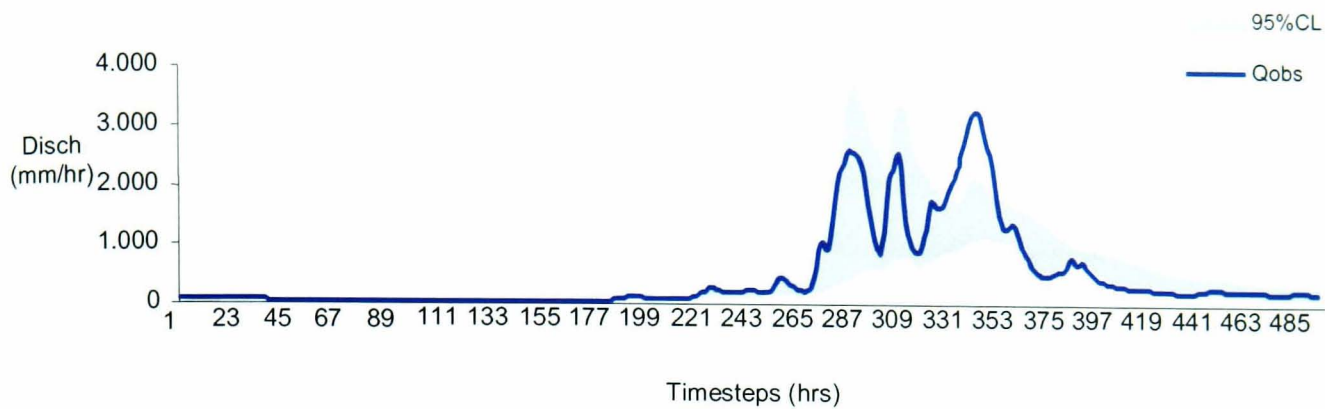


Fig. 5.13 Uncertainty bounds for validation 2 (event 3 – 21/02/99 to 14/03/99).

m (m)	K_0 (m/hr)	SRMAX (m)	CHV2 (m/s)	ETF	Nash Eff (%)
0.02337	63.04206	0.00396	0.9229	1.23921	88.95333
0.02534	50.45237	0.00523	0.94882	1.30811	88.83456
0.02179	120.0933	0.00312	0.96916	0.37796	88.81262
0.02055	148.2845	0.00143	0.98253	0.6146	88.70808
0.02262	81.85835	0.00639	0.86681	0.68152	88.66115
0.01994	141.2355	0.00127	0.8906	0.42718	88.62347
0.02211	169.0842	0.00467	0.86692	0.28084	88.54132
0.01929	186.7633	0.00866	0.86316	0.12421	88.45587
0.02132	91.81033	0.00913	0.78986	0.41233	88.37243
0.0234	131.7382	0.00424	0.85691	1.04313	88.33648

Table 5.5 Ten ‘best’ parameter sets for validation 2.

Fig. 5.15 shows the observed and predicted hydrographs for the ‘best’ parameter set for the validation event – the shaded parameter set in table 5.5. The fit is qualitatively quite good, for the first two peaks, but again the third peak is under-predicted. This predictive failure in the third peak is perhaps attributable to a storage anomaly for this particular event. Over-prediction of the first peak may have resulted in the failure of the model to account for catchment storage and dynamics of the contributing area which, in reality, has expanded, yielding the non-linear result in the third peak. Data quality may have also contributed to the predictive failure of the model at peak 3. With peak flows of 45cumecs, the weir at Kirkby Mills would have exceeded the max discharge for which it was designed to measure (40cumecs). Under such extreme events equipment failure or malfunction would result in unreliable data. Personal observation of the chart record during the event suggests that the flow records might have topped out long before the maximum flood wave had passed. That is, the chart

had exceeded its maximum while on the rising limb, suggesting that it would not have been able to accurately record the higher flows during peak flow. A comparison of the baseflow and saturation excess overland flow contributions (Fig. 5.15c) with that obtained for the ‘optimal’ calibrated parameter set (Fig. 5.12e) reveals that the relative contribution of baseflow during peak flows is much less than for the ‘best’ parameter sets, while the total depths are larger.

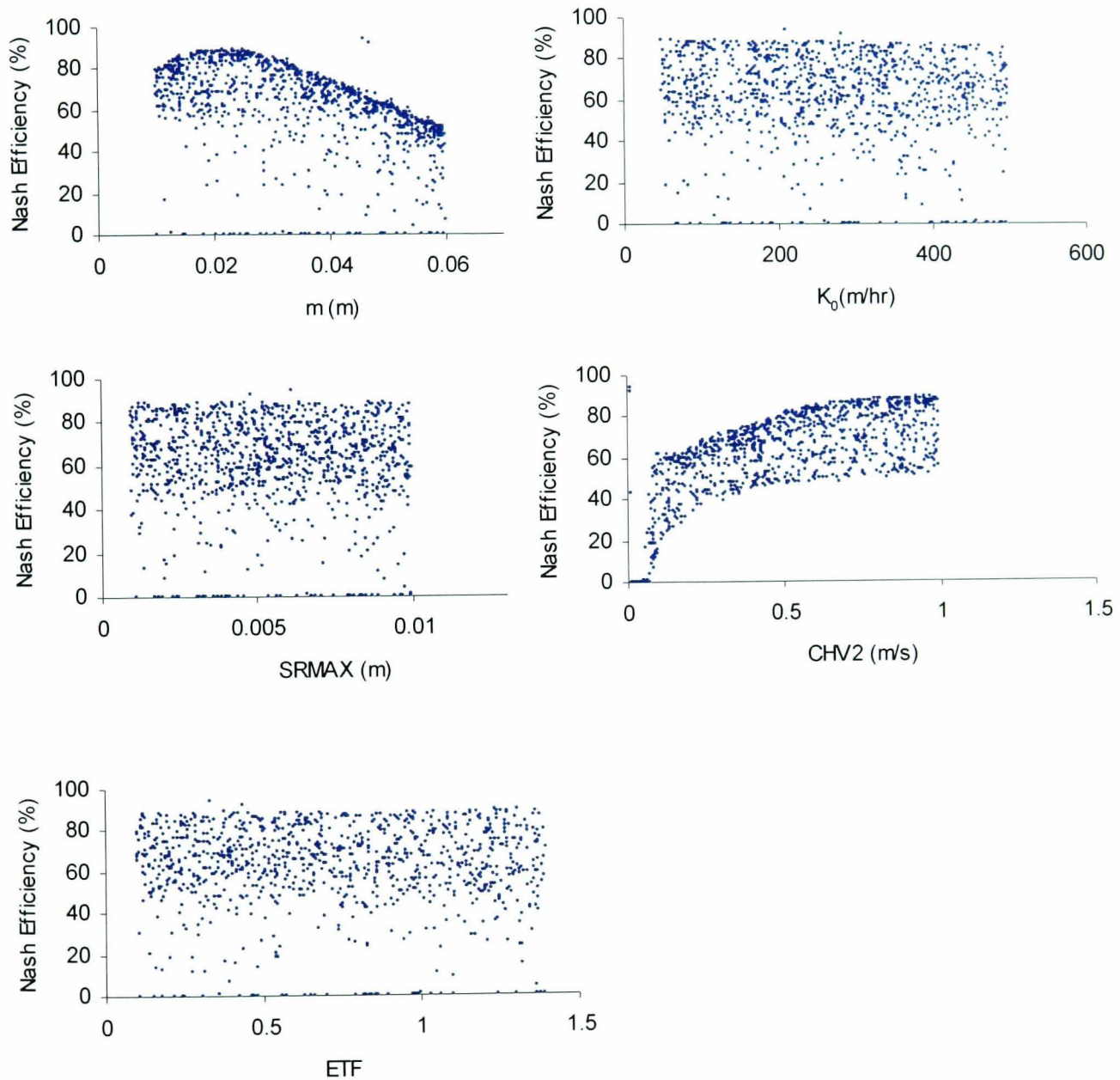


Fig. 5.14 Scatterplots for validation 2 (21/02/99 to 14/03/99).

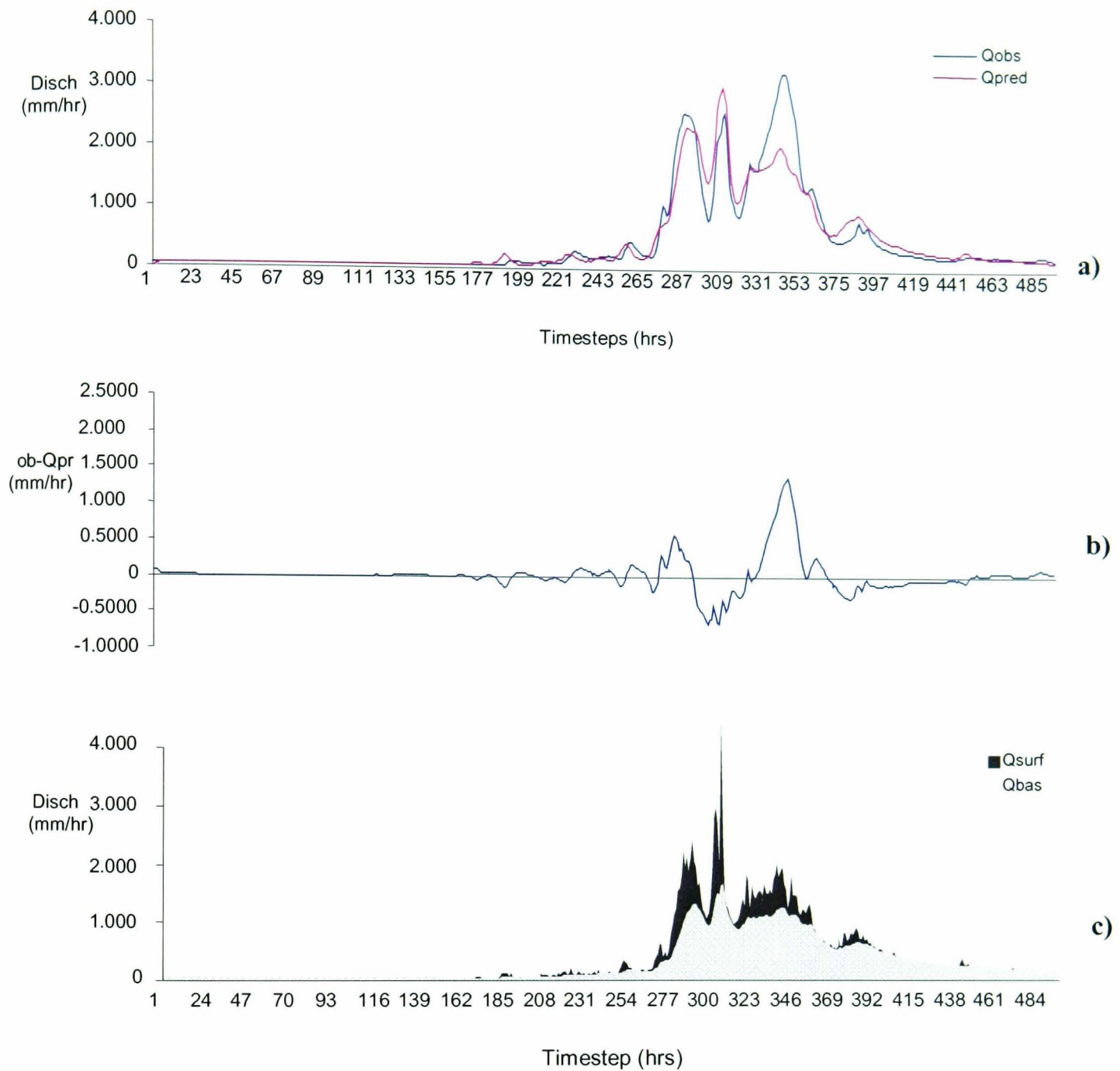
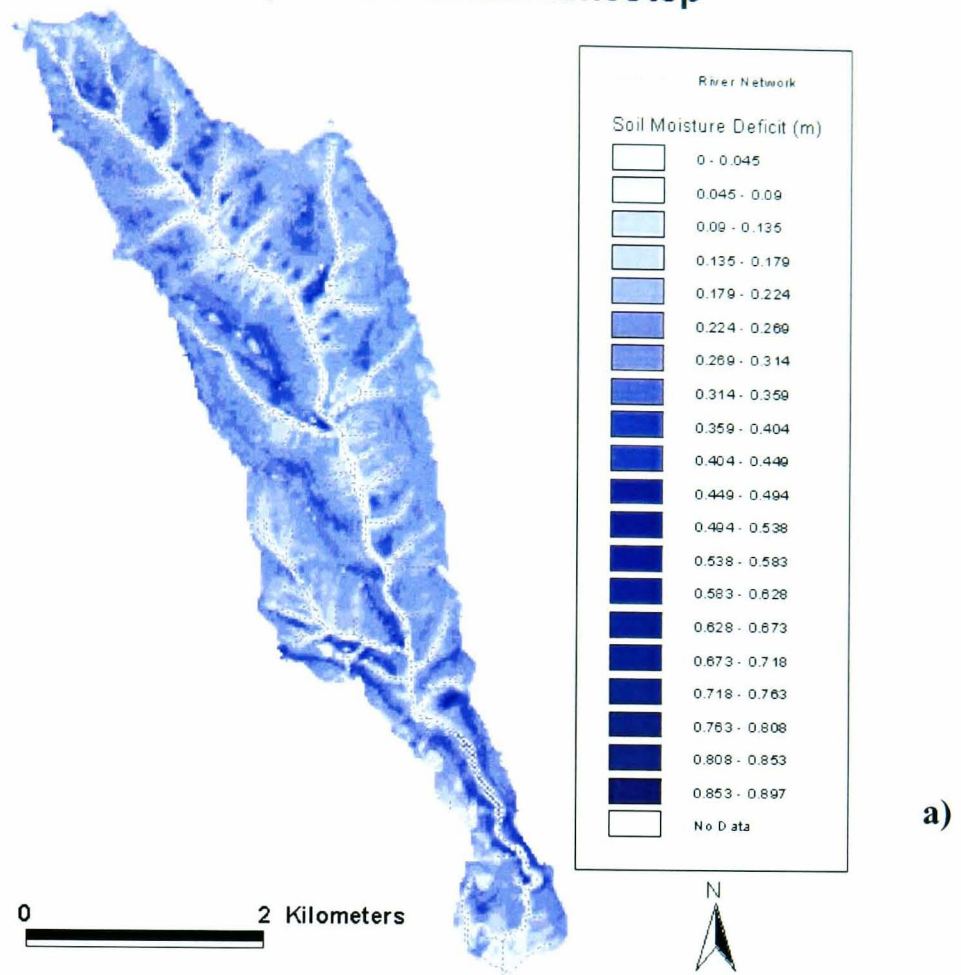


Fig. 5.15 a) Observed and predicted hydrographs for ‘best’ parameter set of validation event 2.
 b) Error in model prediction
 c) Baseflow and saturation excess overland flow contributions.

Soil Moisture Deficit - 'optimum' driest timestep



Soil Moisture Deficit - 'optimum' wettest timestep

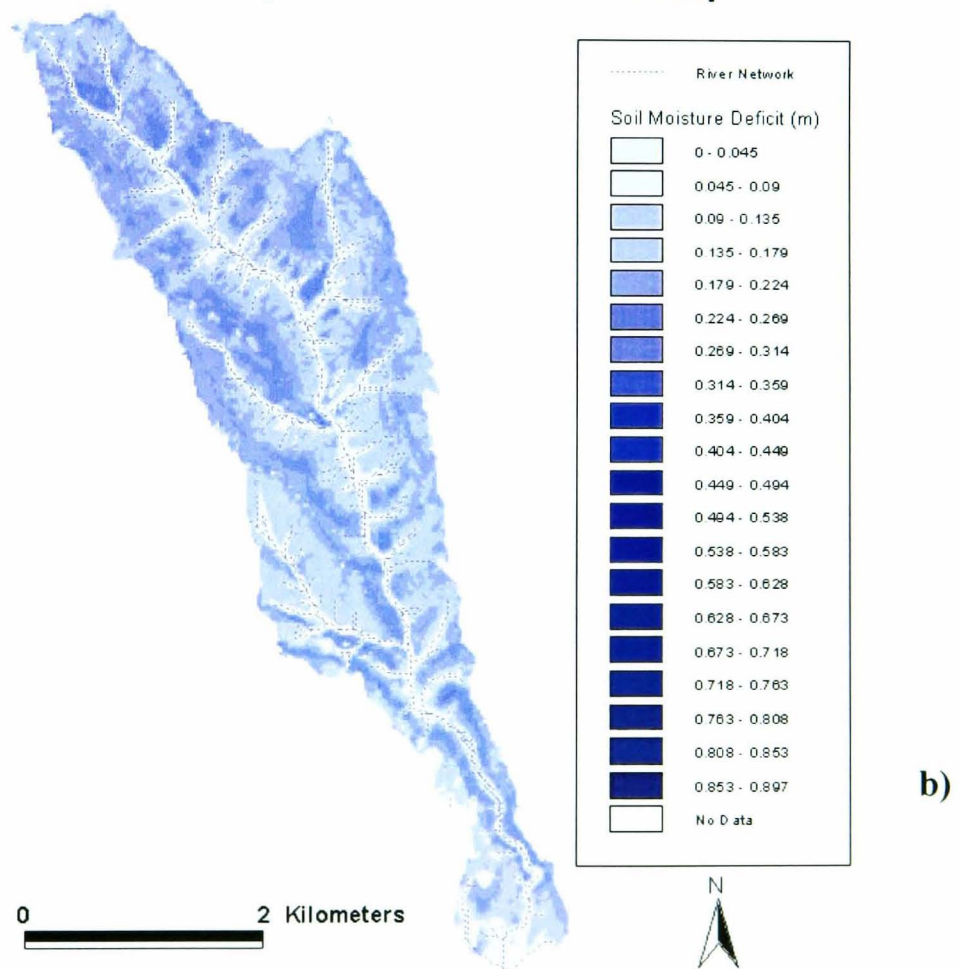
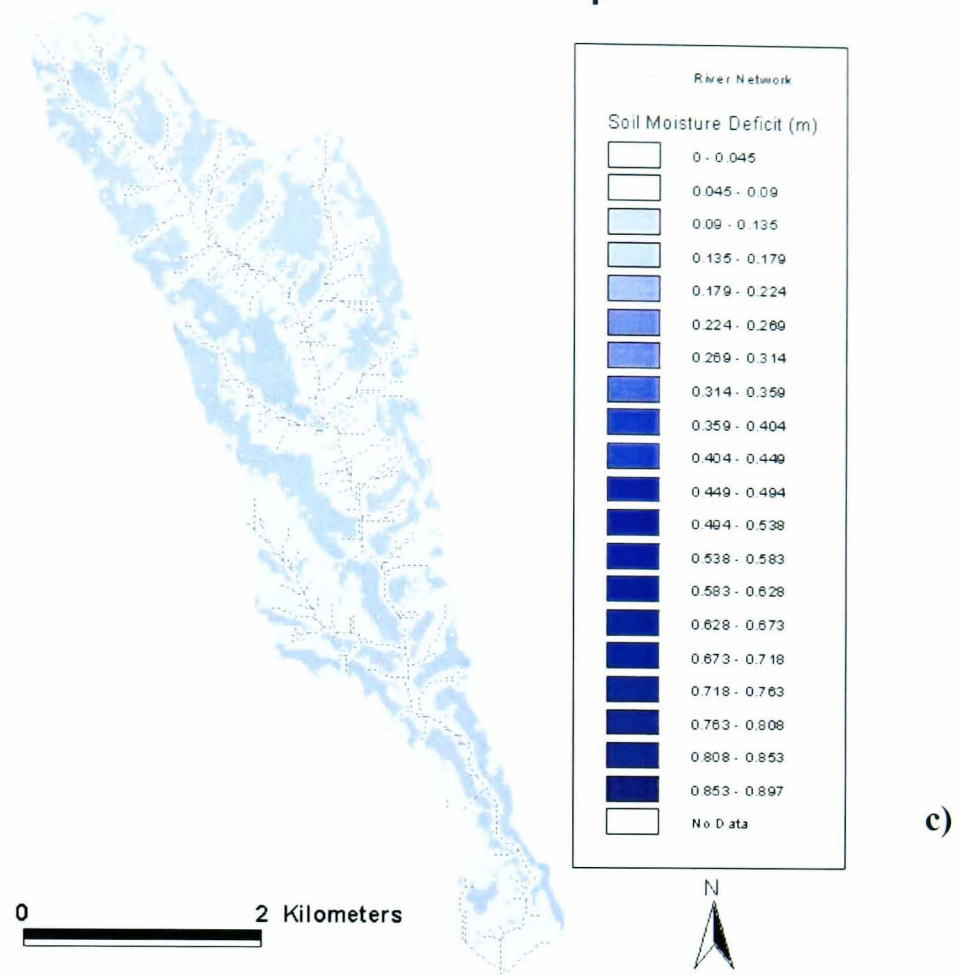


Fig. 5.16 soil moisture deficit for: a) driest interval for calibrated 'optimum' parameter set. b) wettest interval for calibrated 'optimum' parameter set.

Soil Moisture Deficit - 'best' driest timestep



Soil Moisture Deficit - 'best' wettest timestep

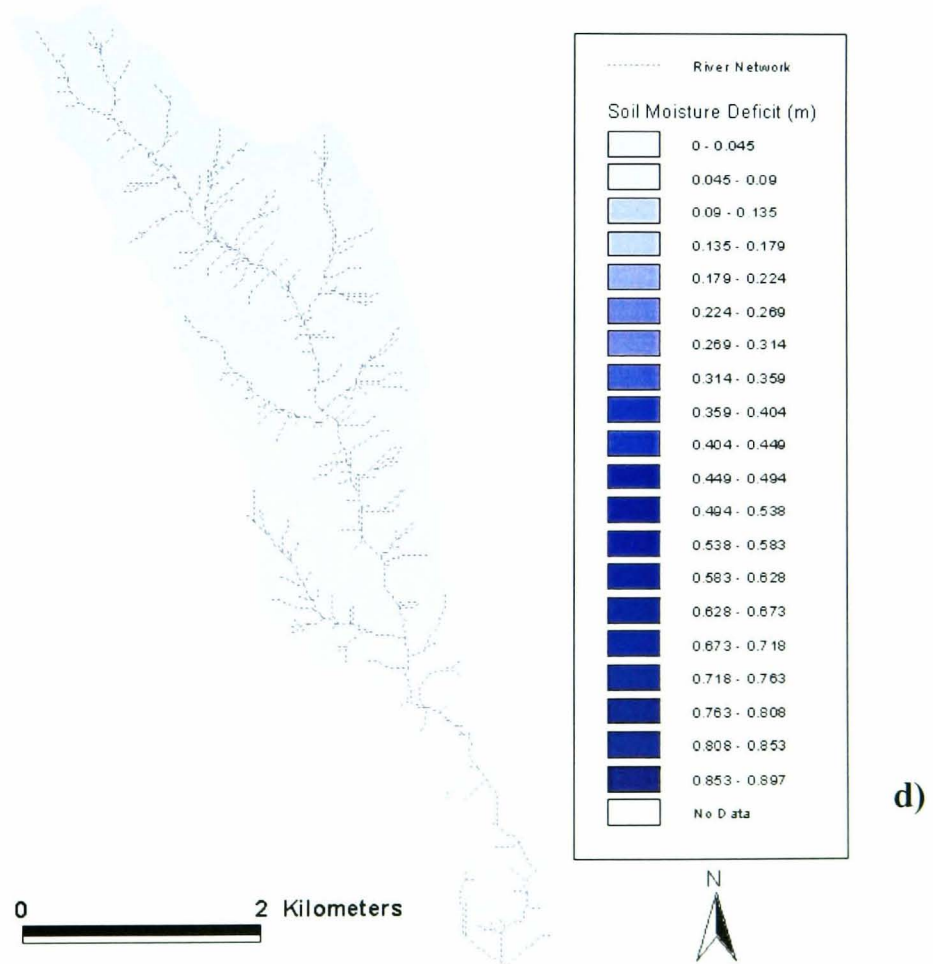


Fig. 5.16 cont'd soil moisture deficit for: c) driest interval for 'best' validated parameter set. d) wettest interval for 'best' validated parameter set.

The spatial distribution of model predictions for the ‘optimal’ calibrated parameter set (Fig. 5.16 a and b) is very different from that for the ‘best’ validated parameter set (Fig. 5.16 c and d). Comparison of Fig. 5.16 a and c shows that the extent of saturation is badly under-predicted everywhere in the catchment for the calibrated ‘optimum’ parameter set at the driest timestep. Similarly, for the wettest timestep (Fig. 5.16b and d), the validated ‘best’ parameter set predicts a completely saturated catchment, while the calibrated ‘optimal’ predicts saturation in the expanded contributing area bordering the channel.

Hence, in addition to the poor qualitative and quantitative fit of the prediction for the calibrated ‘optimum’ parameter set, it also fails to predict the spatial distribution of the runoff contributing areas.

5.3.5 Bayesian Updating using flow data

Recalling Bayes' equation (equation 4.39):

$$L_p(\Theta | Y) = L_y(\Theta | Y)L_o(\Theta) \quad [5.3]$$

the likelihood measures for the original calibration event (04/11/98 to 21/11/98) were used as the prior distribution ($L_o(\Theta)$) of model parameters conditioned upon this set of observations, and were updated using the likelihood measures of validation 1 (10/12/98 to 23/12/98) and validation 2 (21/02/99 to 14/03/99) as $L_y(\Theta|Y)$ – the likelihood of parameters for new observations – both separately and combined.

The combined likelihood measure is given by:

$$L_i = \frac{1}{C} * \frac{Eff1_i}{\sum_1^{N_b} Eff1_i} * \frac{Eff2_i}{\sum_1^{N_b} Eff2_i} * \frac{Eff3_i}{\sum_1^{N_b} Eff3_i}$$

Where $Eff1_i$, $Eff2_i$, $Eff3_i$, are the efficiencies of each i^{th} simulation that is behavioural for all three events; N_b is the number of simulations that are behavioural for all three events; C is $\sum L_i$. Similar combined likelihoods are used for the different combinations of events used in the updating.

Cumulative likelihood distributions are shown in Fig. 5.17 for five of the model parameters. Cumulative likelihoods are based on a separation of the parameter sets into behavioural and non-behavioural (critical Nash efficiency of 40%), and not a separation into different classes as in the sensitivity analysis above. The use of a uniform random sampling strategy in the generation of parameter sets in the original calibration, is equivalent to assuming the same value of the likelihood measure for every parameter set, prior to comparison between the associated simulations and the observed data, and would appear in Fig. 5.17 as straight lines, plotted from lower left to upper right for each parameter. Hence the prior distributions for all parameters are approximately along this line of equal likelihood, while all posterior distributions show some degree of modification in cumulative likelihood as more data is added, with the largest modification obtained when all three events are used.

For m values between 0.03 and 0.04m the distributions for event 1 with either event 2 alone, or event 3 alone, show little modification from the prior distribution. As m increases above 0.05m however, there is a rapid increase in likelihood indicating a critical range between 0.05 and 0.06m. K_0 has a critical value to about 400mhr^{-1} as well as a less critical value of approximately 220mhr^{-1} . $SRMAX$ has a critical range of 0.003 to 0.005m, $CHV2$ is critical at 0.4ms^{-1} , and ETF at 0.3.

The results of the updated distributions reveal that the addition of two different flow observation periods was able to restrict all parameters to smaller ranges. The effect of these parameter modifications on the flow uncertainty limits, are investigated below.

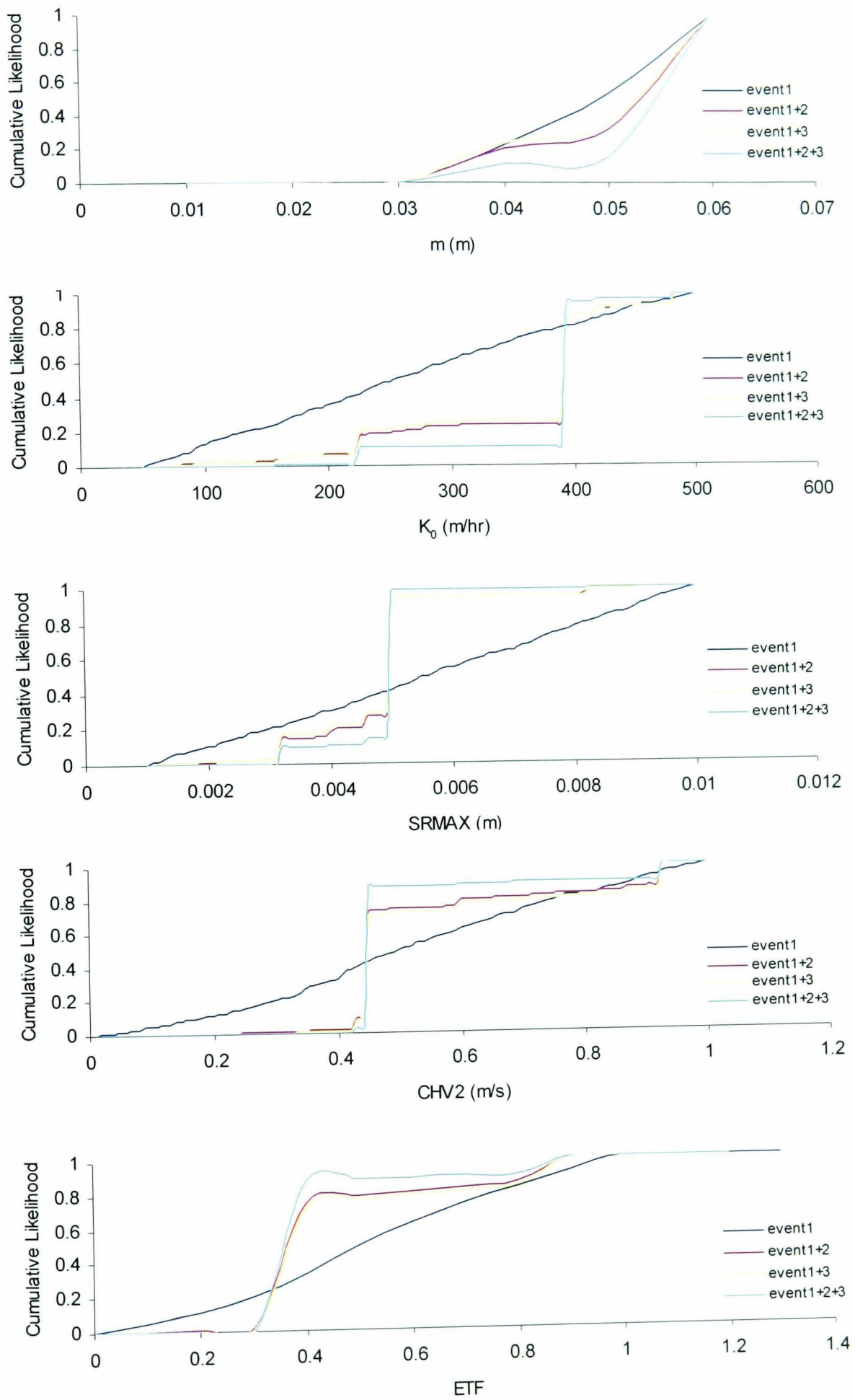


Fig. 5.17 Prior and posterior distribution of cumulative likelihoods.

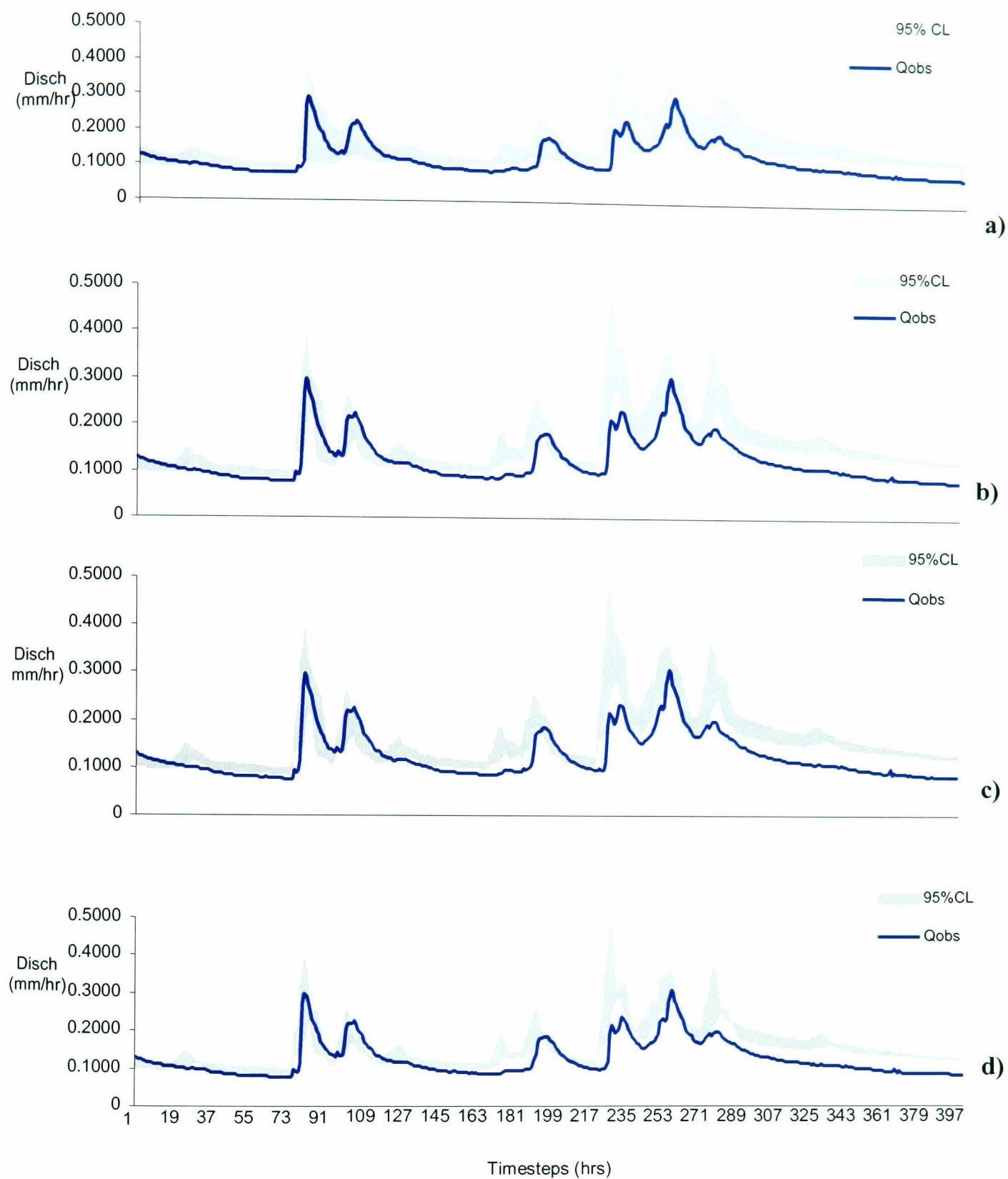


Fig. 5.18 a) Original uncertainty limits for calibrated event (event 1) alone. $N_b=529$.

b) Bayesian updating of event 1 using event 2. $N_b = 527$.

c) Bayesian updating of event 1 using event 3. $N_b = 470$.

d) Bayesian updating of event 1 using both events 2 and 3. $N_b = 468$.

Fig. 5.18 shows the results of Bayesian updating of the calibration uncertainty bounds, using the two additional periods of flow observation. The number of behavioural simulations, N_b , decreased from 529 to 527 when event 2 alone was added, and to 470 when event 3 alone is added. These reductions in the number of behavioural simulations resulted in similar decreases in the width of the uncertainty bounds, particularly in peak flow, as shown in Fig. 5.18b and c. The reduction in uncertainty for both, is mainly due to a higher 5% bound throughout the event. This suggests that the worst parameter sets for events 2 and 3 are better predictors of the system than those of the calibration period. The reduced uncertainty is accompanied by increased predictive failure where reduced uncertainty bounds fail to enclose the observed hydrograph.

The combined likelihoods of all three events resulted in even further restriction of the uncertainty bounds. However, this too is at the expense of predictive success, particularly in peaks four and six, and the recession flows. It should be noted that because the likelihood measure is calculated for an entire simulation, but uncertainty bounds are computed at every timestep, the plotted bounds do not follow any one particular simulation. Hence individual simulations can be more or less dynamic than the uncertainty bounds.

Lamb, *et. al.*, (1998) reported a similar reduction in uncertainty bounds when data from a second flow observation period was used to update uncertainty in the calibration period. As stated earlier, the use of different periods of data for the same response variable to restrict uncertainty bounds is limited in its ability to distinguish model structures and parameter sets in the model validation. Section 5.5.1 examines the use of sediment yield model predictions to restrict hydrological model uncertainty.

The next section presents the results of sediment yield model calibration and validation.

5.4. Sediment Yield Model Results and Analysis

Similar to the hydrological model, the sediment yield model was calibrated and predictive uncertainty analysed using GLUE analysis. The ‘optimum’ hydrological parameter set was used as a fixed input to the model, and sediment yield parameters varied. Calibration was done on the same event for which the hydrological model was calibrated, in order to update the likelihoods of the hydrological model based on its predictive success in the coupled-hydrological model (section 5.5.1). This is done using Bayes’ theorem as above, to reject simulations which do not have good predictive capabilities for both the sediment yield and hydrological responses.

5.4.1 Parameter Sensitivity

Recalling section 4.3, the sediment yield model has three parameters that need calibration. R_0 , the initial maximum rate of sediment accumulation, K_{sed} , the availability rate constant which determines the rate of decrease of accumulation rate, and $CHS2$ the velocity of sediment transport in the channel. K_{sed} and $CHS2$ were determined manually, and used as fixed inputs for the GLUE calibration, so that only R_0 is varied. Hence the fixed input parameter values were:

Parameter	Units	Value
m	m	0.05947
K_0	m hr ⁻¹	271.7395
$SRMAX$	m	0.00372
GWL	m hr ⁻¹	0.0
ETF	N/a	0.76232
V_h	m hr ⁻¹	0.1
V_c	m hr ⁻¹	0.46237
SMF	N/a	9.4x10 ⁻⁵
K_{sed}	m	6.93x10 ⁻⁴
V_{ch}	mhr ⁻¹	0.1
V_{cs}	mhr ⁻¹	0.35

Table 5.6 Parameter values used in the sediment yield model calibration. Hydrological model parameters are the ‘optimised’ values, while the sediment parameter values were determined manually.

The Nash Efficiency (Nash and Sutcliffe, 1970) is again used as the objective function, based on comparison of observed and predicted sediment flux. In general,

low model efficiencies were obtained for the GLUE analysis for the sediment yield model, < 40%. An efficiency of 30% was used as the critical efficiency by which behavioural and non-behavioural simulations were distinguished. The scatterplot of R_0 versus model efficiency (Fig.5.19a) shows that behavioural simulations are obtained for R_0 in the range 4.0×10^{-8} to $9.0 \times 10^{-8} \text{ mhr}^{-1}$.

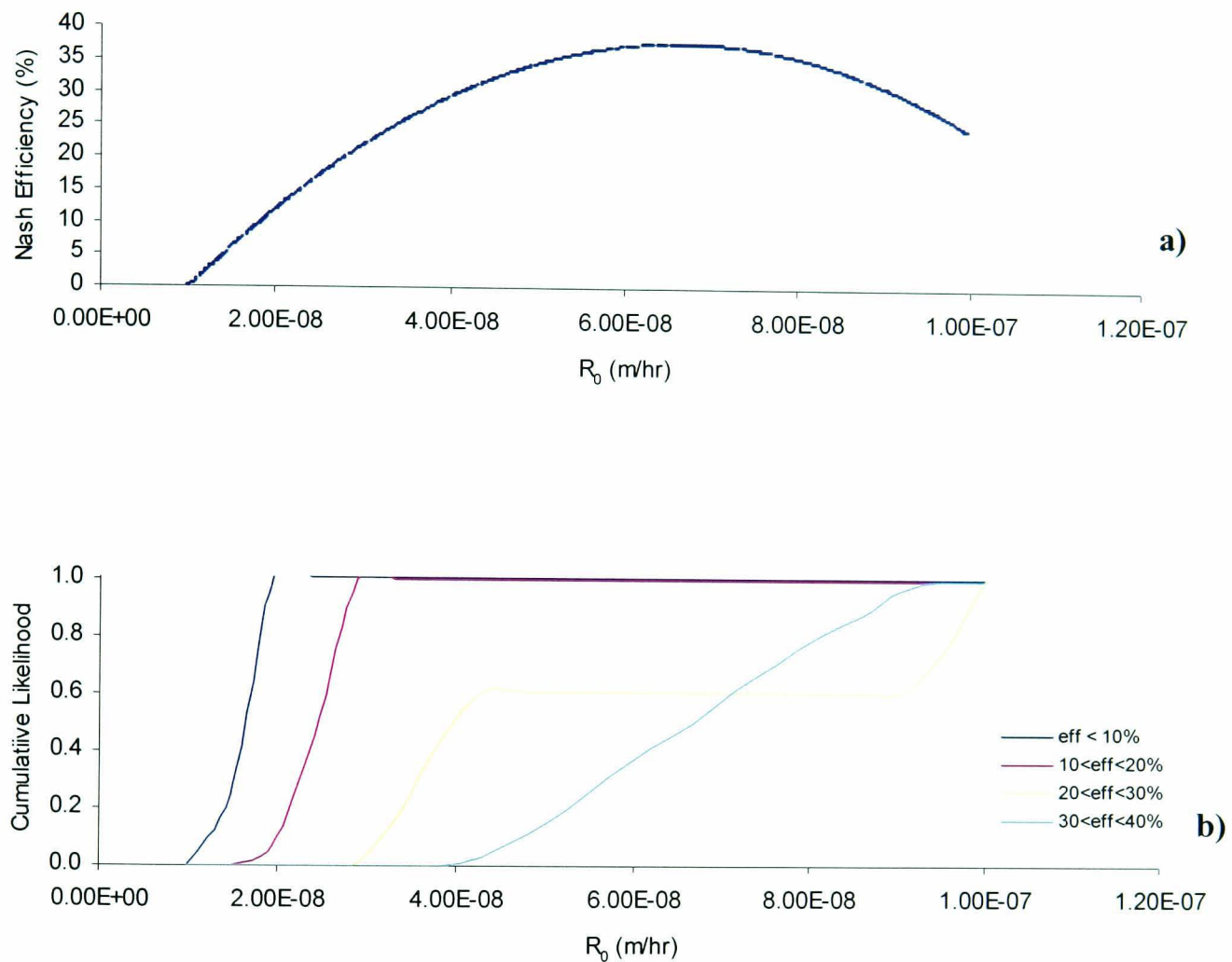


Fig. 5.19 a) Scatter plot of R_0 versus model Efficiency; b) Generalised Sensitivity Analysis for R_0 .

A clear ‘optimum’ R_0 value of $6.7 \times 10^{-8} \text{ mhr}^{-1}$ can be derived from the plot. This seems, at first glance, to be a very low hourly rate of sediment accumulation. However, this value represents the depth of sediment that would become available on the entire grid cell in one hour, and is therefore spread over 2500 m^2 . In reality, available sediment will not necessarily be spread over on the entire $50 \times 50 \text{ m}$ grid cell. Sediment may become available at different rates, on different parts of the grid cell. For example, if sediment accumulated on just one square metre of the entire grid

cell, R_0 would have a value of $1.7 \times 10^{-4} \text{ mhr}^{-1}$. Hence R_0 is dependent on the scale of spatial discretisation. No attempt is made here to determine the extent of that dependence.

Imeson (1970) reported an annual suspended sediment yield of 9100t for the neighbouring Bransdale catchment. Assuming that the majority of sediment is accumulated during approximately 182 days of the year when overland flow is zero, then the average hourly accumulation rate for a 50 x 50m grid cell in Bransdale would be $8.21 \times 10^{-8} \text{ mhr}^{-1}$. This rough estimate assumes, of course, that the sediment delivery ratio is 100% - a somewhat precarious assumption as discussed in section 2.3. However, such an inverse solution shows that the value obtained for Bransdale by working backward in this way, is of the same order of magnitude as the calibrated value for Farndale.

The plot of the Generalised Sensitivity Analysis (Fig. 5.19b) shows that R_0 is a very sensitive parameter. Efficiencies less than 20% are more likely for R_0 values less than $3.0 \times 10^{-8} \text{ mhr}^{-1}$, while higher efficiencies are likely for higher values.

5.4.2 Calibration and Uncertainty Estimation

Fig. 5.20 shows the results of the uncertainty analysis for the sediment yield model for the calibration period (04/11/98 to 21/11/98). The 90 % uncertainty envelope in Fig. 5.20c fails to enclose the observed sedigraph for most of the simulation. Where it does, the limits are wide apart, and although peaks are fairly well timed, peak shape is mis-represented. Sedigraph peaks are generally too broad, and suggest that the duration of elevated sediment flux is over-predicted. The steepness of the rising limbs suggests a failure to represent the, more gradual, observed build up to maximum flux.

Fig. 5.21 is a comparison of the flow-sediment flux relationship for the observed and 'optimum' predicted hydrographs for the first peak. The observed flow-sediment concentration relationship exhibits reverse hysteresis. As observed flow begins to increase, sediment flux stays approximately constant up to a flow of 0.00025 mhr^{-1} , then rises sharply. The maximum observed flux is attained just as flow begins to decrease. The decline in sediment flux along the falling flow limb is relatively slower than on the rising limb, with flux values higher throughout. As explained previously

(section 3.8.2) such reverse hysteresis may be due to the fact that grid cells in the riparian area which contribute more quickly to runoff, are less likely to have large amounts of sediment available for removal. As flow continues to increase and channel-hillslope coupling increases, sediment from the more distant regions of the catchment are carried in overland flow to the channel outlet. The elevated values on the falling limb indicate that more important sediment sources are located further away from the channel network and their contributions arrive at the outlet at a slower rate. It should be noted that the observed flux is derived as a function of observed sediment concentration (in mg l^{-1}) and observed flow. Hence the relationship is doubly dependent on the combined accuracy of the observed variables. The predicted relationship shows a more rapid rise to the maximum sediment flux. This may be a reflection of the rapid rise of the leading slope of the lognormal distribution of arrival times used in the sediment transport component of the sediment yield model. As predicted flow continues to increase, flux falls rising once more before falling with increasing flow. As flow begins to decrease on the falling limb, flux begins to increase again, but is lower than for the corresponding flows on the rising limb. Flow begins to rise again, and it is here that reverse hysteresis is observed, with flux values higher on the final falling limb. The number of additional loops reflects the predictive failure of the model.

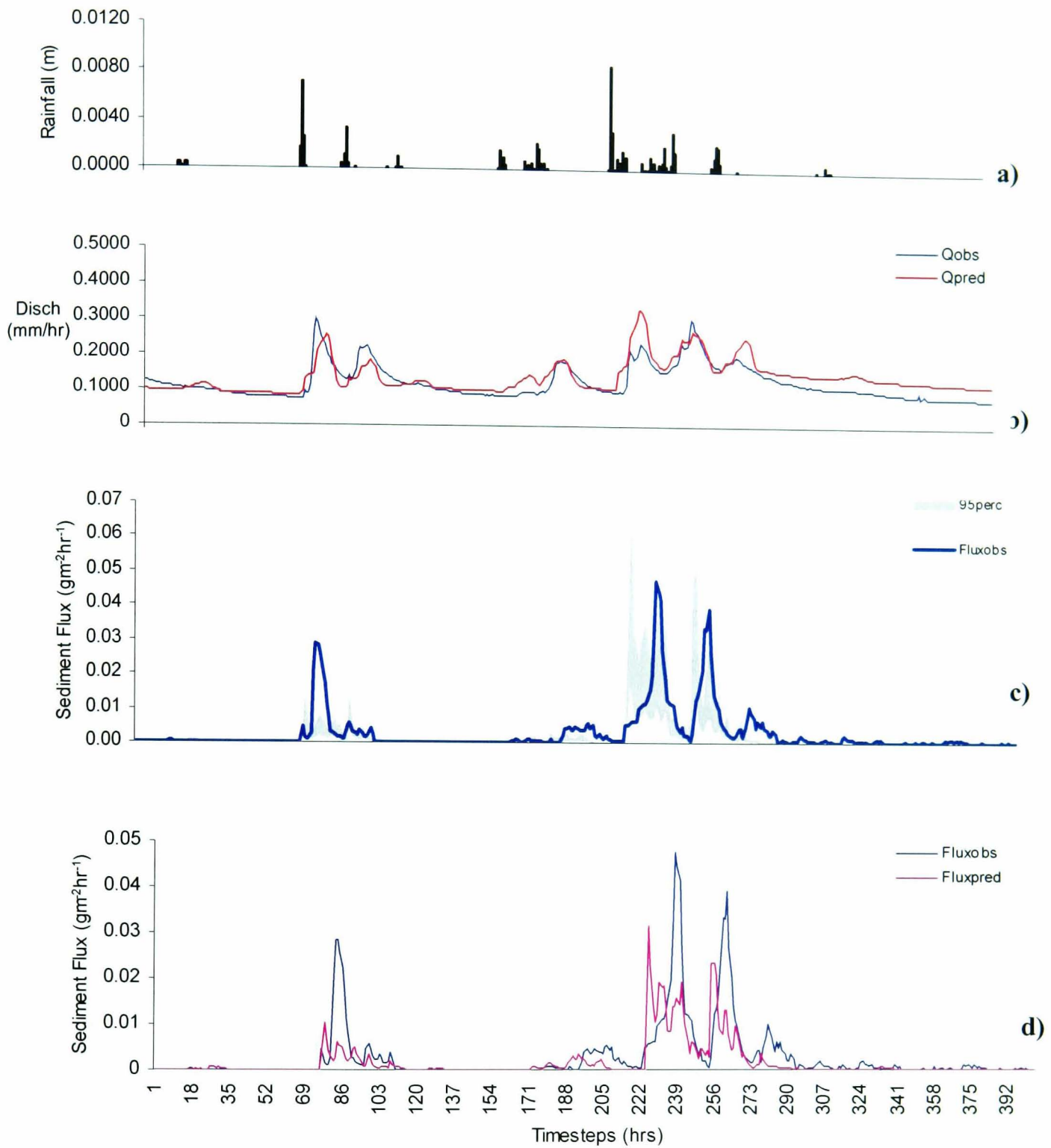


Fig. 5.20 Uncertainty analysis for sediment yield model for 04/11/98 to 21/11/98.

- a) rainfall for the event.
- b) observed and predicted hydrographs.
- c) uncertainty bounds in the sediment flux.
- d) Observed and 'optimum' predicted sedigraphs.

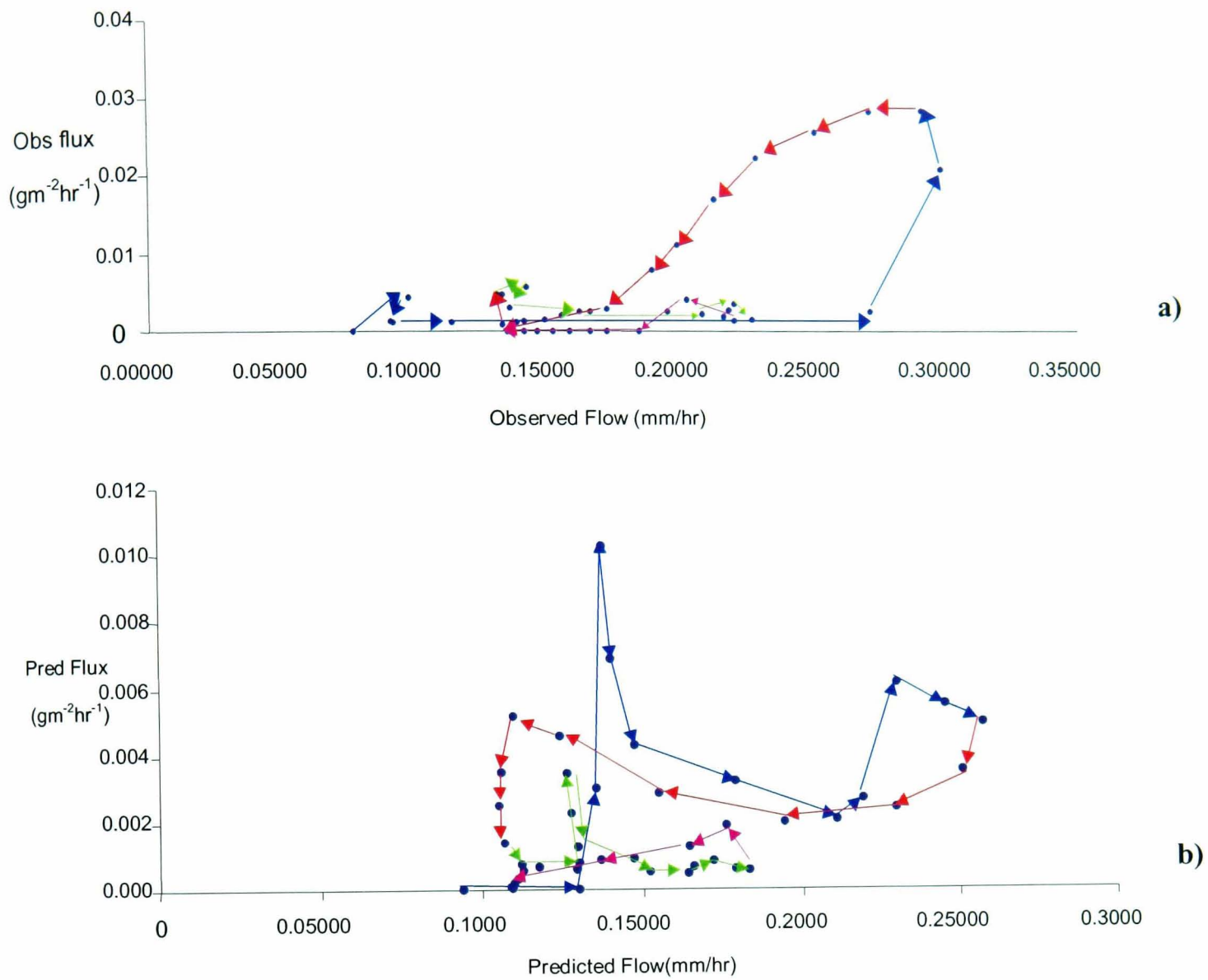


Fig. 5.21 Flow- sediment flux relationships for a) observed and b) predicted hydrographs for peak 1
 —▶ Rising limb of first peak; —▶ falling limb of first peak; —▶ rising limb of second peak; —▶ falling limb of second peak.

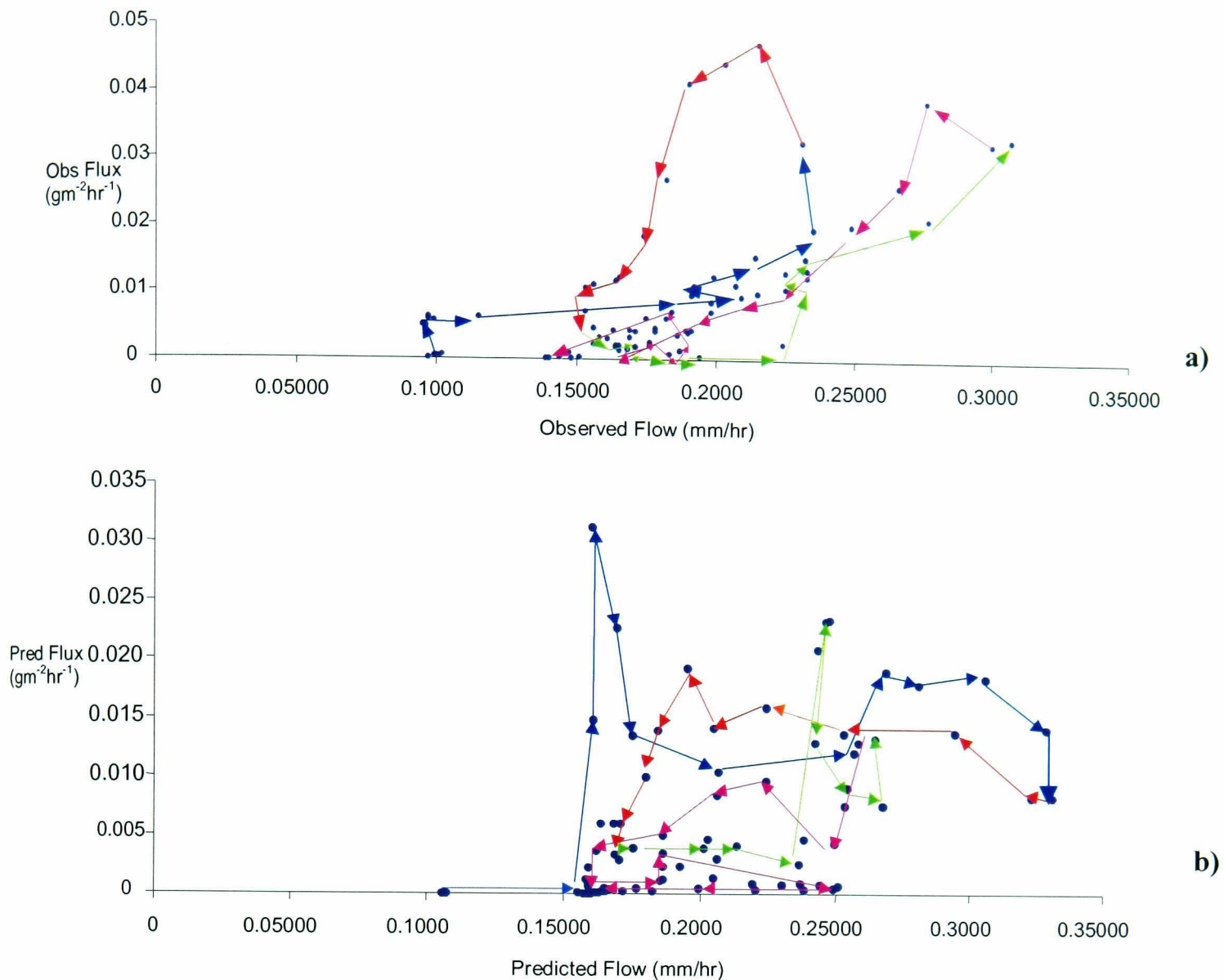


Fig. 5.22 Flow- sediment flux relationships for a) observed and b) predicted hydrographs for peaks 2 and 3. —▶ Rising limb of first peak; —▶ falling limb of first peak; —▶ rising limb of second peak; —▶ falling limb of second peak.

Fig. 5.22 is a comparison of the flow-sediment flux relationship for observed and predicted hydrographs for the double peak ($T=219$ to 287). There is evidence of both reverse hysteresis and exhaustion. For the observed relationship (Fig. 5.22a) sediment flux rises gradually on the rising limb of the first flow peak, then more slowly to the maximum flux just as flow begins to decrease. Sediment flux decline is more gradual on the falling limb of the flow. The second peak flux follows a similar pattern but the effects of exhaustion are reflected in the lower flux values throughout. The predicted relationship is somewhat more complex. Again, the initial increase in flux is very rapid, followed by an equally rapid decline before the first reverse hysteresis loop. This loop exhibits forward hysteresis as peak flow is approached, but reverse hysteresis at lower flows. Flux increases on the rising limb of the second peak to the

maximum flux for this peak, which is less than that of the first, indicating sediment exhaustion as the cells that resulted in the similar rapid response in the first peak are depleted of sediment. Flux falls rapidly with further increase in flow, but rises briefly, just as the second peak flow is attained, indicating the engagement of additional cells with the higher flows. On the falling limb of this peak, flux falls rapidly at first, then more gradually.

The vastly different flow-sediment flux relationships obtained for both peaks is largely due to the rapid initial response at the beginning of each peak, due to the log-normal distribution of arrival times used. The failure to predict the observed reverse hysteresis in the first peak, is due to this rapid response, and the long time taken for the sediment to be dispersed along the falling limb of the lognormal distribution. Similarly, although reverse hysteresis was predicted for half of the first peak of the double peak, and for most of the second peak, the high fluxes predicted at the beginning of the peaks complicated the signal. However, the effect of exhaustion was effectively predicted for the double peak.

In general, failure of the model is largely due to the simplified conceptual nature of the transport component of the sediment yield model. The use of a unit lognormal distribution of sediment arrival times from each grid-cell implies that the general shape of response from any given cell is a multiple of the unit lognormal distribution. It is only the sum of the contributions from different cells (which will vary temporally) which determines the overall shape of the sedigraph peak. In addition, the removal, of all sediment from a grid-cell that contributes runoff, irrespective of the magnitude of the runoff, fails to capture the essential temporal and spatial variation in sediment removal rates due to the variable erosive power of different depths of overland flow. Ideally, some account should be taken of the physical properties that result in such variability, using for example, the unit stream power, which would account for the influence of terrain on soil erosion. Its implementation would require knowledge of the spatial distribution of runoff generation for each grid-cell for each timestep. In addition, simultaneous sediment storage accounting will require cell-by-cell calculations of both flow and flux inputs and outputs which are interdependent. Implementing such a framework will be very difficult within a fully distributed, non steady-state model framework, and would require tremendous computing power.

Spatially Distributed Predictions

Fig. 5.23 are maps of the spatial distribution of accumulated sediment depth at different timesteps during the event, while Fig. 5.24 shows the sediment depth removed from sediment sources. The lowest sediment depths are located in and around the channel network, reflecting the influence of topography on the flow regime which determines the length of the inter-storm period for each grid cell, and hence the rate of accumulation of sediment on each grid cell. Hence, in convergent topography at the bottom of slope and on the valley floor, higher rates of surface saturation results in fewer periods of zero runoff, and hence lower sediment accumulation rates.

Fig. 5.23 shows the spatial distribution of sediment depth at key timesteps in the event. $T=75$ and $T=122$ are the timesteps before and after the first peak, while $T=224$, 248 and 298 are the timesteps before during and after the double peak (fig. 5.20d). At Mapping the spatial distribution of sediment depth at these timesteps permits an analysis of the sediment sources operating at these key timesteps of the event. $T = 75$, the interstorm period is approximately 75 hours, while $T=122$ is the timestep just after the passage of the first sediment peak. The difference between them, Fig. 5.24a indicates that the sediment sources responsible for this peak are along the main channel network. The white areas indicate areas of sediment accumulation during the peak, and these correspond to the hillslope areas where no overland flow is generated.

$T = 224$ marks the beginning of the double peak while $T=248$ is the end of the first of these peaks. Fig. 5.24b shows a similar pattern of spatial distribution of source areas. For the second peak, however, (Fig. 5.24c), source areas are fewer and confined to the main channel in the north of the catchment, and near the outlet. This illustrates the effects of exhaustion on the spatial distribution of sediment, as the inter-storm period after the first peak is too short to allow for replenishment of sediment sources, before the passage of the second peak.

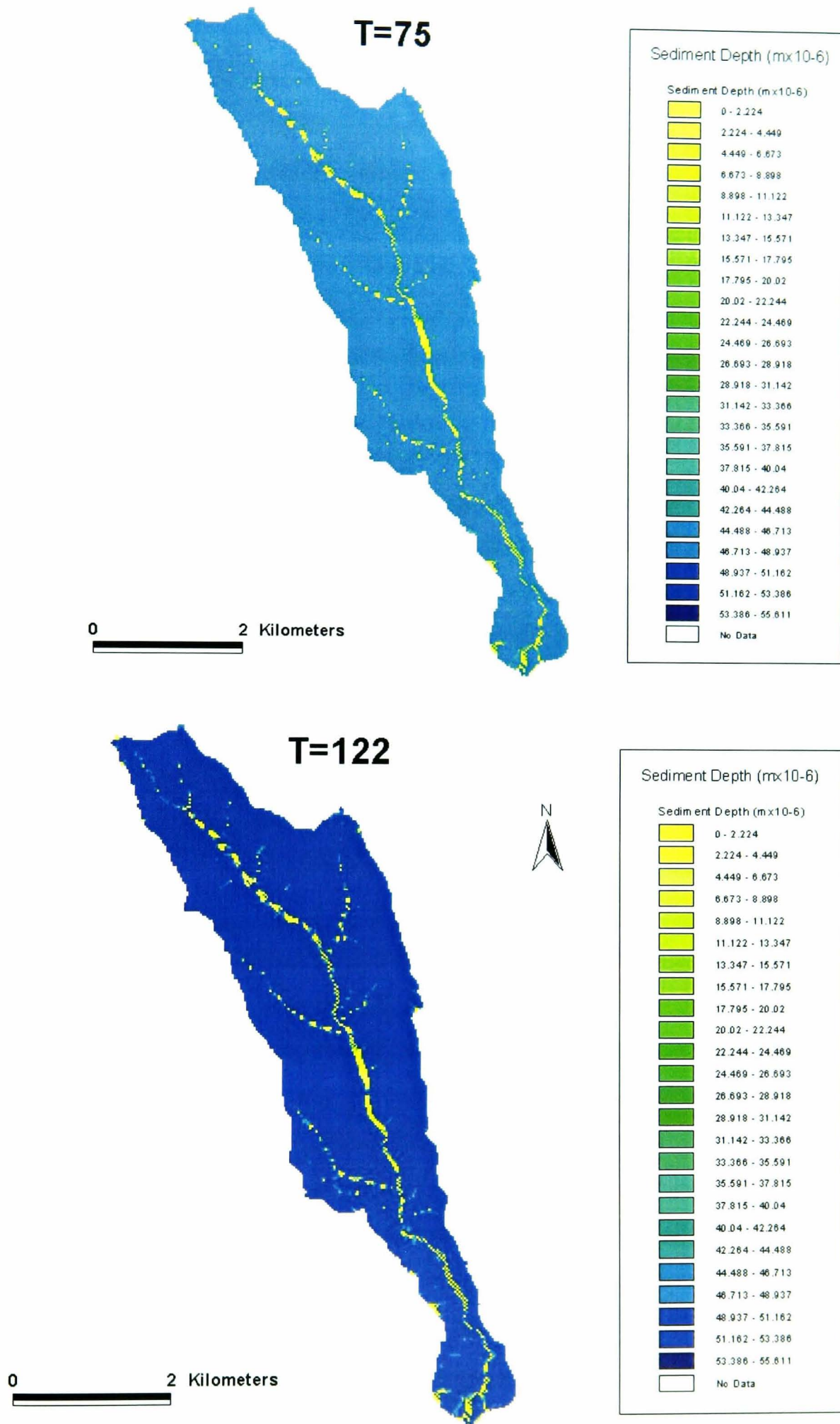


Fig. 5.23 Spatial distribution of accumulated sediment depth at T=75 and 122 hours.

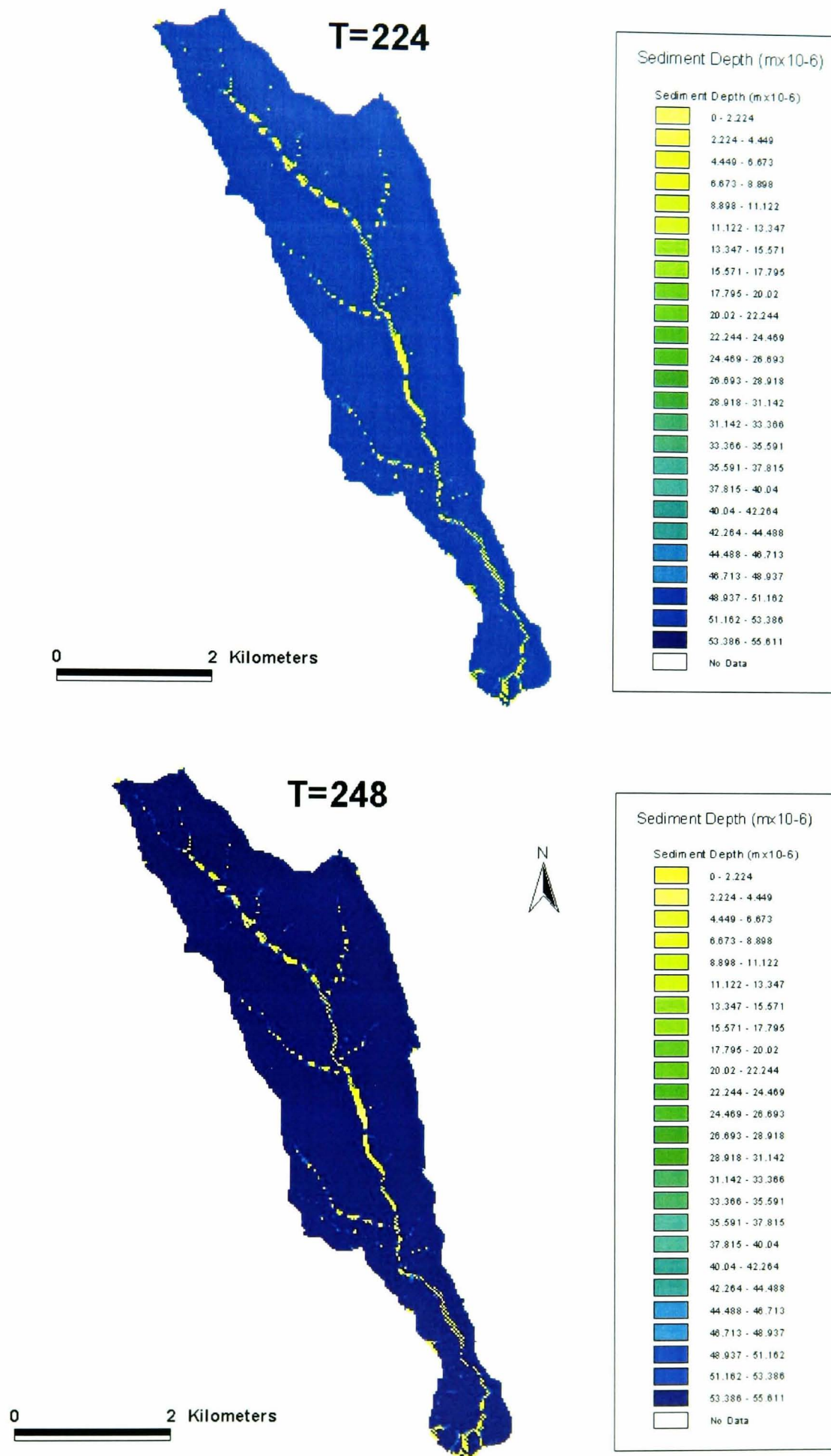


Fig. 5.23 cont'd Spatial distribution of accumulated sediment depth at T=224 and 248 hours.

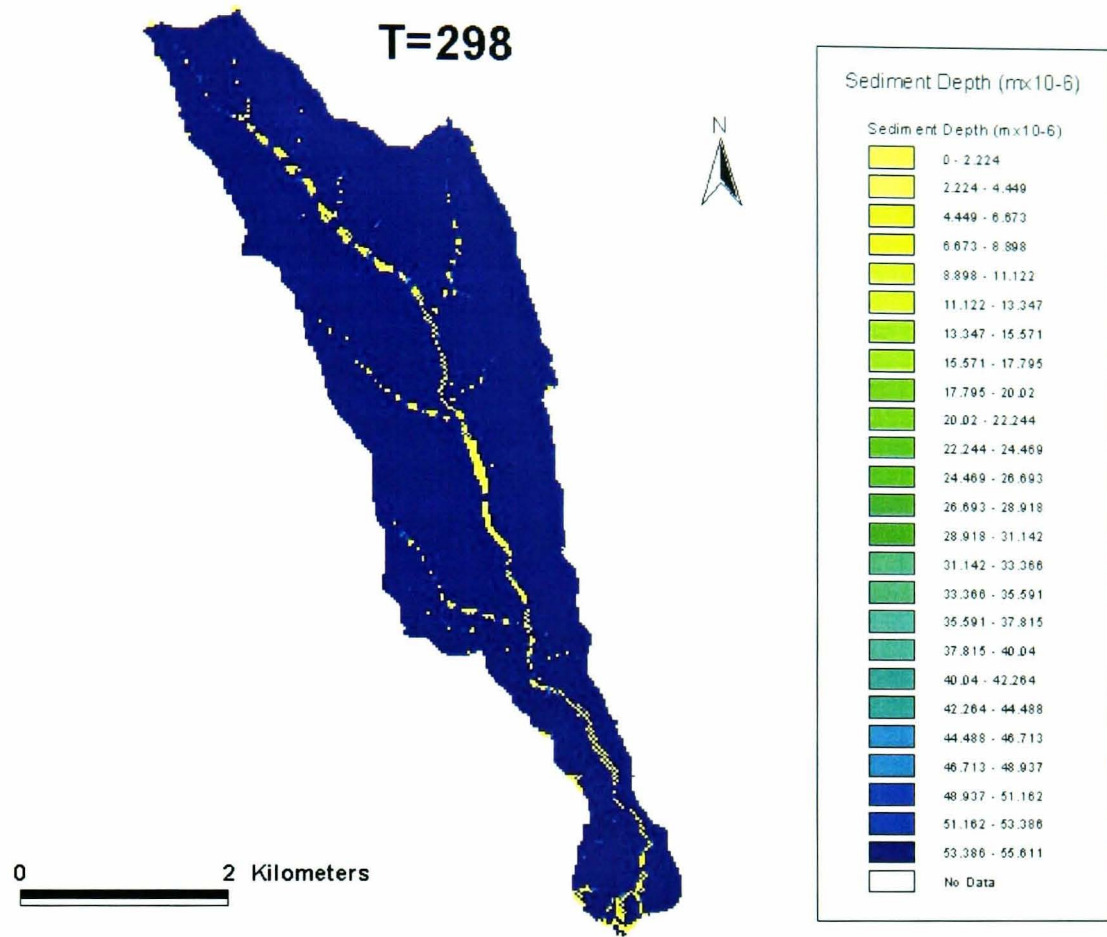


Fig. 5.23 cont'd Spatial distribution of accumulated sediment depth at T=298 hours.

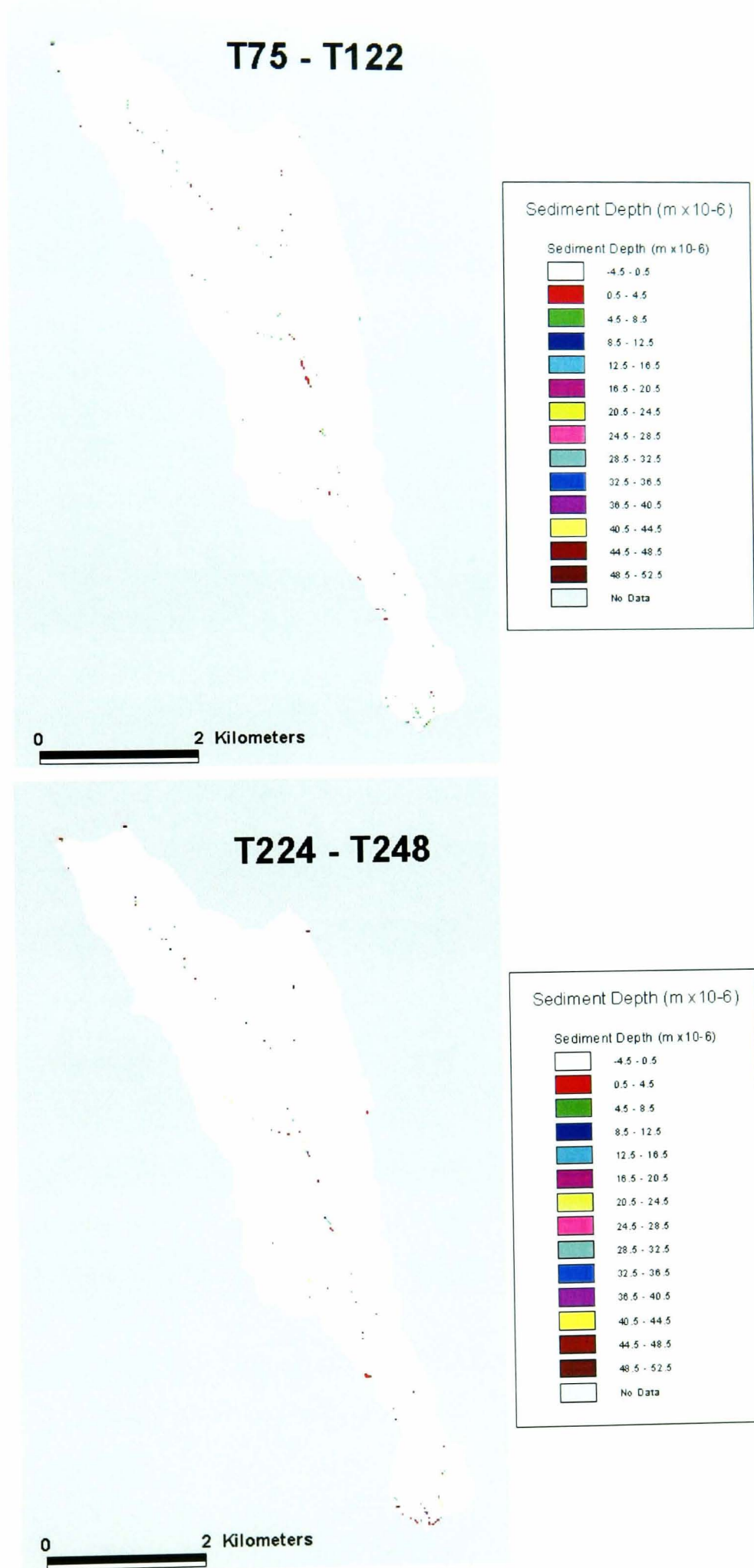


Fig. 5.24 Spatial Distribution of sediment source areas during a) the first peak (T=75 – T=122)
b) the first peak of the double peak (T=224 – T=248)

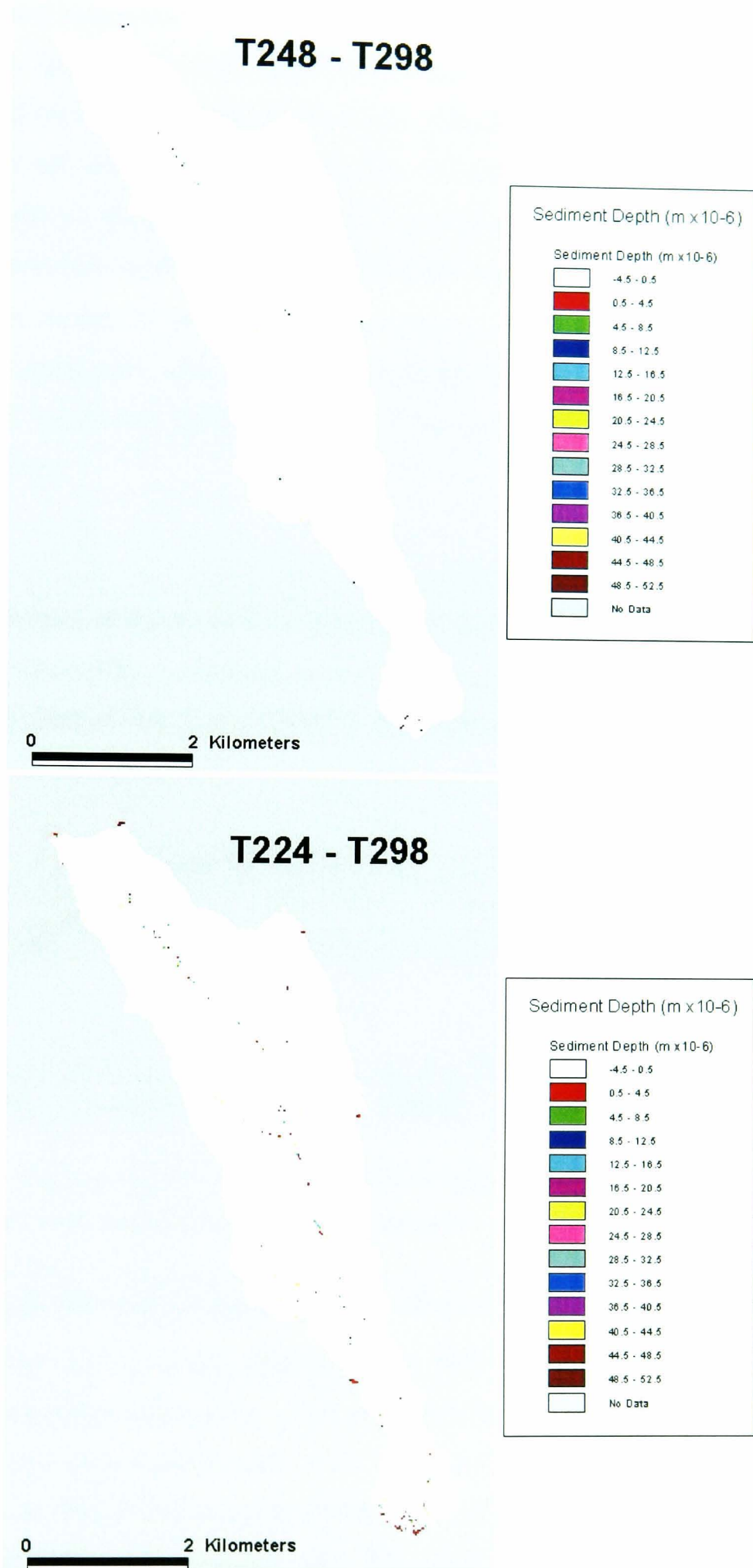


Fig. 5.24 cont'd. Spatial Distribution of sediment source areas during c) the second peak of the double peak (T=248 – T=298) d) the entire double peak (T=224 – T=298).

5.4.3 Sediment Model Validation

Consistent with the approach to the hydrological model validation, the sediment model was validated using a traditional split-sample method, in which the ‘optimal’ calibrated parameter set was applied to independent validation periods. The ‘best’ hydrological parameter set found for each validation period is used as constant input, hence it is the predictive capability of the ‘optimum’ calibrated sediment yield parameter set alone, which is being tested. In addition, uncertainty bounds are derived using the parameter sets from the original calibration Monte Carlo simulations for the validation period, again with individual ‘best’ hydrological parameters for the event.

Validation 1

Fig. 5.25 is the scatterplot of R_0 versus Nash Efficiency for validation 1 (on Event 2). An almost identical scatterplot is obtained as that of the calibration period, with the maximum efficiency attained at $6.21 \times 10^{-8} \text{ mhr}^{-1}$ – very similar to the calibrated value.

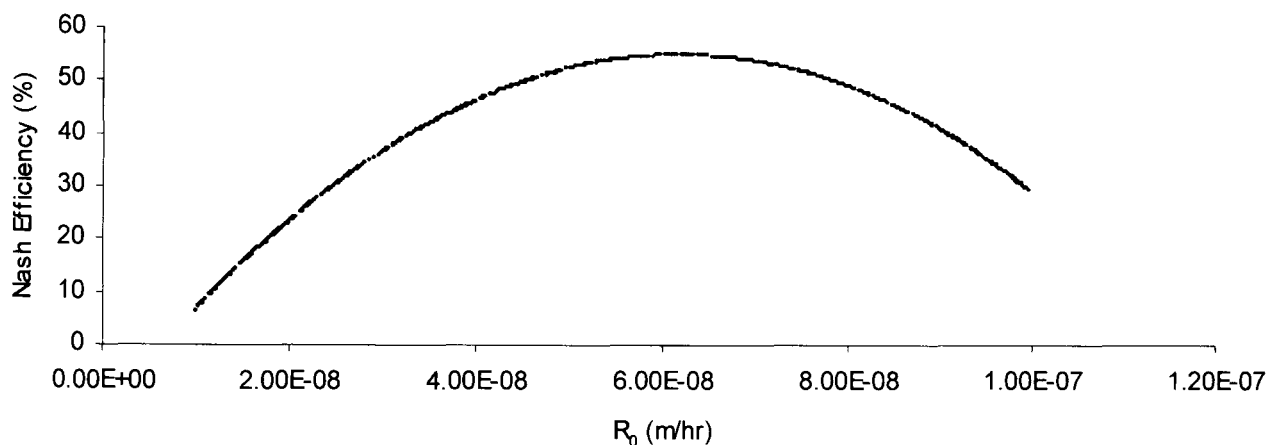


Fig. 5.25 Scatterplot of R_0 versus Nash efficiency for validation period 1.

The uncertainty bounds obtained for the event are qualitatively better than that for the calibration period (Fig. 5.26c). Times-to-peak match well for the entire event, but uncertainty bounds are widest at the peaks. This is largely due to the large uncertainty in predicted peak flows, as is evident in the wide uncertainty limits obtained for the peak flows in Fig. 5.9. Fig. 5.26d is a plot of the observed and predicted sedigraph using the ‘optimum’ calibrated parameter set. Fig. 5.27 is a comparison of the discharge-sediment flux relationships for $T=1$ to 110hrs for the event.

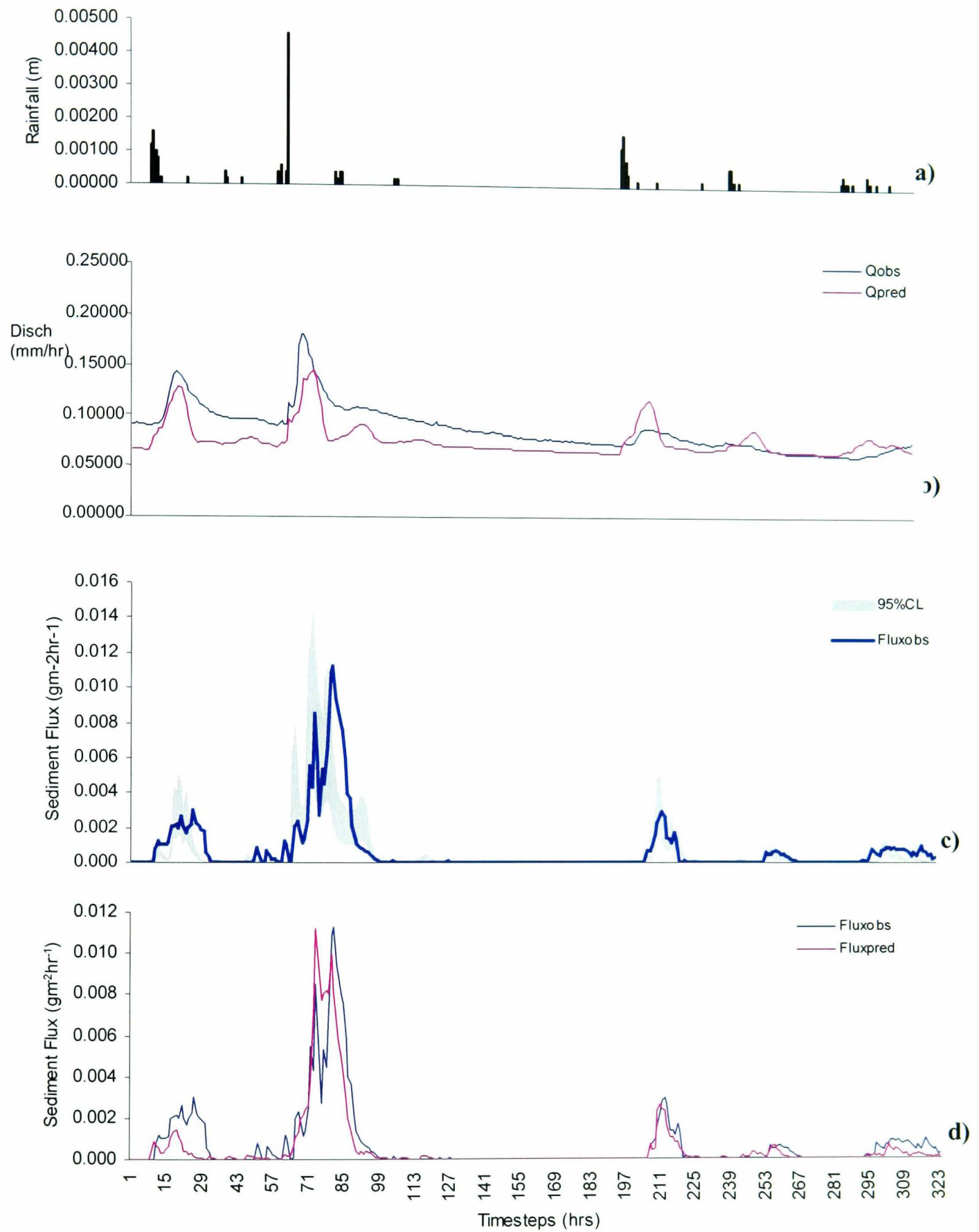


Fig. 5.26 Results of sediment model validation for validation period 1.

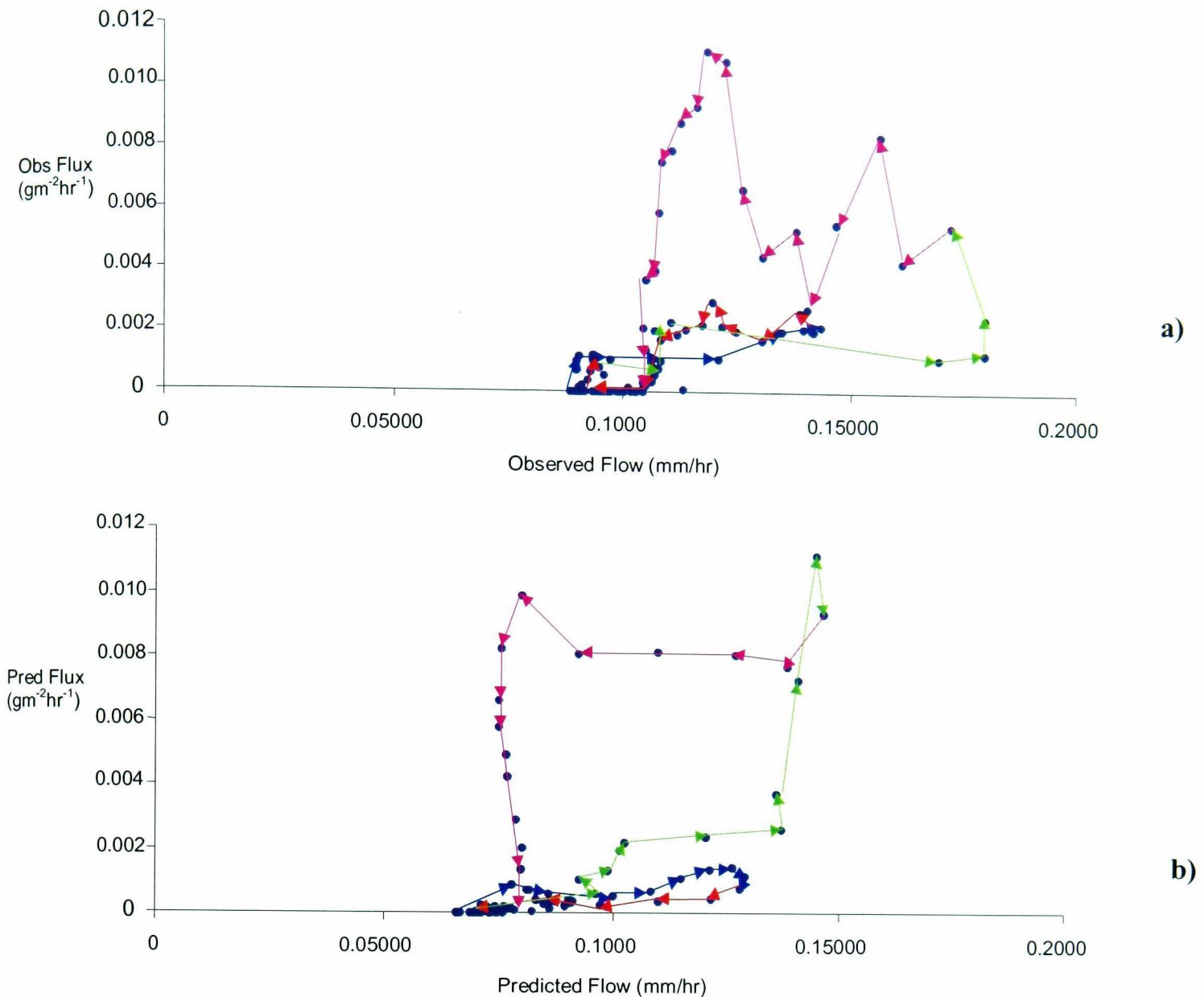


Fig. 5.27 Discharge – Sediment flux relationships for a) observed and b) predicted sedigraphs for T=1 to 110 for validation 1. —▶ Rising limb of first peak; —▶ falling limb of first peak; —▶ rising limb of second peak; —▶ falling limb of second peak.

Fig. 5.27a reveals that observed flux increases gradually on the rising limb of observed flow (blue arrows), followed by a more gradual decrease on the falling limb (red arrows), indicating reverse hysteresis for most of the decline, but forward hysteresis for flows less than 0.00011mhr^{-1} . A similarly gradual increase in predicted flux on the rising limb is predicted (Fig. 5.27b), but both the maximum predicted flow and flux are lower than the observed. Forward hysteresis is predicted for all values of flow.

For the second peak, observed flux increases gradually at first, and then more rapidly as maximum flow is attained on the rising flow limb (green arrows). The

corresponding predicted plot shows a similarly gradual increase in flux with increasing flow. Maximum flux is predicted just before the maximum predicted flow is attained.

Observed flux along the falling limb (purple arrows) is marked by two peaks, the first of which is attained just as flow begins to fall, followed by a sharp decrease in flux, then a rapid rise to the second observed flux peak. Reverse hysteresis is evident in the overall loop. Predicted flux along the falling limb captures this reverse hysteresis. It remains constant for predicted flows between 1.4×10^{-4} and $9.25 \times 10^{-5} \text{ mhr}^{-1}$, and then rises to a maximum before decreasing rapidly with further decrease in flow.

Spatial predictions – Validation 1

Figures 5.28 and 5.29 show the spatial predictions for validation 1. Again, the lowest sediment depths at any timestep are found in, and adjacent to, the channel. Fig. 5.29 indicates that these riparian areas are the main sediment sources for both peaks. There is very little difference between the extent of the source areas for the peaks, due to the low flows that are associated with the event. Hence source area extension is only just discernible in the headward areas of the network.

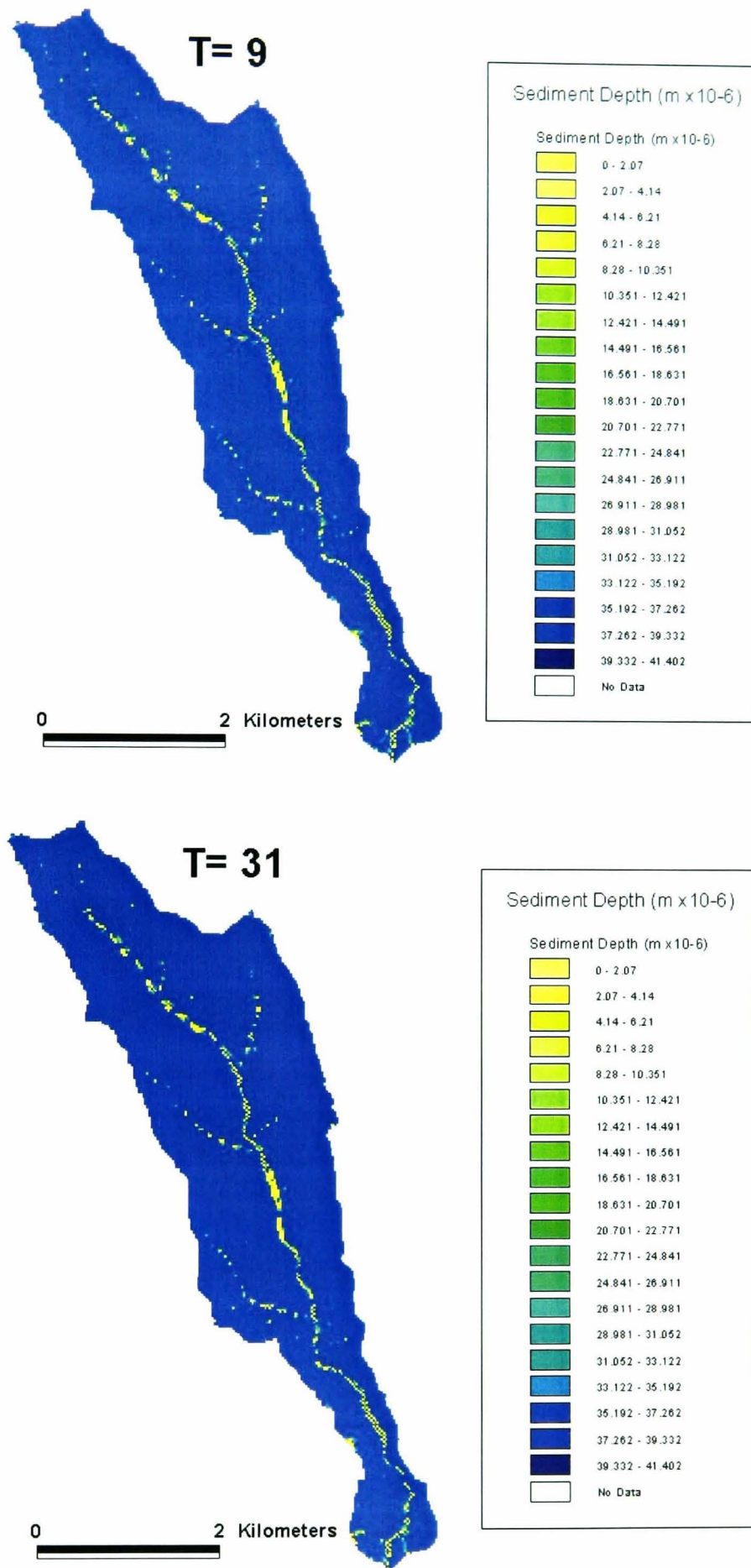


Fig. 5.28 Spatial distribution of accumulated sediment depth at different timesteps for validation 1.

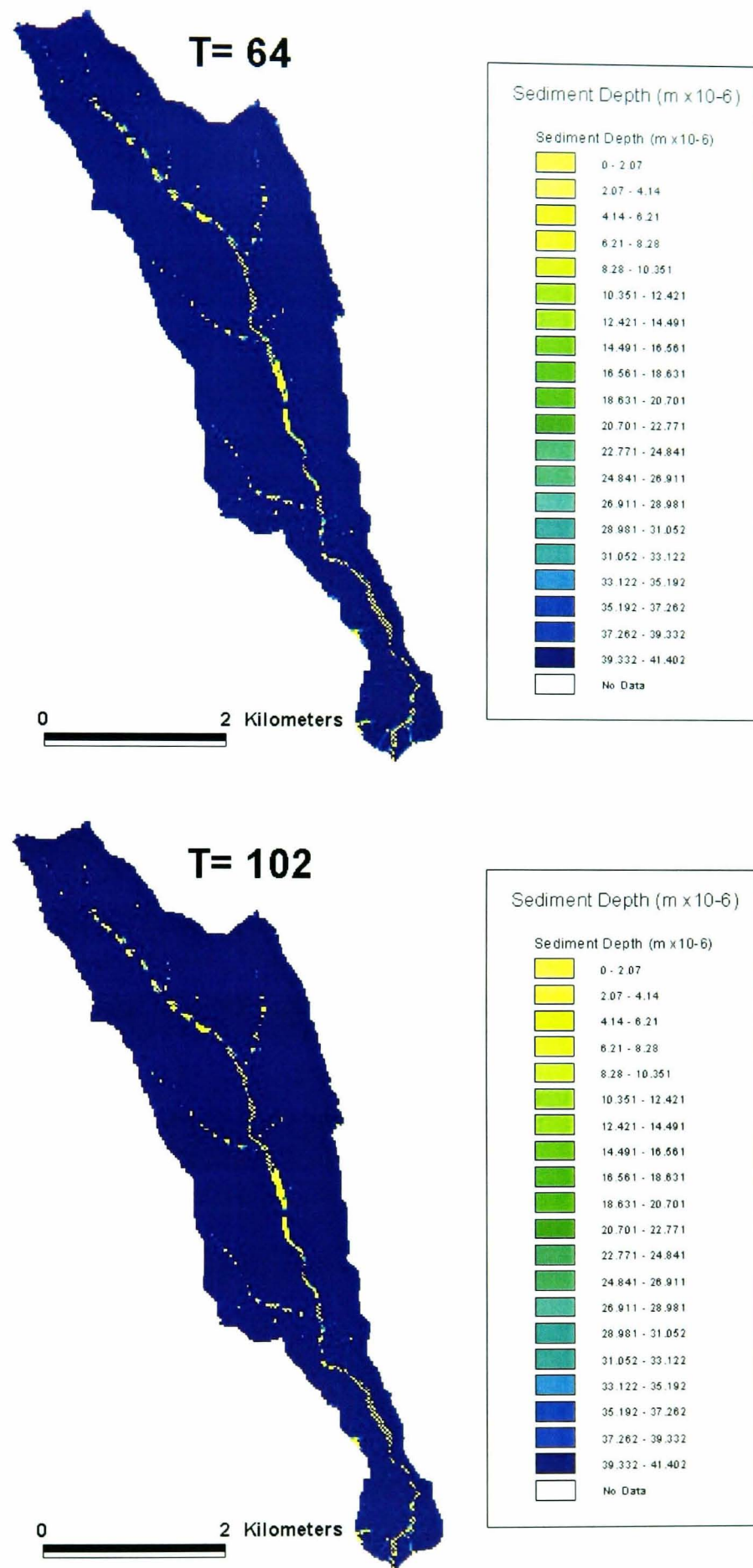


Fig. 5.28 cont'd Spatial distribution of accumulated sediment depth at different timesteps for validation 1.

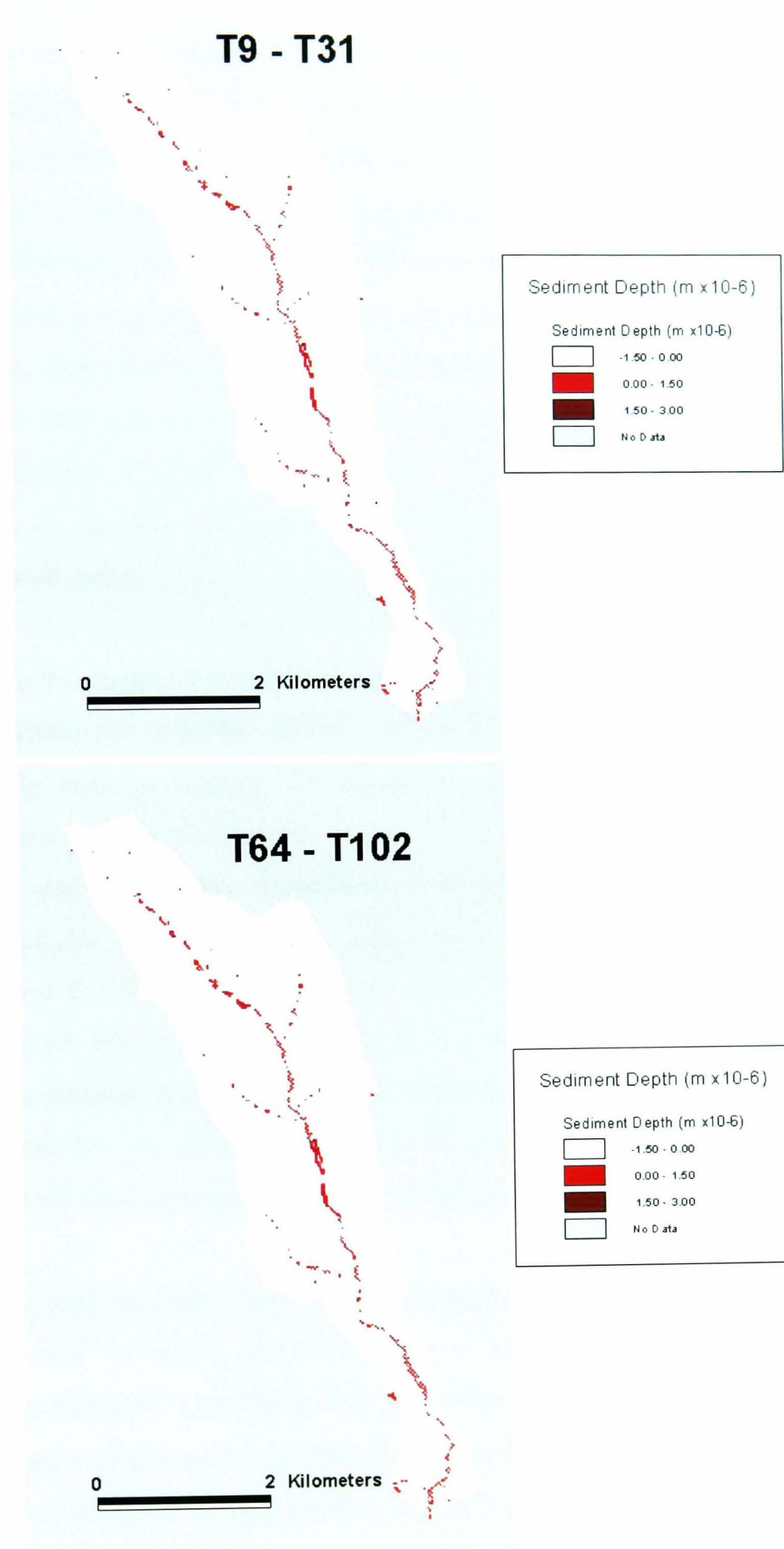


Fig. 5.29 Spatial distribution of sediment source areas for peaks 1 and 2 of event 2.

Validation 2

Fig. 5.30 shows the results for validation 2. Fig. 5.30c is a plot of the observed and predicted hydrographs for a traditional validation. An efficiency of 45% was obtained, which although higher than the calibrated efficiency obtained, is much lower than the maximum efficiency obtained using other parameter sets in the Monte Carlo simulations, as will be seen later. Predictive failure is largely due to the mis-timed peaks. This is because the calibrated channel flow velocity was found to be too low to describe this event, hence the corresponding calibrated sediment channel velocity $CHS2$ (0.35ms^{-1}) is also too low to describe sediment travel rates, resulting in higher times-to-peak than are observed for this event. In addition, the initial sediment accumulation rate, R_0 , and the rate control parameter, K_{sed} , over-estimate the peak sediment flux for both peaks.

Fig. 5.30d and e are the results of the application of 1000 sediment parameter sets that were used to calibrate the sediment model. It should be noted that $CHS2$ was calibrated manually prior to running the model, for this event, given the large discrepancies in times-to-peak found in Fig. 5.30c. A sediment travel velocity, $CHS2$, value of 0.923ms^{-1} was found to best describe the sediment travel for this event. The higher velocity reflects the higher flow rates and hence the higher sediment entrainment and travel velocity. As discussed above, a larger proportion of the catchment is saturated, and hence water makes its way to the outlet faster. This is because of the large number of hillslope cells are ‘converted’ to channel cells, and are actually transferring flow at channel rather than hillslope velocities. Hence the sediment carried in the flow, also gets to the outlet at these higher velocities.

The model was run with the same 1000 simulations used in the calibration, with K_{sed} fixed at $6.21 \times 10^{-4} \text{ mhr}^{-1}$ as before, and $CHS2$ fixed at 0.923ms^{-1} . The optimum R_0 value obtained was $4.09 \times 10^{-8} \text{ mhr}^{-1}$ (Fig. 5.31), with an efficiency of 93.6%. This improved performance of the model for this high magnitude event, may reflect the lower significance of storage of sediment which could affect the earlier simulations.

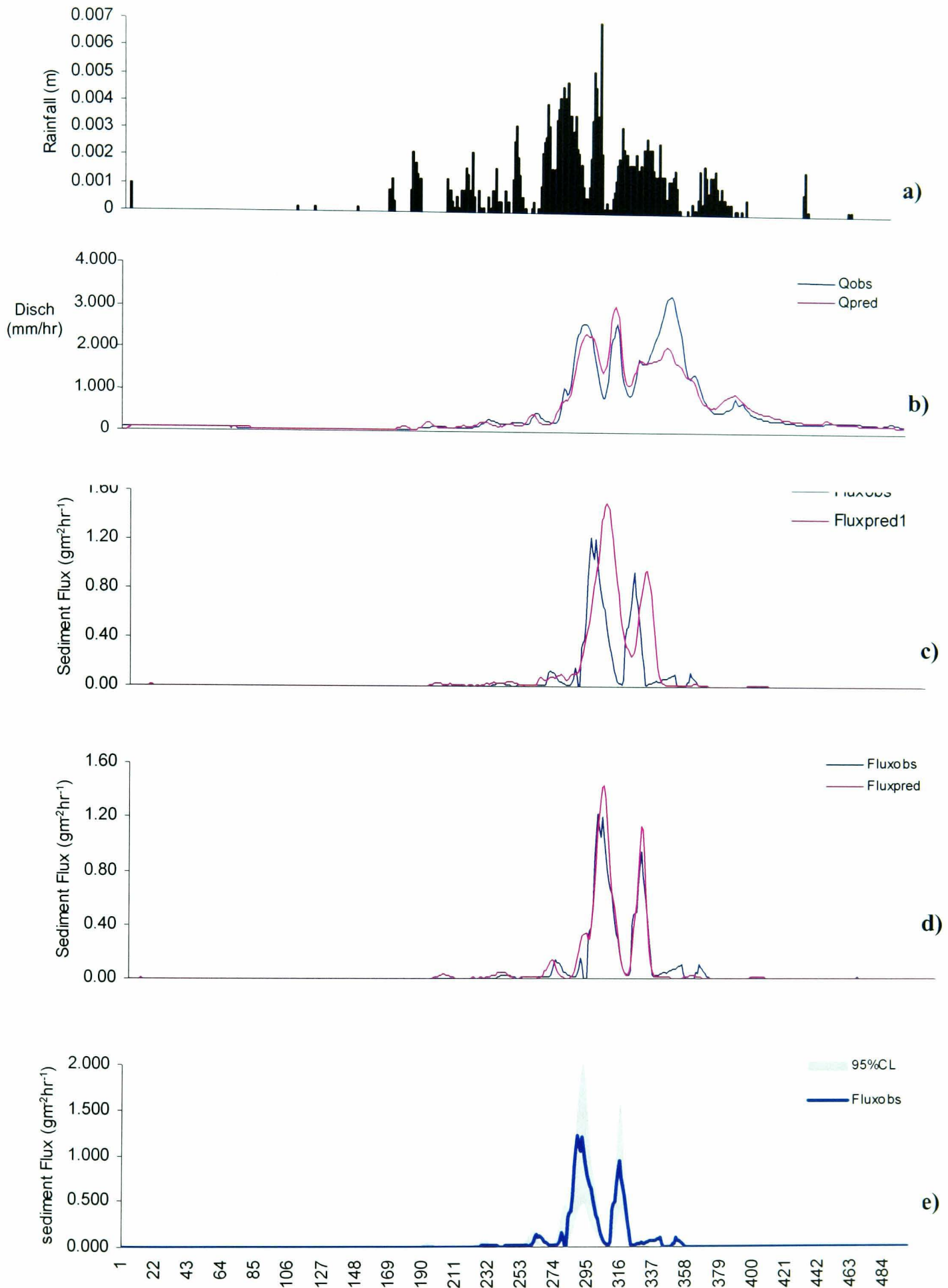


Fig. 5.30 Results of validation 2. a) Rainfall; b) hydrographs; c) uncertainty limits; d) sedigraph using calibrated 'optimum' parameter set; e) sedigraph using 'optimum' validated parameter set for the event.

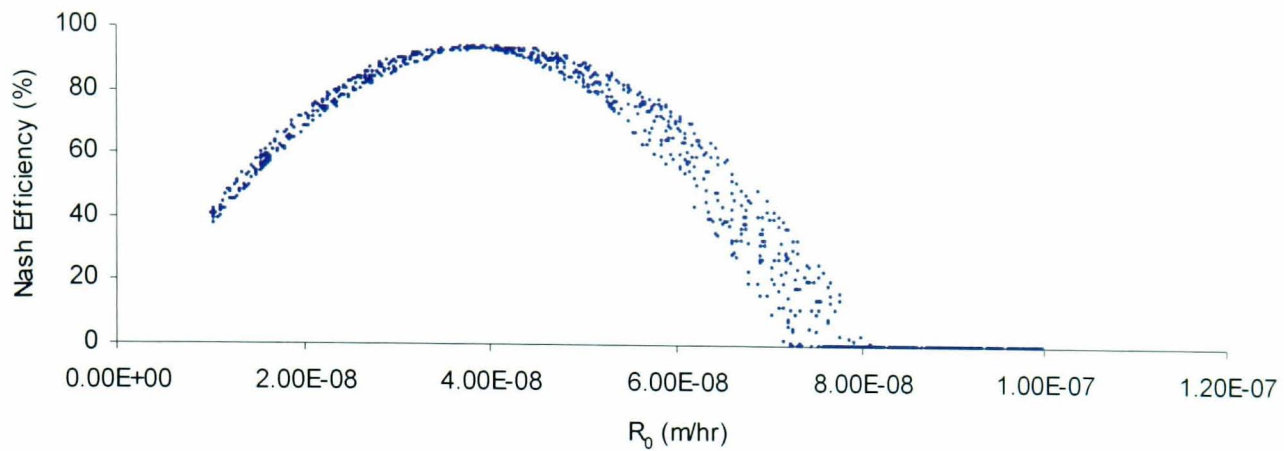


Fig. 5.31 Scatterplot of R_o versus Nash efficiency for validation 2.

Fig. 5.30e shows that the uncertainty envelope encloses both peaks completely, again with the largest uncertainty at peak fluxes. An examination of the discharge-sediment flux relationship for the observed and predicted double peaks (Fig. 5.32a and b) reveals similar patterns for both. Forward hysteresis is observed and predicted on the first peak, while reverse hysteresis is observed and predicted on the second peak. The effects of sediment exhaustion are also evident in both, where sediment flux increases rapidly and almost linearly, with increasing discharge on the rising limb of the first peak (blue arrows). This linear increase reflects the rapid increase in the number of hillslope cells that become saturated as the event progresses. At such rapid increases in discharge, the number of saturated cells becomes the dominant factor for sediment yield rather than the location of saturated cells, as was found in the case for lower flow events. Hence, as the number of saturated cells increases fairly linearly with flow, so too does sediment flux.

As flow decreases on the falling limb of the first peak (red arrows) sediment flux decreases again, approximately linearly (particularly for the observed), with decreasing discharge, with lower flux values than on the rising limb. This forward hysteresis is also indicative of the dominant control of the expansion and contraction of the saturated zone into hillslope cells. As sediment flux increases again on the second loop (green arrows) and decreases to the final minimum (purple arrows), reverse hysteresis and exhaustion are evident. The tighter loops of the observed plot indicates a smaller observed exhaustion effect, with fluxes on the falling limb of the

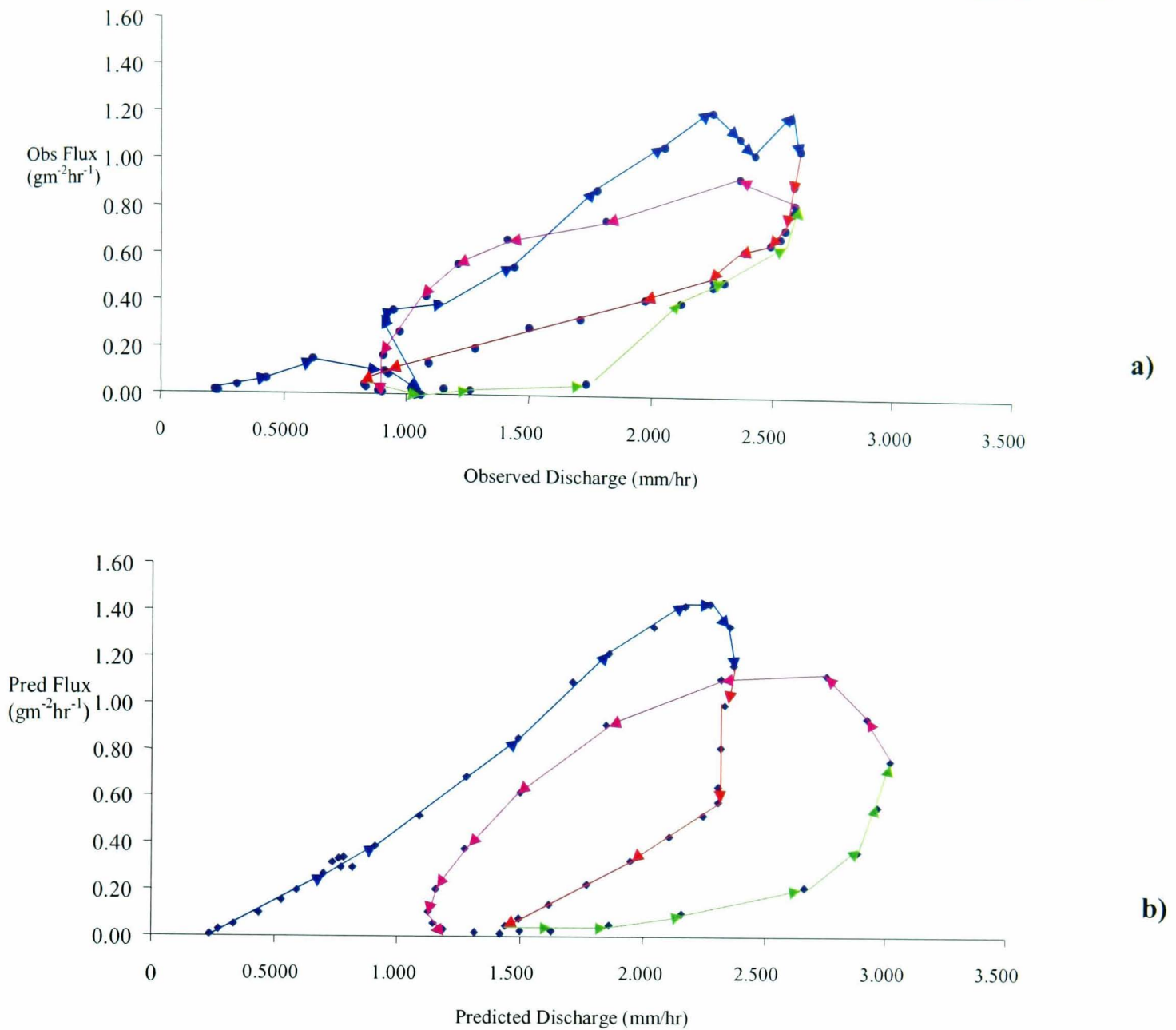


Fig. 5.32 Discharge-sediment flux relationships for a) Observed and b) predicted sedigraphs at $T=274$ to 325.

second observed peak as high as fluxes on the rising limb of the first peak in some cases. However, the maximum fluxes of the second loop for both observed and predicted plots are lower than that of the first loop, although the maximum flows are higher for the second peak than the first, indicating overall exhaustion. A third flow peak is observed (Fig. 5.30b), but is under-predicted. This corresponds to a very small increase in observed flux, which is not predicted. The poorly predicted third flow peak may be partly due to errors in rainfall data, which in turn resulted in the poorly predicted flux, and partly due to errors in observed flow data. The lack of observed flux corresponding to this flow peak is due to equipment failure. However,

it is possible that this is the effect of “ultimate exhaustion”, whereby the catchment, after two sustained flood peaks, is almost completely devoid of sediment by the third peak, and unable to respond.

Spatially distributed predictions

Fig. 5.33 shows the spatial distribution of sediment depth at different timesteps during the event. The maps show a steady expansion in the sediment source areas, from $T=253$ to $T=329$, along the riparian areas adjacent to the channel, and encroaching progressively further up the hillslopes. Expansion is at a decreasing rate, with little or no change between $T=316$ and $T=329$, indicating exhaustion. Fig. 5.34 shows the sediment source areas during the event. Between $T=253$ and $T=289$, on the rising limb of the first peak of the sedigraph sediment sources are in the riparian zone. On the falling limb of the sedigraph, between $T=289$ and $T=310$, sediment sources are further away from the riparian zone, where most of the sediment has already been depleted. The result is an overall sediment source area expanding away from the riparian zone between the start and end of the first peak (between $T=253$ and $T=310$). The sediment source areas for the second peak, are primarily on the hillslopes, indicating exhaustion of sediment in the riparian area during the first peak. The ability to capture the dynamic channel-hillslope coupling which is essential to the sediment delivery process, is evidence of the success of the coupled model. However, because there is no data available to validate the spatial predictions made here, and given the possibility that several different spatial predictions can be obtained for the same hydrograph, it is important to note that there will be uncertainty in the spatial predictions.

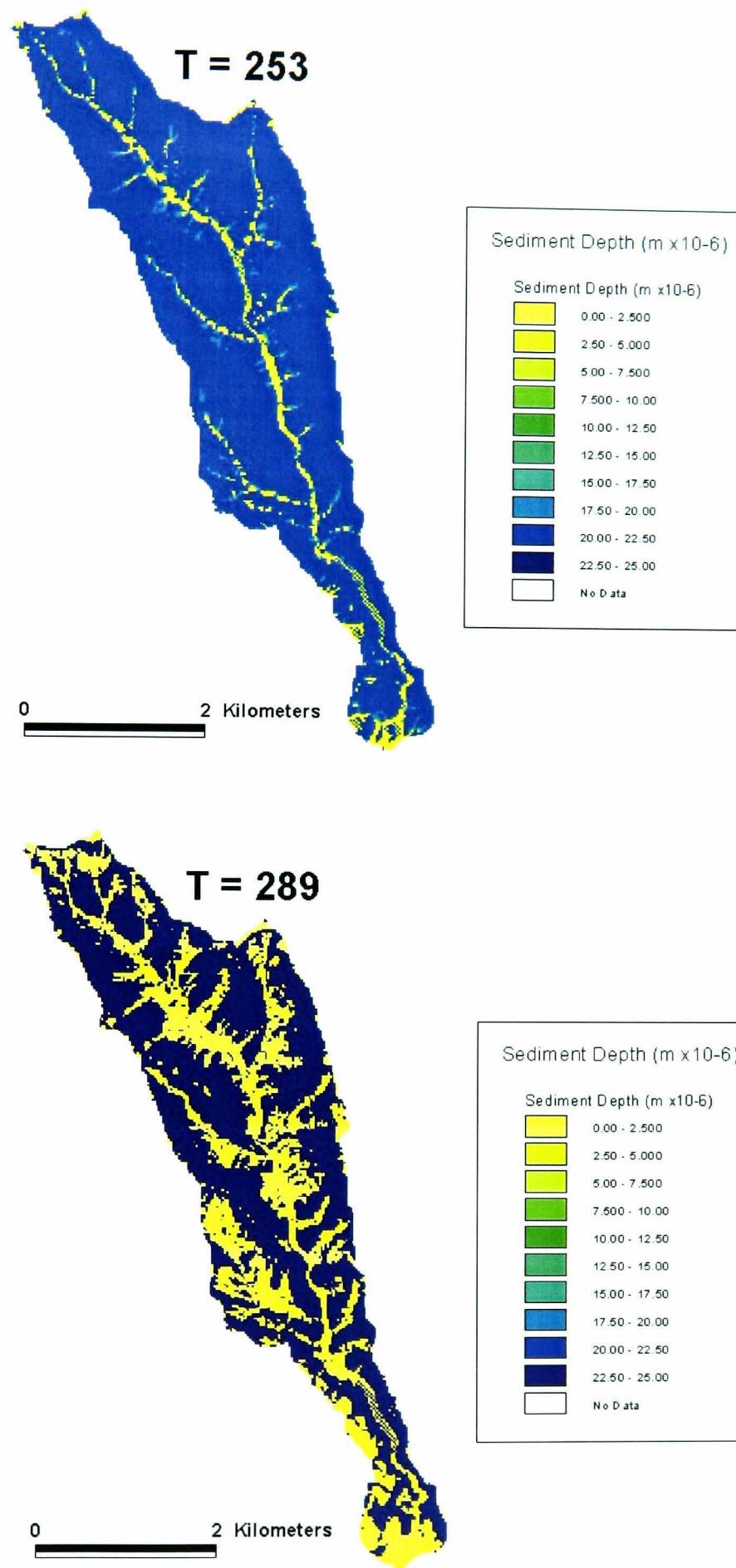


Fig. 5.33 Spatial distribution of accumulated sediment depth at T=253 and 289 for validation 2.

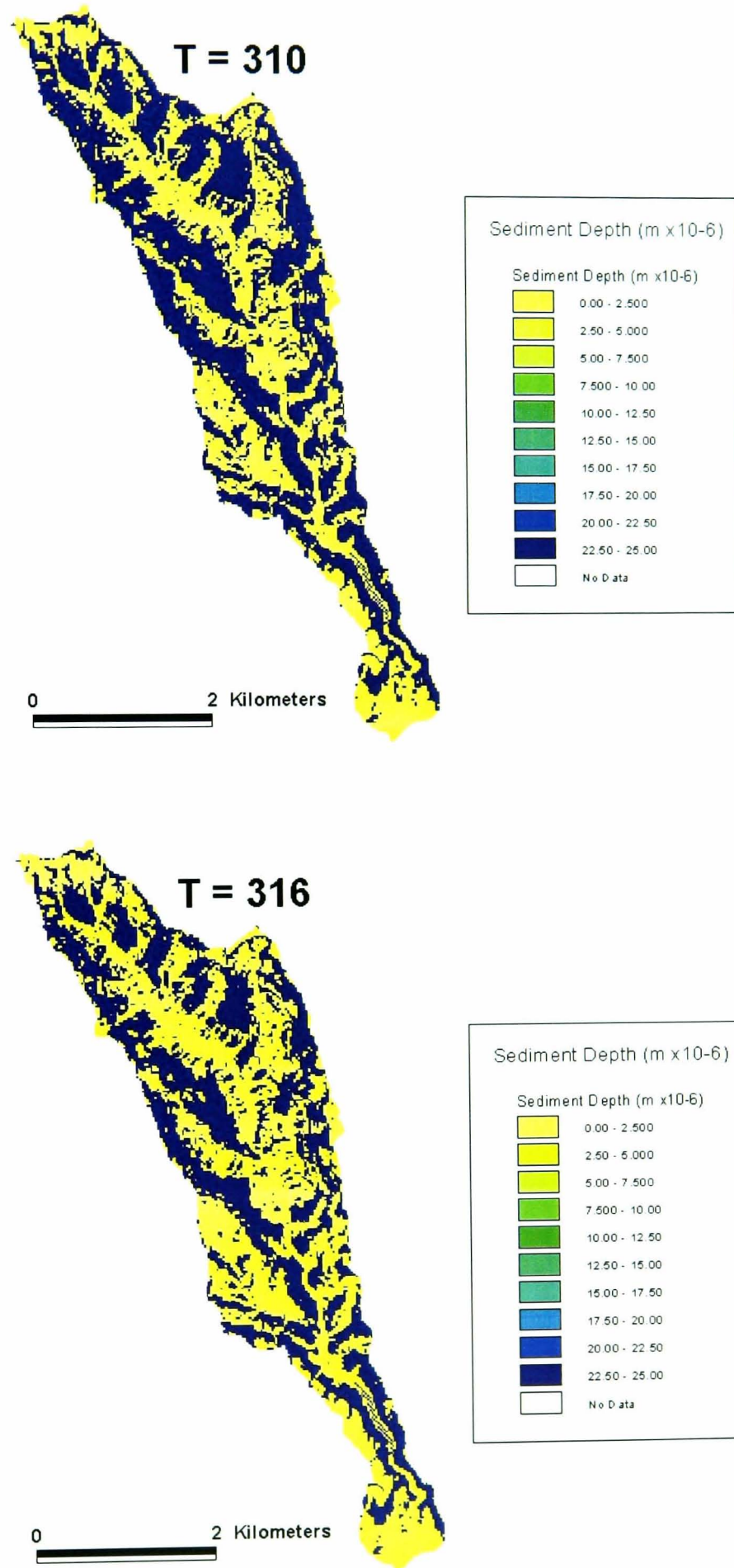


Fig. 5.33 cont'd Spatial distribution of accumulated sediment depth at T=310 and 316 for validation 2.

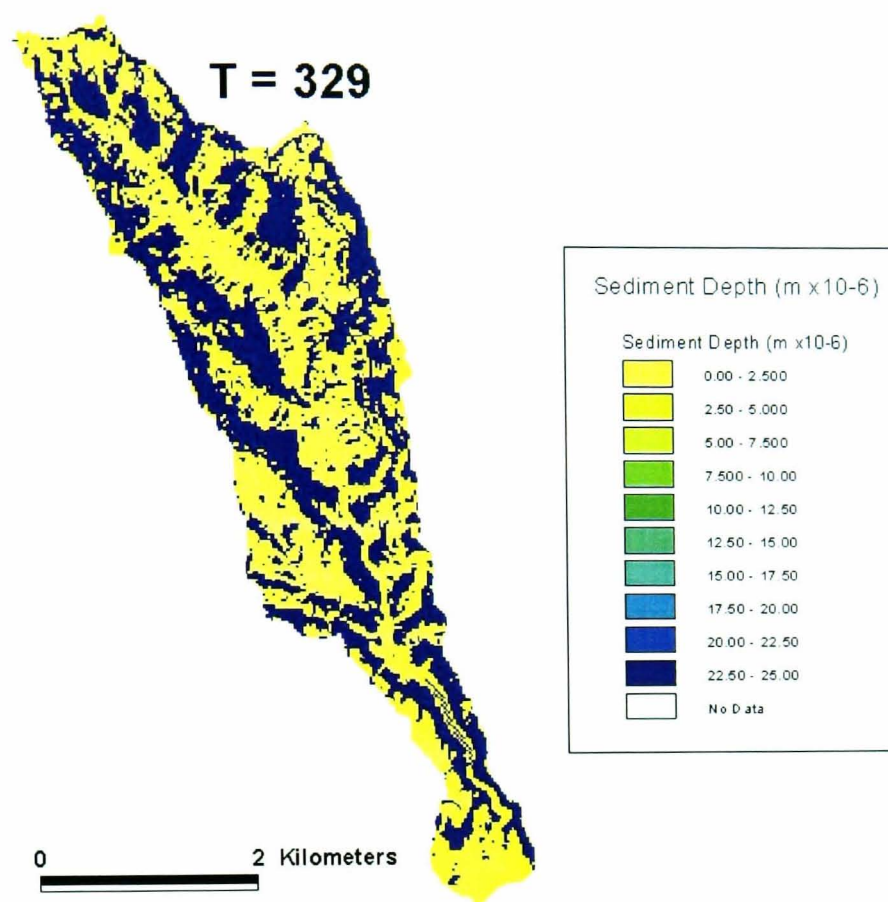


Fig. 5.33 cont'd Spatial distribution of accumulated sediment depth at T=329 for validation 2.

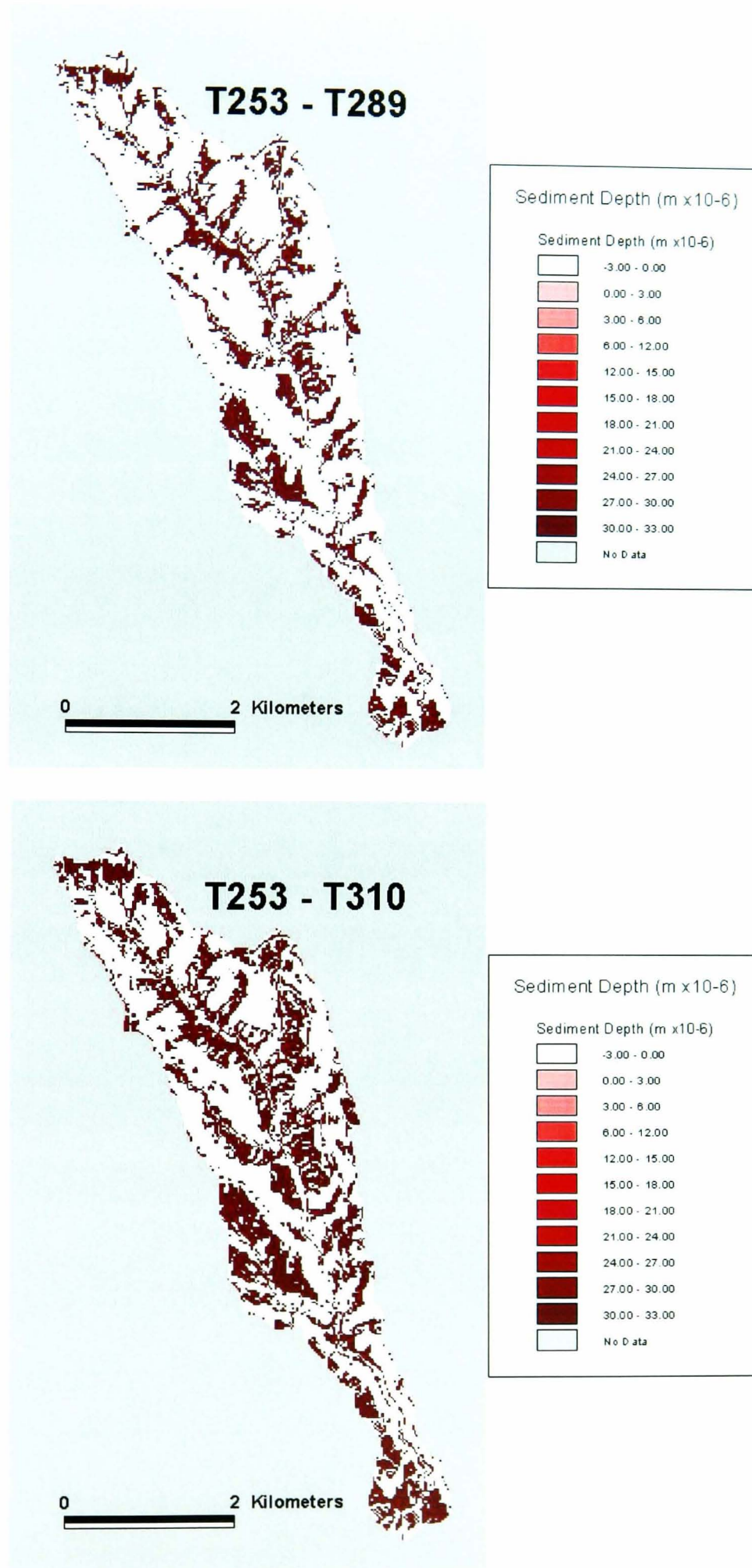


Fig. 5.34 Spatial distribution of sediment source areas for different timesteps in Event 3 – Validation 2

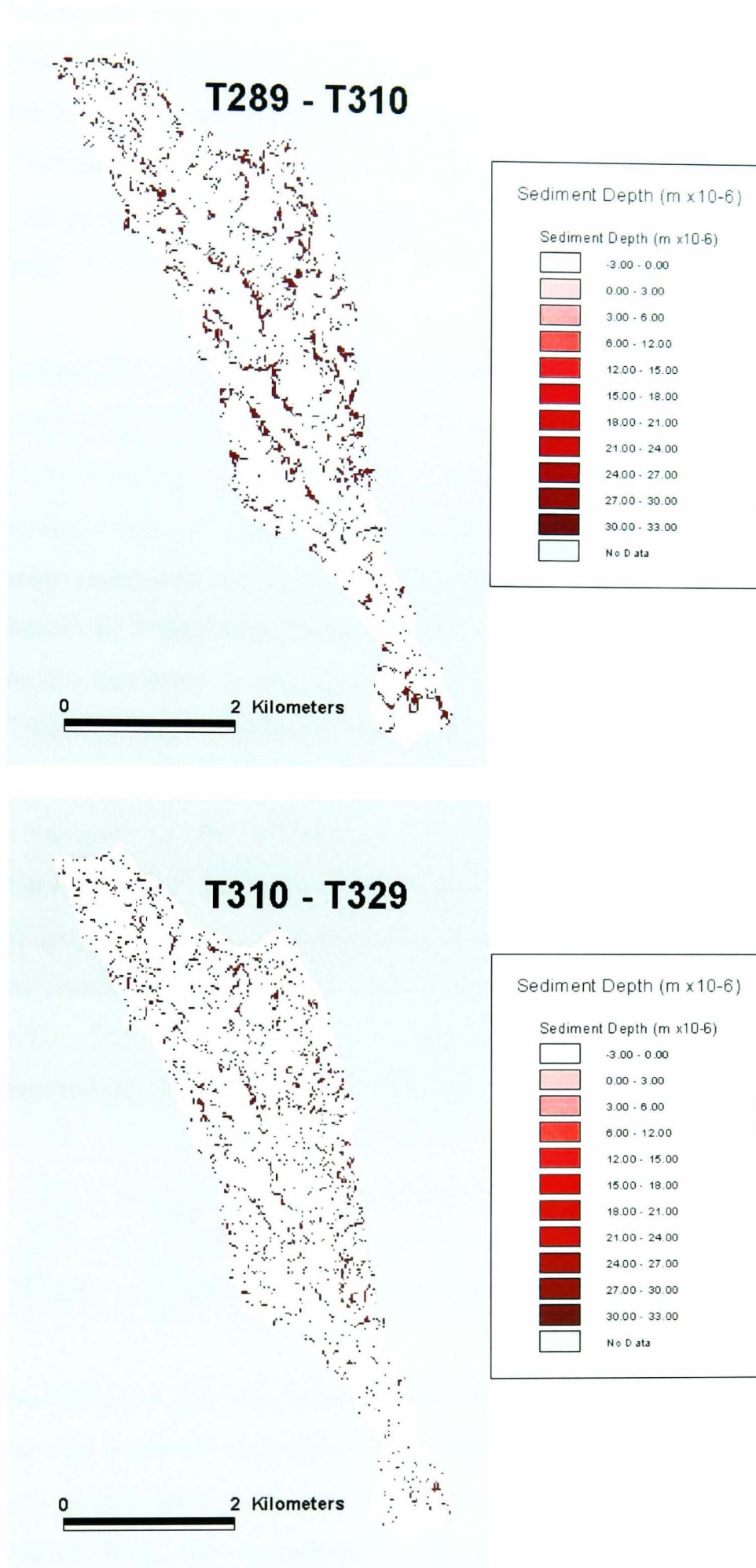


Fig. 5.34 cont'd Spatial distribution of sediment source areas for different timesteps in Event 3 – Validation 2

5.5 Bayesian updating and error propagation in the coupled model

This section describes a joint approach to model conditioning where uncertainty in the hydrological model is updated by considering the joint predictive capability of the hydrological and sediment yield models. In addition, the propagation of model uncertainty from the primary hydrological model to the secondary sediment yield model is investigated.

5.5.1 Updating hydrological predictions using sediment data.

Holding the sediment yield model parameters constant at their calibrated ‘optimum’ values, the original hydrological parameter sets used in the Monte Carlo simulations, are used to vary the hydrology and obtain sediment yield predictions from the coupled hydrological-sediment yield model. The prior likelihood distribution is that based on the original distribution for hydrological parameter sets. New likelihoods are derived based on the predictive capability of each hydrological parameter set with respect to sediment yield. Hence, only simulations which are behavioural for both the hydrological and sediment yield models are retained, where critical Nash efficiencies of 40% and 30% are used for the hydrological and sediment models respectively. Simulations that were previously behavioural for the hydrological model, are deemed non-behavioural if they fail to give behavioural sediment yield predictions. Two different combined likelihood measures are used to update the uncertainty bounds, using Bayes’ equation. The first is based on the average weight of model simulation efficiencies for both models. Thus equation 5.3 becomes:

$$L_{i_{av}} = \frac{1}{C} * \frac{1}{2} \left(\frac{Eff_{i_h}}{\sum_1^{N_{bh-s}} Eff_{i_h}} + \frac{Eff_{i_s}}{\sum_1^{N_{bh-s}} Eff_{i_s}} \right) \quad [5.4]$$

where in this case, Eff_{i_h} and Eff_{i_s} are the hydrological and sediment yield model efficiencies respectively, for the i^{th} simulation, for which both the hydrological model and sediment yield model predictions are behavioural, N_{bh-s} is the number of simulations for which both the hydrological and sediment yield models are behavioural, and C is $\sum L_{i_{av}}$.

The second combined likelihood, uses the product of the respective model efficiency weights to derive new likelihoods. Thus for each behavioural simulation, a posterior likelihood is derived as:

$$L_{imul} = \frac{1}{C} * \frac{Eff_{i_h}}{\sum_1^{N_{bh-s}} Eff_{i_h}} * \frac{Eff_{i_s}}{\sum_1^{N_{bh-s}} Eff_{i_s}} \quad [5.5]$$

where C is $\sum L_{imul}$.

Results and Analysis

Figures 5.35, 5.36 and 5.37 show the cumulative likelihood distributions for prior and posterior likelihoods for the five main model parameters. As stated earlier, all parameters, except m , have prior cumulative distributions that are approximately along the line of equally possible values. The posterior cumulative distributions of all parameters show some modification, for both likelihood measures, with a larger modification for the multiplicative likelihood in all cases. Figs. 5.35a, 5.36a, and 5.37a show that the most rapid increases in the cumulative multiplicative likelihood distributions for m , occur between 0.03 and 0.04m, 0.05 and 0.06 m, and, 0.01 and 0.02 m, for event 1, 2, and 3 respectively, suggesting that their optimum values lie within these ranges. However, it is only for events 1 and 3 that the change from prior to posterior is from higher to lower values. The implication is that sediment yield is better predicted with m values that are lower than those found for the hydrology alone. For event 2, however, the shift is from lower to higher values. The formerly insensitive K_0 is severely restricted by sediment data, showing critical values at 220, 400 and 250mhr⁻¹ for events 1, 2, and 3 respectively. The higher critical K_0 value for event 2, appears to compensate for the increase in m value observed, and is indicative of the interaction between these two parameters. *SRMAX* shows critical values at approximately 0.003, 0.005 and 0.00175m respectively - the lower value for event 3 indicating the lower storage for this large event. *ETF* shows some modification at 0.4 and 0.9 for event 1, 0.4 for event 2, and at 0.9 for event 3.

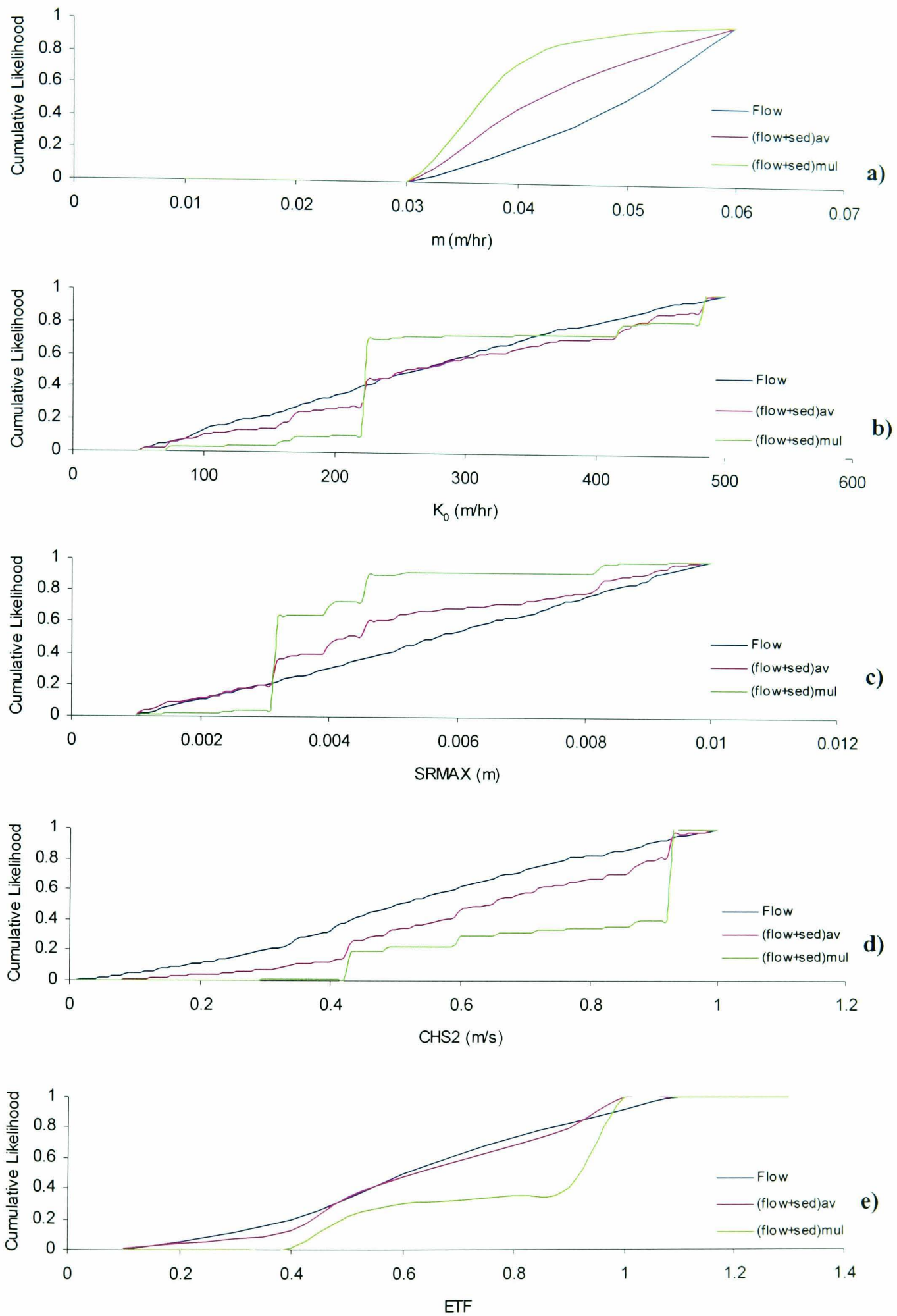
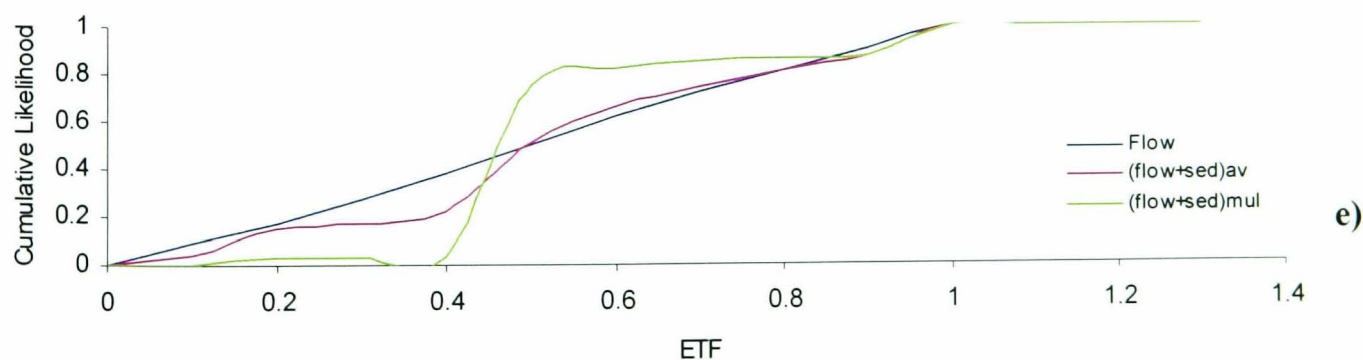
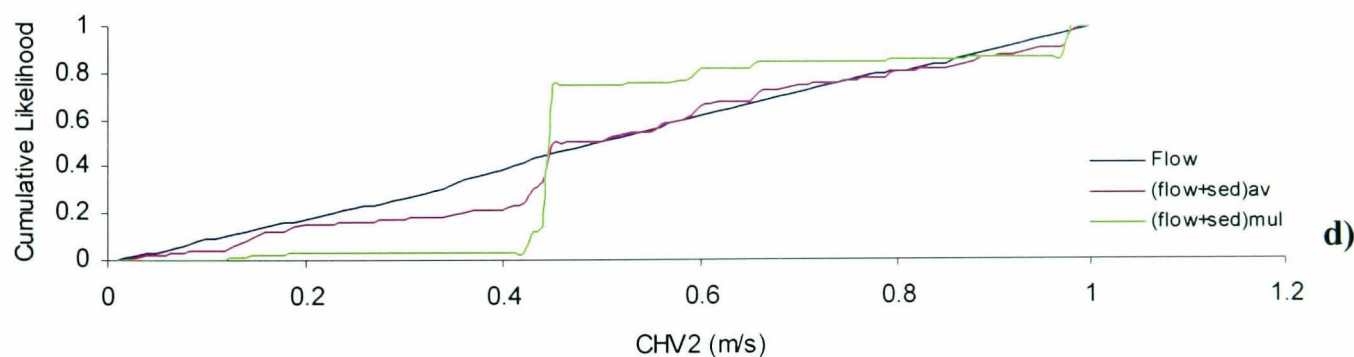
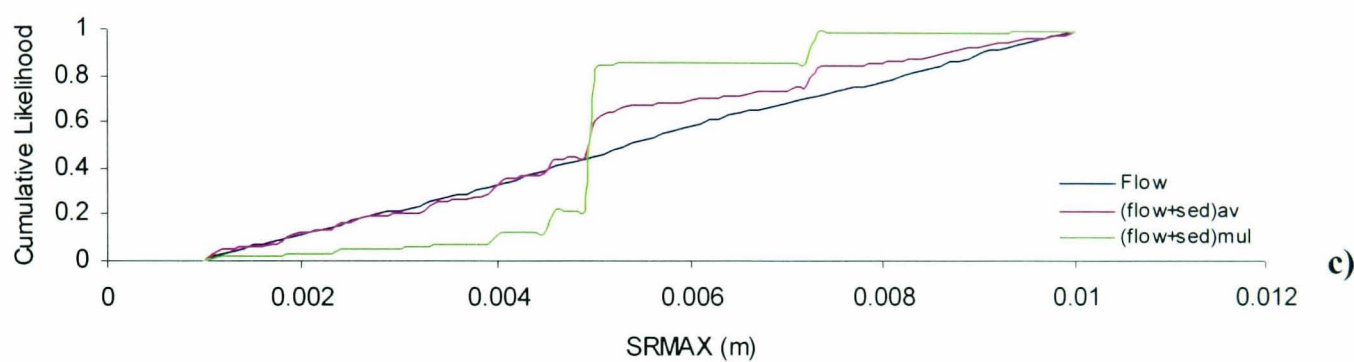
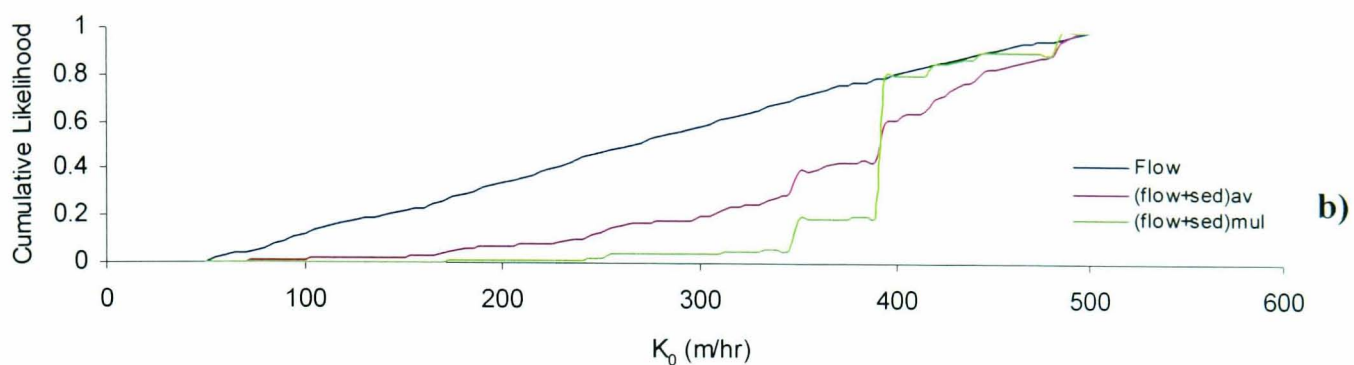
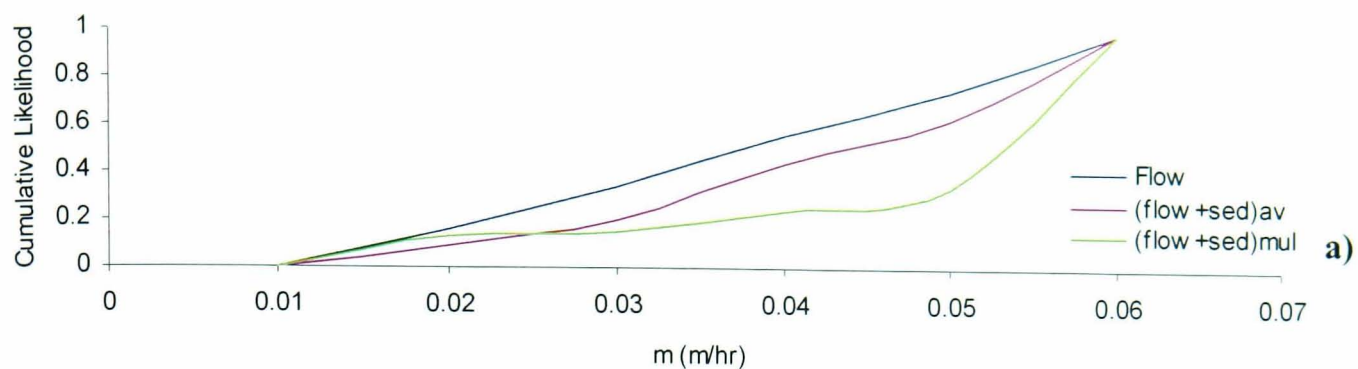
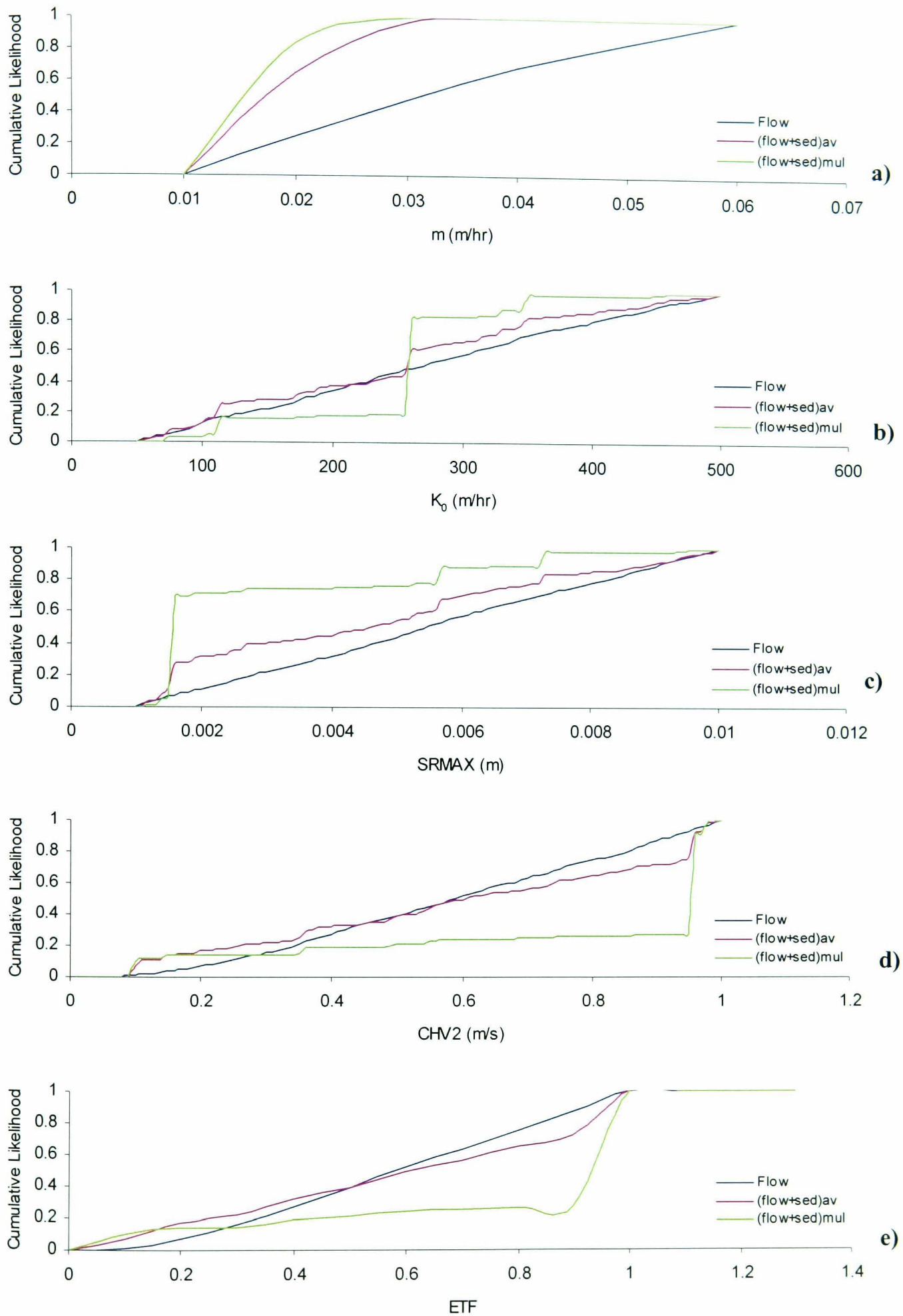


Fig. 5.35 Event 1. Prior and posterior cumulative likelihood distributions for 5 hydrological model parameters, conditioned on flow only, and on flow and sediment data using two different likelihood measures.



5.36 Event 2. Prior and posterior cumulative likelihood distributions for 5 hydrological model parameters, conditioned on flow only, and on flow and sediment data using two different likelihood measures.



5.37 Event 3. Prior and posterior cumulative likelihood distributions for 5 hydrological model parameters, conditioned on flow only, and on flow and sediment data using two different likelihood measures.

These updated distributions suggest that the sediment yield data has helped to constrain the likely values of the hydrological model, and decrease the overall uncertainty. Previously insensitive parameters for which all parameter values were equally likely, have been restricted to critical values, or a smaller range of values, than was the case for distributions conditioned on flow data alone. This is a significant result as it means uncertainty in model predictions will also be constrained.

Figures. 5.38, 5.39 and 5.40 show the uncertainty in the hydrological model conditioned on; a) flow data alone b) flow and sediment data for a combined likelihood derived by equation 5.4, and c) flow and sediment data for a combined likelihood derived by equation 5.5, for events 1, 2, and 3 respectively. There is little difference between uncertainty limits conditioned on flow alone, and on flow and sediment using the average weighted combined likelihood, L_{iav} . For event 1, Fig. 5.39b shows that the lower limit has shifted to higher discharge values. This is indicative of the shift towards lower m and higher K_0 values, resulting in simulations with higher peak flows being retained as behavioural. The effect is only apparent in the modification of the lower limit, because the upper limit would already have been at the maximum peak flow values. A similar modification is observed in event 3, Fig. 5.40b, but only the lower limit of the third peak is affected. For event 2 (Fig. 5.39b) a slight decrease in the upper limit of the recession flows is observed. The higher m and K_0 values for event 2 above have resulted in a deeper soil with reduced recession flow being predicted, which would be most evident in changes to the upper boundary of recession.

The multiplicative likelihood, L_{imul} reduced the width of the uncertainty bounds more significantly for all events. For event 1, uncertainty is reduced throughout the event and particularly in the first and fourth peaks. However, predictive failure is increased in the last three peaks, and for most of the recession flow. Event 2, shows a similar reduction in overall uncertainty, but increased predictive failure, particularly in the recession flows. Reduction in predictive uncertainty in event 3 is less significant than the other two events, and only impacts on the third peak. The more effective reduction of the overall uncertainty for the multiplicative combined likelihood measure, L_{imul} as compared to the average combined likelihood measure, L_{iav} is attributable to the main difference between the two measures.

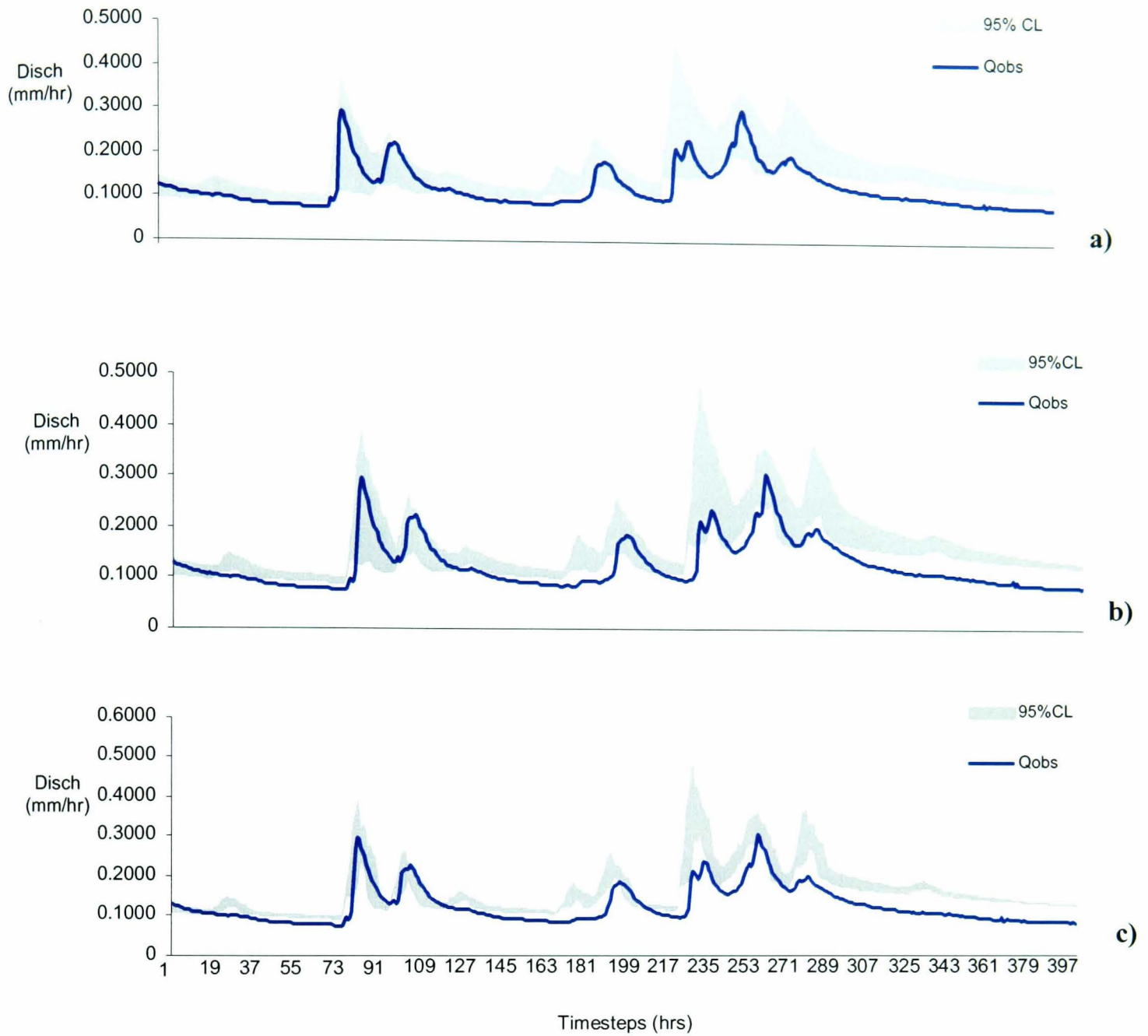


Fig. 5.38 Event 1

- a) Prior uncertainty in hydrological model conditioned on flow alone. $N_b=529$.
- b) Posterior uncertainty in hydrological model conditioned on flow and sediment data.
Combined likelihood, L_{iav} (equation 5.5.1). $N_b=327$.
- c) Posterior uncertainty in hydrological model conditioned on flow and sediment data.
Combined likelihood, L_{imul} (equation 5.5.2). $N_b=327$.

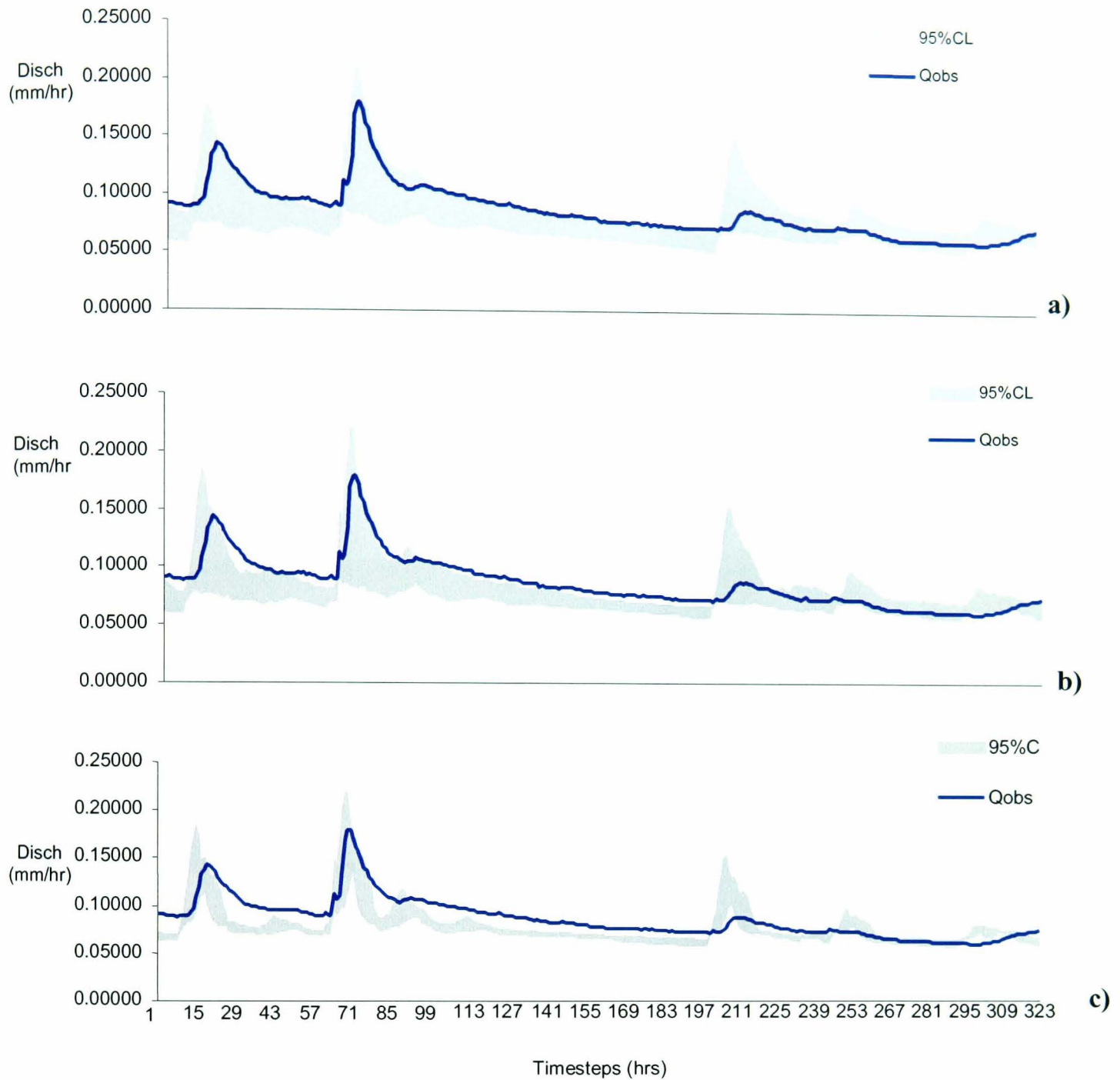


Fig. 5.39 Event 2

- a) Prior uncertainty in hydrological model conditioned on flow alone. $N_b=965$
- b) Posterior uncertainty in hydrological model conditioned on flow and sediment data.
Combined likelihood, L_{iav} (equation 5.5.1). $N_b=374$.
- c) Posterior uncertainty in hydrological model conditioned on flow and sediment data.
Combined likelihood, L_{imul} (equation 5.5.2). $N_b=374$.

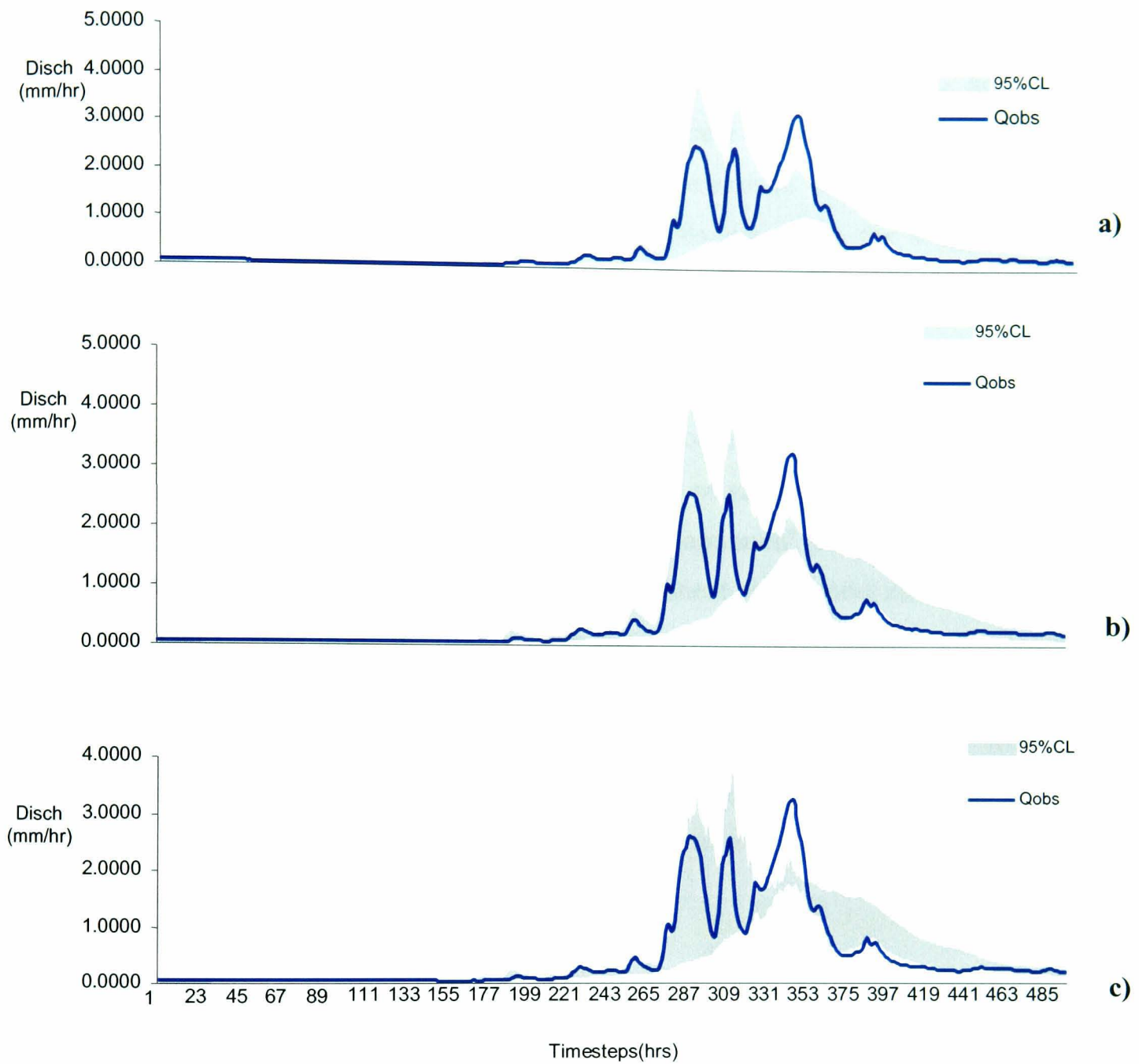


Fig. 5.40 Event 3

- a) Prior uncertainty in hydrological model conditioned on flow alone. $N_b=888$.
- b) Posterior uncertainty in hydrological model conditioned on flow and sediment data.
Combined likelihood, L_{iav} (equation 5.5.1). $N_b=320$.
- c) Posterior uncertainty in hydrological model conditioned on flow and sediment data.
Combined likelihood, L_{imul} (equation 5.5.2). $N_b=320$.

L_{iav} tends to even out the likelihood between the two models. Hence a simulation with a high hydrological efficiency and low sediment yield efficiency, will be averaged out, resulting in little modification to the prior likelihood. L_{imul} , however, has the effect of moderating the high efficiencies where the corresponding sediment model efficiency is low, resulting in a greater decrease in likelihood. Thus the simulations with the highest combined likelihoods are those for which model efficiency is high for both models.

5.5.2 Propagation of Uncertainty to Sediment Yield model

The propagation of uncertainty from the hydrological model to the sediment yield model is investigated here by considering the effect of varying the hydrology, while keeping the sediment yield parameters at their ‘optimum’ calibrated values, on sediment model efficiency. Hence, changes in sediment yield model efficiencies will be due to uncertainty in the hydrology. Note that since this is not an updating of prior sediment yield uncertainty bounds, but the construction of new bounds predicted by the changing hydrology, no combined likelihood measure is used. Uncertainty bounds are constructed based on a simple likelihood which is determined by:

$$L_{is} = \left(\frac{Eff_{i_s}}{\sum_1^{N_{bh-s}} Eff_{i_s}} \right) \quad [5.6]$$

where L_{is} is the likelihood for a given behavioural hydrological parameter set, that results in behavioural sediment yield predictions. All other terms are the same as before.

Figures. 5.41, 5.42 and 5.43 are plots of the uncertainty in the sediment yield model due to uncertainty in the hydrological model. For Event 1, uncertainty bounds do not enclose the observed sedigraph at the peaks, where uncertainty bounds are widest. The uncertainty bounds of Event 2 enclose for most of the observed sedigraph for most of the event, with large uncertainty throughout the main peak. Event 3 has narrow uncertainty bounds that do not enclose peak flows. These results show that uncertainty in hydrological model predictions can lead to significant uncertainty in the sediment yield model.

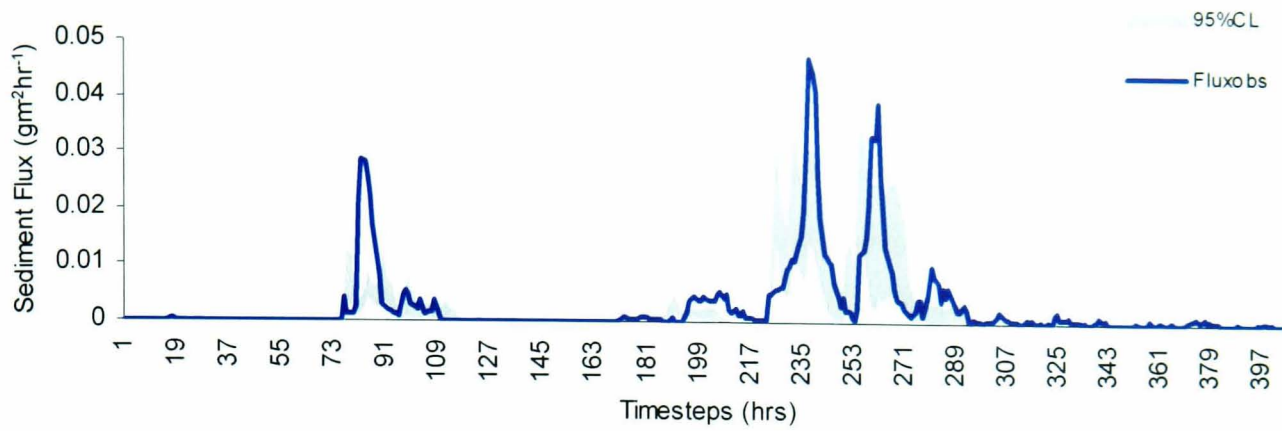


Fig. 5.5.7 Event 1 Uncertainty in sedigraph due to error propagated from hydrological model.

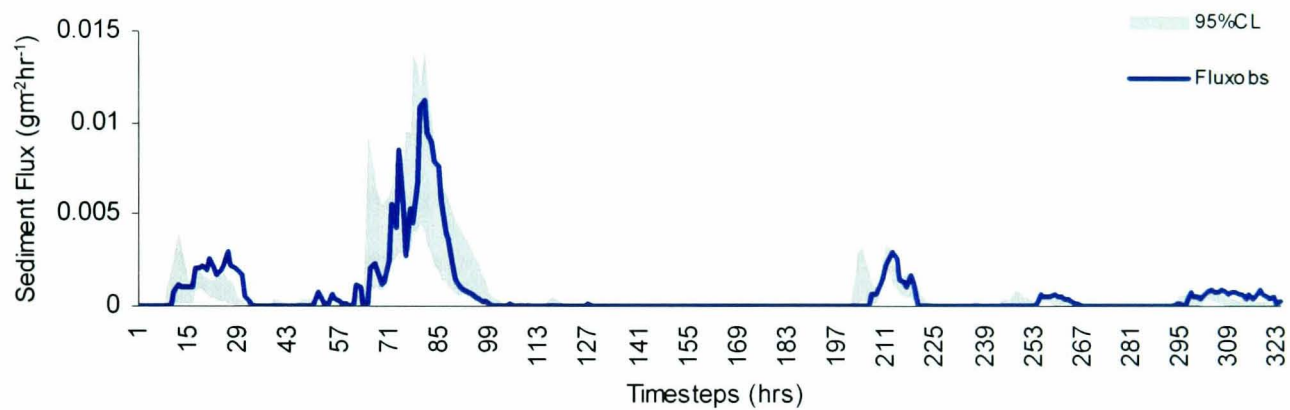


Fig 5.5.8 Event 2 Uncertainty in sedigraph due to error propagated from hydrological model.

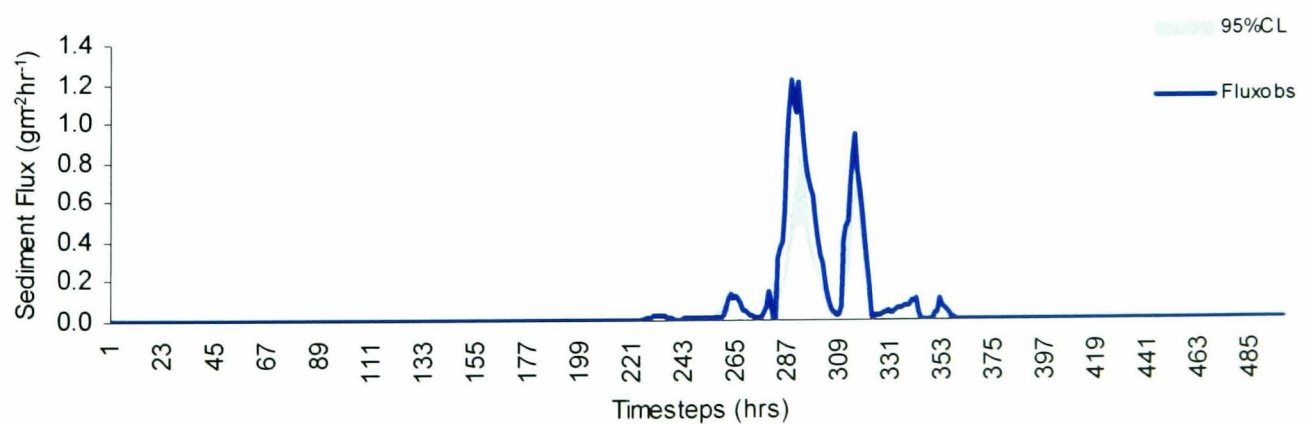


Fig 5.5.9 Event 3. Uncertainty in sedigraph due to error propagated from hydrological model.

5.6 Conclusion

The chapter presented the results of the lumped hydrological and sediment yield model calibration, validation, uncertainty analysis and evaluation of error propagation. Validation tests on the hydrological model (section 5.3.4) highlighted the dangers of applying one ‘optimum’ parameter set derived from one calibration period, to further independent events. The results show that different events may have widely different ‘optimised’ parameter sets. Thus, using the ‘optimised’ parameter set obtained during calibration for a given validation period without ensuring that it is also the ‘optimum’ parameter set for that period may result in very different hydrological temporal and spatial predictions from those of the ‘best’ parameter set for the given event. The analysis also showed that the uncertainty in hydrological prediction can be reduced by using successive events to update uncertainty. The result was that parameter cumulative distributions were significantly altered and uncertainty bounds successively constrained, as more periods of hydrological data are used. This effectively demonstrates that different periods of data with different ‘optimised’ parameter sets can be effectively used to update uncertainty in the hydrological model calibration, and illustrates that uncertainty can be reduced with increased knowledge about the behaviour of the system under different circumstances.

The use of sediment yield predictions to update hydrological model uncertainty resulted in parameter cumulative distributions that restrict hydrological parameter values and effectively reduce hydrological model uncertainty. This suggests, first that the model coupling was successful, and second, that the sediment yield model predictions serve to limit the range of hydrological parameter values that can be considered ‘behavioural’. It has been shown, however, that model coupling, resulted in the propagation of hydrological model error to the sediment yield model. The uncertainty in the hydrological model may have serious implications for the secondary sediment yield model, which uses hydrological model predictions as a primary input, the spatial distribution of which is critical to sediment yield prediction. Thus the sediment yield model uncertainty, while due, in part, to uncertainty in the sediment model parameters and sediment model structure, is also partly due to uncertainty in the hydrological model predictions, particularly the spatial predictions. It is, therefore, important to effectively reduce uncertainty in hydrological model spatial predictions, in order to get the most accurate predictions from the sediment yield

model. The above analysis has not considered the spatial variability in soil hydraulic properties, which can result in considerable variability in hydrological model spatial predictions. Representing heterogeneity in soil hydraulic parameters due to soil and land use variability may be a means of reducing uncertainty in hydrological model spatial and temporal predictions. Soil hydraulic properties may also vary randomly in space.

Chapter 6 examines the effect of using deterministic spatially distributed saturated hydraulic conductivity on hydrological model predictions, and the consequent effect on sediment yield model predictions, while Chapter 7 examines the effect of randomly variable saturated hydraulic conductivity.

CHAPTER 6 – Deterministic Spatial Parameterisation

6.0 Summary

The spatial distribution of hydrological response predicted by the lumped model presented in Chapter 5 is controlled by topography alone. However, soil type and landuse both exert considerable control on saturated hydraulic conductivity, and therefore, on the spatial distribution of hydrological response. A complete deterministic representation of spatially distributed saturated hydraulic conductivity would require extensive monitoring at every point in the parameter space. However, an obvious alternative is to use remote sensing and soil texture maps to spatially parameterise saturated hydraulic conductivity. This chapter presents the results of the deterministic spatial parameterisation of saturated hydraulic conductivity by landuse and soil type, and examines whether the additional information provided by the spatial parameterisation of soil hydraulic parameters is sufficient to reduce model uncertainty in both the hydrological and sediment yield models.

The analytical procedure is the same as that outlined in section 5.0 and the chapter is arranged as follows. The introduction discusses the causes of spatial variability of hydraulic conductivity. This is followed by a discussion of the derivation of spatially variable K_s from remotely sensed imagery and soil texture tables. The results are presented in a similar manner to that of Chapter 5, and the calibration and validation were carried out on the same events used for the lumped parameterisation of Chapter 5 in order to permit comparison. The hydrological model calibration results are presented, followed by the model validation, which is followed by the calibration and validation of the sediment yield model. Each calibration and validation begins with a parameter sensitivity analysis, followed by an uncertainty analysis and the results of spatial predictions. The final section deals with the Bayesian updating of likelihoods, and the propagation of error in the coupled model. This is followed by a general discussion of the benefits of representing the spatial heterogeneity of soil hydraulic properties.

6.1 Introduction

Spatially Distributed Saturated Hydraulic Conductivity

Hydraulic conductivity is primarily a function of grain size. Hence any factors that affect the grain size at the surface will affect the saturated hydraulic conductivity of the surface. These include vegetation cover, soil type, and antecedent soil moisture conditions. Natural vegetation, especially in forests, will usually have leaf litter, humus and other organic matter on the soil surface. Root growth and decay, biological action and burrowing contribute to the surface porosity. This effect also occurs in grass (Hino *et. al.*, 1987) and even in arid scrubland, where infiltration has been found to be nearly three times higher under individual bushes than in the open. In deciduous broad-leaved forests, the leaf litter can produce ‘shingling’ that can have the opposite effect, and prevent infiltration, at least locally (Dingman, 1975). Waxy organic substances produced by vegetation and micro-organisms, makes the ground surface hydrophobic by causing water to ‘bead up’ on impact, preventing infiltration.

Soil properties such as grain size and mineral content that affect swelling and drying may also influence infiltration. Clay minerals in soil may swell when wet, and shrink when dry. Therefore, during the rainy season or during a single rainstorm, swelling can reduce effective surface porosity and permeability and limit infiltration, while during dry periods, polygonal cracks that can accept high infiltration rates, may develop. Where sheet-flow erosion occurs on bare or nearly bare ground, or where mineral grains are brought into suspension by the splashing of raindrops, in-washing of fine sediment into larger pores may effectively reduce the surface pore size and permeability. Anthropogenic modifications to the ground surface such as ploughing, grazing and the use of heavy machinery, may also alter surface porosity, and therefore influence the spatial variability of permeability.

Antecedent soil moisture conditions that cause changes in the local water table can also influence the spatial and temporal variability in saturated hydraulic conductivity. Saturation from below can occur, even in the absence of a local water table, where there is an approximate gradual decrease of porosity and hydraulic conductivity with depth, or where there is a distinct layer with significantly reduced conductivity at depth. Water accumulates from above and ultimately a saturated zone is created. If input continues at a high enough rate, the saturated zone can reach the surface and

prevent further infiltration regardless of the hydraulic conductivity and rate of input. High antecedent water content increases hydraulic conductivity, which tends to increase infiltration rate, by increasing the radius of curvature of the menisci in soil pores. It also reduces the effect of surface tension in drawing water into the soil, which tends to decrease infiltration rate. Furthermore, a soil that is relatively wet at the beginning of an event will more likely become saturated quickly during the event, resulting in a longer period of reduced infiltration. Water content, along with reduced temperatures may also influence infiltration rates significantly, for example, when frozen surface and near-surface soil water render the surface nearly impermeable. However, frost action associated with lower water contents can sometimes markedly increase the surface permeability (Schumm and Lusby, 1963, Dingman, 1975), as the surface produces a polygonal network of cracks that can admit precipitation and meltwater.

Hydraulic conductivity is also affected by other water properties that vary with temperature, e.g. surface tension, density and viscosity. Viscosity at 30°C is less than half that at 0°C, hence hydraulic conductivity at 30°C is about twice that at 0°C, as proven in the laboratory by Klock (1972).

6.2 Distributed Parameterisation

Saturated hydraulic conductivity was distributed on the basis of land use and soil type using two different methods. Parameterisation by landuse employs the use of data derived from remote sensed images, coupled with deterministic field measures of saturated hydraulic conductivity. Digitised soil maps were used in conjunction with soil texture tables to spatially distribute saturated hydraulic conductivity by soil type. It should be noted that it was the ratios of saturated hydraulic conductivity for different soil type and landuse respectively which were used to calibrate the model, rather than the absolute values (see also Brasington and Richards, 1998). The continuing need for calibration necessitates this approach which is clearly not ideal. To spatially distribute parameters in this manner may require extensive fieldwork, in order to fully characterise a given catchment. The use of ratios however minimises the required fieldwork, and when used in conjunction with soil texture tables, and remotely sensed maps, enables spatial parameterisation at smaller scales than would be possible otherwise.

Land use

Vertical saturated hydraulic conductivities for each landuse in the catchment (Fig. 6.1) were estimated from ring infiltrometer tests in the field. The ring infiltrometer forms an impermeable boundary, extending several centimetres into the soil (5cm here) and several centimetres above the surface (10cms), within which ponding due to saturation from above is created by directly flooding the surface. The rate of infiltration is obtained by measuring the rate at which the level of ponded water decreased. Saturated hydraulic conductivity of the near-surface soil was approximated by the infiltration capacity derived from Philip's (1957) model. The general form of the Philip (1957) infiltration model for cumulative infiltration, I (cm), can be expressed as an infinite series in powers of the square-root of time, t (s), as:

$$I = S(\theta_o, \theta_n)t^{1/2} + A_1t + A_2t^{3/2} + \dots \quad [6.1]$$

where $S(\theta_o, \theta_n)$, called sorptivity ($\text{cms}^{-1/2}$) is a function of θ_o and θ_n and is an integral property of the soil hydraulic diffusivity (White and Perroux, 1987). $S(\theta_o, \theta_n)$ is a constant, provided the water content at the inflow end is held constant (Jury *et. al.*, 1991). A_1 (cms^{-1}), A_2 ($\text{cm s}^{-3/2}$), etc., are constants that depend on both the properties of the soil, and θ_o and θ_n . The time derivative of I is the infiltration rate, i (cms^{-1}), which is

$$i = \frac{1}{2}S(\theta_o, \theta_n)t^{-1/2} + A_1 + \frac{3}{2}A_2t^{1/2} + \dots \quad [6.2]$$

For vertical infiltration, equations [6.1] and [6.2] only apply for short time periods when the matric-potential gradient is much greater than the gravity-potential gradient. Terms beyond the first two on the right-hand side of both equations are generally considered to be negligible (Jury, *et. al.*, 1991), and vertical infiltration is usually approximated by the first two terms. For long time periods, as the water content reaches some final value equal to θ_o , the matric-potential gradient approaches zero and gravity becomes the driving force for vertical flow. The vertical infiltration rate will approach some constant value equal to the saturated hydraulic conductivity or the conductivity of the water content at the surface. The time it takes for the infiltration

rate to reach a point where gravity driven flow predominates over flow driven by the matric-potential gradient, t_g , can be found from (Philip, 1969):

$$t_g = \left[\frac{S(\theta_o, \theta_n)}{K(\theta_o)} \right]^2 \quad [6.3]$$

Hence, t_g is also a function of θ_o and θ_n , and will therefore vary, depending on whether the soil is initially ‘wet’ (initial matric-potential gradient is small and therefore a shorter time to gravity flow) or ‘dry’ (initial matric-potential gradient is larger and therefore a longer time to gravity flow). The disadvantage of the Philip infiltration model, as with most theoretical models, is that the assumptions for which it is applicable (i.e. homogeneous, isotropic, infinitely deep soil) rarely (if ever) exist over a large area, because soil types can vary in composition, both areally and at depth, as can vegetation cover, which can significantly influence infiltration rates. Another drawback to this method of obtaining estimates of saturated hydraulic conductivity is that the ring infiltrometer provides essentially point measurements of what is a highly spatially variable parameter. The field survey was designed to capture the most accurate pattern of variability possible. A total of ten ring infiltrometer experiments were conducted for each land use type and the average obtained. This spatial lumping of parameter values is unavoidable and will contribute to model errors. In addition, it is assumed that the ring-infiltration tests were spatially independent of each other. Geostatistical methods for delineating spatial correlation and variability in infiltration rates were not considered, here but, as will be discussed later, saturated hydraulic conductivity may show a high degree of spatial correlation. Loague and Gander (1990) found that the range of spatial correlation of infiltration rates is less than 10m. It was ensured that ring infiltrometer tests were conducted at least 50 m apart.

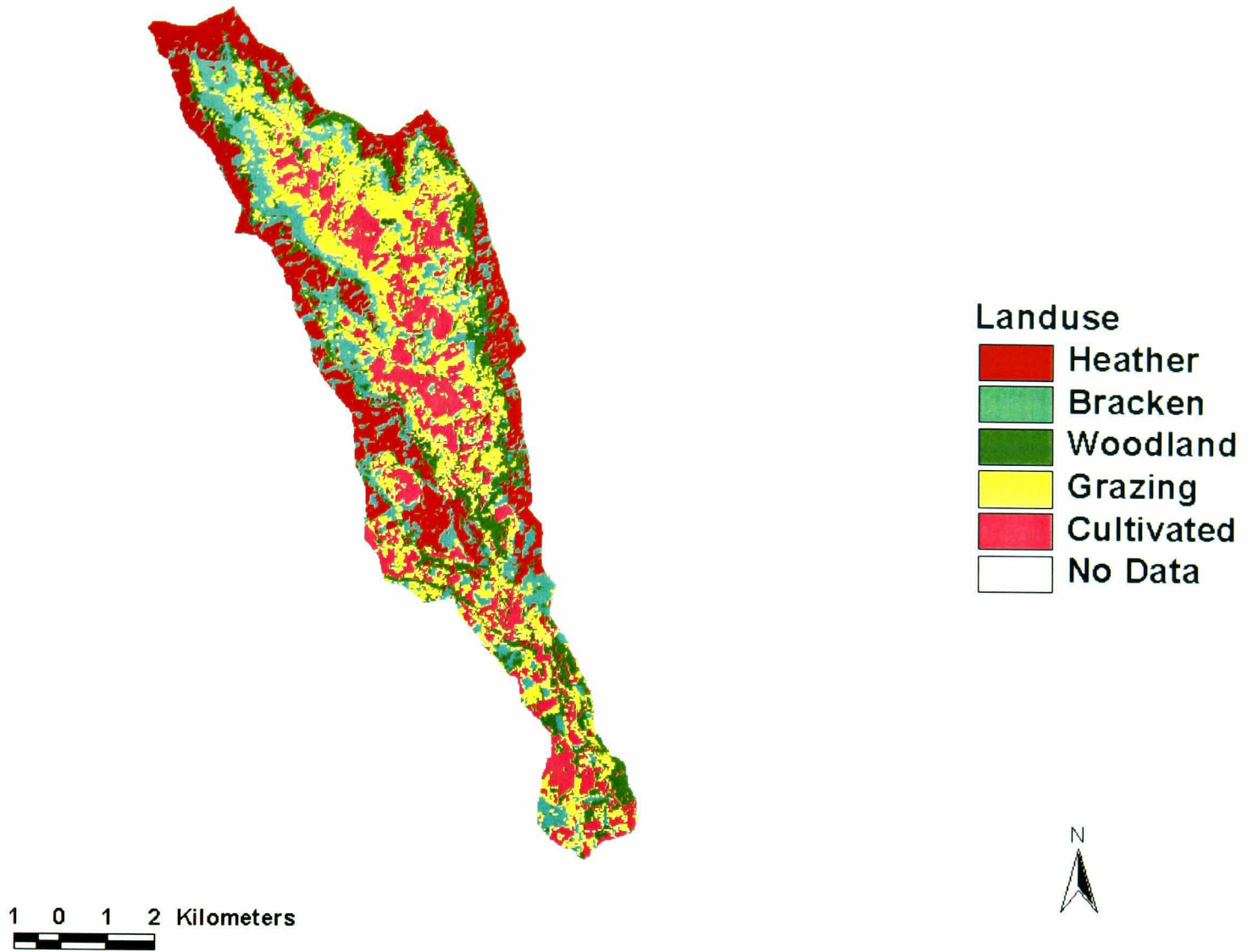


Fig. 6.1 Landuse distribution derived from Landsat image.

Landuse	\bar{K}_s	Variance	Ratios
Heather	0.004	2.67×10^{-6}	1
Bracken	0.008	8.00×10^{-6}	2
Woodland	0.015	7.60×10^{-6}	4
Grazing	0.0024	6.08×10^{-6}	0.6
Cultivated	0.002	4.10×10^{-6}	0.5

Table 6.0a Soil hydraulic properties by land use.

The ratios of saturated hydraulic conductivity obtained were 1:2:4:0.6:0.5 for Heather: Bracken: Woodland: Grazing: Cultivated respectively (Table 6.0a).

Soil Type

Another alternative to direct measurements of soil hydraulic conductivity, is to calculate the conductivity and retention functions from more easily determined soil properties such as texture, bulk density, organic matter and clay mineralogy. Rawls and Brakensiek (1983) reported regression equations for the Brooks-Corey (1964) soil water retention and hydraulic conductivity parameters as a function of soil properties for soils comprising 5-70% sand and 5-60% clay. Hence the basic requirement is the percentage sand and clay of the soil fraction and the soil porosity. They also developed and tabulated the saturated hydraulic conductivity for the USDA soil texture classes (Rawls and Brakensiek, 1982).

The soil classification tables for England and Wales of Avery (1980) were used to determine the saturated hydraulic conductivity of all the soil types within the catchment based on detailed descriptions of each soil type found in the literature. The average saturated hydraulic conductivity was calculated for the top 1m of each soil type, which were lumped into groups of similar values, thus reducing the number of soil types from 14 to 6. Fig. 6.2a is a map of the original digitised catchment soils by name. Fig. 6.2b is a map of soil type classified into 6 soil types according to average K_s values of the top 1m of soil. The catchment comprises 29.5% sandy loam, 54.5% clay, 0.7% clayey loam, 0.9% sandy clay loam, 10.2% silt loam/loam and 4.2% peat. The wide variability in saturated hydraulic conductivity for different soil types (Table 6.0b), especially sandy loams and clay (the two largest groups) can be expected to significantly influence the spatial distribution of saturated areas and hence sediment source areas within the catchment.

Soil type	\bar{K}_s	Ratio
Sandy loam	0.38710	85
Clay	0.00457	1
Clayey loam	0.00882	2
Sandy Clay loam	0.06930	15
Silt loam/loam	0.02272	0.6
Peat	0.00004	0.01

Table 6.0b Soil hydraulic properties by soil type.

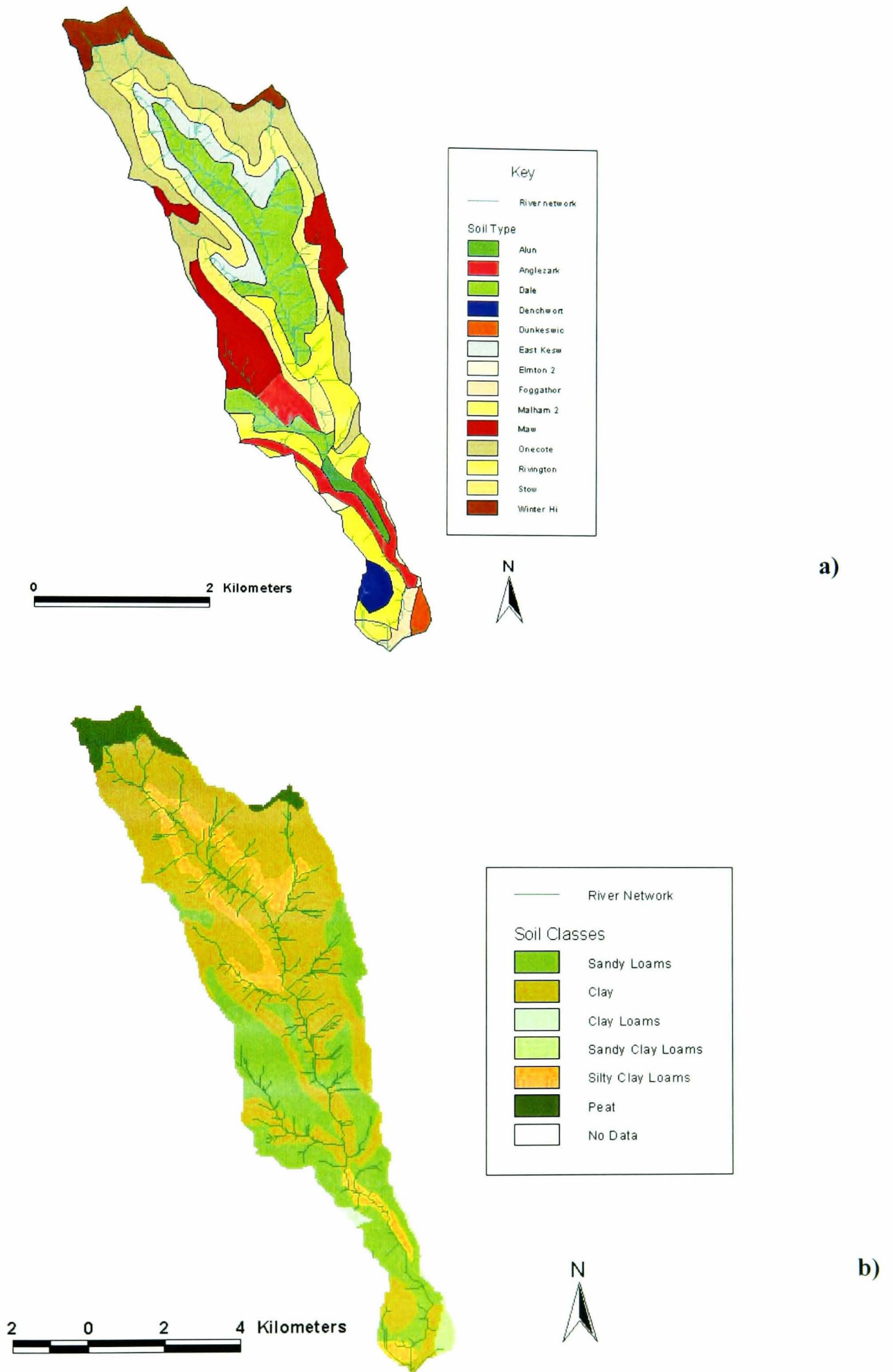


Fig. 6.2 a) Soil names b) Soil reclassified by basic type.

Both methods of spatial parameterisation are prone to errors as they both utilise secondary data sources. As discussed earlier (section 2.10.1), secondary data can add to model uncertainty due to, in the case of remotely sensed data, methods of data extraction and, in the case of the texture tables, the reliability and applicability of the methods and conditions under which tables were derived. An essential aim of this analysis is to examine whether the additional information provided by the spatial parameterisation of soil hydraulic parameters out-weighs the effects of these accompanying data errors, and whether by significant enough margins to justify the use of spatial parameterisations over lumped.

6.3 Hydrological Parameter Sensitivity

The scatterplots (Fig. 6.3) indicate that both the land- and soil-distributed parameterisations are sensitive to m and $CHV2$ with the soil-distributed parameterisation being additionally sensitive to $K_{\theta bar}$. The plots for m are similar to that obtained for the lumped parameterisation (Fig. 5.2), showing a decreasing rate of increase in efficiency with increasing value. This is confirmed by the GSA distributions (Fig. 6.4), which show large degrees of separation between behavioural and non-behavioural simulations – the higher values being associated with behavioural simulations.

The scatterplots for $K_{\theta bar}$, the catchment average saturated hydraulic conductivity, for land-distributed parameterisation shows little sensitivity, but is very sensitive for the soil-distributed parameterisation, which indicates that a catchment average of 1051.33mhr^{-1} gives the highest efficiency. This sensitivity is reflected in the GSA distribution for this parameter, which shows wide variability between behavioural and non-behavioural simulations, in direct contrast to the lumped parameterisation, which is insensitive over the entire range of parameter values considered. The higher degree of sensitivity of the soil-distributed parameterisation compared to both land-distributed and lumped parameterisations reflects the wider variability in saturated hydraulic conductivity ratios for different soil types. The ‘optimum’ value obtained corresponds to values of 3459.5, 40.7, 81.4, 610.5 24.42 and 0.0407mhr^{-1} for sandy loam, clay, clay loam, sandy clay loam, silty clay loam and peat respectively. This wide variability in saturated hydraulic conductivity has significant implications for the

spatial distribution of saturated areas and hence sediment source areas as will be discussed later (section 6.4).

CHV2 shows some sensitivity with maximum efficiency for values in the range 0.4 to 0.45ms^{-1} for both land- and soil-distributed parameterisations. Scatterplots of ETF shows little sensitivity for both parameterisations, but the GSA distributions indicate some separation between behavioural and non-behavioural simulations for both parameterisations. *SRMAX* shows little sensitivity for the land-distributed parameterisation and was fixed at 0.0041m for the soil-distributed parameterisation.

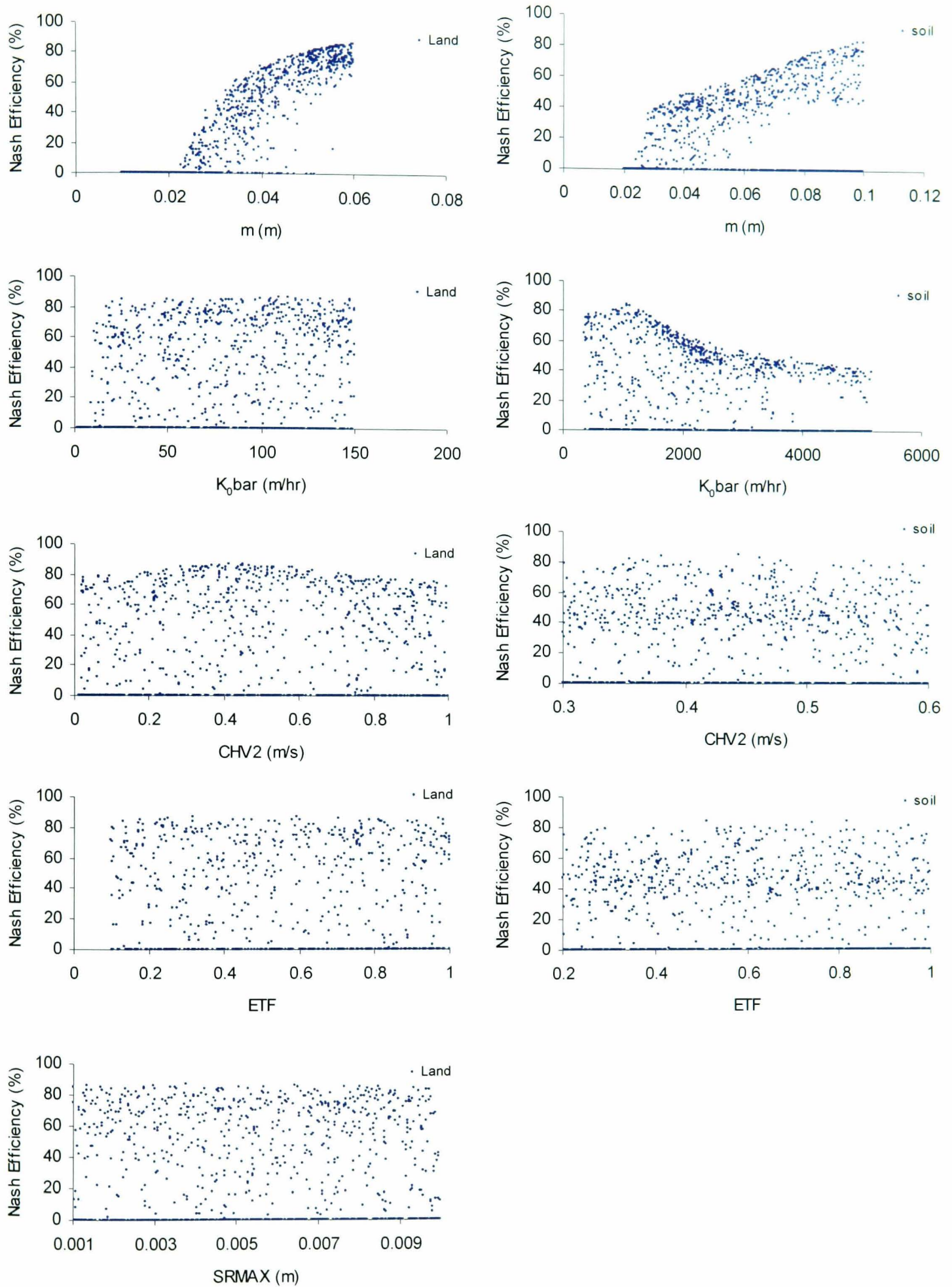


Fig. 6.3 Scatterplots of parameter values versus Nash efficiency for land- and soil-distributed parameterisation.

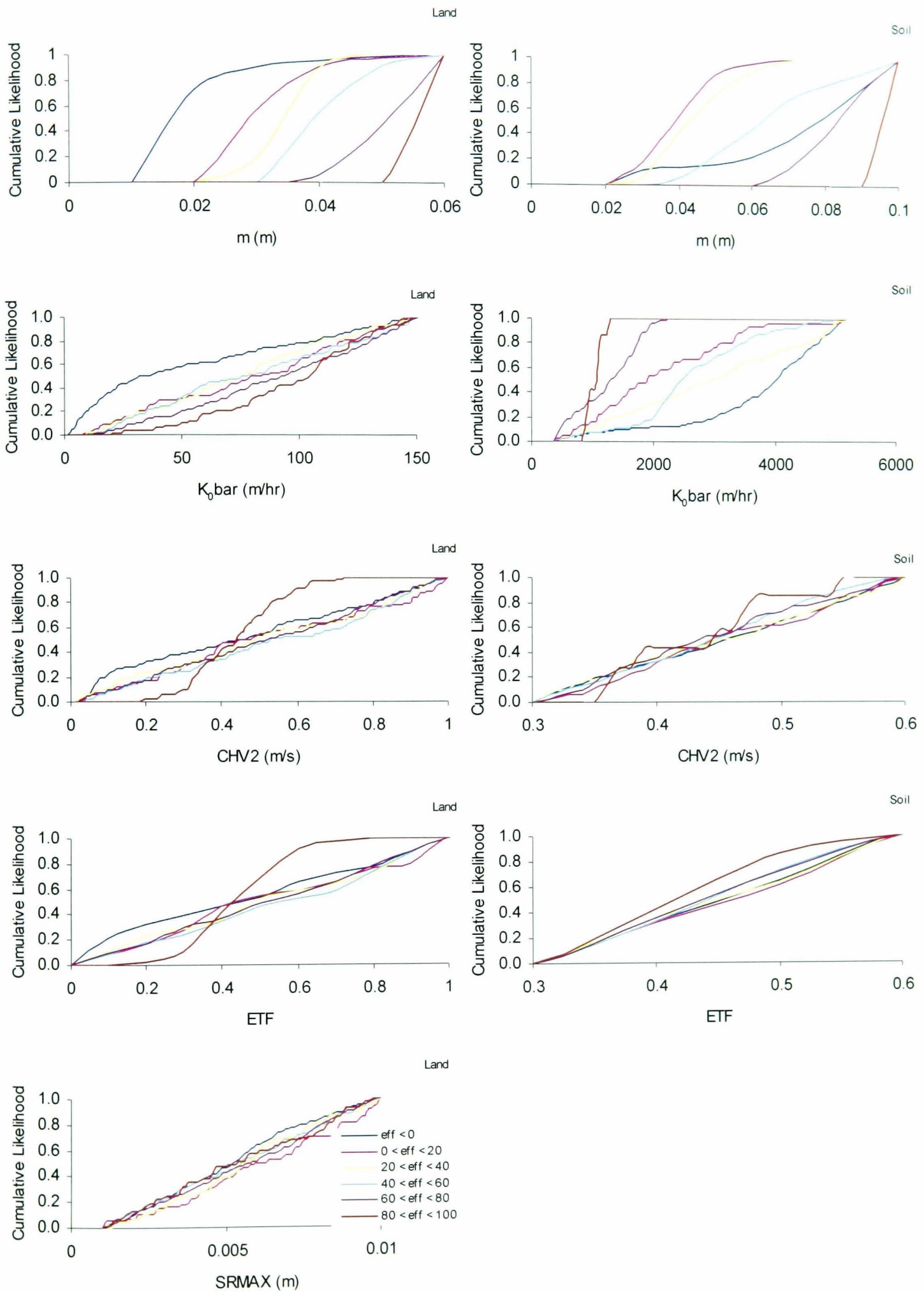


Fig. 6.4 GSA plots for land- and soil-distributed parameterisation.

6.3.1 Hydrological Model Calibration – Results and Uncertainty Analysis

Fig. 6.5 shows the results of model calibration for both parameterisations. The uncertainty bounds in the land-distributed parameterisation (Fig. 6.5a) follows closely, those of the lumped parameterisation represented by the thin red lines in Fig. 6.5a. For the soil-distributed parameterisation, however, uncertainty bounds are wider, with steeper rising and falling limbs. Peaks are rounded instead of spiked, indicating prolonged peak flows, and the lower uncertainty bound follows the observed curve more closely than for the land-distributed parameterisation. Lower recession flow uncertainty bounds are predicted, resulting in the enclosure of the observed recession flow at the end of the event, which was not predicted by either the land-distributed or the lumped parameterisations. The lower recession flows are reflected in the graphs of percentage contributions of base flow and surface runoff, Figs. 6.5e and f, which show a lower proportion of base flow and higher proportion of surface runoff for the soil-distributed parameterisation.

Fig. 6.5c is a plot of the ‘optimum’ hydrographs for the lumped, land- and soil-distributed parameterisations, and the observed hydrograph, and table 6.1 is a summary of the corresponding parameter values, inputs and outputs. The hydrographs for the land and lumped parameterisations are similar. The soil-distributed hydrograph follows the lumped and land hydrographs up to the fourth peak, but the last two peaks are lower. Hence, qualitatively similar hydrographs were obtained for all three parameterisations, with quantitatively similar model efficiencies (Table 6.1).

An examination of the ‘optimum’ parameter sets reveals that while the lumped and land-distributed parameter sets are comparable, the soil-distributed is very different. The largest difference between land and lumped parameter sets is in the K_{ob} values. The catchment average for the land-distributed is 109.59mhr^{-1} , which corresponds to values of 72.81, 145.62, 291.24, 43.69, and 36.41mhr^{-1} for heather, bracken, woodland, grazing and cultivated respectively. Hence heather which is located in the headwaters and on the catchment divide has a saturated hydraulic conductivity half that of bracken located just downslope, and one-quarter that of woodland which is interspersed within the bracken. This would result in run-on during rainfall events, whereby rainfall that is slow to infiltrate the heather, would run-on to bracken and

woodland covered cells where it will infiltrate more quickly. In addition, the lower conductivity heather along the divide and in the headwaters will ‘starve’ the higher conductivity cells under bracken and woodland downslope, of subsurface flow, as its subsurface storage takes a longer time to be replenished. This would have the effect of reducing saturation from below in the bracken and woodland cells, resulting in lower exfiltration flows, which would be particularly pronounced in the inter-storm period when downslope cells depend on subsurface flows from upslope to replenish their soil moisture. Thus Fig. 6.6a and b show the location of low soil moisture deficit cells close to the divide, reflecting higher surface runoff, and cells of higher soil moisture deficit just downslope of them, reflecting lower subsurface recharge from upslope, for both the driest and wettest timesteps.

Grazing and cultivation are mainly located on the valley floor and close to the catchment outlet. Saturated hydraulic conductivities under these landuses are an order of magnitude less than the landuses upslope of them. Hence they will be less able to accept subsurface flow from upslope, which could result in locally perched water tables at the boundary of these cells with the higher conductivity cells, particularly where these boundaries coincide with hollows and swales at the foot of slopes, thus reinforcing the topographic control on saturation. This is reflected in the wider extent of the saturated zone for the driest timestep for the land-distributed model (Fig. 6.6a) compared to the same timestep for the lumped model (Fig. 5.7a). During rainfall events, the direct surface runoff from these cells will be higher, due to their lower infiltration rates. Thus the saturated zone for the wettest timestep (Fig. 6.6b) is also wider than for the same timestep for the lumped model (Fig. 5.7b). Higher rates of direct surface runoff occurring in the riparian area will result in faster times to peak, and this is reflected in the lower calibrated channel velocity (*CHV2*) obtained. The larger extent of the saturated zone means that more soil moisture is available for evapotranspiration. Thus a lower calibrated value is obtained to offset the effect of having a larger surface area contributing to evapotranspiration. All other parameter values are comparable to the lumped parameter set, reflecting their insensitivity in the model.

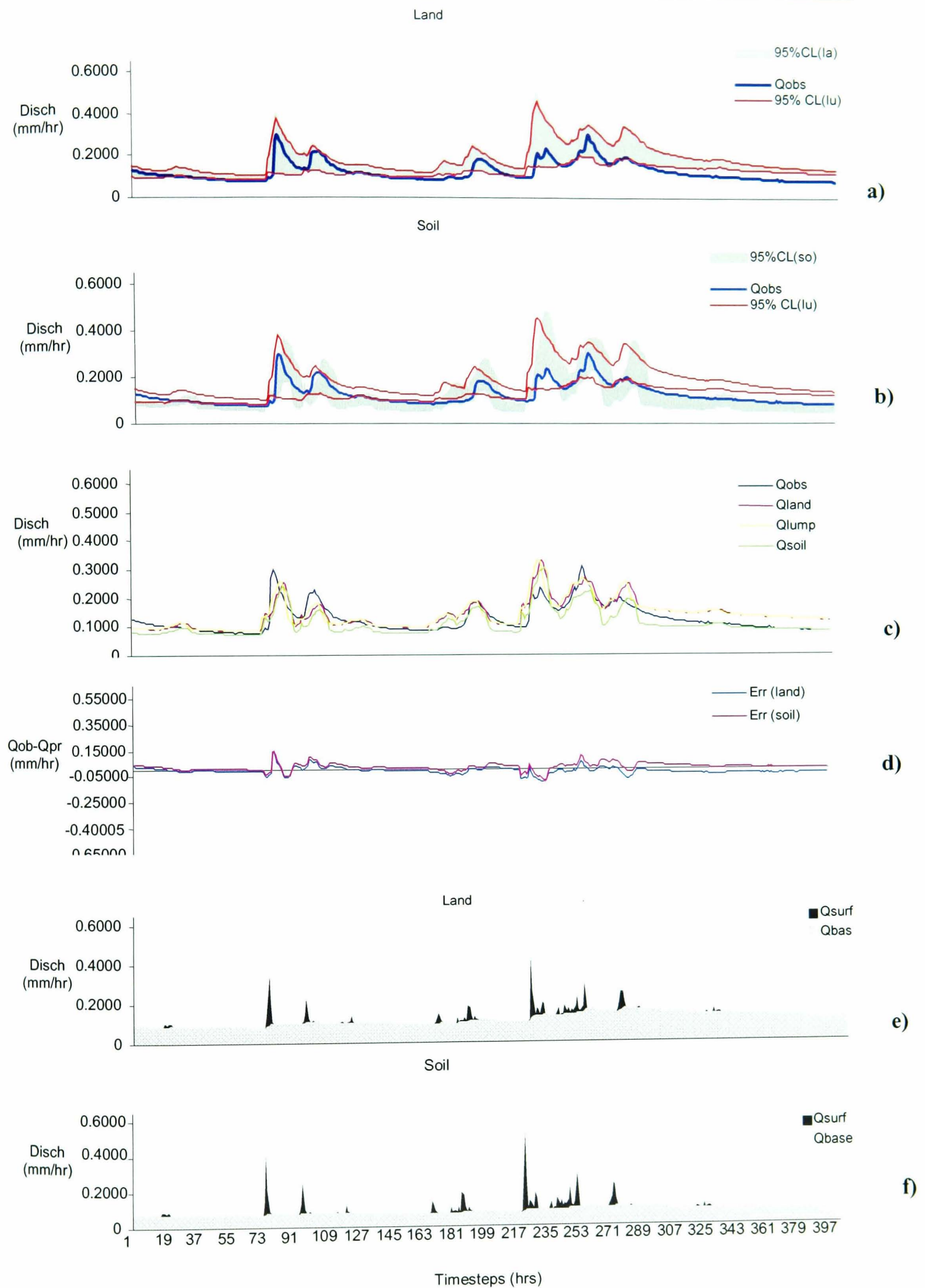


Fig. 6.3.3 Results of calibration for land- and soil-distributed parameterisation. (In e) and f) Q_s and Q_b are surface flow and baseflow respectively). La=land;so=soil;lu=lumped.

Parameter	Observed	Lumped	Land	Soil
m (m)	-	0.05970	0.05981	0.09994
$K_{\theta bar}$ (mhr^{-1})	-	271.7395	109.5864	1051.333
SRMAX (m)	-	0.00372	0.00378	0.0041
CHV2 (ms^{-1})	-	0.46237	0.41436	0.44411
ETF	-	0.76232	0.59224	0.51178
Sum rain (m)	0.0704	-	-	-
Sum discharge (mm)	50.631	56.588	56.719	44.607
Sum Q_b (m)	-	0.048006	0.047177	0.034013
Sum Q_s (m)	-	0.001692	0.002674	0.003575
Nash Eff (%)	-	87.16151	87.10159	86.51292

Table 6.1 Calibrated ‘optimum’ parameter sets for lumped- land- and soil-distributed parameterisations.

The ‘optimum’ soil-distributed parameter set predicts a higher m value, suggesting that a larger average soil depth. The catchment average, saturated hydraulic conductivity, $K_{\theta bar} = 1051.333mhr^{-1}$ corresponds to values of 3459.5, 40.7, 81.4, 610.5, 24.42 and $0.041mhr^{-1}$ for sandy loam, clay, clay loam, sandy clay loam, silty clay loam, and peat respectively. Hence the peat soils have saturated hydraulic conductivity 3 to 5 orders of magnitude less than the other soil types. Located on the gentle to flat slopes of the northern divide where the soil is thin and near the headwaters, they are almost always permanently waterlogged. This is reflected in the low soil moisture deficit (saturated to near-saturated) conditions for both the wettest and driest timesteps (Figs. 6.6c and d) on these soils. The clay soils which occupy most of the northern half of the catchment are better drained than the peats, but less well drained than the sandy loams further south of them. Thus run-on from the north of the catchment would infiltrate the sandy loams quickly. The riparian area in this part of the catchment is severely restricted, with the channel seemingly (but not actually) cut off before “re-appearing” close to the outlet. The ‘optimum’ ETF value is lower than the lumped, again due to the larger saturated area.

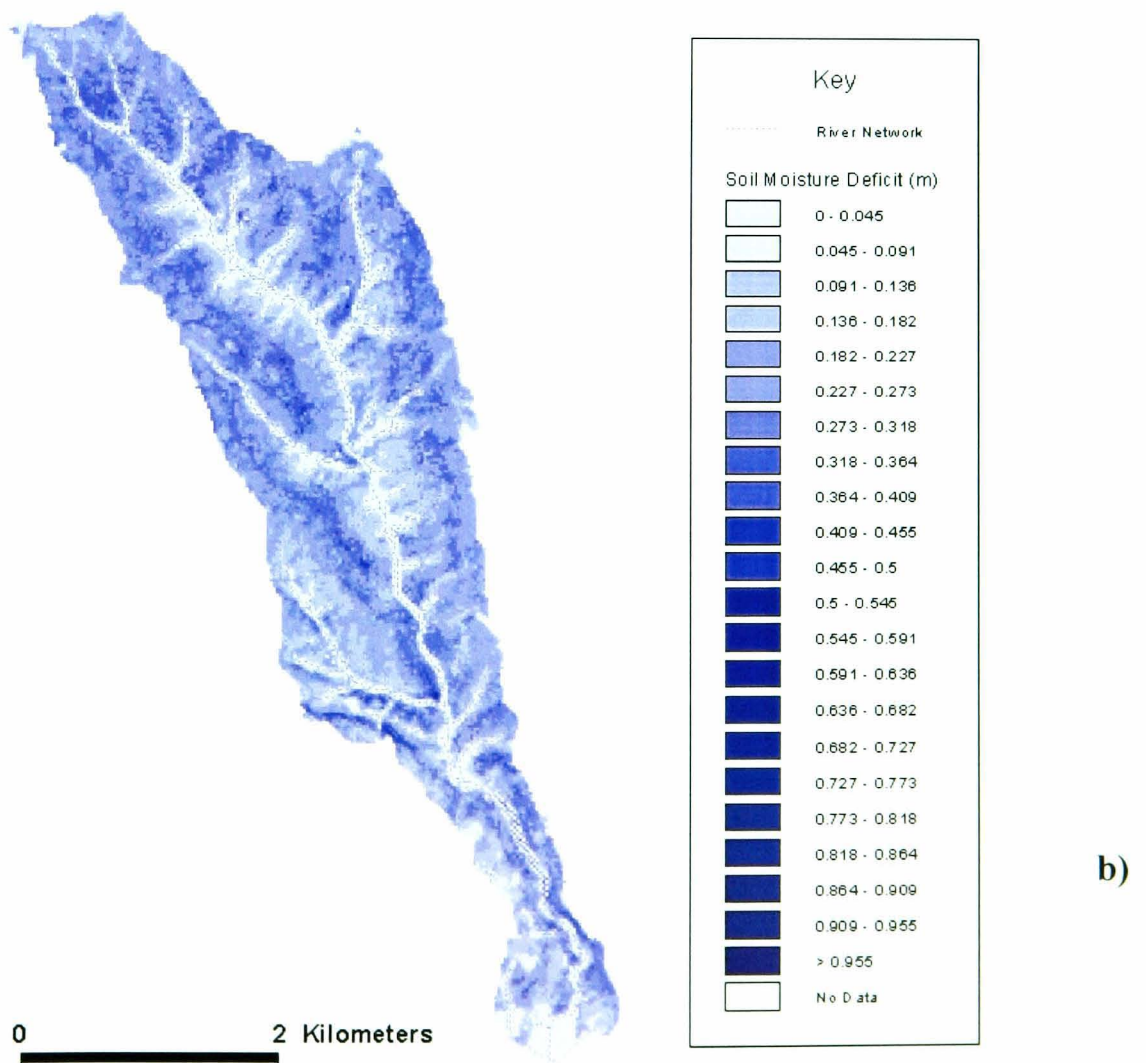
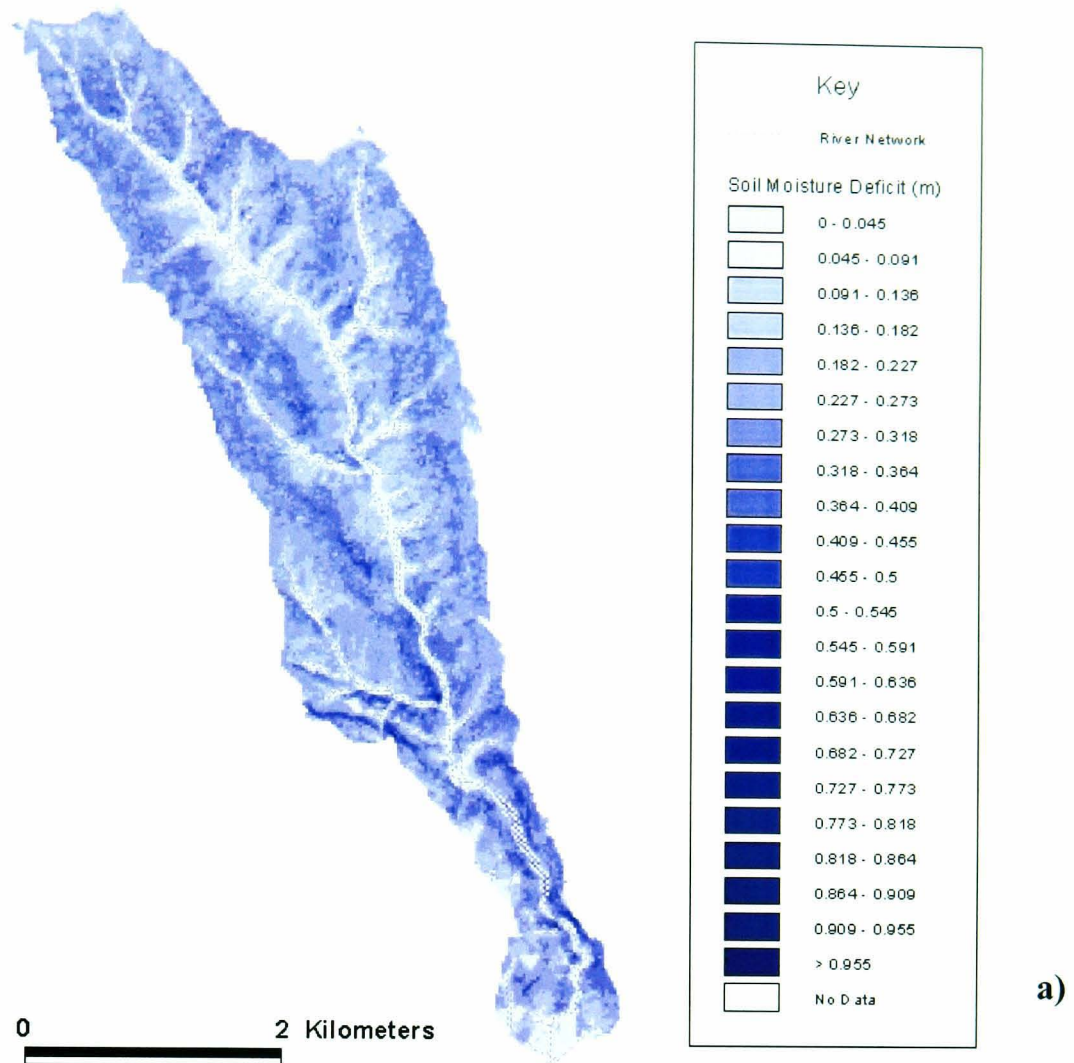


Fig. 6.6 Spatial distribution of soil moisture deficit for the calibration event at a) Driest timestep and

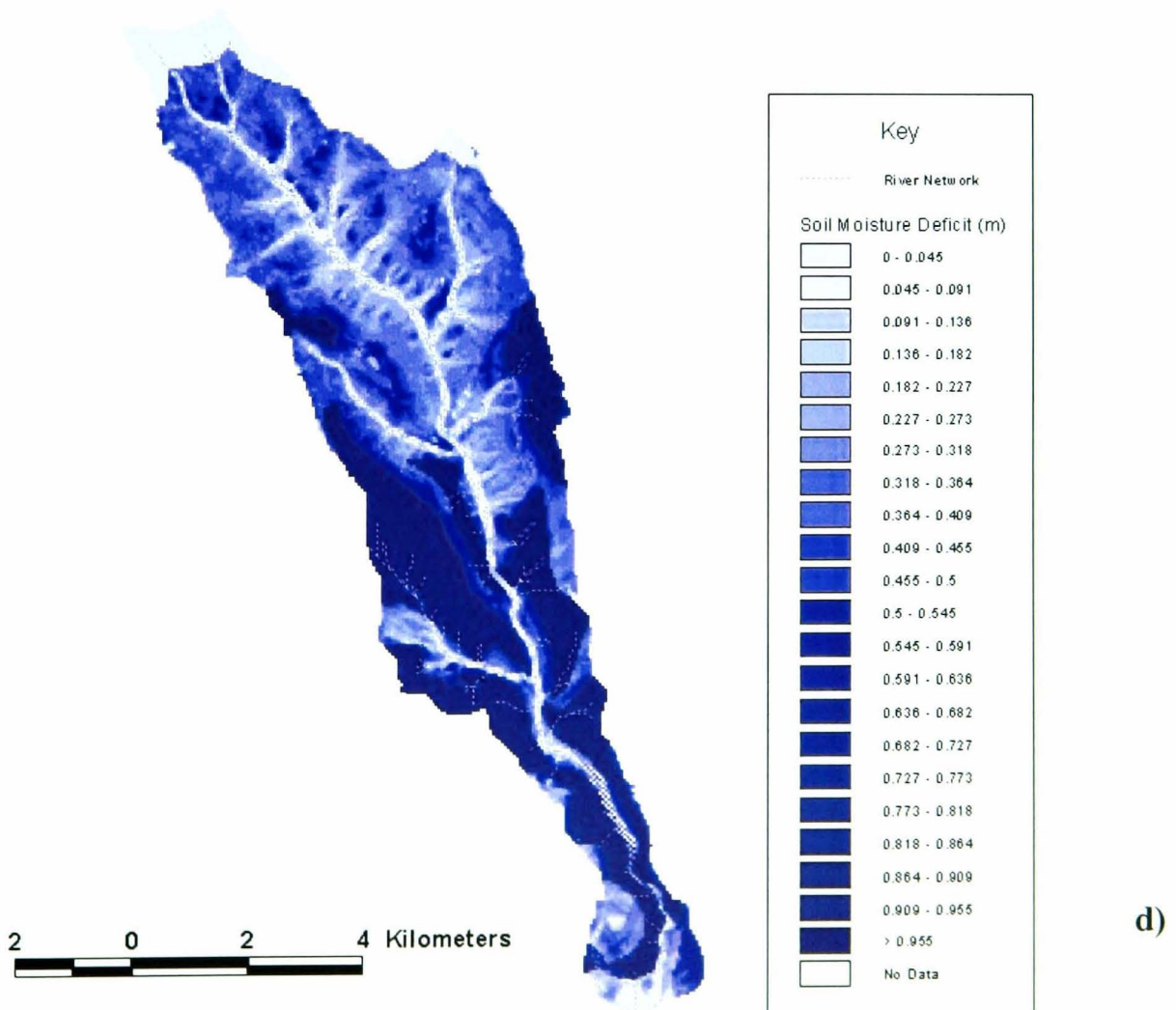
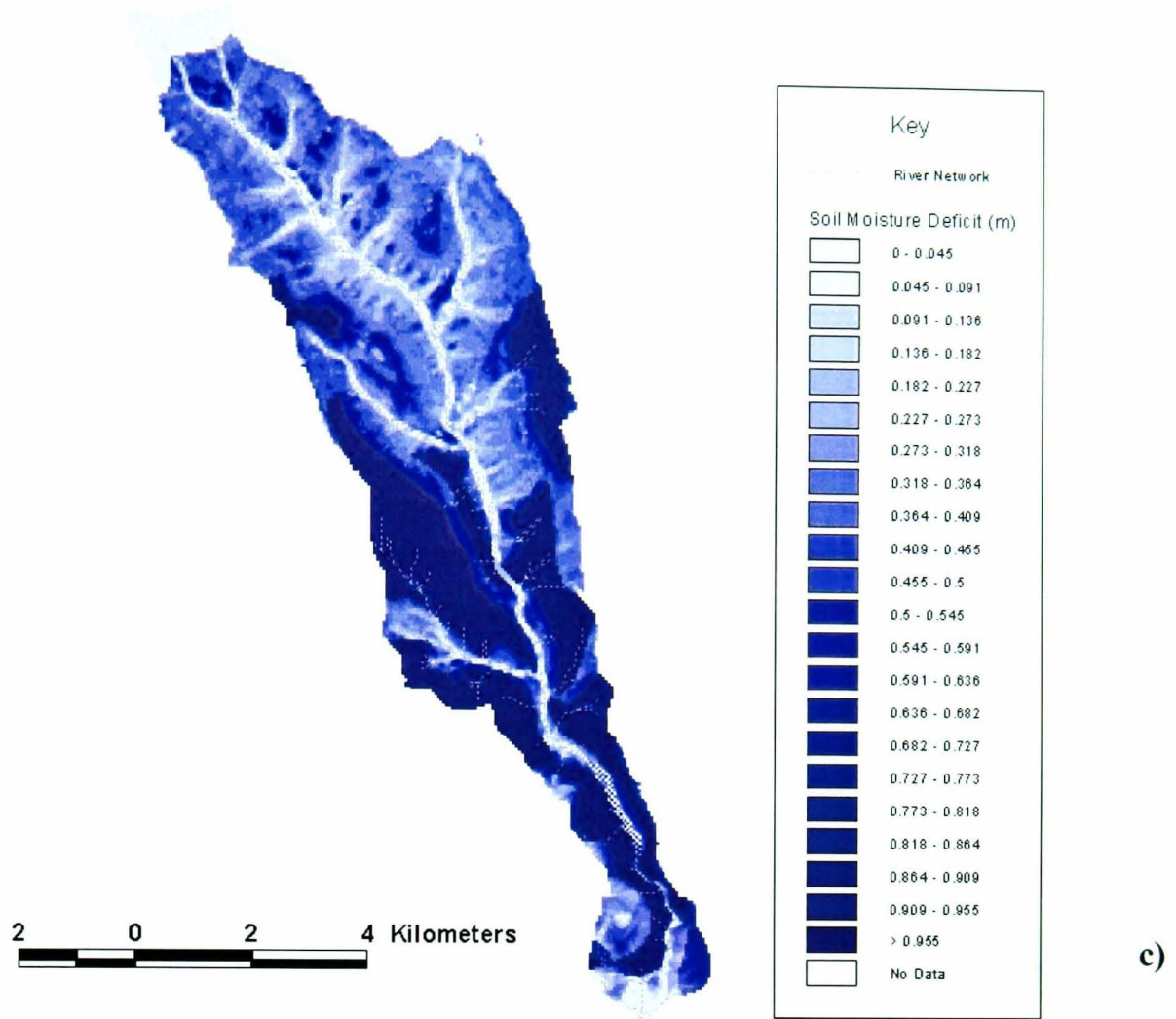


Fig. 6.6 cont'd Spatial Distribution of soil moisture deficit for calibration.

6.4 Model Validation

Validation 1 – Parameter Sensitivity

As seen in the calibration, m is the most sensitive model parameter for both land- and soil-distributed parameterisation (Fig. 6.7). The scatterplot for the soil-distributed parameterisation is much more restricted, with only a narrow band of possible Nash efficiencies for each parameter value. Similar ‘optimised’ values were obtained (Table 6.2).

All other parameters show little or no sensitivity. Mostly high values were obtained for land-distributed $K_{\theta bar}$, while for the soil-distributed parameterisation, efficiency begins to decrease for values of $K_{\theta bar}$ greater than 2000mhr^{-1} .

High efficiencies were obtained for the entire range of $CHV2$ values considered, but between approximately 0.4 and 0.45ms^{-1} , mainly efficiencies greater than 80% are obtained, which is consistent with the optimised channel velocity. Note that the $CHV2$ and $SRMAX$ for the soil-distributed parameterisation were manually fixed at 0.4425ms^{-1} and 0.00517 respectively, prior to the Monte Carlo simulations.

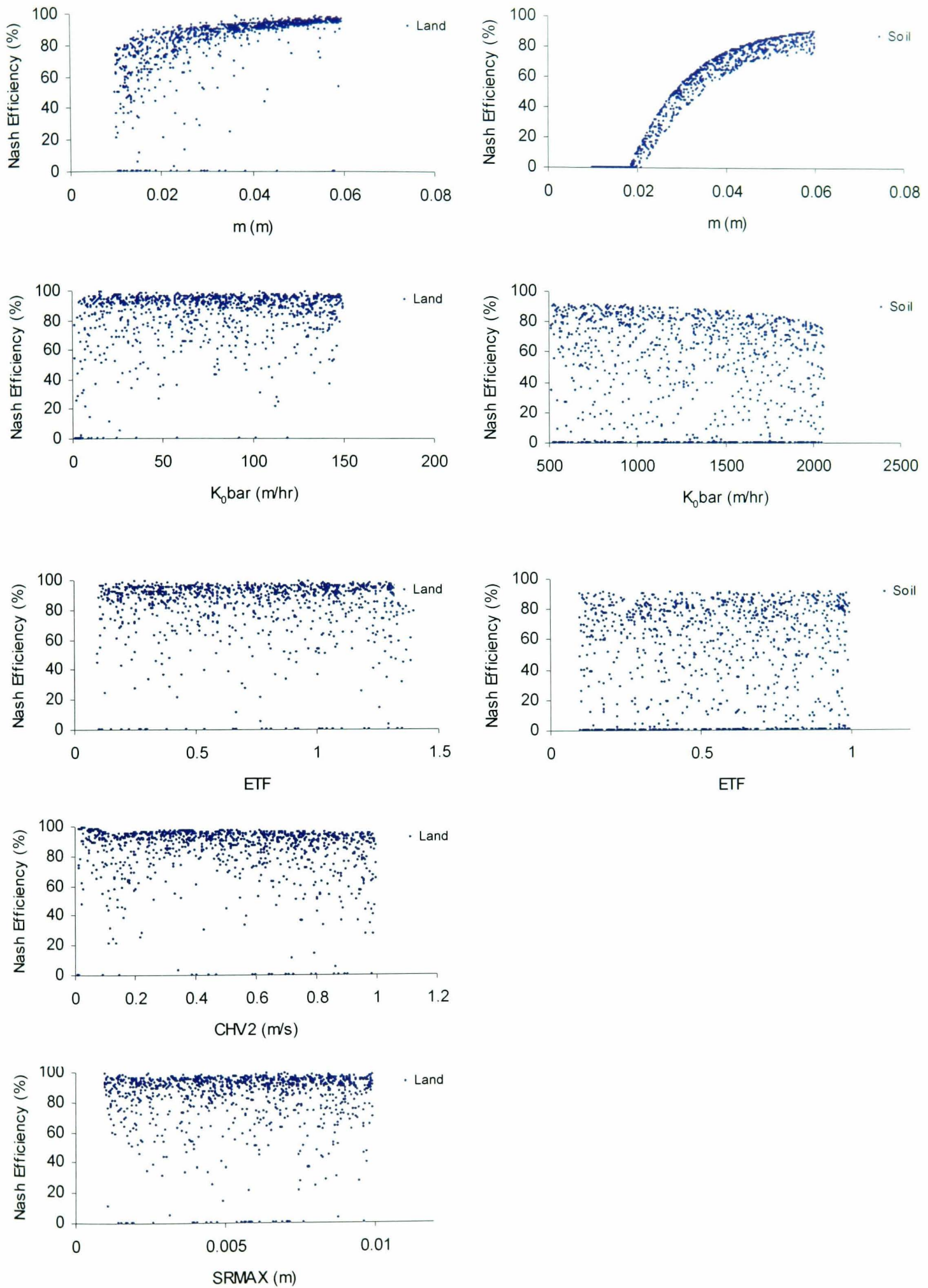


Fig. 6.7 Scatterplots for land- and soil-distributed parameterisation for validation period 1.

Validation 1 – Calibration results and analysis

Land-distributed uncertainty bounds (Fig. 6.8a) completely enclose the observed hydrograph and are widest at the peaks. The bounds follow those of the lumped parameterisation closely. The soil-distributed uncertainty bounds (Fig. 6.8b) however, are of a different shape, with a much gentler slope on the rising limb, and steeper slope on the falling limb for all peaks. The gentler rise to peak flow is due to the primary saturated area – peat - being located on the northern divide of the catchment, and the location of the well drained sandy loams closer to the outlet. This skewness is more discernible in this smaller event, as there is less saturation in the riparian zone so the peak flows are more sensitive to saturation from the distal northern divide. Imeson (1970) working on Bransdale catchment, the neighbouring catchment found that ‘*during dry periods runoff is derived mainly from the numerous peat bogs located along the river headwaters*’. As a result of the skewed peaks, the uncertainty bounds do not enclose the observed peaks, but enclose observed recession flows.

Hydrographs for the ‘optimum’ lumped, land, and soil distributed parameterisations reveals qualitatively similar plots for all three. An examination of the optimised parameter sets (Table 6.2) shows that similar m , $CHV2$ and $SRMAX$ values are obtained. The largest difference in parameter values was obtained for the K_{obar} parameter. The value for the land-distributed parameterisation of 104.5298mhr^{-1} corresponds to values of 69.45, 138.90, 277.79, 41.67, $34,72\text{mhr}^{-1}$ for heather, bracken, woodland, grazing and cultivated respectively. The spatial distribution of soil moisture deficit (Fig. 6.9a and b) reveals a much wetter catchment than that predicted by the lumped model (Fig. 5.11 a and b). Again, the distributed areas are mainly along the riparian areas because, as explained above, land uses have served to reinforce topographic control on hydrological response.

The ‘optimum’ K_{obar} value for the soil-distributed parameterisation, 727.9741mhr^{-1} , corresponds to values of 2395.50, 28.18, 56.36, 422.74, 16.91, 0.28mhr^{-1} for sandy loam, clay, clay lam, sandy clay loam, silty clay loam, and peat respectively.

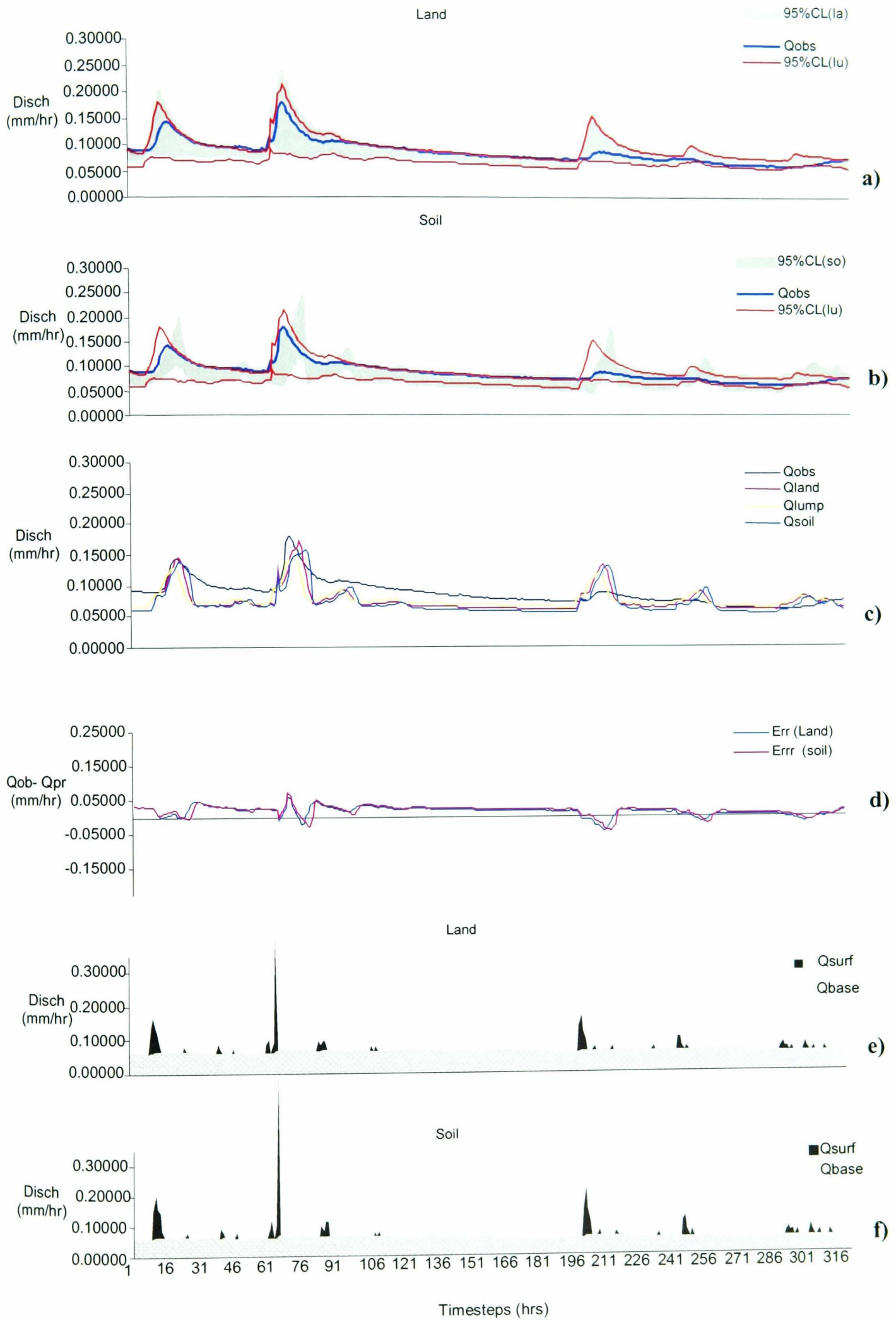


Fig. 6.8 Results for validation 1 for land- and soil-distributed parameterisation.

Parameter	Observed	Lumped	Land	Soil
m (m)	-	0.05732	0.05424	0.05995
K ₀ bar (m/hr)	-	421.351	104.5298	727.9741
SRMAX (m)	-	0.00459	0.00541	0.00517
CHV2 (m/s)	-	0.4229	0.4452	0.4425
ETF	-	0.37655	0.2561	0.17896
Sum rain (m)	0.022	-	-	-
Sum discharge (mm)	28.219	24.678	24.234	23.362
Sum Q _b (m)	-	0.022101	0.020528	0.01923
Sum Q _s (m)	-	0.000429	0.001501	0.002184
Nash Eff (%)	-	96.55	96.14926	91.198

Table 6.2 'Optimum' parameter sets for validation 1 for lumped- land- and soil-distributed parameterisation.

The spatial distribution of soil moisture deficit follows the pattern of soil type closely, with saturation along the riparian area, and in the headwaters on the northern divide. These saturated areas are responsible for the response at the outlet, as the relatively dry slopes in the south of the catchment closer to the outlet are very slow to respond to rainfall input, and accounts for the skewness in the hydrograph peaks mentioned above.

The lower ETF values obtained for the land and soil distributed parameterisations are due to the larger saturated surface areas contributing to evapotranspiration.

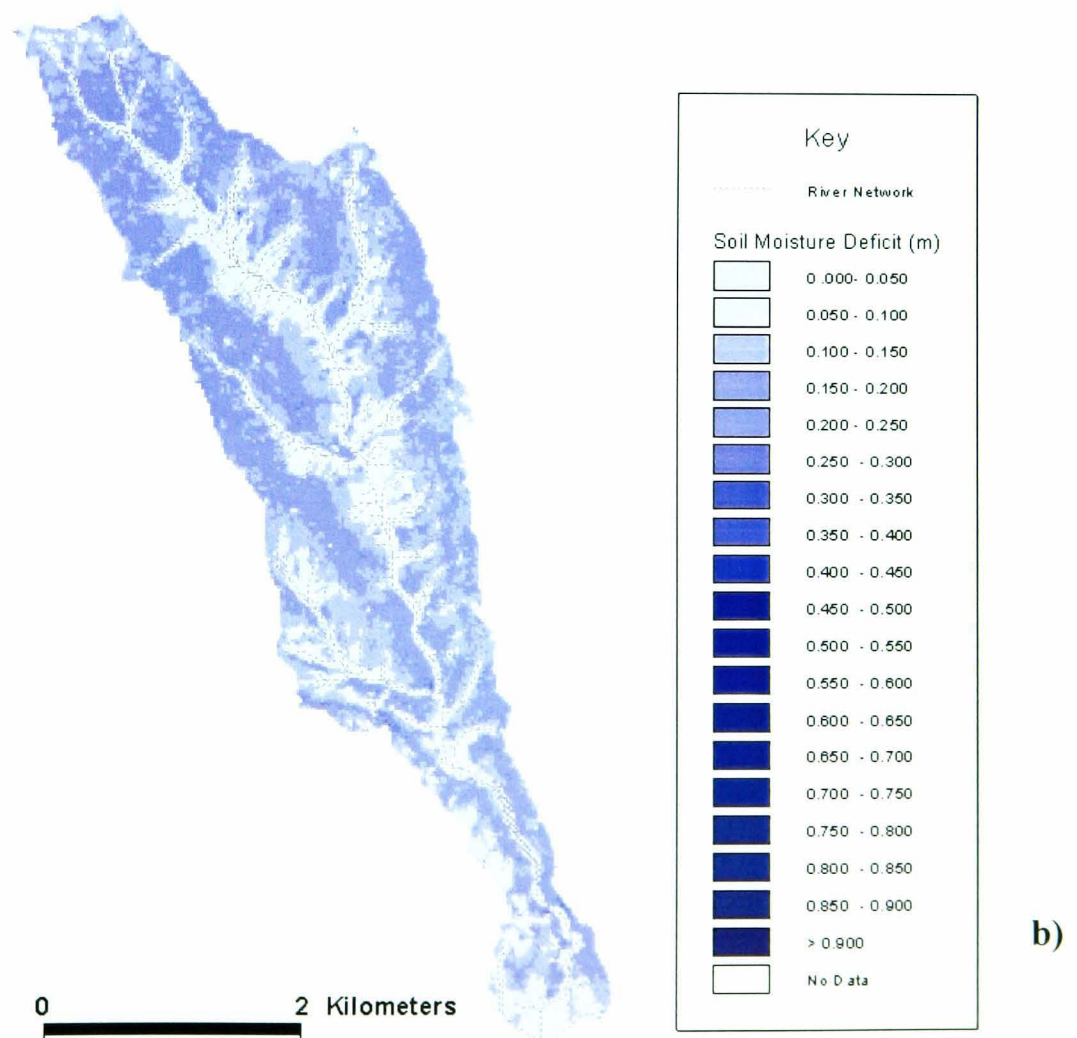
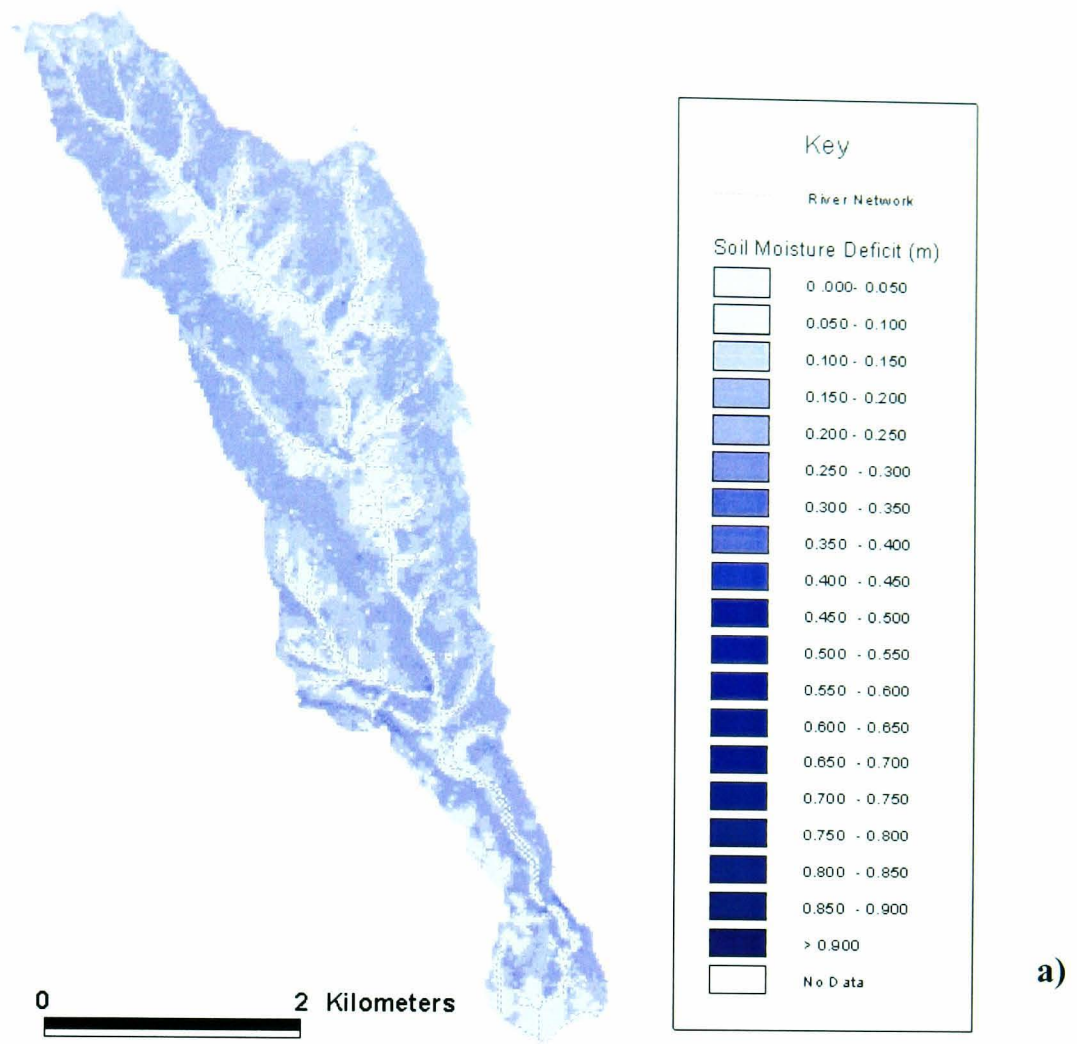


Fig. 6.9 Spatial distribution of soil moisture deficit for validation 1 at a) Driest timestep and b) Wettest timestep for land-distributed parameterisation.

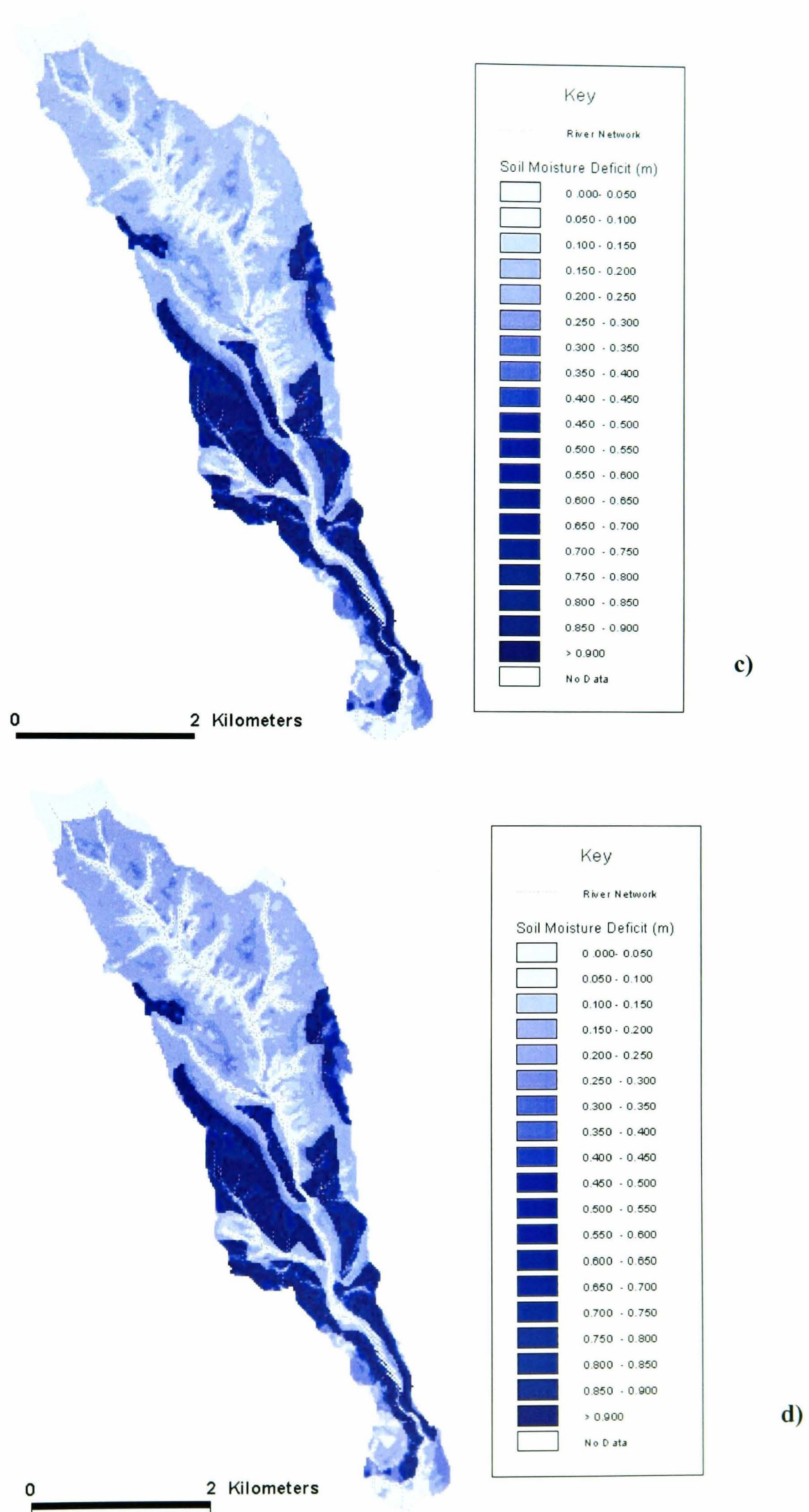


Fig. 6.9 cont'd. Spatial distribution of soil moisture deficit for validation 1 at a) Driest timestep and b)

Validation 2 – Parameter sensitivity

The scatterplot for soil-distributed m is severely constrained compared to the land-distributed plot (Fig. 6.10). For both parameterisations, optimum values are obtained at approximately 0.03m and there is a steady decrease in efficiency for values greater than 0.04m, although the land-distributed plot shows a few simulations with high efficiencies above this value. K_{obar} and $SRMAX$ are insensitive, with efficiencies fairly restricted for the soil-distributed plot. $CHV2$ for land (the value of soil was fixed manually at 0.9263ms^{-1}) shows increasing efficiency with increasing parameter value, and a maximum at approximately 0.9ms^{-1} . As discussed in section 5.3, the increased $CHV2$ value for this event is indicative of the rapid expansion of the channel network into the hillslopes and the inherent difficulties of modelling this dynamic expansion with a static parameterisation of channel and hillslope velocities.

Validation 2 – calibration results and analysis

Again, the uncertainty limits of the land-distributed parameterisation (Fig.6.11a) follow that of the lumped model, enclosing all of the observed hydrograph except the third peak. Uncertainty bounds in the soil-distributed parameterisation (Fig. 6.11b) also enclose all but the third peak of the observed hydrograph, but the bounds are much narrower throughout, with the lower limit following the observed hydrograph more closely than either the lumped or land-distributed models.

Fig. 6.11c shows that the ‘optimised’ hydrographs are qualitatively similar, though peaks for the soil-distributed hydrograph tends to be lower. Comparison of the ‘optimum’ parameter values (Table 6.3) reveals that there is little variability in $CHS2$ with spatial parameterisation. The relative insensitivity of $CHV2$ to spatially distributed saturated hydraulic conductivity reflects the dominance of this parameter in an event of this magnitude.

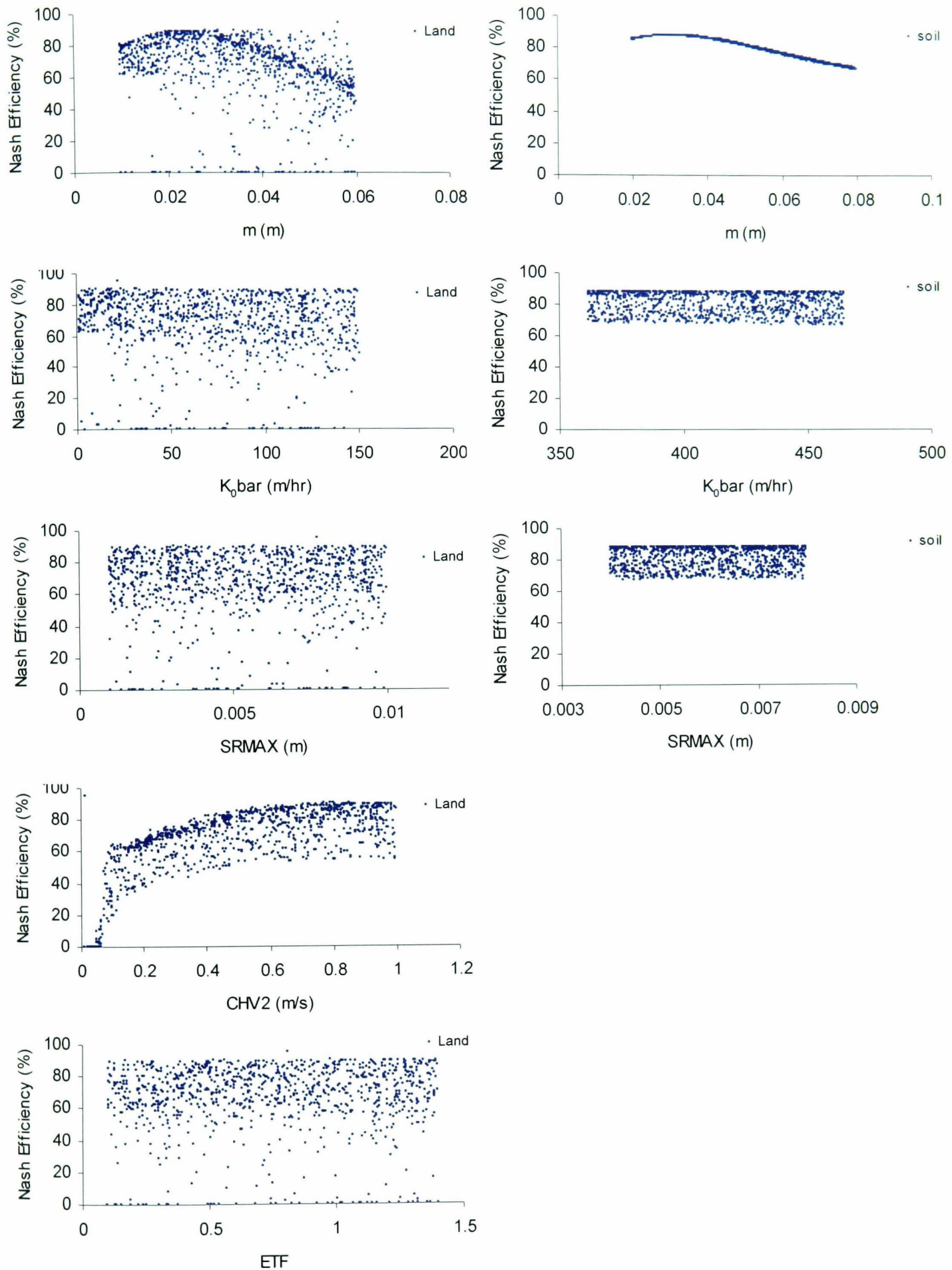


Fig. 6.10 Scatterplots for land- and soil-distributed parameterisation – validation 2.

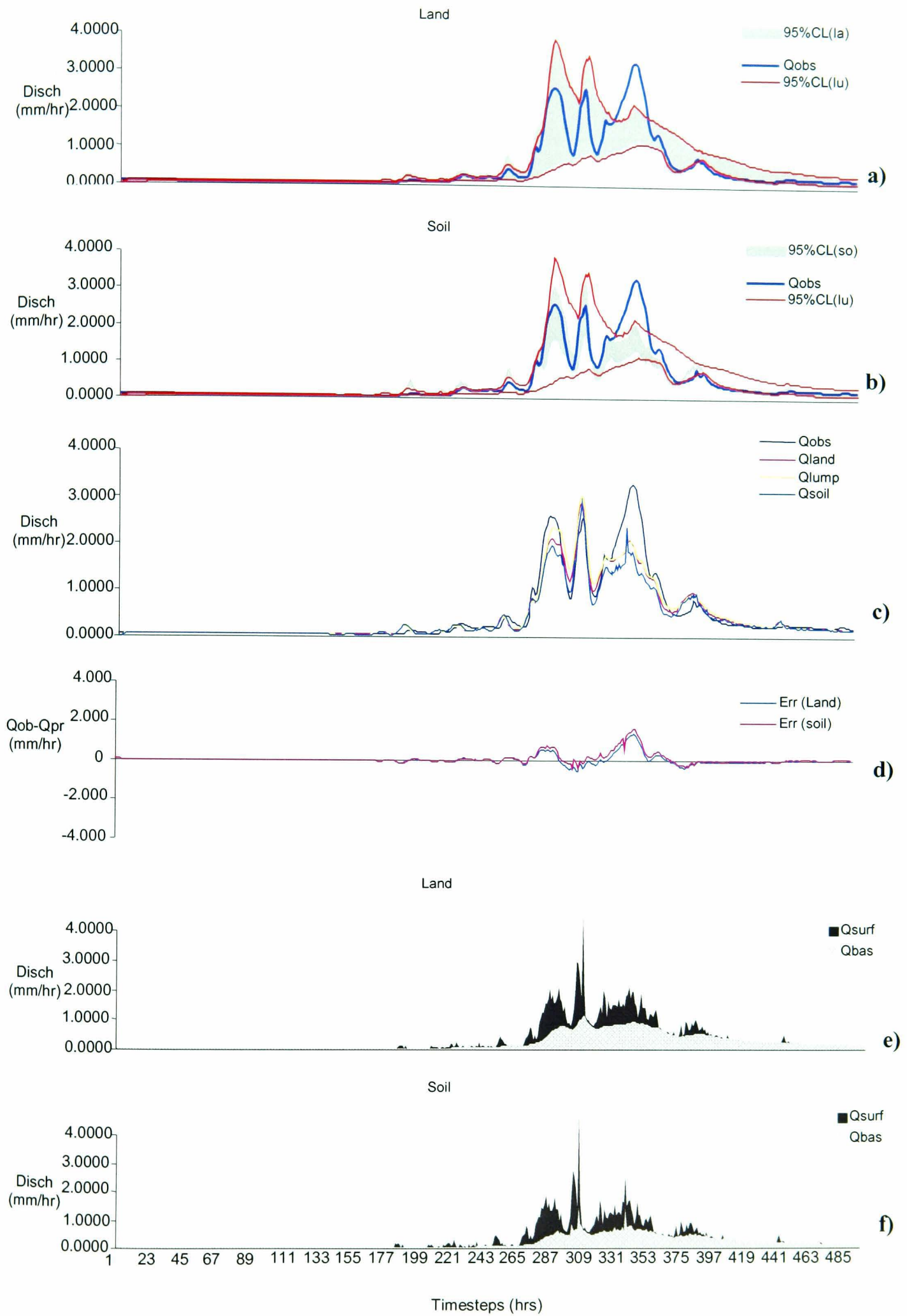


Fig. 6.11 Results of validation 2 for land-distributed parameterisation.

Parameter	Observed	Lumped	Land	Soil
m (m)	-	0.02337	0.03017	0.03182
K_{0bar} (m/hr)	-	63.0421	32.6060	362.381
SRMAX (m)	-	0.00396	0.00647	0.00495
CHV2 (m/s)	-	0.92290	0.89746	0.9263
ETF	-	1.23921	1.2134	0.76235
Sum rain (m)	0.2542	-	-	-
Sum discharge (mm)	240.51	232.801	224.407	202.012
Sum Q_b (m)	-	0.159364	0.1288	0.108279
Sum Q_s (m)	-	0.048692	0.07093	0.068988
Nash Eff (%)	-	88.95	89.43	84.89

Table 6.3 Results of validation 2.

‘Optimum’ parameter values for the land- and lumped parameterisations are similar for all parameters except m and K_{0bar} (Table 6.3). For the land-distributed parameterisation K_{0bar} , 32.606mhr^{-1} , is half the value for the lumped parameterisation, while m is higher than the lumped value. Thus their spatial predictions are also very similar (compare Fig. 6.12 and Fig. 5.16c and d). Everywhere in the catchment is saturated in the wettest timestep (Fig. 6.12b), but for the driest timestep everywhere except the highest ground is saturated (Fig. 6.12a).

The soil-distributed parameterisation predicts a higher K_{0bar} , and lower ETF, as well as lower percentage baseflow (54%) than the land-distributed (58%) or lumped (68%) models (Table 6.3). The spatial predictions for the soil-distributed parameterisation, however, show a similar distribution of saturated areas in the northern half of the catchment only. This suggests that the sandy loams, which comprise the southern half of the catchment, act as buffers that allow much of the upslope runoff to re-infiltrate before reaching the catchment outlet.

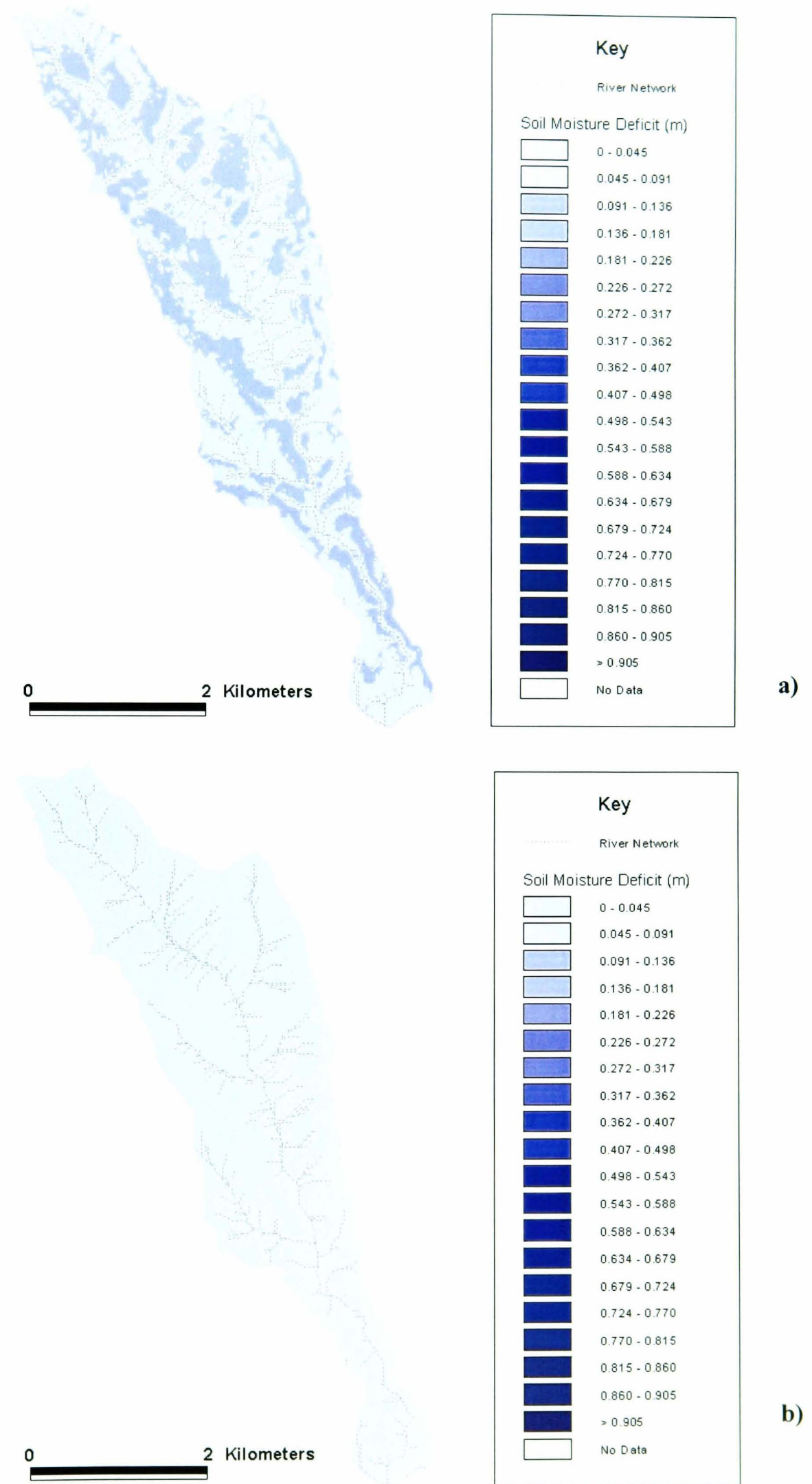


Fig. 6.12 Spatial predictions for validation 2 at a) driest timestep and b) wettest timestep for land-distributed parameterisation

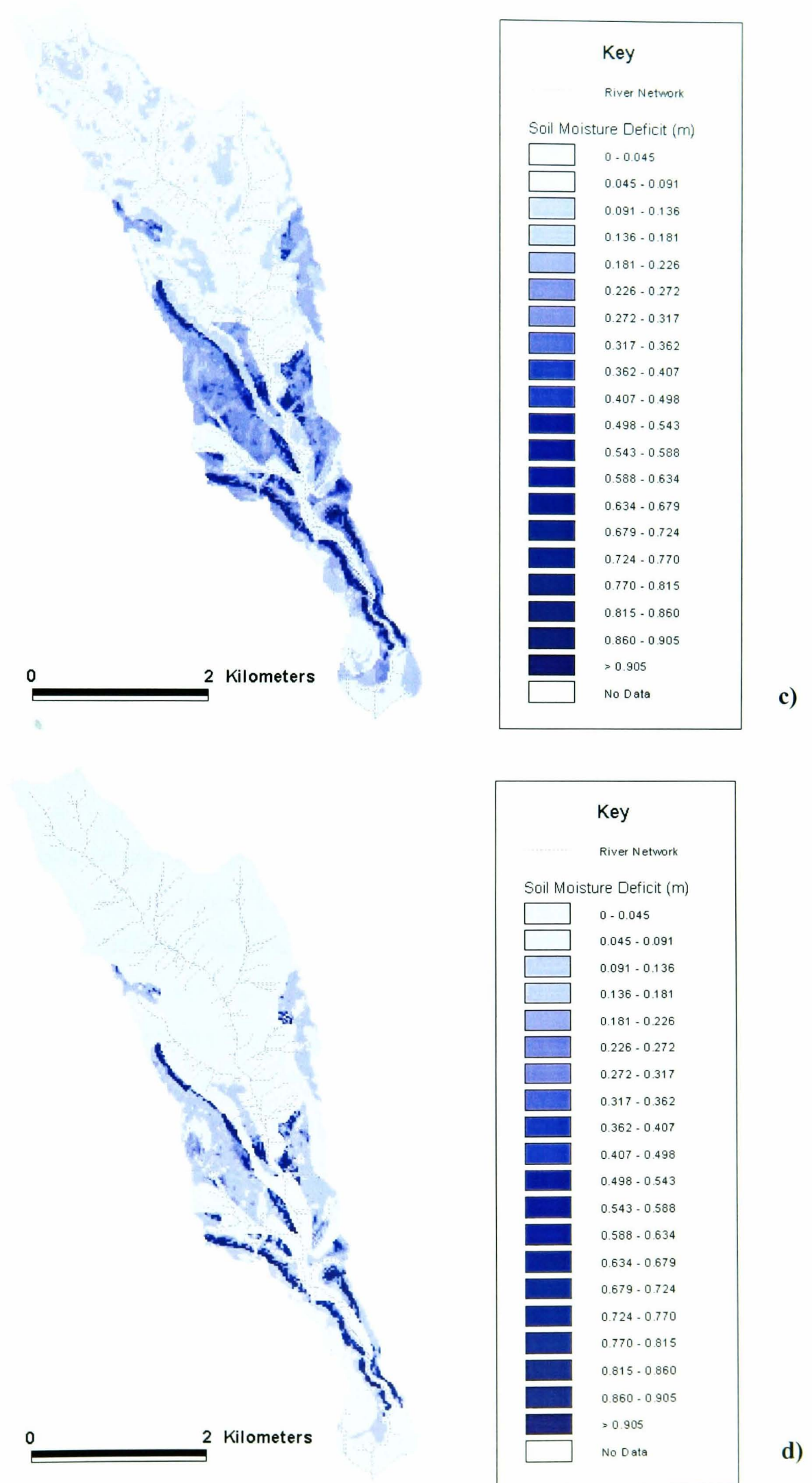


Fig. 6.12 cont'd Spatial predictions for validation 2 at the a) driest timestep b) wettest timestep for soil-distributed parameterisation.

Discussion

The hydrological model calibration and validation results suggest significant model sensitivity to the spatial variation in soil hydraulic properties. While qualitatively similar hydrographs, with similar levels of predictive efficiency, can be obtained from very different spatial parameterisations of the catchment, the spatial predictions of soil moisture are very different. This suggests that the heterogeneity in hydrological processes subsumed by the spatially distributed landuse and soil types significantly differ from the processes predicted by the lumped model. Of great significance is the apparent reinforcement of the topographic control on hydrological response that this particular land use pattern provides. This has resulted in spatial soil moisture distributions that are similar to the lumped model, but which appear to provide a better coupling of the hillslope and channel processes, resulting in a larger expansion of the saturated zone than is predicted by the lumped model. The soil-distributed parameterisation, however, provides a pattern that suggests mechanisms that restrict baseflow in the southern half of the catchment, and which attenuate surface runoff from the northern half of the catchment during flood events. An interesting test would be a detailed study of downstream accumulated runoff over a set of events to determine the key zones of runoff production.

The treatment of landuse and soil type as separate controls on hydrological response is not ideal. In reality, their controls will interact in a non-linear manner to give a hydrological response that may be different from either of the separate responses. In addition, their combined controls may also be temporally variable, for example, on cultivated land, where seasonal changes in land cover occurs, and where grazing patterns are varied seasonally. In order to fully characterise their combined effects, measurements would have to be taken for all combinations of landuse and soil type, and for all temporal possibilities. Hence, the nature of their interaction cannot be easily predicted. The hydrological model equifinality revealed by this analysis, will significantly affect the spatial predictions of sediment source areas and hence the sediment delivery within the catchment. This is examined in the next section.

6.5 Sediment Model Calibration

Parameter Sensitivity

The model is most sensitive to R_0 for both parameterisations (Figs. 6.13 and 6.14). The ‘optimum’ values are approximately $6.6 \times 10^{-8} \text{ mhr}^{-1}$ for the land-distributed, and $6.4 \times 10^{-9} \text{ mhr}^{-1}$ for soil-distributed parameterisations. The reason for this order of magnitude difference will become apparent when the spatial distribution of sediment source areas is examined.

Calibration results and analysis

Fig. 6.15 shows the results of the sediment model calibration for both parameterisations. While the timing of the sedigraphs for the land-distributed peaks (Fig. 6.15b) is correct, the uncertainty bounds fail to predict the shape of the peaks, resulting in steeper rise to peaks and more prolonged (wider) peaks than observed. Uncertainty limits for the soil-distributed parameterisation follow the observed flux more closely with the major peaks predicted and the minor peaks over-predicted. Timing is good in all but the first peak and the main peak starts to rise slightly later than observed.

The plot of ‘optimum’ sedigraphs (Fig. 6.15d) shows that the land-distributed parameterisation is similar to the lumped, except on the last peak, which is better predicted by the land. The ‘optimum’ soil-distributed sedigraph gives the best fit to the observed sediment flux on the major peaks but over-predicts the minor peaks. The total flux predicted by the land-distributed model however, is closest to the observed total with the soil-distributed model over-predicting, and the lumped model under-predicting, the value (Table 6.4). ‘Optimum’ parameter values are comparable for both the land-distributed and lumped models, but the soil-distributed model predicts R_0 and K_{sed} values that are an order of magnitude less, and a larger $CHS2$.

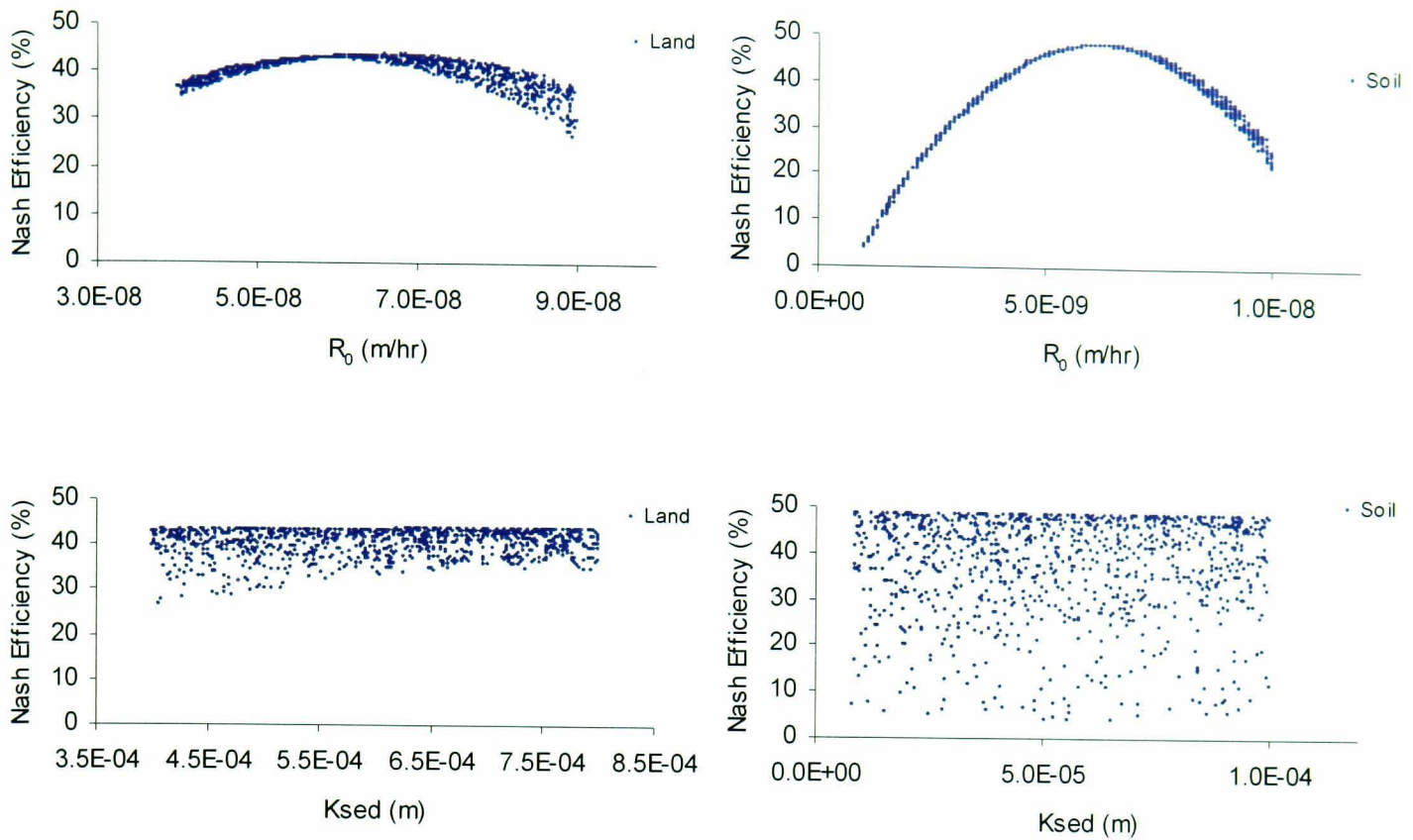


Fig. 6.13 Scatterplots of Parameter values versus Nash Efficiency for land- and soil-distributed parameterisation.

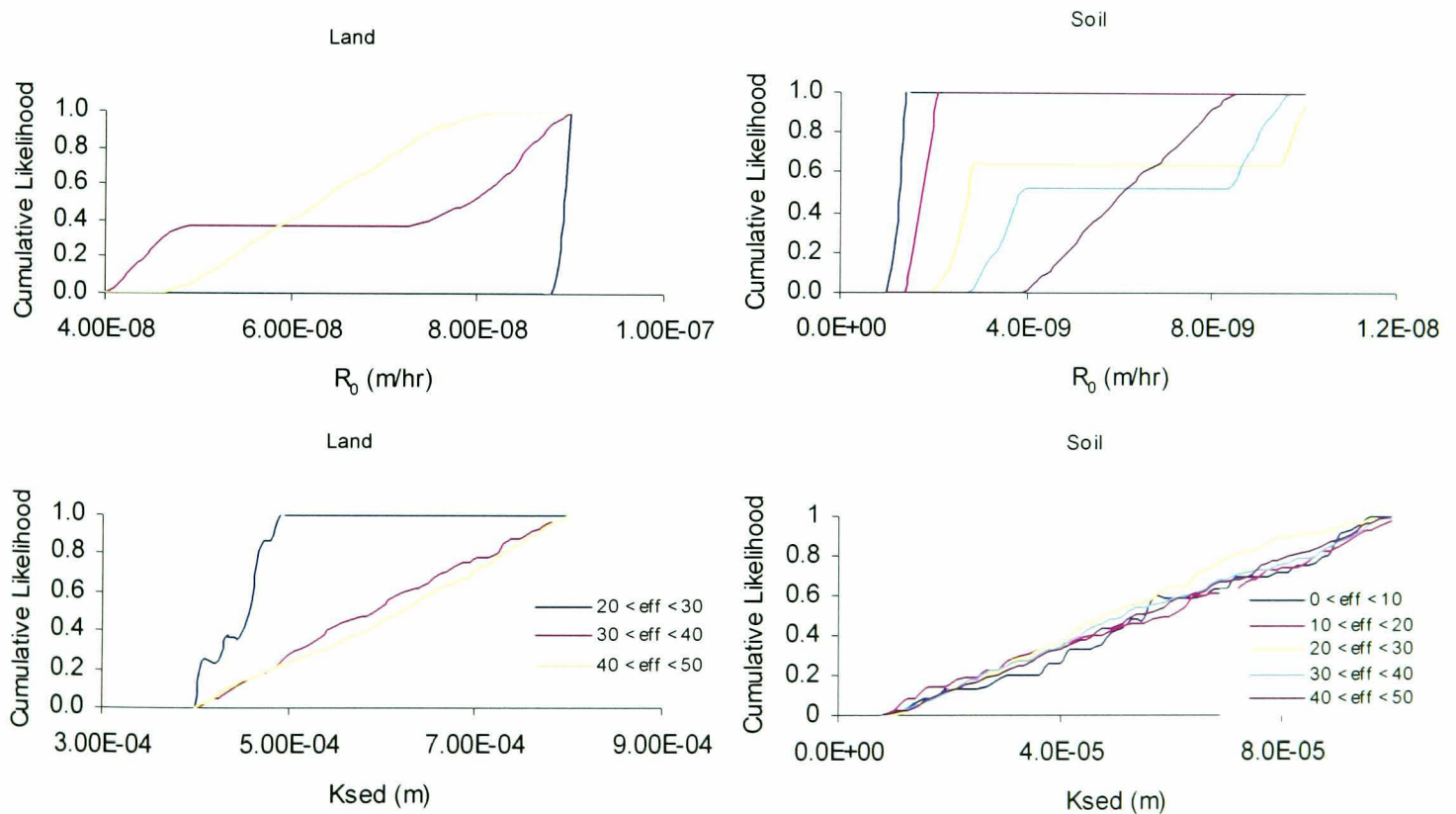


Fig. 6.14 GSA plots for land- and soil-distributed parameterisation for sediment model calibration.

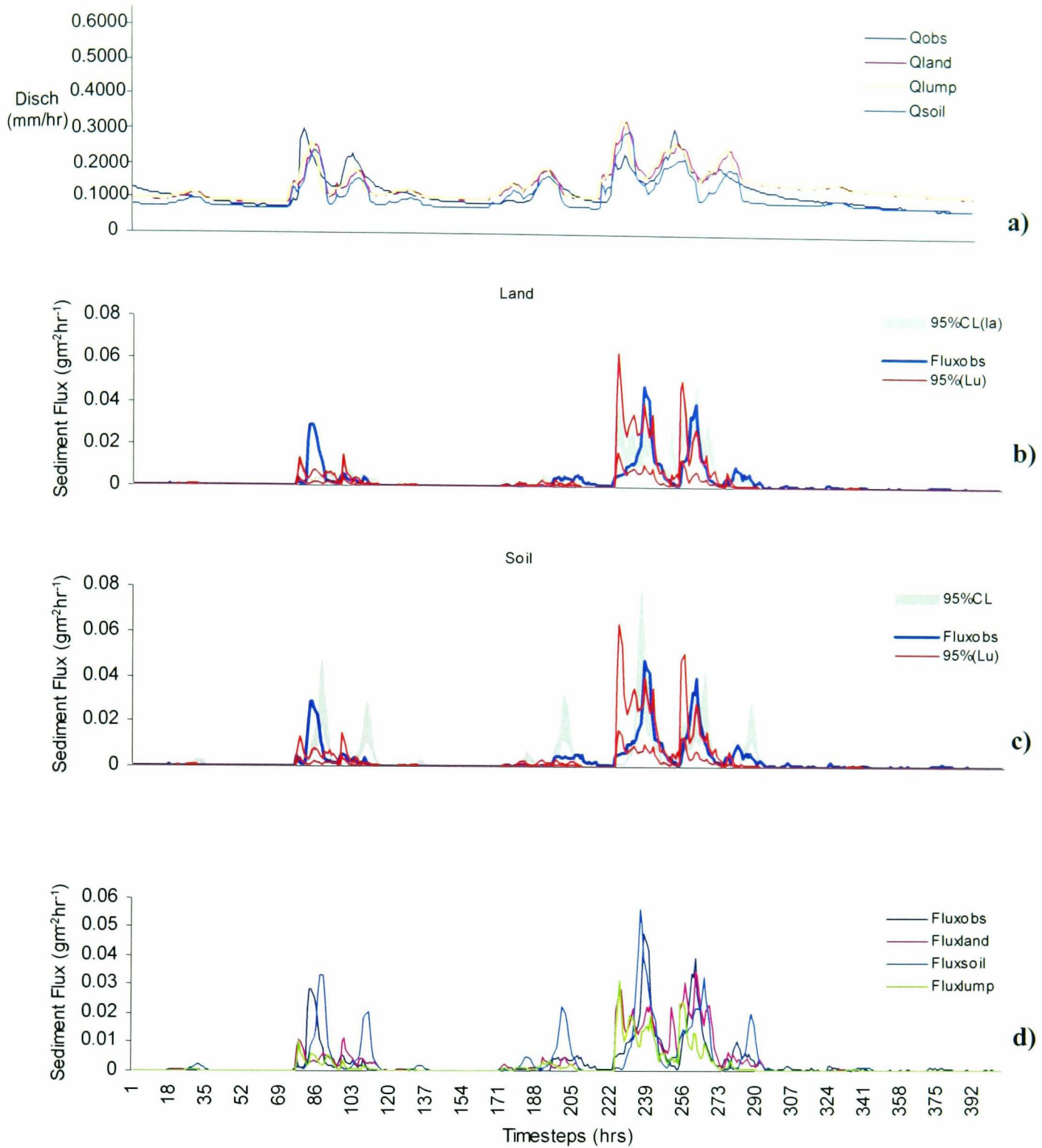


Fig. 6.15 Results of sediment calibration for land- and soil-distributed parameterisation.

- Observed and predicted hydrographs for event using ‘optimum’ land, soil and lumped parameters set.
- Uncertainty bounds for land-distributed sediment flux.
- Uncertainty bounds for soil-distributed sediment flux.
- Observed sediment graph and ‘optimum’ land- and soil-distributed and lumped sediment graphs.

Parameter	Observed	Lumped	Land	Soil
R_0 (m/hr)	-	6.67×10^{-8}	6.6×10^{-8}	6.4×10^{-9}
K_{sed} (m)	-	6.93×10^{-4}	7.86×10^{-4}	9.3×10^{-5}
CHS2 (m/s)	-	0.35	0.35	0.58
Sum Flux ($gm^{-2}hr^{-1}$)	1.125228	0.685066	1.189012	1.365268
Nash Eff (%)	-	37.73	43.84	48.51

Table 6.4 'Optimum' calibrated parameter sets for lumped, land and soil parameterisations.

Spatially Distributed Predictions

The spatial distribution of accumulated sediment depth for the land-distributed parameterisation (Fig. 6.16) reflects the reinforcing effect that landuse has on the topographic control of surface saturation and hence sediment source areas. The lowest sediment depths are located in and around the channel network, where the higher rates of surface saturation result in lower sediment accumulation rates, but more frequent removal of sediment by surface runoff than further upslope. There is little difference in spatial distribution at $T=75$ and $T=122$. However, compared to the same timesteps for the lumped model, there appears to be a more dynamic expansion of sediment source areas on the north-eastern side of the catchment. At $T=248$, just after the passage of the first peak of the double peak, the sediment source area has expanded much more extensively ($T224-T248$, Fig. 6.17) than for the lumped model ($T224-T248$, Fig. 5.23) (note the lighter blue areas indicating lower sediment depth). Similarly, the change in sediment depth over the entire double peak is much larger for the land-distributed parameterisation ($T224-T298$, Fig. 6.17) than for the lumped model ($T224-T298$, Fig. 5.23).

The results suggest that although topography is still the major control on surface saturation and hence sediment source distribution, spatially distributed parameterisation of soil hydraulic conductivity by landuse, enables a better coupling of hillslope and channel processes. The low hydraulic conductivity of the grazing and cultivated areas on the valley floor, results in shorter inter-storm periods than areas further upslope. However, because they produce surface runoff more regularly, sediment yield from these areas is higher, making them primary sediment source areas.

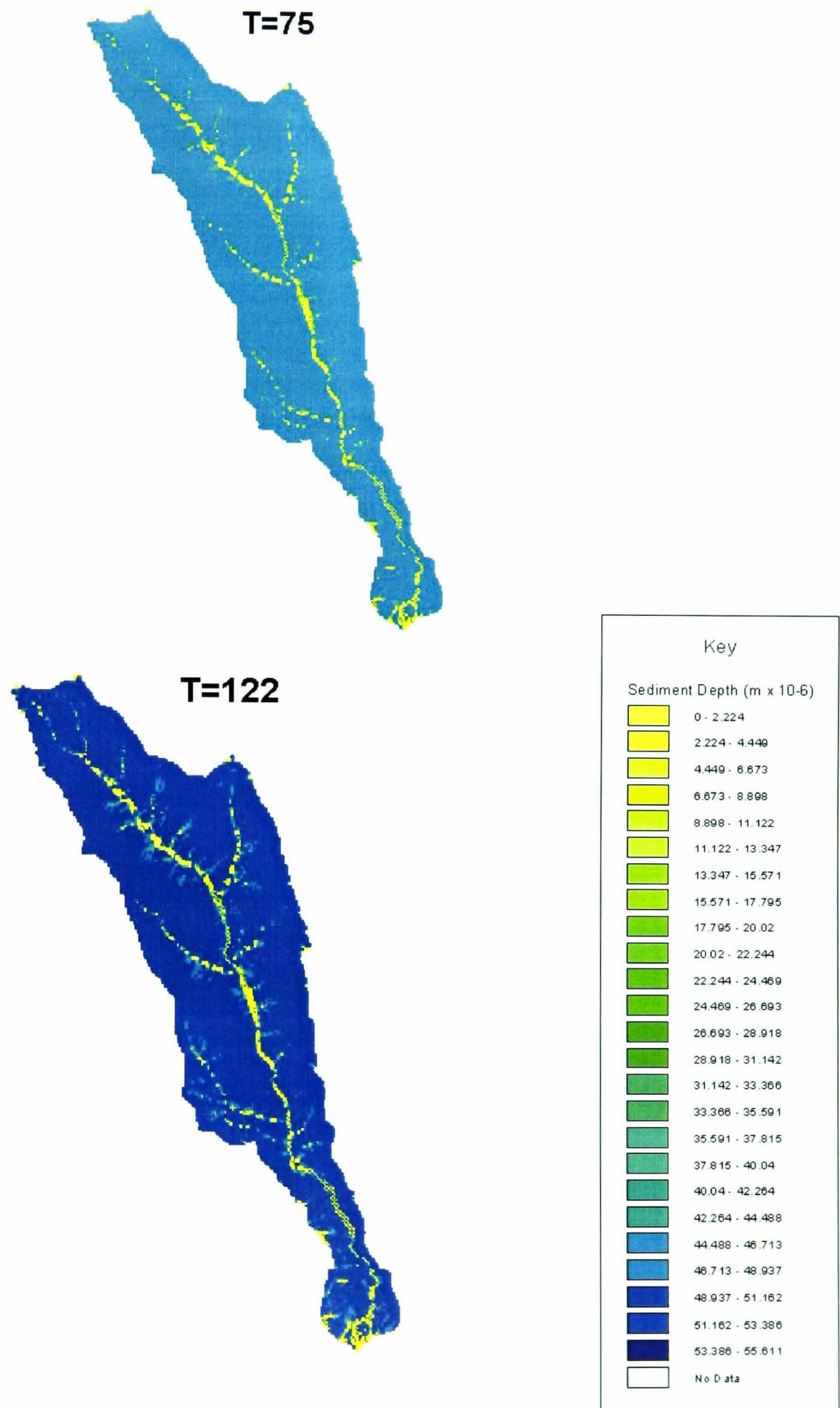


Fig. 6.16 Spatial Distribution of depth of accumulated sediment at T=75 and T=122 hours for the land-distributed parameterisation.

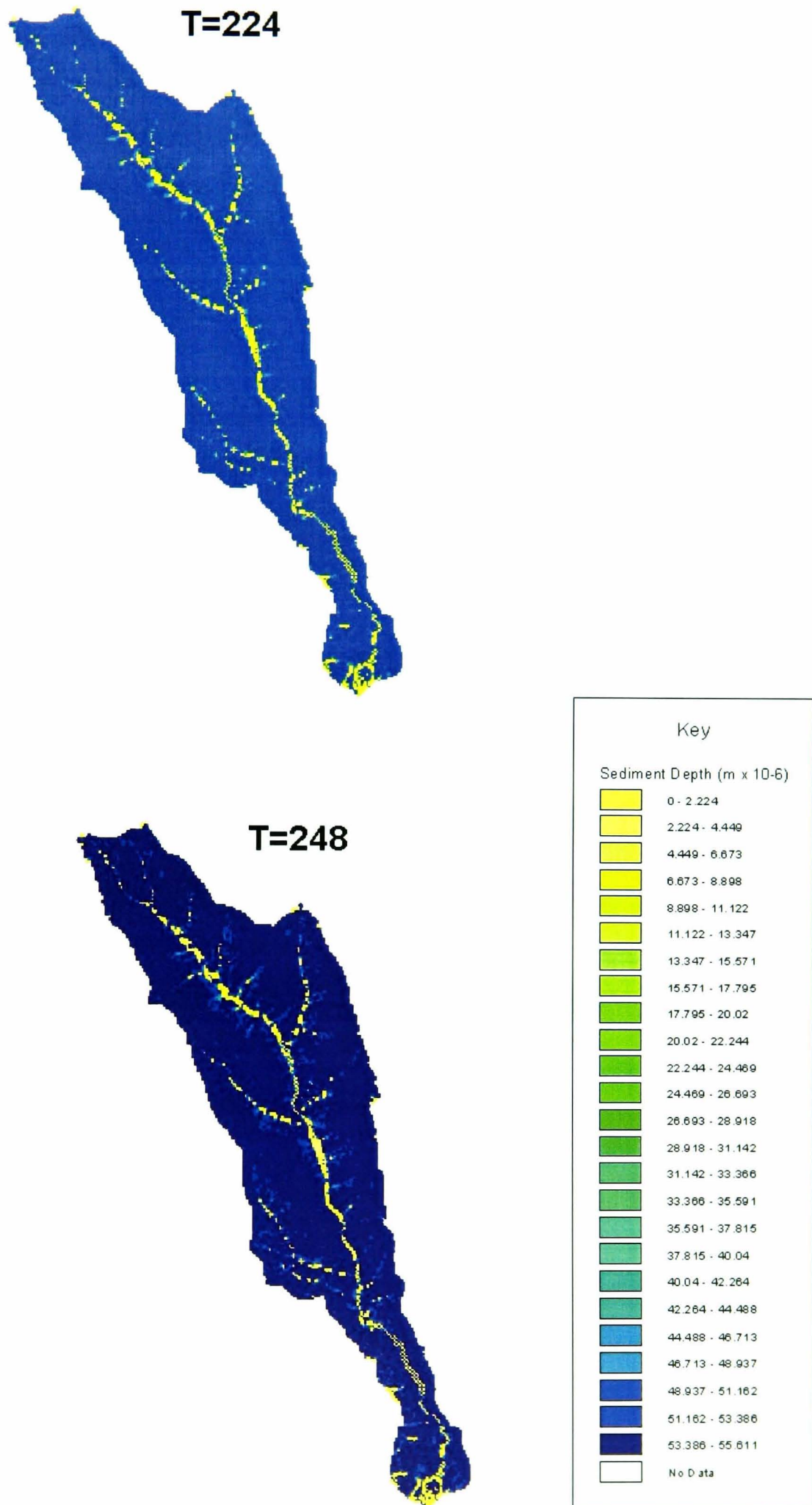


Fig. 6.16 cont'd Spatial distribution of depth of accumulated sediment at T=224 and T=248 hours for the land-distributed parameterisation.

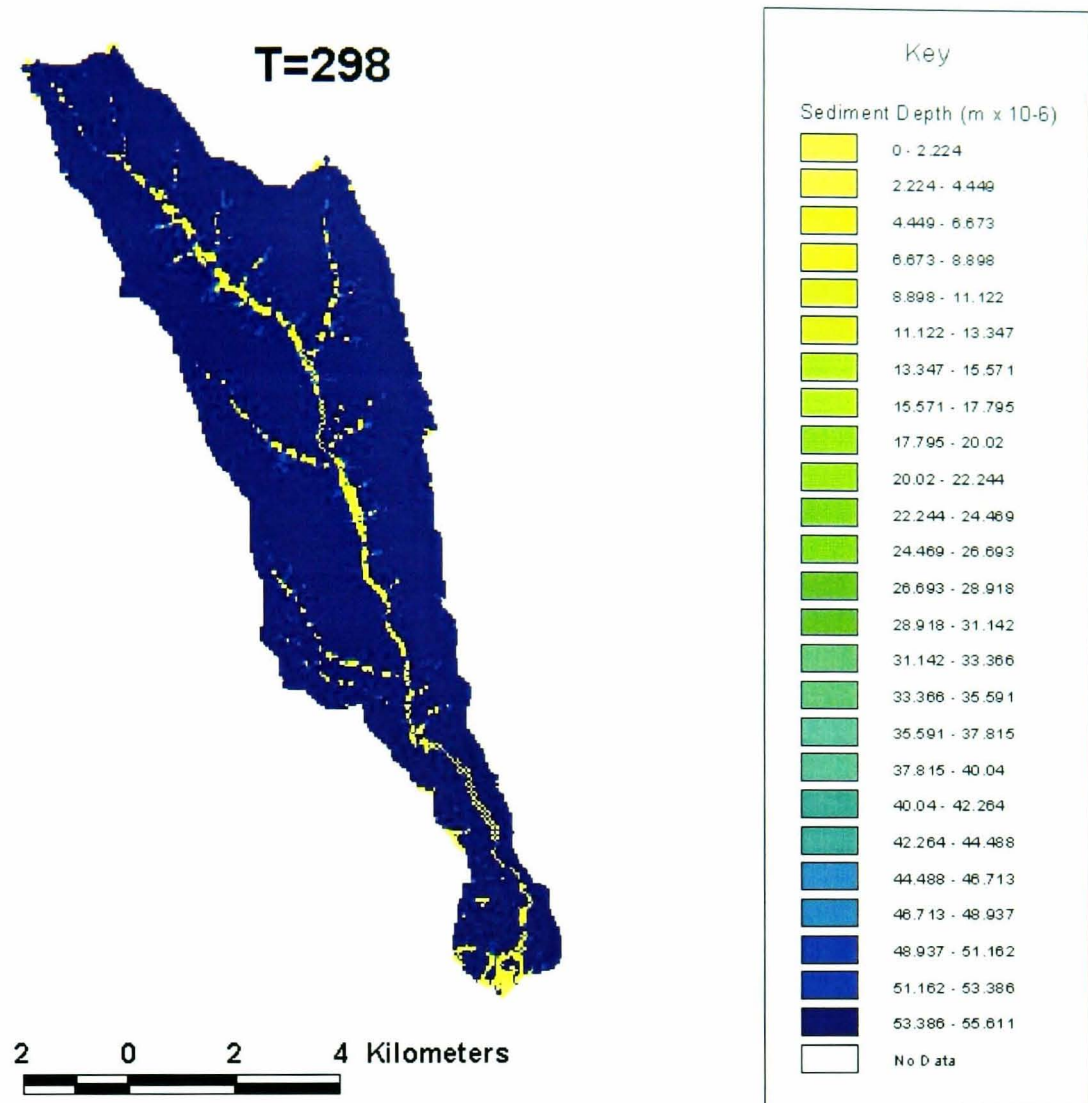


Fig. 6.16 cont'd Spatial distribution of depth of accumulated sediment at T=298 hours for the land-distributed parameterisation.

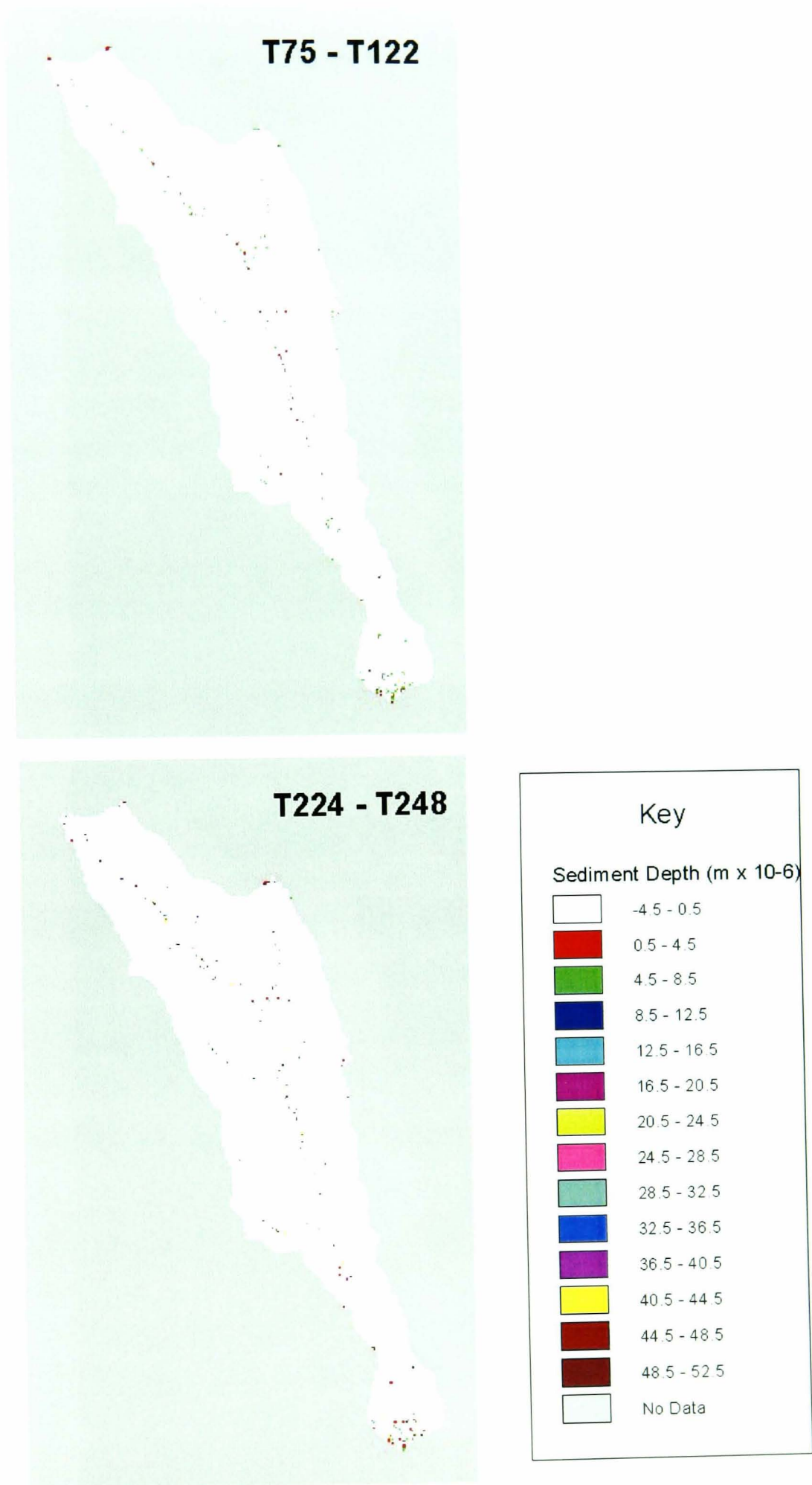


Fig. 6.17 Spatial distribution of sediment source areas for land-distributed parameterisation during:
 a) the first peak (T=75 – T=122) and;
 b) the first peak of the double peak (T=224 – T=248)

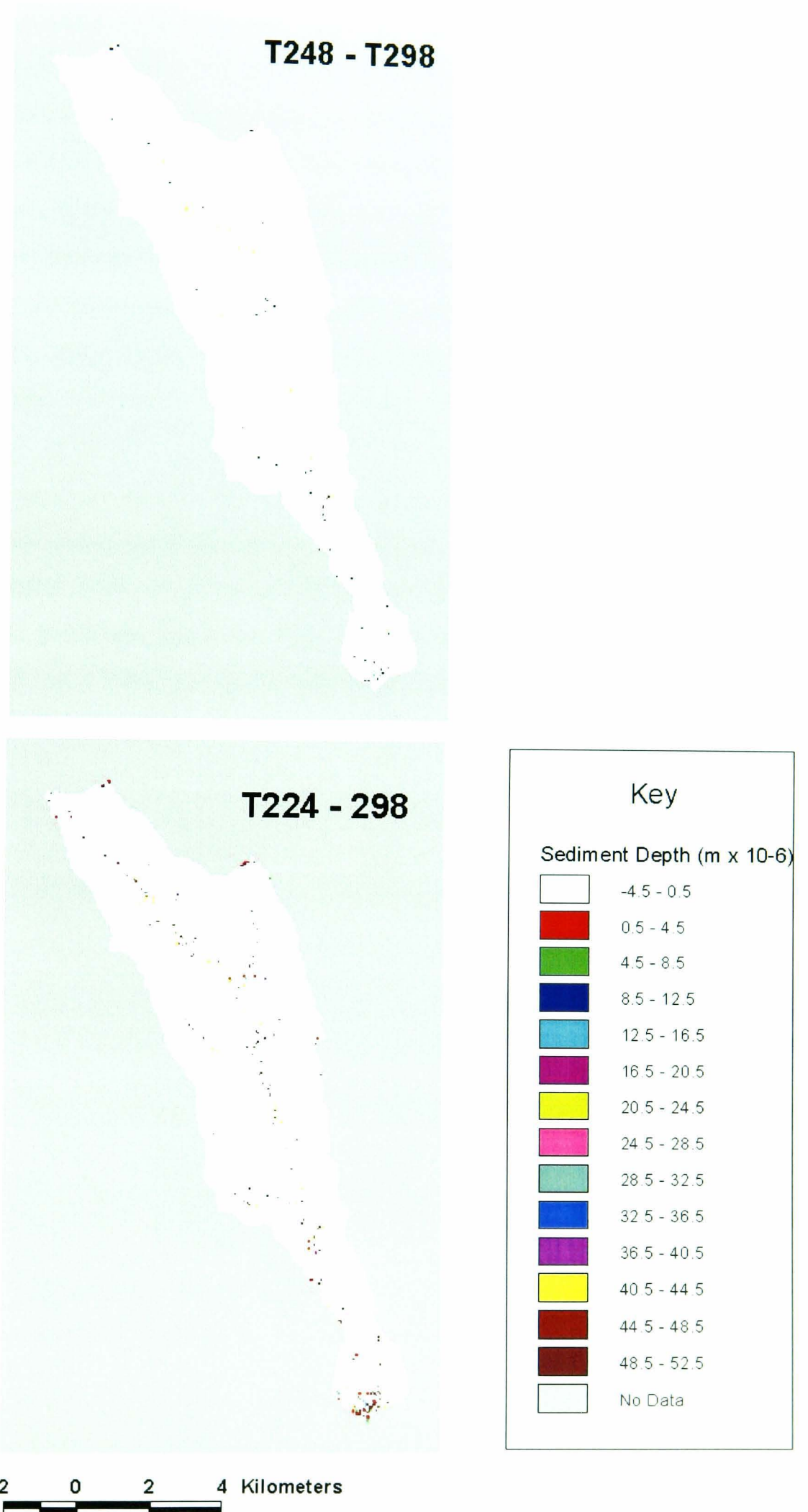


Fig. 6.17 cont'd Spatial distribution of sediment source areas for land-distributed parameterisation during:
 c) the second peak of the double peak (T=248 – T=298) and;
 d) the entire double peak (T=224 – T=298)

The soil-distributed sediment depth maps (Fig. 6.18) are not directly comparable to the lumped or land-distributed maps, as the values are an order of magnitude less. However, the spatial pattern shows a concentration of lower sediment depths in and along the channel network, and in the headwaters on the northern divide. This shows that a larger surface area of the catchment is saturated at any given time (areas of low sediment depth). An examination of the maps of sediment sources for different peaks (Fig. 6.19) shows that the main sediment sources are these saturated areas, mainly in the headwaters, where waterlogged peat contributes runoff and sediment more frequently than any other sources. The larger sediment contributing surface area accounts for the lower ‘optimum’ R_0 values obtained above, as low values, spread over a larger area, compensate for the difference in surface area. For example, for T75 – T122, the soil-distributed parameterisation predicts that 1.99% of the catchment is contributing to sediment yield, compared to 0.75% predicted by the land-distributed parameterisation. The accompanying lower K_{sed} value reflects the inter-dependence of this parameter and R_0 , as a lower rate of decrease of accumulation rate is needed to moderate the effect of lower R_0 values.

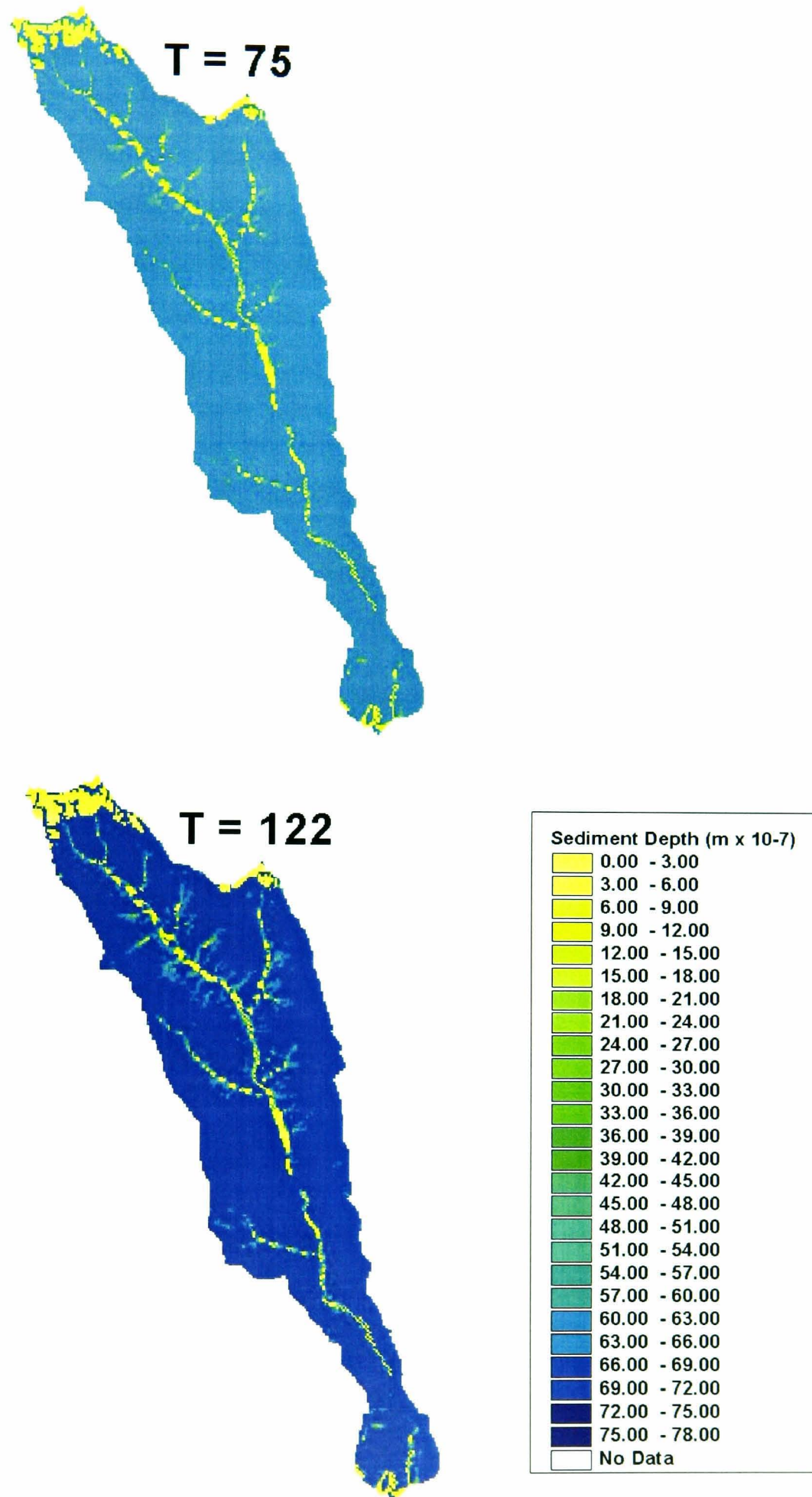


Fig. 6.18 Spatial distribution of depth of accumulated sediment at T=75 and T=122 hours for the soil-distributed parameterisation.

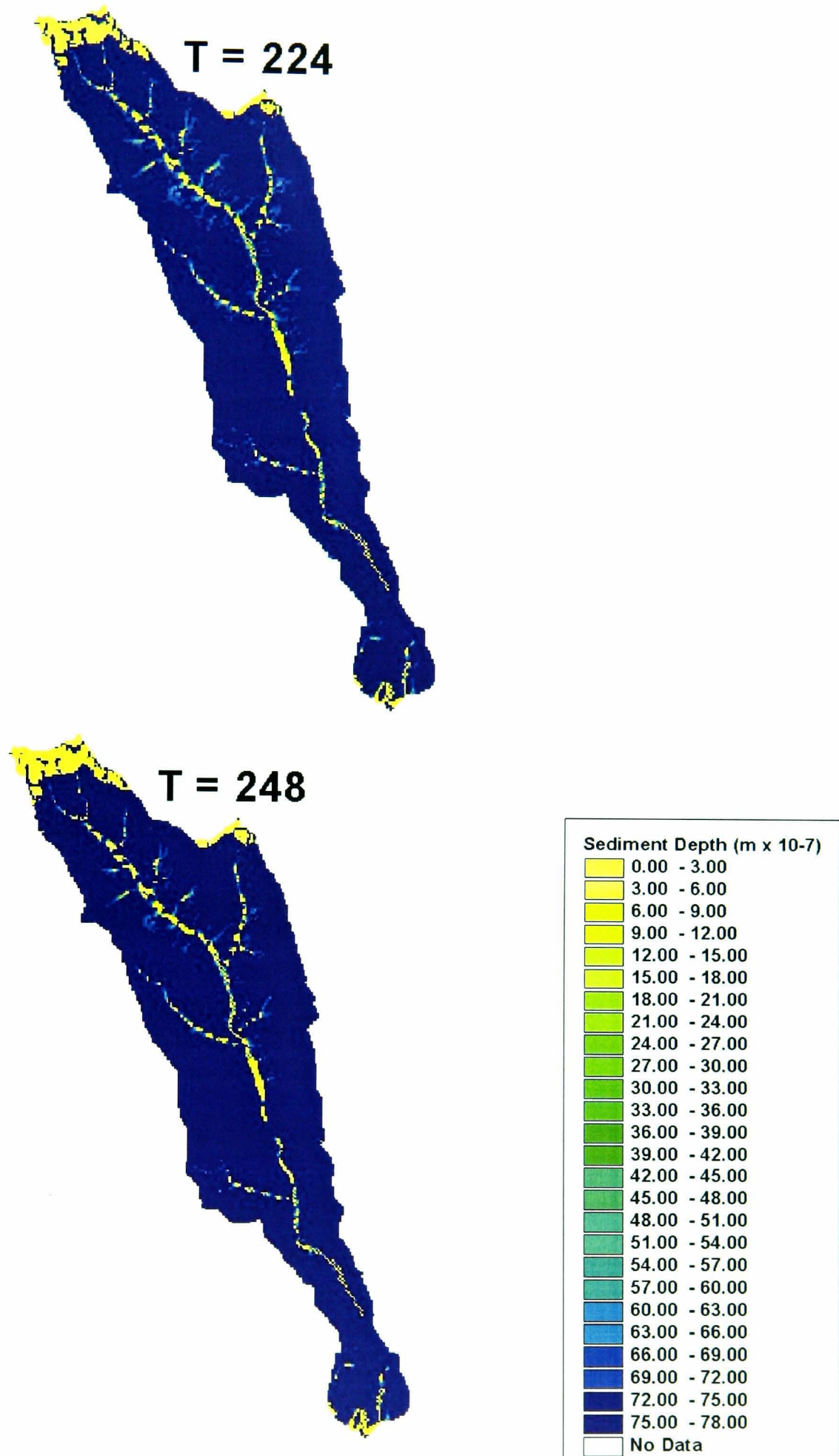


Fig. 6.18 Spatial distribution of depth of accumulated sediment at T=224 and T=248 hours for the soil-distributed parameterisation.

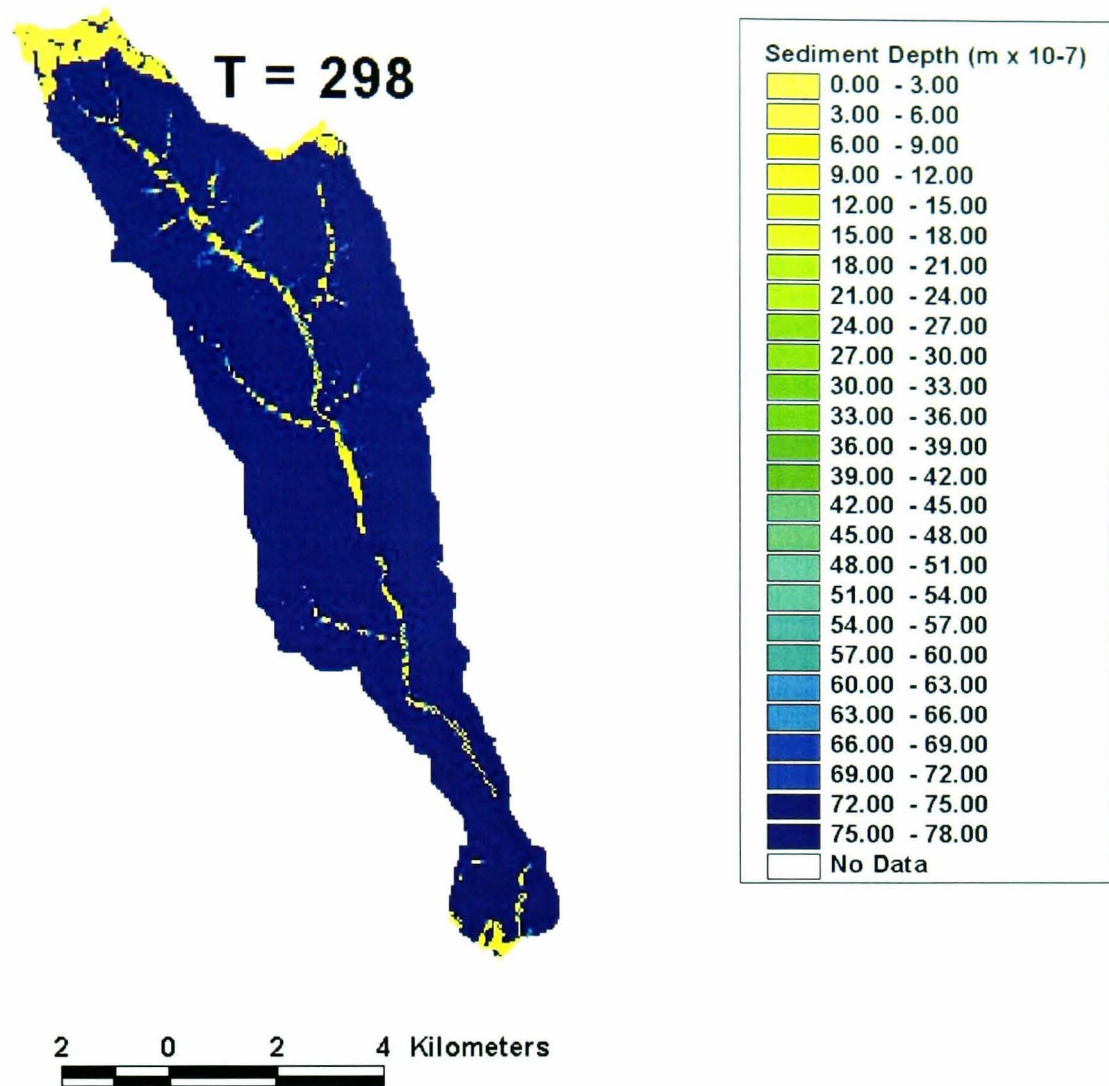


Fig. 6.18 cont'd Spatial distribution of depth of accumulated sediment at T=298 hours for the soil-distributed parameterisation.

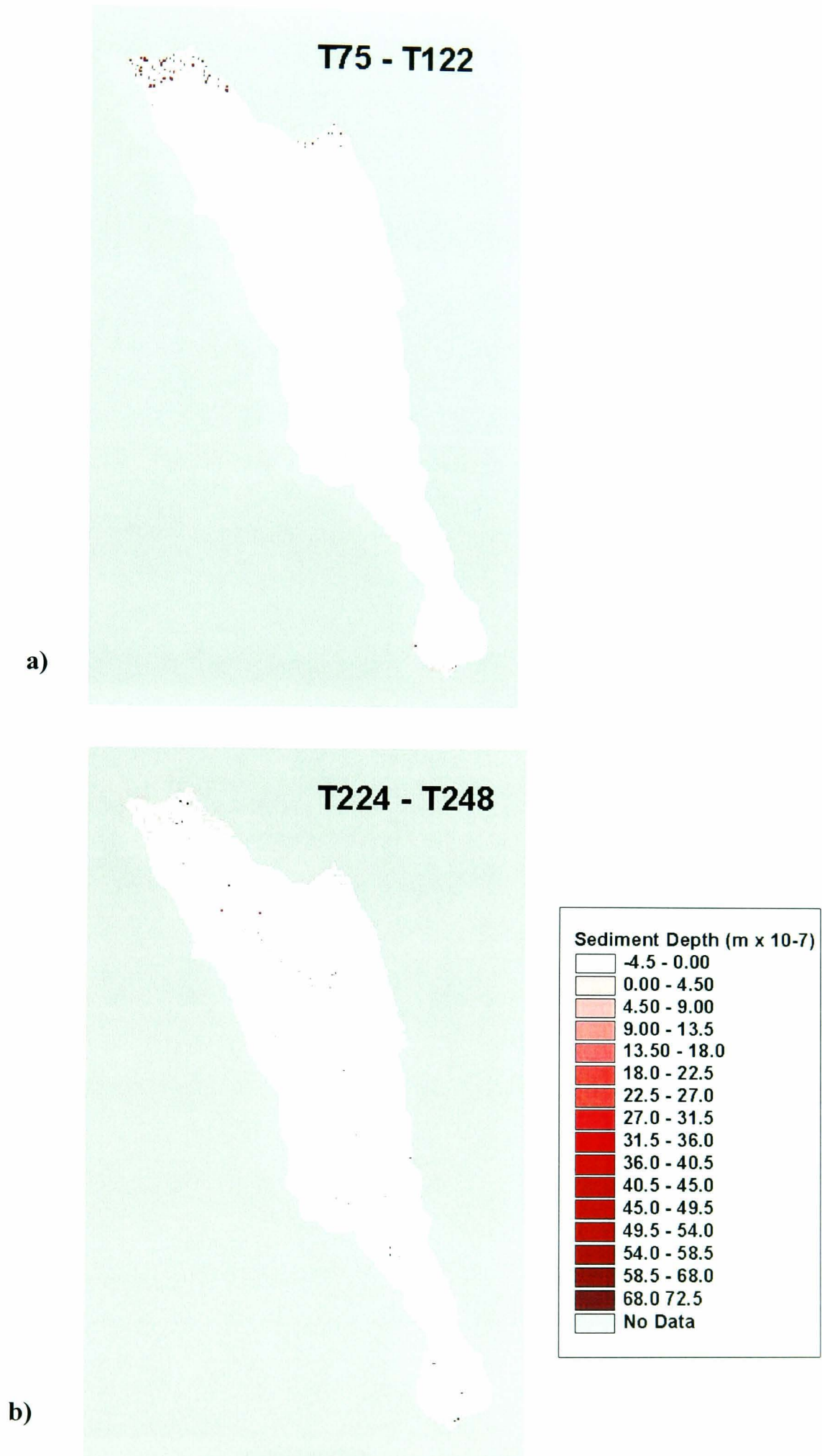


Fig. 6.19 Spatial Distribution of sediment source areas for soil-distributed parameterisation during
a) the first peak (T=75 – T=122)
b) the first peak of the double peak (T=224 – T=248)

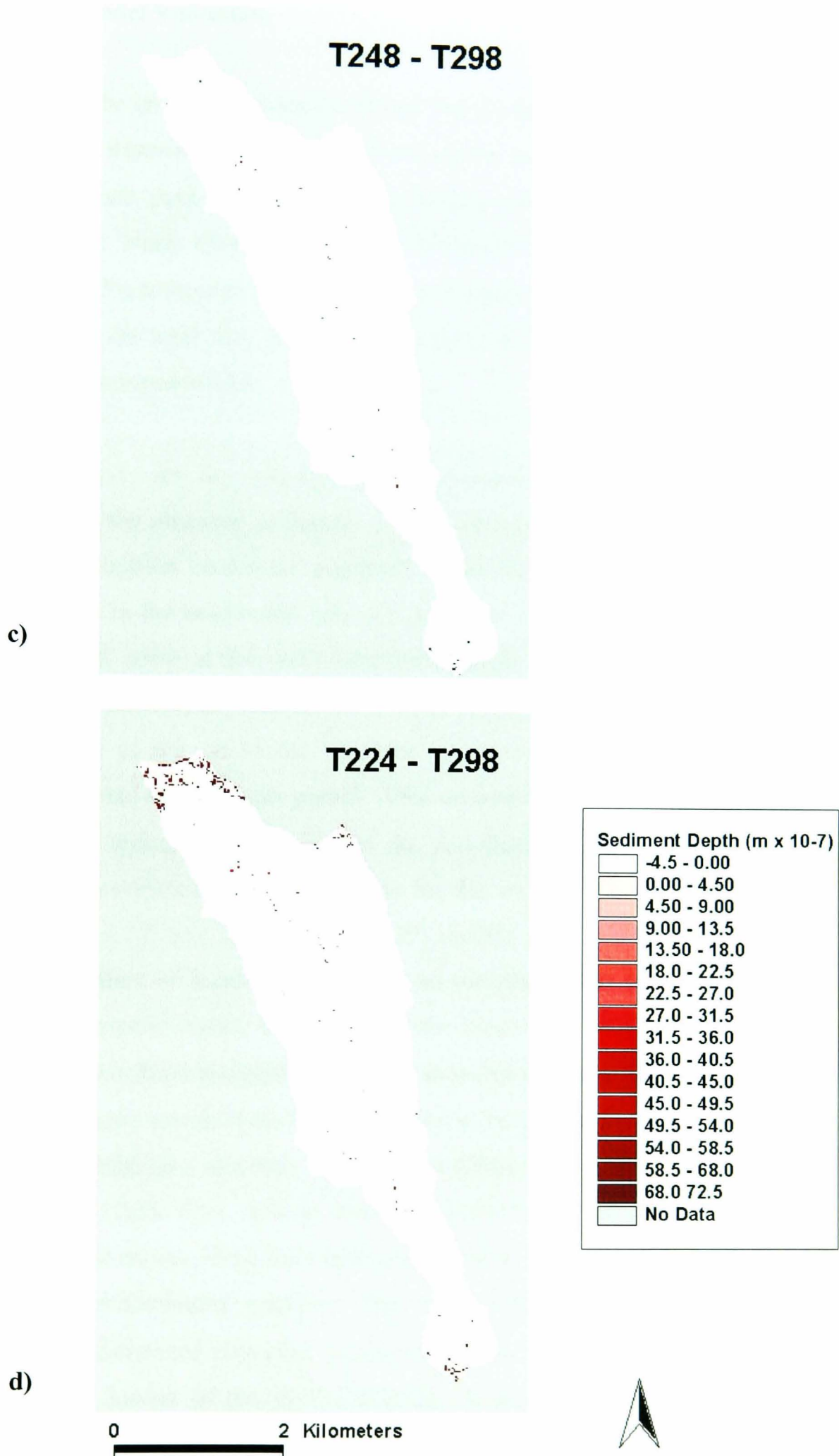


Fig. 6.19 Spatial Distribution of sediment source areas for soil-distributed parameterisation during
 c) the second peak of the double peak (T=248 – T=298)
 d) the entire double peak (T=224 – T=298)

6.6 Sediment Model Validation

Validation 1

Examination of the uncertainty bounds reveals that the land-distributed uncertainty is, qualitatively, an improvement on the lumped model predictions (Fig. 6.20b). The timing of the main peak is better and the bounds enclose most of the observed sedigraph. The Nash efficiency of the ‘optimum’ land-distributed simulation, however, is 44.87% compared to 55.01% for the lumped model. Parameter values are comparable, but the total flux is over-predicted by the land-distributed and under-predicted by the lumped model.

Uncertainty bounds for the soil-distributed parameterisation (Fig. 6.20c) do not enclose much of the observed sedigraph. Peaks are narrow and tall, indicating that higher, shorter duration events are predicted. This suggests that sediment derived from the sources in the headwaters take a longer time to get to the outlet and, once removed, they all arrive at the same time and register a larger maximum. For the lumped and land-distributed parameterisations, however, sediment sources are located in different parts of the catchment, resulting in variable arrival times and, hence, peaks that are spread over a longer period. This is corroborated by the spatial maps of sediment source areas, which show that the soil-distributed (Fig. 6.24) sediment source areas are restricted to the headwaters for this event, while those of the land-distributed (Fig. 6.22) and lumped (Fig. 5.29) models are spread over the channel network. The effect of location of source area on peak width and timing is more evident in this smaller event, because only the areas most susceptible to surface saturation will contribute to sediment yield in an event of this magnitude, and hence the location of these sources becomes the dominant factor controlling sediment flux. The higher sediment channel velocity predicted by the soil-distributed parameterisation (Table 6.5), reflects model compensation for the larger distance of the main sediment source, from the outlet, compared to the average distances for the lumped and land-distributed models. The total sediment flux predicted by the ‘optimum’ soil-distributed parameter set is closest to the observed value, but its efficiency is the lowest of the three (36.73%), reflecting the over-prediction and shorter duration of sediment flux peaks. Again, the lower R_0 and K_{sed} values for the soil-distributed parameterisation are due to the larger surface area over which sediment sources are spread.

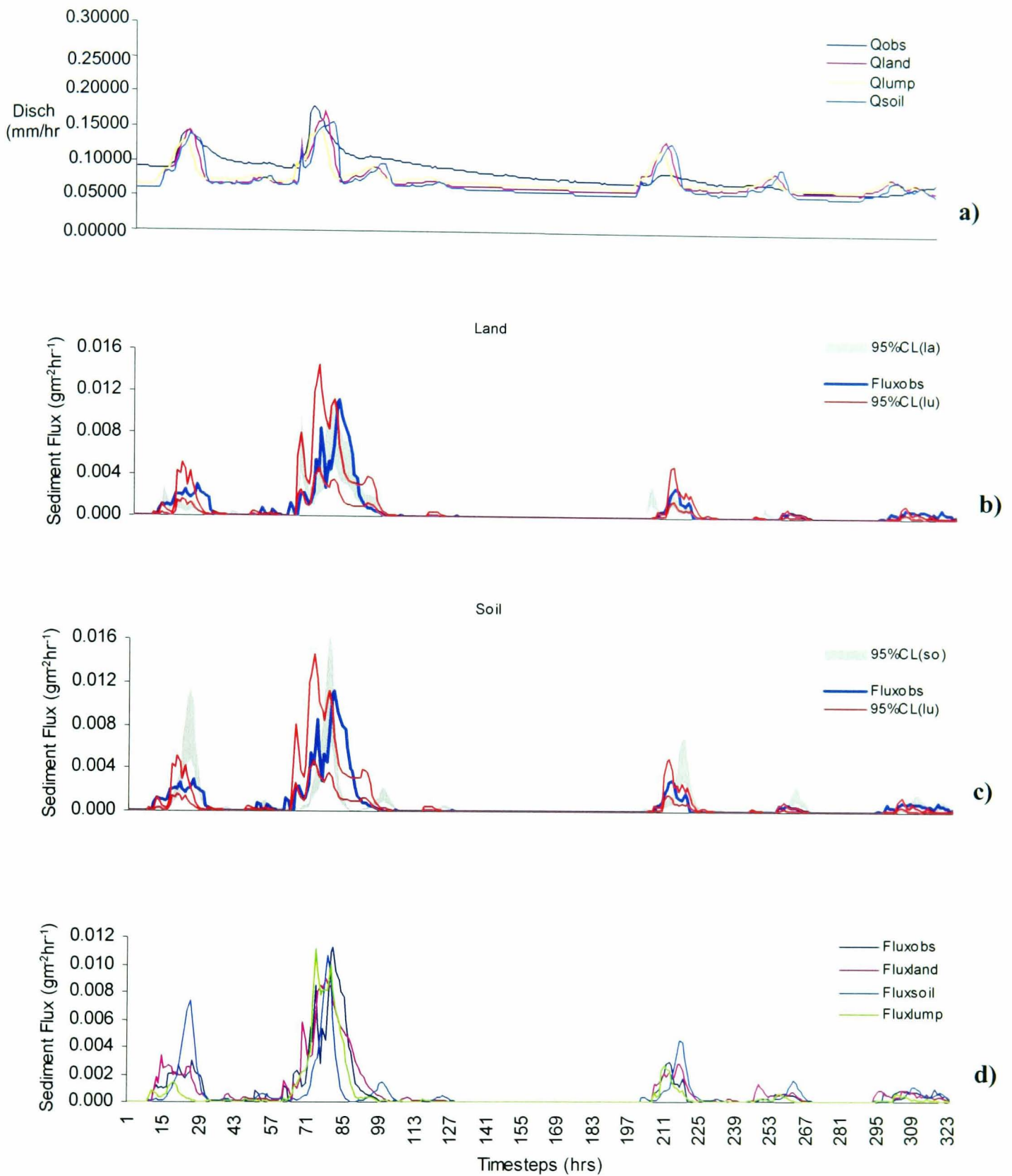


Fig. 6.20 Results of sediment *validation 1* for land- and soil-distributed parameterisation.

- e) Observed and predicted hydrographs for event using ‘optimum’ land, soil and lumped parameters set.
- f) Uncertainty bounds for land-distributed sediment flux.
- g) Uncertainty bounds for soil-distributed sediment flux.
- h) Observed sedigraph and ‘optimum’ land- and soil-distributed and lumped sedigraphs.

Parameter	Observed	Lumped	Land	Soil
R_0 (m/hr)	-	6.21×10^{-8}	5.22×10^{-8}	1.82×10^{-9}
K_{sed} (m)	-	6.93×10^{-4}	7.9×10^{-4}	6.3×10^{-6}
CHS2 (m/s)	-	0.35	0.35	0.44
Sum Flux ($gm^{-2}hr^{-1}$)	0.217205	0.168501	0.250314	0.189137
Nash Eff (%)	-	55.01	44.87	36.73

Table 6.5 ‘Optimum’ parameter sets for lumped, land and soil parameterisations for validation 1.

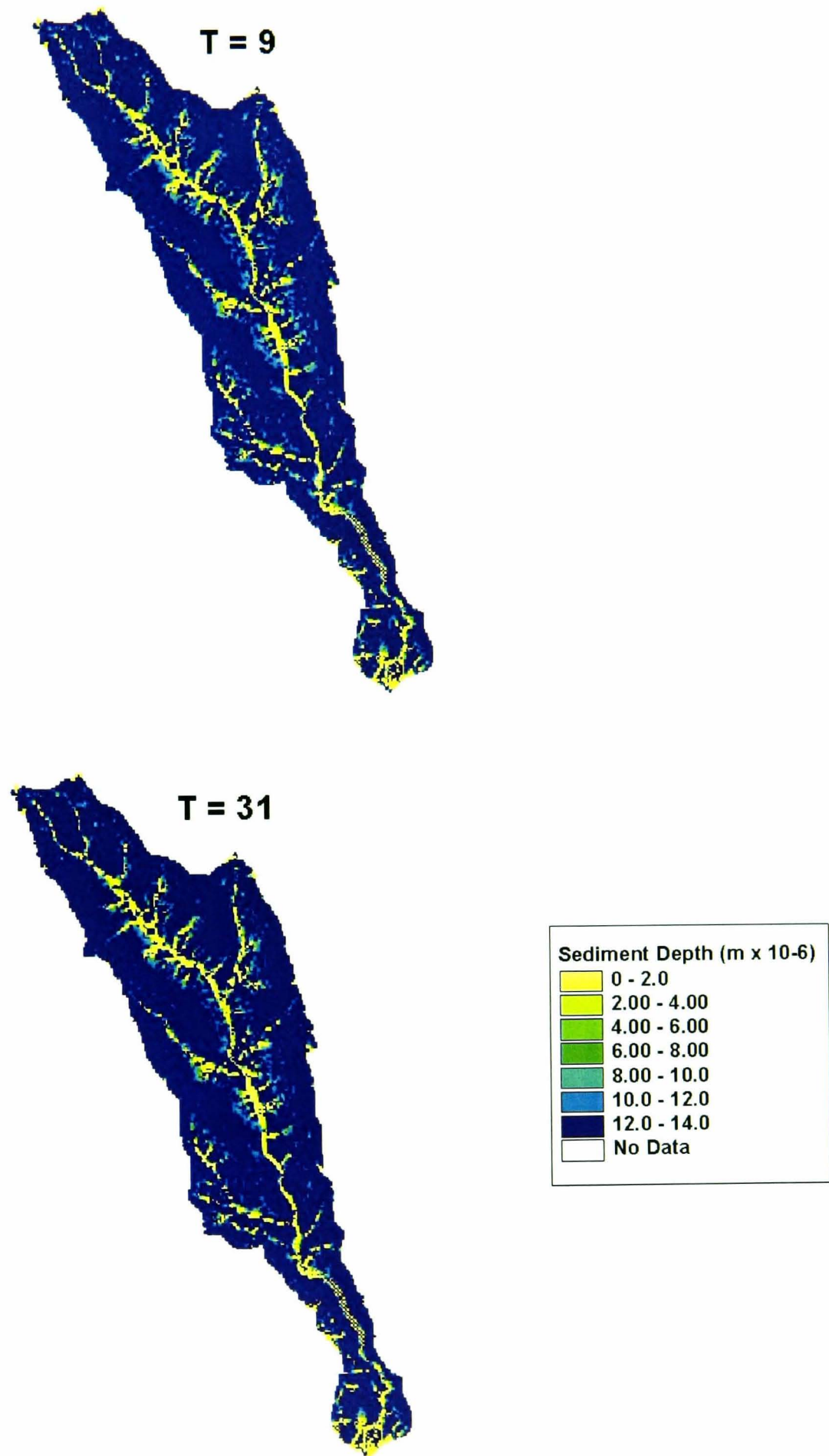


Fig. 6.21 Spatial distribution of sediment depth at T=9 and T=31 hours for validation 1 – land distributed parameterisation.

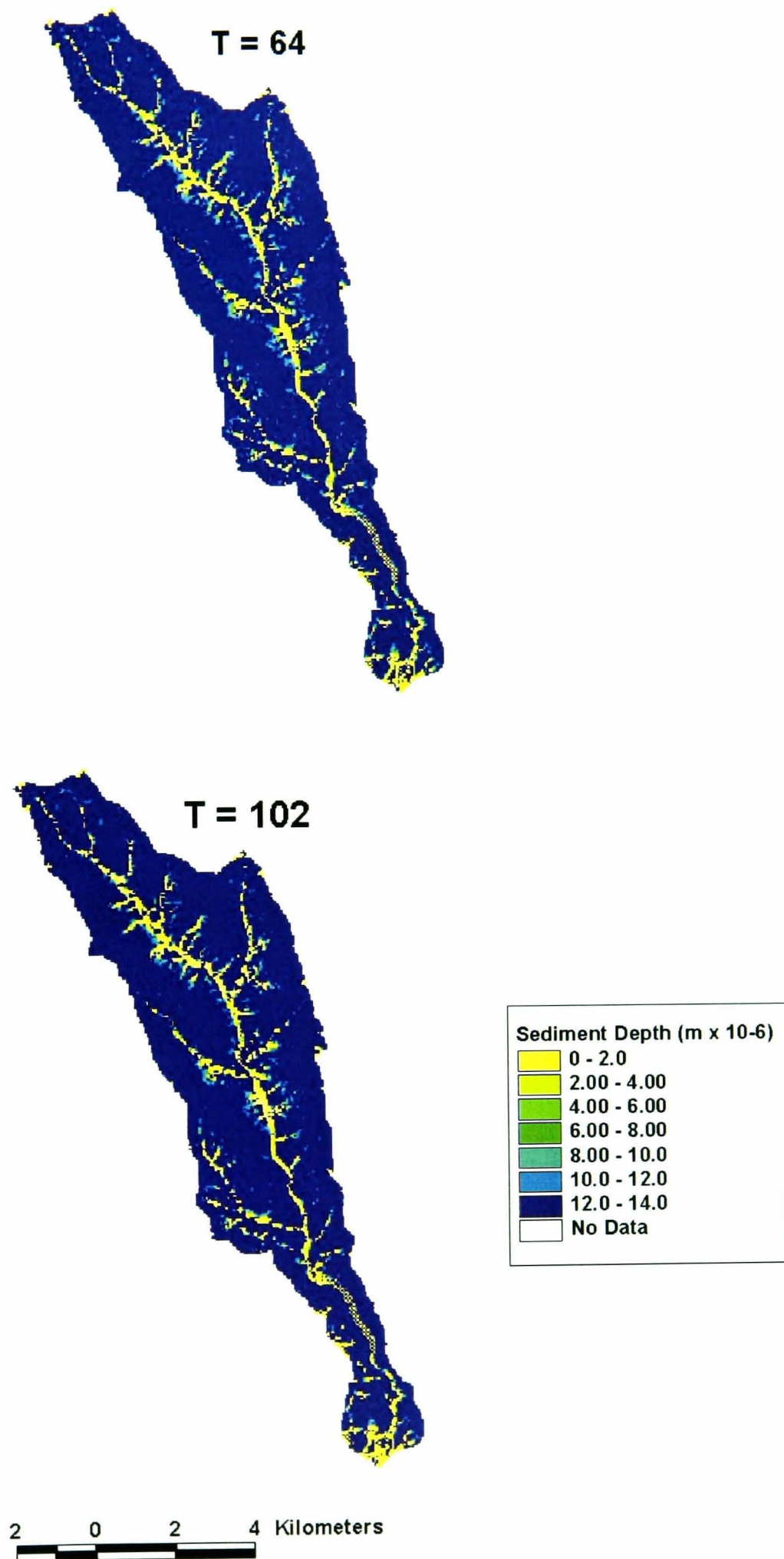


Fig. 6.21 cont'd Spatial distribution of sediment depth at T=64 and T=102 hours for validation 1 – land distributed parameterisation.

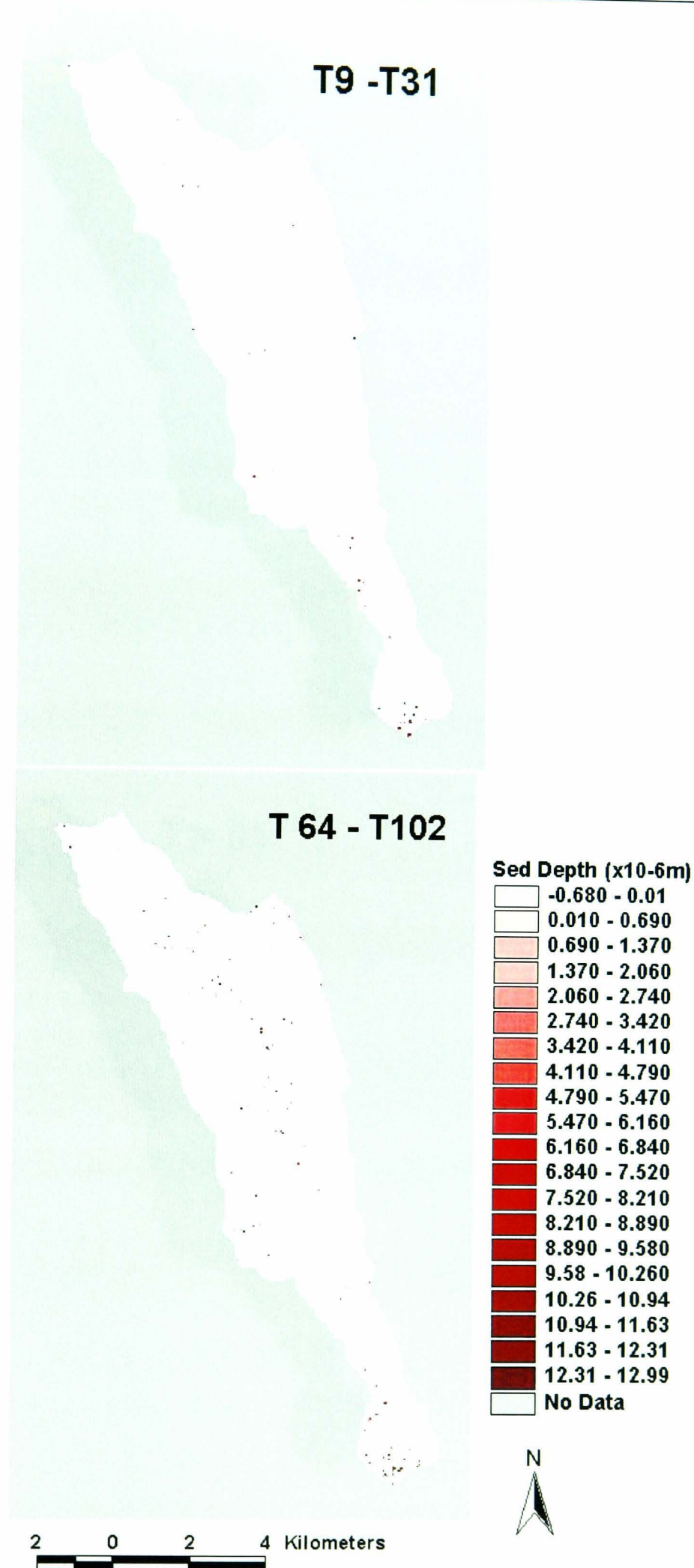


Fig. 6.22 Spatial Distribution of sediment source areas for land-distributed parameterisation - validation 1.

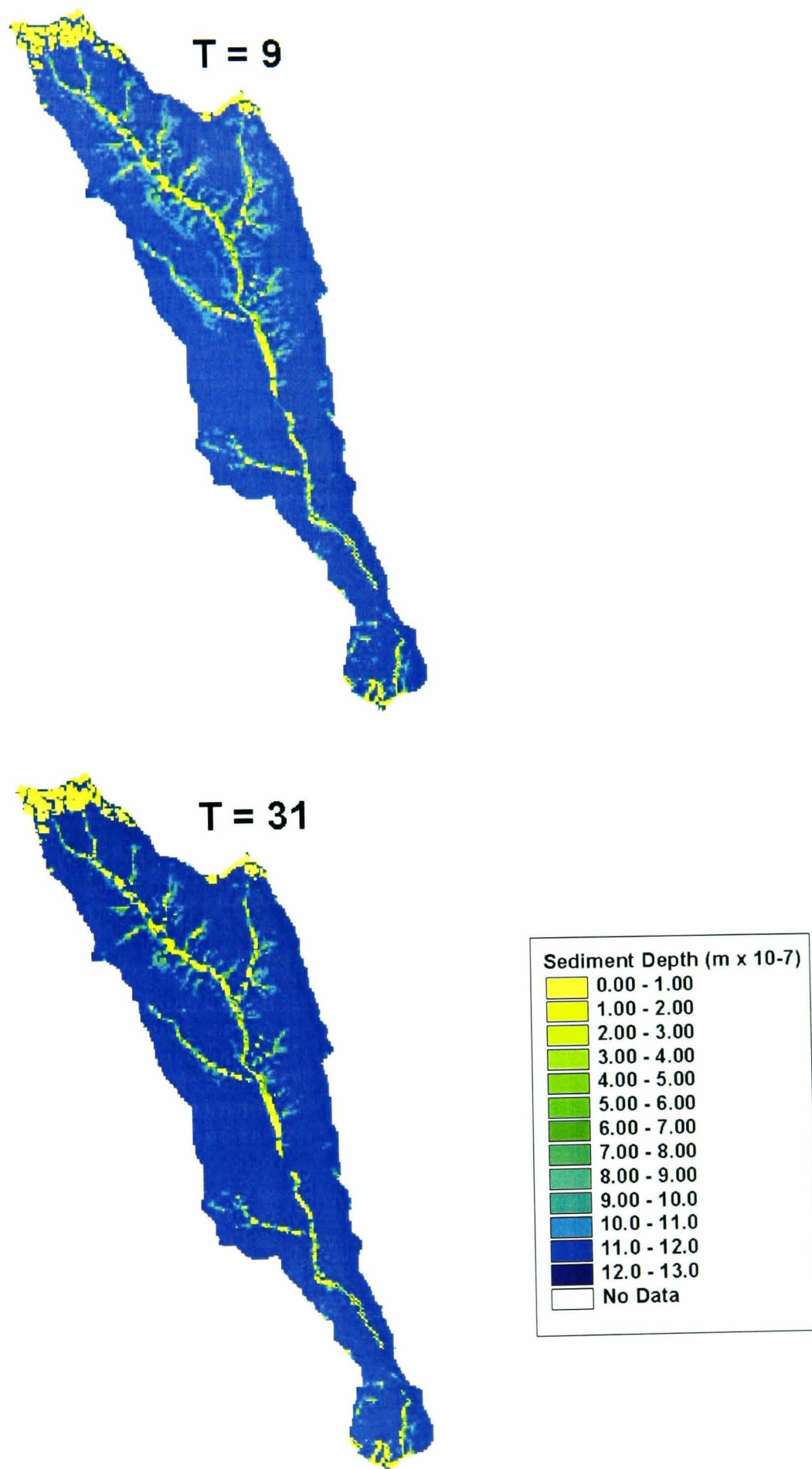


Fig. 6.23 Spatial Distribution of accumulated sediment depth for T=9 and T=31 hours for soil-distributed parameterisation – validation 1.

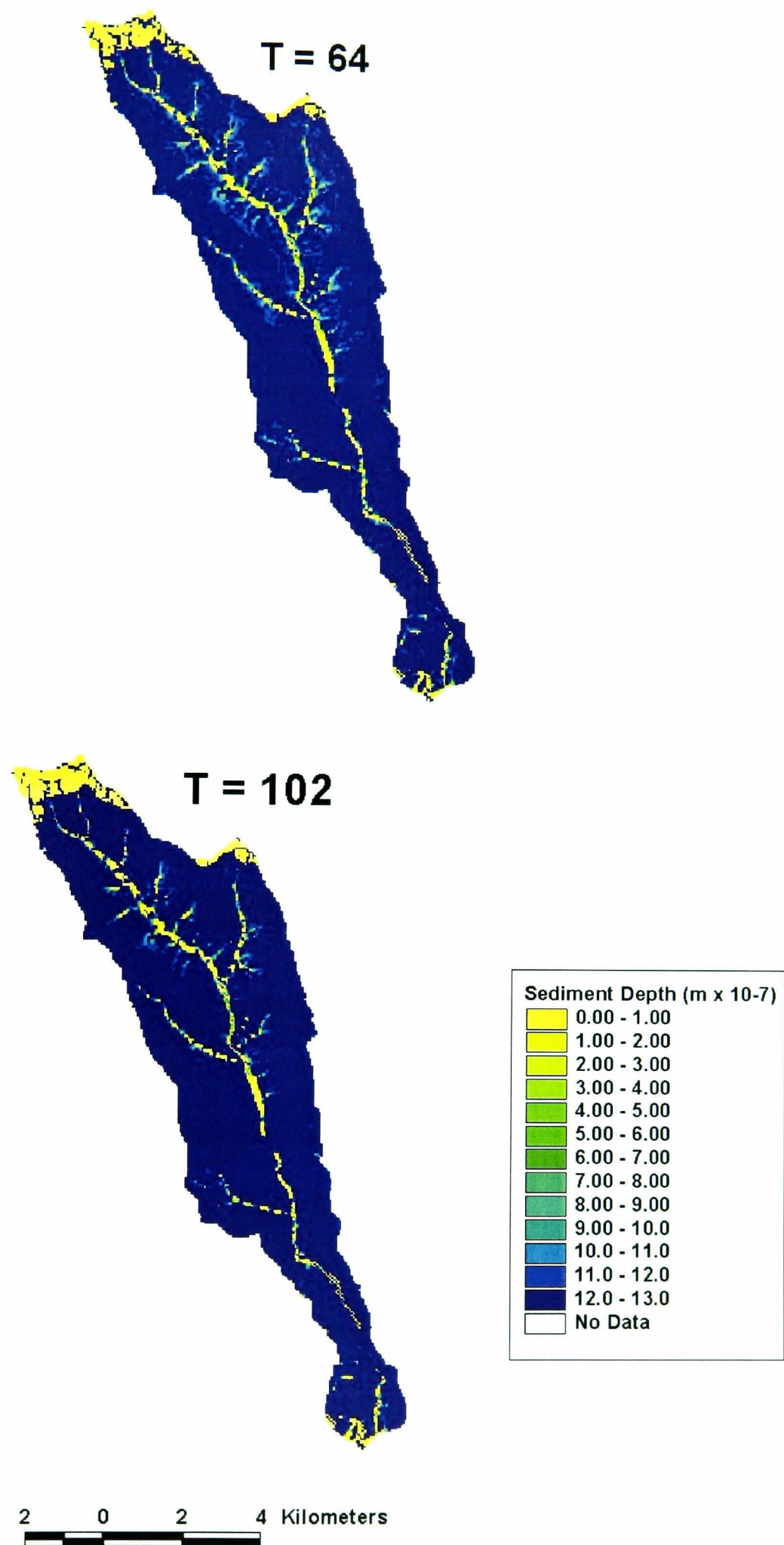


Fig. 6.23 cont'd Spatial Distribution of accumulated sediment depth for T=64 and T=102 hours for soil-distributed parameterisation – *validation 1*.

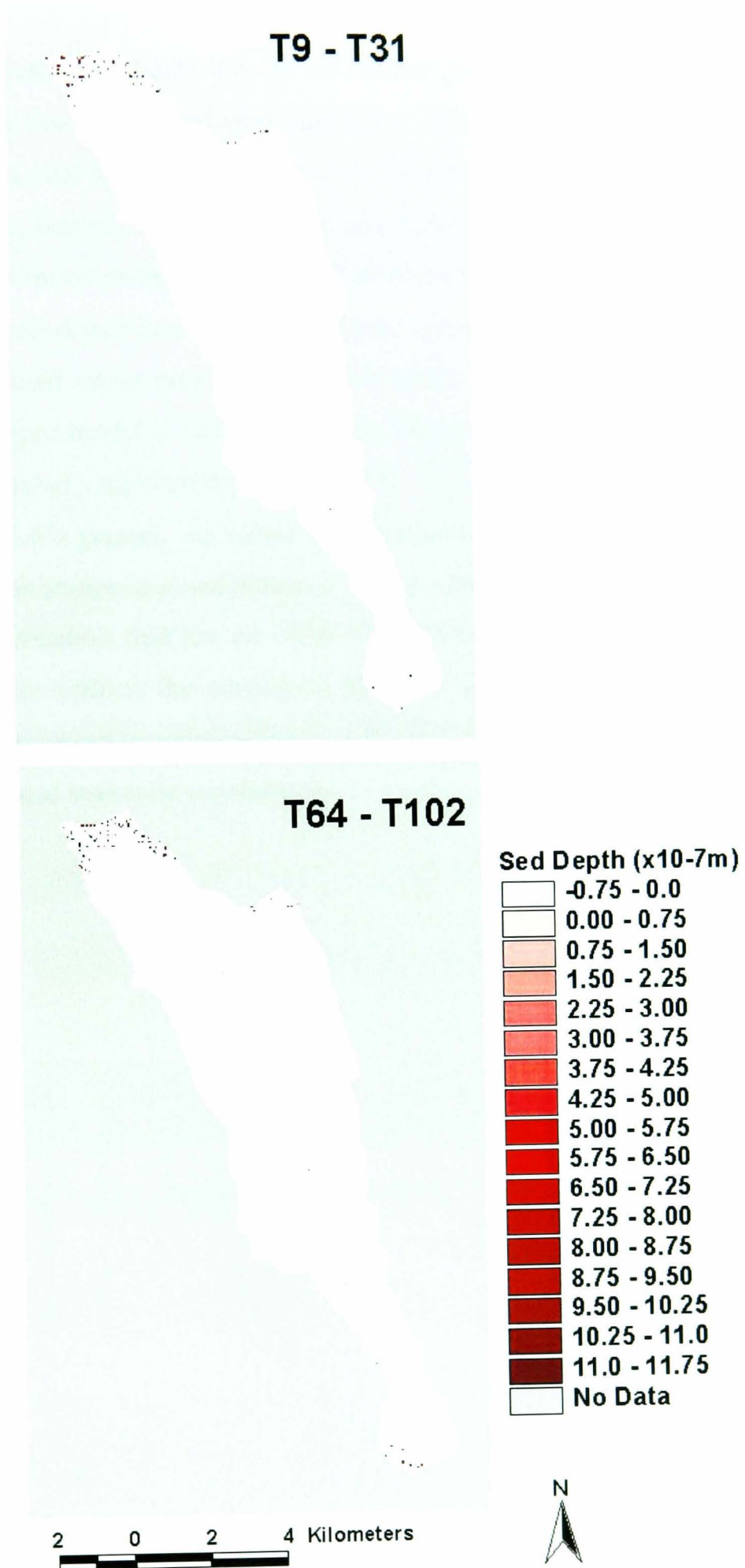


Fig. 6.24 Spatial distribution of sediment source areas for soil-distributed parameterisation – *validation*
1.

Validation 2

The uncertainty bounds of the land- and soil-distributed parameterisations (Fig. 6.25b and c) are similar in extent and predictive capability. Both enclose most of the two main observed peaks, and both are narrower than the lumped parameterisation. The soil-parameterisation, however, has spurious peaks before and after the main peaks. Despite this, the ‘optimum’ sedigraphs (Fig. 6.25d) show that the ‘best’ qualitative fit is obtained for the soil-distributed parameterisation, while the lumped over-predicts, and the land-distributed under-predicts, the main peaks. The total sediment flux predicted by the lumped model is 14% greater than the observed, while that predicted by the land-distributed parameterisation is 1% less, and the soil-distributed parameterisation is 1.6% greater. R_0 values are reasonably similar - a departure from the results of the calibration and *validation 1* which predict R_0 values for the soil-distributed parameterisation that are an order of magnitude less than the land and lumped values. This reflects the magnitude of the event and the fact that a large percentage of the catchment is contributing to sediment yield regardless of the spatial distribution of saturated hydraulic conductivity.

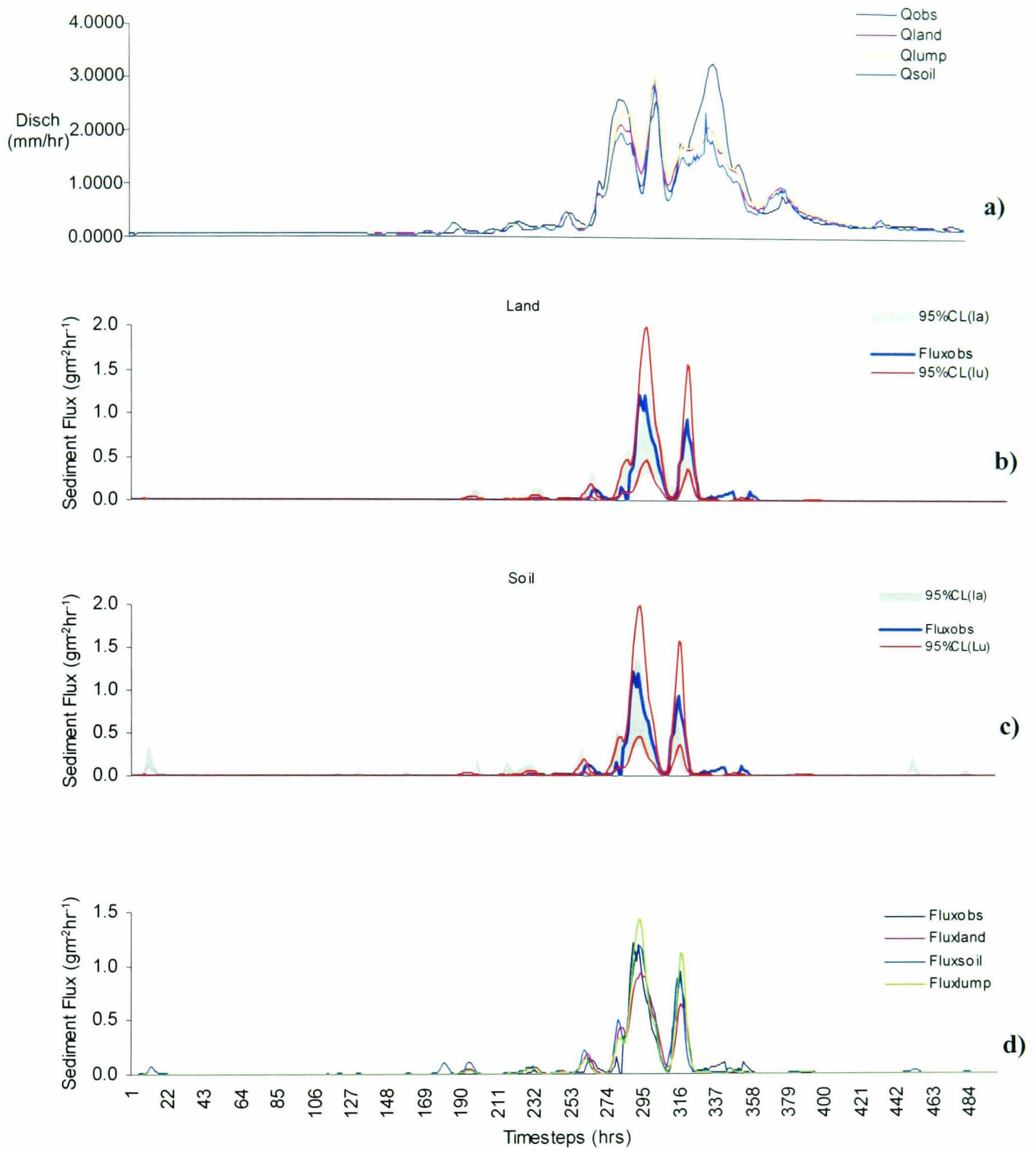


Fig. 6.25 Results of sediment model *validation 2* for land-distributed parameterisation.

- Observed and predicted hydrographs for event using 'optimum' land, soil and lumped parameters set.
- Uncertainty bounds for land-distributed sediment flux.
- Uncertainty bounds for soil-distributed sediment flux.
- Observed sedigraph and 'optimum' land- and soil-distributed, and lumped sedigraphs.

Parameter	Observed	Lumped	Land	Soil
R_0 (m/hr)	-	4.09×10^{-8}	3.39×10^{-8}	4.63×10^{-8}
K_{sed} (m)	-	8.39×10^{-4}	7.8×10^{-4}	6.3×10^{-6}
CHS2 (m/s)	-	0.923	0.78925	1.2
Sum Flux ($gm^{-2}hr^{-1}$)	25.165	28.63	24.898	25.206
Nash Eff (%)	-	93.62	82.425	87.3

Table 6.6 'Optimum' parameter sets for validation 2.

Spatially distributed predictions

The land-distributed spatial predictions of sediment depth (Fig. 6.26) show rapid expansion of sediment source areas along the channel network. Fig. 6.27 illustrates the difference between the lumped and land-distributed predictions. Red areas indicate grid cells for which the lumped sediment depth is greater than the land-distributed, and the blue areas, where the land-distributed is greater than the lumped. At $T=253$, just before the start of the large double peaked event, cells in the riparian area have larger sediment depths than for the land. These are areas along the channel, where saturation (and hence sediment removal) is predicted for the land-distributed model but not for the lumped. As the event progresses, the riparian area remains the area where the lumped model consistently predicts higher sediment depths (and lower removal rates). In areas within heather and bracken further upslope, the land-distributed sediment depths are higher (blue areas), indicating the increasing control that variable land-use has as the storm progresses, and saturated areas expand onto the hillslopes.

The soil-distributed sediment depth distribution (Fig.6.28) shows a similar expansion of sediment source areas as the storm progresses, but mainly in the northern half of the catchment. Fig. 6.29 illustrates this 'north-south divide' more clearly, with higher sediment depth predicted by the lumped model in the north of the catchment, and larger depths predicted by the soil-distributed parameterisation in the drier south.

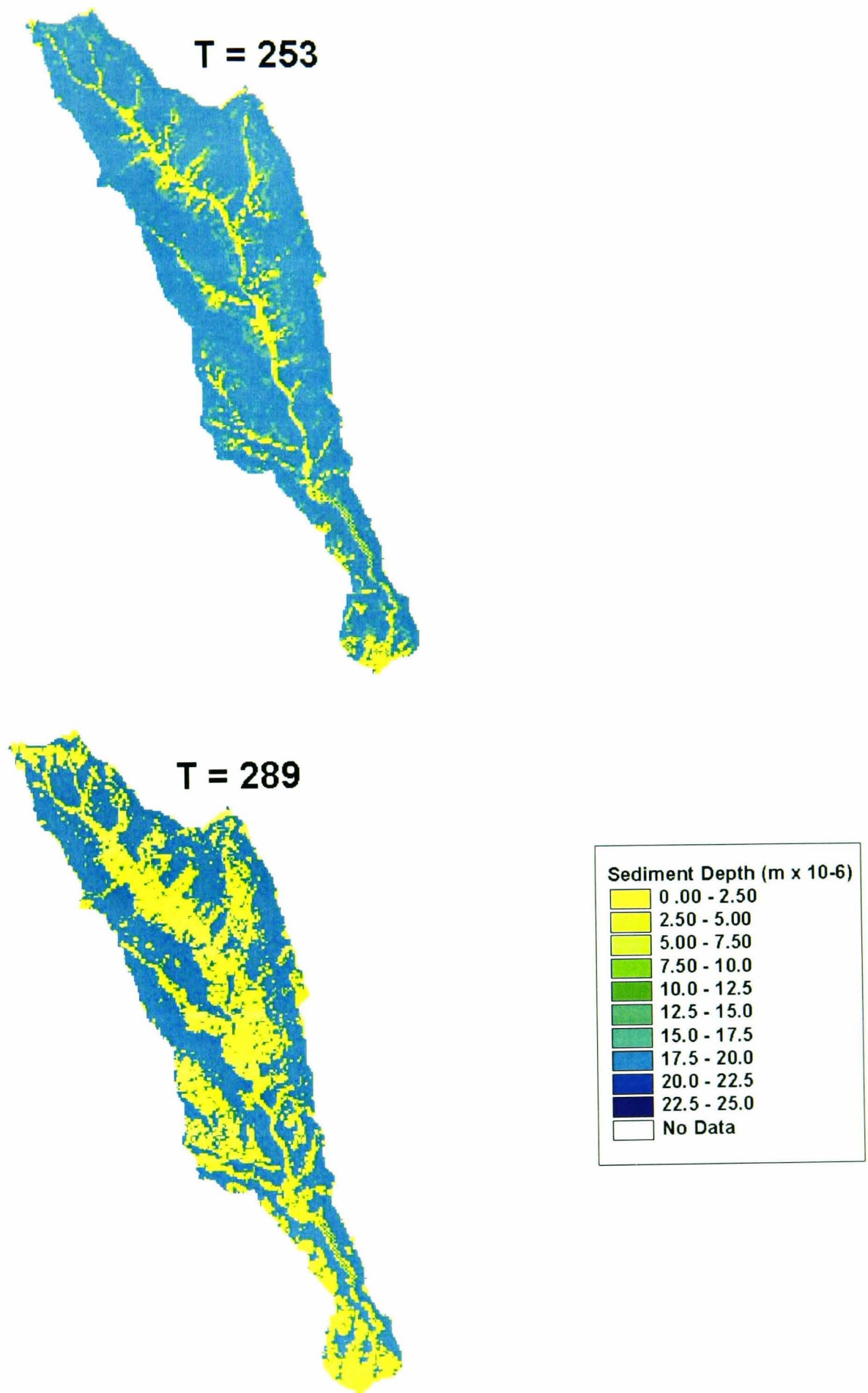


Fig. 6.26 Spatial distribution of sediment depth at T=253 and 289 hours for validation 2 – land-distributed parameterisation

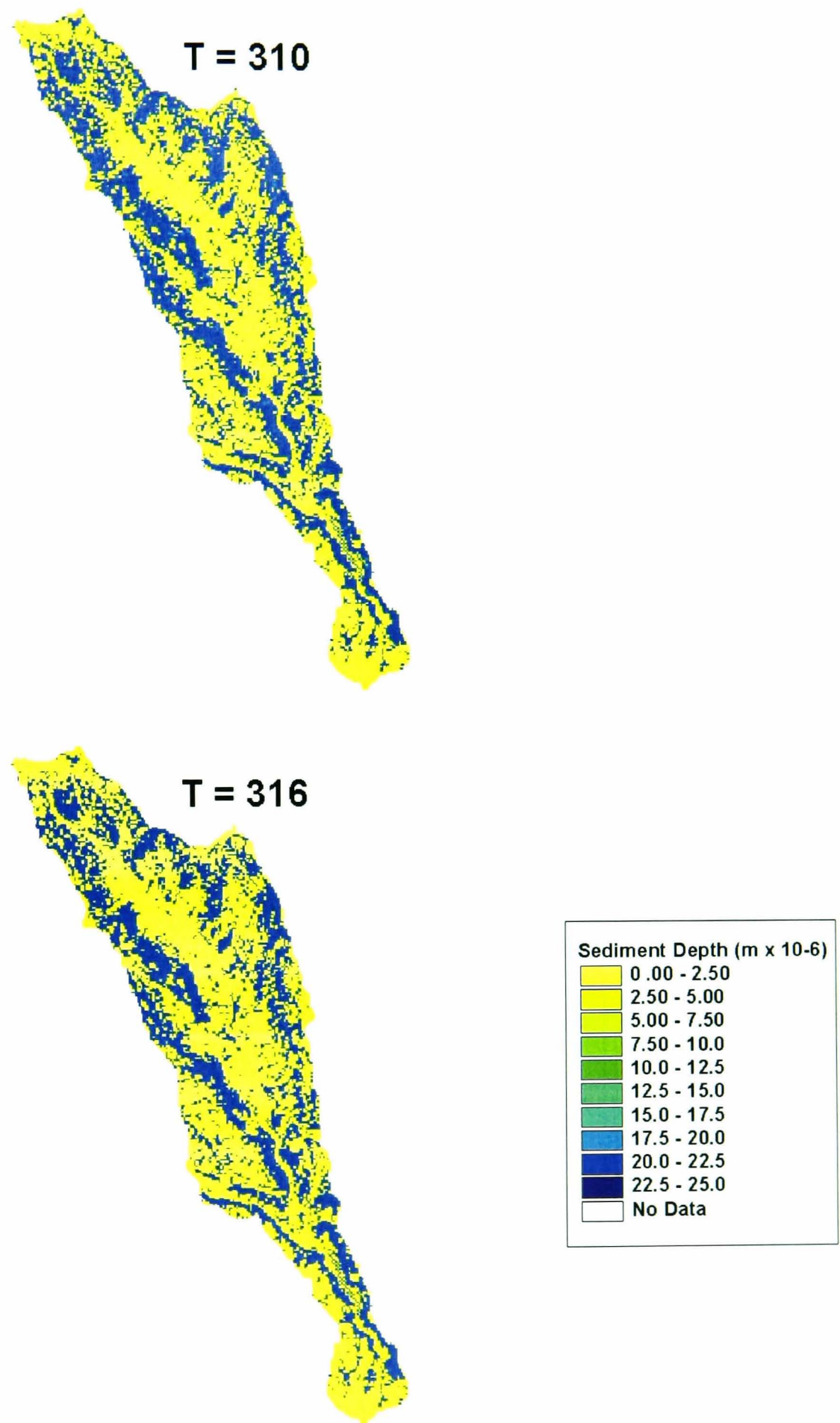


Fig. 6.26 cont'd Spatial distribution of sediment depth at T=310 and 316 hours for validation 2 – land-distributed parameterisation

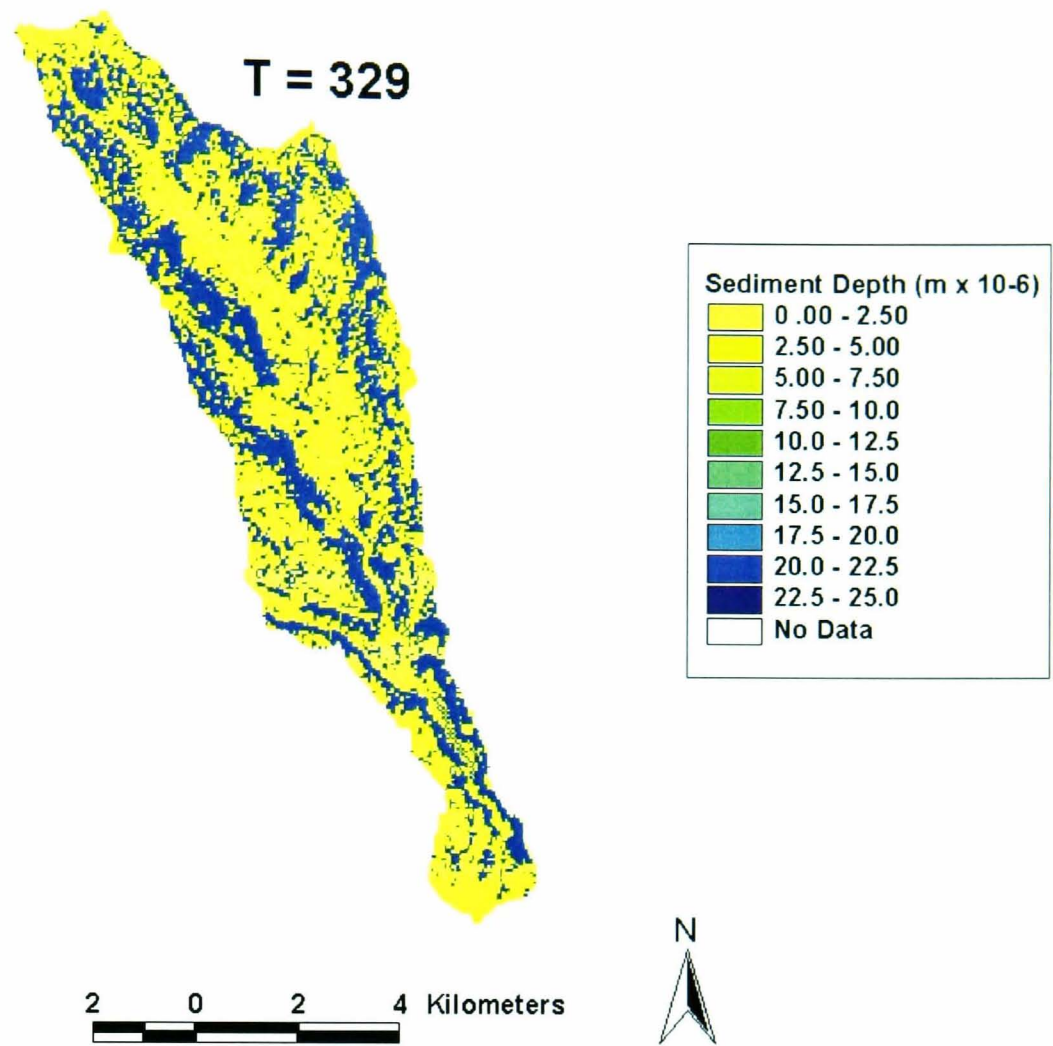


Fig. 6.26 cont'd Spatial distribution of sediment depth at T=329 hours for validation 2 – land-distributed parameterisation

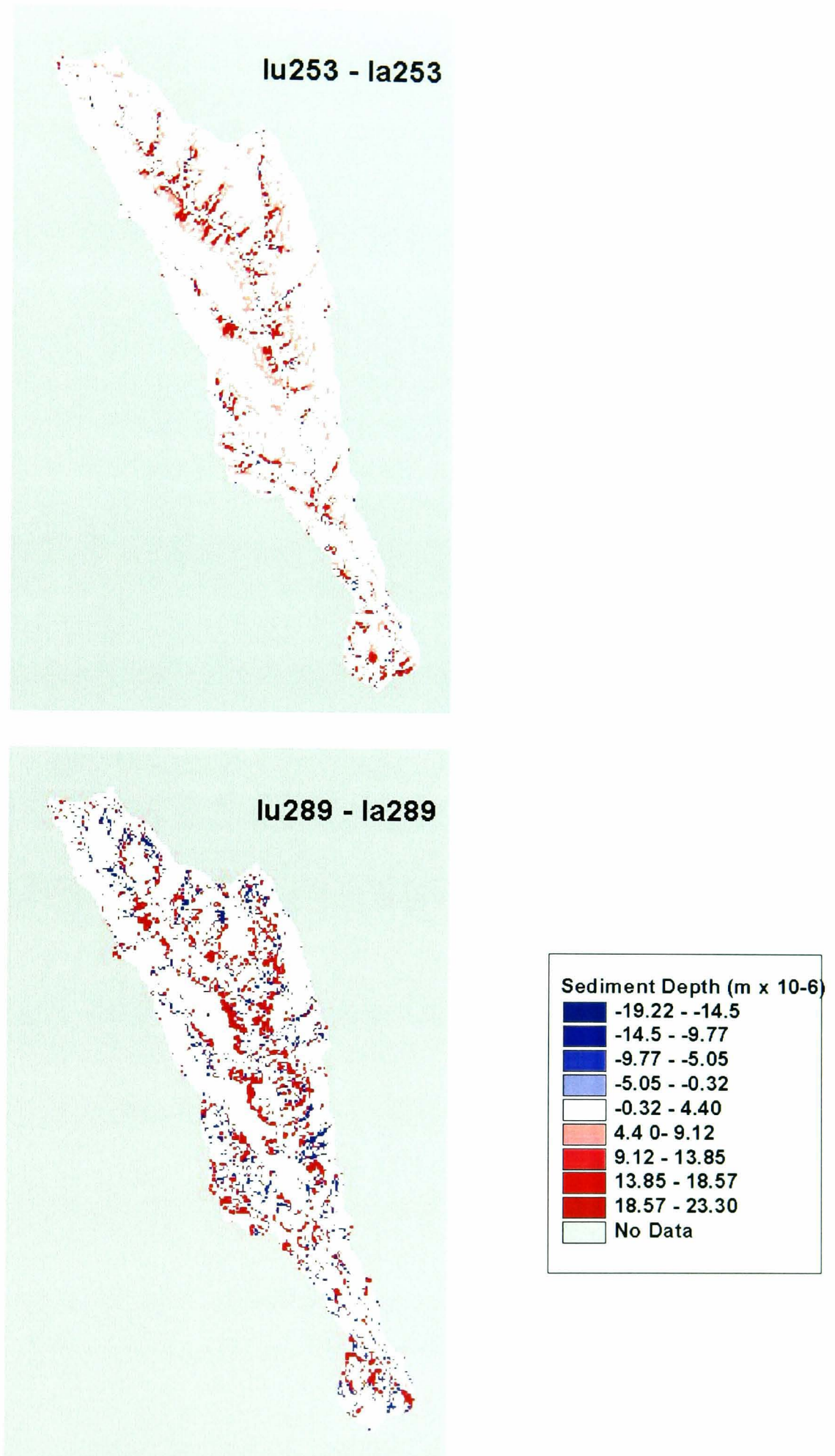


Fig. 6.27 Difference in sediment source areas between land-distributed and lumped parameterisations at T=253 and 289. Validation 2

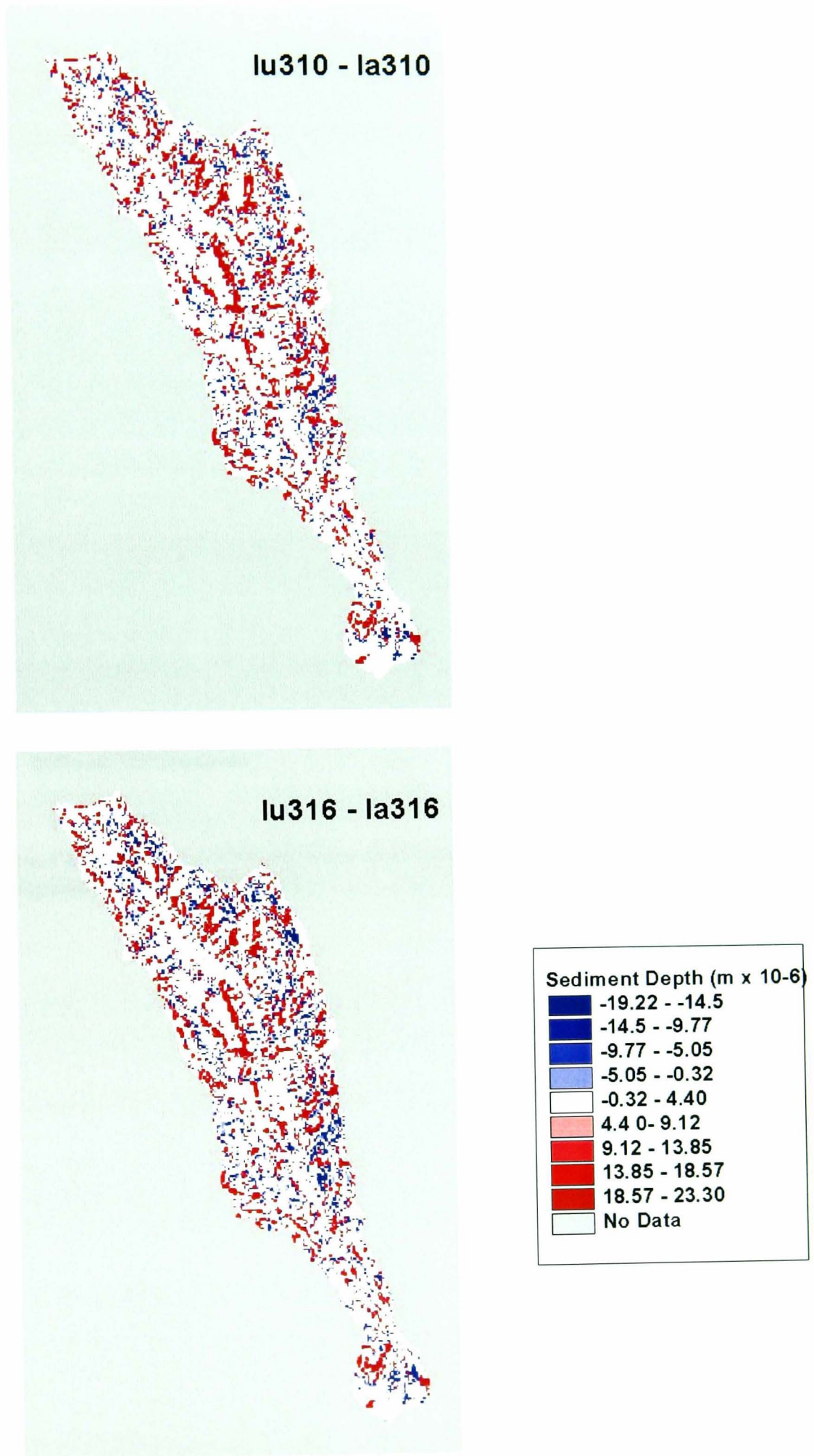


Fig. 6.27 cont'd Difference in sediment source areas between land-distributed and lumped parameterisations at T=310 and 316. Validation 2

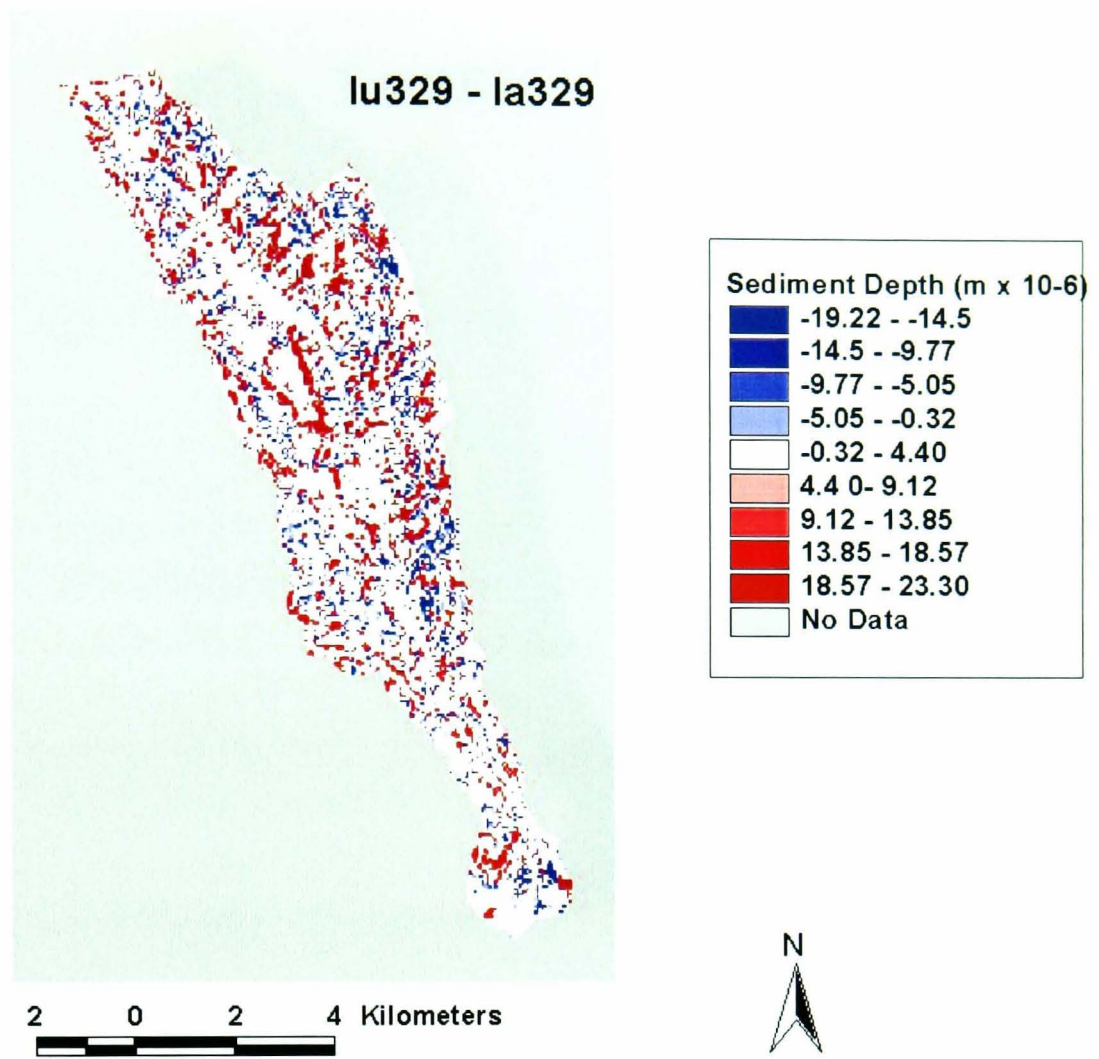


Fig. 6.27 cont'd Difference in sediment source areas between land-distributed and lumped parameterisations at T=329. Validation 2

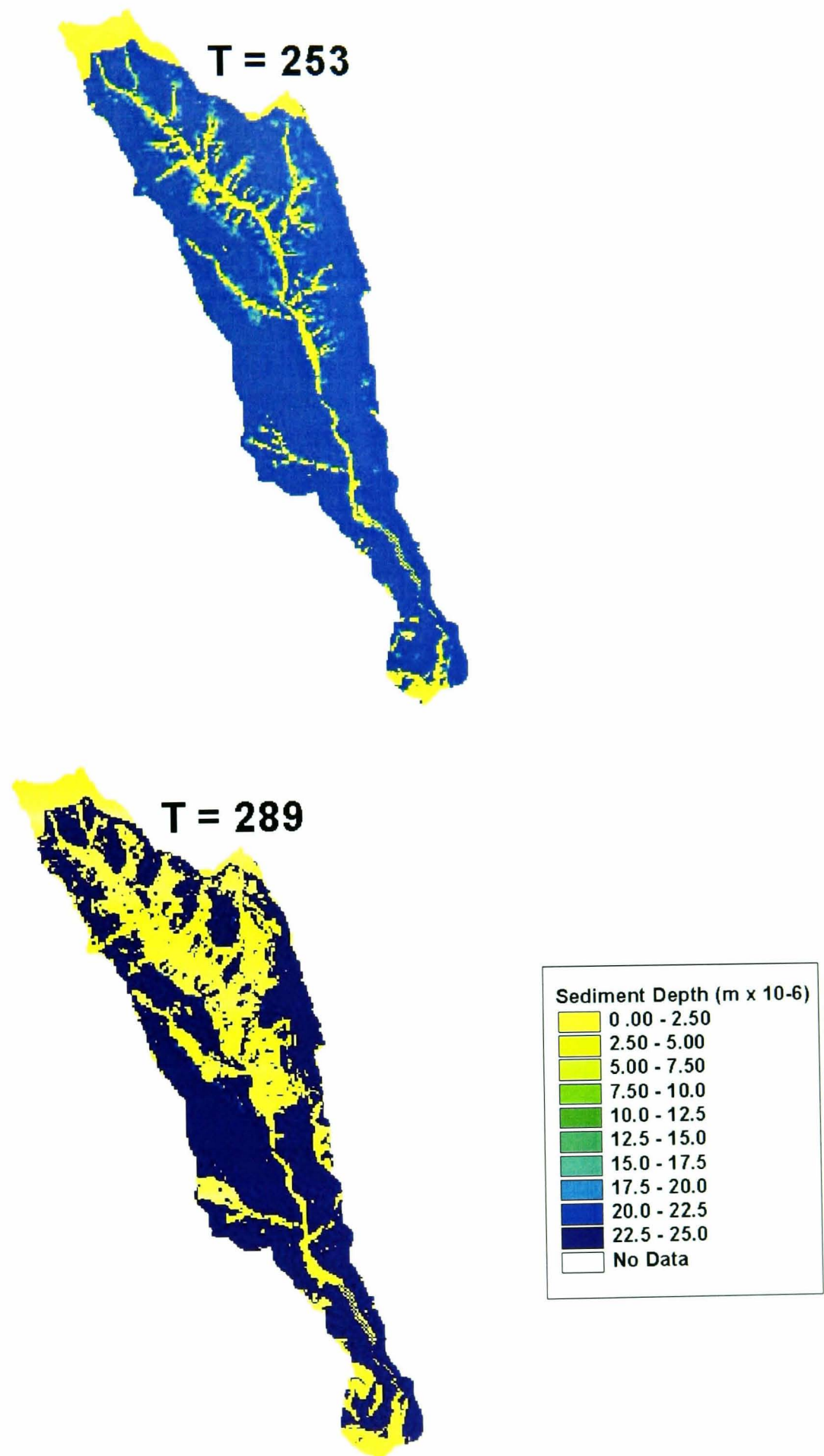


Fig. 6.28 Spatial distribution of sediment depth at T=253 and 289 for validation 2 – soil-distributed parameterisation

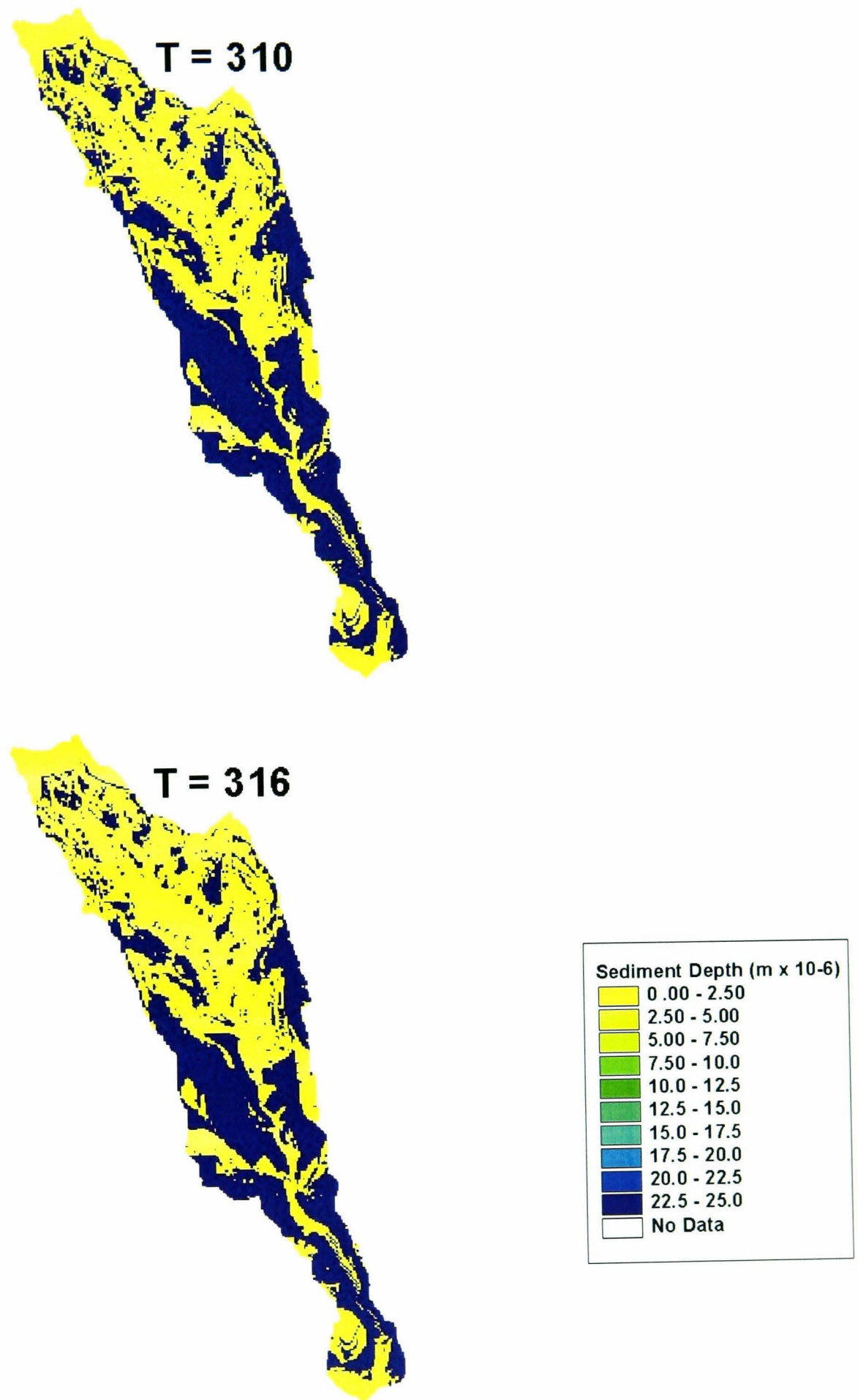


Fig. 6.28 cont'd Spatial distribution of sediment depth at T= 310 and 316 for validation 2 – soil-distributed parameterisation

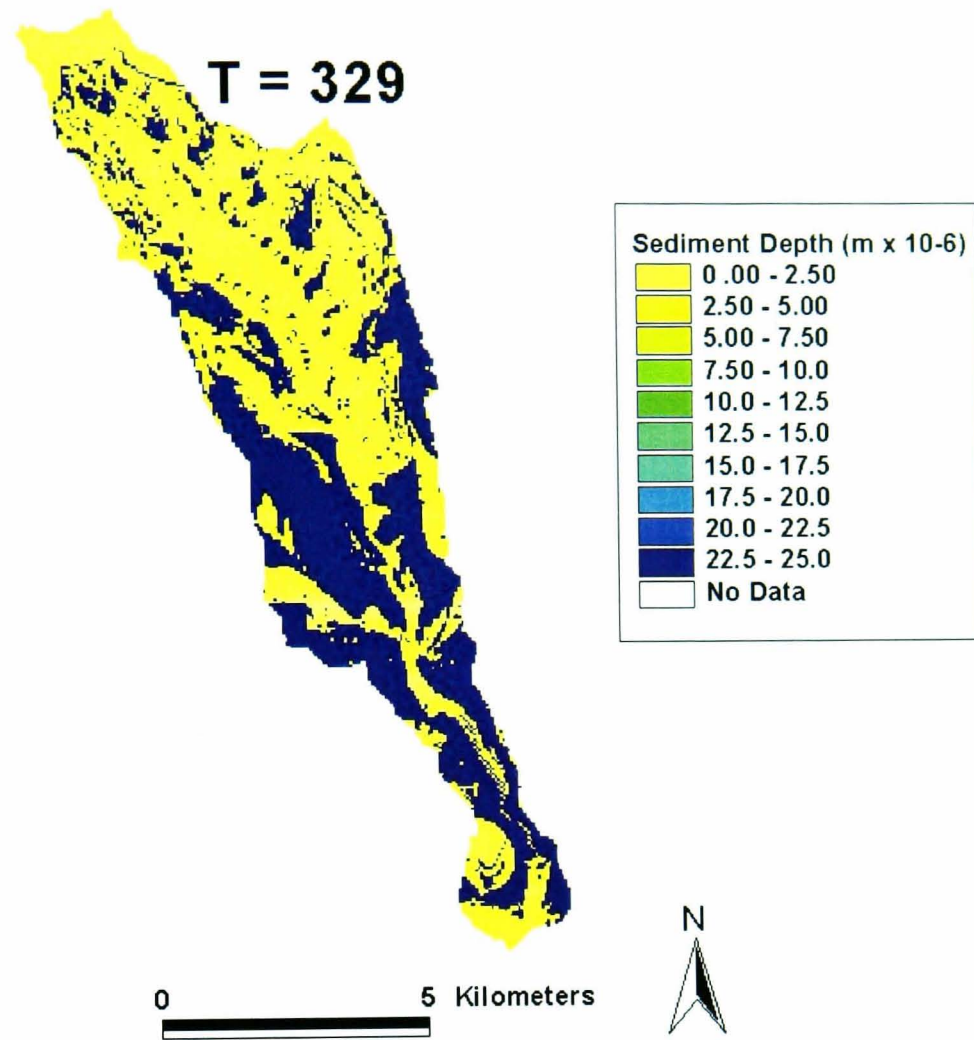


Fig. 6.28 cont'd Spatial distribution of sediment depth at T=329 for validation 2 – soil-distributed parameterisation

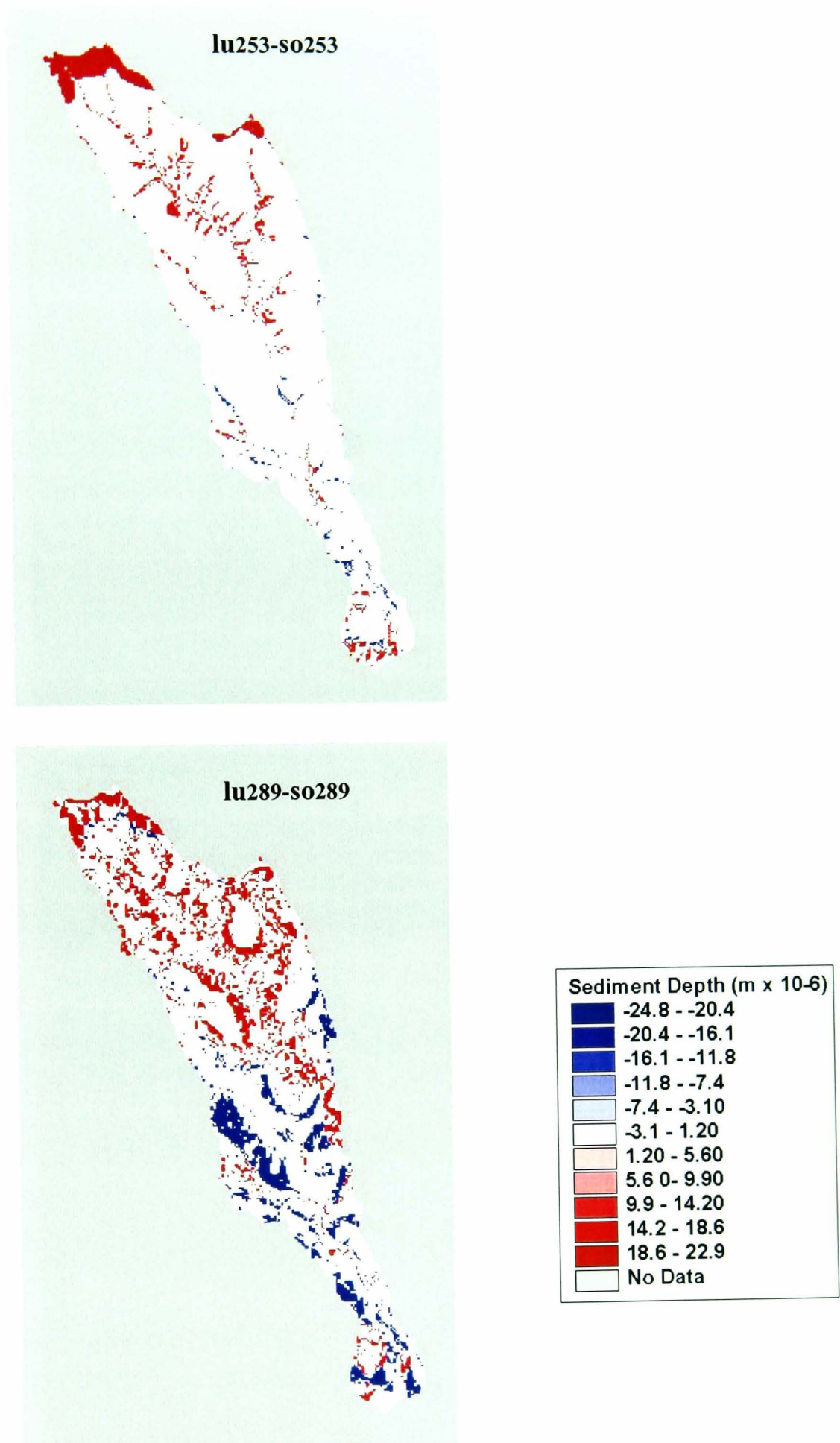


Fig. 6.29 Difference in sediment sources areas between soil-distributed and lumped parameterisations for T=253 and 289. Validation 2.

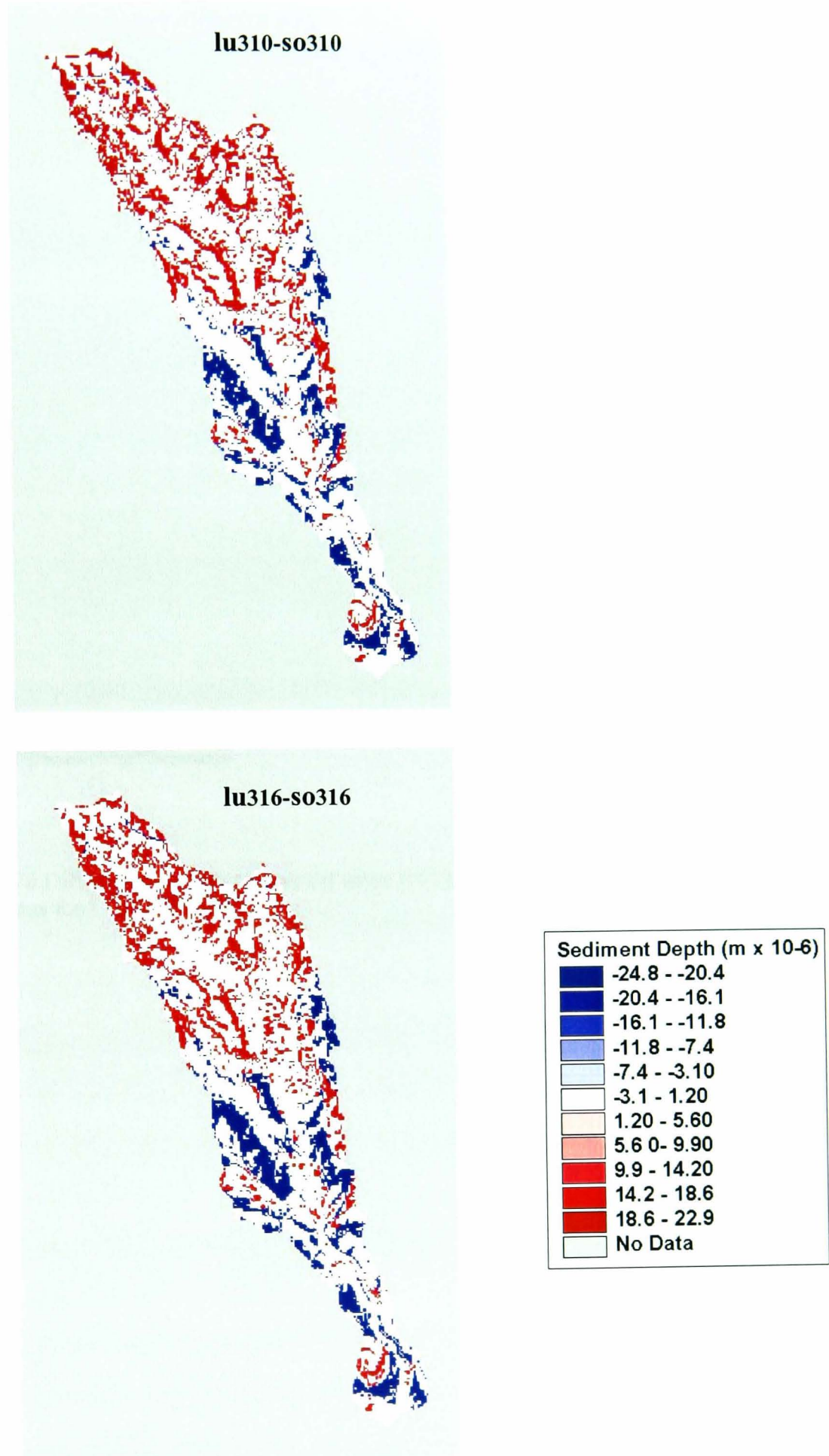


Fig. 6.29 cont'd Difference in sediment sources areas between soil-distributed and lumped parameterisations for T=310 and 316. Validation 2.

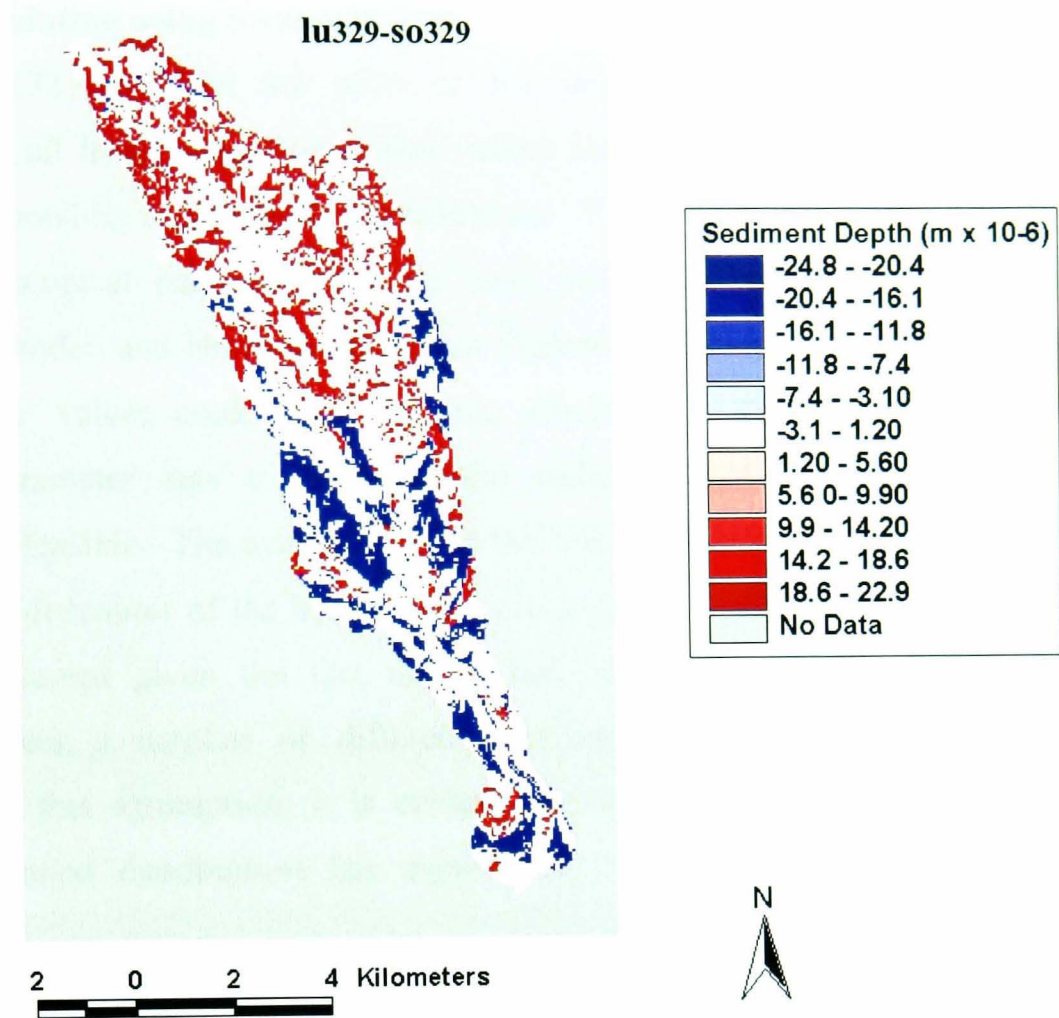


Fig. 6.29 cont'd Difference in sediment sources areas between soil-distributed and lumped parameterisations for T=329. Validation 2.

6.7 Bayesian Updating using Sediment Data

Figures 6.30, 6.32 and 6.34 are plots of the prior and posterior cumulative distributions for all hydrological parameter values for events 1, 2, and 3, updated using the corresponding sediment yield predictions. It should be noted that only the ‘optimum’ hydrological parameter sets for each event was used to calibrate the sediment yield model, and hence the Bayesian Updated likelihoods would be biased to the ‘optimum’ values used. However, the alternative – using all behavioural hydrological parameter sets to calibrate the sediment yield model, was not computationally feasible. The assumption that the ‘optimum’ hydrological parameter set was the best descriptor of the hydrological processes that drive sediment yield is fundamentally flawed given the fact that it has been demonstrated that model equifinality makes a number of different ‘optimum’ parameter sets possible. However, given this assumption, it is evident that the resulting restriction in the parameter likelihood distributions has significantly restricted hydrological model uncertainty.

Event 1

For the land-distributed parameterisation of event 1 (Fig. 6.30), the prior cumulative distribution shows that the most rapid increase in cumulative likelihood is for m greater than 0.05m. The ‘optimised’ value was approximately 0.06m. However, the corresponding posterior distribution, shows that the most rapid increase in cumulative likelihood is between 0.04 and 0.05m. *CHV2*, *ETF* and *SRMAX* have prior cumulative likelihood distributions that predict approximately equal likelihoods for all parameter values, but their posterior cumulative likelihood distributions indicate sharp increases at approximately 0.4ms^{-1} , 0.3 and 0.0025m respectively. More significantly, however, is the apparent deviation from the calibrated $K_{\theta bar}$ value. The prior $K_{\theta bar}$ cumulative likelihood distribution appears to have equal likelihoods for all parameter values between 25 and 150mhr^{-1} , and the optimised value is 109.59mhr^{-1} . However, the posterior distributions indicate a sharp rise in cumulative likelihood at approximately 30mhr^{-1} . This has resulted in updated uncertainty bounds that have higher upper and lower limits (Figs. 6.31a and b), and which do not enclose the observed hydrograph throughout the event. This is particularly evident in Fig. 6.31b - the updated uncertainty bounds predicted by the multiplicative combined likelihood measure.

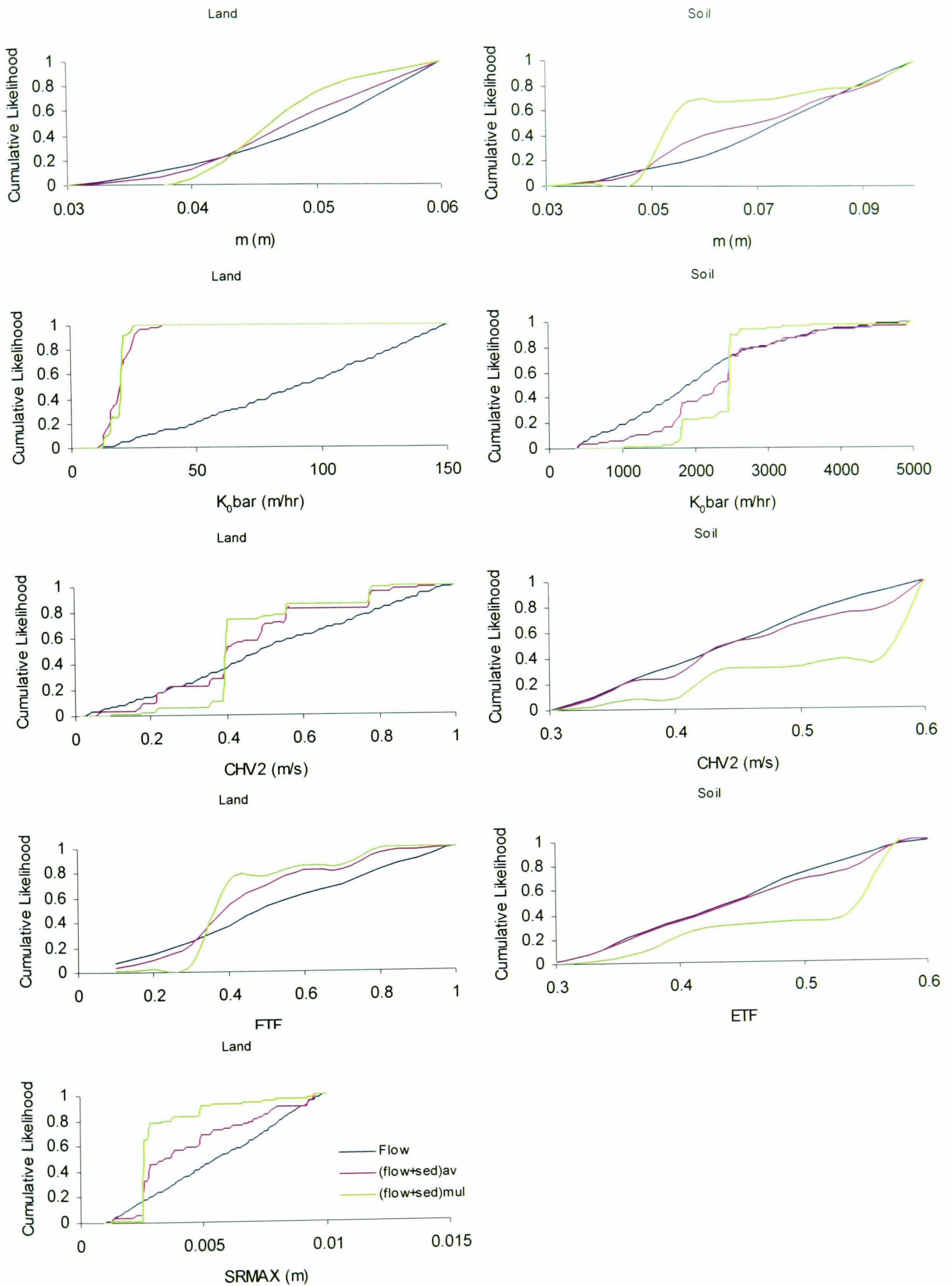


Fig. 6.30 Event 1. Prior and posterior cumulative likelihood distributions for 5 hydrological model parameters conditioned on flow only, and on flow and sediment data using two different likelihood measures.

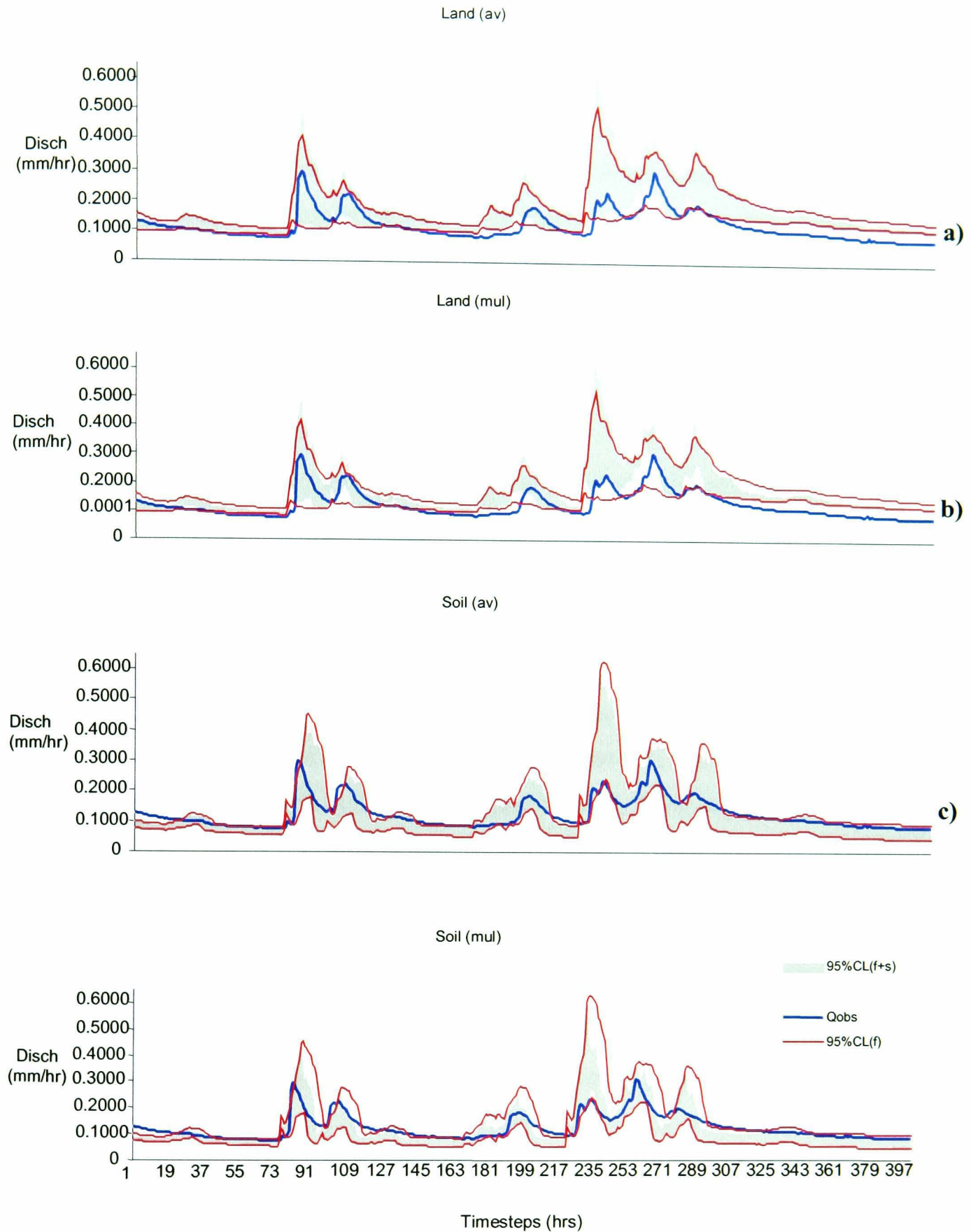


Fig. 6.31 Updated Uncertainty bounds for event 1 for land- and soil-distributed parameterisation using the average and multiplicative likelihoods of equation 5.5.1 and 5.5.2 respectively.

This shift to higher predicted discharge, is due to the lower $K_{\theta bar}$ value predicted by the combined measures and the lower m value which, together, predict shallower soil depths, and hence lower infiltration rates, and higher direct surface runoff. The lower $K_{\theta bar}$ value is due to the fact that most of the sediment sources are located on the valley floor where the lowest hydraulic conductivity land uses are located. Thus, lower catchment average hydraulic conductivities, which can effectively predict the runoff processes of the valley floor, would give higher sediment yield model efficiencies and hence, higher combined likelihoods, particularly for the multiplicative measure.

For the soil-distributed parameterisation, the prior distribution of m shows the highest rate of increase in cumulative likelihood for m greater than 0.06m. The calibrated ‘optimum’ is 0.0994m. The posterior distributions show a sharper increase in m at approximately 0.048m. Posterior distributions for ETF and $CHV2$ have consistently lower likelihoods than their respective prior distributions, suggesting that the combined likelihoods are not effective in reducing the uncertainty in these parameters over the range of parameter values considered. However, the posterior distributions show greater sensitivity than the prior at approximately 0.42 and 0.58ms⁻¹ for $CHV2$, and at 0.55 for ETF . Prior distributions for $K_{\theta bar}$ show a rapid increase in cumulative likelihood between approximately 400 and 2500mhr⁻¹, and the calibrated ‘optimum’ is 1051.33mhr⁻¹, while the posterior distributions show sharp increases at 2500mhr⁻¹. Thus the cumulative likelihoods for the combined measures predict higher infiltration rates, perhaps indicative of the high hydraulic conductivities in the south of the catchment, which restrict the saturated areas, and hence, sediment source areas there. The effect of these changes in ‘optimum’ parameter values on the model uncertainty bounds is shown in Fig. 6.31c and d. Lower limits remain relatively unchanged, while upper limits are considerably lower for the combined measure. Most of the observed hydrograph is enclosed.

In general, the lumped model updated bounds (Fig. 5.38) showed a larger decrease in uncertainty than either the land-distributed or soil-distributed models. However, the soil-distributed model updated uncertainty enclosed most of the observed hydrograph.

Event 2

For the land-distributed parameterisation, the prior distribution for m and K_{0bar} (Fig. 6.32) are all to the left of the posterior distributions, which suggests that the cumulative likelihoods are consistently greater, when flow alone is used to derive uncertainty. This is due to the generally low model efficiencies obtained for the sediment yield model, particularly for this event, which result in lower average and multiplicative combined likelihoods. The linear prior distribution of m is altered to a distribution that shows zero likelihood for all parameters less than 0.04m, and the most rapid increase in likelihood at approximately 0.05m. Similarly, the prior distribution for K_{0bar} indicates that all parameter values are equally likely, while the posterior indicates relative insensitivity between 0 and 100mhr⁻¹, with greatest sensitivity at approximately 145mhr⁻¹ – greater than the ‘optimum’ value. *CHV2* and *ETF* have insensitive prior distributions, which are altered to yield sensitivity at 0.75ms⁻¹ and 0.6 respectively.

The land-distributed uncertainty bounds (Fig. 6.33a and b) are restricted, mainly due to the lower discharges being predicted for the upper bounds. However, the recession flows of the first two peaks are under-predicted. The extent of the restriction obtained for the land-distributed parameterisation is less than that obtained for the lumped model (Fig. 5.39).

For the soil-distributed parameterisation, m , shows relative insensitivity between 0.03 and 0.06m. Posterior distributions show greatest sensitivity between 0.02 and 0.03m, which is lower than the ‘optimum’ value of 0.05995m. Prior cumulative likelihood distribution for K_{0bar} is also linear between approximately 600 and 2000mhr⁻¹, but it altered to give posterior distributions, which increase in cumulative likelihood most rapidly at approximately 750mhr⁻¹ – close to the ‘optimised’ value of 728mhr⁻¹.

The effect on uncertainty bounds is significant (Figs. 6.33 c and d). At peak flow, the upper, and particularly lower, uncertainty bounds have shifted to greater discharge values, while during recession flow, the upper bounds are shifted to lower values. The severe restriction of the width of uncertainty bounds has resulted in vastly increased predictive failure throughout the event. The higher discharge values at

peak flows are due to the lower values to which m has been restricted by the sediment model predictions. Since most of the sediment source areas are located in the northern extreme of the catchment, faster times to saturation and larger extent of saturated areas, would result in higher sediment removal rates, which would favour the sediment yield predictions, resulting in higher sediment yield model efficiencies for lower m values. The result is, faster times to saturation throughout the catchment - the effect of which would be more significant in the northern half of the catchment, where saturated hydraulic conductivities are lower. Hence, during peak flow, northern soils become saturated faster, and the excess rainfall becomes direct runoff, resulting in higher discharges predicted, lower recharge to ground water and hence lower base flow which is manifested in the subsequent recession flows.

The extent to which the uncertainty bounds for this event are constrained is much greater for the soil-distributed parameterisation than for the lumped parameterisation (see Fig. 5.39), but this is accompanied by increased predictive failure.

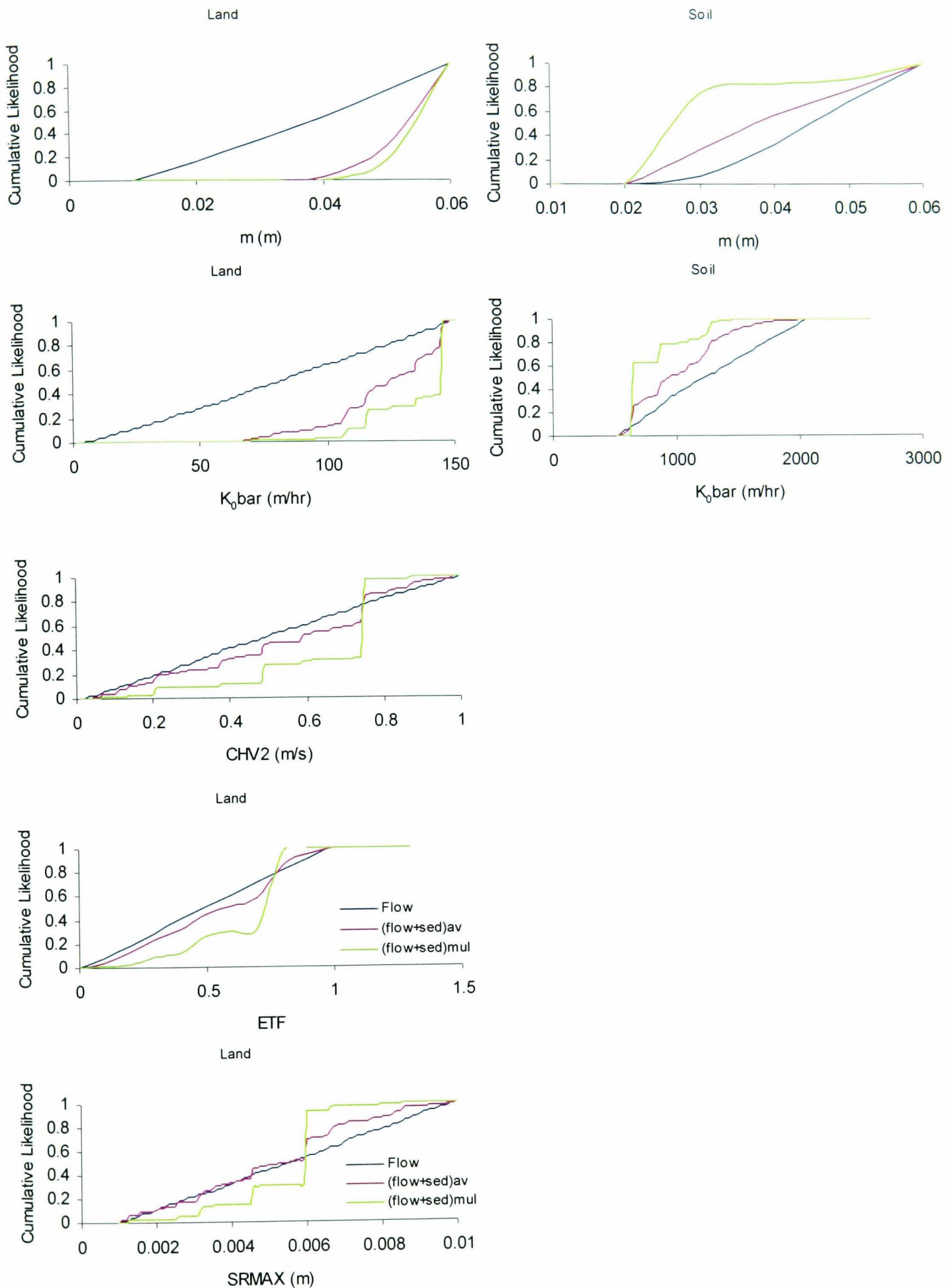


Fig. 6.32 Event 2. Prior and posterior cumulative likelihood distributions for 5 hydrological model parameters, conditioned on flow only, and on flow and sediment data using two different likelihood measures.

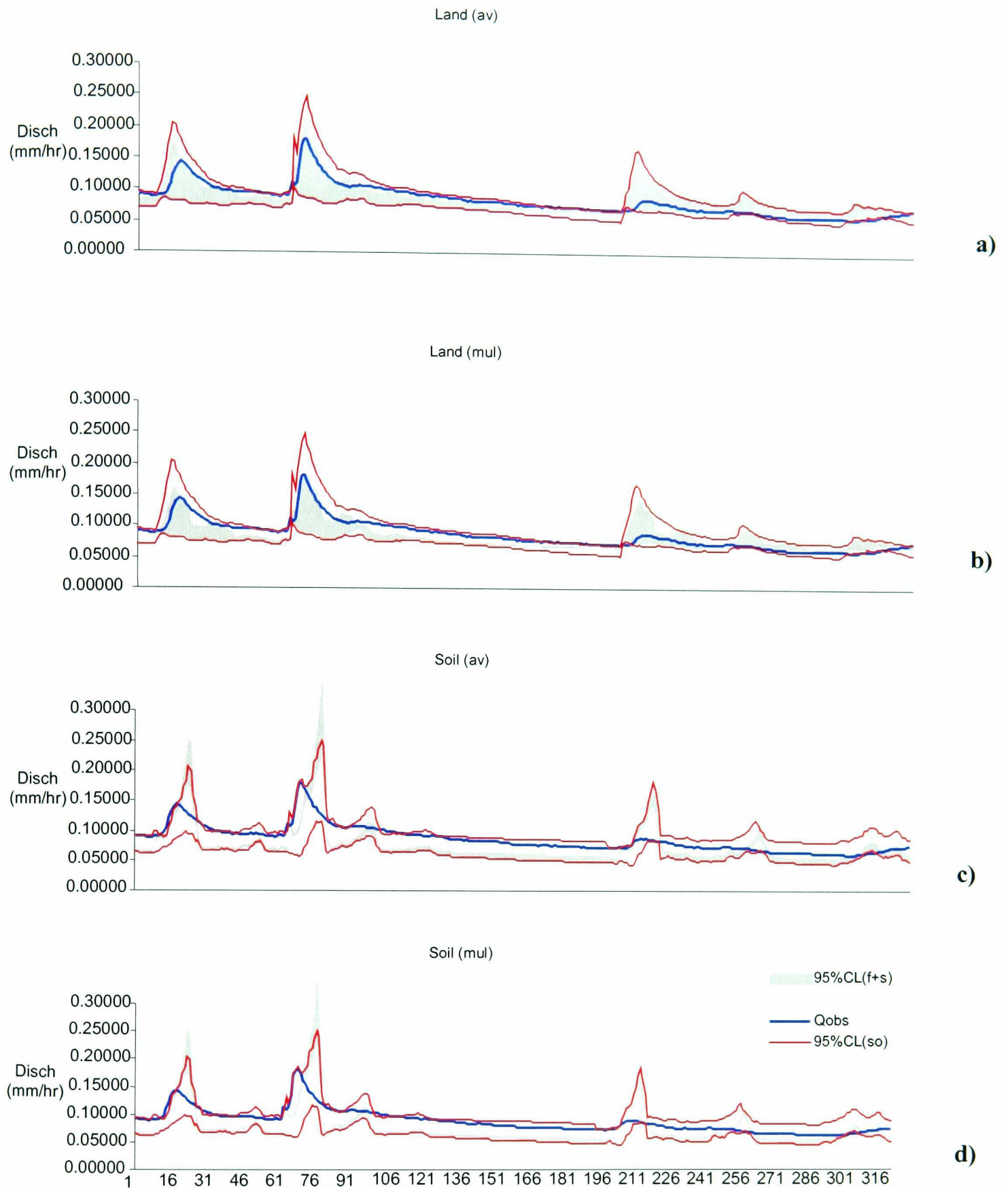


Fig. 6.33 Updated Uncertainty bounds for event 2 for land- and soil-distributed parameterisation using the average and multiplicative likelihoods of equation 5.5.1 and 5.5.2 respectively.

Event 3

Again, all parameters have prior cumulative likelihood distributions which are approximately linear, indicating equal likelihood for all values, but posteriors that show increased rates of increasing cumulative likelihood at certain values of the parameters. For the land-distributed model (Fig. 6.34), parameters are modified to yield greater sensitivity at 0.03m, 60mhr⁻¹, 0.002m, 0.6ms⁻¹ and 0.55 for *m*, *K_obar*, *SRMAX*, *CHV2* and *ETF* respectively. The ‘optimised’ values were 0.03017m, 32.606 mhr⁻¹, 0.00647m, 0.89746 ms⁻¹ and 1.2134 respectively. The resulting uncertainty bounds (fig. 6.35a and b) are constrained with little increase in predictive failure.

For the soil-distributed parameterisation, parameters are modified to 0.0025m, 440mhr⁻¹, and 0.0043m for *m*, *K_obar* and *SRMAX* respectively. The ‘optimised’ values are 0.03182m, 362.4mhr⁻¹, 0.00495m respectively. The resulting uncertainty bounds (Fig, 6.35 c and d) show even further restriction, with no increase in predictive failure. Both models show far greater restriction in uncertainty bounds than for the lumped model (see Fig. 5.40).

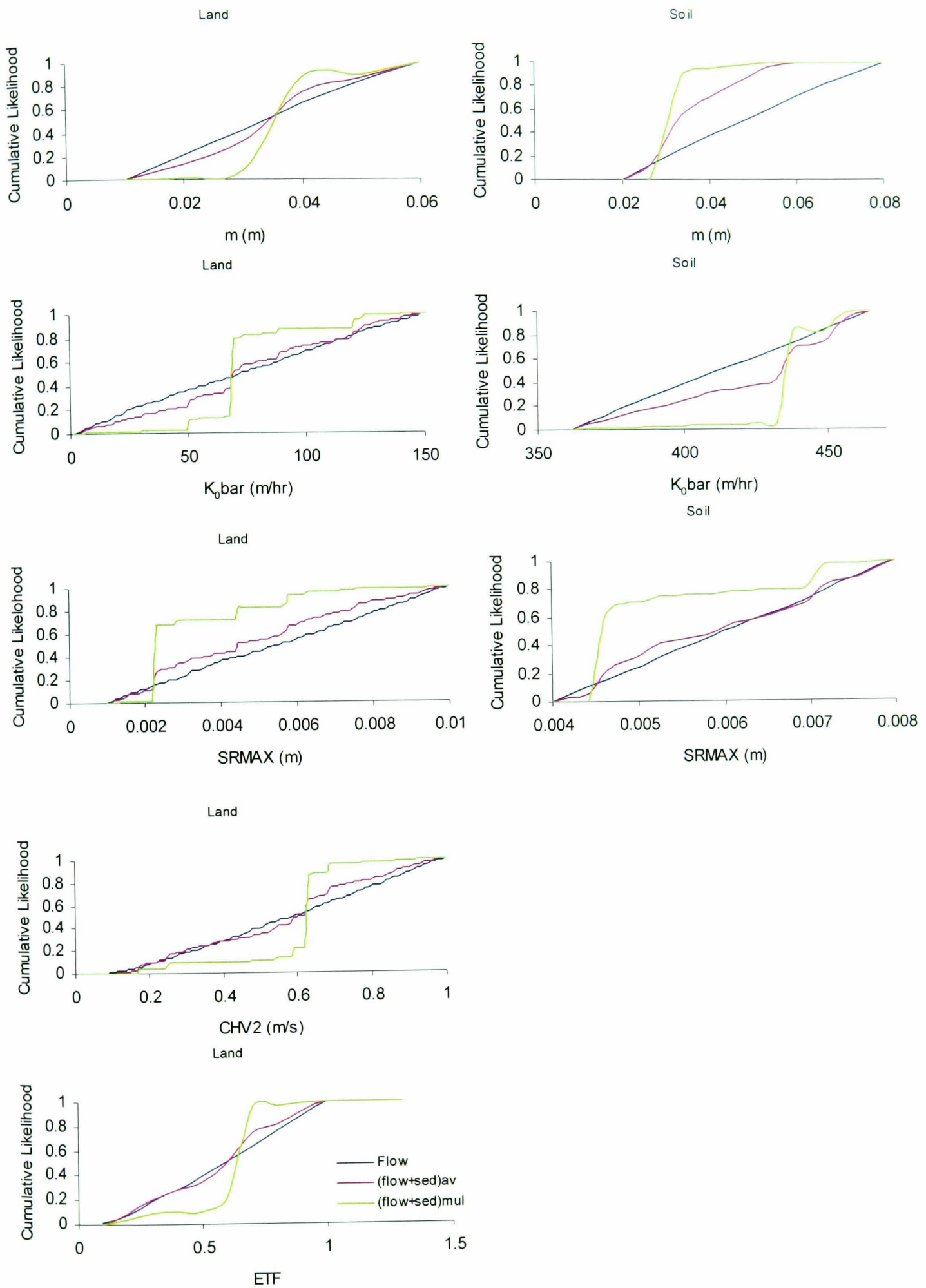


Fig. 6.34 Event 3. Prior and posterior cumulative likelihood distributions for 5 hydrological model parameters, conditioned on flow only, and on flow and sediment data using two different likelihood measures.

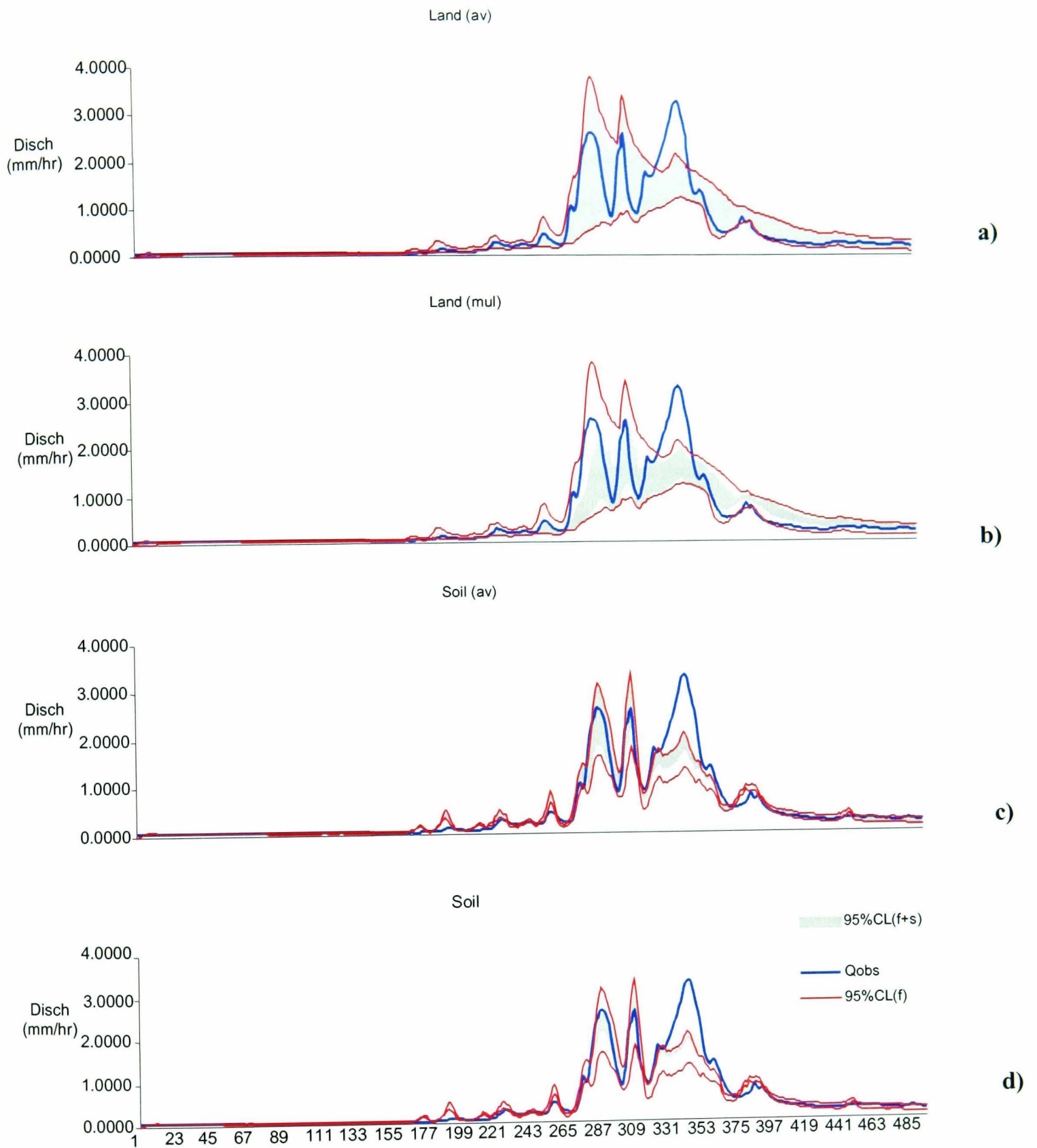


Fig. 6.35 Updated Uncertainty bounds for event 3 for land- and soil-distributed parameterisation using the average and multiplicative likelihoods of equation 5.5.1 and 5.5.2 respectively.

6.8 Propagation of Uncertainty to Sediment Yield Model

Propagation of hydrological model uncertainty to the sediment yield model is analysed in the same way as for the lumped model and is based on equation [5.5.3]. The sediment model parameters are fixed at the ‘optimum’ values and the hydrology varied. The propagated uncertainty bounds are derived based on likelihoods derived from the simulations that are behavioural for both the hydrological and sediment yield models.

Figures 6.36, 6.37 and 6.38 reveal that the propagated uncertainty bounds in the sediment yield are, in some cases (particularly the land-distributed plots for all three events), wider than the uncertainty bounds due to the variability in the sediment yield parameters (Figs. 6.15b and c, Fig. 6.20b and c, and Fig. 6.25b and c). In addition, the soil-distributed model was more effective than the land-distributed for all three events, in reducing the extent of the propagated uncertainty in the sediment yield model, and in some cases the land-distributed parameterisation actually shows greater uncertainty than the lumped.

For Event 1 the land-distributed propagated uncertainty bounds are wider than that of the lumped model (Fig. 6.36a) especially at the last peak. The soil-distributed propagated uncertainty bounds are narrower than those of the lumped model, but there is some over-prediction of minor peaks. For Event 2, the land-distributed propagated uncertainty bounds are similar to those of the lumped, while the soil-distributed propagated uncertainty bounds are very much reduced, resulting in predictive failure particularly at the main peak. The land-distributed propagated uncertainty bounds for Event 3 are narrower than those of the soil- and lumped bounds, and result in predictive failure.

This is the first attempt to quantify the propagated uncertainty from the primary model to a secondary model in a coupled model. The results of both the lumped and distributed parameterisations show that the propagation of uncertainty in the hydrological model can lead to significant uncertainty in the sediment yield model.

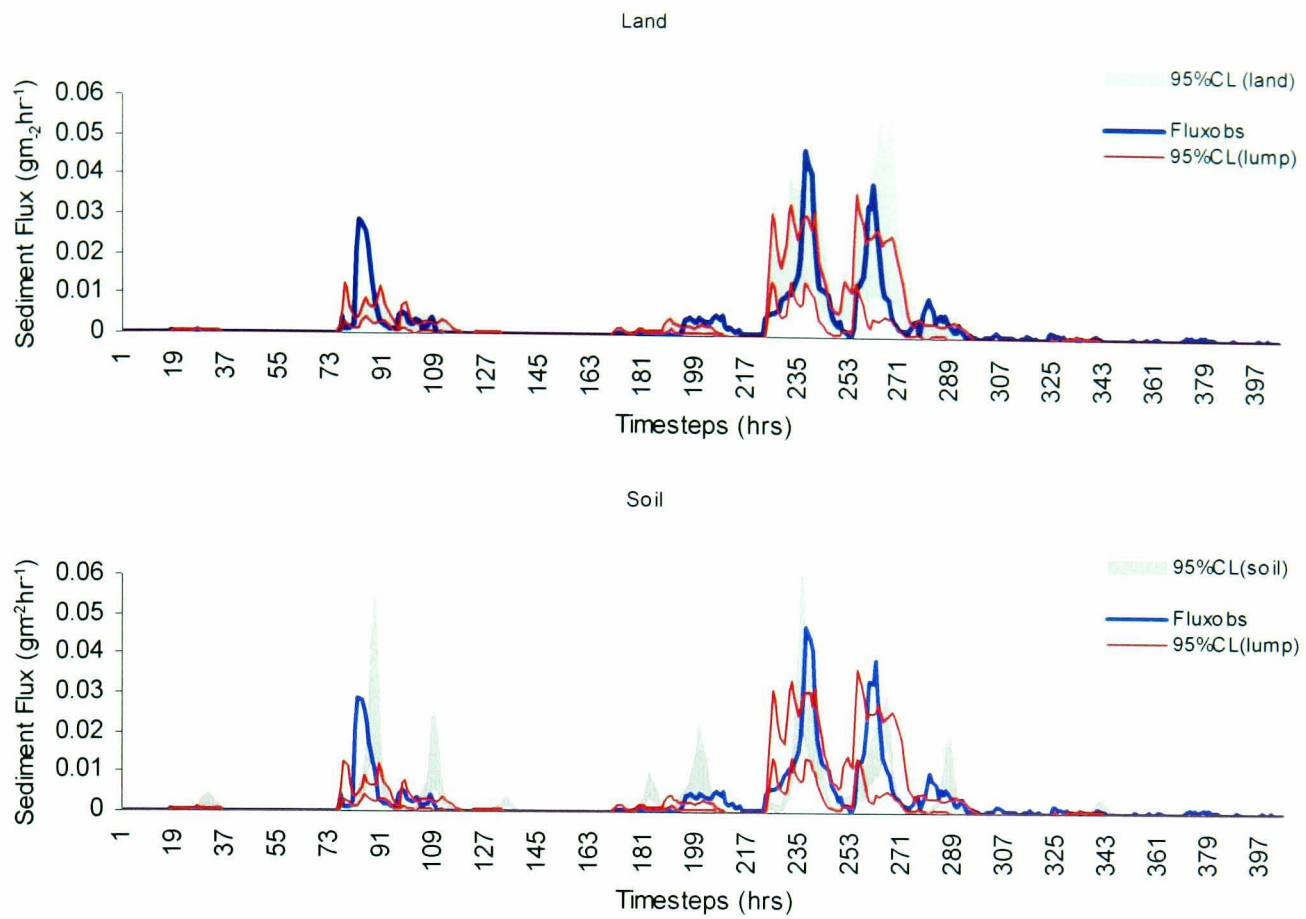


Fig. 6.36 Propagation of uncertainty to sediment yield model – event 1.

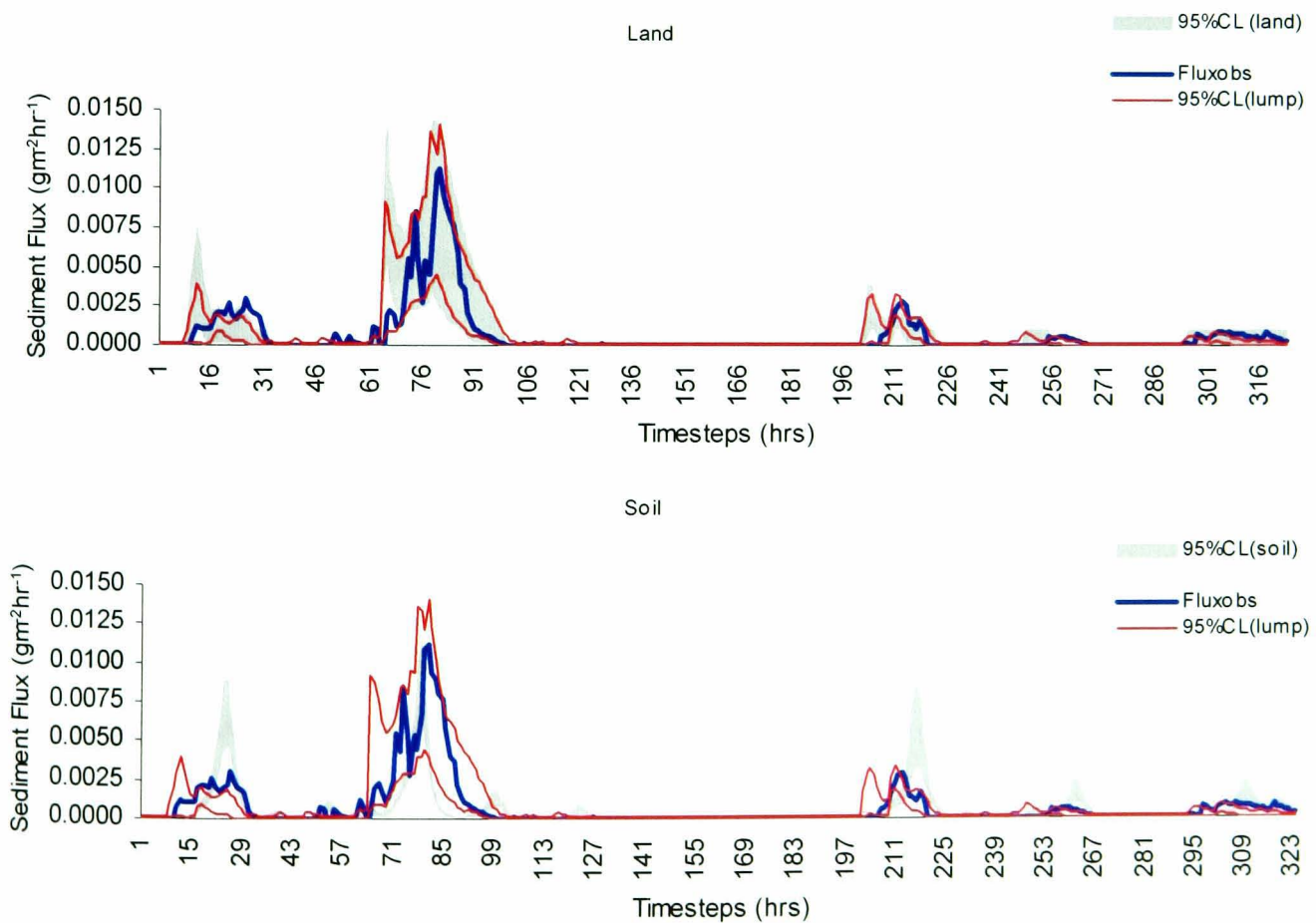


Fig. 6.37 Propagation of uncertainty to the sediment yield model. Event 2.

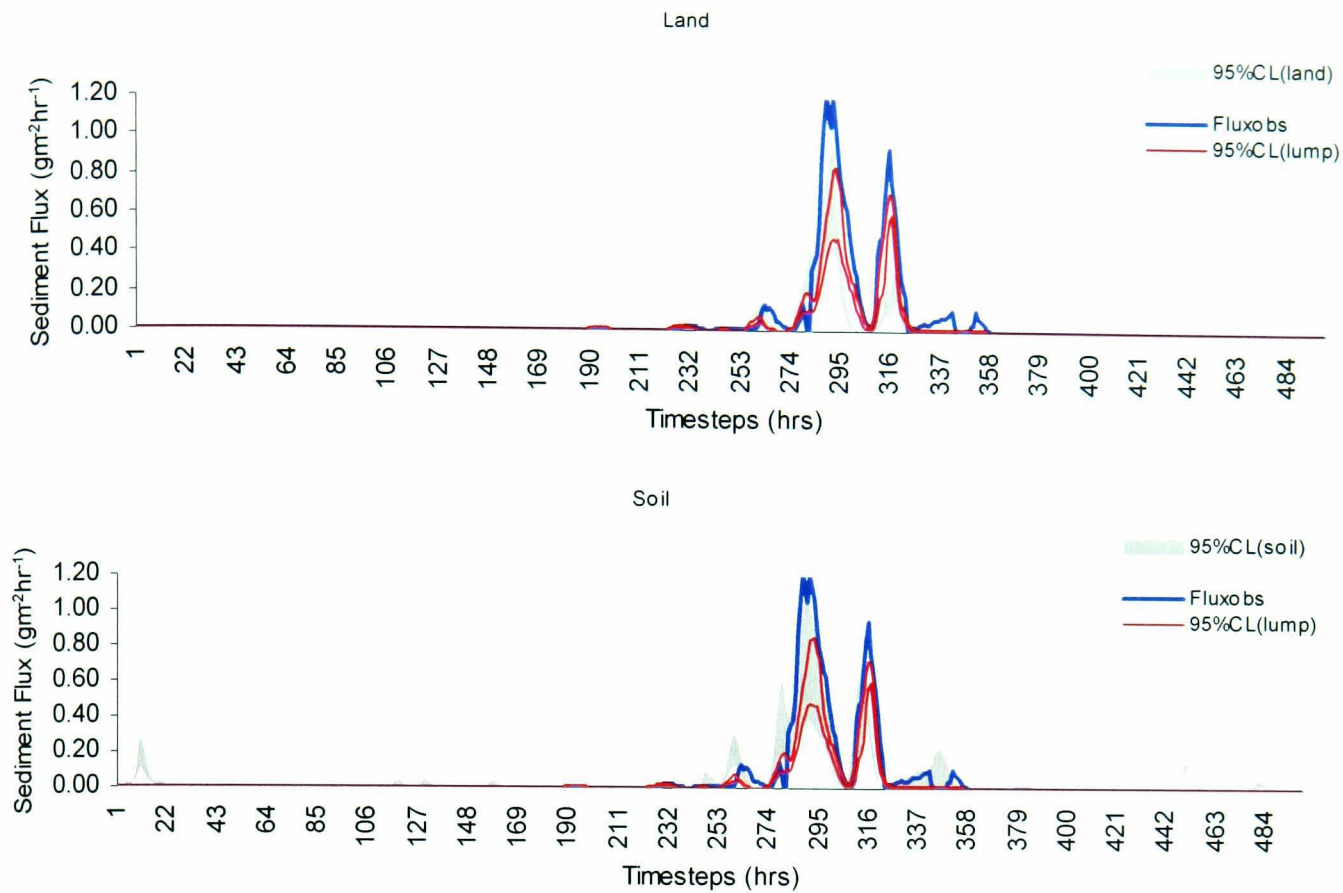


Fig. 6.38 Propagation of uncertainty to sediment yield model. Event 3.

Although the sediment yield model parameters are fixed at their ‘optimum’ values throughout the analysis of propagated uncertainty, the propagated uncertainty can be seen to encompass both the parametric uncertainty of the sediment yield model and that of the hydrological model. This is because the derived ‘optimum’ sediment yield models are dependent on the accuracy of the hydrological model predictions, and therefore inherently carry some uncertainty attributable to them. Hence by holding these already uncertain ‘optimum’ values constant to determine the effect of variable hydrology on sediment model predictions, implies that there is a minimal level of uncertainty that can be expected in the predictions. This perhaps explains why the propagated uncertainty is larger than sediment model parametric uncertainty, which is only one component of propagated uncertainty.

6.9 Conclusion

The main objective of this chapter was to examine whether considering the spatial variability of soil hydraulic properties would reduce uncertainty in the hydrological and sediment yield model predictions.

The two parameterisations considered – landuse and soil type – have had different effects on model uncertainty. It was found that while the land-distributed parameterisation altered the extent of spatial distribution of hydrological response, it did not alter the overall pattern of response, but reinforced topographical controls on hydrological response in the catchment. This did not result in any extensive changes in the uncertainty bounds, of the hydrological model. However, the spatial distribution of soil moisture was altered, with a wider riparian area predicted for the land- than the lumped parameterisation. This resulted in a larger sediment yield source area than the lumped model. Hence the largest difference in spatial predictions of sediment yield were in the riparian zone. The soil-distributed parameterisation, on the other hand, severely altered both the temporal and spatial distribution of hydrological and sedimentological response, and resulted in a more discernible restriction of uncertainty bounds than the land-distributed parameterisation.

The analysis also revealed that both the land- and soil-distributed parameterisations were more effective in reducing the hydrological model uncertainty when the sediment yield model predictions are used to update the hydrological model uncertainty. In addition, the uncertainty propagated from the hydrological to the sediment yield model was found to be greater for the land than the lumped model in most cases, but less for the soil than the lumped parameterisation for most events.

One general conclusion that can be drawn from this analysis is that very different spatial parameterisations resulted in qualitatively and quantitatively similar hydrographs, but very different spatial distributions of runoff production zones. This in turn resulted in spatially and temporally different sediment source areas from those predicted by the lumped model parameterisation.

These results could have serious implications for the prediction of local flooding and soil erosion. They suggest that failure to represent the spatial heterogeneity of soil properties may result in the incorrect predictions of local flooding and soil erosion.

As stated earlier, however, deterministic spatial parameterisation using secondary data sources as done here is prone to error. An alternative is to consider that saturated hydraulic conductivity may vary completely randomly in space. Chapter 7 presents the results of the random spatial parameterisation of saturated hydraulic conductivity.

**PAGE
MISSING
IN
ORIGINAL**

Chapter 7 – Random Spatial Parameterisation

7.0 Summary

Freeze (1975) identified two types of uncertainty associated with deterministic modelling. The first is the uncertainty in the output variables, when input parameters are specified as statistical distributions taken from known populations. The second type is that associated with unknown input population distributions or purely random parameterisations. The former has been dealt with in the two previous chapters in which uncertainty in the output variable (discharge or sediment yield) is derived as a function of the range of input parameter values from known (assumed) populations that give behavioural simulations, for both lumped and deterministic spatial parameterisations. The latter, which Freeze (1975) suggests might also be significant, is the uncertainty associated with the inherent randomness of hydrological systems, and their input variables. Freeze (1975) said of groundwater deterministic models:

'At the very least, we must recognise the uncertainties associated with our deterministic predictions due to the inherent non-uniformity of the porous media and to our uncertainty as to the exact nature of these non-uniformities..... [p. 725]

It is the uncertainty in the nature of these non-uniformities which has led to the application of random spatial parameterisation and input variables in the field of hydrology. This chapter considers the inherent random variability of saturated hydraulic conductivity and examines the effect of its random spatial parameterisation on the model predictions.

7.1 Introduction

The case for Random Spatial parameterisation

Chapter 5 examined the topographical controls on runoff production and showed that runoff is generated from a narrow zone of topographically convergent riparian area cells, which expand onto the hillslopes as the storm progresses only in extreme events. Wolock (1995) showed that distributions of the topographical index exhibited

considerable catchment-to-catchment variability for small catchments ($< 1\text{-}5\text{km}^2$) and much less variability for catchments above 5km^2 . Similarly Woods and Sivapalan (1997) found less variability in the distribution of the index for catchments $> 1\text{km}^2$. These findings suggest that the topographical control can be generalised for large catchments, in keeping with the Representative Elementary Area concept of Wood *et al.* (1988).

Chapter 6 considered the separate control exerted by land use and soil type on runoff production. As stated earlier (section 6.3.2), their controls on runoff production may be interdependent, but deterministic characterisation of every combination of land use and soil type is difficult. To overcome this problem of parameterisation, the occurrence of different soil and vegetation types within a landscape, and hence their combined effect on hydraulic conductivity can be considered probabilistically (Beven, 1991). There will be a certain joint probability of having a particular vegetation cover on soils of given combination of conductivity and moisture characteristics at a certain position within a catchment. Each point in the catchment may also be associated with a probability of receiving a certain storm rainfall volume or temporal pattern of rainfall intensities. In small catchments only a small sample of the individual distributions will be included, particularly where the correlation scales of the individual variables is long relative to the scale of the catchment area. Thus the runoff production for different catchments of the same size may be very different. As scale increases, so does the sample size of properties sampled in each statistically similar catchment area, resulting in similar hydrological response, even though the patterns of properties within the catchments differ. Above a certain scale, the sample may be sufficient that it may no longer be necessary to consider differences due to the pattern of characteristics within each area. This is the Representative Elementary Area (REA) concept proposed by Wood *et al.*, (1988) (see also Butcher *et al.*, 1994; Famiglietti and Wood, 1995; Blöschl *et al.*, 1995; Woods and Sivapalan, 1997; Merz and Plate, 1997; Blöschl, 1999; VandenBygaert and Protz, 1999) by analogy with the representative elementary volume of soil physics. They found that the REA for the volume of storm runoff production for saturation excess and infiltration excess runoff production combined, was of the order of 1km^2 , determined by a minimum in the variance of predicted runoff volumes from areas of the same spatial scale.

The concept of REA is a great simplification as it ignores the effects of channel routing, characteristics that have long or complex correlation structures relative to the catchment scale or else are non-stationary in space. However, it is useful in clarifying the interaction of heterogeneity of catchment characteristics and catchment scale in runoff production. Larger catchments generally have variable rock types, soil series, and hillslope forms, each with different distributions of hydrological parameters. Rainfall inputs may involve correlation structures at multiple scales, with the longer synoptic scales being very much greater than the catchment REA. Non-stationarity and extensive spatial correlation will lead to increased variability in catchment response beyond the scale of the REA, which might then represent the scale at which there is a minimum in the variability in catchment hydrological response.

Thus where catchment hydrological response is the primary factor being modelled, it may be sufficient to model spatially variable hydraulic conductivity stochastically.

Random Variability of Saturated Hydraulic conductivity

Studies into the infiltration process (e.g. by Smith and Hebbert (1979), Sharma *et. al.* (1980), Sharma (1983), Sisson and Wierenga (1981), Vieira *et. al.* (1981), Ahuja *et. al.* (1984), suggest that it should be treated as a stochastic process, and saturated hydraulic conductivity as a statistical variable. Law (1944) was the first to propose a log normal distribution for hydraulic conductivity, on the basis of core analysis dated from a carbonate oil field reservoir. Bulnes (1946) and Warren and Price (1961), also working with oil field cores, supported Law's findings, while Willardson and Hurst (1965) found log normal distributions for the hydraulic conductivity of soils, based on 254 auger hole measurements in 12 fields in Australia and 1498 samples from seven soil types in California. McMillan (1966) analysed the California Department of Water Resources transmissivity maps for the Los Angeles basin and found that hydraulic conductivity was log normally distributed. Bennion and Griffiths (1966) working with 60,000 cores from 2000 wells in a sand and conglomerate oil field reservoir and 24,000 cores from 430 wells in a limestone reservoir found permeabilities to be log normal, although somewhat skewed in some cases. Davis (1969) noted that specific capacities of water wells (which are directly related to formation transmissivities) are usually log-normally distributed. Indirect supporting evidence of the log normal distribution of hydraulic conductivity includes the widely

recognised fact that grain size distributions, which are related to hydraulic conductivity, are log normal, and that in most empirical formulae, hydraulic conductivity is calculated as an exponential function of porosity, which is usually reported as normally distributed. Monte Carlo tests on random block porous media (Warren and Price, 1961; Bouwer, 1969) generally show the geometric mean to be the best estimate of 'effective permeability' in non-uniform media. Aitchison and Brown (1957) provide the theoretical background to show that this conclusion supports a log normal hydraulic conductivity distribution.

Matias *et. al.* (1989) investigated the effect of spatially variable K_s on the ponding time and infiltration rates under constant rainfall, and found that as s.d. of K_s increases, the ponding time becomes shorter, and the infiltration rate lower. They also found that the influence of the skewness coefficient g , is very small for CV=50% (CV is the variation coefficient), as well as for CV=100% when the rainfall rate is high, but there is a trend towards increasing ponding time and the infiltration rate, with higher g . In addition, they showed that there was an asymptotic trend of the temporal evolution of the empirical distribution function of the K_s ($F(K_s)$), which shows that the infiltration process is a probabilistic one, following a pattern, similar to that of K_s . Such similarity growing as rainfall intensity increases. Their results agreed with those of Smith and Hebbert (1979).

The influence of s.d. (or coefficient of variation, CV) on ponding time is higher than that of the skewness coefficient (similar to the effect on infiltration rate), but such influences are smaller when rainfall intensities increase. Matias *et. al.* (1989) used the percentage of catchment area contributing to runoff at the time as a measure of ponding time.

Random Fields

Random fields can be generated to examine typical patterns of fluctuation observed in natural hydrological systems, or estimated from observations, based on minimising the error variance to interpolate between observations (Matheron, 1973; David, 1977; Delhomme, 1978; Journel and Huijbregts, 1978).

In general random fields can be used for many types of assessments in hydrology including:

- a) the assessment of the sensitivity of the natural system to extreme realisation scenarios.
- b) The estimation of measurement and forecast uncertainties resulting from spatial and temporal parameter variability (Monte Carlo simulations).
- c) The interpolation between observations (conditional simulations), i.e. estimated values conditioned on observed data.

Two main types of random field generation (RFG) models can be identified (Haldorsen and Damsleth, 1990). Discrete RFG's, which divide a range of values for a variable into a limited number of classes e.g. number of fracture networks (Geology), and continuous RFG's which describe continuously varying properties, such as hydraulic conductivity, by specifying statistical properties such as the mean, the variability about the mean (s.d.), the spatial persistence of the correlation between neighbouring values (ϵ), and the cross-correlation structure between jointly varying parameters of interest (i.e. correlation between K and θ or K and ψ). Robin *et. al.* (1993) identify a third class which involves a mixture between these two classes. For example, a layered medium of different materials (the discrete variable), with the property of interest varying continuously within each layer.

The theory of continuous random fields, was first applied to multi-dimensional simulation with the development of multi-dimensional spectral techniques for stationary fields (Shinozuka, 1971; Schinozuka and Jan, 1972; Mejia and Rodriguez-Iturbe, 1974). This approach requires significant computer time to generate a large number of realisations for a Monte Carlo model. More commonly used continuous models assume that the variable follows a multivariate normal (or Gaussian) distribution. Multivariate models represent the field only at a number of pre-specified discrete points, and assume stationarity to preserve the covariance of the field between these points (Wilson, 1979). They specify spatial persistence by the auto-covariance function for a single variable or the cross-covariance function for more than one variable. Alternatively, the same information can be specified in the frequency domain by the power and the cross-spectral density functions respectively. The

disadvantage of the Gaussian models is that they sometimes fail to represent reality, especially where discontinuities exist in the real system. Examples of Gaussian RFG's, discussed briefly below, include the following:

1. The matrix decomposition (Clifton and Neuman, 1982; Davis, 1987).
2. The turning bands method (Delhomme, 1979; Mantoglou and Wilson, 1982; Mantoglou, 1987; Thompson *et. al.*, 1989).
3. The spectral method of Mejia and Rodriguez-Iturbe (1974).
4. Nearest neighbours model (Freeze, 1975; Smith and Freeze, 1979a, b; Smith and Schwartz 1981).

The matrix decomposition method essentially involves the construction of the covariance matrix describing the spatial persistence of the field and its subsequent decomposition into an upper and lower triangular matrix. The lower triangular matrix is then multiplied by a vector of random uncorrelated numbers, to produce a random field, which preserves the imposed covariance structure. The disadvantage of the method is that although it is simple, it can be computationally intensive, especially for multi-dimensional systems involving 10's of 1000's of data points. However, it has two main advantages. Firstly, the matrix decomposition step is only to be performed once for Monte Carlo simulations because only backward substitution is required to generate each additional realisation, and secondly, it can be used to generate fields that are correlated with each other. Myers (1982) used this method and incorporated cokriging to include the effects of conditioning.

The turning bands method produces random fields by generating 1-D line processes over discrete bands specified by the power spectral density function. Its basic concept is to transform a multidimensional simulation into the sum of a series of equivalent uni-dimensional simulations, while preserving the statistics of the true field. The turning band method was introduced by Matheron (1973), and has been extensively applied in three-dimensional spatial simulation, particularly in the field of ore mining and energy reserves prospecting (see e.g. David, 1977; Journel and Huijbregts, 1978). Two-dimensional spatial processes that are often encountered in hydrological applications (e.g. saturated hydraulic conductivity, and rainfall fields), however, are much more difficult to simulate using the turning-bands method.

Spectral analysis techniques represent the probabilistic structure of the medium by an explicit function, defined to specify the autocorrelation structure within the medium, which is usually solved by using a perturbation approach. Mantoglou and Wilson (1982) overcame the difficulty of applying the turning bands method to two-dimensional processes, by introducing the spectral equivalent of two-dimensional and one-dimensional processes, permitting the turning bands simulation of any two-dimensional covariance function of a stationary random field. Its major advantage is that it is very computationally efficient as it reduces a 2-D or 3-D problem to a series of 1-D problems (Thompson *et. al.*, 1989). In addition, it enables the generation of fields of irregular geometry, with little additional computational effort. However, a major disadvantage of this method is that the algorithm is complex to implement in practice because the accuracy of the results depends on the discretisation and truncation of the line spectra, the number of bands used to generate the field, and orientation of the bands (Mantoglou and Wilson, 1982). In addition, if not controlled properly, unwanted line-like distortion patterns in the simulated fields and difficulties in anisotropic problems can result. Errors due to discretisation decrease, with increase in the number of runs (Mantoglou and Wilson, 1982). Mantoglou and Wilson (1982) found that evenly spaced lines resulted in a faster rate of convergence of simulated covariance and true covariance than randomly distributed lines, and that the simulated covariance error due to the finite number of lines rapidly approaches zero as $1/L^2$, and the number of lines L increases. They also found that while 16 lines provided very accurate representation of the process, 4 lines was adequate to describe it. Robin *et. al.* (1993) present an algorithm based on the Discrete Fourier Transform (DFT), that can be used to co-generate cross-correlated three-dimensional fields on a regular grid. It is based on the “direct” power spectral estimation method which estimates the spectral density function directly from real data, without using the auto-correlation function as an intermediary step.

In the nearest neighbours method, the conductivity values in each sampled cell of the catchment are related through a simple linear equation expressing the dependence of the conductivity in one cell on conductivity values in surrounding cells.

Interpolation methods

Random parameter values generated at a given scale to reflect the de-correlation length of the parameter can be interpolated to represent the spatial correlation of the parameter. There are two main types of interpolation methods: 1) global (e.g. trend surfaces), and 2) local (e.g. kriging, moving average, weighted moving average).

The global interpolation method, trend surface, uses regression analysis to fit a polynomial equation to the observed data.

For a linear trend:

$$Z^*(x) = \beta_0 + \beta_1 x_1 + \beta_2 x_2 \quad [7.1]$$

For a quadratic trend:

$$Z^*(x) = \beta_0 + \beta_1 x_1 + \beta_2 x_2 + \beta_3 x_1^2 + \beta_4 x_2^2 + \beta_5 x_1 x_2 \quad [7.2]$$

Where $\beta_0, \beta_1, \beta_2, \beta_3, \beta_4, \beta_5$ are regression coefficients.

x_1, x_2 , are horizontal coordinates. Surfaces of higher order can be used (e.g. Hosseini *et. al.*, 1993).

In local interpolation the estimated value of a variable at an unsampled site is estimated from neighbouring values by:

$$Z^*(x) = \sum_{i=1}^n \lambda_i Z(x_i) \quad [7.3]$$

Where $Z(x_i)$ is the observed values of Z at x_i ; $Z^*(x)$ is the estimation of value of Z at x , the coordinates of the estimated point (the initially unknown point); x_i are the coordinates of the observed value i , i.e. coordinates of sampled points for which values are known; n is the number of values used in the estimation; and λ_i is the weight given to observed value i .

Local interpolation methods differ by the number and location of neighbouring points used and by the way weights are assigned to each observed point. For moving average and weighted moving average methods, weights are calculated as:

$$\lambda_i = \frac{D_i^{-\alpha}}{\sum_{i=1}^n D_i^{-\alpha}} \quad [7.4]$$

Where D_i is the distance from observation point i to interpolated site, and α is the distance-weighting exponent. For the moving average method, the same weight is given to each observation ($\alpha=0$, and $\lambda_i = 1/n$). Weighted moving average consist of assigning more weight to closer observation ($\alpha > 0$). The distance-weighting exponent may affect the precision of estimation (Weber and Englund, 1992; Gallichand and Marcotte, 1993).

In kriging, the weights are chosen to minimise the estimated variance (Journel and Huijbregts, 1978), by solving for each estimation point:

$$A\lambda = b \quad [7.5]$$

Where A is the matrix of co-variances between sampling sites; λ is the vector of unknown weights; b is the vector of co-variances between sampling sites and the point being estimated. A and b are constructed using a semi-variogram model that represents the statistical structure of the variable. This model is determined by fitting one of a variety of mathematical functions to the experimental semi-variogram

$$\gamma^*(h) = \frac{1}{2n_p} \sum_{i=1}^{n_p} [Z(x_i) - Z(x_i + h)]^2 \quad [7.6]$$

Where γ^* is the experimental value of semi-variogram; h is the distance vector between sample points; n_p is the number of sample pairs separated by h . Three main shapes of semi-variograms have been identified (Fig. 7.1).

- The spherical model

The ‘ideal’ shape for a semi-variogram is called the spherical or Matheron model, and is given mathematically:

$$\gamma(h) = C \left(\frac{3h}{2a} - \frac{1h^3}{2a^3} \right) \quad h \leq a$$

$$= C \quad h \geq a \quad [7.7]$$

where a is the 'range of influence of a sample' or the de-correlation distance, and C , the sill, is the value of $\gamma(h)$ at which the graph levels off.

- The exponential model

$$\gamma(h) = C[1 - \exp(-h/a)] \quad [7.8]$$

This model rises more slowly from the origin than the spherical and never quite reaches its sill.

- The generalised linear model

$$\gamma(h) = ph^\alpha \quad 0 \leq \alpha < 2 \quad [7.9]$$

where p is the slope of the line.

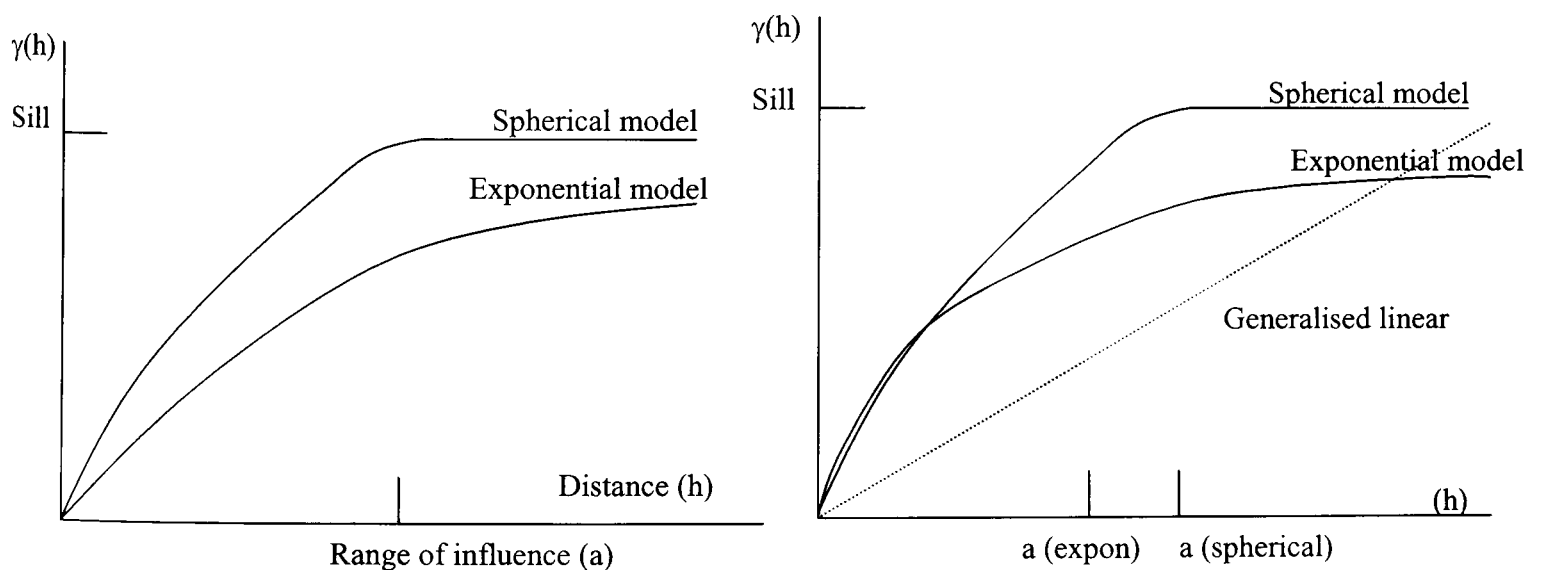


Fig. 7.1a) exponential and spherical models with the same range and sill

b) exponential and spherical models with the same initial slope and sill plus the generalised linear model. After Clark (1979).

Ordinary kriging assumes that, at any point, the expected value of the variable is the same throughout the neighbourhood (1st order stationarity). If this condition is not met, and the expected values change gradually within the neighbourhood, universal kriging is more appropriate because it incorporates this locally changing drift.

Kriging has been used for the study of several soil properties, but few investigations of hydraulic conductivity are reported in the literature. Mulla (1988) and Rogers *et al.* (1991) studied the spatial structure of hydraulic conductivity at field scale (few hectares), while Alemi *et al.* (1988) studied it at project area scale (78 km²). Strzepek *et al.* (1982) were first to suggest kriging as a tool for the design of subsurface drainage systems, and Gallichand *et al.* (1991; 1992a) showed the feasibility of incorporating krigged hydraulic conductivity values into subsurface drainage design for a large (335km²) project in the Nile Delta of Egypt. Studies comparing kriging (Van Kuilenberg *et al.*, 1982; Laslett *et al.*, 1987; Laslett and Mc Bratney, 1990; Gallichand *et al.*, 1992b; Hosseini *et al.*, 1993) to other interpolation methods have shown kriging to be the most precise estimation in most applications. The main advantages of kriging are:

1. Given the basic assumptions, no trend, and a semi-variogram model, kriging always produces the Best Linear Unbiased Estimator (BLUE), and a unique solution.
2. The value at every location is *known* within the kriging system. Hence it is referred to as an 'exact' estimator.
3. The kriging system only needs to be calculated once if regular samples are used.

Hence kriging is applied here to construct grids comprising unique hydraulic conductivity values at each grid cell.

7.2 Method of Random Spatial parameterisation

Random spatial parameterisation of saturated hydraulic conductivity was achieved by generating a unit grid with a mean value of 1. This was done using a random number generator FORTRAN NAG subroutine (G05DEF), which gives log-normally distributed real numbers, called '*K* factors', at equally spaced intervals of 10 grid cells (500m) within the catchment. Using standard kriging functions within Arc View the semi-variogram best suited to the random data points was estimated. Assuming a de-correlation distance of two grid-cells (100m) a smooth surface of saturated hydraulic

conductivity K factors was constructed, for three different standard deviations of K. These grids were then used to spatially distribute the ‘optimised’ lumped K values obtained in chapter 5, to examine the effect of random parameterisation of K, on model results. Figures 7.2, 7.3 and 7.4, show the spatial and frequency distributions of the K factor, and the semi-variograms for three different standard deviations, and Table 7.1 shows their properties.

	Min	Max	Mean	s.d.	Semi Variogram
Grid 1	0.762	1.332	1	0.1	Exponential
Grid 2	0.152	4.291	1	0.6	Exponential
Grid 3	0.072	9.336	1	0.9	Linear with sill

Table 7.1 Statistical properties of K factor grids.

The distributions show typical log-normal variability in saturated hydraulic conductivity, with a tail of high values indicative of a micro-pore/macro-pore sampling problem. Distributing the ‘effective’ calibrated saturated hydraulic conductivity values in this way, enables an examination of the possible stochastic spatial variability that subsumes catchment hydrological response as represented by the lumped model calibrated value. It is also representative of the probabilistic variations in land use and soil type combinations within the catchment and thus represents the ensemble effect of land use and soil type on hydrological response.

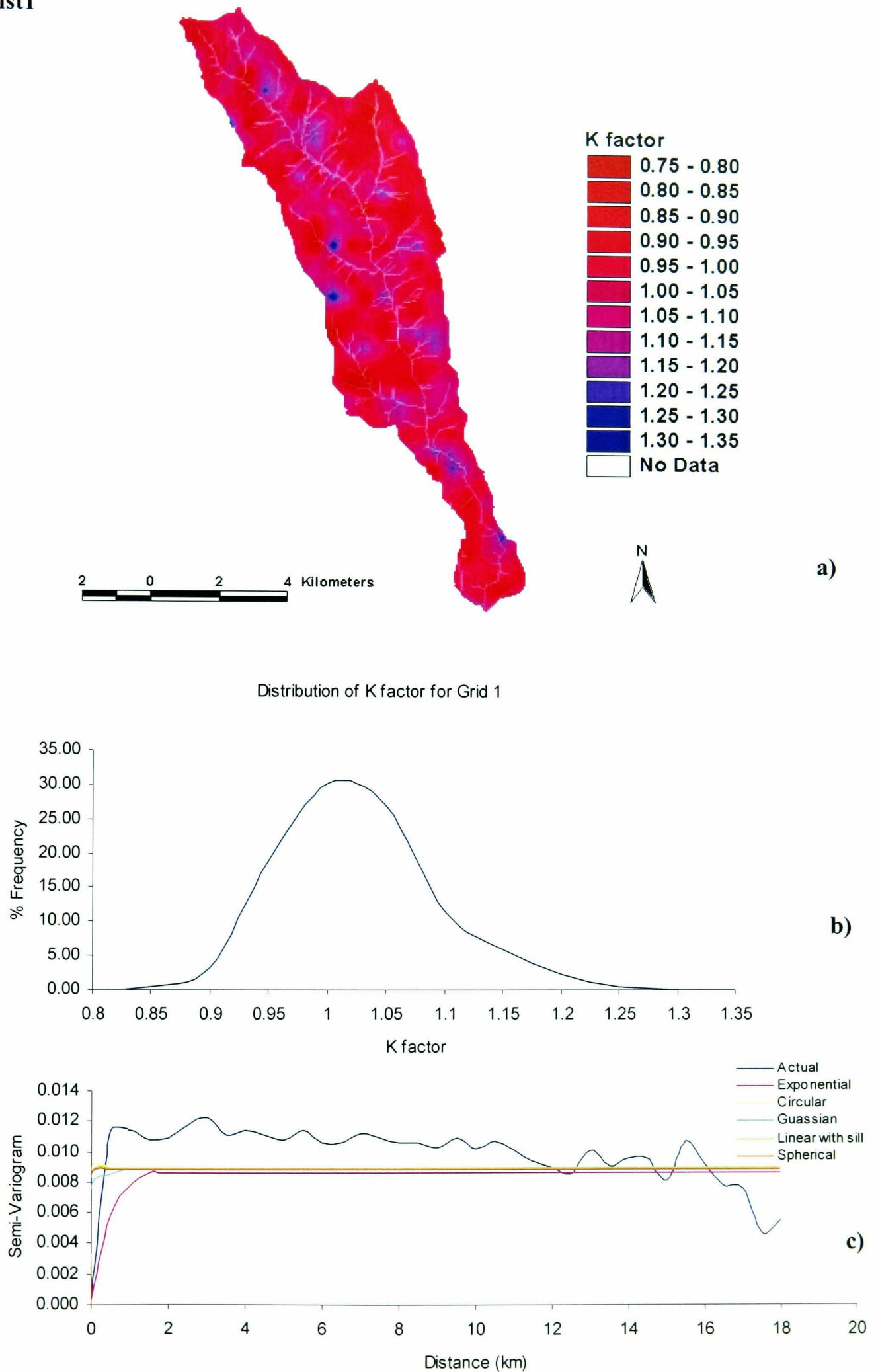
Kdist1

Fig. 7.2 a) Spatial distribution of randomly generated K factor for grid 1. b) Frequency distribution of K factor. c) actual and fitted semi-variograms.

Kdist2

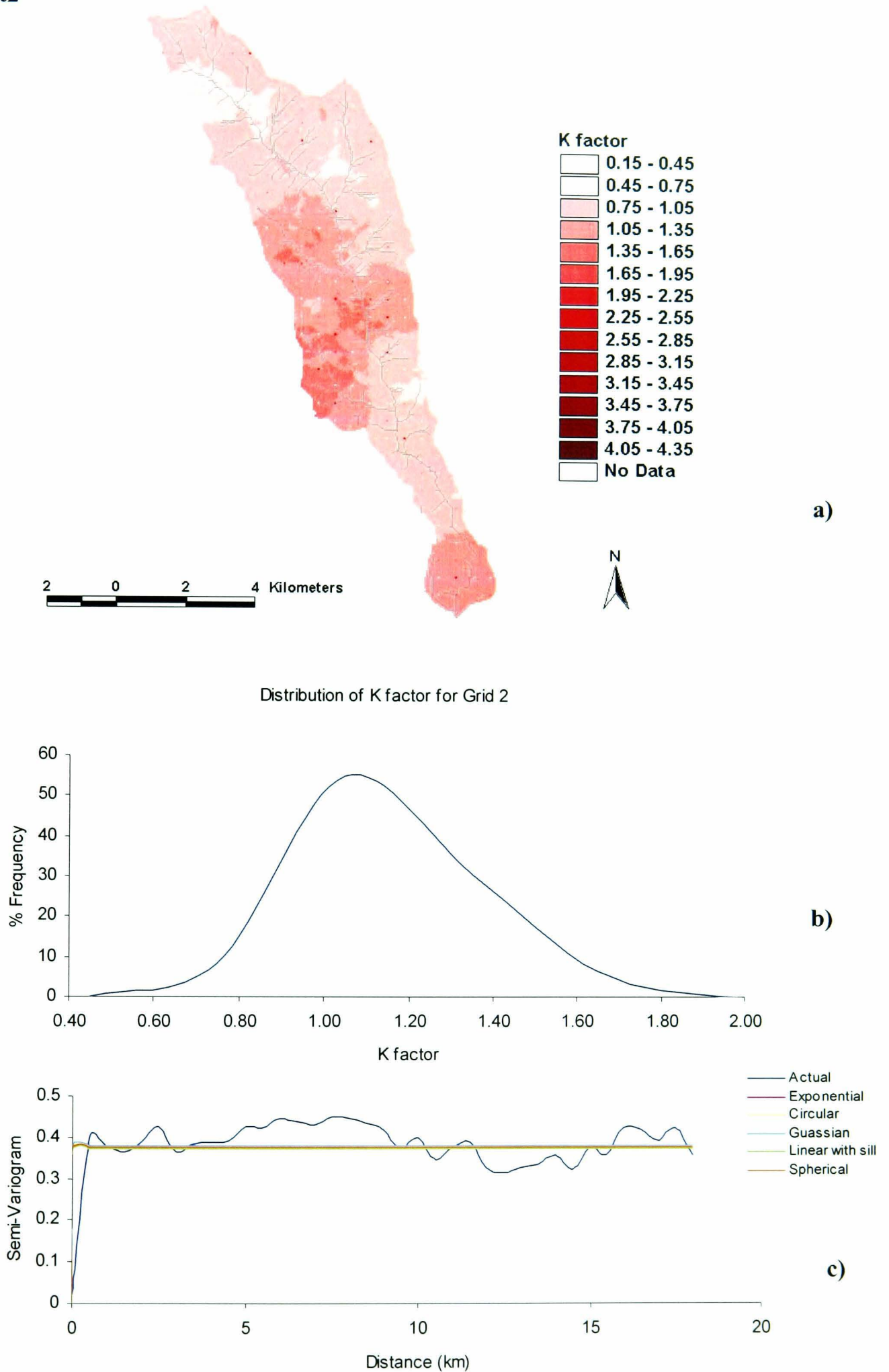


Fig. 7.3 a) Spatial distribution of randomly generated K factor for grid 2. b) Frequency distribution of K factor. c) actual and fitted semi-variograms

Kdist3

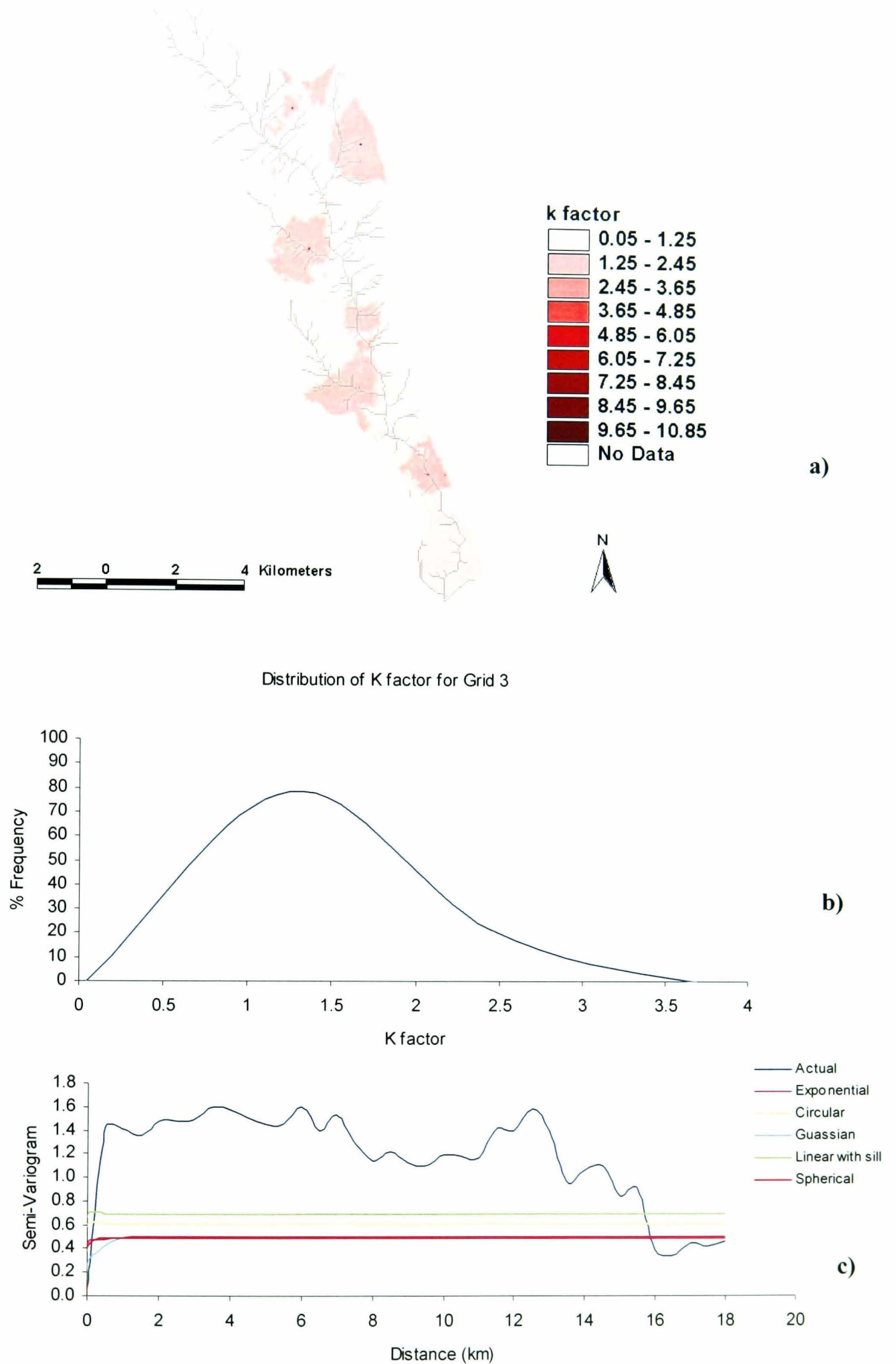


Fig. 7.4 a) Spatial distribution of randomly generated K factor for grid 3. b) Frequency distribution of K factor. c) actual and fitted semi-variograms.

7.3 Results and Discussion

Hydrological Response

Figures 7.5a, 7.6a, and 7.7a show that the hydrographs for randomly distributed saturated hydraulic conductivity, are similar to that for the lumped parameterisation for each event. This suggests that the dominant control on hydrological response might be the statistical ensemble value, rather than the distributed nature of saturated hydraulic conductivity, in keeping with the representative elementary area concept of Wood *et. al.* (1988). However, it is also possible that the extent of the variability of K_s considered may not have been sufficiently large to affect the hydrological response of this catchment. It is conceivable, for example, that if K_s in the riparian area and close to the outlet is several orders of magnitude less than that on the hillslopes, the magnitude and timing of response to rainfall will be different from that of the lumped equivalent K_s , as was the case for the soil-distributed parameterisation in Chapter 6. According to the theory of variable contributing area, it is the rate of runoff from the riparian areas that controls hydrological response. Examination of the randomly parameterised grids (Kdist1, Kdist2, and Kdist3), reveals that for the grid with the largest standard deviation, most of the cells along the channel network have the same low K factor, with the higher values concentrated on three patches on the hillslopes. Thus, the location and extent of the variability of saturated hydraulic conductivity were such that they had little or no effect on the magnitude and timing of the hydrological response, suggesting that topography may still be the dominant factor.

Figures 7.5c, 7.6c, and 7.7c, the frequency distributions of residual soil moisture deficit (random – lumped), show that for events 1, and 3 the distributions for the wettest and driest timesteps have their maxima at different values of residual soil moisture deficit, while all distributions for event 2 have their maxima at the same value. For event 1, the frequency distributions of residual soil moisture deficit for the driest timestep have their maxima at a higher value than that for the wettest timestep, which is at approximately zero. This indicates drier timesteps are more sensitive to the variability in K_s , than wetter timesteps, for this event. Hence at the driest timestep, the random soil moisture deficit is greater than the lumped for most cells in the catchment, and as s.d. of K_s increases, the number of cells with a negative residual deficit increases. For the wettest timestep, approximately 50% of cells have negative

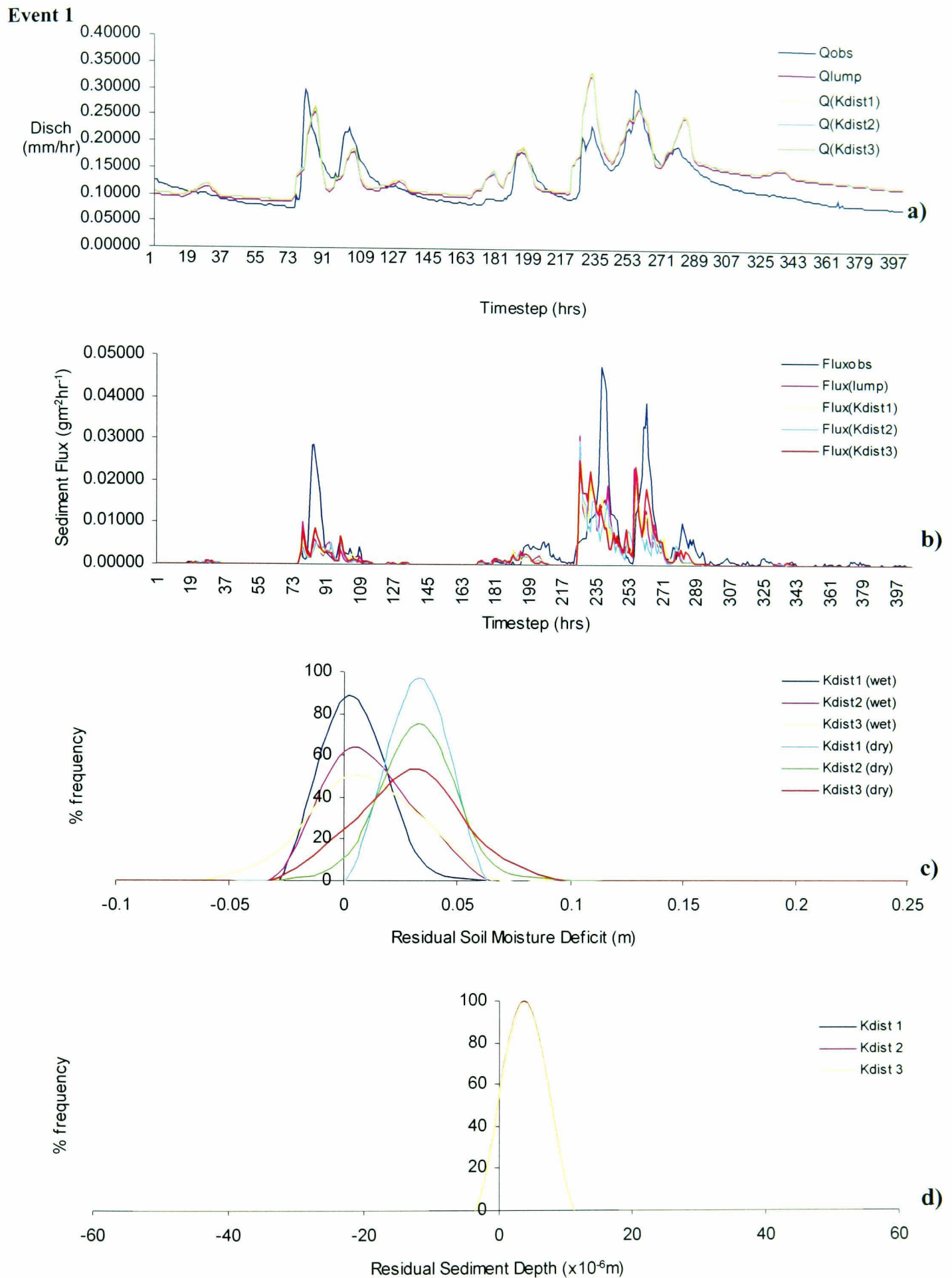


Fig. 7.5 a) Comparison of observed and lumped hydrograph with randomly distributed hydrographs.

b) Comparison of observed and lumped sedigraphs with randomly distributed sedigraphs.

c) Frequency distribution of residual soil moisture deficit for wettest and driest timesteps.

d) Frequency distribution of residual sediment depth for T=343.

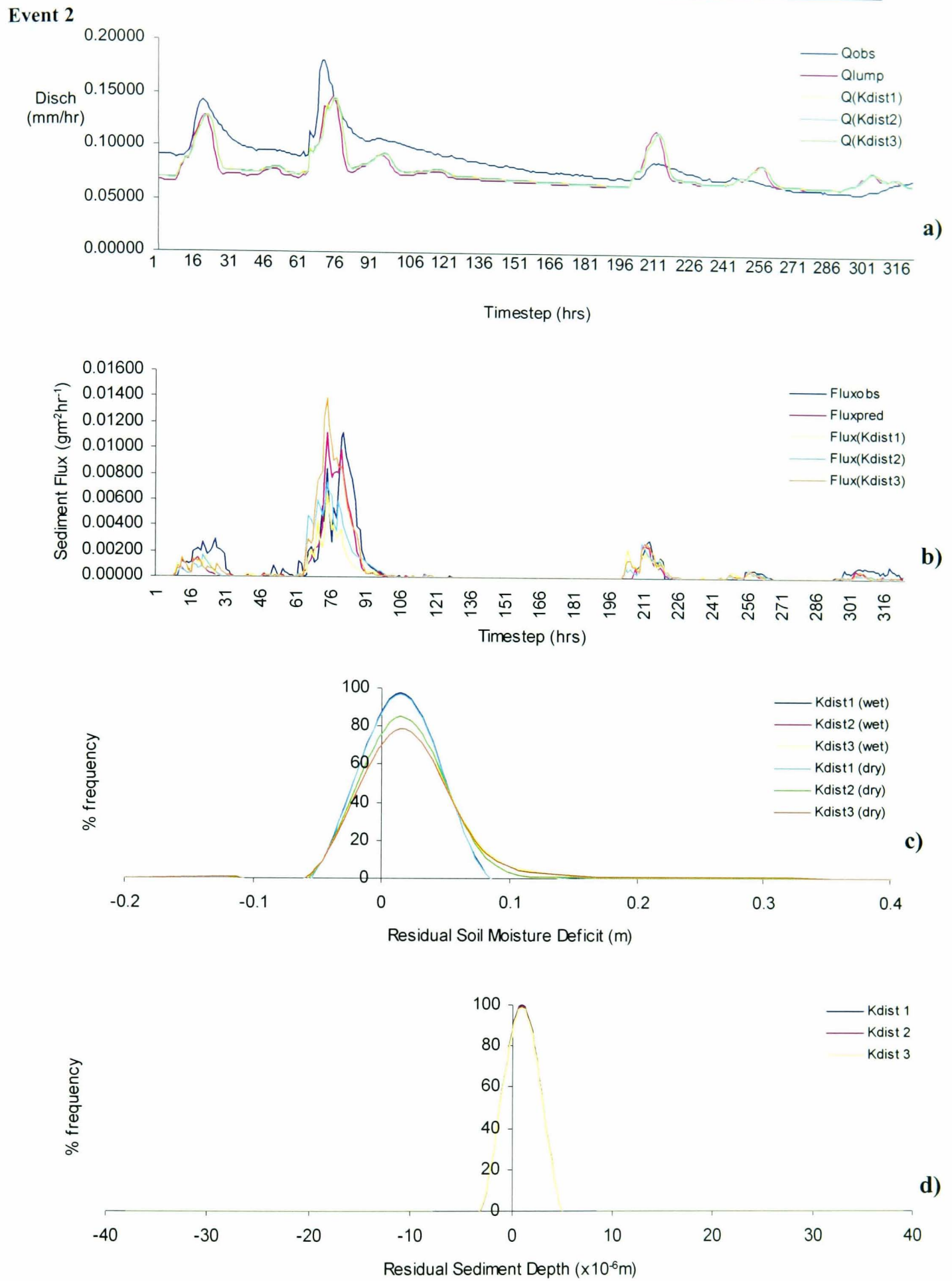


Fig. 7.6 a) Comparison of observed and lumped hydrograph with randomly distributed hydrographs .
 b) Comparison of observed and lumped sedigraphs with randomly distributed sedigraphs.
 c) Frequency distribution of residual soil moisture deficit for wettest and driest timesteps.
 d) Frequency distribution of residual sediment depth for T=343.

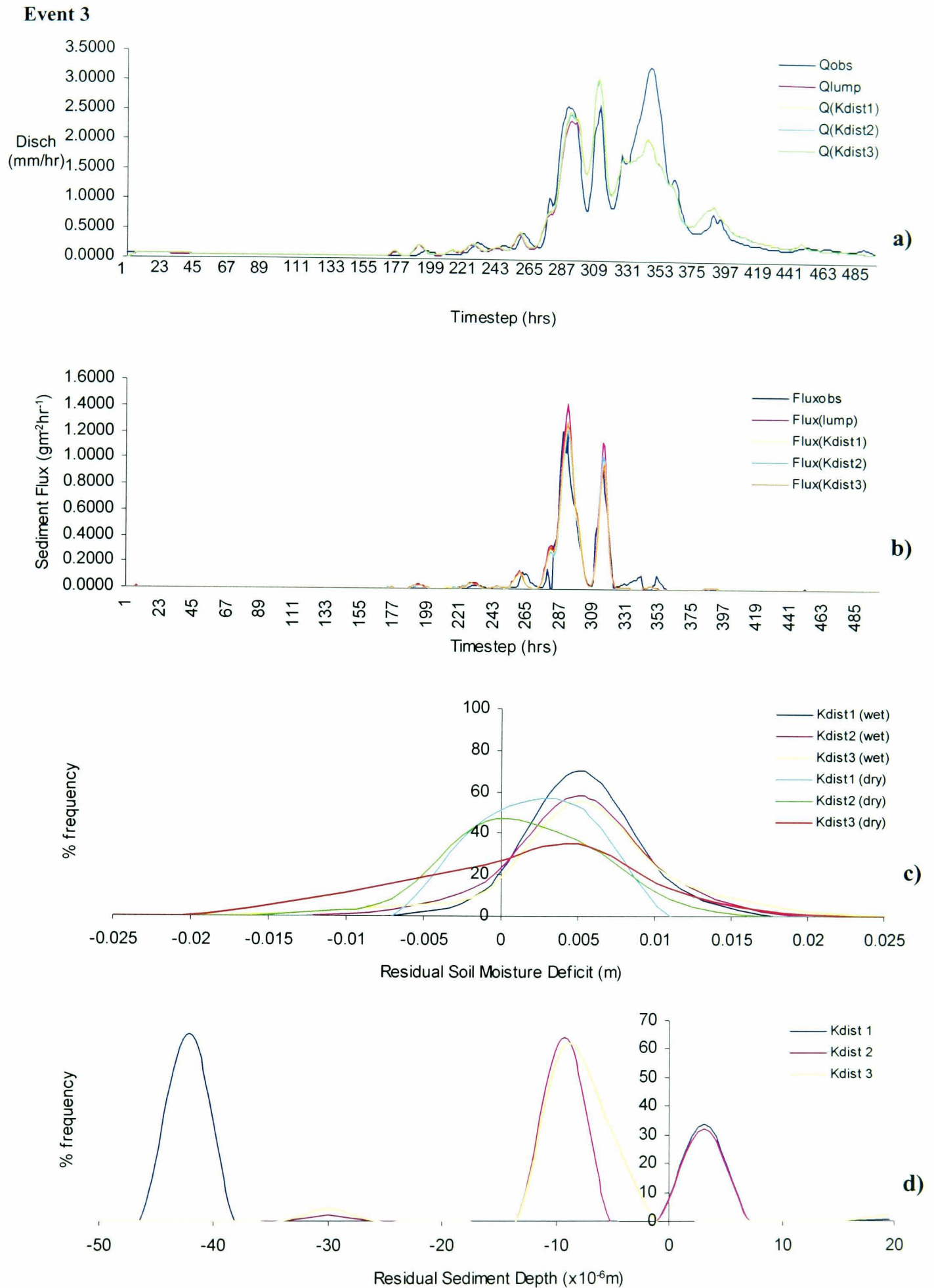


Fig. 7.7 a) Comparison of observed and lumped hydrograph with randomly distributed hydrographs.
 b) Comparison of observed and lumped sedigraphs with randomly distributed sedigraphs.
 c) Frequency distribution of residual soil moisture deficit for wettest and driest timesteps.
 d) Frequency distribution of residual sediment depth for T=343.

residual deficits. For event 3, this pattern is reversed with the wettest timestep having distributions with positive maxima and mostly positive deficits, and the driest having their maxima at lower residual deficits. This reversal suggests that for an event of this magnitude, the wetter timestep is more sensitive to the variability in hydraulic conductivity, perhaps because the number of gridcells involved in the hydrological response is much larger for large events, or as rainfall intensity increases the influence of spatially variable K_s , is reduced. For all three events, the frequency distributions for a given timestep become wider and the maximum decreases as s.d. of K_s increases. Also noticeable is that the frequency of a given residual deficit in the tails of the distributions increases with increasing s.d. of K_s , up to a critical value of residual deficit, as the peak is approached, after which the pattern is reversed. This is because as s.d. of K_s increases, the extreme values of K_s , will result in extremes of soil moisture deficits (higher K_s values giving higher recharge rates, and hence lower soil moisture deficits). At residual deficit values closer to the peak, however, the lower s.d. K_s grids are likely to generate more normal soil moisture deficit values and hence residuals, and will therefore dominate the distribution. That is, for lower s.d. K_s , the number of grid cells with a residual soil moisture deficit closer to the peak, will be greater than that for higher s.d. of K_s , but at more extreme residual values, the more variable K_s distributions, are more likely to have cells with residuals of such extreme magnitudes.

The spatial distribution of residual soil moisture deficit for event 1 (figures 7.8, and 7.9), event 2 (figures 7.10 and 7.11) and event 3 (figures 7.12 and 7.13) show that as s.d. of K_s increases, residuals become more positive, with the highest values of the residual (the more positive) located where there are high values of K_s . This pattern is more pronounced for the wettest timesteps. As observed by Matias *et. al.* (1989), as s.d. of K_s increases, ponding time and hence infiltration rates, decrease, and soil moisture deficit increases. Hence for a given s.d. of K_s , larger residuals of the soil moisture deficit are obtained where there are higher values of K_s , so as s.d. increases, there are more positive residuals within the catchment. Also worth noting, is the increase in near zero residuals, in the wettest timesteps compared to the driest for each event, particularly for event 3. This indicates that for the wetter timesteps, the difference between the lumped and random parameterisations, and hence the effect of spatial variability, is reduced, possibly because for wetter timesteps, rainfall intensity

becomes the dominant factor. For event 3, the random and lumped soil moisture deficits appear to correspond closely at the vastly expanded riparian area that this event generates, resulting in zero or near zero residuals here.

Event 1
Dry

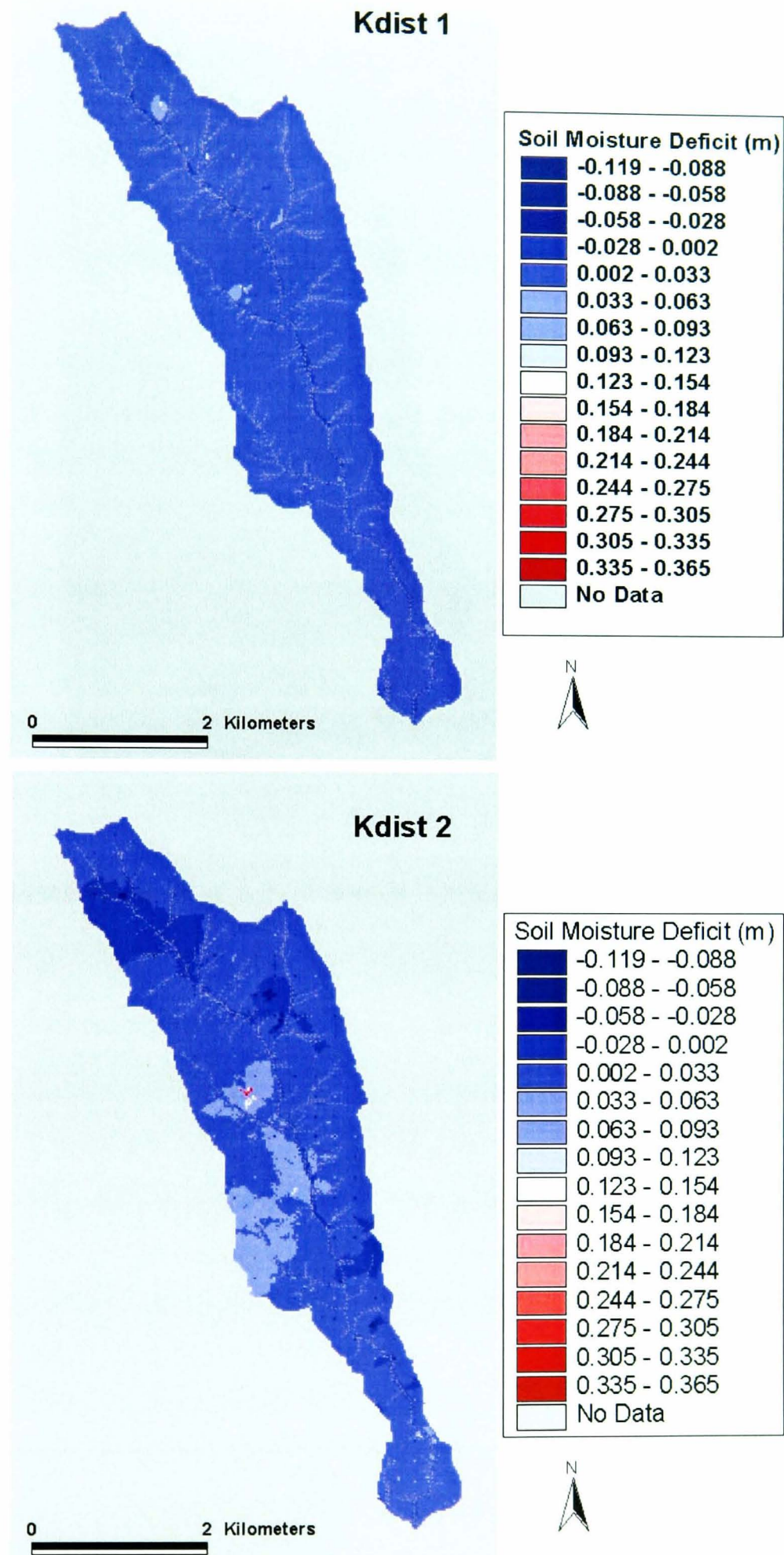


Fig. 7.8 Spatial distribution of residual soil moisture deficit (random - lumped) for the *driest* timestep for event 1.

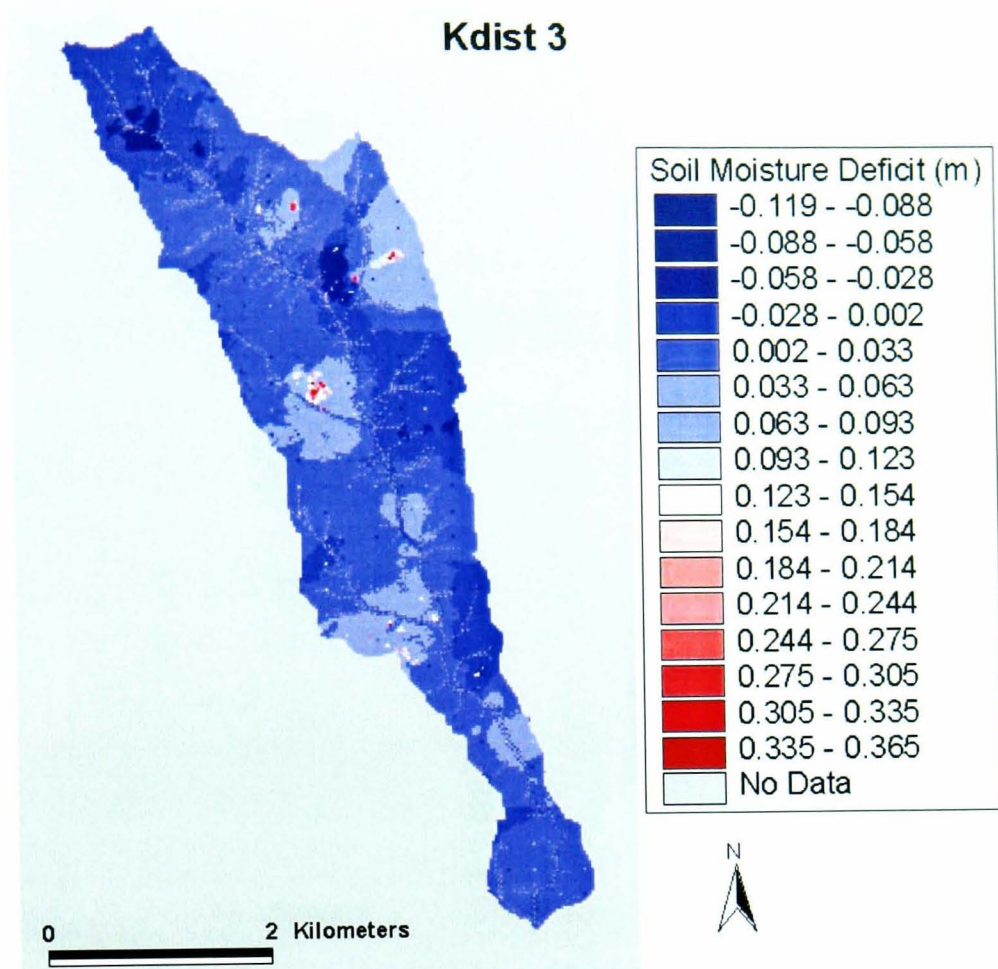


Fig. 7.8 cont'd Spatial distribution of residual soil moisture deficit (random - lumped) for the *driest* timestep for event 1.

Event 1
Wet

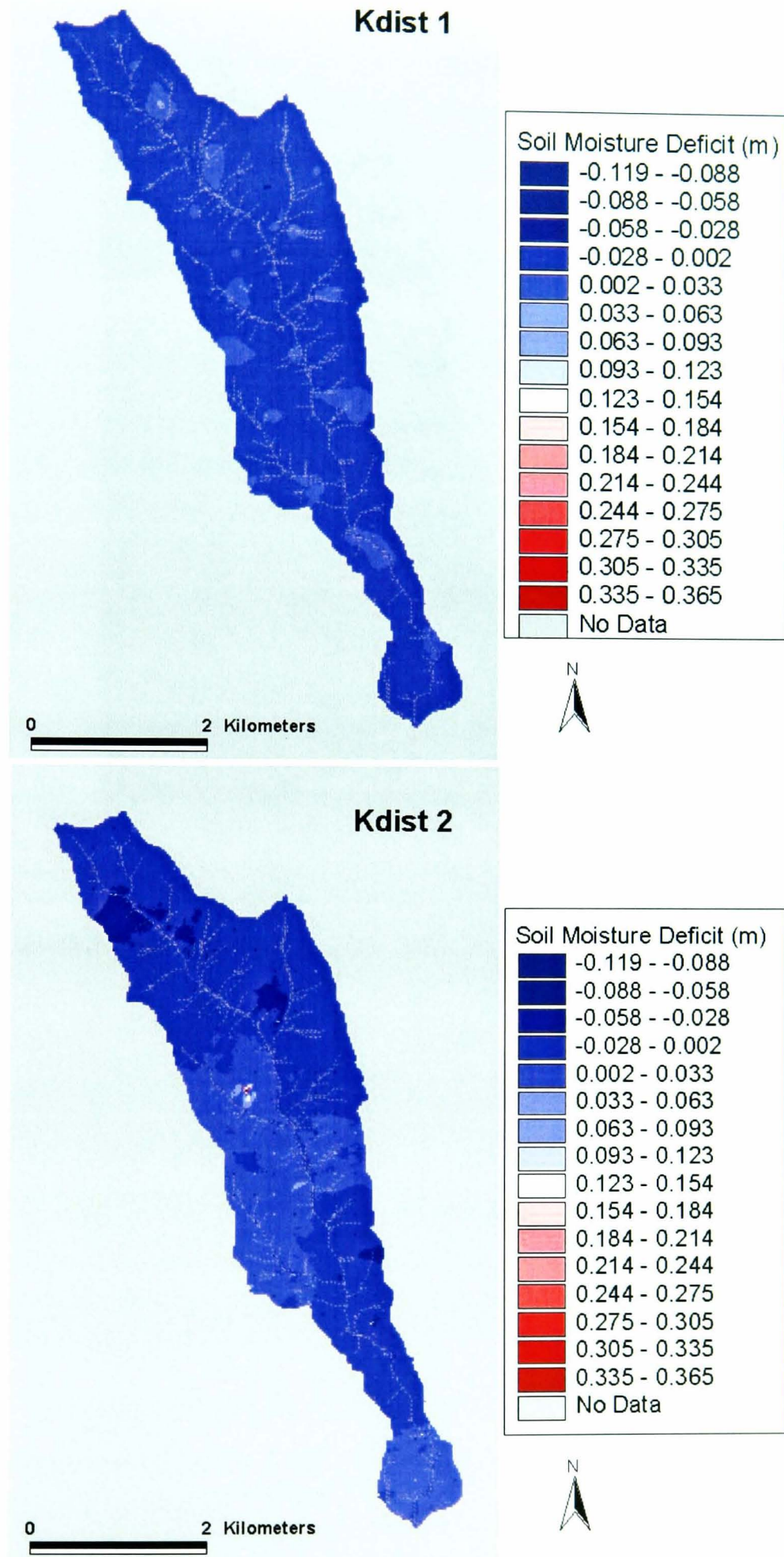


Fig. 7.9 Spatial distribution of residual soil moisture deficit (random – lumped) for the *wettest* timestep for event 1.

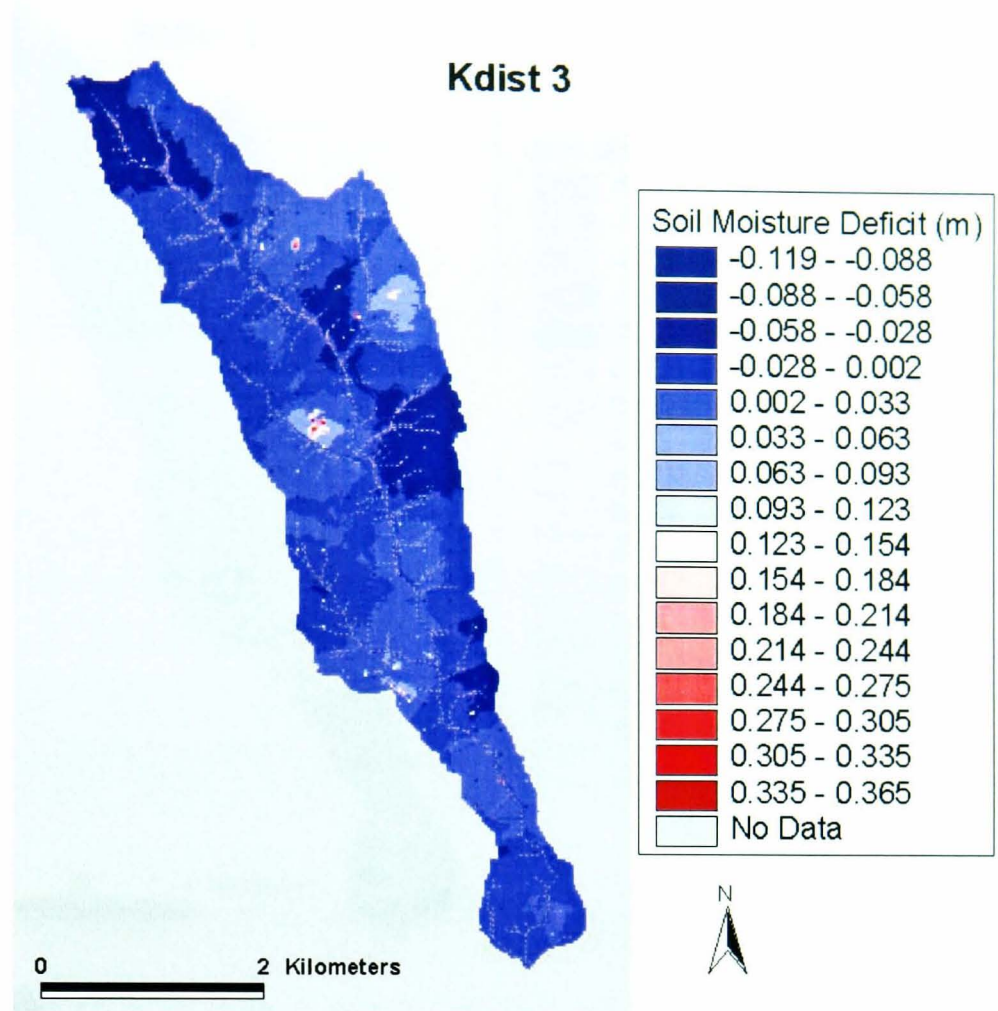


Fig. 7.9 cont'd Spatial distribution of residual soil moisture deficit (random – lumped) for the *wettest* timestep for event 1.

Event 2
Dry

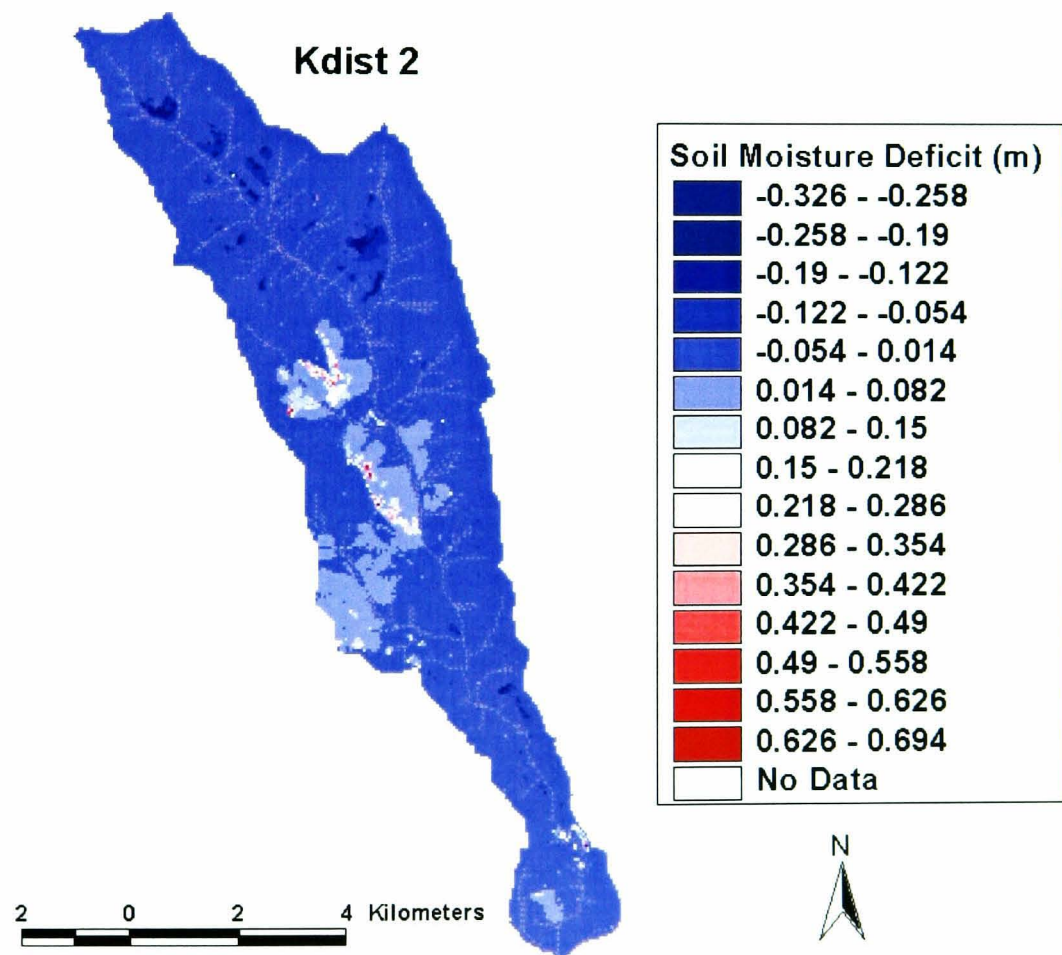
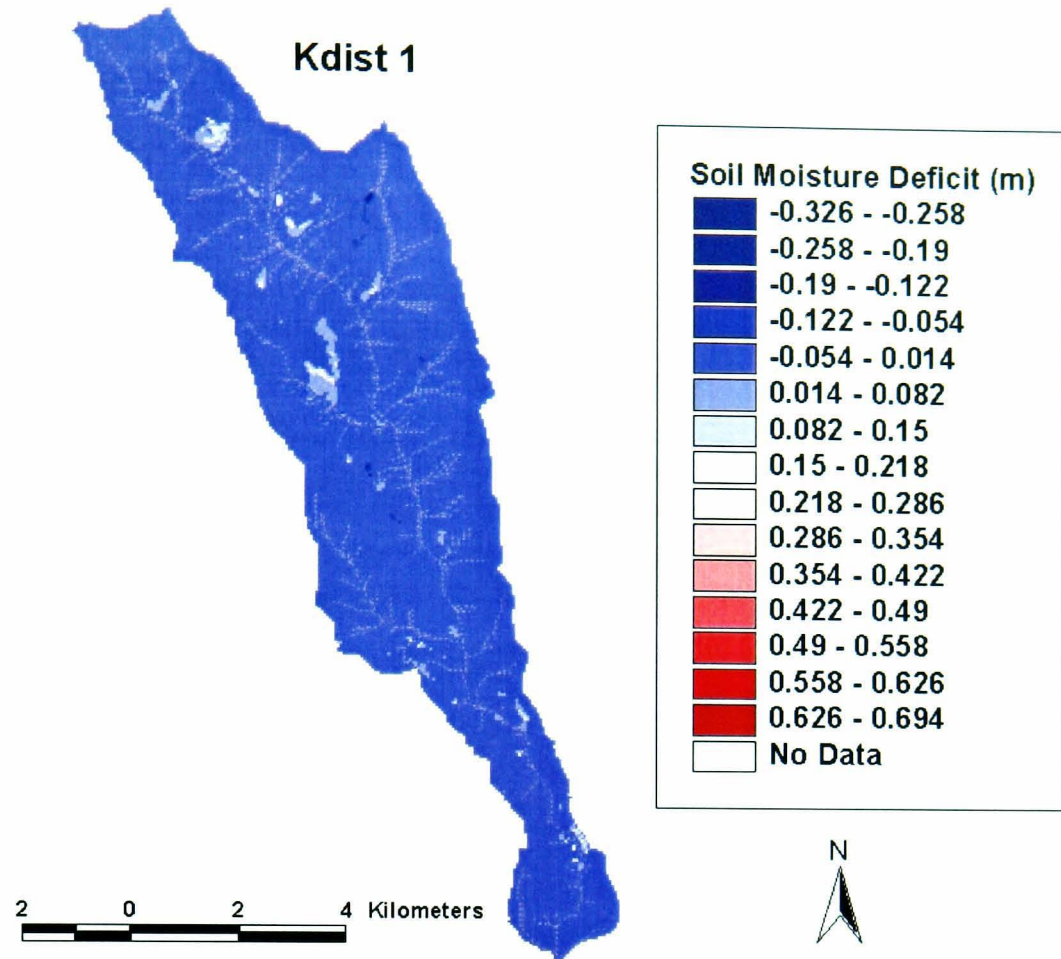


Fig 7.10 Spatial distribution of the residual soil moisture deficit for different random K distributions, at the *driest* timestep – event 2.

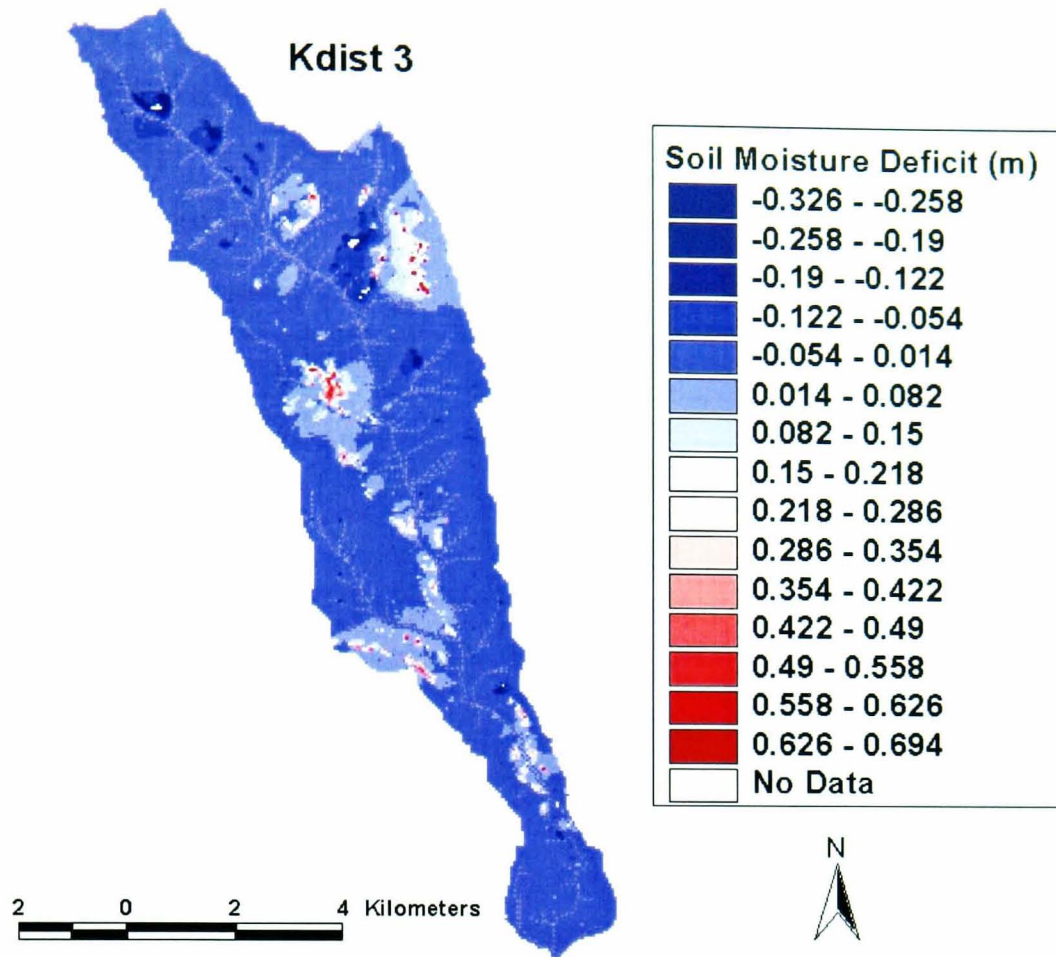


Fig 7.10 cont'd Spatial distribution of the residual soil moisture deficit for different random K distributions, at the *driest* timestep – event 2.

Event 2
Wet

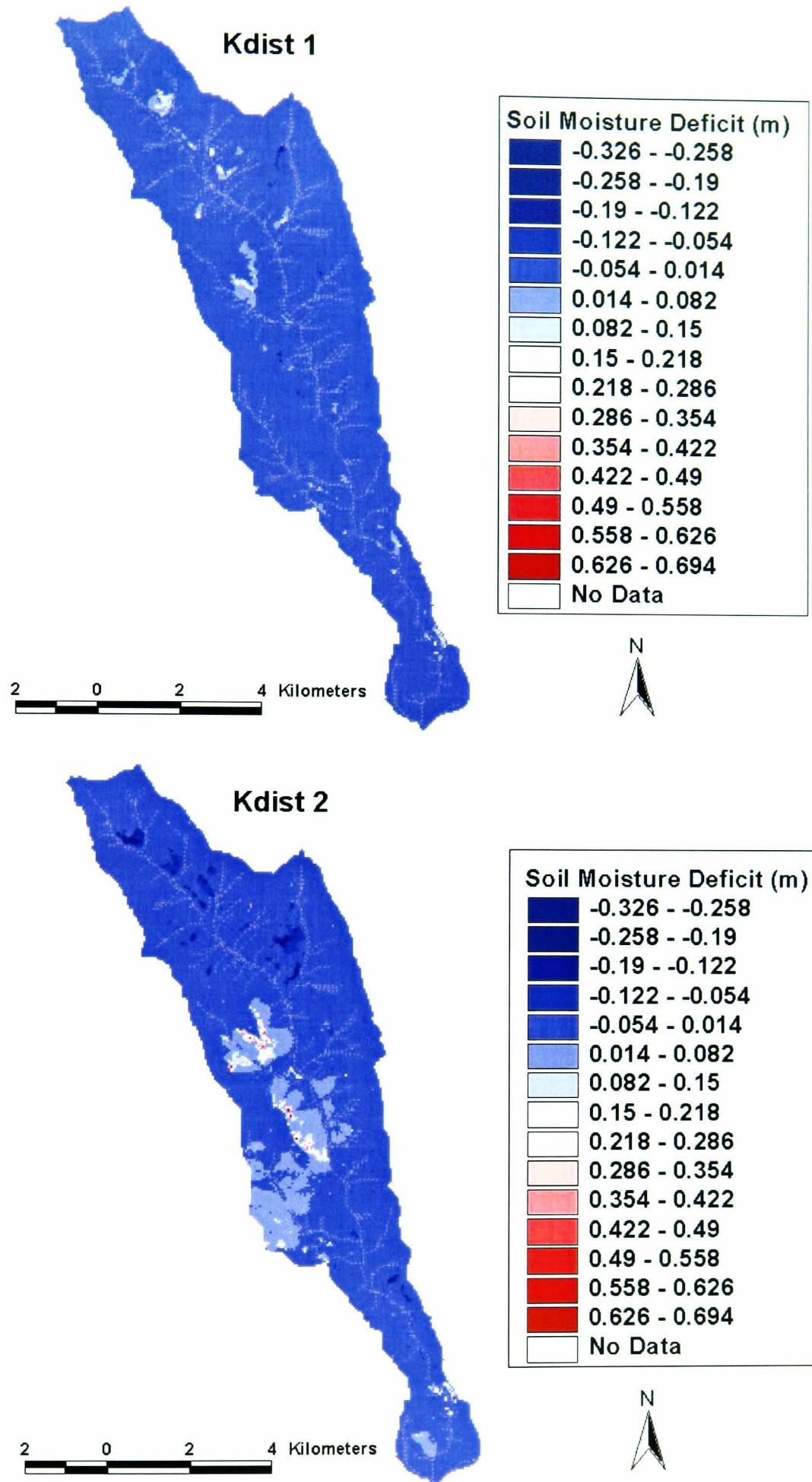


Fig 7.11 Spatial distribution of the residual soil moisture for different random K distributions, at the *wettest* timestep – Event 2.

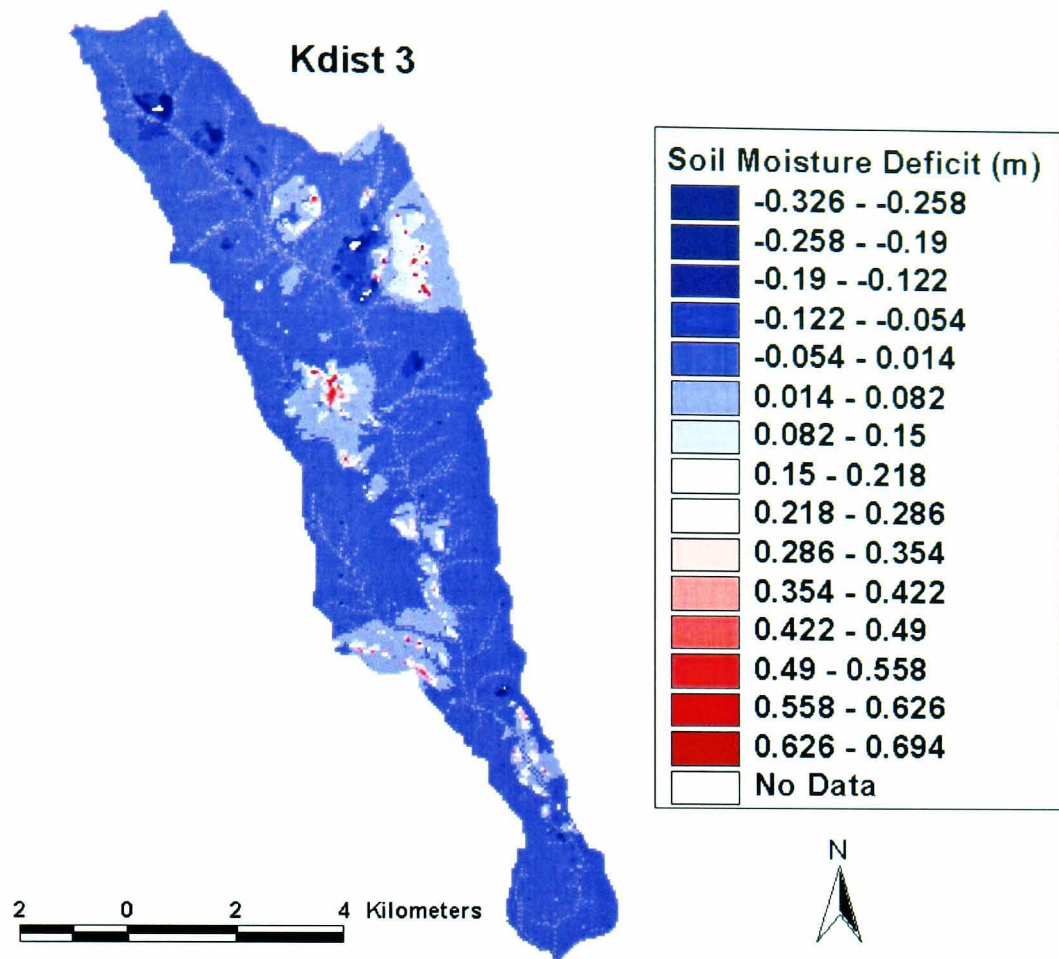


Fig 7.11 cont'd Spatial distribution of the residual soil moisture for different random K distributions, at the *wettest* timestep – Event 2.

Event 3
Dry

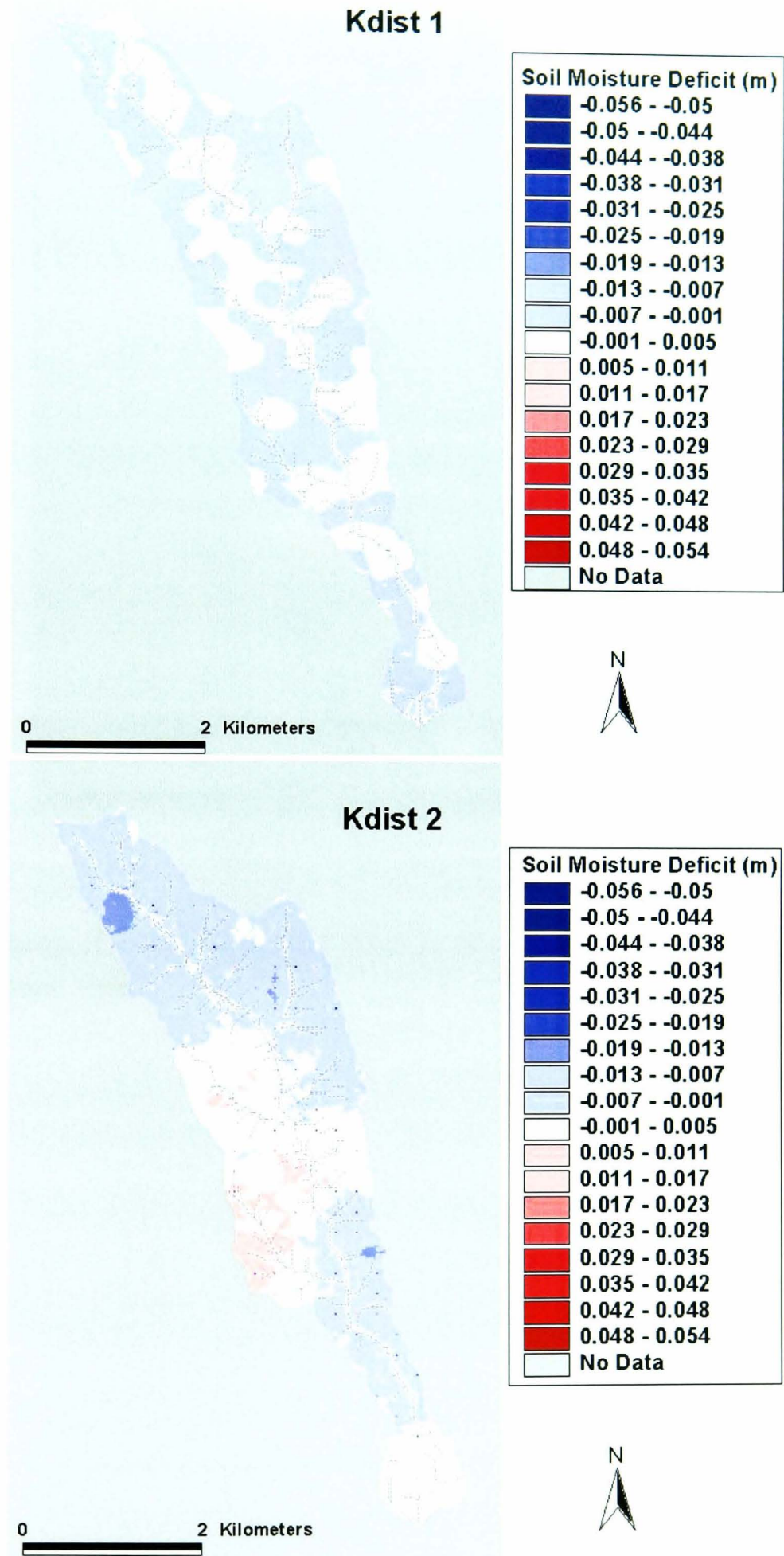


Fig. 7.12 cont'd Spatial distribution of residual soil moisture deficit for the *driest* timestep for the different random K parameterisations - event 3.

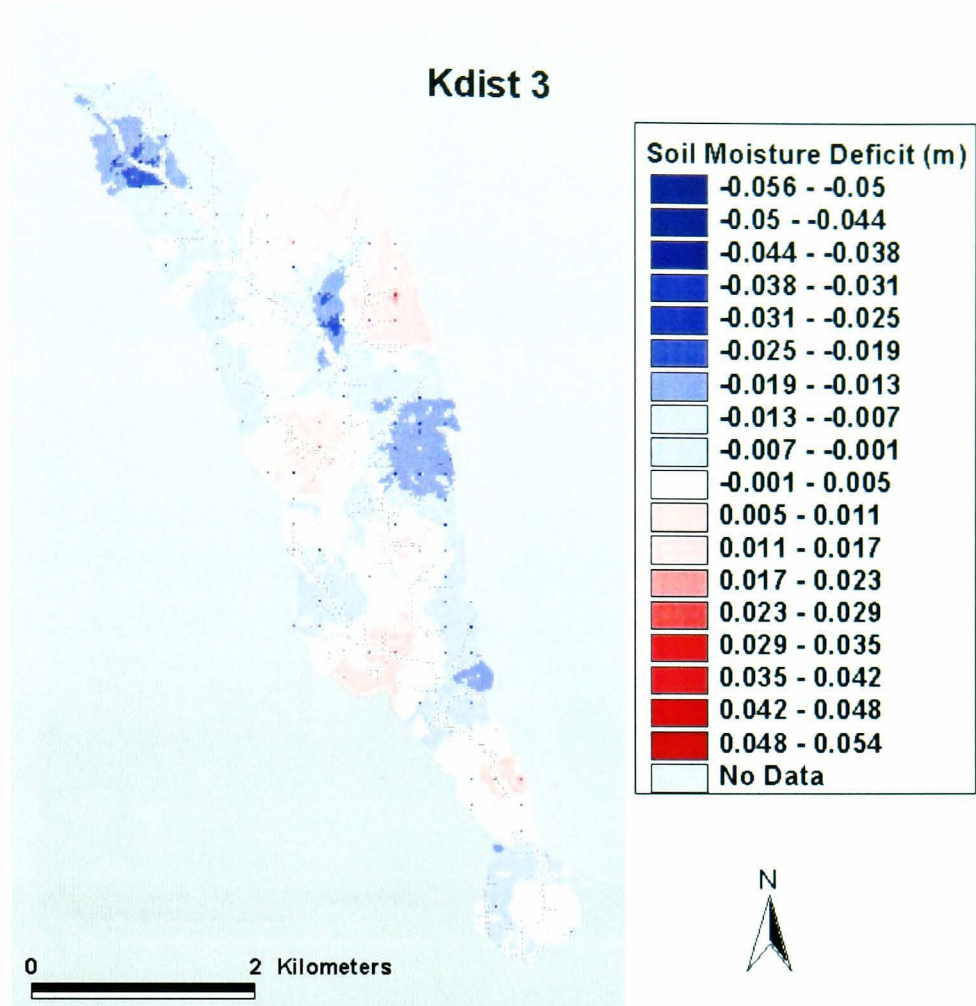


Fig. 7.12 Spatial distribution of residual soil moisture deficit for the *driest* timestep for the different random K parameterisations - event 3.

Event 3
Wet

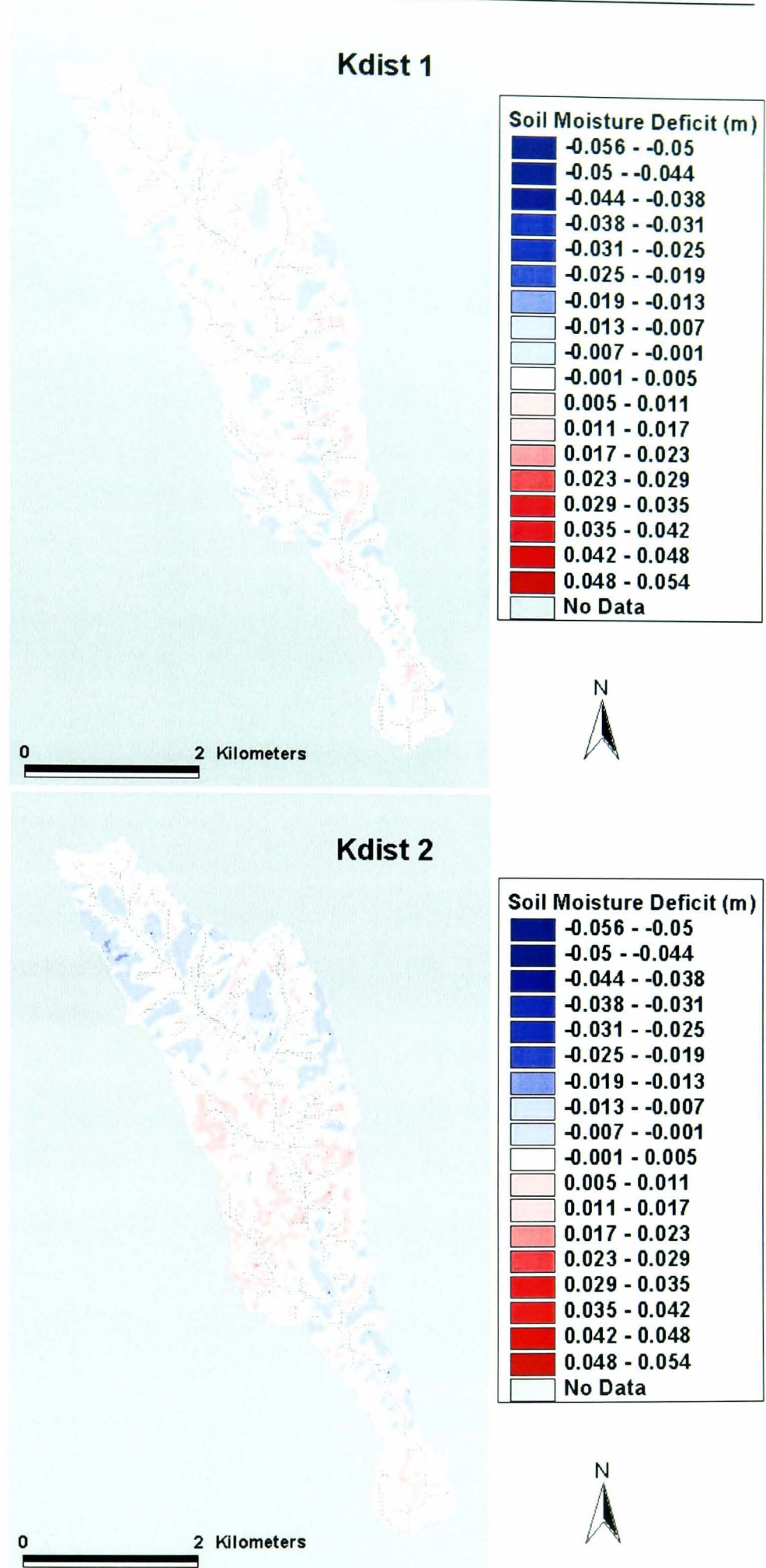


Fig. 7.13 Spatial distribution of residual soil moisture deficit for the *wettest* timestep for the different random K parameterisations – event 3.

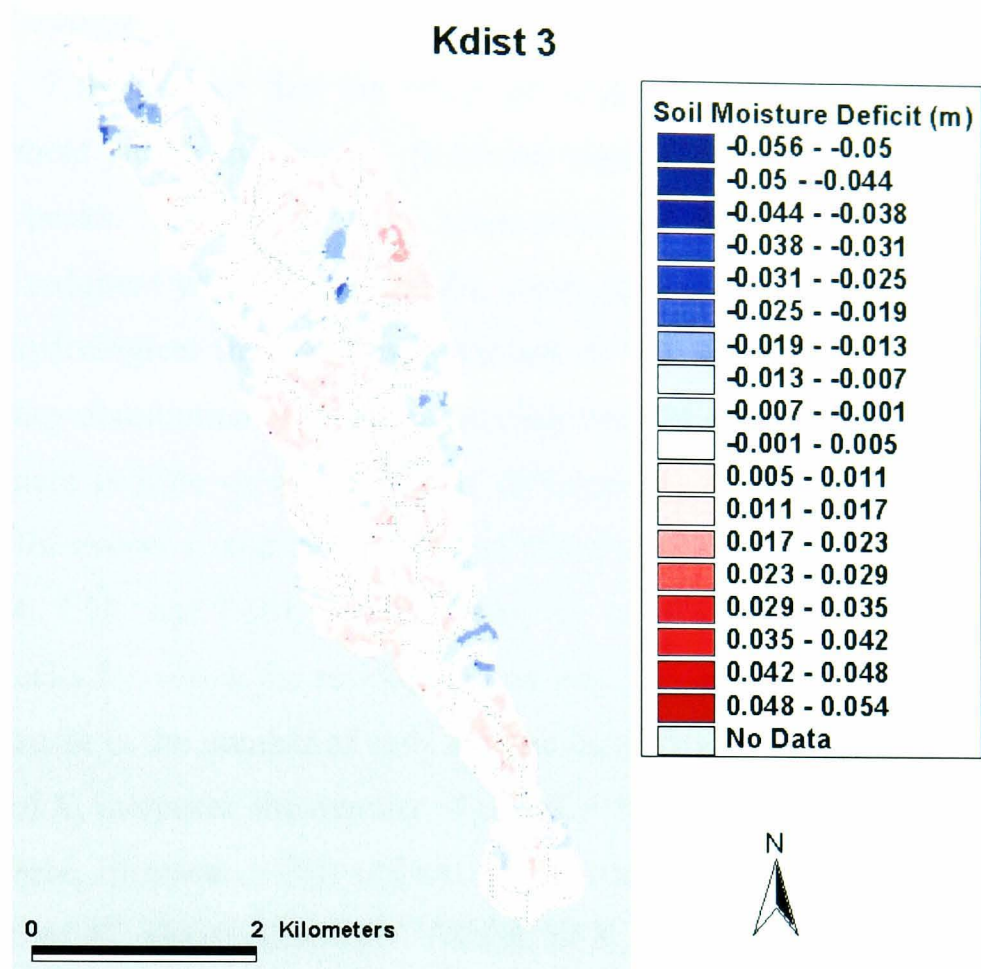


Fig. 7.13 cont'd Spatial distribution of residual soil moisture deficit for the *wettest* timestep for the different random K parameterisations – event 3.

Sedimentological Response

Figures 7.5b, 7.6b, 7.7b indicate that the effect of randomly variable K_s is more significant for sediment yield calculations. Sediment yield increases with s.d of K_s , particularly at the peaks. This reflects the propagation of model error from the hydrological to the sediment yield model, and the manifestation of errors that are not significant to the hydrological model output, but are, to the sediment yield model output. The frequency distribution of residual sediment depth (Figures 7.5d, 7.6d, and 7.7d) shows that there is little or no variability in frequency for different random distributions of K_s for events 1, and 2. The spatial distributions of residual sediment depth (Figures 7.14, 7.15, and 7.16), confirms that, for events 1 and 2, there are a limited number of cells for which the residual is non-zero, located along the channel network, but an increase in the number of cells is more discernible for event 2. It also reveals that, as s.d of K_s increases, the number of cells for which the residual sediment depth is less than zero, increases. This reflects the increase in soil moisture deficit with increasing s.d. of K_s , observed earlier. As s.d. of K_s increases, and infiltration rates decrease, more overland runoff occurs, removing more sediment. Hence the depth of sediment left is lower than for the lumped distribution, resulting in a negative residual. In addition, the largest residuals occur in the riparian areas next to the channel network, the most active sediment sources within the catchment, and hence the most sensitive to the spatial variability of K_s .

Fig. 7.7d shows that for event 3, the frequency distribution for Kdist1 peaks at -40×10^{-6} m, and at 4×10^{-6} m, while that for Kdist2 peaks at -10×10^{-6} m and 4×10^{-6} m, and Kdist 3, at -10×10^{-6} m. For event 3, the spatial distribution of residual sediment depth has near-zero values in channel and riparian areas, but non-zero values on the hillslopes, for all K_s distributions, with a decrease in residual with increase in s.d of K_s . This trend is the reverse of that observed for events 1 and 2, and is perhaps due to the magnitude of the event, and the dominant control of rainfall on the hydrological response, rather than hydraulic conductivity. High intensity rainfall would result in runoff from the expanded contributing area irrespective of the value of the saturated hydraulic conductivity, resulting in residual soil moisture deficit of zero. Thus the predicted sediment removed from these cells is likely to be the same for both the random and lumped models (i.e. all sediment is removed under these conditions).

Event 1

Fig.7.14 Spatial distribution of residual sediment depth for $T=343$ for event 1, for the three different random parameterisations of K .

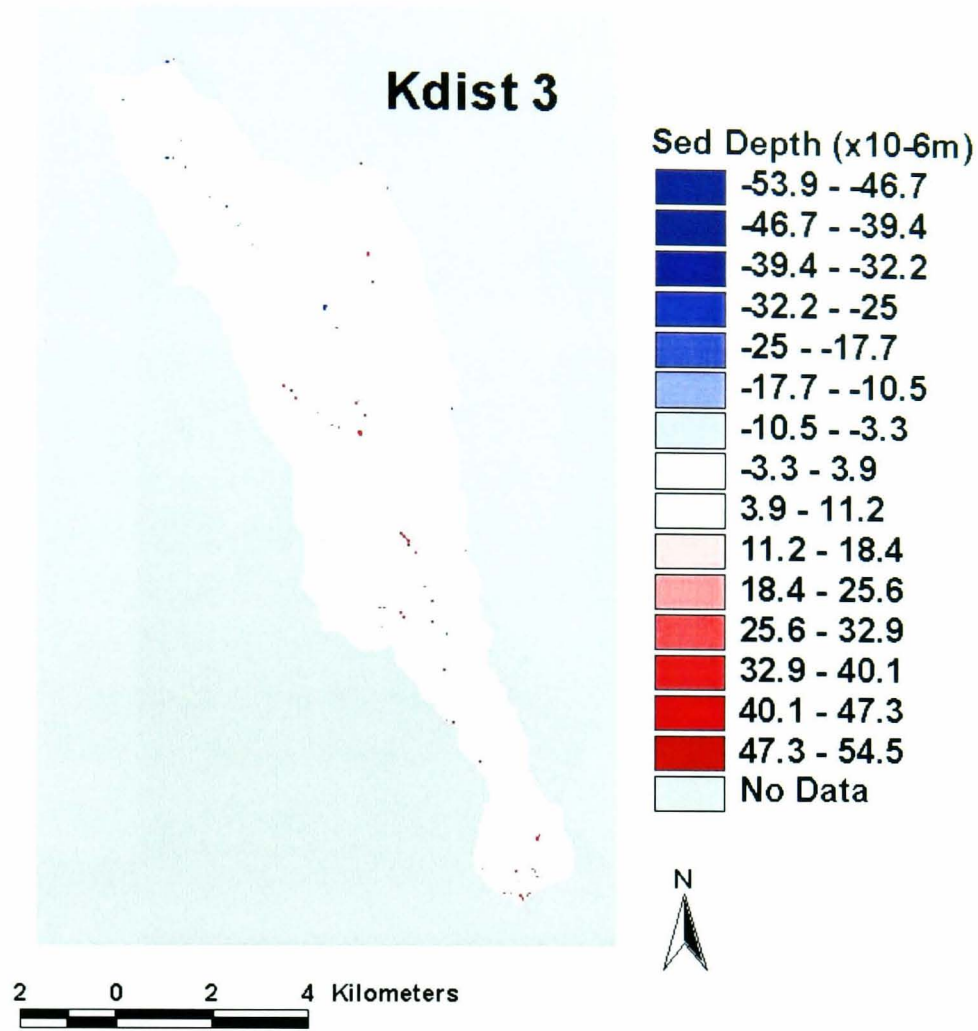


Fig.7.14 cont'd Spatial distribution of residual sediment depth for T=343 for event 1, for the three different random parameterisations of K.

Event 2



Fig.7.15 Spatial distribution of residual sediment for $T=196$ for event 2, for the three different random parameterisations of K

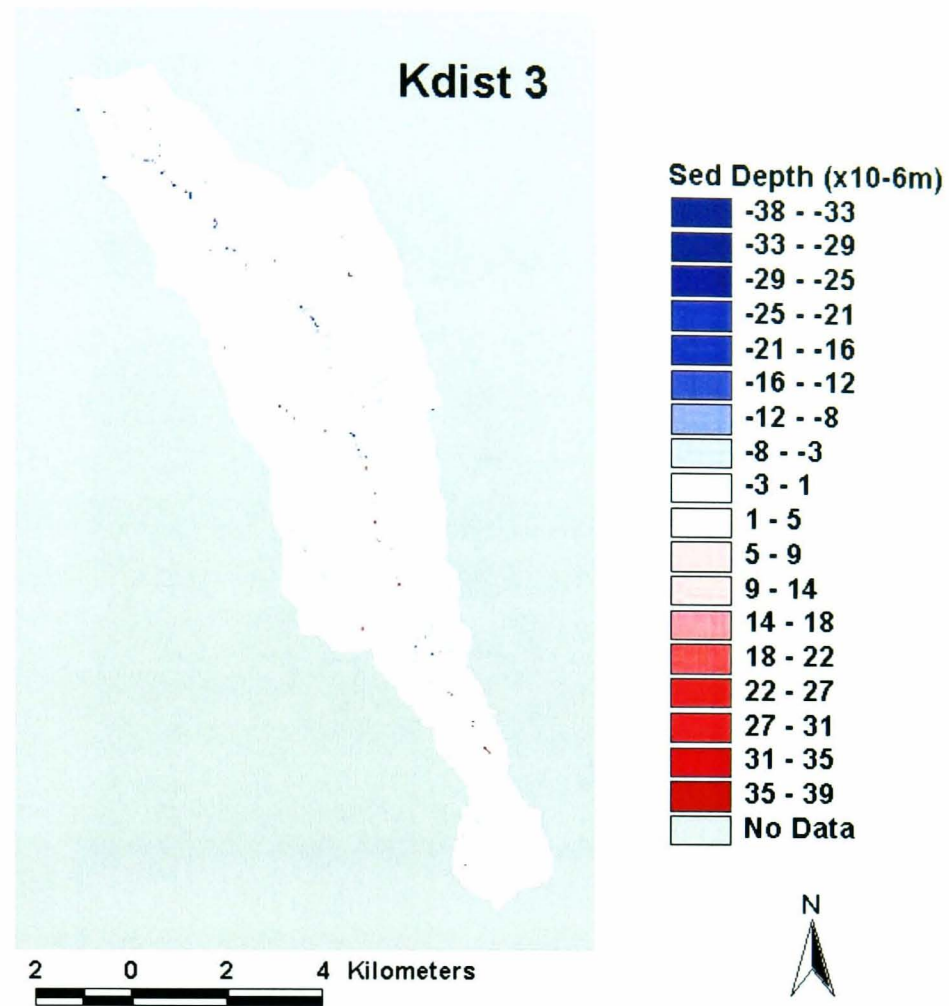


Fig.7.15 cont'd Spatial distribution of residual sediment for T=196 for event 2, for the three different random parameterisations of K

Event 3

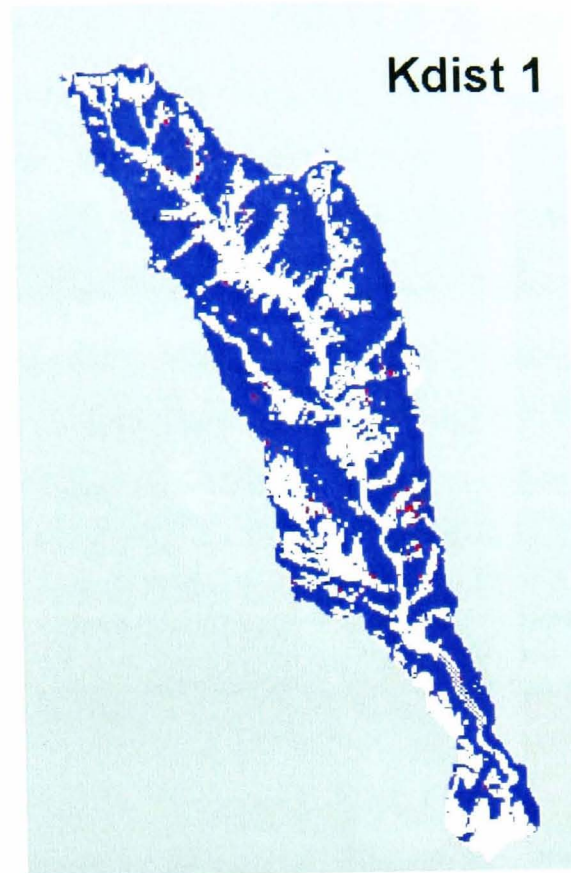


Fig.7.16 Spatial distribution of residual sediment depth for $T=248$ for event 3, for the three different random parameterisations of K

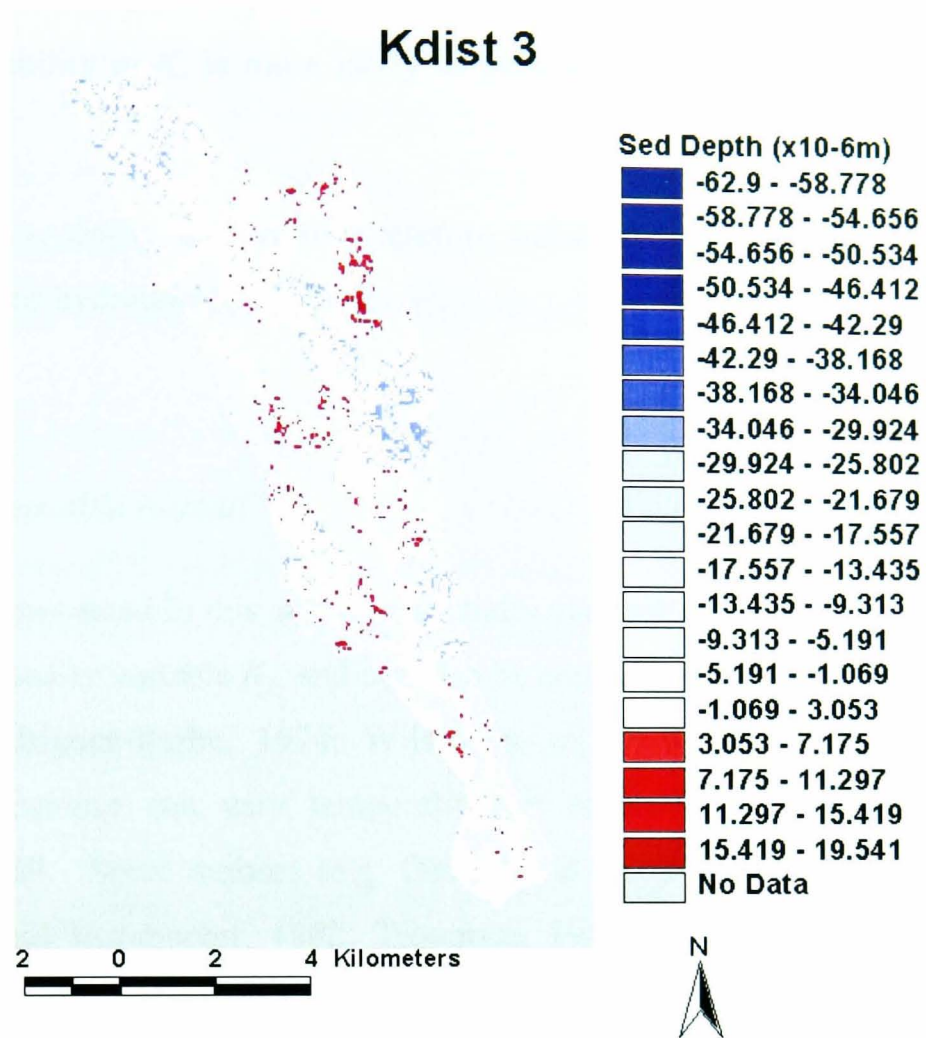


Fig.7.16 cont'd Spatial distribution of residual sediment depth for T=248 for event 3, for the three different random parameterisations of K

The difference in sediment depth are, therefore, more likely to be on the hillslopes where the variability in K_s is more likely to have an effect on predicted runoff and sediment yield.

The temporal variability in rainfall, therefore influences the effect of the spatially variable saturated hydraulic conductivity.

Stochastically variable rainfall

Although not considered in this analysis, spatially variable rainfall, can also influence the effect of spatially variable K_s , and can also be considered a stochastic process (e.g. Mejia and Rodriguez-Iturbe, 1974; Wilson *et. al.* 1979). In some catchments, hydrological response can vary temporally due to the spatial variability of the incoming rainfall. Some authors (e.g. Dawdy and Bergman, 1969; Wilson *et. al.*, 1979; Beven and Hornberger, 1982; Troutman, 1983; Corradini and Singh, 1985; Krajewski *et. al.*, 1991; Seliga *et. al.*, 1992; Obled *et. al.*, 1994) have suggested that natural catchments may show a strong sensitivity to rainfall pattern, and although largely based on numerical experiments, they have shown that temporally and spatially variable rainfall inputs can influence the timing of the simulated basin response and the magnitude of the peak. Surkan (1974) suggests that the sensitivity of peak flow and average flow rates, is maximised when the speed of the storm is comparable with or equal to the average channel flow speed. Similarly, if rainfall is in phase with the runoff generation of a grid cell, the runoff process is reinforced for that grid cell, but not for grid cells that are not in phase with rainfall. Spatially variable rainfall tends to have variable correlation distances, and may also be correlated in time (e.g. Onof and Wheater, 1996). Hence, it is expected that both the spatial and temporal variability of rainfall would result in variability in the hydrological and sedimentological response of the catchment.

7.4 Conclusion

The chapter examined the effect of the random spatial variability of saturated hydraulic conductivity on catchment temporal and spatial hydrological and sedimentological response. The results show that randomly distributing the 'optimised' saturated hydraulic conductivity of the lumped parameterisation, has little effect on the predicted hydrographs. However, the spatial variability in soil moisture deficit, which controls saturation overland flow generation, increases with increasing variability in K_s , indicating that the effects may be localised. This variability in overland flow resulted in variability in the sediment yield, mainly along the channel network where the main sediment sources are located. For the wetter periods of the hydrograph and for larger events, rainfall intensity becomes the dominant control on runoff generation and sediment removal, thus masking the effect of the spatial variability of saturated hydraulic conductivity.

The analysis presented here has a number of limitations including the limited extent of the spatial variability considered, and the exclusion of possibly important spatially variable rainfall. In addition, as has been the case for all of the spatial results presented throughout the thesis, validation of spatial results is not possible because of a lack of data. This is a problem that continues to plague distributed modelling, and although attempts are being made to fill this data need (e.g using remote sensed data), the accessibility, scale and reliability of such data remain problems. However, the results clearly show that random variability of saturated hydraulic conductivity may result in localised variability in hydrological and sedimentological response, which may have considerable consequences for localised flooding and soil erosion. It also demonstrates that the representative elementary area concept may be valid for this catchment, hence it is the statistical ensemble of variability in saturated hydraulic conductivity that dominates the response of the catchment.

CHAPTER 8 - Discussion

8.1 Introduction

Despite the stated advantages that physically-based fully distributed models were expected to provide to model parameterisation, very few models reported in the literature have been applied using parameter values measured or estimated *a priori* (e.g. Beven *et. al.*, 1984; Parkin *et. al.*, 1996; Refsgaard and Knudsen, 1996; Loague and Kyriakidis, 1997). The limitations of both model structures and the data available on parameter values, initial conditions and boundary conditions generally make it difficult to apply a hydrological model without some form of calibration.

Traditional methods of model calibration assume an optimum parameter set and ignore the estimation of predictive uncertainty. Such methods range from simple trial and error, with parameter values adjusted by the user, to the variety of automatic optimisation methods such as hill-climbing techniques, simulated annealing and genetic algorithms (Press *et. al.*, 1992; Sen and Stoffa, 1995; Sorooshian and Gupta, 1995).

Hill-climbing techniques, examples of which include the Rosenbrock method (Rosenbrock, 1960) and the Simplex method (Nelder and Mead, 1965), have been an important area of research since the start of computer modelling in the 1960s. They predict the local gradient of the response surface so that the algorithm knows in which direction to climb, and are therefore most effective when a smooth response surface is obtained. However, while many hydrological models give smooth response surfaces, it becomes more difficult to evaluate or visualise the full shape of the surface as the number of parameters increases.

Several techniques have been applied to the calibration process to surmount the problems associated with complex response surfaces. Simulated annealing and Genetic algorithms, both use randomly distributed sets of parameters in the parameter space to find an optimum state with respect to the performance measure of the optimisation problem. The essence of simulated annealing is that it creates a rule for

the acceptance of new parameter sets. Given a starting parameter set, one or more parameter values are adjusted and the acceptance or rejection of the new parameter set is determined by evaluating the new performance measure relative to the previous performance measure. Successively worse parameter sets may still be accepted, with a probability based on an exponential function of the difference in the performance measure value scaled by a factor, to ensure that the algorithm does not get trapped by a local optimum (see Thyer *et. al.*, 1999; and Kuczera and Parent, 1998). Genetic algorithm (GA) methods also ensure a global optimum is always found. A random population of different parameter sets is chosen as a starting point and then allowed to ‘evolve’ over successive generations or iterations until a global optimum fitness is reached. The algorithms differ in the operations used to evolve the population at each iteration, which include selection, cross-over and mutation (see Davis, 1991; Wang, 1991; Duan *et. al.*, 1992; Forrest, 1993; Sen and Soffa, 1995; Kuczera, 1997; and Franchini and Galeati, 1997).

The automatic optimisation techniques described above are designed to find an optimum parameter set as efficiently as possible. Set theoretic methods based on Monte Carlo simulation suggest, however, that the idea of an optimum parameter set might be illusory, and would be better replaced by a concept of equifinality allowing for the existence of many different acceptable model structures or parameter sets. Set theoretical methods based on Monte Carlo simulation, have been applied in a number of water quality modelling studies (e.g. Klepper *et. al.*, 1991; Rose *et. al.*, 1991; van Straten and Keesman, 1991).

The GLUE methodology provides another way of recognising the possible equifinality of models and parameter sets, and can be used to establish the degree of reliability afforded to different models or parameter sets. The ‘optimum’, given some data for calibration, will have the highest degrees of belief associated with it but there may be many that are almost as good. In most applications of GLUE in rainfall-runoff modelling (Beven and Binley, 1992; Beven, 1993; Romanowicz *et. al.*, 1994; Freer *et. al.*, 1996; Seibert, 1997; Franks *et. al.*, 1998, Dunn *et. al.*, 1999, Cameron *et. al.*, 1999 and Uhlenbrook *et. al.*, 1999) likelihood measures and uncertainty limits have been calculated using observed catchment discharges. In addition, many of

these studies use Bayesian updating to refine uncertainty bounds as more data becomes available.

It could be argued that the GLUE methodology provides the most expedient method to incorporate all available data, and by extension, provides a multiple model approach to prediction, and thus the most exhaustive approach to operational forecasting. However, to what extent has the GLUE approach progressed hydrological modelling, the aim of which is to find the perfect model? To what extent is the identifiability problem an inevitable consequence of modelling non-linear open systems with unknowable spatial and temporally variability? It could be argued that hillslope hydrology has made few conceptual advances since the Variable Saturated Area (VSA) concept, and much of the research has emphasised unique conditions pertinent to a particular catchment without extension to wider theory. There is a danger, that GLUE lets us circumvent some of these difficult issues by permitting a very relativist approach to model application.

8.2 Contribution to the GLUE methodology

The analysis and results presented in this thesis takes the GLUE methodology a number of steps further. First, it has been shown that different events will have different behavioural parameter sets, which may not be applicable to all events. In Chapters 5 and 6 very different behavioural parameter sets were obtained for the calibration event (event 1) and the second validation event (event 3) indicating that the dominant processes were different for the two events. For event 3, the largest of the three events, the more extensive coupling of channel and hillslope cells in the expansion of the saturation zone onto the hillslopes was reflected in the higher channel flow rate, higher infiltration rate and shallower soil depth parameter. While the refinement of behavioural parameter sets during Bayesian updating can be used to take account of the empirical bias of traditional model assessment methods, and provides a means for additional data to be dynamically incorporated, the objective is still to find one group of behavioural parameter sets that would be applicable to all events. However, different events having behavioural parameter sets that are in completely different parts of the parameter space to those derived for the calibration may result in expanded uncertainty bounds when used in Bayesian updating, which may be seen as a failure to constrain the model uncertainty. This suggests that model

equifinality may be taken to the next level, whereby different events occurring in the same catchment may be described by very different groups of behavioural parameter sets. Thus rather than attempting to derive one set of behavioural parameter sets to describe all events, the model calibration process should be geared towards finding different groups of behavioural parameter sets for several different calibration periods which represent the spectrum of events which may occur in the catchment. Model validation would therefore involve an assessment of the type of event under examination, and then a choice of the appropriate group of parameter sets.

Second, most GLUE studies have used discharge data in Bayesian updating with varying degrees of success. The use of discharge data to update calibration period discharge predictions may, however, result in errors due to auto-correlation, as residuals in the new event may be dependent on those of the calibration event. Franks *et. al.*, 1998, however, used some ground based estimates of saturated area for a small part of the Naizin catchment in Brittany, France together with the map of the TOPMODEL index and satellite radar data, to estimate the catchment-wide extent of saturation which was then used as additional information to constrain the model predictions of discharge. They showed that with the addition of this information there was some reduction in uncertainty in discharge predictions and that this was mostly a result of a dramatically reduced feasible range for the effective transmissivity parameter. In their study, the incorporation of the additional information allows the rejection of many of the model parameter sets that, based on fitting discharge observations alone, had previously been considered acceptable. Lamb *et. al.*, 1998, also examined the prediction of the spatially distributed piezometer data which were available for five different discharges. They found that the prediction bounds based on discharges and recording borehole measurements were much narrower than those based on the piezometer data. Beven (2000) suggests that either the model dynamics could not adequately reproduce the pattern of water tables in the catchment, or that local soil heterogeneity was not adequately represented by catchment-scale parameters. These findings suggest that the use of internal state data may require additional local parameter values, and that such local data may not have great value in conditioning the prediction bounds for the catchment discharge.

The above are all applications using spatially distributed data, subject to important scaling issues. A different, catchment scale approach, could involve a multi-criterion analysis using hydrograph separation techniques used to identify flow path end members. This scale of data is similar to the sediment yield data used here, but is clearly more directly related to the hydrological model. Catchment scale hydrograph separation techniques such as that reported by Sklash and Farvolden (1979) have been used to study flow paths and have the advantage that the isotopes used (oxygen and hydrogen) are part of the water molecule and will therefore follow the flow pathways of water in the catchment directly. However, interpretation of the results remain difficult due to spatial and temporal variations in concentrations, and the spatial variability of concentrations of water stored in different soil horizons and parts of the catchment. However, in ideal conditions when there is a strong difference between the concentrations observed in rainfall and the concentrations of water stored in the catchment before an event, the measured concentrations can be used in a simple two-component mixing model to differentiate between the contribution to the hydrograph for an event of the rainfall and the contribution of the water stored in the catchment prior to the event. The technique can be extended by using other environmental tracers to three-component mixing to differentiate rainfall contribution from ‘soil water’ and ‘deep-groundwater’ components, where these components can be differentiated geo-chemically (e.g. Bazemore *et. al.*, 1994).

As an alternative to internal hydrological state variables, the analysis presented here develops a method incorporating the predictions of a secondary sediment model, to update and examine the uncertainty in primary discharge predictions. This type of analysis, based on closely coupled models is becoming more significant as predictive demands extend to secondary processes within the catchment system, including soil erosion and pollutant transport, which depend on the hydrological regime. The analyses in Chapters 5, 6 and 7 demonstrated the dependence of the sediment yield model on accurate hydrological predictions, and the increased sensitivity of sediment yield predictions. Hence there are less hydrological parameter sets that are behavioural for both the hydrological model and sediment yield model, than are behavioural for the hydrological model alone, resulting in narrower uncertainty limits (see sections 5.5.1 and 6.7). In addition, the analysis showed that there were large errors propagated from the hydrological model to the sediment yield. For all

parameterisations, uncertainty bounds in the sediment yield due to hydrological model uncertainty were as wide as uncertainty bounds due to variability of the sediment model parameters alone for some of the events considered (section 5.5.2 and 6.8). This will also be true of coupled rainfall-runoff models, which traditionally make no attempt to account for the uncertainty of the rainfall model predictions before coupling to hydrological models. These findings demonstrate the importance of reducing the uncertainty in primary model predictions before use in secondary models, and the need to ensure that the parameter sets of the primary model are behavioural for both the primary and secondary models.

The use of additional empirical data, either from a second flow event, internal state variables, or secondary process, to constrain model uncertainty in this way raises some interesting issues about the modelling process in general. If we accept that the equifinality problem is endemic to environmental modelling, then an approach based in model falsification requires thoughtful and truly scientific strategies for defining hypotheses and data collection programmes for the most cost-effective refinement of the space of feasible models and parameter sets (Beven, 2000). In doing so, we run the risk of compromising what is accepted as a feasible model or parameter set since, given the approximate nature of environmental models, and rainfall-runoff models in particular, it will generally be the case that we could reject all models if we look at their predictions in enough detail (e.g. Mroczkowski *et. al.*, 1997). Despite the use of methods such as GLUE to take account of model equifinality, it has proven to be difficult to bracket all the discharge and sediment yield observations. This is, in part, a result of data limitations as well as model structural limitations, but it also points to the fact that despite improvements in model calibration techniques, rainfall-runoff modelling is still largely dependent on the accuracy of observed data due to the fact that even the most physically-based models still require calibration.

The results have also shown that model predictive uncertainty can be reduced with increased in the representation of the spatial variability of soil hydraulic parameters. However, the limited increase in parameter spatial variability afforded by landuse and soil type parameterisations, given the scale at which these properties are mapped, coupled with our inability to validate catchment spatial because of a lack of sufficiently detailed measurements, means that completely random spatial

parameterisations could result in the same temporal variation in hydrological response, as that of any spatial parameterisation and even the lumped parameterisation (as shown in Chapter 7).

8.3 The way forward

The above discussion poses a number of questions about the traditional approaches to model calibration in general, and about the more recently developed GLUE methodology in particular.

The GLUE methodology has progressed the field of hydrological modelling by identifying model equifinality as a major issue and providing a method to quantify the effect on model uncertainty. It also espouses the assessment of model uncertainty in modelling exercises – previously ignored or dealt with in only a cursory manner. This suggests therefore, that either the original goal of hydrological modelling, i.e., ‘to find the perfect model’, will have to change in recognition of the fact that our understanding of, and ability to measure, hydrological systems are real limitations to the achievement of this goal, or, we must develop our understanding of hydrological systems and our ability to measure them. While many areas of research are geared towards developing our understanding and measurement techniques, operational hydrology continues to need models that can be applied to the real world with current limited understanding and measurement techniques. Having recognised the existence of model equifinality, and as shown in this thesis, that such equifinality may be more far-reaching than originally thought, we must develop techniques that will allow us to make the best decisions given these limitations.

To this end a new framework for model calibration might usefully be developed to take account of the fact that different groups of behavioural parameter sets will be obtained for different events. Thus, the model could be conditioned on the range of events that have been observed in the study catchment. Subsequent application of the model will therefore require identification of the type of event to be simulated and the appropriate group of behavioural parameter sets to apply. This methodology can be further developed by automating the process of identifying the event type, by training the model to recognise the type of rainfall event, using properties like peak rainfall intensity, and duration.

It is important to recognise, however, that any improvement in model predictions will ultimately depend on the quality of the data used for input to the model and calibration. As seen here, predictive uncertainty can be reduced by spatially parameterising soil hydraulic parameters deterministically and perhaps even stochastically. However, it will be difficult to access any improvements in model spatial predictions without the measurements of spatial hydrological response at the appropriate scale.

While GLUE and similar uncertainty analysis methods have contributed to the wider agenda, increasingly this type of approach is critiqued for its negative and relativistic standpoint, which can be interpreted as accepting all possibilities and then post-processing the results in some probabilistic way. There are good reasons for this view, given the difficulties of establishing parameter values arising from the incommensurable scales in model structures, observations and physical processes. However, what is clear, is that GLUE methods have become popular at a time when process understanding in hydrology has more or less come to a standstill, and it could be argued that this more post-modern perspective reflects a crisis in scientific progress, as much as a measured perspective on dealing with model uncertainty. It may be that we are again at a critical threshold marking a division between approaches applicable to solving problems (operational research) and wider scientific research which seeks broader, less focused goals. The GLUE methodology provides a means to incorporate all data sets and all models as we seek the most inclusive analysis for reliability prediction. On the other hand, we must still strive to resolve the conflicting scales of our tools and the processes we study, seeking the next level of abstraction (beyond the VSA concept) that lies at the heart of dynamic catchment response.

Chapter 9 – Conclusion

The four main objectives of the thesis were:

1. To couple a fully distributed hydrological model to a dynamic, conceptual sediment yield model.
2. To examine the uncertainty in the fully-distributed hydrological model and the sediment yield model.
3. To examine the controls of spatially variable soil hydraulic parameters on hydrological and sedimentological response, and the effectiveness of spatially variable parameterisations in reducing model uncertainty.
4. To examine the propagation of uncertainty from the hydrological model to the sediment yield model.

9.1 Model coupling

A review of the literature on the sediment yield process revealed that catchment sediment yield is a relatively simple process, subsumed by complex spatially and temporally variable processes that control sediment availability, detachment and transport. The dynamic variability of sediment yield is primarily due to the spatio-temporal variability of runoff generation processes, which govern sediment availability, detachment, and transport. This natural coupling of runoff and sediment yield suggests that suspended sediment yield must be modelled as a coupled dynamic, spatially distributed hydrological-sediment yield model. The model developed in this thesis is a fully distributed model based on TOPMODEL (Beven and Kirkby, 1979), developed for unsteady state runoff, and snowmelt contribution to runoff, coupled to a sediment model which represents sediment yield as an availability- and transport-limited process, based on Moore and Clarke (1983) and Moore (1984). The hydrological model represents water fluxes on a cell-by-cell basis using a regular grid discretisation of the catchment, which also permits the representation of spatially variable soil hydraulic parameters. The relaxation of the steady state assumption of TOPMODEL allows for dynamic variation in the upslope contributing area and heterogeneous recharge, while the spatially-distributed snowmelt model developed

here represents seasonal melt contribution to runoff, which was found to be important in this catchment.

The hydrological model was explicitly coupled to the sediment yield model by allowing sediment accumulation on a grid cell once the cell was not producing runoff, and sediment removal in the timestep that the grid cell produced runoff.

9.2 Model Uncertainty

The results revealed significant model uncertainty in both the hydrological and sediment yield models. Hydrological model calibration and validation revealed that uncertainty bounds were widest at the peaks, but failed to effectively predict recession flows, similar to other applications of GLUE methodology to TOPMODEL (e.g. Beven and Binley, 1992; Lamb *et. al.*, 1998; Beven, 1993). Sediment model uncertainty bounds were also widest at the peaks and thinnest during recession. This reflects the uncertainty inherited from the hydrological model, as a wider band of behavioural peak flows predicted a wider band of behavioural peak sediment fluxes. In addition, uncertainty due to simplifying assumptions made about sediment removal and transport have contributed to uncertainty in sedigraphs. The combined uncertainty due to hydrological model uncertainty and sediment yield model uncertainty was reflected in lower model efficiencies and generally poorer qualitative sedigraph fit.

The model validation exercise (section 5.3.4) highlighted the potential dangers of assuming one ‘optimum’ parameter set derived from one calibration period, for all other events. The results showed that the calibrated ‘optimum’ parameter set was not ‘optimum’ for the validation periods, and was particularly dissimilar to the ‘best’ parameter set obtained for Event 3, which resulted in vastly different spatial and temporal hydrological response predictions. Thus models calibrated simply on a split-sample test are, at risk of incorrectly predicting local flooding and soil erosion when the calibrated ‘optimum’ parameter set is applied *carte blanche* to all events. However, calibrating and re-calibrating a model for every event will defeat the purpose of model calibration. One way forward may be to calibrate the model on several different events that represent the range of events, which have occurred in the catchment. Alternatively, different events can be used to update the calibrated model uncertainty.

9.3 The value of additional data

Additional flow and sediment flux data

As discussed in Chapter 1, model uncertainty resulting from an incomplete knowledge of a system can be reduced when additional data becomes available (Moore and Brewster, 1972; Beven and Binley, 1992; Franks and Beven, 1997; Lamb *et. al.*, 1998). Three different types of additional data have been used to update uncertainty in the hydrological model:

1. additional periods of observed streamflow data.
2. sediment yield predictions.
3. Spatially distributed soil hydraulic parameters by land use and soil type, and stochastic spatial parameterisation.

The analysis showed that the use of successive periods of discharge data to update uncertainty bounds, resulted in a reduction in the uncertainty in lumped hydrological predictions. Parameter cumulative distributions were significantly altered and uncertainty bounds successively constrained, as more periods of hydrological data were used. However, this decrease in the width of uncertainty bounds also resulted in increased predictive failure in the recession flow predictions. This is primarily because the reduction in the width of the uncertainty bounds due to parameter refinement was most discernible at the recession flow, where the initial bounds were thinnest. Lamb *et. al.* (1998) found a similar reduction in uncertainty when a second period of observed flow is added.

The use of the results of a secondary model to update uncertainty in the primary model has not been examined in depth before. In a successfully coupled model, the uncertainty from the primary model will be constrained by what is acceptable in the secondary model. That is, a secondary model response, which is more sensitive to hydrological model accuracy than the available observed hydrological response, will serve to constrain the range of behavioural simulations.

The use of sediment yield predictions to update hydrological model uncertainty resulted in a modification of parameter cumulative distributions, limiting the range of hydrological parameter values that were ‘behavioural’, and hence a reduction in hydrological model uncertainty.

The updated parameter cumulative distributions show that previously insensitive parameters for which all parameter values were equally likely, were restricted to critical values, or a smaller range of values, than was the case for distributions conditioned on flow data alone. The uncertainty in the hydrological model decreased when additionally conditioned on sediment flux for both of the likelihood measures considered. Again, the refinement of uncertainty bounds was mainly due to a shift in the lower limit to higher discharge values, and the reduction in hydrological model uncertainty, was accompanied by increased predictive failure of recession flows.

The analysis also examined the propagation of hydrological model uncertainty to the sediment yield model, as a result of direct model coupling. Propagation of hydrological model uncertainty to the sediment yield model was analysed by holding the sediment model parameters constant at the ‘optimum’ values and varying the hydrological parameters. The propagated uncertainty bounds are derived from likelihoods that were behavioural for both the hydrological and sediment yield models. Propagated uncertainty bounds as wide as or wider than those obtained for sediment model uncertainty alone, were obtained. This suggests that a wide range of hydrological parameter sets were found to be behavioural for the sediment yield model. Although the sediment yield model parameters are fixed at their ‘optimum’ values throughout the analysis, the propagated uncertainty can be seen to encompass both the parametric uncertainty of the sediment yield model and that of the hydrological model. This is because the derived ‘optimum’ sediment yield models are dependent on the accuracy of the hydrological model predictions, and therefore inherently carry some uncertainty attributable to them. Hence by holding these already uncertain ‘optimum’ values constant to determine the effect of variable hydrology on sediment model predictions, implies that there is a minimum level of uncertainty that can be expected in the predictions.

The uncertainty in the hydrological model may have serious implications for the secondary sediment yield model, which uses hydrological model predictions as a primary input, the spatial distribution of which is critical to sediment yield prediction. Thus the sediment yield model uncertainty, while due, in part, to uncertainty in the sediment model parameters and sediment model structure, is also partly due to uncertainty in the hydrological model predictions, particularly the spatial predictions.

It is, therefore, important to effectively reduce uncertainty in hydrological model spatial predictions, in order to get the most accurate predictions from the sediment yield model.

9.4 The value of spatially distributed data

Deterministic Spatial parameterisation

Representing heterogeneity in soil hydraulic parameters is another means of reducing uncertainty in hydrological model spatial and temporal predictions. The hydrological model calibration and validation results showed significant model sensitivity to the spatial variation in soil hydraulic properties. The analysis demonstrated that qualitatively similar hydrographs, with similar levels of predictive efficiency, could be obtained from very different spatial parameterisations of the catchment. Thus the heterogeneity in hydrological processes subsumed by the spatially distributed landuse and soil types significantly differ from the processes predicted by the lumped model. Significantly, the pattern of landuse was found to reinforce the topographic control on hydrological response, resulting in spatial soil moisture distributions that are similar to the lumped model, but which appear to provide a better coupling of the hillslope and channel processes. Thus the land-distributed parameterisation predicted a larger expansion of the saturated zone than predicted by the lumped model. The effect of this on hydrological uncertainty bounds was limited, however, with the land-distributed bounds following those of the lumped model very closely, suggesting that the land-distributed parameterisation did not provide any additional information that could reduce hydrological model uncertainty. This is the case for this particular spatial distribution of land use, but may not be the case for others. However, as will be discussed later, the difference in spatial distribution of runoff generation predicted by the land-distributed parameterisation does affect the sediment uncertainty bounds more significantly than was found for the hydrological uncertainty bounds.

The soil-distributed parameterisation resulted in uncertainty bounds that were different in shape from those of the lumped and land-distributed parameterisations, but which predicted the recession flows more effectively than either the lumped- or land-distributed parameterisations did. The soil-distributed parameterisation predicts a pattern that suggests mechanisms that restrict baseflow in the southern half of the catchment, and which attenuate surface runoff from the northern half of the catchment

during flood events. The spatial distribution of catchment runoff generating areas follows the spatial distribution of soil closely, predicting the main saturation areas in the headwaters of the catchment and along the channel network, and dry soils in the south of the catchment, close to the outlet. It is this vastly different spatial distribution of saturated areas which has resulted in the variations in shape of the predicted uncertainty bounds for this parameterisation.

Both land- and soil-distributed parameterisation, were successful in restricting sediment flux uncertainty for all three events. The relatively small reduction in hydrological model uncertainty, resulted in more significant reduction in sediment model uncertainty. The spatial predictions of sediment source areas for the land-distributed reflect the reinforced topographic control on runoff that the land use provides, but it indicates better channel-hillslope coupling as the storm progresses, and the increasing control of landuse on sediment source areas, on the hillslopes. The spatial distribution of sediment source areas for the soil-distributed parameterisation again followed the pattern of soil type more closely.

However, the spatially distributed parameterisations did not successfully reduce the propagated model uncertainty in all events, and instead widened uncertainty bounds in two cases. In general, the soil-distributed parameterisation was more effective in reducing the propagated uncertainty.

Random Spatial parameterisation

The treatment of landuse and soil type as separate controls on hydrological response is not ideal. In reality, their controls will interact in a non-linear manner to give a hydrological response that may be different from either of their separate responses. In addition, their combined controls may also be temporally variable. However, to fully characterise their combined effects, measurements would have to be taken for all combinations of landuse and soil type, and for all temporal possibilities. Hence, the nature of their interaction cannot be easily predicted. It has been argued that in catchments of this size, greater than the representative elementary area, spatially variable saturated hydraulic conductivity can be represented by the statistical distribution of this parameter. Chapter 7 examined the effect of statistical variable saturated hydraulic conductivity on catchment hydrological and sedimentological

response. The results showed that randomly distributing the ‘optimum’ lumped saturated hydraulic conductivity, had little effect on the predicted hydrographs, but resulted in localised spatial variability in soil moisture deficit. The spatial variability in soil moisture deficit, which controls runoff generation, increased with increasing variability in K_s , resulting in variability in sediment yield, mainly along the channel network where the main sediment sources are located. For the wetter periods of the hydrograph and for larger events, rainfall intensity becomes the dominant control on runoff generation and sediment removal, thus masking the effect of the spatial variability of saturated hydraulic conductivity. Thus, the results showed that random variability of saturated hydraulic conductivity may result in localised variability in hydrological and sedimentological response, which may have considerable consequences for localised flooding and soil erosion. It also demonstrates that the statistical ensemble of variability in saturated hydraulic conductivity may be the dominant control on the response of the catchment.

9.5 Limitations

There are a number of limitations with the work presented here. First, the uncertainty analysis requires a larger number of iterations than used here. Most GLUE studies have used greater than 5000 simulations, while only 1000 were used here. This seriously limits the number of random parameter sets, and hence limits the range of behavioural parameter sets obtained. Limitations of computing power and time were the deciding factors in the choice of the number of simulations to use. A workstation capable of running the coupled model 1000 times only became available within the last 12 months of the research period, and even so, it took 3 days to run 1000 simulations.

The second limitation is again related to computing power. Compromises had to be made to both spatial and temporal scales. A grid size resolution of 50x50m was the smallest possible grid that could be used. This would have limited the spatial predictions of the model, by limiting the capability to predict different processes occurring at the sub-grid scale. Similarly, a time step of 1 hour might not have been sufficient to represent transient processes occurring in the catchment at a smaller timescale. Given the sensitivity of both hydrological response and sediment yield to

both spatial and temporal scales as discussed in chapter 2, the compromises made would have limited the accuracy of the predictions.

A third limitation is the lack of spatial data to validate the spatial hydrological and sediment yield predictions. As discussed in chapters 2, 4 and 8, the scale of measurements that would be required to validate spatial predictions made it impossible to carry out during the relatively short time span of this research. Future work may benefit from the increasing availability of remote sensed images and developments in techniques to derived accurate data from such images, to be used in the validation process.

9.6 Thesis conclusions

A conceptual, dynamic sediment yield model has been successfully coupled to a fully-distributed, topography-based hydrological model to provide spatially and temporally variable hydrological and sediment yield predictions. It has been demonstrated that there is significant uncertainty in both models due to uncertainty about individual model structures, parametric uncertainty due to over-parameterisation and parameter interdependence, and uncertainty due to spatial heterogeneity. In addition it has been demonstrated that hydrological model uncertainty is propagated to the sediment yield model.

The use of additional data has been shown to successfully reduce hydrological model uncertainty, thus demonstrating the value of additional data. The use of predictions from the secondary sediment yield model to reduce hydrological model uncertainty is a novel approach which successfully illustrated that the secondary model is an effective regulator of the range of hydrological model predictions that can be considered behavioural. It also illustrated the importance of accurately modelling hydrological response in the coupled model, to reduce the propagated uncertainty to the secondary response.

Another source of additional data was spatially distributed soil type and landuse, which were used to distribute soil hydraulic parameters. These were shown to effectively reduce hydrological model uncertainty, and resulted in spatial distribution

of hydrological and sedimentological responses, which were different from those of the lumped parameterisation. Similarly, the randomly distributed parameterisations, which are more complex and detailed than the lumped parameterisation, but which are a more generalised representation of spatial variability in soil hydraulic parameters, than either the soil or land use distributed parameterisations, illustrated that similar temporal responses can be obtained from very different spatial distributions.

Thus, the Thesis has illustrated that model uncertainty can be reduced by increased knowledge of the system being modelled, as prescribed by Moore and Brewster (1972). However, it brings into question, how much data is sufficient to reduce uncertainty. At the catchment scale, the statistical ensemble variability may be sufficient to represent spatial variability in catchment response.

BIBLIOGRAPHY

- Abbott, M.D., Bathurst, J.C., Cunge, J.A., O'Connell, P.E., Rasmussen, J., 1986. 'An introduction to the European Hydrological System – System Hydrologique European, SHE 1. History and Philosophy of a physically-based, distributed modelling system' in *Journal of Hydrology*, **87** (1-2) pp. 45-59.
- Addison, K., 1987. 'Debris flow during intense rainfall in Snowdonia, North Wales; A preliminary survey' in *Earth Surf. Proc. Lanf.* **12** (5) pp. 561-566.
- Ahuja, R.M., Nancy, J.W., Nielsen, D.R., 1984. 'Scaling soil water properties and infiltration modelling' in *Soil Sci. Soc. Am. J.*, **48** pp. 970-973.
- Aitchison, J., and Brown, J.A.C., 1957. *The lognormal Distribution* 176 pp. Cambridge University Press, London.
- Albaladejo, J., and Stocking, M., 1989. 'Comparative evaluation of two models in predicting storm soil loss from erosion plots in semi-arid Spain'. in *Catena* **16** pp. 227-236.
- Alemi, M.H., Shahriari, M.R., Nielsen, D.R., 1988. 'Kriging and cokriging of soil water properties' in *Soil Technol.* **1** pp. 117-1132.
- Allen, M.W., Mosher, R.R., 1986. 'Monitoring snowpack conditions with an interactive geo-stationary satellite system' in *Proc. Wstern Snow Conf.* (54th annual meeting, Phoenix, Arizona, USA) pp. 51-60.
- Ambroise, B., Beven, K., and Freer, J., 1996. 'Toward a generalization of the TOPMODEL concepts: Topographic indices of hydrological similarity' in *Water Resources Res.* **32** (7) pp. 2135-2145.
- American Society of Civil Engineers (ASCE) 1975. 'Manuals and Reports on Engineering Practice' in *Sediment Engineering* ASCE, New York, NY, no. **54**.
- Anderson, E.A., 1973. 'Normal weather service river forecast system. Snow accumulation and ablation model' in *NOAA Tech. Memorandum NWS Hydro-17*. US Dept. Commerce, Silver Spring, Maryland, USA.
- Anderson, E.A., 1976. 'A point energy and mass balance model of a snow cover. *Noaa Tech. Report NWS* no. **19** US Department of Commerce, Silver Spring, Maryland, USA.
- Anderson, M.G., and Burt, T.P., 1978. 'Toward more detailed field monitoring of variable source areas' in *Water Resources Res.*, **14** (6) pp. 1123-1131.
- Anderson, M.G., 1982. 'Modelling hillslope soil water status during drainage' in *Trans. Inst. Brit. Geogrs.* N.S.7 pp. 337-353.
- Anderson, M.G., and Rogers, C.C.M., 1987. 'Catchment scale distributed hydrological models – a discussion of research directions' in *Progress in Physical Geography* **11** (1) pp. 28-51.
- Ashworth, P.J. and Ferguson, R.I., 1986. 'Interrelationships of channel processes, changes and sediments in a preglacial braided river' in *Geografiska Annaler*, **68A** pp. 361-371.
- Avery, B.W., 1980. *Soil Classification for England and Wales* Soil Survey of Great Britain. Technical monographs; no. **14**. Harpenden.
- Baird, I., Gee, D.M., Anderson, M.G., 1992. 'Ungauged catchment modelling. 2. Utilisation of hydraulic models for validation' *Catena* **19** (1) pp. 33-42.
- Bakr, A.A., Gelhar, L.E., Gutjahr, A.L., MacMillan, J.R., 1978. 'Stochastic analysis of spatial variability in subsurface flows, 1, Comparison of one- and three-dimensional flows' in *Water Resources Res.*, **14** (2) pp. 263-271.

- Barling, R.D., Moore, I.D., Grayson, R.B., 1994. 'A quasi-dynamic wetness index for characterising the spatial distribution of zones of surface saturation and soil water content' in *Water Resources Res.*, **30** pp. 1029-1044.
- Bathurst, J.C., 1986. 'Physically-based distributed modelling of an upland catchment using the Système Hydrologique Européan' in *J. Hydrol.*, **87**, pp. 79-102.
- Bathurst, J.C., 1987. 'Measuring and Modelling bedload transport in channels with coarse bed materials' in Richards, K., (Ed.), *River Channels: Environment and Process*, Blackwell, Oxford, pp. 272-294.
- Bathurst, J.C., and Purnama, A., 1991. 'Design and Application of a sediment and contaminant transport modelling system' in *Sediment and stream water quality in a changing environment: Trends and Explanations*. Proc. Of the Vienna Symp., 1991 IAHS Publ. No. **203** pp. 305-313.
- Bathurst, J.C. and Wicks, J.M., 1991. 'Framework for Erosion sediment yield modelling' in Bowles, D.S. and O'Connell, P.E. (Eds.) *Recent Advances in the Modelling of Hydrologic Systems*. pp. 269-288.
- Bazemore, D.E., Eshleman, K.N., and Hollenbeck, K., 1994. 'The role of soil water in stormflow generation in a forested headwater catchment: synthesis of natural tracer and hydrometric evidence' in *Journal of Hydrology* **162** pp. 47-75.
- Beasley, D.B., Huggins, L.F., and Monke, E.J., 1982. 'Modelling sediment yields from agricultural watersheds' in *J. Soil Wat. Conserv.* **37** (2) pp. 113-117.
- Beck, M.B., Kleissen, F.M., and Wheeler, H.S., 1990. 'Identifying flow paths in models of surface water acidification' in *Review of Geophysics*, **28** (2) pp. 207-230.
- Beck, M.B., 1991. 'Forecasting environmental change' in *Journal of Forecasting*, **10** pp. 3-19.
- Beck, M.B., Jakeman, A.J., MacAleer, M.J., 1993. 'Construction and evaluation of models of environmental systems' in Jakeman A.J., Beck, M.B., MacAleer, M.J. (Eds.) *Modelling Change in Environmental Systems*, pp. 3-35. Wiley, Chicester.
- Bengtsson, L., 1984. 'Modelling snowmelt induced runoff with short time resolution' in *Proceedings, Third International Conference on Urban Storm Drainage* (Goteborg, Sweden, June 4-8) pp. 305-324.
- Bennett, R.J., Chorley, R.J., 1978. *Environmental Systems: philosophy, analysis and control*, London: Methuen.
- Bennion, D.W., and Griffiths, J.C., 1966. 'A stochastic model for predicting variations in reservoir rock properties' in *Trans. AIME*, **237** pp. 9-16.
- Bergström, S., 1976. 'Development and application of a conceptual runoff model for a Scandinavian catchments' in *Dept. Water Resources Engineering, Lund Inst. Technology Bull Ser. A52* Swedish Meteorological and Hydrological Institute, Norrköping, Sweden.
- Best, 1988. 'Sediment transport and bed morphology at river channel confluences' in *Sedimentology* **35** (3) pp. 181-198.
- Beven, K.J., 1977. 'Hillslope hydrographs by the finite element method' in *Earth Surface Processes*, **2**, pp. 13-28.
- Beven, K.J., 1985. 'Distributed Models' in Anderson, M.G., and Burt, T.P. (Eds.) *Hydrological Forecasting*, John Wiley and Sons Ltd.
- Beven, K.J., 1986. 'Hillslope runoff processes and flood frequency characteristics' in Abrahams, A.D. (Ed.) *Hillslope Processes* pp. 187-202, Allen and Unwin, Boston.

- Beven, K., 1989. 'Changing ideas in hydrology – the case of physically-based models' in *Journal of Hydrology*, **105** pp. 157-172.
- Beven, K.J., 1991. 'Spatially distributed modelling: conceptual approach runoff production' in Bowles, D.S., O'Connell, P.E., (Eds.) *Advances in modelling hydrologic systems*, pp. 373-387.
- Beven, K.J., 1993. 'Prophecy, reality and uncertainty in distributed hydrological modelling' in *Advances in WaterResources* **16** (1993) pp.41-51.
- Beven, K.J. (Ed.), 1997. *Distributed Modelling in hydrology: Applications of the TOPMODEL concepts*. Wiley, Chicester.
- Beven, K.J., 2000. *Rainfall-runoff Modelling* John Wiley and Sons, Chichester.
- Beven K.J. and Kirkby, M.J., 1979. 'A physically-based variable contributing area model of basin hydrology' in *Hydrological Sciences Journal* **24** (1): 43-69.
- Beven, K.J., Hornberger, G.M., 1982. 'Assessing the effect of spatial pattern of precipitation in modelling stream flow hydrographs' in *Water Resources Bull.* **18** (5) pp. 823-829.
- Beven, K.J. and Binley, A., 1992. 'The future of distributed models: model calibration and uncertainty prediction' in *Hydrological Processes* vol. **6** pp. 279-298.
- Beven, K.J., Kirkby, M.J., Schofield, N., Tagg, A.F., 1984. 'Testing a physically based flood forecasting model (TOPMODEL) for three UK catchments' in *J. Hydrol.*, **69** pp. 113-143.
- Beven, K.J., Lamb, R., Quinn, P., Romanowicz, R., Freer, J., 1995. 'TOPMODEL' in Singh, V.P. (Ed.) *Computer Models of Watershed Hydrology, Water Resources Publication* pp. 627-668.
- Binley, A., and Beven., K., 1992. 'Three-dimensional modelling of hillslope hydrology' in *Hydrological Processes* **6** (3) pp. 347-359.
- Binley, A.M., Elgy, J., Beven, K.J., 1989. 'A physically-based model of heterogeneous hillslopes. II. Effective hydraulic conductivities' in *Water Resources Res.*, **25** pp. 1227-33.
- Bloschl, G., 1999. 'Scaling issues in snow hydrology' in *Hydrological Processes* **13** (14-15) pp. 2149-2175.
- Bloschl; G., Grayson, R.B., Sivapalan, M., 1995. 'On the representative elementary area (REA) concept and its utility for distributed rainfall-runoff modelling' in *Hydrological Processes* **9** (3-4) pp. 313-330.
- Bobba, G., Singh, V., Bengtsson, L., 1996. 'Application of First-Order and Monte Carlo analysis in watershed water quality models' in *Water Resources Management*, **10** pp.219-240.
- Bouwer, H., 1969. 'Planning and interpreting soil permeability measurements' in *J. Irrig. Drain. Div. ASCE* **95** pp. 391-402.
- Boyce, R.C., 1975. 'Sediment routing with sediment-delivery ratios' in *Present and Prospective Technology for Predicting sediment yields and sources* U.S. Dept. Agric., Publ. ARC-S-40, pp. 61-65.
- Boyle, D.P., Gupta, H.V., Sorooshian, S., 2000. 'Toward improved calibration of hydrologic models: Combining the strengths of manual and automatic methods' in *Water Resources Res.* **36** (12) pp. 3663-3674.
- Boyle, D.P., Gupta, H.V., Sorooshian, S., 2000. 'Towards improved calibration of hydrologic models: Combining the strengths of manual and automatic methods' in *Water Resources Res.*, **36** (12) pp. 3663-3674.

- Brakensiek, D.L., Engleman, R.L., Rawls, W.J., 1981. 'Variation within texture classes of soil-water parameters' in *Transactions of the ASAE*, **24** (2) pp. 335-339.
- Brasington, J., 1997. Monitoring and Modelling runoff response and sediment yield in heterogeneous highland catchments. Unpublished PhD Thesis. University of Cambridge.
- Brasington, J., and Richards, K., 1998. 'Hydrological Modelling in Humid Tropical Catchments' in Harper, D., and Brown, T. (Eds.) *The Sustainable Management of Tropical Catchments*. John Wiley and Sons.
- Brasington, J., and Richards, K., 2000. 'Turbidity and suspended sediment dynamics in small catchments in the Nepal Middle Hills' in *Hydrological Processes* **14** (14) pp. 2559-2574.
- Brooks, R.H., and Corey, A.T., 1964. 'Hydraulic properties of porous media' in *Hydrology Pap. 3* Colorado State University, Fort Collins, CO.
- Brooks, S.M., Richards, K.S., Anderson, M.G., 1993. 'Approaches to the study of hillslope development due to mass movement' in *Progress in Physical Geography*, **17** (1) pp. 32-49.
- Brune, G.M., 1950. 'The dynamic concept of sediment sources' in *EOS Trans. AGU*, **31** (4) pp. 587-594.
- Bruneau, P., Gascuel-Oudou, C., Robin, P., Merot, P., and Beven, K.J., 1995. 'Sensitivity of space and time resolution of a hydrological model using digital elevation data' in *Hydrological Processes*, **9** (1) pp. 69-81.
- Bulnes, A.C., 1946. 'An application of statistical methods to core analysis data of dolomitic limestone' in *Trans. AIME*, **165** pp. 223-240.
- Burges, S.J., and Lettenmaier, D., 1975. 'Probabilistic Methods in Stream Quality Management' in *Water Resources Bulletin*, vol. **11**, no. 1.
- Burns, R.G., 1979. 'An improved sediment delivery model for Piedmont forests'. Georgia Inst. Technol., Atlanta, Ga.
- Burt, T.P., Butcher, D.P., 1986. 'Development of topographic indices for use in semi-distributed hillslope runoff models' in Baltenau, D., and Slaymaker, O. (Eds.) *Geomorphology and Land Management Zeits. Geomorph. Suppl. Vol. 58* pp. 1-19.
- Butcher, B., Hinz, C., Fluhler, H., 1994. 'Sample-size for determination of coarse fragment content in a stony soil' in *Geoderma*, **63** (3-4) pp. 265-275.
- Cameron, D.S., Beven, K.J., Tawn, J., Blazkova, S., and Naden, P., 1999. 'Flood frequency estimation by continuous simulation for a gauged upland catchment (with uncertainty)' in *Journal of Hydrology* **219** pp. 169-187.
- Carbonneau, R., Fortin, J.P., Morin, G., 1977. 'The CEQUEAU model: description and examples of its use in problems related to water resources management' in *Hydrol. Sci. Bull.* **22** (1) pp. 193-203.
- Carbonneau, R., Lardeau, J.P., Obled, C., 1981. 'Problems of modelling a high mountainous drainage basin with predominant snow yields' in *Hydrol. Sci. Bull.* **26** (4) pp. 345-361.
- Chapman, T.G., 1970. 'Optimisation of a rainfall-runoff model for an arid zone catchment' in *IAHS Symposium, Results of research on Representative and experimental basins, Wellington, I*, pp. 126-143.
- Chen, Y.H., 1979. 'Water and sediment routing in rivers' in Shen, H.W. (Ed.) *Modeling of Rivers*, Wiley, New York, pp. 10.1-10.87.
- Chorley, R.J., 1962. 'Geomorphology and general systems theory' in *US Geol. Surv. Prof. Paper 500-1B*, Washington, D.C.

- Chow, V.T. 1964. (Ed.). *Handbook of Applied Hydrology* McGraw Hill, New York, N.Y.
- Clark, I., 1979. *Practical Geostatistics* London: Applied Science Publishers.
- Clarke, R., 1994. *Statistical Modelling in Hydrology* John Wiley and Sons, Chicester.
- Clarke, R.T., 1973. 'A review of some mathematical models used in hydrology, with observations on their calibration and use' in *Journal of Hydrology*, **19** pp. 1-20.
- Clifton, P.M., and Neuman, S.P., 1982. 'Effects of kriging and inverse modelling on conditional simulation of the Avra Valley aquifer in southern Arizona' in *Water Resources Res.* **18** (4) pp. 1215-1234.
- Corr, D., 1993. 'Production of DEMs from ERS-1 radar data' in *Mapping Awareness* **7** pp. 18-22.
- Corradini, C., and Singh, V.P., 1985. 'Effect of spatial variability of effective rainfall on direct runoff by a geomorphologic approach' in *Journal of Hydrology* **81** (1-2) pp. 27-43.
- Culling, W.E.H., 1957. 'Multicycle systems and the equilibrium theory of grade' in *J. Geol.*, **65** pp. 259-274.
- Dagan, G., 1979. 'Models of groundwater flow in statistically homogeneous porous formations' in *Water Resources Research*, **15** (1) pp. 47-63.
- David, M., 1977. *Geostatistical Ore Reserve Estimation* Elsevier Scientific, Amsterdam.
- Davis, L., 1991. *Handbook of Genetic Algorithms*. Van Nostrand Reinhold, New York.
- Davis, M.W., 1987. 'Production of conditional simulations via the LU triangular decomposition of the covariance matrix' in *Math. Geol.*, **19** (2) pp. 91-98.
- Davis, S.N., 1969. 'Porosity and permeability of natural materials' De Wiest, R.J.M. (Ed.) in *Flow Through Porous Media* pp. 54-89.
- Dawdy, D.R., and Lichty, R.W., 1968. 'Methodology of hydrologic model building' in *IAHS Symposium. The Use of Analogue and Digital Models in Hydrology*, IAHS Publ. no. **80**, pp. 347-355.
- Dawdy, D.R., and Bergmann, J.M., 1969. 'Effect of rainfall variability on streamflow simulation' in *Water Resources Res.*, **5** pp. 958-966.
- De Roo, A.P.J., Wesseling, C.G., and Ritsema, C.J., 1996 'LISEM: a single event physically based hydrological and soil erosion model for drainage basins: I. Theory, input and output' in *Hydrological Processes*, **10** pp 1107-1117.
- Delhomme, J.P., 1978. 'Kriging in the Hydrosiences' in *Adv. In Water Resources*, **1** (5) pp. 251-256.
- Delhomme, J.P., 1979. 'Spatial variability and uncertainty in groundwater flow parameters: a geostatistical approach' in *Water Resources Res.*, **15** pp. 269-280.
- Dietrich, W.E., Dunne, T., 1978. 'Sediment budget for a small catchment in mountainous terrain' in *Z. Geomorph. Suppl. Band.* **29** pp. 191-206.
- Dietrich, W.E., Dunne, T., 1993. 'The channel head' in Beven, K.J., Kirkby, M.J. (Eds.) *Channel Network Hydrology*. Wiley, Chichester pp. 175-219.
- Dietrich, W.E., Wilson, C.J., Reneau, S.L., 1986. 'Hollows, colluvium, and landslides in soil mantled landscapes' in Abrahams, A.D. (Ed.) *Hillslope Process*, Allen and Unwin, London.
- Dietrich, W.E., Wilson, C.T., Montgomery, D.R., McKean, J., and Bauer, R., 1992. 'Erosion thresholds and land surface morphology' in *Geology*, **20**, pp. 675-679.
- Dingman, S.L., 1975. 'Hydrologic effects of frozen ground. Hanover, NH: US Army Cold Regions Research and Engineering Laboratory *Special Report* 218.

- Diskin, M.H., 1970. 'Definition and uses of linear regression models' in *Water Resources Res.*, **6** pp. 1668-1673.
- Diskin, M.H., 1990. 'On computer evaluation of Theissen weights' in *J. Hydrol.*, **11** pp. 69-78.
- Dooge, J.C.I., 1973. 'Problems and methods of rainfall-runoff modelling' in US Agr. Res. Serv. Tech. Vol. 1468.
- Douglas, J.R., 1974. 'Conceptual modelling in hydrology' in *Inst. Hydrol. Report*, No. **24**.
- Duan, Q.S., Sorooshian, S., and Gupta, V., 1992. 'Effective and efficient global optimisation for conceptual rainfall-runoff models' in *Water Resources Research* **33** pp. 2559-2562.
- Dunn, S.M., and Ferrier, R.C., 1999. 'Natural flow in managed catchments: a case study of a modelling approach' in *Water Resources Research* **33** pp. 621-630.
- Dunne, T., and Black, R.D., 1970. 'Partial area contributions to storm runoff in a small New England watershed' in *Water Resources Res.*, **6** (5) pp. 1296-1311.
- Dunne, T., and Leopold, L.B., 1978. '*Water in Environmental Planning*', Freeman, San Fransico, 818pp.
- Eagleson, P.S., 1970. *Dynamic Hydrology* Mc Graw Hill, New York, 462pp.
- Engman, E.T., and Gurney, R.J., 1991. 'Recent advances and future implications of remote sensing for hydrologic modelling' in Bowles, D.S., and O'Connell, P.E. (Eds.) *Recent advances in the Modelling of Hydrologic systems*, Kluwer Academic publishers, The Netherlands pp. 471-495.
- Famiglietti, J.S., and Wood, E.F., 1991. 'Evaporation and runoff from large land areas: land surface hydrology for atmospheric general circulation model' in *Surv. Geophys.*, **12** pp. 179-204.
- Famiglietti, J.S., Wood, E.F., 1995. 'Effects of spatial variability and scale in areally averaged evapotranspiration' in *Water Resources Res.*, **31** (3) pp. 699-712.
- Ferguson, R.I. 1986. 'River loads underestimated by rating curves' in *Water Resources Research* **22**, pp. 74-76.
- Ferguson, R.I. 1987. 'Accuracy and precision of methods for estimating river loads' in *Earth Surface Processes and Landforms*, **12**, pp. 95-104.
- Ferro, V., and Minacapilli, M., 1995. 'Sediment delivery processes at basin scale' in *Hydrological Science – des Sciences Hydrologiques* **40**, **6** pp. 703-717.
- Fischer, R.A., 1922. 'On the mathematic foundations of theoretical statistics' in *Phil. Trans. Roy. Soc. London*, **A 222** pp. 309-368.
- Flavelle, P., 1992. 'A Quantative measure of model validation and its potential use for regulatory purposes' in *Advances in Water Resources* **15** (1) pp. 5-14.
- Forrest, S., 1993. 'Genetic algorithms: principles of natural selection applied to computation' in *Science* **261** pp. 872-878.
- Foster, G.R., Meyer, L.D., and Onstad, C.A., 1977. 'An erosion equation derived from basic erosion principles' in *Trans. Am. Soc. Agric. Engrs.* **20** (4) pp. 678-682.
- Fox-Strangways, C., 1892. 'The Jurassic rocks of Britain, vol. I, Yorkshire Memoirs of the Geological Survey of Great Britain' H.M.S.O. London (551pp).
- Franchini, M., Galeati, G., 1997. 'Comparing several genetic algorithm schemes for the calibration of conceptual rainfall-runoff models' in *Hydrological Science Journal* **42** pp.357-380.
- Franks, S. W., and Beven, K.J., 1997. 'Bayesian estimation of uncertainty in land surface-atmosphere flux predictions' in *J. Geophysical Research* **102** (D20) pp. 23991-23999.

- Freebairn, D.M., and Silburn, D.M., and Loch, R.J., 1989. 'Evaluation of three soil erosion models for clay soils' in *Aust. J. Soil Res.*, **27** pp. 199-211.
- Freer, J., Beven, K.J., Ambroise, B., 1996. 'Bayesian estimation of uncertainty in runoff prediction and the value of data: An application of the GLUE approach' in *Water Resources Res.*, **32** (7) pp. 2161-2173.
- Freeze, R.A., 1971. 'Three-dimensional transient, saturated-unsaturated flow in a groundwater basin' in *Water Resources Res.*, **7** (2) pp. 347-366.
- Freeze, R.A., 1972. 'Role of subsurface flow in generating surface runoff. 2. Upstream source areas' in *Water Resources Res.*, **8** pp. 1272-1283.
- Freeze, R.A., 1975. 'A stochastic-conceptual analysis of one-dimensional groundwater flow in nonuniform homogeneous media' in *Water Resources Res.*, **11** (5) pp. 725-741.
- Freeze, R.A., 1980. 'A stochastic-conceptual analysis of rainfall-runoff processes on a hillslope' in *Water Resources Res.*, **16** (2) pp. 391-408.
- Freeze, R.A. and Harlan, R.L., 1969. 'Blue print for a physically-based digitally simulated hydrologic response model' in *Journal of Hydrology*, **9** pp. 237-258.
- Fryer, J.G., Chandler, J.H., Cooper, M.A.R., 1994. 'On the accuracy of heighting from aerial photographs and maps – implications to process modellers' in *Earth Surface Processes and Landforms*, **19** (6) pp. 577-583.
- Gallichand, J., Marcotte, D., 1993. 'Mapping clay content for subsurface in the Nile Delta' in *Geoderma* **58** pp. 165-179.
- Gallichand, J., Marcotte, D., Prashed, S.O., 1992a. 'Including uncertainty and hydraulic conductivity into drainage design' in *J. of Irrig. And Drain. Eng.* **118** (5) pp. 744-756.
- Gallichand, J., Buckland, G.D., Marcotte, D., Hendry, M.J., 1992b. 'Spatial interpolation of soil salinity and sodicity for a saline soil in Southern Alberta' in *Can. J. Soil Sci.* **72** pp. 503-516.
- Gallichand, J., Prasher, S.O., Broughton, R.S., Marcotte, D., 1991. 'Kriging of hydraulic conductivity for subsurface drainage design' in *J. of Irrig. And Drain. Eng.* **117** (5) pp. 667-681.
- Giles, P.T., Chapman, M.A., Franklin, S.E., 1994. 'Incorporation of a digital elevation model derived from stereoscopic satellite imagery in automated terrain analysis' in *Computers and Geosciences* **20** (4) pp. 441-460.
- Gilley, J.E., and Finkner, S.C., 1985. 'Estimating soil detachment caused by raindrop impact' in *Trans. Am. Soc. Agric. Engrs.* **28** pp. 140-146.
- Gilman, K., and Newson, M.D., 1980. 'Soil pipes and pipe flow – a hydrological study in upland Wales' *British Geomorphological Research Group Monograph* no. 1 Norwich:Geo Books.
- Gippel, C.J., 1989. 'The use of turbidimeters in suspended sediment research' in *Hydrobiologia* **176** pp. 465-480.
- Gippel, C.J., 1995. 'Potential of turbidity monitoring for measuring the transport of suspended-solids in streams' in *Hydrological Processes* **9** (1) pp. 83-97.
- Glymph, L.M., 1954. 'Study of sediment yields from watersheds' in *Assemble Generale de Rome 1954, Tome, I* 173-191. IAHS publ. no.36.
- Govers, G., 1990. 'Empirical relationships on the transport capacity of overland flow' in *Erosion, Transport and Deposition. Proc. Of the Jerusalem Workshop.* IAHS Spec. Publ. No. **189** pp. 45-63.
- Grayson, R.B., Moore, I.D., McMahon, T.A., 1992a. 'Physically based hydrologic modelling. 1. A Terrain based model for investigative purposes' in *Water Resources Res.* **28** (10) pp. 2639-2658.

- Grayson, R.B., Moore, I.D., McMahon, T.A., 1992b. 'Physically based hydrologic models, 2. Is the concept realistic?' in *Water Resources Res.*, **28** pp. 2659-2666.
- Gregory, K.J., and Walling, D.E., 1973. '*Drainage basin form and Process: A geomorphological approach*' Arnold, London.
- Gurnell, A., and Midgley, P., 1993. 'A soil erosion and delivery model for the River Test catchment to estimate the effect of land-use change over fifty years' in *BHS 4th National Hydrology Symposium*, Cardiff pp. 5.1-5.7.
- Haines-Young, R.H., Petch, J.R., 1983. 'Multiple working hypotheses: equifinality and the study of landforms' in *Trans, Inst. Br. Geogr.* **8** pp. 458-466.
- Haldorsen, H.H., Damsleth, E., 1990. 'Stochastic Modelling' in *JPT J. Pet. Technol.*, pp. 404-412.
- Hamon, B.V., and Hannan, E.J., 1963. 'Estimating relations between time series' in *Journal of Geophys. Res.*, **81** (21) pp. 6033-6041.
- Hewlett, J.D., 1961. 'Soil Moisture as a source of base flow from steep mountain watersheds' in *U.S.D.A. Southern Forest Exp. Stn. Asheville, N.C., Stn. Pap.*, no. 132.
- Hino, M., Fujita, K., Shutto, H., 1987. 'A laboratory experiment on the role of grass for infiltration and runoff processes' in *Journal of Hydrology* **90** (3-4) pp. 303-325.
- Hogg, H.C., 1986. 'Special Issue on Agricultural and Remote sensing surveys through aerospace remote sensing (Agristars) – Foreward' in *IEEE Transactions on Geoscience and Remote Sensing*, **24** (1) pp. 3-4.
- Hornberger, G.M., and Spear, R.C., 1981. 'An approach to the preliminary analysis of environmental systems' in *J. Environ. Manag.*, **12** pp. 7-18.
- Hornberger, G.M., Beven, K.J., Cosby, B.J., and Sappington, D.E., 1985. 'Shenandoah Watershed study: calibration of a topography-based, variable contributing area hydrological model to a small forested catchment' in *Water Resources Res.*, **21** (12) pp. 1841-1850.
- Hosseini, E., Gallichand, J., Caron, J., 1993. 'Comparison of several interpolators for smoothing hydraulic conductivity data in South Western Iran' in *Journal of Am. Soc. of Agri. Eng.* **36** (6) pp. 1687-1693.
- Howes, S., and Anderson, M.G., 1988. 'Computer simulation in geomorphology' in Anderson, M.G. (Ed.), *Modelling Geomorphological Systems*, John Wiley & Sons Ltd., 421-440.
- Hubbert, M.K., 1940. 'The Theory of groundwater motion' in *Journal of Geology* **48** pp. 785-944.
- Hutchinson, M.F., and Dowling, T.I., 1991. 'A continental assessment of hydrological applications of a new grid-based digital elevation model of Australia' in *Hydrological Processes*, **5** pp. 49-62.
- Imeson, A.C., 1970. *Erosion in three East Yorkshire catchments and variations in the dissolved, suspended and bedload*. Ph.D. thesis University of Hull.
- Ince, S., 1972. 'Uncertainty in Hydraulic Models' in Kiesel and Duckstein (eds.) *Proceedings of the International Symposium on Uncertainty in Hydrologic and Water Resource Systems*, Tuscon Arizona, 11-14 December.
- Jackson, M.C., 1977. 'A method of estimating the probability of occurrence of snow water equivalents in the United Kingdom' in *Hydrol. Sci. Bull.* **22** (1) pp.127-142.
- Jakeman, A.J., and Hornberger, G.M., 1993. 'How much complexity is warranted in a rainfall-runoff model?' in *Water Resources Res.*, **29** pp. 2637-2649.

- Jakeman, A.J., Littlewood, I.G., and Symons, H.D., 1991. 'Features and applications of IHACRES: a PC program for identification of hydrographs and component flows from rainfall, evapotranspiration and streamflow data' in Vichnevetsky, R., Miller, J.J.H (Eds.) *Proceedings of 13th IMACS World Congress on Computations and Applied Mathematics*, Trinity College, Dublin, July 22-26.
- Jakeman, A.J., Littlewood, I.G., Whitehead, P.G., 1993. 'An assessment of the dynamic response characteristics of streamflow in the Balquhider Catchments' in *Journal of Hydrology* **145** (3-4) pp. 337-355.
- Jakeman, A.J., Hornberger, G.M., Littlewood, I.G., Whitehead, P.G., Harvey, J.W., Bencala, K.E., 1992. 'A systematic approach to modelling the dynamic linkage of climate, physical catchment descriptors and hydrologic response components' in *Mathematics and Computers in simulation* **33** (5-6) pp. 359-366.
- Jarvis, M.G., Allen, R.H., Fordham, S.J., Hazelde, J., Moffat, A.J., 1984. *Soil Survey of England and Wales*, Bulletin **15**, Hapendon.
- Jenkins, A.P., Ashworth, P.I., Ferguson, R.I., Grieve, I.C., Rowling, P., and Stott, T.A., 1988. 'Slope failures in the Ochil Hills, Scotland, November 1984' in *Earth Surface Proc. and Landf* **13** (1) pp. 69-76.
- Jonch-Clausen, T., 1979. 'Systeme Hydrologique Europeen: a short description' *SHE report I*, Danish Hydraulics Institute, Horsholm, Denmark.
- Jones, A.J., 1986. 'Some limitations of the a/s index for predicting basin wide patterns of soil water drainage in *Z. Geomorph. Suppl. Band*, **60** pp. 7-20.
- Jordan, J.P., 1994. 'Spatial and temporal variability of stormflow generation processes on a Swiss catchment' in *Journal of Hydrology* **153** pp. 357-382.
- Journel, A.B., and Huijbregts, Ch. J., 1978. *Mining Geostatistics*, Academic, New York.
- Jury, W.A., Gardner, W.R., Gardner, W.H., 1991. *Soil Physics* 5th Edition Wiley, New York.
- Kelley, W.E., and Gultarte, R.C., 1981. 'Erosion resistance of cohesive soils' in Proc. Am. Soc. Civ. Engrs. *J. Hydraul. Div.* **107** (HY10) pp. 1211-1224.
- Kent, P. 1980. British Regional Geology, Eastern England from the Tees to the Walsh. Institute of Geological Sciences. Natural Environment Research Council.
- Kiesel, C.C., 1969. *Time Series analysis of hydrological data, Advances in Hydroscience*, Academic Press, New York and London.
- Kirkby, M.J., 1997. 'TOPMODEL: A personal view' in *Hydrological Processes* **11** pp. 1087-1097.
- Kirkby, M.J., and Chorley, R.J., 1967. 'Throughflow, overland flow and erosion' in *Bull. IASH*, **12** pp. 5-21.
- Kirkby, M.J., and Morgan, R.P.C. (Eds.), 1980. '*Soil Erosion*', John Wiley, New York, USA.
- Klemes, V., 1988. 'Operational testing of hydrological simulation-models' in *Hydrological Sciences Journal-Journal des Sciences Hydrologiques*. **31** (1) pp. 13-24.
- Kleper, O., Scholten, H., and Van de Kamer, J.P.G., 1991. 'Prediction uncertainty in an ecological model of the Oosterschelde estuary' in *Journal and Forecasting* **10** pp. 191-209.
- Kling, G.F., 1974. '*A computer model of diffuse sources of sediment and phosphorous moving into a lake*' PhD. Thesis, Cornell University, Ithaca, New York.

- Klir, G.J., and Folger, T.A., 1988. *Fuzzy Sets, Uncertainty and Information*, Prentice Hall, Englewood Cliffs.
- Klock, G.O., 1972. 'Snowmelt Temperature influence on infiltration and soil water retention' in *Journal of Soil and Water Conservation* **27** pp. 12-14.
- Komura, S., 1976. 'Hydraulics of slope erosion by overland flow' in Proc. Am. Soc. Civ. Engrs. *J. Hydraulic Div.* **102** pp. 1573-1586.
- Krajewski, W.F., Lakshmi, V., Georgakakos, K.P., Jain, S.C., 1991. 'A Monte-Carlo study of rainfall sampling effect on a distributed catchment model' in *Water Resource Res.*, **27** (1) pp. 119-128.
- Kramer, L.A., and Alberts, E.E., 1986. 'C factors for corn under changing management' in *Trans ASCE* **29**, pp. 1590-1596.
- Kuczera, G., and Parent, E., 1998. 'Monte Carlo assessment of parameter uncertainty in conceptual catchment models: the Metropolis algorithm' in *Journal of Hydrology* **211** pp. 69-85.
- Kuczera, G., Raper, G.P., Brah, N.S., Jayasuriya, M.D., 1993. 'Modelling yield changes after strip thinning in a mountain Ash catchment – An exercise in catchment model validation' in *Journal of Hydrology* **150** (2-4) pp. 443-457.
- Kustas, W.P., Rango, A., Uijlenhoet, R., 1994. 'A simple energy budget algorithm for the snowmelt runoff model' in *Water Resources Res.*, **30** (5) pp. 1515-1527.
- Ladson, A.R., and Moore, I.D., 1992. 'Soil-water prediction on the Konza prairie by microwave remote sensing and topographic attributes' in *Journal of hydrology* **138** (3-4) pp. 385-405.
- Lamb, R., 1996. 'Distributed hydrological prediction using generalised TOPMODEL concepts, Ph.D. thesis, Lancaster Univ., Lancaster, England.
- Lamb, R., Beven, K.J., Myrabø, S., 1997. 'Discharge and water table predictions using a generalised TOPMODEL formulation' in *Hydrological Processes* **11** pp. 1145-1167.
- Lamb, R., Beven, K.J., Myrabø, S., 1998. 'Use of spatially distributed water table observations to constrain uncertainty in a rainfall-runoff model' in *Advances in Water Resources* **22** (4) pp. 305-317.
- Lane, L.J., Shirley, E.D., Singh, V.P., 1988. 'Modelling erosion on hillslopes' in Anderson, M.G. (Ed.) *Modelling Geomorphological Systems*, Wiley, Chichester, pp. 287-308.
- Lane, S.N., and Richards, K.S., 1996. 'Linking river channel form and process: Time, space and causality revisited' in *Earth Surface and Landforms*, vol. **22** pp. 249-260.
- Lane, S.N., Richards, K.S. and Chandler, J.H., 1996. 'Discharge and sediment supply controls on erosion and deposition in a dynamic alluvial channel' in *Geomorphology*, **15** pp 1-15.
- Larson, L.W., and Peck, E.L., 1974. 'Accuracy of precipitation measurements for hydrologic modelling' in *Wat. Resour. Res.* **10** (4) pp. 857-863.
- Laslett, G.M., and McBratney, A.B., 1990. 'Estimation and implications of instrumental drift, random measurement error and nugget variance of soil attributes – A case study for soil pH' in *J. of Soil Sci.*, **41** pp. 451-471.
- Laslett, G.M., McBratney, A.B., Pahl, P.J., Hutchinson, M.F., 1987. 'Comparison of several spatial prediction methods for soil pH.' in *J. Soil Sci.*, **38** pp. 325-341.
- Law, J., 1944. 'A statistical approach to the interstitial heterogeneity of sand reservoirs' in *Trans. AIME*, **155** pp.202-222.

- Leaf, C.F., and Brink, G.E., 1973. 'Hydrologic simulation model of Colorado subalpine forest' in Forest Service res. Pap RM-107, US Department of Agric., Fort Collins, Colorado, USA.
- Leavesley, G.H., 1989. 'Problems of snowmelt runoff modelling for a variety of physiographic and climatic conditions' in *Hydrol. Sci. Journal – des Sciences Hydrologiques*, **34** (6) pp. 617-634.
- Leavesley, G.H., Lichty, R.W., Troutman, B.M., Saindon, L.G., 1983. 'Precipitation runoff modelling system: User's manual' *USGS Wat. Resour. Invest. Rep.* 83 4238. US Geological Survey, Reston, Virginia, USA.
- Li, R-M, 1979. Water and sediment routing from watersheds' in Shen, H.W. (Ed.) *Modeling of Rivers*, Wiley, New York, pp. 9.1-9.88.
- Lin, B., Rossow, WB., 1994. 'Observations of cloud liquid water path over oceans – optical and microwave remote-sensing methods' in *Journal of geophysical research – atmospheres* **99** (D10) pp. 20907-20927.
- Littlewood, I. G., Marsh, T. J., 1996. 'Re-assessment of the monthly naturalized flow record for the River Thames at Kingston since 1883 and the implications for the relative severity of historical droughts' in *Regulated Rivers – Research and Management* **12** (1) pp. 13-26.
- Littlewood, I.G., Post, D.A., 1995. 'Comparison of four loss models for timeseries analysis of rainfall streamflow dynamics' in *Environ. Int.* **21** (5) pp. 737-745.
- Loague, K. M., and Gander, G.A., 1990. 'R-5 revisited, 1, Spatial variability of infiltration on a small rangeland watershed' in *Water Resources Res.* **26** (5) pp. 957-971.
- Lui, P.L.F., and Liggett, J.A., 1979. 'Boundary solutions to two problems in porous media' in *J. Hydraul. Div. Proc. Am. Soc. Civ. Eng.*, **105** (HY3), pp. 171-183.
- Lund, J.R., 1992. 'Unverifiable Conclusions. Discussion on Editorial by Thomas M. Walski' in *ASCE Journal of Environmental Engineering*, vol. **118** (3) pp. 459 – 461.
- MAFF, 1984. *Soil Survey of England and Wales: Soils and their uses in Eastern England*. Agriculture and Food Research Council Publ., 450pp.
- Maidment, D.R., Olivera, F., Calver, A., Eatherall, A., Fraczek, W., 1996. 'Unit hydrograph derived from a spatially distributed velocity field' in *Hydrological Processes* **10** (6) pp. 831-844.
- Mandelbrot, B.B., 1970. 'Comments on "Stochastic models in hydrology" by Adrian E. Scheidegger' in *Water Resources Res.*, **6** p. 1791.
- Maner, S.B., 1962. 'Factors influencing sediment delivery rates in the Blackland Prairie land resource area' U.S. Dept. of Agric., Soil Conservation Service, Fort Worth, Texas, USA.
- Mantoglou, A., 1987. 'Digital simulation of multivariate two- and three-dimensional stochastic processes with a spectral turning bands method' in *Math. Geol.*, **19** (2) pp. 129-149.
- Mantoglou, A., and Wilson, J.L., 1982. 'The turning bands method for simulation of random fields using line generation by a spectral method' in *Water Resources Res.*, **13** (5) pp. 1379-1394.
- Martinec, J., 1960. 'The degree-day for snowmelt-runoff forecasting' in *Surface Water, Proceedings of the General Assembly of Helsinki IAHS*, Gentbrugge, Belgium, pp. 468-477.
- Martinec, J., 1989. 'Hour-to-hour snowmelt rates and lysimeter outflow during an entire ablation period' in *Snow Cover and Glacier variations* (Proc. of the Baltimore Symposium, Maryland, May 1989). IAHS Publ. **183** pp. 19-28.

- Martinec, J., and de Quervain, M.R., 1975. 'The effect of snow displacement by avalanches on snow melt and runoff' in *Interdisciplinary Studies of Snow and Ice in Mountain Regions* (Proc. of the Moscow Symposium, August, 1971) IAHS-AISH Publ. **104** pp. 364-377.
- Martinec, J., Rango, A., and Major, E., 1983. 'The snowmelt-runoff model user's manual. *NASA Ref. Pub.* 110 NASA, Washington, D.C., USA.
- Matheron, G., 1973. 'The intrinsic random functions and their applications' in *Adv. Appl. Prob.*, **5** pp. 439-468.
- Matias, P., Correia, F.N., Pereira, L.S., 1989. 'Influence of spatial variability of saturated hydraulic conductivity on the infiltration process' in Morel-Seytoux, H.J., (Ed.) *Unsaturated Flow in Hydrologic Modeling Theory and Practice*. NATO Advance Research Workshop, Arles, France, 1988 pp. 455-467.
- McCool, D.K., Brown, L.C., Foster, G.R., Mutchler, C.K., and Meyer, L.D., 1987. 'Revised slope steepness factor for the Universal Soil Loss Equation' in *Trans ASCE* **30**, pp. 1387-1396.
- McIsaac, G.F., Mitchell, J.K., and Hirschi, M.C., 1987. 'Slope steepness effects on soil loss from distributed lands' in *Trans ASCE* **30**, pp. 1005-1013.
- McMillan, W.D., 1966. 'Theoretical analysis of groundwater basin operations' in *Water Resour. Center Contrib.* **114** 167p. Univ. Calif., Berkley.
- Megahan, W.F., 1983. 'Hydrologic effects of clearcutting and wildlife on steep granitic slopes in Idaho' in *Water Resources Res.* **19** (3) pp. 811-819.
- Megahan, W.F., and King, P.N., 1985. 'Identification of critical areas on forest lands for control of non-point sources of pollution' in *Environmental Management* **9** (1) pp. 7-18.
- Mein, R.G., and Brown, B.M., 1978. 'Sensitivity of optimised parameters in watershed models' in *Water Resources Res.*, **14** pp. 229-269.
- Mejia, J.M., and Rodriguez-Iturbe, I., 1974. 'On the synthesis of random field sampling from the spectrum: A application of the generation of hydrologic spatial processes' in *Water Resources Res.*, **23** (4) pp. 705-711.
- Merz, B., Plate, E. J., 1997. 'An analysis of the effects of spatial variability of soil and soil moisture on runoff' in *Water Resources Res.*, **33**: (12) pp. 2909-2922.
- Mitasova, H., Hofierka, J., Zlocha, M., Iverson, L.R., 1996. 'Modelling topographic potential for erosion and deposition using GIS' in *Int. J. Geographical Information Systems*, **10**. (5) pp. 629-641.
- Monteith, J.L., 1965. 'Evaporation and Environment' in *The state and movement of water in living organisms* 19th Symposium, Soc. of Experimental Biology pp. 205-234.
- Montgomery, D.R., and Dietrich W.E., 1989. 'Source areas, drainage density and channel initiation' in *Water Resources Res.*, **25** (8) pp.1907-1918.
- Montgomery, D.R., and Dietrich W.E., 1994. 'Landscape dissection and drainage area-slope thresholds' in Kirkby, M.J. (Ed.) *Process Models and Theoretical Geomorphology*. Wiley, Chester.
- Montgomery, D.R., and Foufoula-Georgiou, E., 1983. 'Channel Network source representation using digital elevation models' in *Water Resources Res.*, **29**, pp. 3925-3934.
- Moore, I.D., and Burch, G.J., 1986a. 'The physical basis of the length-slope factor in the universal soil loss equation' in *Soil Sci. Soc. Am. J.* **50** pp1294-1298.
- Moore, I.D., and Burch, G.J., 1986b. 'Modelling erosion and deposition: Topographic effects' in *Trans. Am. Soc. Agric. Engrs.*, **29** pp. 1624-1640.

- Moore, I.D., O'Loughlin, E.M., and Burch, 1988. 'A contour-based topographic model for hydrological and ecological applications' in *Earth Surf. Proc. Landf* **13** pp. 305-320.
- Moore, R.J., 1984. 'A dynamic model of basin sediment yield' in *Water Resources Res.*, vol. 20, no. 1 pp. 89-103.
- Moore, R.J., and Clarke, R.T., 1981. 'A distribution function approach to rainfall-runoff modelling' in *Water Resources Res.*, **17** (5) pp. 1376-1382.
- Moore, R.J., and Clarke, R. T., 1983. 'A distribution function approach to modelling basin sediment yield' in *Journal of Hydrology*, **65** pp. 239-257.
- Moore, S.F. and Brewster, J.W., 1972. 'Environmental control systems: Treatment of Uncertainty in Models and data' in Kiesel and Duckstein (eds.) *Proceedings of the International Symposium on Uncertainty in Hydrologic and Water Resource Systems, Tuscon Arizona, 11-14 December*.
- Morgan, R.P., 1982. 'A simple procedure for assessing soil-erosion risk for use in semi-detailed surveys – A case study from Mayaysia' in *Journal of Geological Society*, **139** pp. 657-657.
- Morris, E.M., 1980. 'Forecasting flood flows in the Plynlimon catchments using a deterministic distributed mathematical model' in *Hydrological Forecasting IAHS Publ. no. 129* (Proc. Oxford Symp., April, 1980) pp. 247-255.
- Mroczkowski, M., Raper, G.P., Kuczera, G., 1997. 'The quest for more powerful validation of conceptual catchment models' in *Water Resources Res.* **33** (10) pp. 2325-2335.
- Mulla, D. J., 1988. 'Estimating spatial patterns in water content, matric suction, and hydraulic conductivity' in *Soil Sci. Soc. Am. J.*, **52** (6) pp. 1547-1553.
- Myers, D.E., 1982. 'Matrix formulation of cokriging' in *J. of Int. Assoc. for Math. Geology*, **14** (3) pp. 249-257.
- Mulvaney, T.J., 1851. 'On the use of self-registering rain and flood gauges in making observations of the relations of rain and flood discharges in a given catchment' in *Proc. Inst. Civil. Engs.*, Ireland, **4** pp. 18-31.
- Narasimhan, T.N., and Witherspoon, P.A., 1977. 'Numerical model for saturated-unsaturated flow in deformable porous media. I. Theory' in *Water Resources Res.*, **13** (3), pp. 657-664.
- Nash, J.E., 1960. 'A unit hydrograph study with particular reference to British catchments' in *Proceedings of Institution of Civil Engineers*, **17**: 249-282.
- Nash, J.E., and Suttcliffe, J.V., 1970. 'River flow forecasting through conceptual models 1. A discussion of principles' in *J. Hydrol.*, **10**, pp. 282-290.
- Negev, M., 1967. *A sediment model on a digital computer* Report no. 39 Dept. Civil. Eng., Stanford University, Stanford, USA.
- Nelder, J.A., Wedderburn, R.W.M., 1972. 'Generalized linear models' in *J. Roy. Statist. Soc. A* **135** pp. 370-384.
- Nelder, J.A., and Mead, R., 1965. 'A simplex method for function minimisation' in *Computer Journal* **7** pp. 308-313.
- NERC, 1975. 'Flood Studies Report. 5 volumes. Natural Environment Research Council, U.K.
- Newson, M.D., 1980. 'The geomorphological effectiveness of floods – a contribution stimulated by two recent events in mid-Wales' in *Earth Surface Processes*, **5**, pp. 1-16.
- Nicklin, M.E., Remus, J.I., Conroy, J., 1986. 'Gully bank erosion of loessial soil in urbanising watersheds' in *Drainage basin sediment delivery*, IAHS Publ. no. **159** pp. 141-151.

- Nielsen, D.R., Biggar, J.W., Erh, K.T., 1973. 'Spatial variability of field-measured soil-water properties' in *Hilgardia*, **42** (7) pp. 215-260.
- O'Connell, P.E., 1991. 'A historical perspective' in Bowles, D.S. and O'Connell, P.E., (Eds.) *Recent Advances in the Modelling of Hydrologic Systems*. Kluwer Academic Publ., Dordrecht, pp. 3-30.
- O'Donnell, T., 1966. 'Methods of computation in hydrograph analysis and synthesis' in *Recent Trends in Hydrograph Synthesis, Proceedings Technical Meeting 21*, TNO, The Hague.
- O'Loughlin, E.M., 1981. 'Saturation regions in catchments and their relations to soil and topographic analysis properties' in *Journal of Hydrology* **53** pp. 229-246.
- O'Loughlin, E.M., 1986. 'Prediction of surface saturation zones in natural catchments by topographic analysis' in *Water Resources Res.*, **22** pp. 794-804.
- O'Neill, R.V., and Gardner, R.H., 1979. 'Sources of uncertainty in Ecological Models' in Zeigler, B., Elzas, M., Klir, G., Oren, T (eds.) *Methodologies in Systems Modelling and Simulation, Proc. Of the Symposium on Simulation Methodology, Rehovot, Israel, 13-18 August, 1978*.
- Obled, Ch., and Wendling, J., 1991. Development of TOPMODEL: application to Mediterranean catchments. Role of rainfall spatial variability and further simplifications for operational use. Tech. Rep. TR/89, *Centre for Research on Environmental Systems*, Lancaster University, UK.
- Obled, Ch., Wendling, J., Beven, K.J., 1994. 'The sensitivity of hydrological models to spatial rainfall patterns: an evaluation using observed data' in *Journal of Hydrology* **159** pp. 305-333.
- Olive, L.J., Reiger, A., 1984. 'Variation in suspended sediment concentration during storms in five small catchments in New South Wales' in *Aust. Geogr. Studies* **23** pp. 38-51.
- Onof, C., and Wheeler, H.S., 1996. 'Modelling of the time series of spatial coverage British Rainfall fields' in *Journal of Hydrology*, **176** pp. 115-131.
- Onstad, C.A., Piest, R.F., and Saxton, K.E., 1976. 'Watershed erosion model. Validation for southwest Iowa' in *Proc. Federal Inter-Agency Sedimentation Con. 3rd, Denver, CO, 22-25 Mar. 1976*. Sedimentation Committee, Water Resour. Council. pp. 22-34.
- Osborn, H.B., Simanton, J.R., and Renard, K.G., 1977. 'Use of the Universal Soil Loss Equation in the semiarid southwest' in *Soil Erosion: prediction and control*, Soil Conserv. Soc. Am. Spec. Publ. **21** SCSA, Ankeny, IA.
- Osman, A.M., and Thorne, C.R., 1988. 'Riverbank stability analysis. I. Theory; II. Application' in *Proc. Am. Soc. Civ. Engrs., J. Hydral. Engrs.* **114** (2) pp. 134-172.
- Paola, C., 1996. 'Incoherent structure: turbulence as a metaphor for stream braiding' in Ashworth, P.J. Bennett, S.J., Best, J.L. and McLelland, S.J. (Eds.) *Coherent Flow Structures in Open Channels*, Wiley, Chichester, pp. 705-724.
- Parkin, G., O'Donnell, G., Ewen, J., Bathurst, J.C., O'Connell, P.E., Lavabre., 1996. 'Validation of catchment models for predicting land-use and climate change impacts. 1. Case study for a Mediterranean catchment' in *Journal of Hydrology* **175** pp. 595-613.
- Penman, H.L., 1948. 'Natural evaporation from open water, bare soil and grass' in *Proc. Roy Soc. A.* **193** pp.120-145.
- Philip, J.R., 1957. 'The theory of infiltration. 4. Sorptivity and algebraic infiltration equations' in *Soil Sci.*, **84** pp. 257-64.

- Philip, J.R., 1969. 'The theory of Infiltration' in *Advanced Hydroscience*, 5: pp.215-296.
- Philip, J.R., 1980. 'Field heterogeneity: some basic issues' in *Water Resources Res.*, 16 (2) pp. 443-448.
- Phillips, J.D., 1992. 'Non-linear dynamical systems in geomorphology: revolution or evolution' in *Geomorphology*, 5, pp. 219-229.
- Pickup, G., 1988. 'Hydrology and sediment models' in Anderson, M.G. (Ed.), *Modelling Geomorphological Systems*, Wiley, Chichester, pp. 153-215.
- Piest, R.F., Kramer, L.A. and Heinemann, H.G., 1975. 'Sediment movement from loessial watersheds' in *Present and Prospective Technology for predicting sediment yields and sources* U.S. Dept. of Agric. Publ. ARS-S-40 pp. 130-141.
- Press, W.H., Flannery, B.P., Teukoloskym S.A., and Vetterling, W.T., 1992. *Numerical Recipes: The Art of Scientific Computing* 2nd Edition. Cambridge University Press, Cambridge.
- Quick, M.C., and Pipes, A., 1977. 'U.B.C. watershed model' in *Hydrol. Sci. Bull.* 22 (1) pp. 153-161.
- Quinn, P. F., 1991. *The role of digital terrain analysis in hydrological modelling*. Ph.D. thesis, University of Lancaster, UK.
- Quinn, P.F., Beven, K.J., 1993. 'Spatial and temporal predictions of soil-moisture dynamics, runoff, variable source areas and evapotranspiration for Plynlimon, Mid-Wales' in *Hydrological Processes*, 7 (4) pp. 425-448.
- Quinn, P.F., Beven, K.J., and Culf, A., 1995a. 'The introduction of macroscale hydrological complexity into land surface-atmosphere transfer models and the effect on planetary boundary-layer development' in *Journal of Hydrology*, 166 (3-4) pp. 421-444.
- Quinn, P.F., Beven, K.J., and Lamb, R., 1995b. 'The $\ln(a/\tan\beta)$ index; how to calculate it and how to use it in the TOPMODEL framework' in *Hydrological Processes*, 9 pp. 55-68.
- Quinn, P., Beven, K., Chevalier, P., and Planchon, O., 1991. 'The prediction of hillslope paths for distributed hydrological modeling using digital terrain models' in *Hydrological Processes*, 5, pp. 59-79.
- Rango, A., Feldman, A., George, T.S., Ragan, R.M., 1983. 'Effective use of LANDSAT data in hydrologic-models' in *Water Resources Bulletin* 19 (2) pp. 165-174.
- Rawls, W.J., and Brakensiek, D.L.1982. 'Estimation of soil-water properties' in *Transactions of the ASAE* 25 (5) p. 1316.
- Rawls, W.J., and Brakensiek, D.L., 1983. 'Green-Ampt Infiltration parameters from soils data' in *Journal of Hydraulic Eng. – ASCE* 109 (1) pp. 62-70.
- Refsgaard, J.C., and Knudsen, J., 1996. 'Operational validation and intercomparison of different types of hydrological models' in *Water Resources Res.* 32 (7) pp. 2189-2202.
- Renfro, G.W., 1975. 'Use of erosion equations and sediment-delivery ratios for predicting sediment yield' in *Present and Prospective Tochnology for predicting sediment yields and sources*, U.S. Dept of Agric. ARS-S-40, pp. 33-45.
- Richards, K.S., 1993. 'Sediment Delivery and the drainage network' in Beven, K.J. and Kirkby, M.J. (Eds.), *Channel Network Hydrology*, Wiley, 1993.
- Risse, L.M., Nearing, M.A., Nicks, A.D., Laflen, J.M., 1993. 'Error Assessment in the Universal Soil Loss Equation' in *Soil Soc. Am. J.*, 57 pp 825-833.

- Robin, M.J.L., Gutjahr, A.L., Sudicky, E.A., Wilson, J.L., 1993. 'Cross-correlated random field generator with Direct Fourier Transform Method' in *Water Resources Research*, **29** pp. 2385-2397.
- Rodda, J.C., 1985. *Facets of Hydrology* London: Wiley.
- Rodriguez-Iturbe, I., and Valdes, J.B., 1979. 'The geomorphologic structure of hydrologic response' in *Water Resources Res.*, **15** (6) pp. 1409-1420.
- Roehl, J.E., 1962. 'Sediment source areas, delivery ratios and influencing morphological factors' in *Commission of Land Erosion (Symposium of Bari, 1-8 October, 1962)*, 202-213. IAHS Publ. no. **59**.
- Rogers, J.S., Selim, H.M., Carter, C.E., Fouss, J.L., 1991. 'Variability of auger hole hydraulic conductivity values for a commerce silt loam' in *Trans. of the ASCE* **34** (3) pp. 876-882.
- Rose, K.A., Smith, E.P., Gardner, R.H., Brenkert, A.L., and Bartell, S.M., 1991. 'Parameter sensitivities, Monte Carlo filtering and model forecasting under uncertainty' in *Journal of Forecasting* **10** pp. 117-134.
- Rosenbrock, H.H., 1960. 'An automatic method of finding the greatest or least value of a function in *Computing Journal* **3** pp. 175-184.
- Ross, B.B., Contractor, D.N., and Shanholz, V.O., 1979. 'A finite element model of overland and channel flow for assessing the hydrological impact of land-use change' in *Journal of Hydrology*, **41**, 11-30.
- Russo, D., and Bresler, E., 1981. 'Soil hydraulic properties as stochastic processes: I. An analysis of field spatial variability' in *Soil Soc. Am. J.*, **45** (4) pp. 682-687.
- Sader, S.A., Douglas, A., Liou, W., 1995. 'Accuracy of Landsat-TM and GIS Rule-based methods for forest wetland classification in Maine' in *Remote Sens. Environ.* **53** pp. 133-144.
- Saulnier, G. M., Beven, K., Obled, C., 1997a. 'Including spatially variable effective soil depths in TOPMODEL' in *Journal of hydrology* **202**: (1-4) pp.158-172.
- Saulnier, G. M., Obled, C., Beven, K., 1997b. 'Analytical compensation between DTM grid resolution and effective values of saturated hydraulic conductivity within the TOPMODEL framework' in *Hydrological Processes* **11**: (9) pp. 1331-1346.
- Schumm, S.A., 1960. 'The shape of alluvial channels in relation to sediment types' Professional paper of the *USGS*, 352B, pp. 17-30.
- Schumm, S.A., 1973. *Slope Morphology*, Dowden, Hutchinson and Ross Ltd.
- Schumm, S.A., 1991. *To Diagnose the Earth*. Cambridge University Press, Cambridge, 133 pp.
- Schumm, S.A., and Hadley, R.F., 1957. 'Arroyos and the semi- and cycle of erosion' in *American Journal of Science*, **255**, pp. 161-74.
- Schumm, S. A., and Lustby, 1963. 'Seasonal variation of infiltration capacity and runoff on hillslopes in Western Colorado' in *Journal of Geophysical Research*, **68** pp. 3665-3666.
- Seibert, J., Bishop, K.H., and Nyberg, L. 1997. 'A test of TOPMODEL's ability to predict spatially distributed groundwater levels' in *Hydrological Processes* **11** pp. 1131-1144.
- Seliga, T.A., Aron, G., Aydin, K., White, E., 1992. 'Storm runoff simulation using radar-estimated rainfall rates and a Unit Hydrograph model (SYN-HYD) applied to the GREVE watershed' in *Am. Meteorol. Soc.*, *25th Int. Conf. On Radar Hydrology* pp. 587-590.
- Sempre-Torres, D., 1990. 'Calcul de la lame ruiselee dans la modelisation pluie-debit: limitations des approches globales et introduction simplifiee de la

- topographie et de la variabilité spatiale des pluies' Ph.D. thesis, Institut Mechanique de Grenoble, France.
- Sen, M., and Stoffa, P.L., 1995. *Global Optimisation Models in Geophysical Inversion*. Elsevier, Amsterdam.
- Shannon, C.E. and Weaver, W., 1964. *The Mathematical Theory of Communication*. University of Illinois Press, Urbana.
- Sharma, M.L., 1983. 'Field variability and its hydrological consequences: A synthesis' in *Proc. of Hydrology and Water Resources Symp.* pp. 262-268. The Inst. Of Engineers, Canberra, Australia.
- Sharma, M.L., Luxmore, R.J., 1979. 'Soil spatial variability and its consequences on simulated water balance' in *Water Resources Res.*, **15** pp. 1567-1573.
- Sharma, M.L., Gander, G.A., Hunt, C.G., 1980. 'Spatial variability of infiltration in a watershed' in *Journal of Hydrology*, **45** pp. 101-122.
- Sharma, M.L., Luxmore, R.J., DeAngelis, R., Ward, R.C., and Yeh, G.T., 1987. 'Subsurface water flow simulated for hillslopes with spatially dependent soil hydraulic characteristics' in *Am. Geophys. Union*, pp. 1523-1530.
- Sherman, L.K., 1932. 'Streamflow from rainfall by the unit graph method' in *Eng. News Rec.*, **108**, pp. 501-505.
- Shinozuka, M., 1971. 'Simulation of multivariate and multi-dimensional random process' in *J. Acoust. Soc. Am.*, **49**, pp. 357-367.
- Shinozuka, M., Jan, C.M., 1972. 'Digital simulation of random processes and its applications' in *J. Sound Vib.*, **25** (1) pp. 111-128.
- Seibert, J., 1997. 'Estimation of parameter uncertainty in the HBV model' in *Nordic Hydrology* **28** (4/5) pp. 247-262
- Simons, D.B., and Senturk, F., 1977. *Sediment Transport Technology*, Water Resources Publications, Fort Collins, CO, 807 pp.
- Sisson, J.B., and Wierenga, 1981. 'Spatial variability of steady state infiltration rates as a stochastic processes' in *Soil Sci, Soc. Am. J.* **45** pp. 699-704.
- Sklash, M.G., Farvolden, R.N., 1979. 'The role of groundwater in storm runoff' in *Journal of Hydrology* **43** pp. 45-65.
- Slattery, M.C., Burt, T.P., 1997. 'Particle size characteristics of suspended sediment hillslope runoff and streamflow' in *Earth Surface Processes and Landforms*, vol. **22**, pp.705-719.
- Smerdon, E.T., and Beasley, R.P., 1961. 'Critical Tractive forces in cohesive soils' in *Agricultural Engineering*, **42** (1) pp. 26-29.
- Smith and Woolhiser, 1971. 'Overland flow on an infiltrating surface' in *Water Resources Res.*, **7** (4), pp. 899-913.
- Smith, L., and Freeze, R.A., 1979a. 'Stochastic analysis of steady state groundwater flow in a bounded domain 1. One-dimensional simulations' in *Water Resources Res.*, vol. **15** (3) pp. 521-528.
- Smith, L., and Freeze, R.A., 1979b. 'Stochastic analysis of steady state groundwater flow in a bounded domain 2. Two-dimensional simulations' in *Water Resources Res.*, vol. **15** (6) pp. 1543-1559.
- Smith, L., and Schwartz, F.W., 1981. 'Mass transport, 2, Analysis of uncertainty in prediction' in *Water Resources Res.*, **17** (2) pp. 351-369.
- Smith, R.E., Hebbert, R.H.B., 1979. 'A Monte Carlo analysis of hydrologic effects of spatial variability of infiltration' in *Water Resources Res.*, **15** pp. 419-429.
- Sooroshian, S., and Gupta, V.J., and Fulton, J.L., 1983. 'Evaluation of maximum likelihood parameter estimation techniques for conceptual rainfall-runoff

- models: influence of calibration data variability and length on model credibility' in *Water Resources Res.*, **19** (1): 251-259.
- Sorooshian, S., and Gupta, V.J., 1983. 'Automatic calibration of conceptual rainfall-runoff models: the question of parameter observability and uniqueness' in *Water Resources Res.*, **19** (1): 260-268.
- Sorooshian, S., Gupta, V.J., 1985. 'The analysis of structural identifiability: theory and application to conceptual rainfall-runoff models' in *Water Resources Res.*, **21** (4) pp. 487-495.
- Stephenson, G.R., and Freeze, R.A., 1974. 'Mathematical simulation of subsurface flow contributions to snowmelt runoff, Reynolds Creek, Idaho' in *Water Resources Res.*, **10** (2) pp. 284-294.
- Strzepek, K.M., Wilson, J.L., Marks, D.H., 1982. 'Planning and design of agricultural drainage under uncertainty: A multi-level approach' Report 281. Cambridge MA: Ralph M. Parsons Hydrology and Water resource Systems, Massachusetts Institute of Technology.
- Surkan, A.J., 1969. 'Synthetic hydrographs: Effects of network geometry' in *Water Resources Res.*, **5** (1) pp. 112-128.
- Surkan, A.J., 1974. 'Simulation of storm velocity effects on flow from distributed channel networks' in *Water Resources Res.*, **10** (6) pp. 1149-1160.
- Swift, L.W., 1976. 'Algorithm for solar radiation on mountain slopes' in *Water Resources Res.* **12** (1) pp. 108-112.
- Thompson, A.F.B., Ababou, R., Gelhar, L.W., 1989. 'Implementation of the three-dimensional turning bands random field generator' in *Water Resources Res.* **25** (10) pp. 2227-2243.
- Thompson, N., Barrie, I.A., Ayles, 1981. The Meteorological Office Rainfall and Evaporation Calculation System MORECS. Hydrological Memorandum No. 45, UK Meteorological Office.
- Thorne, C.R., 1982. 'Processes and mechanisms of river bank erosion' in Hey, R.D., Bathurst, J.C., and Thorne, C.R. (Eds.) *Gravel-bed Rivers*, Wiley, Chichester pp. 227-259.
- Thorne, C.R., Zevenbergen, I.W., Grissinger, F.H., Murphy, J.B., 1986. 'Ephemeral gullies as sources of sediment' in *Proc. Fourth Federal Interagency Sed. Conf.* Las Vegas, Nevada, March 26. Vol. 1 pp.3.152-3.161.
- Thyer, M., Kuczera, G., and Bates, B.C., 1999. 'Probabilistic optimisation for conceptual rainfall runoff models: a comparison of the shuffled complex evolution and simulated annealing algorithms' in *Water Resources Research* **35** pp. 767-774.
- Torri, D., and Borselli, F. 1991. 'Overland flow and soil erosion: some processes and their interactions' in *Catena Suppl.* **19** pp. 129-137.
- Trieste, D.J., and Gifford, G.F., 1980. 'Application of the Universal Soil Loss Equation to rangelands on a per storm basis' in *J. Range Management* **33** pp. 66-70.
- Trimble, S.W., 1983. 'A Sediment budget for Coon Creek Basin in the driftless area, Wisconsin, 1853-1977' in *American Journal of Science* **283** (5) pp. 454-474.
- Troutman, B.M., 1983. 'Runoff prediction errors and bias in parameter estimation induced by spatial variability of precipitation' in *Water Resources Res.*, **19** (3) pp. 791-810.
- Tsang, C.F., 1991. 'The modelling process and model validation' in *Groundwater* **29** (6) pp. 825-831.

- Tumeo, M., 1994. 'The meaning of stochasticity, randomness and uncertainty in environmental modeling' in Kippel, K. (ed.) *Stochastic and Statistical Methods in Hydrology and Environmental Engineering*, vol. 2 pp 33-38.
- Uhlenbrook, S., Seibert, J., Leibundgut, C., and Rhode, A., 1999. 'Prediction uncertainty of conceptual rainfall-runoff models caused by problems in identifying parameters and structure' in *Hydrological Science Journal* 44 pp. 779-797.
- United Nations Conference on the Human Environment, Stockholm, 1972. UN Doc. A/Conf/48/14/rev.1.
- US Army, 1956. *Snow Hydrology*. US Army Corps of Engineers, Portland, Oregon, USA.
- US Army, 1975. *Program description and users manual for the SSARR model*, US Army corps of Engineers, Portland, Oregon, USA.
- Valdes, J.B., Fiallo, Y., Rodriguez-Iturbe, I., 1979. 'A rainfall-runoff analysis of the geomorphologic IUH' in *Water Resources Res.*, 15 (6) pp. 1421-1434.
- Van Kuilenberg, J., DeGruijter, J.J., Marsman, B.A., Bouma, J., 1982. 'Accuracy of spatial interpolation between point data on soil moisture supply capacity compared with estimates from mapping units' in *Geoderma*, 27 pp. 311-325.
- Van Rompaey, A.J.J, Govers G., Van Hecke, E., Jacobs, K., 2001. 'The impacts of landuse on the soil erosion risk: a case study in Central Belgium' in *Agricultural Ecosystems and Environment* 83 (1-2) p. 83-94.
- Van Straten., G., and Keesman, K., 1991. 'Uncertainty propagation and speculation in projective forecasts of environmental change: a lake eutrophication example' in *Journal of Forecasting* 10 pp. 163-190.
- VandenBygaart, A. J., Protz, R., 1999. 'The representative elementary area (REA) in studies of quantitative soil micromorphology' in *Geoderma* 89: (3-4) pp. 333-346.
- Vieira, S.R., Nielsen, D.R., Biggar, J.W., 1981. 'Spatial variability of field-measured infiltration rate' in *Soil Sci. Soc. Am. J.*, 45 pp. 1040-1048.
- Wall, G.J., Dickinson, W.T., van Vlie, L.J.P., 1979. 'Agricultural sources of fluvial suspended sediments' *Prog. Water Technol.* 11 (6) pp. 481- 499.
- Walling, D.E., 1977. 'Limitations of the rating curve technique for estimating suspended sediment loads, with particular reference to British rivers' in *IAHS-AISH Publ.*, 122 pp. 34-48.
- Walling, D.E., 1983. 'The Sediment Delivery Problem' in *Journal of Hydrology*, 65 pp. 209-239.
- Walling, D.E. and Webb, B.W., 1982. 'Sediment availability and the prediction of storm-period sediment yields' in *Recent Developments in the Explanation and Prediction of Erosion and Sediment Yield (Proceedings of the Exeter Symposium, July, 1982)*, IAHS Publ. no. 137.
- Walling, D.E., and Webb, B.W., 1983. 'The dissolved load of rivers: a global overview' in *Dissolved loads of rivers and surface water quality/quantity relationship* Proc. Of Hamberg Symp, Aug, 1983. *IAHS Publ.* No. 141 pp.3-20.
- Wang, Q.J., 1991. 'The genetic algorithm and its application to calibrating conceptual rainfall-runoff models' in *Water Resources Research* 27 pp. 2467-2471.
- Ward, R.C., 1984. 'Hypothesis-testing by modelling catchment response' in *Journal of hydrology* 67 pp. 281-305.
- Warren, J.E., and Price, H.S., 1961. 'Flow in heterogeneous porous media' in *Soc. Petrol. Eng. J.*, 1 pp. 153-169.

- Warren, J.E., Skiba, F.F. and Price, H.S., 1961. 'An evaluation of significance of permeability measurements' in *J. Petrol. Technol.*, pp. 739-744.
- Weber, D., and Englund, E., 1992. 'Evaluation and comparison of spatial interpolators' in *Math. Geol.* **24** (4) pp. 381-391.
- Weltz, M.A., Renard, K.G., Simanton, J., 1987. 'Revised USLE for western rangelands' in *U.S. For Serv. Gen. Tech. Rep. Rocky Mountain For. Range Exp. Stn., Fort Collins, Co.* pp. 104-111.
- Wheater, H.S., Bishop, K.H., and Beck, M.B., 1986. 'The identification of conceptual hydrological models for surface water acidification' in *Hydrological Processes*, **1** pp. 89-109.
- Wheater, H.S., Jakeman, A.J., Beven, K.J., 1993. 'Progress and directions in rainfall-runoff modelling' in Jakemen, A.J., Beck, M.B., and Mc Aleer, M.J. (Eds.) *Modelling Change in Environmental Systems*, Wiley and Sons Ltd.
- Wheater, H.S., Shaw, T.L., and Rutherford, J.C., 1982. 'Storm runoff from small lowland catchments in South West England' in *Journal of Hydrology*, **55** pp. 321-337.
- White, I., and Perroux, K.M., 1987. 'Use of sorptivity to determine field soil hydraulic properties' in *Soil Sci. Soc. Am. J.*, **51** (5) pp. 1093-1101.
- Wigmosta, M.S., Vail, L.W., Lettenmaier, D.P., 1994. 'A distributed hydrology-vegetation model for complex terrain' in *Water Resources Research*, **30** (6) pp. 1665-1679.
- Willardson L.S., and Hurst, R.L., 1965. 'Sample size estimates permeability studies' in *J. Irrig. Drain. Div. ASCE* **91** (IRI) pp. 1-9.
- Williams, G.P., 1989. 'Sediment concentration versus water discharge during single hydrologic events in rivers' in *Journal of Hydrology* **111** (1-4) pp. 89-106.
- Williams, J.R., 1975. 'Sediment routing from agricultural watersheds' in *Water Resources Bulletin*, **11**: pp. 965-974.
- Williams, J.R., 1977. 'Sediment delivery ratios determined with sediment and runoff models' in *Erosion and solid matter transport in inland waters (Proc. Paris Symposium, July, 1977)*, 168-179. IAHS Publ. no. **122**.
- Wilson, C.B., Valdes, J.B., and Rodriguez-Iturbe, I., 1979. 'On the influence of the spatial distribution of rainfall on storm runoff' in *Water Resources Res.*, **15** (2) pp. 321-328.
- Wilson, J.L., 1979. 'The synthetic generation of areal averages of random field', paper presented at *Socorro Workshop on Stochastic Methods in Subsurface Hydrology*, New Mex. Tech., Socorro, New Mex.
- Wilson, V., 1958. *British Regional Geology, East Yorkshire and Lincolnshire*: HMSO, London, 94pp.
- Wischmeier, W.H., 1976. 'Use and misuse of the Universal Soil Loss Equation' in *Soil erosion: Prediction and control*, Soil Conserv. Soc. Am. Spec. Publ. **21** SCSA, Ankeny, IA.
- Wischmeier, W.H., and Smith, D.D., 1960. 'A Universal soil-loss equation to guide conservation farm planning' in *7th International Congress of Soil Sci. (Madison, Wisconsin, 1960)*.
- WMO, 1986. *Intercomparison of models of snowmelt runoff*, WMO Operational Hydrology Report no. **23**, WMO Publ. no. 646 World Meteorological Organisation, Geneva, Switzerland.
- Wolman, M.G., and Miller, J.P., 1960. 'Magnitude and frequency of forces in geomorphic processes' in *J. Geology*, **68** pp. 54-74.

- Wolock, D.M., 1995. 'Effects of subbasin size on topographic characteristics and simulated flow paths in Sleepers River watershed, Vermont' in *Water Resources Res.*, **31** (8) pp. 1989-1997.
- Wolock, D.M., and Price, C.V., 1994. 'Effects of digital elevation model map scale and data resolution on a topography-based watershed model' in *Water Resources Res.*, **30** (11), pp. 3041-3052.
- Wood, E.F., and O'Connell, 1985. 'Real-time forecasting' in Anderson, M.G., and Burt, T.P. (Eds.) *Hydrological Forecasting* John Wiley and Sons Ltd.
- Wood, E.F., Lettenmeir, D.P., and Zartarian, V.G., 1992. 'A land-surface hydrology parameterisation with subgrid variability for general circulation models' in *Journal of Geophys. Research* **97** pp. 2717-2728.
- Wood, E.F., Sivapalan, M., Beven, K.J., Band, L., 1988. 'Effects of spatial variability and scale with implications to hydrologic modelling' in *Journal of Hydrology*, **102** pp. 29-47.
- Woods, R.A., and Sivapalan, M., 1997. 'A connection between topographically driven runoff generation and channel network structure' in *Water Resources Res.*, **33** (12) pp. 2939-2950.
- Woolhiser, D.A., 1975. 'Simulation of unsteady overland flow' in Mahmood, K., and Yevjevich, V., (Eds.) *Unsteady Flow in Open Channels*, Water Resources Publications, Fort Collins, CO, vol. **2**. Pp. 485-508.
- Wright, A.C., 1987. 'A model of the distribution of disaggregated soil particles by rainsplash' in *Earth Surf. Proc. and Lanf.*, **12** (6) pp. 583-596.
- Wright, C.W., 1972. 'The Stratigraphy of the Yorkshire Corallian' in *Proc. Yorkshire Geol. Soc.*, Vol. **39**, pp. 225-266.
- Yang, V.Y., 1972. 'Unit stream power and sediment transport' in *J. Hydraul. Div. ASCE* **98** (HY10) pp. 1805-1826.
- Yeh, W.W.G., 1986. 'Review of parameter identification procedure in groundwater hydrology: The inverse problem' in *Water Resources Research*, **22** (2) pp. 95-108.
- Yoo, K.H., and Molnau, M., 1982. 'Simulation of soil erosion from winter runoff in the Palouse Prairie' in *Trans. Am. Soc. Agri. Engrs.*, **25** (6) pp. 1628-1636.
- Young, R.A., and Onstad, C.A., 1982. 'The effect of soil characteristics on erosion and nutrient loss' in *Hydrological Sciences Journal – Journal Des Sciences Hydrologiques*, **27** (2) pp. 235-235.
- Yu, S.L., 1972. 'Uncertainties in Water Quality Modelling, the Case of atmospheric Reaeration' in Kiesel and Duckstein (eds.) *Proceedings of the International Symposium on Uncertainty in Hydrologic and Water Resource Systems, Tuscon Arizona*, 11-14 December.
- Zhang, W., and Montgomery, D.R., 1994. 'Digital elevation model grid size, landscape representation and hydrologic simulations' in *Water Resources Res.*, **30** (4) pp. 1019-1028.
- Zielinski, P.A., 1991. 'On the meaning of Randomness in stochastic environmental models' in *Water Resources Res.*, vol. **27** (7) pp 1607-1611.

APPENDIX 1

HYDROLOGICAL MODEL CODE FOR MONTE CARLO SIMULATION

```

C  A FULLY DISTRIBUTED GRID BASED SOIL MOISTURE ACCOUNTING MODEL
C
C  12.10.99
C
C  INTEGER I,II,N,N2,X,Y,NX,NY,NR,LX,NF
C
C  PARAMETER(PNX=242,PNY=391,PNF=10,PN=9000,PNR=10,
& PN2=10000)
C
C  REAL MDASH2(PN2),K0DASH2(PN2),SRDASH2(PN2),
& CHV2DASH2(PN2),ETFDASH2(PN2),EFF2(PN2)
C
C  COMMON /INTS/ I,II,N,N2,X,Y,NX,NY,NR,LX,NF,
& ZOOM1,ZOOM2
C
C  COMMON /DASH/ PMDASH,PK0DASH,SRDASH,CHV2DASH,
& ETFDASH,EFF,TSTART,IND,RAINAREA(PNX,PNY),
& ETF,CHV1,CHV2,GWL,SMF,
& E(PNX,PNY),DIST1(PNX,PNY),DIST2(PNX,PNY),QOBS(PN),SEDOBS(PN),
& RAIN1(PN),RAIN2(PN),ET(PN),TEMP(PN),RAD(PN),AVERAIN(PN),P1,P2,
& QT(PN),QT2(PN,PN2),AREA,AREA1,AREA2,
& QMIN,QMAX
C
C  COMMON /INICOM/ QBAR,EPT,EA1T,EA2T,EAT,SINIT,SFINAL,SRZINIT,
& SUZINIT,QEXL(PN),ERAIN,SNOW(PNX,PNY),S(PNX,PNY),SRMAX,
& COUNT(PNX,PNY),FEAT(PNX,PNY),SUZ(PNX,PNY),SRZ(PNX,PNY),
& SUMRAIN,SUMQOBS,SUMQPRED,SUMQSF,VAR1,VAR2,VAR3
C-----
C  .. External Functions ..
DOUBLE PRECISION G05DAF
EXTERNAL    G05DAF
C  .. External Subroutines ..
EXTERNAL    G05CCF
C  .. Executable Statements ..
CALL G05CCF(0)
C-----
C
C OPEN HYDROLOGICAL MODEL PARAMETER FILES
C
C  OPEN(1,FILE='grid2.dat',STATUS='UNKNOWN',
& FORM='UNFORMATTED')
READ(1)NX,NY,LX,N,TSTART,NF,IND,N2
CLOSE(1)
C
C  OPEN(3,FILE='feature2.dat',FORM='UNFORMATTED')
OPEN(4,FILE='freedtm2.dat',FORM='UNFORMATTED')
OPEN(5,FILE='hillslope2.dat',FORM='UNFORMATTED')
OPEN(55,FILE='channel2.dat',FORM='UNFORMATTED')
OPEN(7,FILE='rainarea2.dat',FORM='UNFORMATTED')
C
C  AREA=0

```

```

C
DO Y=1,NY
DO X=1,NX
C READ(3)FEAT(X,Y)
READ(4)E(X,Y)
READ(5)DIST1(X,Y)
READ(55)DIST2(X,Y)
READ(7)RAINAREA(X,Y)
c
C J=INT(FEAT(X,Y))
C
S(X,Y)=0.0
SUZ(X,Y)=0.0
SRZ(X,Y)=SRMAX
C
IF(E(X,Y).LT.9000)AREA=AREA+1
IF(RAINAREA(X,Y).EQ.1)AREA1=AREA1+1
IF(RAINAREA(X,Y).EQ.2)AREA2=AREA2+1
ENDDO
ENDDO
C
C-----
C CALCULATE FRACTIONAL RAINAREAS
C
P1=AREA1/AREA
P2=AREA2/AREA
C-----
C CLOSE(3)
CLOSE(4)
CLOSE(5)
CLOSE(55)
CLOSE(7)
C-----
C OPEN(8,FILE='rrdata2.dat',STATUS='UNKNOWN',
& FORM='UNFORMATTED')
C
DO I=1,TSTART-1
IF(IND.EQ.1)THEN
READ(8)QOBS(I),SEDOBS(I),RAIN1(I),ET(I),TEMP(I),RAD(I)
ELSE
READ(8)QOBS(I),SEDOBS(I),RAIN1(I),RAIN2(I),ET(I),TEMP(I),RAD(I)
ENDIF
ENDDO
C
DO I=1,N
IF(IND.EQ.1)THEN
READ(8)QOBS(I),SEDOBS(I),RAIN1(I),ET(I),TEMP(I),RAD(I)
ET(I)=ET(I)*ETF
ELSE
READ(8)QOBS(I),SEDOBS(I),RAIN1(I),RAIN2(I),ET(I),TEMP(I),RAD(I)
AVERAIN(I)=(RAIN1(I)*P1)+(RAIN2(I)*P2)
ET(I)=ET(I)*ETF
ENDIF
C-----
C CALCULATE MIN AND MAXIMUM DISCHARGES
C
QMIN=0.00006
QMAX=0.00030
C
C

```

```

IF(QOBS(I).LT.QMIN)THEN
QMIN=QOBS(I)
ZOOM1=I
ENDIF
IF(QOBS(I).GT.QMAX)THEN
QMAX=QOBS(I)
ZOOM2=I
ENDIF
C
ENDDO
CLOSE(8)
C-----
C OPEN RESULTS FILES FOR THE PARAMETER SEARCH
C
OPEN(997,FILE='parameters.dat',FORM='UNFORMATTED')
OPEN(998,FILE='discharges.dat',FORM='UNFORMATTED')
OPEN(999,FILE='max_params.dat',FORM='UNFORMATTED')
C-----
C
MAXEFF=0.0
C
DO II=1,N2
C
PMDASH = G05DAF(0.01D0,0.06D0)
PK0DASH = G05DAF(50.0D0,500.0D0)
SRDASH = G05DAF(0.001D0,0.01D0)
C CHV1DASH = G05DAF(0.01D0,1.0D0)
CHV2DASH = G05DAF(0.01D0,1.0D0)
ETFDASH = G05DAF(0.1D0,1.4D0)
C
C-----
C
CALL INIMOD
C
CALL HYDROMOD
C-----
C
MDASH2(II)=PMDASH
K0DASH2(II)=PK0DASH
SRDASH2(II)=SRDASH
CHV1DASH2(II)=CHV1DASH
CHV2DASH2(II)=CHV2DASH
ETFDASH2(II)=ETFDASH
EFF2(II)=EFF
C-----
C
C SEARCH FOR GLOBAL OPTIMAL PARAMETER VALUES
C
MAXEFF=0.0
C
IF(EFF2(II).GT.MAXEFF)THEN
MAXM=MDASH2(II)
MAXK0=K0DASH2(II)
MAXSRMAX=SRDASH2(II)
MAXEFF=EFF2(II)
C MAXCHV1=CHV1DASH2(II)
MAXCHV2=CHV2DASH2(II)
MAXETF=ETFDASH2(II)
ENDIF
C

```

```

C-----
C
C CLOSE PARAMETER SEARCH LOOP
C
C ENDDO
C
C-----
C
C WRITING PARAMETER SEARCH VALUES AND OBJECTIVE F TO FILE
C
C-----
C DO II=1,N2
C WRITE(997)MDASH2(II),K0DASH2(II),SRDASH2(II),
C & CHV2DASH2(II),ETFDASH2(II),EFF2(II)
C
C DO I=1,N
C WRITE(998)QT2(I,II)
C ENDDO
C ENDDO
C
C
C WRITE(999)MAXM,MAXK0,MAXSRMAX,MAXCHV2,MAXETF,
C & MAXEFF
C-----
C
C CLOSE(997)
C CLOSE(998)
C CLOSE(999)
C
C STOP
C END
C-----
C SET INITIAL VALUES FOR STORAGES AND TOTALS
C
C SUBROUTINE INIMOD
C
C INTEGER I,II,N,N2,X,Y,NX,NY,NR,LX,NF
C
C PARAMETER(PNX=242,PNY=391,PNF=10,PN=9000,PNR=10,
C & PN2=10000)
C
C REAL QBAR,EPT,EA1T,EA2T,EAT,SINIT,SFINAL,SRZINIT,SUZINIT,
C & ERAIN
C
C COMMON /INTS/ I,II,N,N2,X,Y,NX,NY,NR,LX,NF,
C & ZOOM1,ZOOM2
C
C COMMON /INICOM/ QBAR,EPT,EA1T,EA2T,EAT,SINIT,SFINAL,SRZINIT,
C & SUZINIT,QEXL(PN),ERAIN,SNOW(PNX,PNY),S(PNX,PNY),SRMAX,
C & COUNT(PNX,PNY),FEAT(PNX,PNY),SUZ(PNX,PNY),SRZ(PNX,PNY),
C & SUMRAIN,SUMQOBS,SUMQPRED,SUMQSF,VAR1,VAR2,VAR3
C
C
C DO Y=1,NY
C DO X=1,NX
C
C J=INT(FEAT(X,Y))

```

```

S(X,Y)=0.0
SUZ(X,Y)=0.0
SRZ(X,Y)=SRMAX
COUNT(X,Y)=0.0
SNOW(X,Y)=0.0
ENDDO
ENDDO
C
NR=0
QBAR=0.0
EPT=0.0
EA1T=0.0
EA2T=0.0
EAT=0.0
SINIT=0.0
SFINAL=0.0
SRZINIT=0.0
SRZFINAL=0.0
SUZINIT=0.0
SUZFINAL=0.0
QEXL(1)=10.0
ERAIN=0.0
QV=0.0
SUMRAIN=0.0
SUMQOBS=0.0
SUMQPRED=0.0
SUMQSF=0.0
SUMQEX=0.0
VAR1=0.0
VAR2=0.0
VAR3=0.0
C
END
C
C-----
C
C-----
C
SUBROUTINE HYDROMOD
C
C-----
INTEGER I,II,N,N2,X,Y,IX,IY,NX,NY,LX,N,NF,NR,
& ZOOM1,ZOOM2,IND,DELAY,TSTART
C
PARAMETER(PNX=242,PNY=391,PNF=10,PN=9000,PNR=10,
& PN2=10000)
C
REAL CL,TT,DH1,DH2,
& QSF(PN),QPRED(PN),QS(PN),
& QSFAREA(PN),QEXAREA(PN),QTAREA(PN),
& HEAD,PQSF,PQEX,QEXFIL,QSOF,NTOT,NQSF,
& NQEX,BALANCE,BALANCE1,DELTAS,PRECIP,EA1,EA2,EVAP,E2,
& EA1T,EA2T,EAT,QV,CUME(PNX,PNY),SRZINIT,
& TEMP2(PNX,PNY),M,K0,CHV1,
& MELT(PNX,PNY),PRECIP2(PNX,PNY)
C
COMMON /INTS/ I,II,N,N2,X,Y,NX,NY,NR,LX,NF,
& ZOOM1,ZOOM2
C
COMMON /DASH/ PMDASH,PK0DASH,SRDASH,CHV2DASH,

```

```

& ETFDASH, EFF, TSTART, IND, RAINAREA(PNX, PNY),
& ETF, CHV1, CHV2, GWL, SMF,
& E(PNX, PNY), DIST1(PNX, PNY), DIST2(PNX, PNY), QOBS(PN), SEDOBS(PN),
& RAIN1(PN), RAIN2(PN), ET(PN), TEMP(PN), RAD(PN), AVERAIN(PN), P1, P2,
& QT(PN), QT2(PN, PN2), AREA, AREA1, AREA2,
& QMIN, QMAX
C
COMMON /INICOM/ QBAR, EPT, EA1T, EA2T, EAT, SINIT, SFINAL, SRZINIT,
& SUZINIT, QEXL(PN), ERAIN, SNOW(PNX, PNY), S(PNX, PNY), SRMAX,
& COUNT(PNX, PNY), FEAT(PNX, PNY), SUZ(PNX, PNY), SRZ(PNX, PNY),
& SUMRAIN, SUMQOBS, SUMQPRED, SUMQSF, VAR1, VAR2, VAR3
C
C-----
C
C ASSIGN NEW NAMES TO PARAMETERS TO BE VARIED
C
M=PMDASH
K0=PK0DASH
SRMAX=SRDASH
C CHV1=CHV1DASH
CHV2=CHV2DASH
ETF=ETFDASH
C-----
C
GWL=0.0
SMF=0.000094
CHV1=0.1
C-----
C CALCULATE CELL DISTANCES AND CONTOUR LENGTHS
C
C (CARDINAL)
DX1=LX
CL1=LX*0.5
C (DIAGONAL)
DX2=LX*1.41421
CL2=LX*0.707
C
C-----
C OPEN FILES FOR OUTPUT MAPS
C
C OPEN(20, FILE='map1.dat')
C OPEN(21, FILE='map2.dat')
C OPEN(22, FILE='cume.dat')
C-----
C INITIALISE SETTINGS FOR STORAGES AND TOTALS
C
NR=0
QBAR=0.0
EPT=0.0
EA1T=0.0
EA2T=0.0
EAT=0.0
SINIT=0.0
SFINAL=0.0
SRZINIT=0.0
SRZFINAL=0.0
SUZINIT=0.0
SUZFINAL=0.0
QEXL(1)=10.0
ERAIN=0.0

```

```

QV=0.0
COUNT(X,Y)=0
SNOW(X,Y)=0.0
SUMRAIN=0.0
SUMQOBS=0.0
SUMQPRED=0.0
SUMQSF=0.0
SUMQEX=0.0
VAR1=0.0
VAR2=0.0
VAR3=0.0
C
C-----
C
C START MAIN PROGRAM LOOP - DO 10
C
C-----
C
  DO 10 I=1,N
C
C START INITIAL SOIL DRAINAGE UNTIL QEX = QOBS(1), AND THEREFORE
C AUTOMATICALLY SET THE SOIL MOISTURE DISTRIBUTION
C
2  IF(I.EQ.1)THEN
    IF(QEXL(I).GT.QOBS(1))THEN
      RAIN1(I)=0.0
      RAIN2(I)=0.0
      ET(I)=0.0
      START=1.0
      DO JI=1,N
        QT(JI)=0.0
        QS(JI)=0.0
      ENDDO
    ELSE
      START=2.0
      ET(I)=ET(I)
      RAIN1(I)=RAIN1(I)
      RAIN2(I)=RAIN2(I)
    ENDIF
  ENDIF
C
  NTOT=0.0
  NQSF=0.0
  NQEX=0.0
C
C-----
C START INTERNAL GRID LOOP FOR EACH TIMESTEP OF THE SIMULATION
C
  DO Y=1,NY
    DO X=1,NX
C
      IF(E(X,Y).GE.9998.0)GOTO 1
      EVAP=ET(I)
      IF(IND.EQ.1)PRECIP=RAIN1(I)
      IF(IND.EQ.2)THEN
        IF(RAINAREA(X,Y).EQ.1)THEN
          PRECIP=RAIN1(I)
        ELSE
          PRECIP=RAIN2(I)
        ENDIF
    ENDIF

```

```

      ENDIF
C
C-----
C CALCULATE DEPTH OF SNOWMELT RUNOFF
C
      TEMP2(X,Y)=TEMP(I)-0.0065*(E(X,Y)-110)
      IF(TEMP2(X,Y).LE.0.0)THEN
          SNOW(X,Y)=SNOW(X,Y)+PRECIP
          PRECIP2(X,Y)=0.0
          MELT(X,Y)=0.0
          COUNT(X,Y)=COUNT(X,Y)+1
      IF((TEMP2(X,Y).GT.0.0).AND.(COUNT(X,Y).GT.10))THEN
          SNOW(X,Y)=SNOW(X,Y)+PRECIP
          PRECIP2(X,Y)=0.0
          MELT(X,Y)=0.0
          COUNT(X,Y)=COUNT(X,Y)-1
          IF(COUNT(X,Y).LT.0)THEN
              COUNT(X,Y)=0
          ENDIF
      IF((TEMP2(X,Y).GT.0.0).AND.(COUNT(X,Y).LE.10))THEN
          MELT(X,Y)=1*((SMF*(TEMP2(X,Y)-0))+(0.00125* $\text{RAD}(I)$ *(1-0.8))
&-(0.0000000558*((TEMP2(X,Y)+273)**4)))
          PRECIP=PRECIP
          COUNT(X,Y)=COUNT(X,Y)-1
          IF(COUNT(X,Y).LT.0)THEN
              COUNT(X,Y)=0
          ENDIF
      IF((MELT(X,Y).GT.0.0).AND.(MELT(X,Y).LT.SNOW(X,Y)))THEN
          PRECIP2(X,Y)=MELT(X,Y)+PRECIP
          SNOW(X,Y)=SNOW(X,Y)-MELT(X,Y)
          MELT(X,Y)=0.0
      IF((MELT(X,Y).GT.0.0).AND.(MELT(X,Y).GE.SNOW(X,Y)))THEN
          MELT(X,Y)=SNOW(X,Y)
          PRECIP2(X,Y)=MELT(X,Y)+PRECIP
          SNOW(X,Y)=0.0
          MELT(X,Y)=0.0
      ENDIF
      ENDIF
      ENDIF
      ENDIF
      ENDIF
C
      PRECIP2(X,Y)=MELT(X,Y)+PRECIP
C-----
      SUMOUT=0.0
      SUMIN=0.0
      QEXFIL=0.0
      QSOF=0.0
      QTOT=0.0
      QV=0.0
      EA1=0.0
      EA2=0.0
      E2=0.0
C-----
C START INTERNAL MOVING WINDOW FOR FLOW ROUTING CALCULATIONS
C
      DO IX=-1,1
      DO IY=-1,1
C
      IF ((IX.EQ.0).AND.(IY.EQ.0))      GOTO 20

```

```

IF ((X+IX.EQ.0).OR.(X+IX.EQ.NX+1)) GOTO 20
IF ((Y+IY.EQ.0).OR.(Y+IY.EQ.NY+1)) GOTO 20
IF (E(X+IX,Y+IY).GE.9999.0) GOTO 20
C
IF ((IX.EQ.0).OR.(IY.EQ.0))THEN
DX=DX1
CL=CL1
ELSE
DX=DX2
CL=CL2
ENDIF
C
C J=INT(FEAT(X,Y))
C K=INT(FEAT(X+IX,Y+IY))
DH1=E(X,Y)-S(X,Y)
DH2=E(X+IX,Y+IY)-S(X+IX,Y+IY)
HEAD=(DH1-DH2)/DX
C
C IF SLOPE IS > 0.0 - THEREFORE DOWNSLOPE - CALCULATE FLOWS IN
C FROM (X,Y)
C
IF(HEAD.GT.0.0)THEN
QB=K0*M*ABS(HEAD)*(EXP(-S(X,Y)/M))
SUMOUT=SUMOUT+QB/CL
C
ELSE
C
QB=K0*M*ABS(HEAD)*(EXP(-S(X+IX,Y+IY)/M))
SUMIN=SUMIN+QB/CL
C
ENDIF
20 ENDDO
ENDDO
C
C-----
C COMPUTE SATURATED ZONE WATER BALANCE AND DETERMINE EXFILTRATION
C
S(X,Y)=S(X,Y)-SUMIN+SUMOUT+GWL
C-----
C A) CALCULATIONS FOR INITIALLY UNSATURATED AREAS; THEREFORE
C
IF(S(X,Y).LT.0.0)GOTO 99
C
C-----
C ROOT ZONE STORE CALCULATIONS
C
C J=INT(FEAT(X,Y))
IF(COUNT(X,Y).GT.5)THEN
SRZ(X,Y)=SRZ(X,Y)+0.9*PRECIP2(X,Y)
ELSE
SRZ(X,Y)=SRZ(X,Y)+PRECIP2(X,Y)
ENDIF
C
IF(SRZ(X,Y).GT.SRMAX)THEN
SUZ(X,Y)=SUZ(X,Y)+SRZ(X,Y)-SRMAX
SRZ(X,Y)=SRMAX
ENDIF
C
C COMPUTE EVAPORATION FROM ROOT ZONE STORE AT POTENTIAL RATE
C AND COMPUTE RESIDUAL EVAP POTENTIAL IF ET(I) IS UNSATISFIED

```

```

C
EA1=EVAP*(SRZ(X,Y)/SRMAX)
IF(EA1.GT.SRZ(X,Y))EA1=SRZ(X,Y)
SRZ(X,Y)=SRZ(X,Y)-EA1
EA1T=EA1T+EA1
C
C-----
C UNSATURATED ZONE STORE CALCULATIONS
C
C A) SATURATION FROM ABOVE
C
IF(SUZ(X,Y).GT.S(X,Y))THEN
QSOFSUZ(X,Y)-S(X,Y)
SUZ(X,Y)=S(X,Y)
ENDIF
C
C B) UNSATURATED ZONE RECHARGE TO SATURATED ZONE
C
QV=K0*(EXP(-S(X,Y)/M))
IF(QV.GT.SUZ(X,Y))QV=SUZ(X,Y)
SUZ(X,Y)=SUZ(X,Y)-QV
C
C C) EVAPORATION
C
IF((S(X,Y)-SUZ(X,Y)).GE.SRMAX) GOTO 40
C
C RESIDUAL EVAP POTENTIAL
C
E2=EVAP-EA1
C
C DEFICIT FROM SURFACE IS
C
DFS=S(X,Y)-SUZ(X,Y)
C
C WATER AVAILABLE FOR EVAPORATION IS
C
EXAV=SRMAX-DFS
IF(E2.GE.EXAV)EA2=EXAV
IF(E2.LT.EXAV)EA2=E2
EA2T=EA2T+EA2
C
C ADDITIONAL EVAP IS SUBTRACTED FROM QV
C
QV=QV-EA2
C
GOTO 40
C-----
C
C SATURATED ZONE CALCULATIONS
C
99 CONTINUE
C-----
C
C A) CALCULATE EXFILTRATION FLOW
C
IF(S(X,Y).LT.0.0)THEN
QEXFIL= -S(X,Y)
S(X,Y)=0.0
ENDIF

```

```

C
C B) CALCULATE SATURATION EXCESS OVERLAND FLOW
C
  IF(COUNT(X,Y).GT.5)THEN
  SRZ(X,Y)=SRZ(X,Y)+0.9*PRECIP2(X,Y)
  ELSE
  SRZ(X,Y)=SRZ(X,Y)+PRECIP2(X,Y)
  ENDIF
  IF(SRZ(X,Y).GT.SRMAX)THEN
  SUZ(X,Y)=SUZ(X,Y)+SRZ(X,Y)-SRMAX
  SRZ(X,Y)=SRMAX
  ENDIF
  QSOF=SUZ(X,Y)
  SUZ(X,Y)=0.0
C
C C) CALCULATE EVAPORATION
C
  EA1=EVAP*(SRZ(X,Y)/SRMAX)
  IF(EA1.GT.SRZ(X,Y))EA1=SRZ(X,Y)
  SRZ(X,Y)=SRZ(X,Y)-EA1
  EA1T=EA1T+EA1
C
C D) RESIDUAL EVAPORATION POTENTIAL EXTRACTED FROM SAT ZONE
C
  E2=EVAP-EA1
  EXAV=SRMAX
  IF(E2.GE.EXAV)EA2=EXAV
  IF(E2.LT.EXAV)EA2=E2
  S(X,Y)=S(X,Y)+EA2
  EA2T=EA2T+EA2
C
40 CONTINUE
C
  S(X,Y)=S(X,Y)-QV
C
C-----
C
C CALCULATE FLOW ROUTING TO THE GAUGE
C
  IF(COUNT(X,Y).GT.5)THEN
  QTOT=QEXFIL+QSOF+0.1*PRECIP2(X,Y)
  ELSE
  QTOT=QEXFIL+QSOF
  ENDIF
C-----
C A) TIME TO CHANNEL
C
  T1=(DIST1(X,Y)/CHV1)
C
C B) TIME IN CHANNEL
C
  T2=(DIST2(X,Y)/CHV2)
C
C C) TOTAL TRAVEL TIME
C
  TT=T1+T2
  DELAY=INT((TT/3600)+1)
  IF(DELAY.GT.NR)NR=DELAY
C
C D) CALCULATE TIME DELAYED DISCHARGE

```

```

C
  QT(I+DELAY-1)=QT(I+DELAY-1)+QTOT
  QS(I+DELAY-1)=QS(I+DELAY-1)+QEXFIL
C
C-----
C CALCULATE FLOW TOTALS IN TIMESTEP
C
  QEXL(I)=QEXL(I)+QEXFIL
  QSF(I)=QSF(I)+QSOF
C
C CALCULATE PERCENTAGE CONTRIBUTING AREA
C
  IF(QEXFIL.GT.0.0)NQEX=NQEX+1
  IF(QSOF.GT.0.0)NQSF=NQSF+1
  IF(QTOT.GT.0.0)NTOT=NTOT+1
C
C-----
C CALCULATE FINAL WATER STORAGE
C
  IF(I.EQ.N)THEN
    SRZFINAL=SRZFINAL+SRZ(X,Y)
    SUZFINAL=SUZFINAL+SUZ(X,Y)
    SFINAL=SFINAL+S(X,Y)
  ENDIF
C-----
C SUM GRIDCELL EVAPORATION
C
  if(srz(x,y).gt.srmax)write(*,*)'help'
  CUME(X,Y)=CUME(X,Y)+EA1+EA2
C
C-----
C CLOSE GRIDCELL LOOP
C
1  ENDDO
  ENDDO
C-----
C WRITE SOIL MOISTURE MAPS AT THE SPECIFIED TIMES – WHEN IN SINGLE
C PARAMETER SET MODE
C
C DO Y=1,NY
C DO X=1,NX
C
C IF(I.EQ.35)THEN
C IF(E(X,Y).GT.500)THEN
C SWRITE=-9999.0
C ELSE
C SWRITE=S(X,Y)
C ENDIF
C WRITE(20,*)SWRITE
C ENDIF
C
C
C IF(I.EQ.323)THEN
C IF(E(X,Y).GT.500)THEN
C SWRITE=-9999.0
C ELSE
C SWRITE=S(X,Y)
C ENDIF
C WRITE(21,*)SWRITE
C ENDIF

```

```

C
C
C  ENDDO
C  ENDDO
C
C-----
C CONVERT ALL SUMMED DATA BACK TO DEPTHS BY DIVIDING BY THE AREA
C
  EPT=EPT+ET(I)
  QBAR=QBAR+QOBS(I)
  QPRED(I)=QSF(I)+QEXL(I)
C
  QEXL(I)=QEXL(I)/AREA
  QSF(I)=QSF(I)/AREA
  QPRED(I)=QPRED(I)/AREA
  QT(I)=QT(I)/AREA
  QS(I)=QS(I)/AREA
C
  QSFAREA(I)=100*(REAL(NQSF/AREA))
  QEXAREA(I)=100*(REAL(NQEX/AREA))
  QTAREA(I)=100*(REAL(NTOT/AREA))
C
C2-----
C
C  IF(IND.EQ.1)THEN
C  WRITE(*,2000)I,RAIN1(I),QOBS(I),QT(I),QPRED(I)
C  ELSE
C  WRITE(*,2000)I,AVERAIN(I),QOBS(I),QT(I),QPRED(I)
C  ENDIF
C
C2000 FORMAT(1X,'T='1X,I4,1X,'RAIN=',1X,F7.5,1X,'OBS=',1X,F7.5,1X,
C  &'QT=',1X,F7.5,1X,'QPRED=',1X,F7.5,1X)
C
C-----
C
  IF(I.EQ.1)THEN
  IF(QEXL(I).LT.QOBS(1))START=2.0
  ENDIF
C
  IF(I.EQ.1)THEN
  IF(START.EQ.1.0)THEN
  GOTO 2
  ELSE
  START=0.0
  DO Y=1,NY
  DO X=1,NX
  IF(E(X,Y).LT.9000)THEN
  SINIT=SINIT+S(X,Y)
  SRZINIT=SRZINIT+SRZ(X,Y)
  SUZINIT=SUZINIT+SUZ(X,Y)
  ENDIF
  ENDDO
  ENDDO
  ENDIF
  ENDIF
C-----
C
C CLOSE TIMESTEP LOOP
C
10 CONTINUE

```

```

C-----
QBAR=QBAR/N
EA1T=EA1T/AREA
EA2T=EA2T/AREA
EAT=EA2T+EA1T
SINIT=SINIT/AREA
SFINAL=SFINAL/AREA
SRZINIT=SRZINIT/AREA
SRZFINAL=SRZFINAL/AREA
SUZINIT=SUZINIT/AREA
SUZFINAL=SUZFINAL/AREA
C
C CLOSE(20)
C CLOSE(21)
C
C-----
SUMRAIN=0.0
SUMQOBS=0.0
SUMQPRED=0.0
SUMQSF=0.0
SUMQEX=0.0
VAR1=0.0
VAR2=0.0
VAR3=0.0
C
C DO Y=1,NY
C DO X=1,NX
C IF(E(X,Y).EQ.9999)CUME(X,Y)=-9999.0
C WRITE(22,*)CUME(X,Y)
C ENDDO
C ENDDO
C
C OPEN(9,FILE='results.dat',STATUS='UNKNOWN')
C OPEN(10,FILE='pcarea.dat',STATUS='UNKNOWN')
C WRITE(9,*)' RAIN QOBS QT QPRED QEX
C & QSF QS'
C WRITE(9,*)' ---- ---- ---- ---- ---
C & ---- ----'
C
C DO I=1,N
C
C IF(IND.EQ.1)THEN
SUMRAIN=SUMRAIN+RAIN1(I)
ELSE
SUMRAIN=SUMRAIN+AVERAIN(I)
ENDIF
C
SUMQOBS=SUMQOBS+QOBS(I)
SUMQPRED=SUMQPRED+QPRED(I)
SUMQSF=SUMQSF+QSF(I)
SUMQEX=SUMQEX+QEXL(I)
SUMGWL=GWL*N
C
C IF(I.GT.NR)THEN
VAR1=VAR1+((QOBS(I)-QT(I))**2)
VAR2=VAR2+((QOBS(I)-QBAR)**2)
VAR3=VAR3+((QOBS(I)-QPRED(I))**2)
ENDIF
C
C IF(IND.EQ.1)THEN

```

```

C WRITE(9,1000)RAIN1(I),QOBS(I),QT(I),QPRED(I),QEXL(I),QSF(I),QS(I)
C ELSE
C WRITE(9,1000)AVERAIN(I),QOBS(I),QT(I),QPRED(I),QEXL(I),QSF(I),
C & QS(I)
C ENDIF
C
C1000 FORMAT(1X,F10.7,TR3,F10.7,1X,F10.7,1X,F10.7,1X,F10.7,1X,F10.7,
C & 1X,F10.7,1X)
C WRITE(10,1001)QEXAREA(I),QSFAREA(I),QTAREA(I)
C1001 FORMAT(F7.3,1X,F7.3,1X,F7.3)
C
C-----
C WRITE MONTE CARLO SIMULATED DISCHARGES TO FILE
C
C QT2(I,II)=QT(I)
C
C-----
C ENDDO
C
C EFF=100*((VAR2-VAR1)/VAR2)
C
C CLOSE(9)
C CLOSE(10)
C CLOSE(22)
C
C COMPUTE FLOW AND PREDICTION STATISTICS
C
C RCOBS =(SUMQOBS/SUMRAIN)*100
C RCPRED=(SUMQPRED/SUMRAIN)*100
C PQSF=(SUMQSF/SUMQPRED)*100
C PQEX=(SUMQEX/SUMQPRED)*100
C
C OPEN(11,FILE='suminfo.dat',STATUS='UNKNOWN')
C WRITE(11,*)'THE FOLLOWING SIMULATION RESULTS WERE OBTAINED'
C WRITE(11,*)'-----'
C WRITE(11,*)
C WRITE(11,1002)SUMRAIN,SUMQOBS,SUMQPRED,EPT,EAT,EA1T,EA2T,
C & SUMQSF,SUMQEX,SUMGWL
C1002 FORMAT(1X,'TOTALS WERE AS FOLLOWS'//
C & 1X,'RAINFALL      =',F10.6,/
C & 1X,'OBSERVED FLOW   =',F10.6,/
C & 1X,'PREDICTED FLOW  =',F10.6,/
C & 1X,'POTENTIAL ET    =',F10.6,/
C & 1X,'ACTUAL ET       =',F10.6,/
C & 1X,'ACTUAL ET FROM SRZ =',F10.6,/
C & 1X,'ACTUAL ET FROM SAT =',F10.6,/
C & 1X,'SAT EXCESS FLOW  =',F10.6,/
C & 1X,'EXIFLTRATION    =',F10.6,/
C & 1X,'TOTAL GWL       =',F10.6,/)
C
C WRITE(11,1003)VAR1,VAR3,VAR2,EFF,RCOBS,RCPRED,PQSF,PQEX
C1003 FORMAT(1X,'THE FOLLOWING STATISTICS WERE COMPUTED'//
C & 1X,'SUM OF SQUARED ERRORS =',F10.6,/
C & 1X,'SSE (UNROUTED)      =',F10.6,/
C & 1X,'SUM OF MEAN ERRORS  =',F10.6,/
C & 1X,'EFFICIENCY %        =',F10.6,/
C & 1X,'OBS RUNOFF COEFF    =',F10.6,/
C & 1X,'PRED RUNOFF COEFF   =',F10.6,/
C & 1X,'PERCENTAGE QSF     =',F10.6,/
C & 1X,'PERCENTAGE QEX     =',F10.6,/)

```

```
C
C WRITE(11,1004)ZOOM1,ZOOM2
C1004 FORMAT(1X,'SOIL MOSITURE DEFICIT MAPS WERE CREATED AT:-'//
C & 1X,'OBSERVATION NUMBER   =',I4,/
C & 1X,'OBSERVATION NUMBER   =',I4,/)
C
C
C MASS BALANCE CALCULATION
C INPUTS-OUTPUTS=CHANGE IN STORAGE
C
C BALANCE1=SUMRAIN-SUMQPRED-EAT-SUMGWL
C DELTAS= (SINIT-SFINAL)+(SRZFINAL-SRZINIT)+(SUZFINAL-SUZINIT)
C BALANCE=BALANCE1-DELTAS
C
C WRITE(11,1005)BALANCE,SRZINIT,SRZFINAL,SUZINIT,SUZFINAL,
C & SINIT,SFINAL
C1005 FORMAT(1X,'THE MASS BALANCE FOR THE SIMULATION IS',//
C & 1X,'BALANCE (M)           =',F20.6,/
C & 1X,'SRZ IN                 =',F20.6,/
C & 1X,'SRZ OUT                =',F20.6,/
C & 1X,'SUZ IN                 =',F20.6,/
C & 1X,'SUZ OUT                =',F20.6,/
C & 1X,'SOIL DEFICIT IN       =',F20.6,/
C & 1X,'SOIL DEFICIT OUT      =',F20.6)
C
C CLOSE(11)
C
C END
```

APPENDIX 2

Coupled Hydrological-sediment yield model code

```

C  A FULLY DISTRIBUTED GRID BASED SOIL MOISTURE
C  ACCOUNTING MODEL
C  SEDIMENT YIELD MODEL
C
C
C  INTEGER I,II,N,N2,X,Y,NX,NY,NR,LX,NF
C
C  PARAMETER(PNX=242,PNY=391,PNF=10,PN=9000,PNR=10,
& PN2=2000,PNR2=10)
C
C  REAL EFFSS2(PN2),
& R0DASH2(PN2),KSEDASH2(PN2),CHS2DASH2(PN2)
C
C  COMMON /INTS/ I,II,N,N2,X,Y,NX,NY,NR,NR2,LX,NF,
& ZOOM1,ZOOM2
C
C  COMMON /DASH/ R0DASH,PKSEDASH,CHS2DASH,
& EFF,EFFSS,ISTART,IND,RAINAREA(PNX,PNY),PM(PNF),
& PK0(PNF),ETF,CHV1,CHV2,GWL,SMF,R0(PNF),PKSED(PNF),
& E(PNX,PNY),DIST1(PNX,PNY),DIST2(PNX,PNY),QOBS(PN),
& SEDOBS(PN),RAIN1(PN),RAIN2(PN),ET(PN),TEMP(PN),
& RAD(PN),AVERAIN(PN),P1,P2,AREA,AREA1,AREA2,
& QSSC2(PN,PN2),QMIN,QMAX
C
C  COMMON/INICOM/
& QBAR,EPT,EA1T,EA2T,EAT,SINIT,SFINAL,SRZINIT,
& SUZINIT,QEXL(PN),ERAIN,SNOW(PNX,PNY),S(PNX,PNY),SRMAX,
& COUNT(PNX,PNY),FEAT(PNX,PNY),SUZ(PNX,PNY),SRZ(PNX,PNY),
& SUMRAIN,SUMQOBS,SUMQPRED,SUMQSF,VAR1,VAR2,VAR3,VAR4,VAR,
& DTOT(PNX,PNY),TS(PNX,PNY),DSED(PNX,PNY),SEDREM(PNX,PNY),
& QSED(PN),QSSC(PN)
C-----
C  .. External Functions ..
DOUBLE PRECISION G05DAF,G05DEF
EXTERNAL      G05DAF,G05DEF
C  .. External Subroutines ..
EXTERNAL      G05CCF
C  .. Executable Statements ..
CALL G05CCF(0)
C-----
C
C  OPEN HYDROLOGICAL MODEL PARAMETER FILES
C
C  OPEN(1,FILE='grid.dat',STATUS='UNKNOWN')
READ(1,*)NX,NY,LX
READ(1,*)N,ISTART,NF,IND,N2
CLOSE(1)
C
C  OPEN(3,FILE='feature.dat')
OPEN(4,FILE='freedtm.dat')
OPEN(5,FILE='hillslope.dat')
OPEN(55,FILE='channel.dat')
OPEN(7,FILE='rainarea.dat')
C

```

```

AREA=0
C
DO Y=1,NY
DO X=1,NX
READ(3,*)FEAT(X,Y)
READ(4,*)E(X,Y)
READ(5,*)DIST1(X,Y)
READ(55,*)DIST2(X,Y)
READ(7,*)RAINAREA(X,Y)
C
J=INT(FEAT(X,Y))
C
S(X,Y)=0.0
SUZ(X,Y)=0.0
SRZ(X,Y)=SRMAX
C
IF(E(X,Y).LT.9000)AREA=AREA+1
IF(RAINAREA(X,Y).EQ.1)AREA1=AREA1+1
IF(RAINAREA(X,Y).EQ.2)AREA2=AREA2+1
ENDDO
ENDDO
C
C-----
C CALCULATE FRACTIONAL RAINAREAS
C
P1=AREA1/AREA
P2=AREA2/AREA
C-----
C CLOSE(3)
CLOSE(4)
CLOSE(5)
CLOSE(55)
CLOSE(7)
C-----
C OPEN(8,FILE='rrdata.dat',STATUS='UNKNOWN')
C
DO I=1,ISTART-1
IF(IND.EQ.1)THEN
READ(8,*)QOBS(I),SEDOBS(I),RAIN1(I),ET(I),TEMP(I),RAD(I)
ELSE
READ(8,*)QOBS(I),SEDOBS(I),RAIN1(I),RAIN2(I),ET(I),TEMP(I),RAD(I)
ENDIF
ENDDO
C
DO I=1,N
IF(IND.EQ.1)THEN
READ(8,*)QOBS(I),SEDOBS(I),RAIN1(I),ET(I),TEMP(I),RAD(I)
ET(I)=ET(I)*ETF
ELSE
READ(8,*)QOBS(I),SEDOBS(I),RAIN1(I),RAIN2(I),ET(I),TEMP(I),RAD(I)
AVERAIN(I)=(RAIN1(I)*P1)+(RAIN2(I)*P2)
ET(I)=ET(I)*ETF
ENDIF
C-----
C CALCULATE MIN AND MAXIMUM DISCHARGES
C
QMIN=0.00006
QMAX=0.00300
C
IF(QOBS(I).LT.QMIN)THEN

```

```

QMIN=QOBS(I)
ZOOM1=I
ENDIF
IF(QOBS(I).GT.QMAX)THEN
QMAX=QOBS(I)
ZOOM2=I
ENDIF
C
ENDDO
CLOSE(8)
C-----
C OPEN RESULTS FILES FOR THE PARAMETER SEARCH
C
OPEN(997,FILE='sedparams.dat')
OPEN(998,FILE='sedyield.dat')
OPEN(999,FILE='max_params.dat')
C-----
C
MAXEFF=0.0
C
C-----
DO II=1,N2
C
R0DASH=G05DAF(0.80D-08,4.50D-08)
PKSEDASH=G05DAF(3.0D-04-4.80D-04)
CHS2DASH=G05DAF(0.1-1.0)
C
C-----
CALL INIMOD
C
CALL HYDROMOD
C-----
C
R0DASH2(II)=R0DASH
KSEDASH2(II)=PKSEDASH
CHS2DASH2(II)=CHS2DASH
EFF2(II)=EFF
EFFSS2(II)=EFFSS
C
C-----
C
SEARCH FOR GLOBAL OPTIMAL PARAMETER VALUES
C
C
IF(EFFSS2(II).GT.MAXEFF)THEN
MAXR0=R0DASH2(II)
MAXKSED=KSEDASH2(II)
MAXEFFSS=EFFSS2(II)
MAXCHS2=CHS2DASH2(II)
ENDIF
C
C-----
C
CLOSE PARAMETER SEARCH LOOP
C
ENDDO
C
C-----
C

```

```

C WRITING PARAMETER SEARCH VALUES AND OBJECTIVE F TO FILE
C
C-----
C
  DO II=1,N2
  WRITE(997,1000)R0DASH2(II),KSEDASH2(II),CHS2DASH2(II),EFFSS2(II)
1000 FORMAT(1X,F12.10,1X,F10.7,1X,F10.7,1X,F10.3)
C
C
  DO I=1,N
  WRITE(998,1001)QSSC2(I,II)
1001 FORMAT(1X,F10.3)
  ENDDO
  ENDDO
C
C
  WRITE(999,*)MAXR0,MAXKSED,MAXCHS2,MAXEFFSS
C-----
C
  CLOSE(997)
  CLOSE(998)
  CLOSE(999)
C
  STOP
  END
C-----
C SET INITIAL VALUES FOR STORAGES AND TOTALS
C
  SUBROUTINE INIMOD
C
  INTEGER I,II,N,N2,X,Y,NX,NY,NR,LX,NF
C
  PARAMETER(PNX=242,PNY=391,PNF=10,PN=9000,PNR=10,
& PN2=2000,PNR2=10)
C
  REAL QBAR,EPT,EA1T,EA2T,EAT,SINIT,SFINAL,SRZINIT,SUZINIT,
& ERAIN
C
  COMMON /INTS/ I,II,N,N2,X,Y,NX,NY,NR,NR2,LX,NF,
& ZOOM1,ZOOM2
C
  COMMON /INICOM/ QBAR,EPT,EA1T,EA2T,EAT,SINIT,SFINAL,SRZINIT,
& SUZINIT,QEXL(PN),ERAIN,SNOW(PNX,PNY),S(PNX,PNY),SRMAX,
& COUNT(PNX,PNY),FEAT(PNX,PNY),SUZ(PNX,PNY),SRZ(PNX,PNY),
& SUMRAIN,SUMQOBS,SUMQPRED,SUMQSF,VAR1,VAR2,VAR3,VAR4,VAR5,
& DTOT(PNX,PNY),TS(PNX,PNY),DSED(PNX,PNY),SEDREM(PNX,PNY),
& QSED(PN),QSSC(PN)
C
C
  DO Y=1,NY
  DO X=1,NX
C
  J=INT(FEAT(X,Y))
  S(X,Y)=0.0
  SUZ(X,Y)=0.0
  SRMAX=SRDASH
  SRZ(X,Y)=SRMAX
  COUNT(X,Y)=0.0

```

```

SNOW(X,Y)=0.0
DTOT(X,Y)=0.0
DSED(X,Y)=0.0
SEDREM(X,Y)=0.0
TS(X,Y)=0
ENDDO
ENDDO
C
DO I=1,N
QSED(I)=0.0
QSSC(I)=0.0
ENDDO
C
NR=0
NR2=0
QBAR=0.0
EPT=0.0
EA1T=0.0
EA2T=0.0
EAT=0.0
SINIT=0.0
SFINAL=0.0
SRZINIT=0.0
SRZFINAL=0.0
SUZINIT=0.0
SUZFINAL=0.0
QEXL(1)=10.0
ERAIN=0.0
QV=0.0
SUMRAIN=0.0
SUMQOBS=0.0
SUMQPRED=0.0
SUMQSF=0.0
SUMQEX=0.0
VAR1=0.0
VAR2=0.0
VAR3=0.0
VAR4=0.0
VAR5=0.0
C
END
C-----
C
SUBROUTINE HYDROMOD
C-----
C
INTEGER I,II,N,N2,X,Y,IX,IY,NX,NY,LX,N,NF,NR,
& ZOOM1,ZOOM2,IND,DELAY,ISTART,NR2
C
PARAMETER(PNX=242,PNY=391,PNF=10,PN=9000,PNR=10,
& PN2=2000,PNR2=10)
C
REAL CL,TT,DH1,DH2,
& QSF(PN),QPRED(PN),QS(PN),QT(PN),
& QSFAREA(PN),QEXAREA(PN),QTAREA(PN),
& HEAD,PQSF,PQEX,QEXFIL,QSOFF,NTOT,NQSF,
& NQEX,BALANCE,BALANCE1,DELTAS,PRECIP,EA1,
& EA2,EVAP,E2,NSED,NCON,R02,PKSED2,

```

```

& EA1T,EA2T,EAT,QV,CUME(PNX,PNY),SRZINIT,
& TEMP2(PNX,PNY),M,K0(PNF),CHS1,CHS2,SEDFIN,
& MELT(PNX,PNY),PRECIP2(PNX,PNY)
C
COMMON /INTS/ I,II,N,N2,X,Y,NX,NY,NR,NR2,LX,NF,
& ZOOM1,ZOOM2
C
COMMON /DASH/ R0DASH,PKSEDASH,CHS2DASH,
& EFF,EFFSS,ISTART,IND,RAINAREA(PNX,PNY),PM(PNF),
& PK0(PNF),ETF,CHV1,CHV2,GWL,SMF,R0(PNF),PKSED(PNF),
& E(PNX,PNY),DIST1(PNX,PNY),DIST2(PNX,PNY),QOBS(PN),SEDOBS(PN),
& RAIN1(PN),RAIN2(PN),ET(PN),TEMP(PN),RAD(PN),AVERAIN(PN),P1,P2,
& AREA,AREA1,AREA2,QSSC2(PN,PN2),
& QMIN,QMAX
C
COMMON /INICOM/ QBAR,EPT,EA1T,EA2T,EAT,SINIT,SFINAL,SRZINIT,
& SUZINIT,QEXL(PN),ERAIN,SNOW(PNX,PNY),S(PNX,PNY),SRMAX,
& COUNT(PNX,PNY),FEAT(PNX,PNY),SUZ(PNX,PNY),SRZ(PNX,PNY),
& SUMRAIN,SUMQOBS,SUMQPRED,SUMQSF,VAR1,VAR2,VAR3,VAR4,VAR5,
& DTOT(PNX,PNY),TS(PNX,PNY),DSED(PNX,PNY),SEDREM(PNX,PNY),
& QSED(PN),QSSC(PN)
C
DOUBLE PRECISION QSEDU(PN),
& QSEDAREA(PN),SUMQSSC,QSSCU(PN)
C
C
C-----
C
C ASSIGN NEW NAMES TO PARAMETERS TO BE VARIED
C
M=0.03966
K0(1)=7.50368
K0(2)=2*K0(1)
K0(3)=4*K0(1)
K0(4)=0.6*K0(1)
K0(5)=0.5*K0(1)
SRMAX=0.00574
CHV2=0.78925
ETF=0.56688
C-----
C
GWL=0.0
SMF=0.000094
CHV1=0.1
C-----
R02=R0DASH
PKSED2=PKSEDASH
CHS1=0.1
CHS2=CHS2DASH
C
C CALCULATE CELL DISTANCES AND CONTOUR LENGTHS
C
C (CARDINAL)
DX1=LX
CL1=LX*0.5
C (DIAGONAL)
DX2=LX*1.41421
CL2=LX*0.707
C
C INITIALISE SETTINGS FOR STORAGES AND TOTALS

```

```

C
NR=0
NR2=0
QBAR=0.0
QSSCBAR=0.0
EPT=0.0
EA1T=0.0
EA2T=0.0
EAT=0.0
SINIT=0.0
SFINAL=0.0
SRZINIT=0.0
SRZFINAL=0.0
SUZINIT=0.0
SUZFINAL=0.0
SEDFIN=0.0
QEXL(1)=10.0
ERAIN=0.0
QV=0.0
C
C INITIALISE SPATIAL STORAGES
C
DO Y=1,NY
DO X=1,NX
C
DTOT(X,Y)=0.0
DSED(X,Y)=0.0
SEDREM(X,Y)=0.0
TS(X,Y)=0
COUNT(X,Y)=0
SNOW(X,Y)=0.0
SRZ(X,Y)=SRMAX
ENDDO
ENDDO
C
C-----
C
C START MAIN PROGRAM LOOP - DO 10
C
C-----
C
DO 10 I=1,N
C
C START INITIAL SOIL DRAINAGE UNTIL QEXL = QOBS(1), AND THEREFORE
C AUTOMATICALLY SET THE SOIL MOISTURE DISTRIBUTION
C
2 IF(I.EQ.1)THEN
IF(QEXL(I).GT.QOBS(1))THEN
RAIN1(I)=0.0
RAIN2(I)=0.0
ET(I)=0.0
START=1.0
DO JI=1,N
QT(JI)=0.0
QS(JI)=0.0
ENDDO
ELSE
START=2.0
ET(I)=ET(I)
RAIN1(I)=RAIN1(I)

```

```

RAIN2(I)=RAIN2(I)
ENDIF
ENDIF
C
NTOT=0.0
NQSF=0.0
NQEX=0.0
NSED=0.0
NCON=0.0
C
C-----
C START INTERNAL GRID LOOP FOR EACH TIMESTEP OF THE SIMULATION
C
DO Y=1,NY
DO X=1,NX
C
IF(E(X,Y).GE.9998.0)GOTO 1
EVAP=ET(I)
IF(IND.EQ.1)PRECIP=RAIN1(I)
IF(IND.EQ.2)THEN
IF(RAINAREA(X,Y).EQ.1)THEN
PRECIP=RAIN1(I)
ELSE
PRECIP=RAIN2(I)
ENDIF
ENDIF
C
PRECIP=RAIN1(I)
C-----
C CALCULATE DEPTH OF SNOWMELT RUNOFF
C
TEMP2(X,Y)=TEMP(I)-0.0065*(E(X,Y)-110)
IF(TEMP2(X,Y).LE.0.0)THEN
SNOW(X,Y)=SNOW(X,Y)+PRECIP
PRECIP2(X,Y)=0.0
MELT(X,Y)=0.0
COUNT(X,Y)=COUNT(X,Y)+1
IF((TEMP2(X,Y).GT.0.0).AND.(COUNT(X,Y).GT.10))THEN
SNOW(X,Y)=SNOW(X,Y)+PRECIP
PRECIP2(X,Y)=0.0
MELT(X,Y)=0.0
COUNT(X,Y)=COUNT(X,Y)-1
IF(COUNT(X,Y).LT.0)THEN
COUNT(X,Y)=0
ENDIF
IF(TEMP2(X,Y).GT.0.0)THEN
MELT(X,Y)=1*((SMF*(TEMP2(X,Y)-0))+(0.00125* $RAD(I)$ *(1-0.8))
&-(0.0000000558*((TEMP2(X,Y)+273)**4)))
PRECIP=PRECIP
COUNT(X,Y)=COUNT(X,Y)-1
IF(COUNT(X,Y).LT.0)THEN
COUNT(X,Y)=0
ENDIF
IF((MELT(X,Y).GT.0.0).AND.(MELT(X,Y).LT.SNOW(X,Y)))THEN
PRECIP2(X,Y)=MELT(X,Y)+PRECIP
SNOW(X,Y)=SNOW(X,Y)-MELT(X,Y)
MELT(X,Y)=0.0
IF((MELT(X,Y).GT.0.0).AND.(MELT(X,Y).GE.SNOW(X,Y)))THEN
MELT(X,Y)=SNOW(X,Y)
PRECIP2(X,Y)=MELT(X,Y)+PRECIP

```

```

        SNOW(X,Y)=0.0
        MELT(X,Y)=0.0
    ENDIF
ENDIF
ENDIF
ENDIF
ENDIF
C
    PRECIP2(X,Y)=MELT(X,Y)+PRECIP
C-----
    SUMOUT=0.0
    SUMIN=0.0
    QEXFIL=0.0
    QSOF=0.0
    QTOT=0.0
    QV=0.0
    EA1=0.0
    EA2=0.0
    E2=0.0
C-----
C START INTERNAL MOVING WINDOW FOR FLOW ROUTING CALCULATIONS
C
    DO IX=-1,1
    DO IY=-1,1
C
    IF ((IX.EQ.0).AND.(IY.EQ.0))    GOTO 20
    IF ((X+IX.EQ.0).OR.(X+IX.EQ.NX+1)) GOTO 20
    IF ((Y+IY.EQ.0).OR.(Y+IY.EQ.NY+1)) GOTO 20
    IF (E(X+IX,Y+IY).GE.9999.0)    GOTO 20
C
    IF ((IX.EQ.0).OR.(IY.EQ.0))THEN
        DX=DX1
        CL=CL1
    ELSE
        DX=DX2
        CL=CL2
    ENDIF
C
    J=INT(FEAT(X,Y))
    K=INT(FEAT(X+IX,Y+IY))
    DH1=E(X,Y)-S(X,Y)
    DH2=E(X+IX,Y+IY)-S(X+IX,Y+IY)
    HEAD=(DH1-DH2)/DX
C
C-----
C IF SLOPE IS > 0.0 - THEREFORE DOWNSLOPE - CALCULATE FLOWS IN
C FROM (X,Y)
C
    IF(HEAD.GT.0.0)THEN
        QB=K0(J)*M*ABS(HEAD)*(EXP(-S(X,Y)/M))
        SUMOUT=SUMOUT+QB/CL
C
    ELSE
C
        QB=K0(K)*M*ABS(HEAD)*(EXP(-S(X+IX,Y+IY)/M))
        SUMIN=SUMIN+QB/CL
C
    ENDIF
20  ENDDO
    ENDDO

```

```

C
C-----
C COMPUTE SATURATED ZONE WATER BALANCE AND DETERMINE EXFILTRATION
C
  S(X,Y)=S(X,Y)-SUMIN+SUMOUT+GWL
C
C-----
C A) CALCULATIONS FOR INITIALLY UNSATURATED AREAS; THEREFORE
C
  IF(S(X,Y).LT.0.0)GOTO 99
C
C-----
C ROOT ZONE STORE CALCULATIONS
C
  J=INT(FEAT(X,Y))
  IF(COUNT(X,Y).GT.5)THEN
    SRZ(X,Y)=SRZ(X,Y)+0.9*PRECIP2(X,Y)
  ELSE
    SRZ(X,Y)=SRZ(X,Y)+PRECIP2(X,Y)
  ENDIF
C
  IF(SRZ(X,Y).GT.SRMAX)THEN
    SUZ(X,Y)=SUZ(X,Y)+SRZ(X,Y)-SRMAX
    SRZ(X,Y)=SRMAX
  ENDIF
C
C COMPUTE EVAPORATION FROM ROOT ZONE STORE AT POTENTIAL RATE
C AND COMPUTE RESIDUAL EVAP POTENTIAL IF ET(I) IS UNSATISFIED
C
  EA1=EVAP*(SRZ(X,Y)/SRMAX)
  IF(EA1.GT.SRZ(X,Y))EA1=SRZ(X,Y)
  SRZ(X,Y)=SRZ(X,Y)-EA1
  EA1T=EA1T+EA1
C
C-----
C UNSATURATED ZONE STORE CALCULATIONS
C
C A) SATURATION FROM ABOVE
C
  IF(SUZ(X,Y).GT.S(X,Y))THEN
    QSOF=SUZ(X,Y)-S(X,Y)
    SUZ(X,Y)=S(X,Y)
  ENDIF
  IF(QSOF.LE.0.0)THEN
    TS(X,Y)=TS(X,Y)+1
    DSED(X,Y)=R02*EXP(-PKSED2*TS(X,Y))
    DTOT(X,Y)=DTOT(X,Y)+DSED(X,Y)
    SEDREM(X,Y)=0.0
  ELSE
    SEDREM(X,Y)=DTOT(X,Y)
    DTOT(X,Y)=0.0
    TS(X,Y)=0.0
  ENDIF
C
C B) UNSATURATED ZONE RECHARGE TO SATURATED ZONE
C
  QV=K0(J)*(EXP(-S(X,Y)/M))
  IF(QV.GT.SUZ(X,Y))QV=SUZ(X,Y)
  SUZ(X,Y)=SUZ(X,Y)-QV
C

```

```

C C) EVAPORATION
C
C IF((S(X,Y)-SUZ(X,Y)).GE.SRMAX) GOTO 40
C
C RESIDUAL EVAP POTENTIAL
C
C E2=EVAP-EA1
C
C DEFICIT FROM SURFACE IS
C
C DFS=S(X,Y)-SUZ(X,Y)
C
C WATER AVAILABLE FOR EVAPORATION IS
C
C EXAV=SRMAX-DFS
C IF(E2.GE.EXAV)EA2=EXAV
C IF(E2.LT.EXAV)EA2=E2
C EA2T=EA2T+EA2
C
C ADDITIONAL EVAP IS SUBTRACTED FROM QV
C
C QV=QV-EA2
C
C GOTO 40
C-----
C
C SATURATED ZONE CALCULATIONS
C
C 99 CONTINUE
C-----
C
C A) CALCULATE EXFILTRATION FLOW
C
C IF(S(X,Y).LT.0.0)THEN
C QEXFIL=-S(X,Y)
C S(X,Y)=0.0
C ENDIF
C
C B) CALCULATE SATURATION EXCESS OVERLAND FLOW
C
C IF(COUNT(X,Y).GT.5)THEN
C SRZ(X,Y)=SRZ(X,Y)+0.9*PRECIP2(X,Y)
C ELSE
C SRZ(X,Y)=SRZ(X,Y)+PRECIP2(X,Y)
C ENDIF
C IF(SRZ(X,Y).GT.SRMAX)THEN
C SUZ(X,Y)=SUZ(X,Y)+SRZ(X,Y)-SRMAX
C SRZ(X,Y)=SRMAX
C ENDIF
C QSOF=SUZ(X,Y)
C IF(QSOF.GT.0.0)THEN
C SEDREM(X,Y)=DTOT(X,Y)
C DTOT(X,Y)=0.0
C TS(X,Y)=0
C ENDIF
C SUZ(X,Y)=0.0
C
C C) CALCULATE EVAPORATION
C

```

```

EA1=EVAP*(SRZ(X,Y)/SRMAX)
IF(EA1.GT.SRZ(X,Y))EA1=SRZ(X,Y)
SRZ(X,Y)=SRZ(X,Y)-EA1
EA1T=EA1T+EA1
C
C D) RESIDUAL EVAPORATION POTENTIAL EXTRACTED FROM SAT ZONE
C
E2=EVAP-EA1
EXAV=SRMAX
IF(E2.GE.EXAV)EA2=EXAV
IF(E2.LT.EXAV)EA2=E2
S(X,Y)=S(X,Y)+EA2
EA2T=EA2T+EA2
C
40 CONTINUE
C
S(X,Y)=S(X,Y)-QV
C
C-----
C
C CALCULATE FLOW ROUTING TO THE GAUGE
C
IF(COUNT(X,Y).GT.5)THEN
QTOT=QEXFIL+QSOF+0.1*PRECIP2(X,Y)
ELSE
QTOT=QEXFIL+QSOF
ENDIF
C-----
C A) TIME TO CHANNEL
C
T1=(DIST1(X,Y)/CHV1)
T12=(DIST1(X,Y)/CHS1)
C
C B) TIME IN CHANNEL
C
T2=(DIST2(X,Y)/CHV2)
T22=(DIST2(X,Y)/CHS2)
C
C C) TOTAL TRAVEL TIME
C
TT=T1+T2
TT2=T12+T22
DELAY=INT((TT/3600)+1)
DELAY2=INT((TT2/3600)+1)
IF(DELAY.GT.NR)NR=DELAY
IF(DELAY2.GT.NR2)NR2=DELAY2
C
C D) CALCULATE TIME DELAYED DISCHARGE
C
QT(I+DELAY-1)=QT(I+DELAY-1)+QTOT
QS(I+DELAY-1)=QS(I+DELAY-1)+QEXFIL
QSED(I+DELAY2-2)=QSED(I+DELAY2-2)+0.0096*SEDREM(X,Y)
QSED(I+DELAY2-1)=QSED(I+DELAY2-1)+0.40357*SEDREM(X,Y)
QSED(I+DELAY2)=QSED(I+DELAY2)+0.2663*SEDREM(X,Y)
QSED(I+DELAY2+1)=QSED(I+DELAY2+1)+0.1500*SEDREM(X,Y)
QSED(I+DELAY2+2)=QSED(I+DELAY2+2)+0.0890*SEDREM(X,Y)
QSED(I+DELAY2+3)=QSED(I+DELAY2+3)+0.0417*SEDREM(X,Y)
QSED(I+DELAY2+4)=QSED(I+DELAY2+4)+0.01976*SEDREM(X,Y)
QSED(I+DELAY2+5)=QSED(I+DELAY2+5)+0.01223*SEDREM(X,Y)
QSED(I+DELAY2+6)=QSED(I+DELAY2+6)+0.00784*SEDREM(X,Y)

```

```

C
C-----
C CALCULATE FLOW TOTALS IN TIMESTEP
C
  QEXL(I)=QEXL(I)+QEXFIL
  QSF(I)=QSF(I)+QSOFF
  QSEDU(I)=QSEDU(I)+SEDREM(X,Y)
C
C CALCULATE PERCENTAGE CONTRIBUTING AREA
C
  IF(QEXFIL.GT.0.0)NQEX=NQEX+1
  IF(QSOFF.GT.0.0)NQSF=NQSF+1
  IF(QTOT.GT.0.0)NTOT=NTOT+1
  IF(SEDREM(X,Y).GT.0.0)NSED=NSED+1
C
C-----
C CALCULATE FINAL WATER STORAGE
C
  IF(I.EQ.N)THEN
    SRZFINAL=SRZFINAL+SRZ(X,Y)
    SUZFINAL=SUZFINAL+SUZ(X,Y)
    SFINAL=SFINAL+S(X,Y)
    SEDFIN=SEDFIN+DTOT(X,Y)
  ENDIF
C
C-----
C SUM GRIDCELL EVAPORATION
C
  if(srz(x,y).gt.srmax)write(*,*)'help'
  CUME(X,Y)=CUME(X,Y)+EA1+EA2
C
C-----
C CLOSE GRIDCELL LOOP
C
1  ENDDO
  ENDDO
C
C-----
C WRITE SOIL MOISTURE MAPS AT THE SPECIFIED TIMES – ENABLED WHEN RUNNING
C MODEL FOR SINGLE PARAMETER SET
C
C DO Y=1,NY
C DO X=1,NX
C
C IF(I.EQ.253)THEN
C IF(E(X,Y).GT.500)THEN
C SWRITE=-9999.0
C ELSE
C SWRITE=S(X,Y)
C ENDIF
C WRITE(20)SWRITE
C ENDIF
C
C IF(I.EQ.253)THEN
C IF(E(X,Y).GT.500)THEN
C SWRITE=-9999.0
C ELSE
C SWRITE=SEDREM(X,Y)
C ENDIF
C WRITE(23)SWRITE
C ENDIF
C

```

```

C IF(I.EQ.310)THENC
C IF(E(X,Y).GT.500)THEN
C SWRITE=-9999.0
C ELSE
C SWRITE=S(X,Y)
C ENDIF
C WRITE(21)SWRITE
C ENDIF
C
C IF(I.EQ.310)THEN
C IF(E(X,Y).GT.500)THEN
C SWRITE=-9999.0
C ELSE
C SWRITE=SEDREM(X,Y)
C ENDIF
C WRITE(24)SWRITE
C ENDIF
C
C ENDDO
C ENDDO
C
C-----
C CONVERT ALL SUMMED DATA BACK TO DEPTHS BY DIVIDING BY THE AREA
C
  EPT=EPT+ET(I)
  QBAR=QBAR+QOBS(I)
  QSSCBAR=QSSCBAR+SEDOBS(I)
  QPRED(I)=QSF(I)+QEXL(I)
  QSSC(I)=2.65E06*(QSED(I)/QT(I))
  QSSCU(I)=2.65E06*(QSEDU(I)/QPRED(I))
C
  QEXL(I)=QEXL(I)/AREA
  QSF(I)=QSF(I)/AREA
  QPRED(I)=QPRED(I)/AREA
  QT(I)=QT(I)/AREA
  QS(I)=QS(I)/AREA
C
  QSFAREA(I)=100*(REAL(NQSF/AREA))
  QEXAREA(I)=100*(REAL(NQEX/AREA))
  QTAREA(I)=100*(REAL(NTOT/AREA))
  QSEDAREA(I)=100*(REAL(NSED/AREA))
C  QSSCAREA(I)=100*(REAL(NSED/AREA))
C
C2-----
C WRITE FLOW TIME-SERIES RESULTS – ENABLED WHEN IN SINGLE PARAMETER MODE
C
C IF(IND.EQ.1)THEN
C WRITE(*,2000)I,RAIN1(I),QOBS(I),QT(I),QPRED(I),QSED(I),QSSC(I)
C ELSE
C WRITE(*,2000)I,AVERAIN(I),QOBS(I),QT(I),QPRED(I),QSED(I),QSSC(I)
C ENDIF
C
C2000 FORMAT(1X,'T='1X,I4,1X,'RAIN='1X,F7.5,1X,'OBS='1X,F7.5,1X,
C &'QT='1X,F7.5,1X,'QPRED='1X,F7.5,1X,'QSED='1X,F7.5,1X,
C &'QSEDCON='1X,F7.5,1X)
C
C-----
C
  IF(I.EQ.1)THEN
  IF(QEXL(I).LT.QOBS(1))START=2.0

```

```

ENDIF
C
IF(I.EQ.1)THEN
IF(START.EQ.1.0)THEN
GOTO 2
ELSE
START=0.0
DO Y=1,NY
DO X=1,NX
IF(E(X,Y).LT.9000)THEN
SINIT=SINIT+S(X,Y)
SRZINIT=SRZINIT+SRZ(X,Y)
SUZINIT=SUZINIT+SUZ(X,Y)
ENDIF
ENDDO
ENDDO
ENDIF
ENDIF
C-----
C
C CLOSE TIMESTEP LOOP
C
10 CONTINUE
C-----
QBAR=QBAR/N
QSSCBAR=QSSCBAR/N
EA1T=EA1T/AREA
EA2T=EA2T/AREA
EAT=EA2T+EA1T
SINIT=SINIT/AREA
SFINAL=SFINAL/AREA
SRZINIT=SRZINIT/AREA
SRZFINAL=SRZFINAL/AREA
SUZINIT=SUZINIT/AREA
SUZFINAL=SUZFINAL/AREA
SEDFIN=SEDFIN/AREA
C
CLOSE(20)
CLOSE(21)
CLOSE(23)
CLOSE(24)
CLOSE(25)
C
C-----
SUMRAIN=0.0
SUMQOBS=0.0
SUMQPRED=0.0
SUMQSF=0.0
SUMQEX=0.0
SUMQSED=0.0
SUMQSSC=0.0
VAR1=0.0
VAR2=0.0
VAR3=0.0
VAR4=0.0
VAR5=0.0
C
C DO Y=1,NY
C DO X=1,NX
C IF(E(X,Y).EQ.9999)CUME(X,Y)=-9999.0

```

```

C WRITE(22)CUME(X,Y)
C ENDDO
C ENDDO
C
C OPEN(9,FILE='results.dat',STATUS='UNKNOWN')
C OPEN(10,FILE='pcarea.dat',STATUS='UNKNOWN',FORM='UNFORMATTED')
C OPEN(99,FILE='sediment.dat',STATUS='UNKNOWN',FORM='UNFORMATTED')
C WRITE(9,*) RAIN QOBS QT QPRED QEX
C & QSF QS'
C WRITE(9,*)' ---- ---- ---- ---- ----
C & ---- ----'
C WRITE(99)' SEDOBS QSED QSEDU QSSC
C & QSSCU'
C WRITE(99)' ----- ---- ---- ----
C & -----'
C
C DO I=1,N
C
C IF(IND.EQ.1)THEN
SUMRAIN=SUMRAIN+RAIN1(I)
ELSE
SUMRAIN=SUMRAIN+AVERAIN(I)
ENDIF
C
SUMQOBS=SUMQOBS+QOBS(I)
SUMQPRED=SUMQPRED+QPRED(I)
SUMQSF=SUMQSF+QSF(I)
SUMQEX=SUMQEX+QEXL(I)
SUMQSED=SUMQSED+QSED(I)
SUMQSSC=SUMQSSC+QSSC(I)
SUMGWL=GWL*N
C
IF(I.GT.NR)THEN
VAR1=VAR1+((QOBS(I)-QT(I))**2)
VAR2=VAR2+((QOBS(I)-QBAR)**2)
VAR3=VAR3+((QOBS(I)-QPRED(I))**2)
ENDIF
IF(I.GT.NR2)THEN
VAR4=VAR4+((SEDOBS(I)-QSSC(I))**2)
VAR5=VAR5+((SEDOBS(I)-QSSCBAR)**2)
ENDIF
C
C IF(IND.EQ.1)THEN
C WRITE(9,1000)RAIN1(I),QOBS(I),QT(I),QPRED(I),QEXL(I),QSF(I),QS(I)
C ELSE
C WRITE(9,1000)AVERAIN(I),QOBS(I),QT(I),QPRED(I),QEXL(I),QSF(I),
C & QS(I)
C ENDF
C
C1000 FORMAT(1X,F10.7,TR3,F10.7,1X,F10.7,1X,F10.7,1X,F10.7,1X,F10.7,
C & 1X,F10.7,1X)
C WRITE(10)QEXAREA(I),QSFAREA(I),QTAREA(I),QSEDAREA(I),QSSCAREA(I)
C1001 FORMAT(F7.3,1X,F7.3,1X,F7.3,1X,F7.3,1X,F7.3)
C
C WRITE(99)SEDOBS(I),QSED(I),QSEDU(I),QSSC(I),QSSCU(I)
C1010 FORMAT(1X,F10.5,1X,F10.7,1X,F10.7,1X,F10.5,1X,F10.5,1X)
C
C-----
C ASSIGN QSED TO 2-D ARRAY

```

```

C
C QSSC2(I,II)=QSSC(I)
C
C ENDDO
C
C EFF=100*((VAR2-VAR1)/VAR2)
C EFFSS=100*((VAR5-VAR4)/VAR5)
C
C CLOSE(9)
C CLOSE(10)
C CLOSE(99)
C CLOSE(22)
C
C COMPUTE FLOW AND PREDICTION STATISTICS
C
C RCOBS =(SUMQOBS/SUMRAIN)*100
C RCPRED=(SUMQPRED/SUMRAIN)*100
C PQSF=(SUMQSF/SUMQPRED)*100
C PQEX=(SUMQEX/SUMQPRED)*100
C PSED=(SUMQSED/SUMRAIN)*100
C
C WRITE SUMMARY RESULTS FILE – ENABLED IN SINGLE PARAMETER SET MODE
C
C OPEN(11,FILE='suminfo.dat',STATUS='UNKNOWN')
C WRITE(11,*)'THE FOLLOWING SIMULATION RESULTS WERE OBTAINED'
C WRITE(11,*)'-----'
C WRITE(11,*)
C WRITE(11,1002)SUMRAIN,SUMQOBS,SUMQPRED,EPT,EAT,EA1T,EA2T,
C & SUMQSF,SUMQEX,SUMGWL
C1002 FORMAT(1X,'TOTALS WERE AS FOLLOWS'//
C & 1X,'RAINFALL      =',F10.6,/
C & 1X,'OBSERVED FLOW   =',F10.6,/
C & 1X,'PREDICTED FLOW  =',F10.6,/
C & 1X,'POTENTIAL ET    =',F10.6,/
C & 1X,'ACTUAL ET       =',F10.6,/
C & 1X,'ACTUAL ET FROM SRZ =',F10.6,/
C & 1X,'ACTUAL ET FROM SAT =',F10.6,/
C & 1X,'SAT EXCESS FLOW  =',F10.6,/
C & 1X,'EXIFLTRATION    =',F10.6,/
C & 1X,'TOTAL GWL       =',F10.6,/)
C
C WRITE(11,1003)VAR1,VAR3,VAR2,EFFSS,EFF,RCOBS,RCPRED,PQSF,PQEX,PSED
C1003 FORMAT(1X,'THE FOLLOWING STATISTICS WERE COMPUTED'//
C & 1X,'SUM OF SQUARED ERRORS =',F10.6,/
C & 1X,'SSE (UNROUTED)      =',F10.6,/
C & 1X,'SUM OF MEAN ERRORS  =',F10.6,/
C & 1X,'EFF % FOR SEDIMENT  =',F10.6,/
C & 1X,'EFFICIENCY %        =',F10.6,/
C & 1X,'OBS RUNOFF COEFF    =',F10.6,/
C & 1X,'PRED RUNOFF COEFF   =',F10.6,/
C & 1X,'PERCENTAGE QSF      =',F10.6,/
C & 1X,'PERCENTAGE QEX      =',F10.6,/
C & 1X,'PERCENTAGE QSED     =',F10.6,/)
C
C WRITE(11,1004)ZOOM1,ZOOM2
C1004 FORMAT(1X,'SOIL MOSITURE DEFICIT MAPS WERE CREATED AT:-'//
C & 1X,'OBSERVATION NUMBER  =',I4,/
C & 1X,'OBSERVATION NUMBER  =',I4,/)
C
C

```

```
C MASS BALANCE CALCULATION
C INPUTS-OUTPUTS=CHANGE IN STORAGE
C
  BALANCE1=SUMRAIN-SUMQPRED-EAT-SUMGWL
  DELTAS= (SINIT-SFINAL)+(SRZFINAL-SRZINIT)+(SUZFINAL-SUZINIT)
  BALANCE=BALANCE1-DELTAS
C
C  WRITE(11,1005)BALANCE,SRZINIT,SRZFINAL,SUZINIT,SUZFINAL,
C &      SINIT,SFINAL
C1005 FORMAT(1X,'THE MASS BALANCE FOR THE SIMULATION IS',//
C &      1X,'BALANCE (M)          =',F20.6,/
C &      1X,'SRZ IN              =',F20.6,/
C &      1X,'SRZ OUT              =',F20.6,/
C &      1X,'SUZ IN              =',F20.6,/
C &      1X,'SUZ OUT              =',F20.6,/
C &      1X,'SOIL DEFICIT IN     =',F20.6,/
C &      1X,'SOIL DEFICIT OUT    =',F20.6)
C
C  CLOSE(11)
C
C  STOP 'SIMULATION TERMINATED'
END
```